



HAL
open science

Mechanistic modeling and optimization of vaccine response in infectious diseases: application to HIV, Ebola and Sars-CoV-2

Marie Alexandre

► **To cite this version:**

Marie Alexandre. Mechanistic modeling and optimization of vaccine response in infectious diseases: application to HIV, Ebola and Sars-CoV-2. Statistics [stat]. Université de Bordeaux, 2022. English. NNT: 2022BORD0157 . tel-04403589v1

HAL Id: tel-04403589

<https://inria.hal.science/tel-04403589v1>

Submitted on 18 Jan 2024 (v1), last revised 25 Jan 2024 (v2)

HAL is a multi-disciplinary open access archive for the deposit and dissemination of scientific research documents, whether they are published or not. The documents may come from teaching and research institutions in France or abroad, or from public or private research centers.

L'archive ouverte pluridisciplinaire **HAL**, est destinée au dépôt et à la diffusion de documents scientifiques de niveau recherche, publiés ou non, émanant des établissements d'enseignement et de recherche français ou étrangers, des laboratoires publics ou privés.



Distributed under a Creative Commons Attribution 4.0 International License

THÈSE PRÉSENTÉE POUR OBTENIR LE GRADE DE
DOCTEUR DE L'UNIVERSITÉ DE BORDEAUX

ÉCOLE DOCTORALE SOCIÉTÉS, POLITIQUE, SANTÉ PUBLIQUE
SPÉCIALITÉ SANTÉ PUBLIQUE, OPTION BIOSTATISTIQUE

Par Marie ALEXANDRE

MODÉLISATION MÉCANISTE ET OPTIMISATION DE
LA RÉPONSE VACCINALE CONTRE LES MALADIES
INFÉCTIEUSES : APPLICATION AU VIH, À EBOLA ET
AU SARS-COV-2

Mechanistic modeling and optimization of vaccine response in
infectious diseases: application to HIV, Ebola and SARS-CoV-2

Sous la direction de Rodolphe THIÉBAUT et Mélanie PRAGUE

Soutenue le 10 mai 2022 à Bordeaux

Membres du jury

OPATOWSKI Lulla, Professeure, Université Versailles-Saint-Quentin-en-Yvelines, Paris Rapporteuse
GRAW Frederik, Doctor, Heidelberg University, Heidelberg..... Rapporteur
PROUST-LIMA Cécile, Directrice de recherche, Inserm U1219, Bordeaux..... Présidente du Jury
WHITE Michael, Docteur, Institut Pasteur, Paris Examineur
HEFFERNAN Jane Marie, Professor, York University, Toronto Examinatrice
PRAGUE Mélanie, Chargée de recherche, Inria, Bordeaux..... Co-directrice de thèse
THIÉBAUT Rodolphe, PU-PH, Inserm U1219, Bordeaux..... Directeur de thèse
GUEDJ Jérémie, Directeur de recherche, Inserm U1137, Paris..... Invité

Contents

Remerciements	7
Scientific production	11
Abbreviations and Notations	14
Résumé substantiel	17
Introduction	23
PART I Biological and mathematical background	27
Chapter 1: Biological background in immunology and vaccinology	29
1.1 The immune system	30
1.1.1 The innate immune response	30
1.1.2 The adaptive immune response	31
1.1.2.1 The main actors of the adaptive immunity	31
1.1.2.2 The phases and the properties of the adaptive immunity	34
1.2 Vaccination	36
1.2.1 Principle and brief history of vaccination	36
1.2.2 Vaccine strategies	37
1.2.3 Clinical trials and vaccine development	39
1.2.3.1 The relevance of pre-clinical studies in vaccine development	39
1.2.3.2 The different phases of the vaccine clinical trials	40
1.2.3.3 Evaluation of vaccine efficacy	41
Chapter 2: Mathematical and statistical modelling of infectious disease dynamics	47
2.1 The role of mathematical modelling	48
2.2 Descriptive models for longitudinal data in epidemiology	49
2.2.1 Incomplete longitudinal data	50
2.2.2 The linear Mixed-Effects models	51
2.2.2.1 General model	51
2.2.2.2 Statistical inference and model estimation using maximum likelihood estimation	53
2.2.2.3 Optimization algorithms	54
2.2.2.4 Model with censored data	57
2.2.2.5 Estimation of individual parameters	58
2.2.3 Surrogate endpoint in causal modeling framework	59
2.2.3.1 Introduction to the causal inference / paradigm of causal agent	60

2.2.3.2	Direct and indirect causal effects	61
2.2.3.3	Analytic methods of estimation	62
2.2.3.4	Limits of the causal inference	63
2.3	Modeling of biological processes via mechanistic modelling	64
2.3.1	The different type of mechanistic models	65
2.3.2	The ordinary differential equations system in population approach	66
2.3.3	Estimation methods of NLME-ODE	68
2.3.3.1	The Expectation-maximization (EM) algorithm	69
2.3.3.2	Estimation with Monolix: the SAEM algorithm	70
2.3.3.3	Extensions of the SAEM algorithm	72
2.3.3.4	Model with censored data	73
2.3.4	Mechanistic models describing within-host infectious disease dynamics	74
 PART II Viral dynamics		78
 Chapter 3: Evaluation of therapeutic vaccine efficacy in HIV-infected patients		80
3.1	Biological and clinical context	81
3.1.1	General introduction on HIV infection	81
3.1.1.1	Epidemiological context	81
3.1.1.2	Some generalities about the virus	82
3.1.1.3	HIV replication cycle	82
3.1.1.4	Natural HIV disease progression and immune response	84
3.1.2	Treatment strategy	85
3.1.2.1	Antiretroviral therapies	85
3.1.2.2	Therapeutic vaccines as functional cure against HIV	86
3.1.2.3	Analytical treatment interruption	87
3.2	Optimization of the choice of primary endpoint in HIV therapeutic vaccine trial	88
3.3	Perspectives	109
 Chapter 4: Endpoints in HIV therapeutic vaccine trials		110
4.1	Introduction of the context	111
4.2	Between-group comparison of area under the curve in clinical trials with censored follow-up	113
4.3	Perspectives	132
 Chapter 5: Mechanistic correlates of protection in vaccine trial: application to SARS-CoV-2.		136
5.1	Biological and clinical context	137
5.1.1	General introduction on COVID-19	137
5.1.1.1	The COVID-19 pandemics	137
5.1.1.2	The SARS-CoV-2 virus	137
5.1.2	Vaccine development	139
5.1.2.1	An unprecedented worldwide effort	139
5.1.2.2	The necessity to identify immune correlates of protection	141
5.2	Editorial about within-host models and their application on SARS-CoV-2	142
5.3	Model building strategy in mechanistic model to identify mechanistic correlates of protection in NHP preclinical trials	146
5.4	Perspectives	195

PART III Humoral response dynamics	201
Chapter 6: Evaluation of the longevity of the humoral immune response of Ebola vaccine	203
6.1 Biological and clinical context	204
6.1.1 General introduction on Ebola virus disease	204
6.1.2 Ebola outbreaks and actual epidemiological context	204
6.1.3 Ebola vaccine development	205
6.2 Evaluation of the durability of the humoral response	208
6.3 Perspectives	230
General discussion and conclusion	233
Bibliography	239
Appendices	267
Appendix A: Supplementary Materials - Between-group comparison of area under the curve in clinical trials with censored follow-up: Application to HIV therapeutic vaccines	267
Appendix B: Poster PAGE2019 - Modeling Viral Load Rebound in HIV Therapeutic Vaccine Studies	287

Remerciements

Je souhaite tout d'abord remercier Rodolphe Thiébaud, mon directeur de thèse. Merci de m'avoir accueilli au sein de ton équipe et de la confiance que tu m'as portée tout au long de cette thèse. Malgré ton emploi du temps surchargé, tu as toujours su trouver du temps quand il le fallait, que ce soit pour discuter des travaux, de mes projets futurs (même pour parler de charpente) ou de s'assurer de mon bien-être au sein de l'équipe. Je te remercie également pour ton enthousiasme communicatifs pour la recherche et pour toutes ces discussions passionnantes et très éclairantes qui ont toujours su me booster quand une petite baisse de régime pouvait se faire ressentir. Merci pour ta bienveillance, tes conseils et les opportunités que tu m'as offertes au cours de ces trois années.

Je souhaite également remercier Mélanie Prague, ma co-directrice de thèse. A la suite de mon stage de M1, tu m'as proposé de continuer de m'encadrer pour ces 3 années de thèse. Ce jour-là, tu m'as offert l'opportunité de réaliser mon vœux le plus cher, que je peux concrétiser aujourd'hui grâce à toi. Merci d'avoir toujours été là et de m'avoir remotivé quand j'en avais besoin, de m'avoir guidé sur tous ces travaux et de m'avoir fait bénéficier de tout ton savoir-faire. Je te remercie également de m'avoir encouragé à avancer sur des projets qui me tiennent à cœur, que ce soit d'un point de vue professionnel ou plus personnel. Merci pour tes conseils et ton aide si précieux dans la rédaction de ce manuscrit et tout au long de cette thèse. J'espère que l'on aura l'opportunité de continuer à travailler ensemble encore longtemps.

I would like to sincerely thank Lulla Opatowski and Frederik Graw who accepted to judge my thesis as main examiners. I am really grateful for the interest you have on my work and it is an honour to benefit from our great expertise in mathematical modelling of infectious diseases.

I would also like to warmly thank Michael White and Jane Heffernan who accepted to judge my thesis. Michael White, I really appreciated the discussion we had follow-

ing my presentation in Paris and it will be a real pleasure to meet you again and benefit from your great knowledge in epidemiology and infectious diseases. Jane Heffernan, I had the opportunity to see some presentations of your work about mathematical modelling of infectious disease during your stay in the SISTM team and I am looking forward to benefit from your thought on this work.

Je souhaite également remercier Cécile Proust-Lima et Jérémie Guedj qui ont respectivement accepté de faire partie de mon jury de thèse en tant qu'examinatrice et invité. Outre votre participation à mon jury de thèse, je souhaite particulièrement vous remercier de m'avoir suivi au cours de ces trois années en tant que membres de mon comité de thèse. Merci pour ces échanges passionnants et pour l'intérêt que vous avez montré envers mon travail. Je vous remercie également pour vos conseils toujours très pertinents et votre bienveillance au cours de ces trois années. J'ai hâte d'avoir de nouveau votre retour sur ces travaux.

Je tiens à remercier sincèrement tous les collaborateurs avec qui j'ai pu travailler au cours des différents projets. Tout d'abord le Vaccine Research Institute qui m'a donné la possibilité de travailler avec eux, en me donnant l'accès un grand nombre de jeux de données pour le VIH (LIGHT, ILIADE, DALIA), sans qui les travaux que nous avons pu réaliser n'auraient pas eu lieu, mais également l'opportunité de participer à l'élaboration du protocole d'un nouvel essai clinique. Je remercie également le VRI et le CEA de m'avoir fait confiance sur le projet du développement du vaccin α CD40.RBD contre le SARS-CoV-2 en me confiant la modélisation des données de l'essai préclinique. Je tiens tout particulièrement à remercier Yves Lévy pour sa confiance et sa bienveillance au cours de ces trois années. Vous avez toujours montré un grand intérêt pour mes résultats et fait l'effort de comprendre les travaux de modélisation dont ils résultaient. Je remercie également Roger Legrand pour cette collaboration réellement enrichissante sur le projet du vaccin α CD40.RBD. Merci à Romain Marlin pour sa disponibilité sans faille, pour son aide et pour toutes ces discussions passionnantes sur les données et sur la mise en place des nouveaux essais. Je remercie aussi tous les collaborateurs des projets EBOVAC. Merci pour ces discussions scientifiques captivantes au cours des différents workshops, et notamment à Thierry van Effeltherre et son retour toujours pertinent sur notre travaux de modélisation. Je suis également très reconnaissante envers l'Inria qui a financé cette thèse et qui nous a donné l'opportunité d'accéder à la plateforme Plafrim pour mener à bien nos travaux de recherches dans les meilleures conditions. J'en profite d'ailleurs pour remercier les membres de l'Inria qui gèrent Plafrim pour leur disponibilité et leur aide dans la prise en main de la plateforme, même quand notre utilisation

des serveurs n'était pas très optimale.

Je souhaite également remercier chaleureusement Audrey et Sandrine pour toute leur aide administrative, que ce soit pour les déplacements professionnels, les réunions ou la mise en relation avec le service RH. Merci pour votre disponibilité sans faille. Sandrine, je souhaiterais également te remercier pour ton aide précieuse au cours des multiples déménagements. Malgré la situation chaotique, tu as toujours été présente pour nous aider à tout gérer tout en gardant ta bonne humeur.

Merci à toutes les personnes de l'équipe avec qui j'ai eu l'occasion de travailler et d'interagir au cours de divers projets : Chloé, Irène, Laura R, Edouard, Linda, Quentin et Mathieu. Merci également à Anton pour son expertise sur les projets EBOVAC et de son temps pour m'expliquer tous ces projets. Je souhaite aussi remercier Panthéa pour son aide dans la gestion et la mise en ligne de données sur Labkey et du temps qu'elle a pris pour m'expliquer comment utiliser la plateforme. Je remercie également tous les collègues du bureau John Snow durant ces années qui ont permis de travailler dans une bonne ambiance, malgré la longue période de télétravail qui nous quelque peu séparé: Chloé, Irène, Hadrien, Solenne, Jean-Nöel, Laura V, Maria, Quentin, Benjamin, Mélanie H, Mélanie D, Clément, Kalidou, Hélène, Myrtille, Bruno, Iris, et tous ceux que j'ai pu oublier. Merci à tous les permanents, doctorants et ingénieurs de l'équipe SISTM, actuels et anciens, que je n'ai pas encore cité, Robin, Boris, Louis, Marine, Marta, . . . , qui participent à la bonne cohésion de cette équipe extraordinaire.

J'ai une pensée toute particulière pour Guillemette Chapuisat pour m'avoir encadré au cours de multiples stages au sein de l'équipe d'analyse appliquée de l'I2M durant mes six années d'études à Marseille. Merci de m'avoir donné l'opportunité de découvrir le monde de la recherche et de m'avoir fait confiance tout au long de ces années. Tu as été d'un grand soutien dans des moments très difficiles, que tes conseils et ta bienveillance m'ont permis de surmonter. Je te remercie également pour tes conseils précieux au cours de cette thèse.

Mes remerciements vont également à toute ma famille qui a toujours été présente au long de ces années. Je pense en particulier à Jean-François, Sylvie, Amandine et Sébastien pour ces soirées jeux de société, à Isabelle, Karim, Nora, Max et Sacha pour ces invitations du dimanche qui m'ont permis de me vider l'esprit. Merci à Roger avec qui il semblerait que nous partageons la passion des biostatistiques et des applications en santé publiques, et qui m'a offert l'opportunité de faire ce stage de M1 à l'origine de cette thèse au sein de l'équipe SISTM. A Paul et Linda et à leur bonne humeur commu-

Remerciements

nicative qui malgré la distance ont toujours été là. Un grand merci à ma grand-mère Nicole pour son soutien indéfectible. Pour finir, je remercie mes parents qui m'ont toujours soutenu dans mes choix et ont toujours été mon pilier, mon frère Jonathan, Jessica, et leur petit ange Mia, et mon frère Arnaud et ces soirées passées au téléphone à me raconter les anecdotes invraisemblables sur ses élèves de CM2. A tous, je vous dis merci.

A toi, dont le simple sourire avait la faculté de nous faire oublier tous nos problèmes, à toi avec qui aucune barrière n'existait, à toi qui a toujours fait preuve d'une force à toute épreuve malgré les difficultés que la vie a mis sur ta route, à toi qui m'a permis d'être qui je suis aujourd'hui et m'a donné la force d'avancer pour en arriver là. A toi, la personne la plus importante de ma vie, aujourd'hui tu n'es plus là, mais cette thèse elle est pour toi.

Project reference: L'EUR DPH bénéficie d'une aide de l'État gérée par l'Agence Nationale de la Recherche au titre du programme d'investissement d'avenir portant la référence 17-EURE-0019. This PhD program is supported within the framework of the PIA3 (Investment for the future). Project reference 17-EURE-0019.

Scientific production

Articles

- ▷ [Alexandre, M., Prague, M., & Thiébaud, R. \(2021\). Between-group comparison of area under the curve in clinical trials with censored follow-up: Application to HIV therapeutic vaccines. *Statistical Methods in Medical Research*, 30\(9\), 2130-2147. <https://doi.org/10.1177/09622802211023963>](#)
- ▷ [Prague, M., Alexandre, M., Thiébaud, R., & Guedj, J. \(2022\). Within-host models of SARS-CoV-2: What can it teach us on the biological factors driving virus pathogenesis and transmission?. *Anaesthesia Critical Care & Pain Medicine*, 101055. <https://doi.org/10.1016/j.accpm.2022.101055>](#)
- ▷ [Alexandre, M., Marlin, R., Prague, M., Coleon, S., Kahlaoui, N., Cardinaud, S., ... & Thiébaud, R. \(2021\). SARS-CoV-2 mechanistic correlates of protection: insight from modelling response to vaccines. *bioRxiv* <https://doi.org/10.1101/2021.10.29.466418>, *In revision in Elife*](#)
- ▷ [Alexandre, M., Prague, M., Thiébaud, R., & EBOVAC 1 and EBOVAC 2 consortia. Evaluation and prediction of the long-term humoral immune response induced by the two-dose heterologous Ad26.ZEBOV, MVA-BN-Filo vaccine regimen against Ebola., *In preparation for submission*. Available in section 6.2](#)
- ▷ [Alexandre, M., Prague, M., Thiébaud, R., coauthors & VRI studygroup. Optimization of the choice of primary endpoint in HIV therapeutic vaccine trials, *In preparation for submission*. Available in section 3.2.](#)

Communications

Oral communications at international conferences

- ▷ [Alexandre Marie](#), Richert Laura, Lévy Yves, Prague Mélanie, Thiébaud Rodolphe. [Evaluation of primary endpoint assessing HIV therapeutic vaccine efficacy during analytical treatment interruption studies](#). *Workshop on Virus Dynamics, 4th*, Paris, France, 2019.
- ▷ [Alexandre Marie](#), Prague Mélanie, Thiébaud Rodolphe and the VRI/CEA group. [Accounting for time-dependant confounding variables in mechanistic ODE model: simulations and application to vaccine trial](#). *International Society for Clinical Biostatistics (ISCB)*, Lyon, France, 2021 (Online).
- ▷ [Alexandre Marie](#), Prague Mélanie, Clairon Quentin, Van Effelterre Thierry, Thiébaud Rodolphe. [Dynamics of the humoral immune response to a two-dose heterologous vaccine regimen against Ebola virus](#). *Population Approach Group in Europe (PAGE)*, 2021 (Online).
- ▷ [Alexandre Marie](#), Prague Mélanie, Clairon Quentin, Van Effelterre Thierry, Thiébaud Rodolphe. [Dynamics of the humoral immune response to a two-dose heterologous vaccine regimen against Ebola virus](#). *Workshop on Modelling Immunity*, Toronto, Canada, 2021 (Online).
- ▷ Thiébaud Rodolphe, [Alexandre Marie](#), Prague Mélanie. [Viral dynamics as an outcome in HIV therapeutic vaccine trials: from AUC to dynamical modelling](#). *Computational and Methodological Statistics (CMstatistics)*, London, UK, 2021 (Online)

Oral communications at national conferences

- ▷ [Alexandre Marie](#), Prague Mélanie, Thiébaud Rodolphe. [Comparaison d'AUC entre groupe de traitement dans des essais avec censure de suivi : Application aux vaccins thérapeutiques contre le VIH](#). *Young Statisticians and Probabilists (YSP)*, France, 2021 (Online)
- ▷ [Alexandre Marie](#), Prague Mélanie, Thiébaud Rodolphe. [Méthodes de comparaison d'aires sous la courbe dans des essais cliniques avec arrêt prématuré du suivi : Application aux vaccins thérapeutiques contre le VIH](#). *Journées de Statistique (JDS)*, Nice, France, 2021 (Online).

Written communications (poster) at international conferences

- ▷ [Alexandre Marie](#), Prague Mélanie, Lévy Yves, Thiébaud Rodolphe. [Modelling Viral load Rebound in HIV Therapeutic Vaccine Studies](#). *Population Approach Group in Europe (PAGE)*, Stockholm, Sweden, 2019.
- ▷ [Alexandre Marie](#), Prague Mélanie, Lévy Yves, Thiébaud Rodolphe. [Comparison of AUC in clinical trials with follow-up censoring: Application to HIV therapeutic vaccines](#). *International Society for Clinical Biostatistics (ISCB)*, Krakow, Poland, 2020 (Online).

Invited talk at French seminar

- ▷ [Alexandre Marie](#). [Mechanistic modelling and optimization of vaccine response in HIV](#). *Summer School MPCl - "Science and Health"*, Marseille, France, 2019

Abbreviations and Notations

ACE2	Angiotensin-converting enzyme 2
AIC	Akaike information criterion
AIDS	Acquired immunodeficiency syndrome
ART	Antiretroviral treatment
ASCs	Antibody-secreting cells
ATI	Analytical treatment interruption
AUC	Area under the curve
BIC	Bayesian information criterion
cART	Combined antiretroviral therapy
CD	Cluster of differentiation
CoP	Correlate of protection
CoR	Correlate of risk
DCs	Dendritic cells
DNA	Deoxyribonucleic acid
DRC	Democratic republic of Congo
EBE	Empirical bayes estimate
EBOV	Ebola virus
EM	Expectation-Maximization
EMA	European Medicines Agency
EUA	Emergency use authorization
EUL	Emergency use listin
EVD	Ebola virus disease
FDA	Food and Drug Administration
GP	Glycoprotein
HAART	Highly active antiretroviral treatment
HIV	Human Immunodeficiency Virus
IFN	Interferon
Ig	Immunoglobulin

IL	Interleukin
LMEM	Linear mixed-effects model
LOD	Limit of detection
MAR	Missing at random
MCAR	Missing completely at random
mCoP	mechanistic correlate of protection
MEM	Mixed-effects model
MLE	Maximum likelihood estimate
MNAR	Missing not at random
nAUC	Normalized area under the curve
nCoP	non-mechanistic correlate of protection
NHP	Non-human primate
NK	Natural Killer
NLME-ODE	ODE-based Non-linear mixed-effects model
NLMEM	Non-linear mixed-effects model
NP	Nucleoprotein
ODE	Ordinary differential equation
PD	Pharmacodynamic
PK	Pharmacokinetic
RBD	Receptor binding domain
RCT	Randomized controlled trial
RMSE	Root mean squared error
RNA	Ribonucleic acid
SAEM	Stochastic approximation Expectation-Maximization
SARS-CoV-2	Severe acute respiratory syndrome coronavirus 2
TNF	Tumor necrosis factor
VoC	Variant of concern
WHO	World health organization

Résumé substantiel

Introduction

Ces dernières années, et particulièrement dans le contexte de l'épidémie mondiale de COVID19, la vaccination s'est révélée être un réel succès dans la prévention et le contrôle des maladies infectieuses et constitue un élément clé dans l'amélioration de la santé publique mondiale. En plus du développement médical et biologique, de nouveaux outils statistiques sont nécessaires pour fournir une compréhension quantitative des mécanismes d'action et d'efficacité des vaccins. En effet, l'un des principaux défis que peuvent relever ces outils analytiques est l'accélération du développement vaccinal et donc du processus long et coûteux des études précliniques et cliniques. A ce titre, dans ce travail, nous nous intéressons plus particulièrement à deux questions applicatives : comment évaluer la protection conférée par la vaccination et quelle est la durée de l'immunité conférée par la vaccination ? Bien que chaque partie soit motivée par une application et profondément ancrée dans l'analyse de données cliniques, l'accent est mis sur la combinaison et le développement de méthodes statistiques originales. En particulier, nos travaux sont centrés sur l'utilisation de modèles mécanistes, c'est-à-dire des modèles à effets mixtes non linéaires basés sur des équations différentielles, et l'utilisation de leurs capacités prédictives. Le manuscrit est divisé en six chapitres dont le contenu est décrit ci-dessous.

Chapitre 1: Contexte en immunologie et vaccinologie.

Dans ce chapitre, nous introduisons le contexte biologique général dans lequel s'inscrit cette thèse. En particulier, nous présentons quelques notions clés en immunologie et les principaux mécanismes biologiques entrant en jeu dans l'établissement et le maintien d'une réponse immunitaire efficace suite à une infection virale ou vaccination. L'intérêt majeur que représente la vaccination dans la lutte contre les maladies infectieuses est ensuite abordé en introduisant les principes de cette stratégie de santé publique ainsi

que le long processus et les challenges que représente le développement vaccinal.

Chapitre 2 : Contexte en mathématique et biostatistiques.

Ce chapitre décrit les méthodes mathématiques et statistiques mobilisées dans les travaux de modélisation réalisés dans cette thèse. En effet, l'objectif de cette thèse porte sur l'analyse de l'efficacité vaccinale, que ce soit en termes de protection ou de la longévité de la réponse immunitaire induite par la vaccination. Dans cette perspective, l'ensemble des travaux reposent sur l'analyse longitudinale de marqueurs immunologiques et virologiques. Ainsi, nos méthodes se placent donc dans le contexte des modèles à effets mixtes. Nous présentons dans ce chapitre deux approches auxquelles nous avons recouru : des modèles descriptifs représentés principalement par les modèles de régressions à effets mixtes, et les modèles dynamiques dits mécanistes basés sur des systèmes d'équations différentielles ordinaires. Pour ces deux approches, nous présentons le cadre mathématique ainsi que les techniques d'estimation utilisées. Par ailleurs, nous introduisons le cadre général de la modélisation causale nécessaire à la bonne compréhension du contexte dans lequel s'inscrit l'identification de corrélats de protection, ainsi que son lien avec les modèles mécanistes et leurs capacités de prédiction.

Chapitre 3 : Evaluation de l'efficacité d'un vaccin thérapeutique chez les patients infectés par le VIH.

Dans ce chapitre, on s'intéresse au développement de vaccins thérapeutiques contre le VIH et à l'évaluation de leur efficacité au cours d'essais cliniques. Requérant l'interruption d'antirétroviraux (ART) chez des individus infectés par le VIH, ces essais peuvent présenter un risque significatif pour les patients qui subissent un rebond virologique. Ainsi, les ART sont souvent repris de manière précoce pour protéger le patient dès que leur charge virale devient trop importante. Un choix optimal des critères de reprise de traitement et de jugement de l'efficacité est donc nécessaire. La charge virale d'équilibre après plusieurs semaines sans traitement, couramment défini comme le critère optimal de jugement de l'efficacité du vaccin à contrôler ce rebond, ne peut pas toujours être observé. Nous présentons donc une analyse descriptive de données longitudinales de charges virales dans de multiples essais afin de trouver le meilleur descripteur virologique de substitution pour cette charge virale d'équilibre. Son application sur les trajectoires virales obtenues au cours de trois essais vaccinaux permet

d'identifier l'aire sous la courbe (AUC) comme un critère de substitution optimal. Une analyse de l'impact de critères de reprise précoce des ART sur la relation charge virale d'équilibre/AUC montre l'intérêt d'un niveau de censure de charge virale au moins supérieur à 100 000 cp/mL (i.e., niveau de charge viral pour laquelle la reprise des ART est encouragée) ainsi que le recours à une mesure de confirmation avant toute reprise des ART.

Chapitre 4 : Critère d'évaluation dans les essais thérapeutiques vaccinaux pour le VIH

Dans ce chapitre, on s'attache à développer un test statistique robuste permettant de comparer entre plusieurs groupes de traitements des mesures synthétiques de dynamiques longitudinales, telles que l'aire sous la courbe du marqueur d'intérêt (AUC). En particulier, on s'intéresse au cas de données longitudinales impactées par des données manquantes de type MAR monotone par sortie d'étude qui induisent un biais dans le calcul de l'AUC. On propose alors un test paramétrique basé sur des modèles à effets mixtes à splines pour rendre compte de ce biais. Au cours d'un travail de simulation d'essais à 2 bras de randomisation, on démontre les bonnes propriétés statistiques de ce test vis-à-vis de méthodes ad hoc classiquement utilisées ainsi que d'un test non-paramétrique. Par continuité avec le chapitre précédent, on applique cette méthodologie dans le cadre de deux essais cliniques développant des vaccins thérapeutiques contre le VIH requérant des périodes d'interruption de traitement antirétroviraux (ART) pour rendre compte de l'efficacité vaccinale. L'AUC est alors utilisé comme critère de jugement et le niveau de charge virale comme critère de reprise précoce des ART et donc de sortie d'étude. Un travail préliminaire en vue de l'extension de cette méthode à des modèles mécanistes basés sur des équations différentielles ordinaires est également proposé en fin de chapitre consistant en une comparaison de trois modèles servant à décrire le rebond de charge virale.

Chapitre 5 : Définition de corrélats de protection mécanistes dans les essais vaccinaux: application au SARS-CoV-2.

Dans ce chapitre, on s'intéresse à l'évaluation de l'efficacité vaccinale dans le cadre de la pandémie actuelle de SARS-CoV-2. Après avoir présenté le contexte de développe-

ment vaccinal sans précédent dans lequel s'inscrit ce travail, nous rappelons la nécessité que représente la connaissance de corrélats de protection (CoP) dans l'accélération du processus de développement vaccinal. En particulier, nous mettons en avant l'absence d'identification de CoP causalement liés avec l'effet protecteur des vaccins, aussi appelés CoP mécanistes. Nous nous attachons ensuite à montrer l'apport qu'a représenté la modélisation mécaniste intra-hôte dans la compréhension des mécanismes biologiques et immunologiques liés à cette infection virale, ainsi que sur les mécanismes de transmission au sein d'une population. Par la suite, nous proposons une méthode d'identification de CoP mécaniste, au sein d'essais précliniques, couplant une modélisation de la dynamique virale par modèles mécanistes et une analyse approfondie de marqueurs immunologiques se basant sur un algorithme de sélection de covariables dépendantes du temps. Par application de cette méthode sur les données de trois essais vaccinaux, nous pointons la robustesse des résultats trouvés par cette méthode vis-à-vis des approches purement descriptives couramment utilisées ainsi que son apport à identifier les mécanismes immunologiques sous-jacents.

Chapitre 6 : Evaluation de la longévité de la réponse humorale: application au virus Ebola.

Contrairement aux chapitres précédents se focalisant majoritairement sur la dynamique virale, dans ce chapitre, on s'intéresse à l'évaluation de la longévité de la réponse immunitaire humorale induite par la vaccination contre le virus Ebola. En particulier, on se focalise sur la stratégie vaccinale prime/boost hétérologue à deux doses impliquant les vecteurs viraux Ad26.ZEBOV et MVA-BN-Filo développée par Janssen Pharmaceutical et testée au cours de multiples essais cliniques de phase I à III. On présente un modèle mécaniste, basé sur des équations différentielles ordinaires, décrivant la dynamique des anticorps issus de deux populations sécrétrices (ASC), qui a été préalablement estimé sur des données de trois essais de phase I ayant 1 an de suivi. En se basant maintenant sur des données collectées chez 498 individus au cours de 3 essais de Phase II/IIB suivis jusqu'à 2 ans après la première vaccination, nous démontrons la robustesse de ce modèle ainsi que sa bonne qualité de prédiction à long-terme. Profitant du nombre plus conséquent de participants ainsi que du suivi à plus long terme, nous ré-estimons le modèle en utilisant une approche populationnelle. En particulier, nous démontrons une survie plus longue des ASC à longue durée de vie que préalablement estimée et nous confirmons une persistance plus longue des anticorps chez les européens que les africains. Par ailleurs, un effet de l'âge et du sexe des participants est identifié sur la

décroissance de la dynamique humorale. Une estimation de ce modèle sur des données à plus long terme ainsi que l'estimation de modèles couplant à la fois l'établissement et le maintien de la réponse humorale permettrait de confirmer et affiner ces résultats et sont évoqués en fin de chapitre.

Conclusion

De nombreuses perspectives de développement sont envisageables pour la suite de ces travaux, que ce soit dans la compréhension des réponses immunologiques déclenchées par la vaccination ou dans le développement d'outils mathématiques et statistiques efficaces pour optimiser l'évaluation des vaccins préventifs et thérapeutiques. Tout d'abord, l'utilisation de modèles mécanistes dotés de capacités prédictives permet de réaliser des simulations, ce qui peut constituer une formidable opportunité pour optimiser la conception des essais cliniques et ainsi accélérer le développement des vaccins. De même, ils pourraient être utilisés pour la médecine personnalisée. Notre travail méthodologique sur la dérivation de modèles mécanistes à partir de données ouvre cette voie à leur utilisation dans de tels domaines. Une extension sérieuse qui pourrait ajouter de la valeur à ce travail est de considérer des méthodes de moyenne de modèles, plutôt que des méthodes de sélection de modèles comme cela a été fait dans ce travail lors de la construction d'un modèle pour expliquer les données. En particulier, cela permettrait de prendre en compte la mauvaise spécification du modèle et l'incertitude. Enfin, nous nous sommes concentrés sur les dynamiques intra-hôte dans ce travail. Des modèles multi-échelles, qui tiennent compte de la propagation des maladies infectieuses entre les hôtes, les données génomiques qui tiennent compte de la diversité des patients et les données phylogénétiques qui tiennent compte de la diversité virale, pourraient être développés davantage et représentent une direction de recherche future intéressante.

Introduction

In recent years, and particularly in the context of the global COVID19 epidemic, vaccination has proven to be a real success in preventing and controlling infectious diseases and is a key element in improving global public health. However, much progress remains to be made to develop effective strategies against specific infectious diseases. In particular, the development of prophylactic vaccines that prevent an individual's viral infection and/or therapeutic vaccines that help the immune system to fight the virus once the infection is established still require significant development work in the case of viral infections such as chronic diseases like HIV, sporadic diseases like Ebola, or even the recent case of COVID19. On top of medical and biological development, **new statistical tools are needed to provide a quantitative understanding of vaccines mechanisms of action.**

One of the main challenge that can be addressed with analytical tools is **the acceleration of the lengthy and costly process of preclinical and clinical studies** evaluating the tolerability, safety, immunogenicity, and ultimately the efficacy of a tested strategy. During this process, many questions arise regarding the optimal strategy, which is relatively dependent on the vaccine developed and the infection targeted. As we saw in the case of SARS-CoV-2, the choice of vaccine type, a homologous or heterologous strategy, and thus the sequence of vaccines, as well as the number of injections and the time between each injection, is essential. However, exploring all possibilities of combinations in clinical trials is not feasible. Computer-based simulations also known as *in silico* approaches can further explore these scenarios. Furthermore, in addition to the development of effective vaccines, the ability to evaluate their efficacy in clinical trials is a critical element. Therefore, the definition of good criteria for endpoints, which may extend to the identification of correlates of protection, is necessary. A correlate of protection is defined as an immunological marker statistically associated with the clinical outcome of interest and causally related to vaccination and induced protection. The identification of the latter can then allow a significant acceleration of the process of evaluating new vaccine candidates, especially in specific populations often at risk,

such as the elderly, pregnant women, children, or immunocompromised individuals. In this context, **mathematical and statistical tools are crucial in understanding the complex mechanisms of interaction between the virus and the immune system of an infected or susceptible host and in elucidating the role of vaccination in these interactions.**

Two main questions are addressed in this thesis. The first is the **evaluation of protection conferred by vaccination**, which is a multi-layer question. It also depends on what is the clinical outcome of interest. Protection provided by a vaccine can be different against disease acquisition (or eradication in case of therapeutic vaccine), symptomatic infection or death. In this work, we define the efficacy of a vaccine as the potential to prevent or clear an infection. To investigate this question, we model the viral dynamics observed during preclinical and/or clinical trials using so-called dynamical mechanistic models or more descriptive mathematical models in order to identify/define and evaluate optimal criteria for the efficacy of the tested vaccines. Of course, there is no general method to achieve the general goal of evaluation of protection conferred by vaccination. Answers are problem-specific and may depend on the disease biology and outcome of interest. In this thesis, we focused on two main topics. In the field of HIV, in collaboration with the Vaccine Research Institute, in the context of a therapeutic vaccine trial against HIV EHVA T02, we investigated what could be the best primary endpoint and how to analyse trials in which interruption of antiretroviral treatment is required. Indeed, it creates a problem of non-ignorable missing data since individual who drops out of the study are likely to be the one for which the vaccine was the less effective. In the field of SARS-CoV-2, jointly with the Vaccine Research Institute and CEA as part of a preclinical study on non-human primates (NHPs), we propose a model building strategy to elicit mechanistic correlates of protection within a large number of immunological markers. Once efficacy against an infection has been proven, it is important to focus on the problem of **longevity of immunity conferred by vaccination**, which is the second problem addressed in these works. When investigating longevity, data accumulate with time. It is important to develop statistical analysis that are sequential and allow to predict long-term abilities and evaluate the quality of model prediction on subsequent data collection. In collaboration with Janssen Pharma as well as other academic partners such as the College of Oxford or the London School of Hygiene & Tropical Medicine under the European projects EBOVAC 1 and EBOVAC 2, funded by the Innovative Medicines Initiative Ebola+, we proposed a pipeline of sequential analyses to test the robustness of long-term predictions and used statistical tools to determine the factors that explain the variability of response observed in participants.

The manuscript is divided into three parts with six chapters. Although each part is motivated by an application and deeply rooted in the analysis of clinical data, the focus is on the combination and the development of original statistical methods.

The first part consists of two chapters (Chapter 1 and 2) and aims to introduce the main biological and mathematical concepts necessary to fully understand the context of the work performed. In particular, in the first chapter we introduce the key concepts of immunology that are essential to understand the principle of vaccination, focusing especially on the immunological mechanisms involved in the vaccine strategies used in our work. We also present the different steps of the vaccine development process and the need to identify correlates of protection when evaluating vaccine efficacy. In the second chapter, we present the framework of **linear and nonlinear mixed-effects models** and extend it to the so-called **mechanistic model based on ordinary differential equations**. We present **methods of inference** for estimation of parameters that are then used as a "black-box" in the following chapters. We also define some concepts of **causality** that are essential in order to ensure the **predictive capability** of our models.

The second part (Chapter 3, 4 and 5) of the manuscript contains the three chapters that summarize the work done on the development of mathematical and statistical tools to analyze viral dynamics and to determine optimal criteria for the clinical studies endpoints and immunological correlates of protection. Chapters 3 and 4 focus on the development of therapeutic HIV vaccines. Chapter 3 presents **a comprehensive descriptive data analysis of multiple clinical trials** that allow to identify the optimal endpoint for HIV vaccine trials with interruption of antiretroviral treatment to assess vaccine efficacy. Chapter 4 develops **a robust statistical test** to compare these criteria between treatment groups **in presence of informative study drop-out**. In Chapter 5, we propose **a model building strategy in mechanistic models** to define immunological correlates of protection against SARS-CoV-2 among numerous time-varying immune markers. As a prelude to this work, we present an editorial on the benefits of **within-host modeling** in the SARS-CoV-2 pandemic.

Finally, the third part contains a single chapter (Chapter 6) dedicated to assess the longevity of the humoral immune response elicited by vaccination. Accordingly, in Chapter 6, we present **a pipeline of analysis using mechanistic models** to predict long-term immunity based on phase I data, confirm the predictions on subsequent trials in phase II and investigate possible factors of variability in the long-term responses.

PART I

Biological and mathematical background

Chapter 1

Biological background in immunology and vaccinology

Abstract: In this chapter, we introduce the general biological context in which this work operates. In particular, we introduce some key concepts of immunology and the main biological mechanisms involved in the establishment and maintenance of an effective immune response after viral infection or vaccination. We then discuss the great interest in vaccination in the fight against infectious diseases by presenting the principles of this public health strategy and the long process and challenges of vaccine development.

Keywords: Immune system ; dendritic cell ; B lymphocyte ; antibodies ; T lymphocyte ; vaccine development ; efficacy ; correlate of protection

In this chapter, we introduced key concepts of immunology and vaccinology that are used in the various modeling proposed in the research presented in chapters 3, 4, 5 and 6. Of course, not all the mechanisms are presented in details here and a very good introduction can be found in [Abbas et al., 2017]. In particular, the key components of interest are the dendritic cells for intervening in the elaboration of promising vaccines encountered in this thesis for HIV (see chapter 3) and SARS-CoV-2 (see chapter 5), the B cell responses to understand the modeling work of humoral response for Ebola (see chapter 6) and T cells and inflammatory markers measured as covariates in preclinical study on correlates of protection (see chapter 5).

1.1 The immune system

The immune system is the body's main defense against infections and is composed of cells and molecules responsible for immunity by detecting and responding to various pathogenic microbes (e.g. viruses, bacteria, fungi, toxins) [Chaplin, 2010]. Their coordinated response against invading pathogens elicits an immune response. Immunity is mediated by two sequential but deeply connected immune responses: innate immunity (also called 'natural immunity') followed by adaptive immunity ('acquired immunity' or 'specific immunity') [Hoebe et al., 2004].

1.1.1 The innate immune response

Innate immunity is the first line of defense against microbes by providing a quick and non-specific response to infections. This immune response has a dual role: (1) a defensive function resulting in the recognition and the early elimination of pathogens, and (2) a warning function aiming at alerting and stimulating the adaptive immune system.

In addition to the physical and chemical barriers (e.g. skin and mucosal surfaces) preventing the entry of microbes into the organism, these two functions are fulfilled by phagocytes and natural killer (NK) cells. Phagocytes, including neutrophils, monocytes, macrophages and dendritic cells (DCs), aim at identifying and ingesting pathogens. Among them, DCs play a major role in the initiation of the immune response due to their large ability to recognize microbes. Like all so-called antigen-presenting cells, DCs present at their surface fragment of pathogens, called antigens. By presenting them to the naive cells (cells that have never encountered the antigen) of adaptive immunity and by secreting proteins called cytokines, DCs have the essential role to initiate and enhance the immune response specific to these antigens. Finally, NK cells directly elim-

inate infected cells and secrete cytokines that stimulate the other actors of the innate response, like macrophages [Lodoen and Lanier, 2006].

1.1.2 The adaptive immune response

1.1.2.1 The main actors of the adaptive immunity

In contrast to innate immunity, adaptive immunity is stronger and antigen-specific. The main components of the adaptive immune response are a type of white blood cell, called lymphocytes, including NK cells, B lymphocytes, and T lymphocytes (also called "B cells" and "T cells", respectively). Lymphocytes express at their surface diverse membrane receptors enabling them to recognize a large number of antigens and activate an immune response specific to each of them. Adaptive immunity can be splitted into two types: humoral immunity (also called "antibody-mediated immunity") and cellular immunity (also called "cell-mediated immunity").

Humoral immunity is mediated by Y-shaped proteins called antibodies, also called immunoglobulins (Ig). Their main purpose is to prevent the spread of infection by binding to extracellular pathogens and neutralizing their infectivity, either by tagging antigens or infected cells and promoting their elimination by phagocytosis, or by neutralizing them directly. Different classes of antibodies exist with distinct properties and functionalities. However, in the scope of this thesis, we will focus exclusively on IgG, the most abundant class, as no data on other types were encountered in our work. Antibodies are produced by B cells and can be found in two distinct forms: membrane-bound antibodies located on the surface of B cells and secreted circulating antibodies that can be found in the blood and mucosal secretions. Initially produced in the bone marrow, B cells undergo a complex series of maturation and differentiation steps, from stem cells to antibody-secreting plasma cells (ASCs). Membrane-bound antibodies are produced by immature and mature B cells (before activation) and aim at initiating the humoral immune response by triggering maturation of B cells through antigen binding. Activation of mature B cells, leading to their differentiation into ASCs, is followed by the production of highly antigen-specific IgG (also called affinity maturation), which improves the quality of the humoral response. These circulating IgG are characterized by a half-life, defined as the time required to divide the number of antibodies by 2, ranging from 20 to 30 days [Mankarious et al., 1988]. **The evaluation of the durability of the humoral response after vaccination is a question we are addressing in this thesis (Chapter 6).**

Although antibodies are the first line of defense to block infection and eliminate extracellular pathogens, they are powerless against intracellular pathogens, such as viruses, that infect and replicate directly in the infected cells. In this case, cell-mediated immunity is required. As shown in Figure 1.1, cellular immunity is mediated by T lymphocytes. T cells aim at eliminating the reservoir of infection inaccessible to circulating antibodies by inducing the lysis of infected cells or the destruction of pathogens hidden within phagocytes. To initiate antigen-specific cellular immunity, similar to B cells, naive T lymphocytes must recognize antigens presented by antigen-presenting cells inducing their activation, proliferation, and finally their differentiation into effector cells. The latter are able of eliminating intracellular pathogens. T cells can be derived into distinct sub-populations of cells, each of which has specific functions. In our work, we focused only on the two main classes: helper T cells, also called CD4+ T cells as they express the cluster of differentiation (CD) 4 glycoprotein at their surface, and cytotoxic T cells, referred as CD8+ T cells as expressing the CD8 glycoprotein at their surface. The role of CD4+ T cells is to recruit and mediate functions of other immune cells by secreting different types of cytokines (e.g. interleukin-2 (IL-2) or interferon γ (IFN- γ), among others). In particular, CD4+ T cells stimulate the activation and the differentiation of macrophages or NK cells to enhance pathogen elimination by phagocytosis, stimulate antibody production by helping B cells to differentiate into ASCs or enhance differentiation of T cells into effector cells. CD8+ T cells represent the first line of defense against intracellular pathogens by killing infected cells via three different pathways: 1) secreting cytokines to activate macrophages and induce inflammation, 2) secreting cytotoxic granules inducing deterioration and apoptosis of target cells and 3) directly eliminating infected cells via receptor binding inducing signalling cascade leading to target cell apoptosis. To avoid excessive activation of the immune system and an uncontrolled inflammatory process, a sub-population of CD4+ T cells called regulatory T cells aims at regulating the immune response to pathogens and self-antigens [Kondělková et al., 2010]. As immunosuppressive T cells, regulatory T cells inhibit T cell proliferation and cytokine production to maintain homeostasis and self tolerance.

As widely mentioned, the functions of both innate and adaptive immune cells are mediated by proteins called cytokines, which are considered as the main actors of the inflammatory response (or inflammation). This inflammation involves the development of a pathogen-specific humoral and cellular immune response by recruiting and activating lymphocytes, macrophages, and plasma cells at the site of infection. Most cytokines are called interleukin (IL) as they are mostly produced by macrophages, DCs, NK cells, and T cells, and act on them. Initially produced at the site of infection, they can elicit

1.1. The immune system

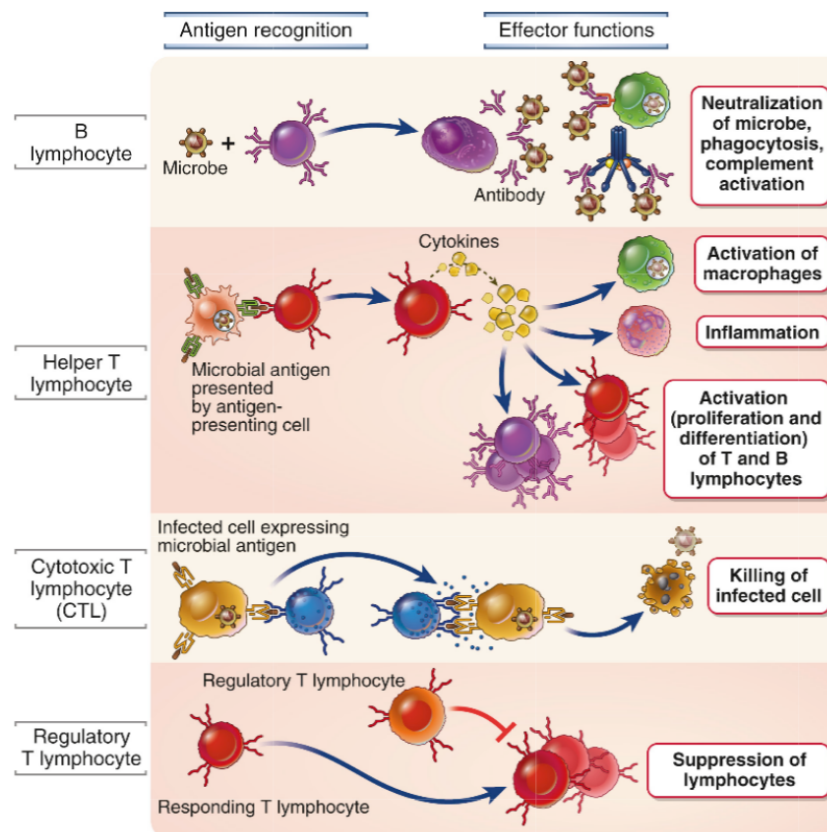


Figure 1.1 – Classes of lymphocytes and their functions in adaptive immunity. Taken from [Abbas et al., 2017].

both local and systemic actions. Without trying to provide an exhaustive list of all cytokines, we focus on cytokines encountered in our projects (mostly in Chapter 5 as immune markers, or in Chapter 3 as immunotherapy against HIV).

- ▷ *Interleukin-2 (IL-2)* is secreted by T lymphocytes, NK cells and, DCs and has a multivariate function in the immune system. In particular, it triggers the activation of multiple immune cells such as T cells and is essential to their differentiation into memory cells [Gaffen and Liu, 2004]. Due to its central role in the immune system and especially on T cells, this cytokine has been widely studied as an immunotherapy for HIV. **The reader can refer to the work conducted in Chapter 3 for an example of a clinical trial assessing the efficacy of IL-2 immunotherapy.**
- ▷ *Interleukin-8 (IL-8)* is produced by multiple cells such as monocytes, neutrophils, epithelial and endothelial cells, and plays an important role in inflammation. In addition, it contributes to the recruitment of T cells and non-specific inflammatory cells into the site of inflammation [Qazi et al., 2011].
- ▷ *Interleukin-10 (IL-10)* is secreted by a variety of cells, but in the majority by CD4+

T cells, monocytes, macrophages and DCs. Among its various functions in the inflammatory response, this cytokine aims at enhancing B cell survival, production, and proliferation, as well as antibody production, and inhibits the synthesis of pro-inflammatory cytokines by macrophages like IL-2, IFN- γ , TNF- α [Iyer and Cheng, 2012].

- ▷ *Interleukin-12 (IL-12)* is produced by dendritic cells. It stimulates the production of IFN- γ by NK cells and T cells and promotes the differentiation of naive CD4+ T cells (also called T helper 1 cells) into effector cells [McNab et al., 2015].
- ▷ *Interleukin-13 (IL-13)* is produced by CD4+ T cells and mast cells and aims at regulating the functions of B cells and monocytes by activating them and regulating their secretion of inflammatory cytokines [Zurawski and de Vries, 1994].
- ▷ *Interferon γ (IFN- γ)* is produced by macrophages, NK cells and T cells, activates macrophages and stimulates both dendritic cells and macrophages in the activation and differentiation of T cells (especially CD4+ T cells) through the production of IL-12. It also enhances the recognition of antigens by T cells and promotes antibody response by acting on B cells. Finally, it mediates the interaction between NK cells and macrophages to avoid excessive activation of macrophages [Market et al., 2020].
- ▷ *Tumor necrosis factor α (TNF- α)* is produced mainly by macrophages and dendritic cells but also NK and T cells. In addition to stimulating phagocyte recruitment and activation, TNF- α also enhances the ability of macrophages and endothelial cells to secrete chemokines. Finally, in severe infection, TNF can result in the systemic effects of the inflammatory response [Feghali et al., 1997] such as fever, the production of acute-phase proteins, similar to IL-6, and cachexia. It can also cause septic shock.

1.1.2.2 The phases and the properties of the adaptive immunity

Following the exposure of the human body to a foreign pathogen and its detection by the main actors of innate immunity, the response of adaptive immunity is progressively established in five consecutive phases: 1) antigen recognition, 2) lymphocyte activation, 3) antigen elimination (effector phase), 4) apoptosis of effector cells and 5) activation of memory lymphocytes. The different phases are presented in Figure 1.2. Adaptive immunity is triggered by recognition of the pathogen by naive lymphocytes. This initial phase relies on the first fundamental characteristic of the adaptive immune response: its *specificity*. This property derives from a single lymphocyte precursor cell that, even before encountering the antigen, develops many mature lymphocytes with surface receptors, each specific for a single antigen. A clone will refer in the following

1.1. The immune system

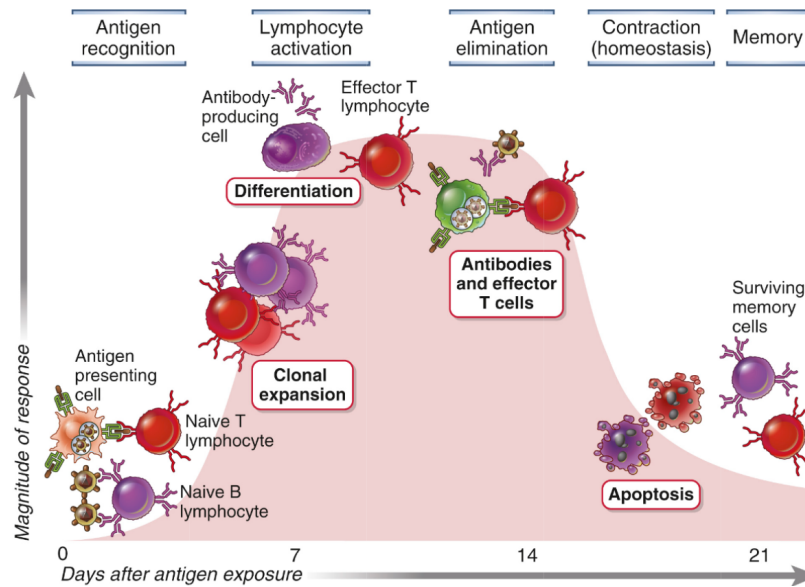


Figure 1.2 – The 5 phases of adaptive immunity. Taken from [Abbas et al., 2017].

to a population of lymphocytes with identical antigen receptors and thus their specificity. The ability of the immune system to recognize a large number of antigens results in the diversity of the lymphocyte reservoir. Once captured, antigen-presenting cells present them to B cells and T cells. Accordingly, the presented antigens lead to the selection of a pre-existing clone of specific lymphocytes and stimulate the proliferation and differentiation of this clone into effector cells. This second phase is characterized by a sharp increase of the immune response. This process is called the *clonal expansion*. Although both B cells and T cells exhibit antigen-receptors at their surface, the major difference is that B cells can only recognize free and unprocessed antigens, whereas T cells can only recognize antigens associated with infected cells. As antigens are eliminated by both humoral and cell-mediated immune responses, the immune response progressively declines. This decline is driven by the elimination of the effector cells by apoptosis, until reaching a steady state referred as homeostasis. At the end of the immune response, a small proportion of these antigen-specific B and T cells survives and remains in the immune system. These cells, known as memory cells, are responsible for the second fundamental characteristic of the immune system: its *memory* of prior exposures to a specific antigen. This specificity of the immune system, referred as immunological memory, is responsible for its ability to induce a faster and more efficient immune response at each exposure. This latter is essential for the success of vaccination, the cornerstone of this thesis.

1.2 Vaccination

1.2.1 Principle and brief history of vaccination

Vaccination is one of the brightest successes in the history of public health, saving nowadays millions of lives every year [D'Argenio and Wilson, 2010]. It consists in protecting people from infection by stimulating their immune response through exposure to attenuated or killed pathogens.

The initial idea of manipulating the immune system to control infectious diseases arised centuries ago over the world. However, the concept of variolation (also called 'en-grafting') largely widespread in Europe at the beginning of the 18th century, when an epidemic of smallpox ravaged the world [Riedel, 2005]. Empirically discovered, immunization against smallpox following natural infection led to the commonly used procedure of subcutaneous inoculation of a small amount of the virus into non-immune individuals. Based on the observation that people initially infected with cowpox developed resistance to smallpox, Edward Jenner extended this concept, leading to its landmark publication in 1798 on *vaccination* [Riedel, 2005; Plotkin, 2014]. This discovery enabled the worldwide eradication of smallpox in 1980 [Henderson, 1980]. Over the years, advances in immunology, virology, and molecular biology enabled a rapid vaccine development that led to the control of dozens of infectious diseases, including diphteria, tetanus, measles, polio, yellow fever, *Haemophilus influenzae* type b, and hepatitis B, among others [Delany et al., 2014; Plotkin and Plotkin, 2004; Bloom et al., 2017]. Until the second half of the 20th century, vaccine development was mostly based on the principle of immunological memory using inactivated toxins (e.g. tetanus toxoid), live-attenuated viruses (e.g. smallpox, polio, rabies, yellow fever), or inactivated/killed pathogens (e.g. cholera, influenza). By inoculating a weakened version of the live virus, these vaccines stimulate immunity of healthy people without causing serious infection due to the removal of their infectivity and pathogenicity [Plitnick, 2013; Delany et al., 2014]. Based on this concept, the best vaccines are those that stimulate the humoral response through the production of plasma cells secreting neutralizing antibodies with high-affinity (called long-lived plasma cells), and memory B-cells [Abbas et al., 2017]. Despite their widely approved efficacy and ability to reduce mortality, these vaccines show limitations. As a matter of fact, live viral vectors can present high reversion to natural virulence through mutations reactivating their pathogenicity (e.g. oral polio vaccine). Moreover, the development of immunity against the viral vector, resulting either from prior immunization (e.g. infection or vaccination) or from unexpected viral antigens injected with the vaccine, could counteract the vaccine efficacy [Ulmer et al., 2012]. Furthermore, in some cases, the humoral response might appear harmless in

protecting people from pathogens. Indeed, while inactivated vaccines can either display poor immunogenicity due to their nature or even induce the targeted pathology [Brisse et al., 2020], host protection should be conducted by cellular immunity and not humoral immunity as is the case with most parasites [Germain, 2010]. During the 20th century, a new type of vaccine was developed to overcome all potential pathogen-induced diseases: the subunit vaccine (also referred as 'protein-based vaccine'). These vaccines, which contain only purified fragments (antigens) of pathogens, can safely stimulate the immune system [Iwasaki and Omer, 2020]. However, their poor natural immunogenicity and low-affinity of antibody responses (resulting from T cell-independent antibody responses) must be compensated by their combination with proteins called adjuvants to induce strong and long-term protective effects [Foged, 2011]. The first subunit vaccines developed were composed of bacterial polysaccharide antigens and were used against meningococcus, pneumococcus and *Haemophilus influenzae* [Plotkin, 2014]. To induce a strong immune response against the targeted pathogens, the most recent vaccine platforms directly integrate the genetic material of the targeted virus. These include replicating and non-replicating viral vectors that integrate viral genetic material inside another harmless virus that may or may not self-replicate, as well as RNA- and DNA-based vaccines. **The development of these vaccine platforms is broadly discussed in Chapters 5 and 6 focusing exclusively on SARS-CoV-2 for mRNA- and DNA-based vaccines and on Ebola virus disease for replicating or non-replicating viral vectors.**

1.2.2 Vaccine strategies

The initial purpose of vaccine development was to administrate a preventive treatment, also called a 'prophylactic' approach, against infectious diseases to reach both individual and herd immunity [Sela and Hilleman, 2004; Kayser and Ramzan, 2021]. Over the years, the development of numerous safe and effective prophylactic vaccines led to the eradication, or at least control, of vaccine-preventable infectious diseases. **In this thesis, we will focus on Ebola and SARS-CoV-2 for preventive vaccine strategies.** Nowadays, the use of vaccines has been extended by the development of therapeutic vaccines. Similar to prophylactic vaccines, the mechanism of action of therapeutic vaccines relies on the stimulation of the adaptive immune response during persistent infection to reduce the viral burden. However, therapeutic vaccines are still at an early stage of development [Boukhebbza et al., 2012], with only a few products on the market [Sela and Hilleman, 2004], although many of them have been evaluated [Leal et al., 2020]. **In our work, we focused exclusively on HIV for therapeutic vaccine de-**

velopment (see chapters 3 and 4). In the specific case of HIV, the development of an effective therapeutic vaccine is a public health priority as it represents the best opportunity to slow down the epidemic [Girard and Koff, 2018]. In recent years, many vaccine candidates have been investigated, including classical strategies, such as inactivated viruses or protein subunits, or new promising strategies such as cell-mediated immune-based vaccines (e.g. dendritic cell-based vaccines [Sadat Larijani et al., 2019]) or broadly neutralizing antibodies [Sok and Burton, 2018]. However, none provided real evidence of efficacy and/or long-term control of infection. The failure of vaccines is likely related to mechanisms of immune evasion by HIV. Among other mechanisms, we can mention (1) its ability to persist in a latent state in the immune system by directly integrating the genome of long-lived host immune cells, (2) its short viral generation time resulting in a rapid replication rate and high mutation and recombination rates, rendering the virus nearly invisible to the immune system, or (3) its ability to spread from cell to cell within the host, protecting it from the immune effector cells [Girard and Koff, 2018; Kirchhoff, 2010]. Accordingly, optimal HIV vaccine candidates should be able to elicit both humoral and cellular responses.

In parallel with the choice of the optimal viral vector, the development of effective vaccines relies on the optimization of the design of vaccine strategies. In particular, some vaccine candidates will appear as inefficient to generate an effective and long-term protection against infection after a single dose of the active agent and therefore require multiple doses. In that vein, the so-called multi-doses vaccine regimens have proven to be a highly effective approach to induce both humoral and cellular immune responses [Kardani et al., 2016]. In this type of strategy, multiples factors will influence the outcome and should then be carefully defined to optimize the immunization approach. The first factor is the number of viral vectors involved in the immunization strategy. Indeed, while the prime/boost homologous strategies (i.e. single viral vaccine) can elicit efficient protection against a particular infectious disease, the combination of multiple vaccines may elicit a stronger immune response against the pathogen. These strategies are called prime/boost heterologous vaccine strategies. In addition to the choice between homologous and heterologous strategies, factors such as the total number of doses, the order of vector injections, the interval between two vaccinations, among others, should be carefully selected. **For instance, in this thesis, we especially worked on a prime/boost heterologous vaccine regimen against Ebola virus involving two viral vectors, the adenovirus Ad26.ZEBOV and viral vector MVA-BN-Filo, as the first and second injections, respectively, with an optimal interval of 56 days between the two doses. The reader can refer to this work in chapter 6.**

1.2.3 Clinical trials and vaccine development

The development of new drugs and vaccines is a long and complex process that usually requires 10 to 15 years. Typically, this process consists of four phases, referred as clinical trials, which are conducted sequentially to evaluate the safety, toxicity, immunogenicity (i.e., the ability to induce an immune response), efficacy, and effectiveness of the drug in humans [FDA, 2021] (Figure 1.3). Both vaccine efficacy and effectiveness are related to the effects of a vaccine on specific outcomes but may often be confusedly used. The major difference is that the term efficacy is used to talk about the action of a vaccine in a specific population under controlled conditions (e.g. controlled clinical trials), while the term effectiveness is more related to a "real-world" view of vaccine effects. [Weinberg and Szilagyi, 2010; WHO, 2021d]. Considering only data collected in controlled trials in our projects, the evaluation of effectiveness has been considered as out of the scope of this manuscript.

The entire vaccine development process is strictly regulated by the public health regulatory authorities. They set the guidance to be followed and are the only authorities able to license a product and thus approve it for the market. Among the well-known regulatory authorities over the world, we can mention the U.S. Food and Drug Administration (FDA) for the United States [Cohn et al., 2018], the European Medicines Agency (EMA) for Europe [Johansen et al., 2018], including the Safety of Medicine and Health Products in France.

1.2.3.1 The relevance of pre-clinical studies in vaccine development

In vaccine development, clinical trials are mostly preceded by nonclinical studies called 'preclinical studies'. Two types of studies are commonly conducted: *in-vitro* studies in laboratories using human tissue- or cell-cultures, or *in-vivo* studies on animals. The purpose of these studies is to evaluate the toxicity, safety and immunogenicity of the tested vaccine before any test on humans [Wright, 2017]. To this end, pharmacokinetics, pharmacodynamics, and toxicology studies are performed. In particular, these preclinical studies allow us to identify some biological, chemical, and physical properties of the molecule of interest as well as its mechanism of action [Honek, 2017]. Being easier to implement, these studies offer the opportunity to evaluate and compare multiple vaccine strategies and/or study designs that could be more difficult to conduct on humans. Accordingly, these studies can provide guidance for clinical trial design. Coupled with toxicity studies [Ochoa, 2002], single- and multiple-dose range-finding studies (e.g. dose-escalation studies) [Wexler and Bertelsen, 2011; Iasonos and O'Quigley, 2014] are performed to quantify a safe starting dose for clinical trials. Similar to clinical

trials, preclinical studies are conducted in compliance with the guidelines defined by the Good Laboratory Practice as well as with guidelines on animal experimentation defined by the national authorities [WHO, 2007]. In the frame of this thesis, we had the opportunity to be enrolled in a project developing a new vaccine strategy against SARS-CoV-2 that is currently being evaluated in preclinical studies in non-human primates (NHPs). The related work is available in Chapter 5.

1.2.3.2 The different phases of the vaccine clinical trials

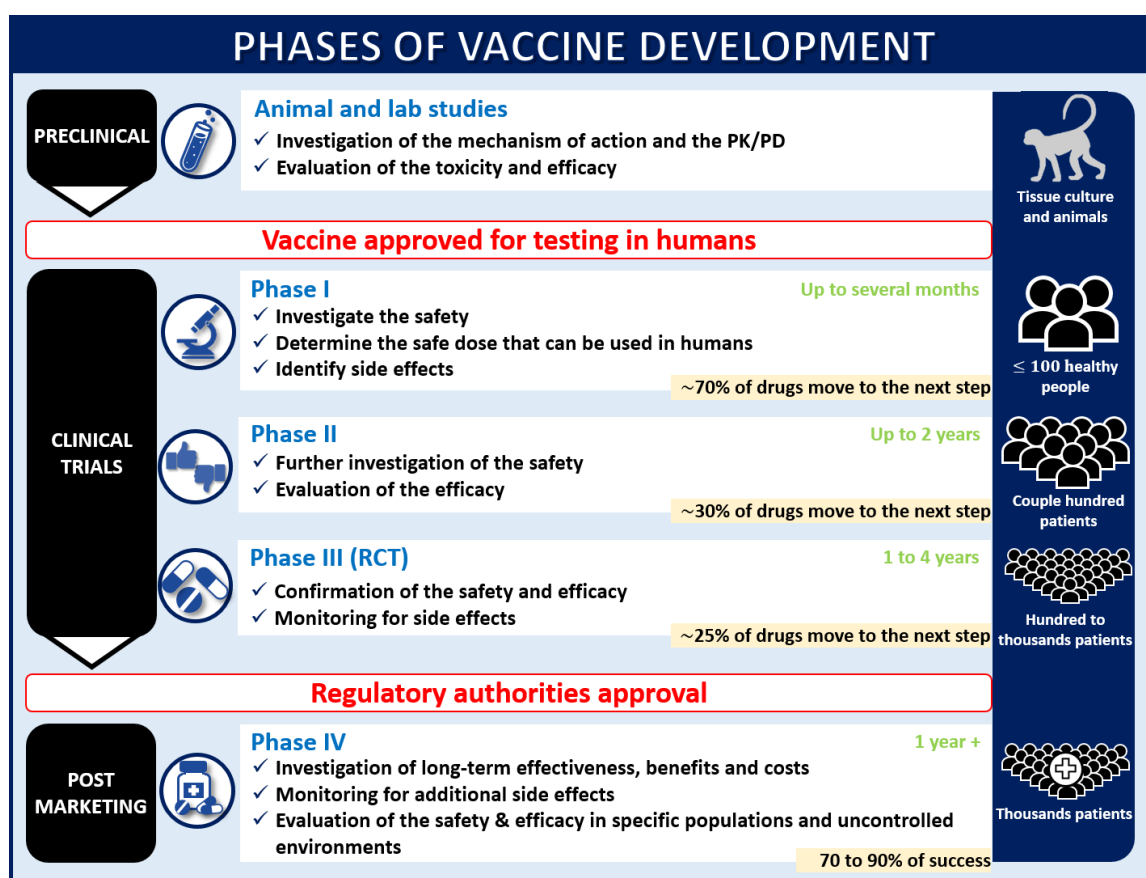


Figure 1.3 – Phases of a new vaccine development

The Phase I clinical trial represents an exploratory phase enrolling a small group of participants (less than one hundred), usually healthy volunteers, and aims at finding a proper way to administrate the vaccine by evaluating its safety and tolerability. Among these clinical trials, the Phase I First-in-Human studies can be conducted in the early phase of a new vaccine development, to mainly evaluate its pharmacokinetic (PK) and pharmacodynamics (PD) in humans [Wexler and Bertelsen, 2011]. Despite the fact that First-in-Human studies are essential in the development of new vaccines, Goetz

[et al. \[2010\]](#) highlights the specificity of vaccine development, especially in infectious diseases, compared with more traditional drug development (e.g. cancer treatment, monoclonal antibodies), and the resulting lack of general guidance in this particular case.

The phase II clinical trials are conducted on a larger number of participants (couple hundred), and often represent the first opportunity to test the medication on patients affected by the studied disease, like for therapeutic vaccines, or are still tested on healthy volunteers in the case of prophylactic vaccines. Although the safety is further assessed, these trials are specifically designed to get information about the vaccine-induced immune response in the targeted population and start to assess its efficacy (usually based on immune markers in Phase II). In addition to multiple dose testing, Phase II studies can be conducted to evaluate the vaccine efficacy in various and specific populations (e.g. infants, children, elderly, immuno-compromised, pregnant women).

The phase III studies (or "pivotal" studies) are performed on a large number of subjects (from hundreds to thousands) and aim at formally evaluating the vaccine efficacy (based on clinical outcomes) before its approval by authorities. Once approved, Phase IV studies are conducted on thousands of volunteers to evaluate its effectiveness (see [Figure 1.3](#)). We are not going into further details for these last two phases as only Phase I and II studies were considered in our work.

1.2.3.3 Evaluation of vaccine efficacy

Through the different phases of clinical trials leading to the approval of the new products, both safety and efficacy of vaccines need to be proven. To demonstrate vaccine benefit, investigators have to specify and describe in the protocol criteria in accordance with the objective of the trial reflecting its clinical outcome (i.e., a measure of how patients feel, function, or survive). These criteria, referred as endpoints, can then be defined either as a direct/true endpoint if they directly characterize the clinical outcome (e.g. survival), or as a surrogate endpoint if they represent a substitute of the clinical outcome [[FDA, 2018](#)]. In clinical trials, surrogate endpoints are widely related to the notion of biomarkers, which have been defined by the WHO as "*any substance, structure, or process that can be measured in the body or its products and influence or predict the incidence of outcome or disease*" [[WHO, 2001](#)].

In Phase I and Phase II studies, primary (related to the primary objective) and secondary endpoints are typically safety and immunogenicity endpoints [[Hudgens et al., 2004](#)]. In Phase IIb and Phase III trials, the clinical outcome of vaccination is the vaccine efficacy, also referred to as the percent reduction in the chance of developing clin-

ical disease (also referred as "incidence", e.g. hospitalization, symptoms) among vaccinated people compared to unvaccinated in clinical trials [Weinberg and Szilagyi, 2010; Hanquet et al., 2013; Fine et al., 2018]. As a matter of fact, in addition to its safety and immunogenicity, the efficacy of a vaccine must be proven in order to be licensed. Nevertheless, the evaluation of the vaccine efficacy as clinical measure requiring large-scale controlled clinical trials, this one can only be directly observed under specific and limited conditions (geographic regions, target populations, vaccine formulation, ...) [Gilbert et al., 2008; Qin et al., 2007], due to resource limitations and sometimes ethical reasons. This is particularly true in the case of low incidence, as with Ebola, or when other vaccines are available, as with SARS-CoV-2. Consequently, the identification of immunological surrogate endpoints/markers that could be used to predict vaccine-induced benefits is a crucial goal of vaccine research. Besides accelerating the clinical vaccine development, identification of immunological surrogate endpoints progressively enhances our understanding of the immune system, making the development of new vaccine strategies/platforms possible. Nevertheless, the validation of such relationship between the immune marker and vaccine efficacy is quite challenging [Qin et al., 2007] and additional methods need to be developed to address this question.

In this manuscript, we will use the terminology introduced by Plotkin and Gilbert [2012]. The definition of the different types of immune surrogate endpoints is quite hierarchical and relies on the conceptual link between the treatment, the immune marker, and the vaccine efficacy (protective effect). In particular, the type, the strength of these links, and the amount of information required to evaluate them are key components [Gilbert et al., 2008]. We refer to as an immune correlate any surrogate endpoint that allows us to predict an important clinical outcome without measuring a clinical benefit itself [Guideline, 1997]. As defined in Table 1.1 and in Figure 1.4, immune correlates can be splitted into two categories according to their property to be directly impacted by the treatment (also called "intervention"). First, as defined by Qin et al. [2007], a biomarker will be categorized as a correlate of risk (CoR) if this latter is correlated with the clinical outcome used to quantify the vaccine efficacy. Consequently, a CoR is not necessary directly related to the treatment and can only reflect its effect on the clinical outcome. For example, in 1943, a clinical trial evaluating a vaccine against influenza was conducted, using the incidence of hospitalizations as primary efficacy endpoint. In this trial, antibody titers against the Weiss strain A were assessed as CoR eliciting a statistically significant inverse association between antibody titers (immune marker) and the incidence (clinical outcome) [Salk et al., 1945]. On the other side, we will define as a correlate of protection (CoP) any immune correlate that can be used to reliably predict vaccine-induced protection. In particular, all CoPs are assumed to be CoRs. In the liter-

ature, this definition of CoP corresponds to the “surrogate of protection” defined by [Qin et al. \[2007\]](#). Nevertheless, it is important to notify that the definition of CoP and surrogate defined by [Plotkin and Plotkin \[2008\]](#) is quite different. Namely, we referred as CoP any biomarker that is statistically correlated with the vaccine efficacy, without any specification about the causation of this link. As defined in [Plotkin and Gilbert \[2012\]](#), a CoP can directly refer to the mechanism of protection induced by the vaccine and is then causally responsible for the protective effect. In that case, this CoP is identified as a mechanistic CoP (mCoP). Otherwise, this latter is defined as a non-mechanistic CoP (nCoP) and is thus only correlated with the vaccine efficacy, without causal relationship. These types of CoP refer to the notion of CoP and surrogate defined by Plotkin in 2008 and 2010 [[Plotkin and Plotkin, 2008](#); [Plotkin, 2010](#)], respectively. The figure 1.4 displays this hierarchical link between the CoR, CoP, mCoP and nCoP. However, mCoP, and nCoP are a partition (in mathematical sense) of the set of CoP meaning that a CoP is either a mCoP or a nCoP (further details about causality and surrogacy are given in section 2.2.3).

Table 1.1 – Definitions and properties of immune surrogate endpoints

Term	Definition	Reference
Immune correlate	Surrogate endpoint predicting either the clinical outcome used to measure vaccine efficacy or directly the vaccine efficacy	[Guideline, 1997]
CoR (correlate of risk)	Immune marker statistically correlated with the clinical outcome of interest, but not necessary with the treatment itself (=Predictor of clinical outcome)	[Qin et al., 2007] [Gilbert et al., 2008]
CoP (correlate of protection)	Immune marker statistically correlated with vaccine efficacy that may or may not be mechanistically and causally responsible for protection (=Predictor of protection)	[Plotkin and Gilbert, 2012] [Qin et al., 2007] [Gilbert et al., 2008] [Prentice, 1989]
mCoP (mechanistic CoP)	A CoP that is mechanistically and causally responsible for protection (=Protective immune function)	[Plotkin and Gilbert, 2012] [Plotkin, 2010] [Plotkin and Plotkin, 2008]
nCoP (non-mechanistic CoP)	A CoP that is not mechanistically and causally responsible for protection (= immune function related to protection)	[Plotkin and Gilbert, 2012] [Plotkin, 2010] [Plotkin and Plotkin, 2008]
Properties	Absolute CoP	A CoP that always provides approximately 100% of protection (= threshold level of immune response correlated with protection)
	Relative CoP	A CoP that usually provides protection but not always (= a variable level of immune response correlated with protection)

VE: Vaccine efficacy ; RCT: Randomized controlled trial.

The immune system corresponds to the collaboration of various different types of cells to protect an individual against foreign pathogens. Consequently, the protection induced by a vaccine could result from many different immune responses. Nevertheless, the majority of approved vaccines target the humoral response by enhancing the production of antibodies. Consequently, nowadays, antibodies have been widely studied

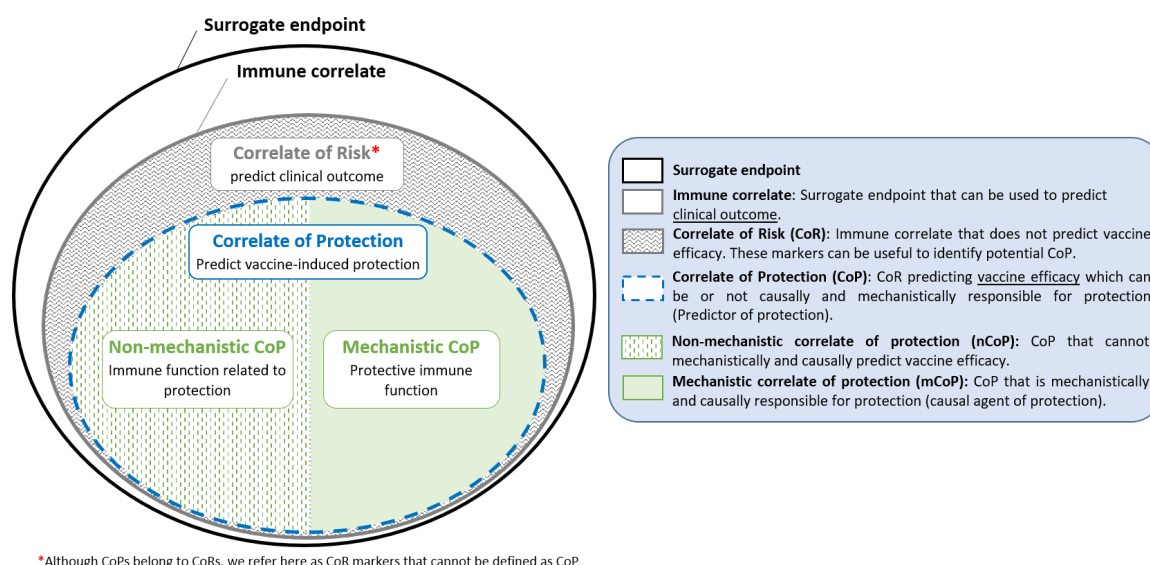


Figure 1.4 – Nested nomenclature of immune correlates.

and identified as CoP, whether as mCoP or nCoP, for various infectious diseases, such as smallpox, diphtheria, Haemophilus influenzae type b, measles, rubella, and polio [Plotkin and Plotkin, 2008]. For many of them, the level of antibody response required to guarantee protection after vaccination has been quantified (see Table 4 in [Plotkin and Plotkin, 2008]). These CoPs are then qualified as absolute. However, it is important to notice that in some cases, a CoP can also be relative which means that a certain level of the immune marker can be identified for which protection is almost always reached but in some punctual cases, this level appears as ineffective and a higher response is required.

Finally, it is important to understand that a single vaccine may be associated with different CoPs. Indeed, depending on the context and correlate of interest (e.g., infection, disease, hospitalization, ...), different immune markers can be identified. Moreover, for a given infectious disease, CoPs may vary between the response elicited by the vaccine and the immune response elicited by a natural infection. For example, in the case of measles vaccines, it has been shown that an antibody titer between 120 and 200 mIU/ml, and thus vaccines that elicit a titer greater than 200 mIU/ml, provide protection against clinical symptoms but insufficient protection against infection with measles [Chen et al., 1990]. As might be expected, the relevance of a CoP may also depend on the vaccine platform used against a particular infection, due to the vaccine's different mechanism of action and depending on the target population (e.g., immunocompromised, elderly, infants) or the challenging dose. Accordingly, identifying at least one relevant CoP for a vaccine candidate is a major challenge.

In this thesis, we focus mainly on three infectious diseases: HIV, Ebola, and SARS-Cov-2. As will be described in detail in the next chapters, no CoPs have yet been clearly identified for these three infectious diseases, although there is ample evidence of a strong link between vaccine-induced protection and binding and/or neutralizing antibody levels, particularly in the case of Ebola and SARS-CoV-2.

One of the most challenging aspect of vaccine development in many important pathogens is their antigenic variability, which mainly results from a high mutation rate and a genetic instability [Servín-Blanco et al., 2016]. Although a wide scale of variability may be observed between pathogens, for highly variable pathogens, such as HIV and SARS-CoV-2, it confer to viruses the ability to escape protective immune responses established by prior infection or vaccination. Accordingly, it can have a large impact on vaccine design, efficacy and on the longevity of its induced immune response. **Despite its crucial aspect on vaccine development and identification of CoP, antigenic variability was not integrated in our work. In the case of SARS-CoV-2, our analyses included only data collected after infection with a single known strain (wild-type) while, in our work on HIV, we focused on the identification of an efficacy of a vaccine in a given RCT (i.e. comparing vaccine and placebo on the same and single strain) and never tried to compare vaccines from various trials with each other.**

Chapter 2

Mathematical and statistical modelling of infectious disease dynamics

Abstract: The aim of this thesis work is to analyze the efficacy of vaccines, whether in terms of protection or longevity of the immune response induced by vaccination. In this regard, all work is based on longitudinal analysis of immunological and virological markers. Thus, our methods are in the realm of mixed-effects models. We present in this chapter two approaches that we use: descriptive models, mainly represented by mixed-effects regression models, and the so-called mechanistic dynamics, based on systems of ordinary differential equations. For these two approaches, we present both the mathematical framework and the inference techniques used. In addition, we present the general framework of causal modeling, which is necessary for a good understanding of the context in which the identification of the correlates of protection takes place, as well as for the use of mechanistic models and their predictive ability.

Keywords: Mathematical modelling ; longitudinal data ; within-host modelling ; mixed-effects model ; maximum likelihood ; mechanistic model ; ordinary differential equation ; SAEM algorithm ; missing data ; censored data ; causal inference

This chapter presents the general tools that have been pooled together for the research and provides an overview of the current state of the art. Moreover, all the methods of estimation are generally presented as "black boxes" in our different papers. However, in the context of this thesis, we have deepened our understanding of these algorithms, that is why we decided to present them in this chapter.

2.1 The role of mathematical modelling

Since the dawn of time, the world, and by extension mankind, has faced countless outbreaks of infectious diseases. Despite the amazing discovery of vaccination, which successfully allowed the eradication of smallpox and the control of many other infectious diseases, endemic and epidemic infections are ubiquitous in our modern world. Emerging infectious diseases such as HIV, influenza A strains, the Ebola virus with the 2014/2016 West Africa outbreak, or more recently the SARS-CoV-2 pandemics, represent a major threat to human health and worldwide challenge to daily life. These last decades, the massive apparition of infectious diseases and their spread over the world could result, at least in part, from our modern lifestyle which tends to enhance their emergence and their spread [Heesterbeek et al., 2015]: population growth, urbanization with intensive national and international travel or rural modernization with increasing production especially in cattle farming (new infections mostly arise from wildlife and livestock). Over the last years, substantial efforts have been made in many fields and interdisciplinary collaborations have been developed to tackle pandemics. In addition to vaccine development, technical and theoretical progress in scientific fields such as medicine, immunology, molecular biology, genetics, computer science, mathematics, data management, but also in economy, sociology, anthropology, ecology, among others, enabled the establishment of a global infectious disease surveillance network [Grassly and Fraser, 2008; Siettos and Russo, 2013]. Moreover, these advances provided an improved understanding of the immune system, infections, and the underlying biological processes or factors that could influence some of their features, such as duration or infectiousness. Nevertheless, the multi-scale nature of the interaction between the host and the pathogen (also called "within-host" interaction) and between hosts themselves (also called "inter-host" interaction) at both individual and population level significantly increase the complexity to fully understand the underlying immune mechanisms and control infectious disease outbreaks. Furthermore, although vaccine development experienced major breakthroughs these last decades, it remains a time consuming process from the theoretical development to the commercial production and distribution, and faces many challenges such as with highly antigenically

variable pathogens (e.g. HIV, malaria). In this context, mathematical, statistical and computational tools are fundamental in public health strategies in various countries. Firstly introduced in 1766 by Bernoulli to study the benefit of vaccination against smallpox [Dietz and Heesterbeek, 2002], mathematical modelling is today a key feature to analyze infectious disease epidemiology and widely help to define and take important decisions. In combination with valuable data, mathematical models allow to synthesis information, better understand epidemiological/immunological processes and test many scientific hypotheses. Despite the interest that both inter- and intra-host modelling scale could offer, we only focused on within-host modelling in the framework of this PhD.

2.2 Descriptive models for longitudinal data in epidemiology

In epidemiology and more specifically in clinical trials, longitudinal data are really common. Collected in longitudinal studies, data consist in series of time-dependent repeated measurements of variables of interest for each subject enrolled in the study. Outcomes of interest are thus measured repeatedly over time for each individual. For example, in clinical trials evaluating HIV vaccine candidates, the two outcomes most commonly used to account for the clinical progression are viral loads and concentrations of CD4+ T cells (also called CD4 count) [Boscardin et al., 1998]. In addition to the outcome of interest, multiple variables can also be measured individually over time, such as immune markers investigated as surrogate endpoints. For example, similar to HIV trials, viral load measurements are widely used in SARS-CoV-2 studies to evaluate the progression and severity of infection [Fajnzylber et al., 2020; Shenoy, 2021; Yu et al., 2020a]. Nevertheless, trajectories of immune markers such as binding or neutralizing antibody titers can also be collected [Roosendaal et al., 2021; Chia et al., 2021]. Over the years, multiple methods have been developed to analyze this type of data and quantify the potential effect of a treatment. In this manuscript, we will mainly focus on **two types of modelling approaches to evaluate this effect**. These two approaches rely on **the modelling of individual trajectories** of our outcomes using multiple types of mathematical models, but are distinguished by the methods used to detect the treatment effect. While the first approach aims at **summarizing trajectories by a single variable compared between groups of treatment**, the second one focuses on the identification of this effect by directly **integrating covariates into the modelling process** (e.g. adjustment of model parameters for groups of treatment).

2.2.1 Incomplete longitudinal data

In longitudinal studies, whether in observational or experimental studies, the incompleteness of data is a recurrent problem [Rubin, 1976]. Although missing data are less common in controlled trials due to the establishment of protocols defining the number, frequency, time-window or type of measurements, among others, for each subject, these latter are likely to exist in practice. Among the most common reasons inducing missing data, participants can be absent at specific visits, or can decide to prematurely leave the study, whether for medical or personal reasons. In the case of survey data, missing data can also occur when some parts of the questionnaire remain incomplete. Regardless of the reason, missing data irretrievably lead to a loss of information. Consequently, statistical analyses of incomplete data without any consideration for missingness patterns often result in biased results [Ibrahim and Molenberghs, 2009]. To better integrate missing data in the analysis, Little and Rubin [Rubin, 1976; Little and Rubin, 2019] classified them into three categories according to their underlying processes. In order to define these categories, we first introduce the notations used in Little and Rubin [2019] to describe missing data. We note \mathbf{Y} the vector of responses (outcome) which can be partitioned into two sub-vectors such that $\mathbf{Y} = (\mathbf{Y}^o, \mathbf{Y}^m)$ with \mathbf{Y}^o and \mathbf{Y}^m being the vectors of observed and unobserved (=missing) responses, respectively. We define the vector \mathbf{X} as an exploratory variable assumed to be completely observed and independent of \mathbf{Y} and the variable \mathbf{R} as the following indicator variable: $R(t) = 1$ if $Y(t)$ is observed ($Y(t) \in \mathbf{Y}^o$) and $R(t) = 0$ if $Y(t)$ is missing ($Y(t) \in \mathbf{Y}^m$). Based on these definitions, missing data are said *monotone* if from a given missing observation, all data presumably observed after this one are also missing. Monotone data are also termed as *dropout*. Mathematically, data follow a monotone missing pattern if $\exists T \forall t \geq T, R(t) = 0$ or $\mathbb{P}(R(t)|R(s) = 0, s < t) = 1$. Otherwise, data are said *non-monotone* or *intermittent*. According to the classification of Little and Rubin, data are defined as:

- ▷ *missing completely at random* (MCAR) if the mechanism of missingness is independent on the date meaning that the variable \mathbf{R} does not depend on \mathbf{Y} :

$$\mathbb{P}(R|Y^o, Y^m, X) = \mathbb{P}(R|X)$$

- ▷ *missing at random* (MAR) if the mechanism of missingness depends on previous observations but not on missing data meaning that \mathbf{R} depends on \mathbf{Y}^o but not on \mathbf{Y}^m :

$$\mathbb{P}(R|Y^o, Y^m, X) = \mathbb{P}(R|Y^o, X)$$

- ▷ *missing not at random* (MNAR) if \mathbf{R} depends on both observed and missing responses.

These data are also called *informative* missing data.

While no bias is introduced with MCAR data, missingness should be carefully considered for MAR and MNAR data. In addition to missing data, the presence of a limit of detection (LOD) in assays quantifying outcomes and immune markers of interest can result in the left-censoring of data and biased estimates, if ignored. The consideration of left-censored data is particularly relevant in the case of HIV viral load measurements [Hughes, 1999, 2000; Jacqmin-Gadda et al., 2000; Lynn, 2001]. The efficacy of antiretroviral treatments allows a fast decrease of the HIV RNA load, until becoming undetectable, but still present. Consequently, censored data should be carefully taken into account in the estimation of the model parameters used, for example, to evaluate a treatment efficacy and avoid as far as possible the introduction of a bias in this estimation.

In the case of our work conducted on HIV, we will place in MAR setting with left-censored data (see chapters 3 and 4).

2.2.2 The linear Mixed-Effects models

In longitudinal studies, the models that are the most commonly used to describe and model individual trajectories over time are the mixed-effect models (MEMs) [Vonesh and Chinchilli, 1996]. As a matter of fact, despite the relevance of using standard regression models in many fields, repeated measurements collected for each individual cannot be independently interpreted, as required by this type of model. MEMs have then been introduced to account for within-subject correlations [Pinheiro, 2005; Laird and Ware, 1982]. Consequently, they are built to incorporate the two sources of variation found in longitudinal data: the between-individual and the within-individual variations [Wu, 2009].

2.2.2.1 General model

In this section, we will exclusively focus on the linear MEMs which correspond to the models used in chapter 4 to describe HIV viral load dynamics in therapeutic vaccine trials.

In the following, let us denote Y the variable of outcomes with Y_{ij} being the observation of Y for the i th subject at the time t_{ij} , where $i = 1, \dots, N$ and $j = 1, \dots, n_i$ with N and n_i being the number of subjects and the number of measures for the subject i , respectively. For sake of simplicity without loss of generality to a broader framework, lets

assume Y defined as a single variable outcome. In other words, we limit this mathematical framework to univariate models, even though every results remain valid or have been extended to multivariate models [Thiébaud et al., 2003, 2005]. We define X and Z as the matrices of explanatory variables for fixed and random effects, respectively. Explanatory variables can be defined as fixed variables in time, such as an intercept or an indicator variable accounting for group of treatment (1=treatment, 0=control), or as time-dependent variables, such as the time itself, polynomials or any more complex functions of time such as splines (see Chapter 4) [Wand, 2003; Mackenzie et al., 2005; Welham et al., 2007].

Introduced by Harville [1977] and Laird and Ware [1982], the standard linear mixed-effects model (LMEM), assuming a Gaussian distribution of the variable Y , is defined as follows

$$Y_{ij} = \mathbf{X}_{ij}^T \boldsymbol{\beta} + \mathbf{Z}_{ij}^T \boldsymbol{\gamma}_i + \varepsilon_{ij} \quad \text{with } \varepsilon_{ij} \sim \mathcal{N}(0, \omega^2) \text{ and } \boldsymbol{\gamma}_i \sim \mathcal{N}(\mathbf{0}, \boldsymbol{\Sigma})$$

where $\mathbf{X}_{ij} \in \mathbb{R}^p$ and $\mathbf{Z}_{ij} \in \mathbb{R}^q$ are the vectors of explanatory variables for fixed and random effects for the subject i at time t_{ij} ; and $\boldsymbol{\beta} \in \mathbb{R}^p$ is the vector of the fixed effect parameters. The vectors $\boldsymbol{\gamma}_i \in \mathbb{R}^q$ are vectors of random effect parameters assumed to be identically and independently distributed (iid) and assumed to be normally distributed with an unstructured covariance matrix $\boldsymbol{\Sigma}$. Finally, we assume a constant error model with the residual errors ε_{ij} independent of the random effects $\boldsymbol{\gamma}_i$. By denoting $\mathbf{Y}_i = (Y_{i1}, Y_{i2}, \dots, Y_{in_i})^T$ the outcome variable specific to the i th subject, $\mathbf{X}_i \in \mathcal{M}_{n_i \times p}$ and $\mathbf{Z}_i \in \mathcal{M}_{n_i \times q}$ its matrices of explanatory variables such that $\mathbf{X}_i = (\mathbf{X}_{i1}^T, \mathbf{X}_{i2}^T, \dots, \mathbf{X}_{in_i}^T)$ and $\mathbf{Z}_i = (\mathbf{Z}_{i1}^T, \mathbf{Z}_{i2}^T, \dots, \mathbf{Z}_{in_i}^T)$, and $\boldsymbol{\varepsilon}_i = (\varepsilon_{i1}, \varepsilon_{i2}, \dots, \varepsilon_{in_i})^T$, the LMEM can be written in matrix formulation as

$$\mathbf{Y}_i = \mathbf{X}_i \boldsymbol{\beta} + \mathbf{Z}_i \boldsymbol{\gamma}_i + \boldsymbol{\varepsilon}_i \quad \text{with } \boldsymbol{\varepsilon}_i \sim \mathcal{N}(\mathbf{0}, \boldsymbol{\Omega}) \text{ and } \boldsymbol{\gamma}_i \sim \mathcal{N}(\mathbf{0}, \boldsymbol{\Sigma}) \quad (2.1)$$

Given the random effects, the model can be re-written under the marginal formulation [Jones and Boadi-Boateng, 1991] as:

$$\mathbf{Y}_i = \mathbf{X}_i \boldsymbol{\beta} + \boldsymbol{\varepsilon}_i \quad \text{with } \boldsymbol{\varepsilon}_i \sim \mathcal{N}(\mathbf{0}, \mathbf{V}_i = \mathbf{Z}_i \boldsymbol{\Sigma} \mathbf{Z}_i^T + \boldsymbol{\Omega})$$

Initially developed in a Gaussian context, the framework of the LMEM has been progressively extended to be applied in broader contexts. McCullagh and Nelder [2019]

introduced the framework of the generalized mixed-effects models given the opportunity to analyze other types of distribution of the outcomes, such as Binomial distribution [Williams, 1982; Stiratelli et al., 1984] for binary data or Poisson distribution for count data [Breslow, 1984]. Keeping the Gaussian distribution for the outcome, LMEM have also been extended to account for non-linearity in the model parameters [Lindstrom and Bates, 1990; Vonesh and Carter, 1992; Davidian and Gallant, 1993]. However, in this section, we are not going into further details about the non-linear mixed effects models. Nevertheless, these latter are further presented in section 2.3, in particular with the **description of the NLME-ODE framework that we used in our modeling work available in chapters 5 and 6.**

2.2.2.2 Statistical inference and model estimation using maximum likelihood estimation

The major problem in statistics is that data are generated by a process (or population) with unknown properties (e.g. unknown probability distributions). Statistical inference refers to the process of analyzing these data to learn information/properties about this underlying process (or population). Considering the problem where our observations Y_{ij} are assumed to be generated by MEM, we aim at estimating model parameters using observations. This procedure is also referred as the *inverse problem*. Although we are mostly interested in LMEMs, in this section, the general framework of MEM is considered, as similar methods can be applied. Let us denote θ the vector of parameters to estimate. In the model 2.1, this vector is defined as $\theta = (\beta, \Sigma, \Omega)$.

In statistics, the maximum likelihood estimation is an approach commonly used to estimate the vector θ . This approach consists of calculating the observed likelihood (i.e. the likelihood of the observations), labelled $p(\theta; \mathbf{Y})$, and to estimate θ as the parameters maximizing this observed likelihood. By assumption of independence between individuals, the observed likelihood can be defined as

$$\mathcal{L}(\mathbf{Y}; \theta) = p(\theta; \mathbf{Y}) = \prod_{i=1}^N p(\theta; \mathbf{Y}_i) \quad (2.2)$$

where $p(\theta; \mathbf{Y}_i)$ is the observed individual likelihood for the individual i which can be computed by integration over the random effects γ_i . Assuming that the pairs (\mathbf{Y}_i, γ_i) are mutually independent, the individual likelihood can be written as:

$$p(\theta; \mathbf{Y}_i) = \int_{\mathbb{R}^q} p(\mathbf{Y}_i, \gamma_i; \theta) d\gamma_i = \int_{\mathbb{R}^q} p(\mathbf{Y}_i | \gamma_i; \theta) p(\gamma_i; \theta) d\gamma_i$$

with $p(\mathbf{Y}_i, \gamma_i; \boldsymbol{\theta})$ being the joint distribution of (\mathbf{Y}_i, γ_i) , $p(\mathbf{Y}_i|\gamma_i; \boldsymbol{\theta})$ is the conditional distribution of the observations given the individual parameters and $p(\gamma_i; \boldsymbol{\theta})$ is the density function of the random effects (i.e. distribution of the individual parameters within the population). Based on these definitions, the observed log-likelihood of a general MEM can be written as:

$$\begin{aligned} L(\mathbf{Y}; \boldsymbol{\theta}) = \log p(\boldsymbol{\theta}; \mathbf{Y}) &= \sum_{i=1}^N \log \int_{\mathbb{R}^q} p(\mathbf{Y}_i|\gamma_i; \boldsymbol{\theta})p(\gamma_i; \boldsymbol{\theta})d\gamma_i \\ &= \sum_{i=1}^N \log \int_{\mathbb{R}^q} \prod_{j=1}^{n_i} p(Y_{ij}|\gamma_i; \boldsymbol{\theta})p(\gamma_i; \boldsymbol{\theta})d\gamma_i \end{aligned} \quad (2.3)$$

Once the integral evaluated, the estimation of the parameter $\boldsymbol{\theta}$ is defined as the maximum likelihood estimates (MLE), meaning the parameter $\boldsymbol{\theta}$ belonging to the set Θ maximizing the observed likelihood, and labelled $\hat{\boldsymbol{\theta}}$ such that:

$$\hat{\boldsymbol{\theta}} = \arg \max_{\boldsymbol{\theta} \in \Theta} L(\mathbf{Y}; \boldsymbol{\theta})$$

To perform the maximization of the observed likelihood (or log-likelihood), iterative optimization algorithms are commonly used, such as the well-known Newton-Raphson algorithm [Lindstrom and Bates, 1988] (see section 2.2.2.3 for more details about these algorithms).

In the case of LMEM, the use of normal density functions provides a closed-form of the integral allowing an exact numerical computation of the integral defined in equation 2.3. **This is in particular the method that we used in chapter 4 to estimate our aforementioned splines-based MEM.** A closed-form of the log-likelihood is more difficult to obtain in a more general framework, especially in non-linear models. Consequently, numerical approximations of the log-likelihood, and more precisely of the integral, must be performed. The reader can refer to section 2.3 for further details about the methods and numerical approximations that are commonly used in the case of non-linear MEM (NLMEM).

2.2.2.3 Optimization algorithms

To maximize the likelihood, iterative algorithms have been developed. The most efficient algorithm is the Newton-Raphson algorithm [Lindstrom and Bates, 1988] which belongs to the class of the Newton's algorithms. These algorithms rely on the maximiza-

tion of a continuous and twice differentiable function (the observed log-likelihood) by moving step by step on the surface to maximize. At each iteration k , the direction of the displacement is defined according the gradient of the function to optimize and the curvature of this function. We aim at calculating the MLE defined by:

$$\hat{\boldsymbol{\theta}} = \arg \max_{\boldsymbol{\theta} \in \Theta} L(\mathbf{Y}; \boldsymbol{\theta})$$

where $L(\mathbf{Y}; \boldsymbol{\theta})$ is the observed log-likelihood. Consequently, by denoting $\boldsymbol{\theta}^{(k)}$ the vector of parameters estimated at the k th iteration, the general equation of displacement of the Newton-Raphson algorithm is given by:

$$\boldsymbol{\theta}^{(k+1)} = \boldsymbol{\theta}^{(k)} + \mathbf{H}^{-1}(\boldsymbol{\theta}^{(k)}) \mathbf{U}(\boldsymbol{\theta}^{(k)}) \quad (2.4)$$

where the function \mathbf{U} is the gradient (first derivative) of the observed likelihood and \mathbf{H} is the Hessian matrix. Assuming a population of N independent subjects and as described in Equation 2.2, the global observed likelihood can be expressed as the product of the observed individual likelihood. The observed log-likelihood $L(\mathbf{Y}; \boldsymbol{\theta})$ can then be defined by summing the contribution of all the N subject as:

$$L(\mathbf{Y}; \boldsymbol{\theta}) = \sum_{i=1}^N \log p(\boldsymbol{\theta}; \mathbf{Y}_i) = \sum_{i=1}^N L_i(\mathbf{Y}_i; \boldsymbol{\theta}) \quad (2.5)$$

Assuming the log-likelihood as twice-differentiable and noting $P = |\boldsymbol{\theta}|$ the size of the vector $\boldsymbol{\theta}$, the gradient and the Hessian can be written as:

$$\begin{aligned} \mathbf{U} : \mathbb{R}^P &\longrightarrow \mathbb{R}^P & ; & \quad \mathbf{H} : \mathbb{R}^P &\longrightarrow \mathbb{R}^P \times \mathbb{R}^P \\ \boldsymbol{\theta} &\longmapsto \left(\frac{\partial L(\mathbf{Y}; \boldsymbol{\theta})}{\partial \theta_p} \right)_{p=1, \dots, P} & & \boldsymbol{\theta} &\longmapsto \left(\frac{\partial^2 L(\mathbf{Y}; \boldsymbol{\theta})}{\partial \theta_p \partial \theta_q} \right)_{\substack{p=1, \dots, P \\ q=1, \dots, P}} \end{aligned} \quad (2.6)$$

Numerically, the derivatives are approximated by multivariate finite differences such as:

$$\begin{aligned} \frac{\partial L(\mathbf{Y}; \boldsymbol{\theta})}{\partial \theta_p} &\approx \frac{L(\mathbf{Y}; (\theta_1, \dots, \theta_p + d\theta_p, \dots, \theta_P)) - L(\mathbf{Y}; (\theta_1, \dots, \theta_p - d\theta_p, \dots, \theta_P))}{2d\theta_p} \\ \frac{\partial^2 L(\mathbf{Y}; \boldsymbol{\theta})}{\partial \theta_p \partial \theta_q} &\approx \frac{L(\mathbf{Y}; (\theta_1, \dots, \theta_p + d\theta_p, \dots, \theta_q + d\theta_q, \dots, \theta_P)) - L(\mathbf{Y}; (\theta_1, \dots, \theta_p + d\theta_p, \dots, \theta_P))}{d\theta_p d\theta_q} \\ &\quad - \frac{L(\mathbf{Y}; (\theta_1, \dots, \theta_q + d\theta_q, \dots, \theta_P)) - L(\mathbf{Y}; (\theta_1, \dots, \theta_P))}{d\theta_p d\theta_q} \end{aligned}$$

where $d\theta_p$ and $d\theta_q$ are infinitesimal movements on the surface to approximate, respectively in the direction of θ_p and θ_q . To ensure the stability of the algorithm, the Hessian matrix must be positive-definite, which is the case while the model is quite well speci-

fied. In the case of model misspecification, various algorithms have been proposed to correct the equation of displacement and retrieve a positive-definite matrix. The general form of the equation of displacement is given by

$$\boldsymbol{\theta}^{(k+1)} = \boldsymbol{\theta}^{(k)} + \omega_k \mathbf{G}^{-1}(\boldsymbol{\theta}^{(k)}) \mathbf{U}(\boldsymbol{\theta}^{(k)}) \quad (2.7)$$

where ω_k is called the learning rate and quantifies the size of the displacement on the surface to ensure the convergence of the algorithm towards at least a local extremum and \mathbf{G} is the matrix defining the curvature. The matrix $\mathbf{G}(\boldsymbol{\theta})$ is then build to be definite-positive and such $\mathbf{G}(\boldsymbol{\theta}^{(k)})$ tends to $\mathbf{H}(\hat{\boldsymbol{\theta}})$ when $\boldsymbol{\theta}^{(k)}$ tends to $\hat{\boldsymbol{\theta}}$. In particular, the Marquardt algorithm [Marquardt, 1963] ensures this property, by applying a slight correction of the Hessian matrix such that $\mathbf{G}(\boldsymbol{\theta}^{(k)}) = \mathbf{H}(\boldsymbol{\theta}^{(k)}) + \lambda_P \mathbf{I}$, where \mathbf{I} is the identity matrix. Many other versions of this algorithm have been developed to propose different approximations of the Hessian matrix [Berndt et al., 1974; Commenges et al., 2006; Hedeker and Gibbons, 1994]. Others such as the simplex method developed by Nelder and Mead in 1965 [Nelder and Mead, 1965] can be used to maximize the likelihood without calculation of the derivatives. Although this method is usually less time consuming, it can also be less efficient leading to false convergence. To tackle this issue, stochastic version of the algorithm has been proposed [Barton and Ivey Jr, 1991].

These algorithms are used to maximize the likelihood, whether in a linear or a non-linear framework like NLME-ODE (see section 2.3).

Once the parameter $\boldsymbol{\theta}$ estimated, its standard deviation, i.e. the uncertainty of the estimates, is typically estimated using the Fisher Information matrix. Confidence intervals and statistical tests, such as Wald test, on fixed parameters can then be performed. By definition, whether for LMEM, generalized LMEM or non-linear MEM, the Fisher Information matrix \mathbf{I} is defined as minus the expected Hessian matrix of the observed log-likelihood, such as:

$$\mathbf{I}(\hat{\boldsymbol{\theta}}) = \left(-\mathbb{E} \left(\frac{\partial^2 L(\mathbf{Y}; \boldsymbol{\theta})}{\partial \boldsymbol{\theta}_p \partial \boldsymbol{\theta}_q} \right) \right)_{\substack{p=1, \dots, P \\ q=1, \dots, P}}$$

The variance-covariance matrix of the estimated parameters $\boldsymbol{\theta}$ is then defined as the inverse of the Fisher information matrix: $\boldsymbol{\Gamma}(\hat{\boldsymbol{\theta}}) = [\mathbf{I}(\hat{\boldsymbol{\theta}})]^{-1}$. Generally, a closed form of the observed log-likelihood being not available, different approaches have been developed to approximate the Fisher Information matrix. In particular, in the case of non-linear MEM, the most commonly used approaches rely on the linearization of the system using for example the methods FO, FOCE [Mentre et al., 1997; Retout et al., 2001; Lei et al., 2010]. Alternative methods based on stochastic approximation of the likelihood are

also quite common (e.g. Laplace approximation or SAEM) [Ueckert and Mentré, 2017; Savic and Lavielle, 2009] (see [Bazzoli et al., 2009] for the comparison of multiple first order approximation methods and stochastic approximation approaches).

2.2.2.4 Model with censored data

In the presence of censored data, a reliable inference of model parameters, that can be used to evaluate the efficacy of a treatment, is more complex and requires special attention. Many methods have been proposed to account for left-censored data in the estimation of the parameters. These latter have been mostly developed to handle left-censoring in HIV RNA. In addition to *ad hoc* approaches replacing censored data by the LOD or LOD/2, or multiple imputations methods [Schafer, 1997, 1999; Rubin, 2004], likelihood-based methods have been proposed, adapting the computation of the observed likelihood to left-censored data [Hughes, 1999; Jacqmin-Gadda et al., 2000; Thiébaud and Jacqmin-Gadda, 2004; Lyles et al., 2000]. In particular, two main formulations of the observed likelihood have been proposed. Considering the notations defined in section 2.2.2.1, let Y_{ij} be the measure for the subject i at the time t_{ij} , $i = 1, \dots, N$ and $j = 1, \dots, n_i$. For each subject i , the vector \mathbf{Y}_i can be written as $\mathbf{Y}_i = (\mathbf{Y}_i^{obs}, \mathbf{Y}_i^{cens})$ where \mathbf{Y}_i^{obs} is a vector of size n_i^{obs} gathering observed responses (i.e. observations that have been really quantified) and \mathbf{Y}_i^{cens} is a vector of size n_i^{cens} gathering censored responses. The general idea consists in considering the contribution of the censored responses to the likelihood as the probability that the censored response should be lower than the censoring threshold while the contribution of observed responses remains unchanged. In the first approach, developed by [Hughes, 1999] and [Jacqmin-Gadda et al., 2000; Thiébaud et al., 2003], the likelihood is formulated given the observed responses, \mathbf{Y}_i^{obs} . We note \mathbf{C}_i the vector of size n_i^{cens} of censoring thresholds for the subject i . At each time t_{ij} , we observe $\max(C_{ij}, Y_{ij})$ given the following formulation of the likelihood:

$$p(\mathbf{Y}; \boldsymbol{\theta}) = \prod_{i=1}^N p(\mathbf{Y}_i^{obs}; \boldsymbol{\theta}) \Phi(\mathbf{C}_i | \mathbf{Y}_i^{obs}; \boldsymbol{\theta})$$

where $\Phi(\cdot)$ is the multivariate cumulative distribution function (CDF) such that $\Phi(\mathbf{C}_i) = \mathbb{P}(\mathbf{Y}_i^{cens} > \mathbf{C}_i)$. By definition of the CDF, the likelihood can be written as:

$$p(\mathbf{Y}; \boldsymbol{\theta}) = \prod_{i=1}^N p(\mathbf{Y}_i^{obs}; \boldsymbol{\theta}) \int_{\mathcal{H}} p(\mathbf{u} | \mathbf{Y}_i^{obs}; \boldsymbol{\theta}) d\mathbf{u}$$

where $\mathcal{H} = H_1 \times \cdots \times H_{n_i^{cens}}$ with $H_d =] - \inf; C_{id}]$ and $\mathbf{u} = (u_1, \cdots, u_{n_i^{cens}})$. Consequently, the computation of the likelihood requires numerical integration which can be extremely time-consuming for a large number of censored data. In that case, the calculation can be reduced using the second approach. This latter was proposed by [Lyles et al. \[2000\]](#), in which the likelihood is formulated given the random effects. We define the dichotomic variable $\delta_{ij} = 1$ if the observation Y_{ij} is detectable (i.e. $Y_{ij} > \text{LOD}$) and 0 if Y_{ij} is left-censored. Considering notations aforementioned, the observed likelihood can be written as an adaptation of the equation 2.3 as:

$$p(\mathbf{Y}; \boldsymbol{\theta}) = \prod_{i=1}^N \int_{\mathbb{R}^q} \prod_{j=1}^{n_i} p(Y_{ij} | \gamma_i; \boldsymbol{\theta})^{\delta_{ij}} \Phi(Y_{ij} | \gamma_i; \boldsymbol{\theta})^{(1-\delta_{ij})} p(\gamma_i; \boldsymbol{\delta}) d\gamma_i \quad (2.8)$$

In this expression, we can see that a detectable observation only contributes to the conditional density function $p(Y_{ij} | \gamma_i; \boldsymbol{\theta})$, while an undetectable value only contributes to the univariate cumulative distribution function $\Phi(Y_{ij} | \gamma_i; \boldsymbol{\theta})$. This formulation of the likelihood also requires numerical integration. Efficient for LMEM, these approaches remain more difficult to apply for NLMEM because of the non-linearity of the regression function in the random effects. Afterwards, several methods have been proposed to obtain reliable estimation of the model parameters with left-censored data and NLMEM. These methods are discussed later in section 2.3.3.4.

2.2.2.5 Estimation of individual parameters

When the parameters of the model $\boldsymbol{\theta}$ have been estimated, we can perform the estimation of the individual parameters. In particular, for each subject i , we can estimate its random effects γ_i . To this end, Empirical Bayes estimates (EBE) [[Laird and Ware, 1982](#); [Morris, 1983](#)] framework is applied. By definition, the estimated random effects correspond to the expectation of the posterior distribution of γ_i given the observation and the parameters $\boldsymbol{\theta}$: $\hat{\gamma}_i = \mathbb{E}(\gamma_i | \mathbf{Y}_i, \hat{\boldsymbol{\theta}})$. While a closed form of this expectation can easily be computed in LMEM, in non-linear or non-Gaussian framework, its computation requires an approximation of the conditional distribution. Using the Bayes law, the conditional distribution of the random effects given the observations can be re-written as

$$p(\boldsymbol{\gamma}_i | \mathbf{Y}_i; \hat{\boldsymbol{\theta}}) = \frac{p(\mathbf{Y}_i | \boldsymbol{\gamma}_i; \hat{\boldsymbol{\theta}})p(\boldsymbol{\gamma}_i; \hat{\boldsymbol{\theta}})}{p(\mathbf{Y}_i; \hat{\boldsymbol{\theta}})}$$

Both the conditional distribution of the observation given the random effects ($p(\mathbf{Y}_i | \boldsymbol{\gamma}_i; \hat{\boldsymbol{\theta}})$), and the density function of the random effects can be calculated by a closed form. The density function of the observation $p(\mathbf{Y}_i; \hat{\boldsymbol{\theta}})$ can be more difficult to estimate. However, this latter being independent on the random effects $\boldsymbol{\gamma}_i$, the EBE can be directly estimated as the mode of the conditional distribution as

$$\begin{aligned} \hat{\boldsymbol{\gamma}}_i^{\text{mode}} &= \arg \max_{\boldsymbol{\gamma}_i \in \mathbb{R}^q} p(\boldsymbol{\gamma}_i | \mathbf{Y}_i; \hat{\boldsymbol{\theta}}) \\ &= \arg \max_{\boldsymbol{\gamma}_i \in \mathbb{R}^q} p(\mathbf{Y}_i | \boldsymbol{\gamma}_i; \hat{\boldsymbol{\theta}})p(\boldsymbol{\gamma}_i; \hat{\boldsymbol{\theta}}) \end{aligned}$$

Similar to the maximization of the likelihood, optimization algorithms can be used to maximize the conditional distribution.

In this thesis, we were particularly interested in the evaluation of vaccine efficacy and the identification of surrogate/immune markers that could be associated with the vaccine-induced protection. Consequently, despite the relevance of using classic regression models to analyze data and identify treatment effects in randomized placebo-controlled, the identification of correlate of protection (CoP) and more specifically of mechanistic CoP, requires the identification of a causal association between the surrogate endpoint and the vaccine efficacy. To this end, a mathematical framework has been widely developed over the years to account for causal modeling. Although causal models have not been directly studied in this thesis, the general framework of causal modeling has been presented to better understand the properties and the type of relationship that surrogate outcome should have to be evaluated as CoP. Thereafter, these properties will be used in association with the mechanistic mathematical framework (see chapter 5) to propose an alternative approach to identify mCoP.

2.2.3 Surrogate endpoint in causal modeling framework

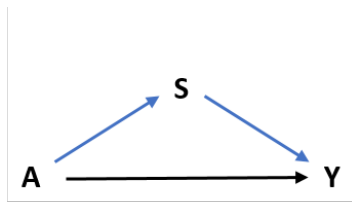
The identification of an immune marker that could be used to predict the level of protection induced by a vaccine is crucial in vaccine development. Nevertheless, good correlate of protection are quite difficult to identify and quantify in many cases. This difficulty mainly results from the various degree of surrogacy that can exist between an immune marker and the true clinical outcome. Mathematical frameworks have been

introduced to validate the use of an immune marker as surrogate marker and to characterize its degree of surrogacy. As briefly introduced in the previous chapter, the surrogacy relies on two major concepts: 1) the paradigm of prediction (often referred as "association") including correlate of risk and non-mechanistic CoP, and 2) the paradigm of causality including mechanistic CoP [Holland, 1986; Joffe and Greene, 2009]. Both concepts of surrogacy are relevant in vaccine development and distinct mathematical frameworks are required to assess their related immune markers. While the associational inference requires quite standard statistical analysis like regression models, correlations, descriptive analysis, classic statistical test (e.g student t-test, Wilcoxon rank test)[Pearl, 2010; Corey et al., 2015; Lumley et al., 2020; Corbett et al., 2021a], the paradigm of causal inference requires more sophisticated mathematical tools which are more broadly presented in the following.

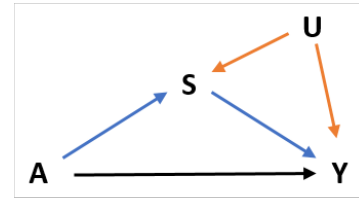
For sake of consistency, we denote by A the treatment variable, Y the outcome of interest and S the surrogate marker we are evaluating. For a given surrogate S , we aim at identifying whether S is only able to relate the association between A and Y or is able to causally link these two variables making of S a valid surrogate endpoint. Without loss of generality, we assume the case of a RCT with a dichotomic variable of treatment ($A = 0$: control group, $A = 1$: treatment group). While Y refers to the true/clinical outcomes in most cases, biomarkers could also be used as study endpoints. **That is especially the case in HIV vaccine trials, as developed in Chapter 3.**

2.2.3.1 Introduction to the causal inference / paradigm of causal agent

The crucial distinction between the concepts of association and causation relies on the fact that, while the relationships between variables of interest are evaluated under static conditions in the first case, these relationships as well as their dynamics are inferred under changing conditions in the second one. The basis of the causality concept is that, contrary to associational assumptions, causal assumptions cannot be verified outside controlled experimental studies. The first mathematical formulation of a causal relationship was introduced by Wright [1921] with structural equation models and graphical models called "path diagram". This latter is a graphical representation of the situation highlighting causal relationships that could or could not exist between variables exposure. Now a days, path diagrams correspond to directed acyclic graphs [Robins, 1987; Pearl, 1995].



(a) Naive causal relationship.



(b) Causal relationship impacted by a confounding variable, U .

Figure 2.1 – Causal diagrams for surrogate outcomes. Causal relationships between the treatment A and the clinical outcome Y with the immune marker S (mCoP) defined as a mediating variables. The direct effect of treatment is represented by the path $A \rightarrow Y$ (black arrow), the indirect effect by the path $A \rightarrow S \rightarrow Y$ (blue arrows) and the effect of the confounding variables by the paths $U \rightarrow S$ and $U \rightarrow Y$ (orange arrows).

2.2.3.2 Direct and indirect causal effects

Let us assume a mediation analysis relating a naive causal relationship between the variables A and Y and involving a mediating variables, such as the mCoP (S) (see Figure 2.1(a)). The so-called causal effect of A on Y is defined as the *total effect* (TE) of A on Y and is given by $\mathbb{E}(Y|A = a_1) - \mathbb{E}(Y|A = a_0)$, with a_0 and a_1 being two values of treatment post-intervention such as $a_0 = 0$ and $a_1 = 1$ in the case of RCT with placebo group. Nevertheless, when the effect of A on Y is mediated by a surrogate marker, the causal effect is partitioned into two effects: the direct and the indirect effect. The direct effect (DE) corresponds to the effect of A that is not mediated by other variables in the model (i.e. surrogate assumed as fixed) and can be written as $DE = \mathbb{E}(Y|A = a_1, S = s) - \mathbb{E}(Y|A = a_0, S = s)$, with s being the value of the surrogate fixed by physical intervention. At the opposite, the indirect effect (IE) is seen as the effect of the change of the value of the surrogate marker in the control group: $IE = \mathbb{E}(Y|A = a_0, S = s_1) - \mathbb{E}(Y|A = a_0, S = s_0)$. The total effect of A on Y is then defined as $TE = DE + IE$. Further formal definitions of the direct and indirect effects have been rigorously exposed in [Pearl, 2001; Robins and Greenland, 1992; Aalen et al., 2012; Pearl, 2011], in particular for non-linear systems. In the configuration presented in Figure 2.1(a), the immune marker, and more specifically the mCoP, is considered as a true mCoP if the direct effect is negligible. However, this diagram is usually an incomplete version of the real situation. Indeed, as displayed in Figure 2.1 (b), the effect of S on the outcome Y can be impacted by confounding variables U . For example S and Y can result from a common cause [Joffe and Greene, 2009]. These confounding variables can then be measured or not. Nevertheless, the absence of adjustment of statistical model for variables U modifies the relationships

between A , Y and S leading to a potential bias of effect mediated by S . Extensive works have been conducted to incorporate confounding in causal analysis [Rosenbaum, 1984; Robins, 1986; Pearl et al., 2000; Frangakis and Rubin, 2002].

2.2.3.3 Analytic methods of estimation

Two different analytic methods can be used in large clinical trials to evaluate whether an immune correlate can be defined as mCoP or not. The first approach relies on the three criteria required by Prentice [Prentice, 1989] to validate surrogate as a true mCoP: (a) S must be identified as a CoR in each of the treatment and control group, meaning that S must be correlated with Y , (b) S must be impacted by the vaccination A and (c) the relationship between S and Y must be the same within the two groups meaning that the effect of A on Y should be totally mediated by S : $Y \perp\!\!\!\perp A | S$ (conditioned on S the direct effect of A on Y must be null). This approach to identify a mCoP leads to the definition of a *statistical* mCoP (mCoP^S) [Qin et al., 2007].

The second approach, defining a mCoP as *principal* (mCoP^P), refers to the counterfactual approach which was initially introduced by Neyman [1923] and often termed as Rubin's model [Holland, 1986; Rubin, 1974, 1977, 1978]. The previous approach aimed at identifying causal effect at group level by comparing outcomes between individuals randomly assigned to groups of treatments. On the contrary, the counterfactual approach aims at identifying causal effect at individual level by answering the question *What is the effect that the treatment of interest has on a specific subject ?* However, that is a question that experimental studies can not answer directly, as an individual can only belong to a single group. This approach is then based on the concept of actual and counterfactual outcomes for a given individual, which are respectively the true observed outcome and the one that should have been observed if this individual had received the other treatment. Based on this definition, the causal effect is defined as the difference of the actual and the counterfactual outcomes [Frangakis and Rubin, 2002; Joffe and Greene, 2009; Aalen et al., 2012; Dawid, 2000]: Causal Effect = $Y_{a=1} - Y_{a=0}$. Nevertheless, the estimation of this causal effect being impossible to estimate at an individual level in most cases, the counterfactual theory focuses on the average causal effects: $\mathbb{E}(Y_{a=1} - Y_{a=0}) = \mathbb{E}(Y_{a=1}) - \mathbb{E}(Y_{a=0})$. Although well defined theoretically, this approach can be performed only in RCT, to either be able to fully control experimental conditions (e.g. by blocking biological pathways in a given group to mimic the counterfactual outcome) [Aalen et al., 2012] or to be able to make the strong assumption that the control group represents a good counterfactual for the treatment group.

To assess an immune marker as a mCoP in Phase IV trials, meta-analysis approach are usually performed [Qin et al., 2007; Gilbert et al., 2008]. However, this manuscript

being exclusively focused on the evaluation of the vaccine efficacy in RCT, we shall not get into more details.

2.2.3.4 Limits of the causal inference

The identification of mCoP faces many difficulties, whether for statistical or principal ones. The first limitation impacting both types of mechanistic CoP corresponds to their high sensitivity to the existence of confounding variables and thus the necessity to adjust causal effects on all these variables [Frangakis and Rubin, 2002; Gilbert et al., 2008]. Apart from that, the major problem to identify a mCoP^S is linked to Prentice's first criteria and its necessity to observe variability in the immune response of unvaccinated while subjects have not been exposed to the pathogen. In the case of the counterfactual approach, the difficulty relies on the principle of the approach itself as it imposes either to make the strong assumption that the placebo group is a good counterfactual for the treatment group, or to manipulate/hold the value of the surrogate at an inconsistent level for treatment group (e.g. high viral load for HIV-infected patient taking antiretroviral treatment in the case of HIV). This approach can then be ethically questionable under certain conditions [Aalen et al., 2012] and results may be difficult to interpret. However, the major limitation of this approach remains the *surrogate paradox* introduced by Chen et al. [2007] and defined as follows:

"It is possible that a treatment has a positive averaged effect on the surrogate, which in turn is strongly and positively associated with the true endpoint, but the treatment has a negative averaged effect on the true endpoint. [Chen et al., 2007]"

Without going into further details, the reader can refer to [VanderWeele, 2013] for a deeper understanding of this paradox and to [Moore, 1997] for the most well-known case in which the surrogate paradox was involved.

In longitudinal studies, the time is a relevant parameter that should be taken into account in the identification of a valid CoP and consequently in the causal inference. Despite the absence of consideration for time in many statistical analysis, the counterfactual framework was extended to time-varying treatment and surrogate/confounders [Robins, 1986; Pearl and Robins, 1995; Arjas and Parner, 2004; Robins and Hernán, 2009] ; and a global review is available in [Richardson and Rotnitzky, 2014]. Over the years, many methods have been developed to account for time-dependent processes and their interaction in the establishment of causation, such as marginal structural models or structural nested models and their respective integration of time-dependent confounders via g-estimation or the inverse-probability of treatment weights [Robins et al., 1992; Robins, 1997, 2000]. Nevertheless, most of them have been developed in the

case of discrete time-dependent variables. In the continuity of these works, some other works have been conducted to extend the Robin's theory of causal inference to dynamical problems, in the sense of time continuous processes [Gill and Robins, 2001; Lok et al., 2004]. However these processes were still based on random variables. Thereafter, the development of dynamical models allowed to analysis causality in a time continuous way [Commenges and Gégout-Petit, 2009; Aalen et al., 2012].

2.3 Modeling of biological processes via mechanistic modelling

The introduction of stochastic processes and the concept of system enabled to extend the notion of causality to dynamical problems and progressively led to the use of dynamical models in this mathematical framework [Aalen, 1987; Aalen et al., 2008; Granger, 1969; Aalen and Frigessi, 2007]. In addition, the consideration of the notion of system gave the opportunity to incorporate phenomenological knowledge and physical meaning in the process instead of only describe data. Let us denote $\mathbf{X} = (\mathbf{X}_k, k = 1, \dots, K)$ a multivariate stochastic process describing a system of K components, with $\mathbf{X}_k = (X_{kt})_{t \geq 0}$, and their relationships called "direct influence". Contrary to causal models introduced in the previous section, a component X_j can influence another component X_k and in the same time, X_k can also influence X_j . Similarly to directed acyclic graphs and "path diagrams", graphical models have been developed to represent the stochastic processes. In particular, Fosen et al. [2006] and Didelez et al. [Didelez, 2007, 2008] respectively introduced the "dynamical path diagram" and the directed (possibly) cyclic diagram. According to the Doob-Meyer decomposition [Aalen, 1987], the stochastic process \mathbf{X} can be derived as the sum of a stochastic term \mathbf{M}_t (sequence of random variables called martingale) and predictable/deterministic term $\mathbf{\Lambda}_t$ such as:

$$\mathbf{X}_t = \mathbf{\Lambda}_t + \mathbf{M}_t, \quad t \geq 0 \quad (2.9)$$

Commonly, the process $\mathbf{\Lambda}_t$ is characterized as a (multivariate) function of the components X_{kt} . **In the framework of this thesis, we focused on mechanistic dynamical models which correspond to a subset of those dynamical models.** The term mechanistic refers to the fact that the processes running inside the system are described by differential equations.

2.3.1 The different type of mechanistic models

Mechanistic models are widely used to investigate processes in finance, engineering and science, whether in physics, biology or epidemiology, as they are built to express physical law. By definition, differential equations are equations describing the relationship between the components/variables of the process and their changes over time using derivatives. Accordingly, the differential equations characterizing the system evolve in a time continuous way and the deterministic process Λ_t defined in equation 2.9 is assumed to be differentiable such as $\Lambda_t = \int_0^t \lambda_u du$. Nevertheless, observations are measured at discrete timepoints. Moreover, in cases of complex systems (e.g. multivariate systems), observations may not correspond directly to the components of the system. Consequently, the basic structure of a mechanistic model for a given system is the combination of a system of differential equations and an equation, potentially multivariate, for the observations, linking them to the components of the system. A mechanistic model can then be written as follows:

$$d\mathbf{X}_t = \Lambda(\mathbf{X}_t; \Psi(t)) dt + d\mathbf{M}_t, \quad \forall t \geq 0 \quad (2.10)$$

$$\mathbf{Y}_j = \mathbf{f}(\mathbf{X}_{t_j}; \Psi(t_j)) + \varepsilon_j \quad \forall j \in \{1, \dots, m\} \quad (2.11)$$

where Ψ is the vector of parameters, Λ is the function representing deterministic law of evolution of the system, \mathbf{Y}_j is the vector of observations at time t_j , \mathbf{f} is a known function linking observations to the components of the system, and ε_j is a measurement error. Based on this general definition of a mechanistic model, different types of differential equations can be distinguished [Commenges and Gégout-Petit, 2009] such as ordinary differential equations (ODEs), partial differential equations or stochastic differential equations. **In this thesis, we only focused on ODEs.** These equations are defined as deterministic equations, meaning without stochastic process, such as in equation 2.9, $M = 0$. Although the system described by the system of ODEs can depend on multiple variables, ODEs only involve first order derivations with respect to only one variable, usually the time. In life science, the first ODE-based model was introduced by Lotka [Lotka, 1925] and Volterra [Volterra, 1926] to describe the system of predation of a specie by another. Since then, ODEs have been widely used in epidemiology to describe viral infection (e.g. HIV infection) by modelling virus transmission or the effect of drug therapy [Perelson and Ke, 2021]. ODEs are also a key point in pharmacology to study the pharmacokinetic process of a drug called ADME for absorption, distribution, metabolism, excretion [Zarnitsyna et al., 2021]. **In the scope of this thesis, we used these equations in the study of the three viral infections HIV, SARS-CoV-2 and**

Ebola infections, as shown in appendix B for HIV and in chapters 5 and 6 for SARS-CoV-2 and Ebola respectively.

2.3.2 The ordinary differential equations system in population approach

In the context of a population approach, we consider a mechanistic model defined as an ODE-based non-linear mixed-effects models (NLME-ODE) and build as the combination of three modeling layers. Using the notations previously defined in section 2.2.2, let us consider N independent subjects longitudinally monitored over time. Assuming a multivariate outcome for each individual, we note Y_{ijm} the observation for the i th subject at the time t_{ij} measured for the m th marker, such that $\mathbf{Y}_{ij} = (Y_{ij1}, \dots, Y_{ijM})^T$ where $i \in \{1, \dots, N\}$, $j \in \{1, \dots, n_{im}\}$ and $m \in \{1, \dots, M\}$, with M being the number of markers measured in the study and n_{im} the number of observations for the m th marker for the subject i . The first layer of the mechanistic model used to model these observations consists in a mathematical model based on a system of ODEs describing the dynamics of the biological process, $\mathbf{X}(t)$. This ODEs system is composed of K components (also called compartments) such as $\mathbf{X}(t) = (X_1(t), \dots, X_K(t))^T$, for $t \in \mathbb{R}^+$.

$$\begin{cases} \frac{dX_k}{dt} &= \mathcal{F}_k(\mathbf{X}(t), \boldsymbol{\Psi}, t), & k \in \{1, \dots, K\} \\ X_k(0) &= \mathcal{H}_k(\boldsymbol{\Psi}), & X_k \in \mathbf{X} \end{cases} \quad (2.12)$$

with $\boldsymbol{\xi} \in \mathbb{R}^{n_p}$ the vector of biological parameters, and $\mathcal{F} = (\mathcal{F}_1, \dots, \mathcal{F}_K)$ and $\mathcal{H} = (\mathcal{H}_1, \dots, \mathcal{H}_K)$ two vector-valued functions with values in \mathbb{R}^K , assumed to be bijective and at least twice differentiable. To respect some biological or computational constraints, transformation functions can be applied to parameters. For example, a logarithmic transformations is usually applied to ensure the positivity of the parameters, while logit or probit transformations are considered for parameters with values in $]0; 1[$. In complex ODEs models, the \log_{10} transformation can sometimes be used to improve the convergence of the model estimation. We define the transformation function \mathbf{h} as:

$$\begin{aligned} \mathbf{h} : \mathbb{R}^p &\longrightarrow \chi^p \subset \mathbb{R}^p \\ \boldsymbol{\Psi} &\longmapsto \mathbf{h}(\boldsymbol{\Psi}) = (h_p(\Psi_p))_{p=1, \dots, n_p} \end{aligned}$$

with $h_p(\cdot)$ being the transformation function applied to the p th parameters with $h_p(\Psi_p) = \tilde{\Psi}_p$. To account for inter-individual variability in the population approach, the second layer of the mechanistic model consists in a statistical model describing each parameter

of the compartmental model by a linear mixed-effects model which can depend on covariates. By definition of a LMEM, we can define each parameter Ψ_p for each subject i as:

$$\tilde{\Psi}_p^i = \tilde{\Psi}_{p_0} + \beta_p^T \mathbf{Z}_p^i + u_p^i \quad (2.13)$$

where $\tilde{\Psi}_{p_0}$ is the intercept (fixed effect) representing the mean value of the parameter, \mathbf{Z}_p^i and β_p are respectively the vectors of n_e explanatory variables which can potentially dependent on time and regression coefficients related to the parameter Ψ_p , and u_p^i is the individual random effect assumed to be normally distributed with a variance ω_p^2 . For each individual, this equation can be re-written in matrix formulation as $\tilde{\Psi}^i = \tilde{\Psi}_0 + \mathbf{A}_i \boldsymbol{\beta} + \mathbf{u}_i$ where random effects are assumed to be independent such as $\mathbf{u}^i \sim \mathcal{N}(\mathbf{0}, \boldsymbol{\Omega})$ with $\boldsymbol{\Omega}$ defined as a diagonal matrix, and applied only on a subset of n_q parameters ($n_q \leq n_p$). Assuming the independence of individuals and combining equations 2.12 and 2.13 allows to define the ODE system for the subject i which can be written as:

$$\begin{cases} \frac{dX_k^i}{dt} &= \mathcal{F}_k(\mathbf{X}^i(t), \boldsymbol{\Psi}^i, t), & k \in \{1, \dots, K\} \\ X_k^i(0) &= \mathcal{H}_k(\boldsymbol{\Psi}^i), & X_k \in \mathbf{X} \end{cases} \quad (2.14)$$

Finally, the third layer of the model is the observational model. As previously introduced in equation 2.11, this model aims at linking observations with ODE compartments using link functions f_m evaluated at discrete time of observations t_{ijm} . Commonly, the link functions are chosen to ensure normality and heteroscedasticity of the measurement errors [Box and Cox, 1964] (e.g. \log_{10} transformation of the viral load or the fourth root transformation of the CD4 count in the case of HIV infection). To account for measurement errors, the structural model $\mathbf{f} = (f_1, \dots, f_M)$, $m = 1, \dots, M$, is augmented by a residual error model $\mathbf{g} = (g_1, \dots, g_M)$. The observational model can then be written as :

$$Y_{ijm} = f_m(\mathbf{X}^i(t_{ijm}), \boldsymbol{\Psi}^i) + g_m(\mathbf{X}^i(t_{ijm}), \boldsymbol{\Psi}^i, \boldsymbol{\xi}_m) \varepsilon_{ijm} \quad (2.15)$$

where the intra-individual errors ε_{ijm} are assumed to be i.i.d $\varepsilon_{ijm} \sim \mathcal{N}(0, 1)$, the link functions f_m are usually non-linear functions of $(\boldsymbol{\Psi}_0, \boldsymbol{\beta}, \mathbf{u}_i)$ and the variance functions g_m are dependent on f_m and a parameter vector $\boldsymbol{\xi}_m$. Common choices for the error model are $g_m = a + b f_m^c$ with $\boldsymbol{\xi}_m = (a, b, c) = (a, 0, 0)$ for a constant error model to assume homogeneous variances and $\boldsymbol{\xi}_m = (a, b, c) = (0, b, 0)$ for a proportional error model or $\boldsymbol{\xi}_m = (a, b, c) = (0, 0, c)$ for a power model to introduce heterogeneous variances. In this mathematical framework, we essentially focus on the so-called *inverse*

problem which consists in inferring the values of the model parameters using the observations. In other words, we want to use the observed data to estimate the parameters of the model built to describe those same data. We denote θ the vector of unknown parameters to be estimated in this mechanistic model:

$$\theta = [\Psi_0, \beta, \Omega, \xi] = \left[(\Psi_{p0})_{p=1 \dots n_p}, (\beta_{p,e})_{\substack{p=1 \dots n_p \\ e=1 \dots n_e}}, (\omega_p)_{p=1 \dots n_q}, (\xi_m)_{m=1 \dots M} \right]$$

The mechanistic model resulting from the three modeling layers given by equations 2.13, 2.14, and 2.15 corresponds to a multivariate non-linear mixed-effects model. **This type of mathematical modelling was considered in the two chapters 5 (SARS-CoV-2) and 6 (Ebola), as well as a small modeling work conducted in the case of HIV infection and therapeutic vaccine (see Appendix B).**

2.3.3 Estimation methods of NLME-ODE

Many methods have been developed to numerically approximate the log-likelihood and estimate the parameters in NLMEM. The first ones were based on the approximation of the log-likelihood by linearization of the model, such as the "First-Order" (FO) linearization developed by Sheiner and Beal [Sheiner and Beal, 1980; Beal and Sheiner, 1982], the "First-Order Conditional Estimate" (FOCE) linearization proposed by Lindstrom and Bates [1990] or even the Laplace's approximations [Tierney and Kadane, 1986; Wolfinger, 1993]. These methods aim at approximating the NLMEM by its first order Taylor approximation to be able to apply the classic methods of the LMEM framework thereafter, as presented in section 2.2.2.2. Although these methods are quite easy to implement and are less time consuming than methods based on the exact maximum likelihood, these latter can induce a large bias in the approximation of the observed likelihood [Davidian and Gallant, 1992]. Consequently, alternative and more efficient methods have been developed on the exact formulation of the maximum likelihood. Among the most common methods, we can identify the Gaussian quadrature developed by Davidian and Gallant [1992] in which the integral is approximated by a weighted sum evaluated at specific points of domain of integration. This method has been proven more effective than the aforementioned approximations [Lesaffre and Spiessens, 2001] and is widely used nowadays [Guedj et al., 2007]. Other methods based on simulations, such as the importance sampling [Geweke, 1989] (also called Monte-Carlo approximation) [Pinheiro and Bates, 1995], appear as quite efficient. Nevertheless, the log-likelihood being defined as a multiple integral on \mathbb{R}^q , similarly to the Gaussian quadrature, these methods are extremely time-consuming as soon as the number of ran-

dom effects q becomes significant [Vonesh et al., 2002]. An alternative approach to the maximum likelihood estimate has been proposed by Dempster et al. [1977] to overcome the issue in the numerical computation of the likelihood: the Expectation-Maximization (EM) algorithm.

2.3.3.1 The Expectation-maximization (EM) algorithm

The EM algorithm is an iterative algorithm relying on the concept that observations can be viewed as incomplete data and that a closed-form of the observed likelihood can be obtained from the complete data. Let us denote \mathbf{X} the complete data such that $\mathbf{X} = (\mathbf{Y}, \phi)$ with \mathbf{Y} being the observed data and ϕ the non-observed or the latent data. The objective of the EM algorithm is to compute the maximum likelihood estimator of θ by maximizing the observed likelihood $p(\theta; \mathbf{Y})$. However, this algorithm relies on the concept that the complete likelihood defined as $p(\mathbf{Y}, \phi; \theta)$ is easier to compute than the observed likelihood $p(\theta; \mathbf{Y}) = \int p(\mathbf{Y}, \phi; \theta) d\phi$. The complete data being not available, the algorithm simplifies the computation of the likelihood by its expectation given the observations, enabling in the same time to retrieve the targeted observed likelihood. In the context of a mixed-effects model, the non-observed data are characterized by the random effects, which by definition can not be observed.

At each iteration k of the iterative algorithm, two steps are performed to compute the MLE: the Expectation step (E-step) and the Maximization step (M-step).

- ▷ **Expectation-step:** Computation of the expectation of the complete log-likelihood with respect to the distribution of the non-observed data ϕ , given the observed data \mathbf{Y} , and the current estimated parameter $\theta^{(k-1)}$:

$$\begin{aligned} Q(\theta|\theta^{(k-1)}) &= \mathbb{E}(\log\{p(\mathbf{Y}, \phi; \theta)\}|\mathbf{Y}, \theta^{(k-1)}) \\ &= \int \log p(\mathbf{Y}, \phi; \theta) p(\phi|\mathbf{Y}; \theta^{(k-1)}) d\phi \end{aligned} \quad (2.16)$$

- ▷ **Maximization-step:** Update of the current value of the parameters by maximizing the Q-function:

$$\theta^{(k)} = \arg \max_{\theta \in \Theta} Q(\theta|\theta^{(k-1)})$$

In the cases in which the maximization of the Q-function remains difficult, Dempster et al. [1977] derived a generalized EM algorithm. Instead of targeting the maximization of the Q-function, this version of the algorithm only focuses on its improvement at each step such that $Q(\theta^{(k)}|\theta^{(k-1)}) \geq Q(\theta|\theta^{(k-1)})$. In addition to the generalized EM, many extended version of the algorithm have been developed. For example, Silverman

et al. [1990] and Nychka [1990] proposed a smoothed version of the algorithm (EMS) to account for the specific case of indirect observations and non-parametric curves describing observations, by adding a smoothing step after the E and M steps. Other versions of the EM algorithms have been proposed such as the adaptation of the algorithm for the penalized likelihood [Green, 1990; Van Dyk and Tang, 2003] or the adaptation of the M-step of the algorithm to incorporate prior information on the distribution of the parameters given rise to the maximum *a posteriori* estimation of θ [Green, 1990; Wang and Gindi, 1997]. In addition to this non-exhaustive list of extended algorithms, three major stochastic versions of the algorithm have been developed: the stochastic version of the EM algorithm (SEM) [Broniatowski et al., 1983; Celeux and Diebolt, 1988, 1992; Celeux et al., 1995]; the stochastic approximation EM (SAEM) algorithm [Delyon et al., 1999] and the MCEM algorithm approximating the E-step by numerical Monte-Carlo simulation [Wei and Tanner, 1990; Levine and Casella, 2001]. These algorithms have been developed for the cases in which the computation of the expectation of the likelihood requires numerical computation of the integrals. That is especially true in the case of non-linear models.

2.3.3.2 Estimation with Monolix: the SAEM algorithm

In this manuscript, parameter estimation of ODE system was performed using the Stochastic Approximation Expectation-Maximization (SAEM) [Delyon et al., 1999] algorithm implemented in the software Monolix (Non-linear mixed-effects models or "MOdèles NOn LInéaires à effets miXtes in French) [Kuhn and Lavielle, 2005]. Developed by ©Lixoft, Monolix is widely used for model based drug development, whether for preclinical or clinical PK/PD modeling.

For sake of simplification of the writing, we assume in the rest of the chapter a mechanistic model with an univariate response Y ($m = 1$). However, the methods described in this section can be expanded to multivariate models.

The SAEM algorithm

In the case of non-linearity, the evaluation of the Q-function can not be performed in a closed form. Consequently, the SAEM consists in replacing calculation of the integral (see equation 2.16) by splitting the E-step into two steps: 1) a simulation step to generate realizations of the incomplete data (Ψ) using their posterior distribution given the observed data and 2) a stochastic averaging procedure. At each iteration k , the algorithm is defined as follows:

- ▷ **Simulation-step:** Generation of $m(k)$ realizations $\{\Psi^{(k,l)}, l = 1, \dots, m(k)\}$ of the random parameters under the conditional distribution $p(\Psi|Y; \theta^{(k-1)})$

- ▷ **Stochastic approximation-step:** Update of the current approximation of $Q(\theta|\theta^{(k-1)})$, labeled $Q_k(\theta)$, according to

$$Q_k(\theta) = Q_{k-1}(\theta) + \gamma_k \left(\frac{1}{m^{(k)}} \sum_{l=1}^{m^{(k)}} \log p(\mathbf{Y}, \Psi^{(k,l)}; \theta) - Q_{k-1}(\theta) \right) \quad (2.17)$$

where $(\gamma_k)_{k \geq 1}$ is a decreasing sequence of positive step size.

- ▷ **Maximization-step:** Update of the current value of the parameters by maximizing the approximation of the Q-function $Q_k(\theta)$:

$$\theta^{(k)} = \arg \max_{\theta \in \Theta} Q_k(\theta)$$

Delyon et al. [1999] demonstrated the ability of the SAEM algorithm to converge to a maximum (at least local) of the observed likelihood under general conditions.

Likelihood computation

By independence of N individuals, the complete likelihood is defined as:

$$p(\mathbf{Y}, \Psi; \theta) = \prod_{i=1}^N \prod_{j=1}^{n_i} p(\mathbf{Y}_{ij}, \Psi_i; \theta) \quad (2.18)$$

Considering the framework given by equations 2.13, 2.14 and 2.15 in an univariate form, the complete log-likelihood can be written as:

$$\begin{aligned} \log p(\mathbf{Y}, \Psi; \theta) = & - \sum_{i=1}^N \sum_{j=1}^{n_i} \log \left[g \left(\mathbf{X}^i(t_{ij}, \tilde{\Psi}_i), \xi \right) \right] - \frac{1}{2} \sum_{i=1}^N \sum_{j=1}^{n_i} \left(\frac{Y_{ij} - f \left(\mathbf{X}^i(t_{ij}, \tilde{\Psi}_i) \right)}{g \left(\mathbf{X}^i(t_{ij}, \tilde{\Psi}_i), \xi \right)} \right)^2 \\ & - \frac{N}{2} \log(|\Omega|) - \frac{1}{2} \sum_{i=1}^N \left(\tilde{\Psi}_i - \bar{\mathbf{A}}_i \bar{\beta} \right)^T \Omega^{-1} \left(\tilde{\Psi}_i - \bar{\mathbf{A}}_i \bar{\beta} \right) - \frac{N_{tot}}{2} \log(\sigma^2) + cte \end{aligned} \quad (2.19)$$

where $N_{tot} = \sum_{i=1}^N n_i$ is the total number of observations, $\mathbf{X}^i(t_{ij}, \tilde{\Psi}_i)$ represents the trajectories predicted by the ODE system for the subject i at time j with the individual parameters $\tilde{\Psi}_i$; $\bar{\mathbf{A}}_i = [1 \ \mathbf{A}_i]$ and $\bar{\beta} = (\tilde{\Psi}_0, \beta)^T$ such that $\tilde{\Psi}_i = \bar{\mathbf{A}}_i \bar{\beta}$.

At each realization m of the k th iteration, the stochastic approximation-step consists in updating the current value of $Q_k(\theta)$ by evaluating the complete log-likelihood given in equation 2.19 with $\Psi = \Psi^{(k,l)}$. Mostly considered in the scope of this thesis, we will assume in the following a constant residual error model such that $g = a$. As

defined, the complete model belongs to the exponential family reducing the stochastic approximation-step to the update of three sufficient statistics as defined by [Duval and Robert-Granié, 2007; Lavielle and Mentré, 2007; Duval et al., 2009]. Let us define $\mathbf{S}_{1,i}^{(k)} = \mathbb{E}[\Psi_i | \mathbf{Y}; \boldsymbol{\theta}^{(k-1)}]$, $\mathbf{S}_{2,i}^{(k)} = \mathbb{E}[\sum_i \Psi_i \Psi_i^T | \mathbf{Y}; \boldsymbol{\theta}^{(k-1)}]$ and $\mathbf{S}_{3,i}^{(k)} = \mathbb{E}[\sum_{i,j} (Y_{ij} - f(\mathbf{X}^i(t_{ij}, \tilde{\Psi}_i)))^2 | \mathbf{Y}; \boldsymbol{\theta}^{(k-1)}]$, with $\tilde{\mathbf{S}}_{1,i}^{(k)}$, $\tilde{\mathbf{S}}_{2,i}^{(k)}$ and $\tilde{\mathbf{S}}_{3,i}^{(k)}$ being respectively their stochastic approximations. The update of the stochastic approximation of the Q-function defined in equation 2.17 is equivalent to the following updates:

$$\tilde{\mathbf{S}}_{1,i}^{(k)} = \tilde{\mathbf{S}}_{1,i}^{(k-1)} + \gamma_k \left(\frac{1}{m(k)} \sum_{l=1}^{m(k)} \Psi_i^{(k,l)} - \tilde{\mathbf{S}}_{1,i}^{(k-1)} \right) \quad (2.20)$$

$$\tilde{\mathbf{S}}_{2,i}^{(k)} = \tilde{\mathbf{S}}_{2,i}^{(k-1)} + \gamma_k \left(\frac{1}{m(k)} \sum_{l=1}^{m(k)} \sum_i \Psi_i^{(k,l)} \Psi_i^{(k,l)T} - \tilde{\mathbf{S}}_{2,i}^{(k-1)} \right) \quad (2.21)$$

$$\tilde{\mathbf{S}}_{3,i}^{(k)} = \tilde{\mathbf{S}}_{3,i}^{(k-1)} + \gamma_k \left(\frac{1}{m(k)} \sum_{l=1}^{m(k)} \sum_{i,j} \left[Y_{ij} - f(\mathbf{X}^i(t_{ij}, \tilde{\Psi}_i^{(k,l)})) \right]^2 - \tilde{\mathbf{S}}_{3,i}^{(k-1)} \right) \quad (2.22)$$

Based on these approximations, the value of $\boldsymbol{\theta}^{(k)}$ provided by the maximization-step is given by the following equations, with $\boldsymbol{\mu} = (\Psi_0, \boldsymbol{\beta})$:

$$\begin{aligned} \boldsymbol{\mu}^{(k)} &= \left(\sum_{i=1}^N \bar{\mathbf{A}}_i^T \bar{\mathbf{A}}_i \right)^{-1} \sum_{i=1}^N \bar{\mathbf{A}}_i^T \tilde{\mathbf{S}}_{1,i}^{(k)} \\ \boldsymbol{\Omega}^{(k)} &= \text{diag} \left(\frac{1}{N} \left[\tilde{\mathbf{S}}_{2,i}^{(k)} - \sum_{i=1}^N (\bar{\mathbf{A}}_i \boldsymbol{\mu}^{(k)}) \tilde{\mathbf{S}}_{1,i}^{(k)T} - \sum_{i=1}^N \tilde{\mathbf{S}}_{1,i}^{(k)} (\bar{\mathbf{A}}_i \boldsymbol{\mu}^{(k)})^T + \sum_{i=1}^N (\bar{\mathbf{A}}_i \boldsymbol{\mu}^{(k)}) (\bar{\mathbf{A}}_i \boldsymbol{\mu}^{(k)})^T \right] \right) \\ a^{(k)} &= \sqrt{\frac{\tilde{\mathbf{S}}_{3,i}^{(k)}}{N_{tot}}} \end{aligned}$$

For models that do not belong to the exponential family (e.g. with $g = a + bf^c$) the quantity $\mathbf{S}_{3,i}^{(k)}$ can not be approximated by a stochastic approach and consequently the M-step can not directly be performed. Newton's-like optimization algorithms presented in section 2.2.2.3 can be used to overcome this problem [Duval et al., 2009].

2.3.3.3 Extensions of the SAEM algorithm

In general cases, the conditional distribution of the random effects given the observations required for the simulation-step of the SAEM algorithm is not known in a closed form. Consequently, the simulation step can not be performed directly as aforementioned presented. To overcome this problem, Kuhn and Lavielle [2004] proposed

to combine the SAEM algorithm with a Markov Chain Monte Carlo (MCMC) procedure. To this end, at each iteration k of the algorithm, the simulation step of the SAEM algorithm is replaced by L iterations of the Hastings-Metropolis algorithm [Chib and Greenberg, 1995]. The reader may refer to the following articles for more details about the MCMC-SAEM algorithm [Duval and Robert-Granié, 2007; Duval, 2008; Duval et al., 2009; Kuhn and Lavielle, 2004].

2.3.3.4 Model with censored data

In the presence of left-censored data, the estimation problem with non-linear MEM requires further development. While some efficient methods have been proposed to handle this problem in the linear framework, the introduction of non-linearity in the random effects make the problem more complex. To overcome the difficulty of the non-linearity, many authors proposed to approximate the likelihood using a linearized version of the model function f [Beal and Sheiner, 1982; Lindstrom and Bates, 1990; Wolfinger, 1993; Wu and Wu, 2001]. Nevertheless, as previously mentioned these linearization algorithms tend to induce a bias in the estimation of the model parameters. Taken advantage of the framework of incomplete data introduced by the EM algorithms, other authors proposed adapted versions of the EM algorithm to deal with censored data. These algorithms rely on the fact that both individual parameters and censored data can be seen as non-observed data. Accordingly, considering the notations introduced in section 2.2.2.4, for each subject i , complete data can be written as $(\mathbf{Y}_i^{obs}, \mathbf{Y}_i^{cens}, \Psi_i)$ with both \mathbf{Y}_i^{cens} and Ψ_i seen as unobserved data. Based on the theory of incomplete data, the observed likelihood can then be written as:

$$p(\mathbf{Y}; \theta) = \prod_i^N \int \int p(\mathbf{Y}_i^{obs}, \mathbf{Y}_i^{cens}, \Psi_i; \theta) d\Psi_i d\mathbf{Y}_i^{cens}$$

where $p(\mathbf{Y}_i^{obs}, \mathbf{Y}_i^{cens}, \Psi_i; \theta)$ is the likelihood of the complete data for the subject i . Similarly to the method proposed by Lyles et al. [2000] for linear models (see equation 2.8), the complete likelihood can be written according to the conditional distribution of the observed and censored data:

$$p(\mathbf{Y}_i^{obs}, \mathbf{Y}_i^{cens}, \Psi_i; \theta) = \prod_{j=1}^{n_i} p(Y_{ij}^{obs} | \Psi_i; \theta)^{\delta_{ij}} p(Y_{ij}^{cens} | \Psi_i; \theta)^{(1-\delta_{ij})} p(\Psi_i; \theta)$$

with $\delta_{ij} = 1$ if Y_{ij} is observed and 0 if Y_{ij} is left-censored, $p(Y_{ij}^{obs} | \Psi_i; \theta) = \pi(Y_{ij}^{obs}; f(\Psi_i t_{ij}), g^2(\Phi_i, t_{ij}, \xi))$ and $p(Y_{ij}^{cens} | \Psi_i; \theta) = \pi(Y_{ij}^{cens}; f(\Psi_i, t_{ij}), g^2(\Phi_i, t_{ij}, \xi))$ where $\pi(x; m, v)$ is the probability density function of the Gaussian distribution evaluated at x with mean m

and variance v . Considering this expression of the complete likelihood, [Samson et al. \[2006\]](#) proposed an extension of the SAEM algorithm to deal with left-censored data which is currently implemented on Monolix. The reader can refer to the paper [[Samson et al., 2006](#)] for a deeper understanding of the algorithm.

2.3.4 Mechanistic models describing within-host infectious disease dynamics

In the analysis of various infectious diseases such as HIV, hepatitis B and C, influenza, Zika or more recently SARS-CoV-2, mechanistic models are widely used to improve our understanding of the dynamics of these infections. The majority of the models that are used today to study the underlying biological mechanisms of these infections arise from the first models that have been built with the emergence of HIV and the development of antiretroviral treatments. Thereafter these latter have been progressively extended and applied to other infections. Moreover, the reader can refer to the following reviews for an exhaustive description of the models that have been developed in the last decades [[Xiao et al., 2013](#); [Ciupe and Heffernan, 2017](#); [Best and Perelson, 2018](#); [Conway and Ribeiro, 2018](#); [Perelson and Ke, 2021](#)].

The first modeling works, conducted by [Ho et al. \[1995\]](#), [Wei et al. \[1995\]](#) and [Perelson et al. \[1996\]](#), aimed at developing simple models to describe the viral dynamics during the acute phase of the infection and led to the standard model of viral dynamics, named "target-cell model", presented by Perelson [[Perelson et al., 1996](#)]. This well-known three-compartment model, describing the interaction between the virus and its target cells, is characterized by a sharp increase of the viral load until reaching the peak of the dynamics before progressively stabilizing at a constant level of viruses for a long period of time, also called viral setpoint. In the model, the setpoint is depicted by a steady-state (an equilibrium point) and corresponds to the chronic phase of the HIV infection. This model describes the interaction between the virus (V), its target cells (T), which are predominantly CD4+ T cells in the case of HIV, and infected target cells (I). The model can be written as:

$$\begin{cases} \frac{dT}{dt} = \lambda_T - \mu_T T - \beta VT \\ \frac{dI}{dt} = \beta VT - \delta I \\ \frac{dV}{dt} = \pi I - cV \end{cases}$$

where the target cells are produced at a constant rate λ_T , are eliminated at a rate μ_T per cell and become infected with a true infection rate β when free HIV virions interact with them. Infected cells are thus generated at a rate βVT and eliminated at a rate δ per cell. Finally, viruses are produced by infected cells at a rate π and are cleared at a rate c per virion. The integration of both natural production and elimination of target cells in this model allows to take into account the stabilisation of the viral dynamics during the chronic phase in untreated patients and accordingly the definition of a non-trivial steady state (i.e. with V not null).

Since 1996, numerous extensions of the target-cell model have been proposed integrating progressively knowledge learnt on the HIV virus and its interaction with the immune system but also by using this model to describe the viral dynamics for other diseases. As a matter of fact, in the case of acute infections (i.e. without chronic phases) such as influenza, Zika or more recently SARS-CoV-2, the natural mechanisms of replenishment and elimination of target cells are considered as negligible ($\lambda_T \approx \mu_T \approx 0$) during the short infectious period [Perelson and Ke, 2021]. The dynamics of the target cells being only defined by the term of infectivity βVT , the resulting model, known as "limited target-cell model", describe a viral dynamics that progressively tends toward the trivial equilibrium state (i.e. with $V = 0$). **The reader can refer to Chapter 5 for an application of the target-cell limited model in the case in SARS-CoV-2 infection.** To take into account the time required for a newly infected cell to produce infectious virions, representing the time of the virus replication cycle, Herz et al. [1996] introduced the notion of the "eclipse phase". Initially introduced into the standard model by transforming it into a system of delayed differential equations, many other solutions have been proposed since then, as presented in [Best and Perelson, 2018]. In this manuscript, the eclipse phase has been integrated by dividing infected cells I into two states, each described by an ODE-compartment: latent infected cells (I_1), meaning unproductively infected cells, that become productively infected cells (I_2) after an eclipse phase lasting $1/k$ days (see chapter 5). Other types of target cells can be distinguished in the model to describe the complex interactions of the virus with its host. For example, Prague et al. [2012] included quiescent CD4+ T cells (Q) in the model to account for CD4+ T cells that have the ability to proliferate but, being not activated, can not be infected by the virus [Commenges et al., 2008]. The inclusion of HIV reservoir in the model, meaning latent infected cells, could be made by including quiescent infected cell compartment [Luo and Zurakowski, 2008]. Other models have been proposed to integrate the effect of the innate immune response on the viral dynamics by adding compartments for IFN γ its cytotoxic effect on infected cells or directly IFN γ producing

cells (macrophages, NK cells) [Xu and Sneppen, 2021]. Finally, bigger models have also been proposed to couple both the viral and the adaptive immune dynamics. For example, some of them described the effect of effector cells (e.g. CD8+ T cells) on infected cells [Prague et al., 2019] while others included interactions with the humoral immune response (antibodies, B-cells, ASCs) [Ciupe et al., 2014; Wang and Zou, 2012]. **In the frame of this thesis, a mechanistic model including only the dynamics of the humoral response has been consider in a work conducted to assess the longevity of the humoral response (see Chapter 6).** Target cell models have also widely been adapted to model and study the effect of drug therapies on the viral dynamics. However, this type of model is outside the scope of the work carried out in this thesis and the reader can refer to the aforementioned reviews papers for a broader description.

In the four following chapters, we present the different works conducted during this thesis that aim at providing answers to the two main questions addressed in this manuscript: the evaluation of the protection induced by vaccination (chapters 3, 4 and 5) and of the longevity of the immunity conferred by vaccination (Chapter 6).

PART II

Viral dynamics

Chapter 3

Evaluation of therapeutic vaccine efficacy in HIV-infected patients

Abstract: This chapter focuses on the development of therapeutic HIV vaccines and the evaluation of their efficacy in clinical trials. Because these trials require interruption of antiretroviral treatment (ART) in HIV-infected individuals, they expose patients to a significant risk because they experience virologic rebound. In this case, ART is often resumed early to protect the patient when viral load exceeds a certain threshold. Optimal choice of ART resumption criteria and endpoint in the study is therefore necessary. The viral set point, i.e., the equilibrium viral load after several weeks without ART, which is commonly defined as the optimal criterion for evaluating the efficacy of the vaccine in controlling this rebound, cannot always be observed. We therefore present a descriptive analysis of longitudinal viral load data from multiple studies to find the best surrogate virologic descriptor for the setpoint. Application to viral load trajectories collected in three vaccine trials allowed identification of the area under the curve (AUC) as this optimal descriptor. Analysis of the impact of ART resumption criteria on the relationship between setpoint and AUC revealed that viral load censoring of at least 100,000 cp/ml (i.e. the minimal viral load for which ART resumption is indicated) and confirmatory measurement before restart ART are of interest.

Keywords: HIV ; therapeutic vaccine ; antiretroviral treatment ; ATI ; viral rebound ; virological descriptor ; criteria endpoint ; setpoint ; AUC ; descriptive analysis

Dissemination:

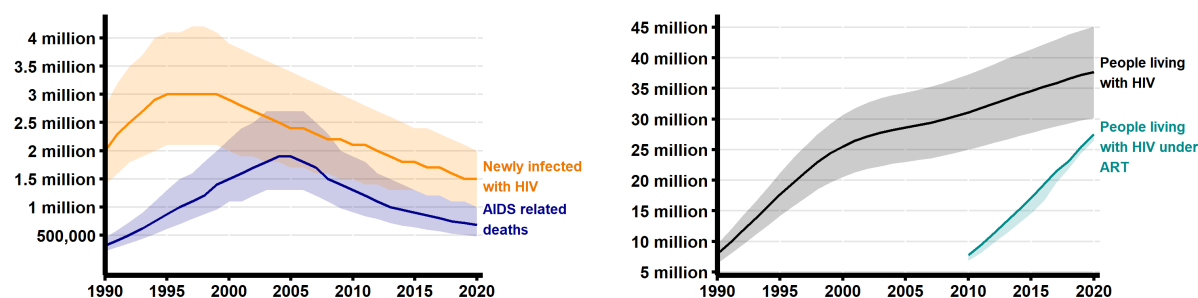
- ▷ **Article in preparation** [Alexandre Marie](#), [Prague Mélanie](#), [Thiébaud Rodolphe](#), coauthors and VRI studygroup, [Optimization of the choice of the primary endpoint in HIV therapeutic vaccine trials](#).
- ▷ **Written communication (poster) at international conference** [Alexandre M](#), [Prague M](#), [Lévy Y](#), [Thiébaud R](#). [Modelling Viral load Rebound in HIV Therapeutic Vaccine Studies](#). *Population Approach Group in Europe (PAGE)*, Stockholm, Sweden, 2019.
- ▷ **Oral communication at international conference** [Alexandre M](#), [Richert L](#), [Lévy Y](#), [Prague M](#), [Thiébaud R](#). [Evaluation of primary endpoint assessing HIV therapeutic vaccine efficacy during analytical treatment interruption studies](#). *Workshop on Virus Dynamics, 4th*, Paris, France, 2019.
- ▷ **Invited talk at French seminar** [Alexandre M](#). [Mechanistic modelling and optimization of vaccine response in HIV](#). *Summer School MPCI - "Science and Health"*, Marseille, France, 2019

3.1 Biological and clinical context

3.1.1 General introduction on HIV infection

3.1.1.1 Epidemiological context

The human immunodeficiency virus (HIV) has been discovered in the early 1980s [Barré-Sinoussi et al., 1983; Gallo et al., 1983]. Since its declaration as pandemic in 1987 [Mann et al., 1988], many programs have been developed to generate a global mobilization of people, institutions and resources against acquired immunodeficiency syndrome (AIDS). Recently in 2021, the UNAIDS *new Global AIDS Strategy 2021–2026*, has been adopted in Geneva [UNAIDS, 2021d]. The overall objective of this program is *to get every country and every community on track to end AIDS as a public health threat by 2030* [UNAIDS, 2021b]. In 2020, global HIV statistics established that 79.3 million [55.9 million - 110 million] people have been infected since its emergence [UNAIDS, 2021a] and 36.3 million [27.2 million - 47.8 million] AIDS-related deaths have been reported [UNAIDS, 2021e]. As shown in Figure 3.1, the creation of prevention programs allowed to decrease by 29% the number of new infections since 2010 (from 2.1 million [1.5 million - 2.9 million] to 1.5 million [1 million - 2 million]). Moreover, the development of efficient treatment and their intensive use, as shown by the significant increase of the percentage of HIV-infected people living with ART ranging from 25% [18% - 30%] in 2010 to 73% [56% - 88%], led to the decrease of 48% of the number of AIDS-related deaths since 2010 (from 1.3 million [910 000 - 1.9 million] to 680 000 [480 000 - 1 million]).



(a) Evolution of the numbers of newly HIV-infected people (in orange) and AIDS-related deaths (in blue), from 1990 to 2020.

(b) Evolution of the number of people living with HIV (in black) and among them, those with ART (in cyan), from 1990 to 2020.

Figure 3.1 – Global summary of the AIDS epidemic since 1990. Prevalence, incidence, related deaths and drug use against HIV/AIDS in the world, from 1990 to 2020. Solid lines represent the estimates and the shaded areas the boundaries around these estimates based on the best available information. Data used for these figures were extracted from the spreadsheet available in [UNAIDS, 2021c].

3.1.1.2 Some generalities about the virus

Human immunodeficiency virus is a retrovirus that causes HIV infection by targeting cells of the human immune system. Belonging to the subfamily of lentivirus, HIV is characterized by a long incubation period from infection to the apparition of the first clinical symptoms and therefore to the most advanced stage of HIV infection: AIDS. HIV can be divided into two main types (also called strains): HIV-1 and HIV-2, both of them leading to AIDS. Nevertheless, HIV-1 strain being the most widespread and virulent type inducing approximately 95% of HIV infections over the world and our works involving data only from this specific strain, we will exclusively focus on HIV-1 in the manuscript. HIV-1 has been classified into four phylogenetic lineages [Hemelaar, 2012]: Group M (for "major) which is mostly responsible for the pandemic and can be subdivided into nine subtypes (A-K), Group O (for "outlier") that causes hundred thousands cases in West-Central Africa [D'arc et al., 2015], Group N (for "non-M and non-O") identified in dozen of people in Cameroun and Group P newly discovered in 2009 in Cameroonians individuals [Plantier et al., 2009]. Divided into nine groups (A-I), only two of them (A and B) are characterized as pandemic while the others appeared as mostly asymptomatic lineages [Visseaux et al., 2016]. All of this genetic diversity represents a major challenge in the development of an effective vaccine.

3.1.1.3 HIV replication cycle

An HIV virion is a spherical membrane-enveloped particle containing a genome composed of two identical single-stranded RNA molecules encapsulated within a capsid along with enzymes important for virus replication. HIV virions infect the host by directly targeting its immune system and its immune cells expressing CD4 glycoprotein at their surface. Accordingly, CD4+ T lymphocytes represent the main HIV target, along with monocytes, macrophages or DCs. Without going into too much details (the reader can refer to [NIH, 2021b] for further details) and as displayed in Figure 3.2, the HIV replication cycle can be divided into seven steps: 1) the binding of the virus to its target cell, 2) its entry into the cytoplasm of this cell after fusion of cell membranes, 3) the release of the viral genome into the cytoplasm of the host-cell (uncoating) and its reverse transcription into proviral DNA, 4) integration of the viral DNA into the genome of the infected cell, 5) the replication of the viral genetic material by the infected cell, 6) the synthesis of new viral structural proteins and the formation of a non-infectious virion and 7) the release of this virion out of the infected cell and its maturation into an infectious one (budding). One of the greatest strengths of HIV is its ability to escape the human host's immune system due to its huge genetic variability [Bebenek et al., 1989;

3.1. Biological and clinical context

Sarafianos et al., 2009], resulting from a high rate of mutations [Preston, 1996] and a rapid rate of replication [Ho et al., 1995; O'Brien and Hendrickson, 2013].

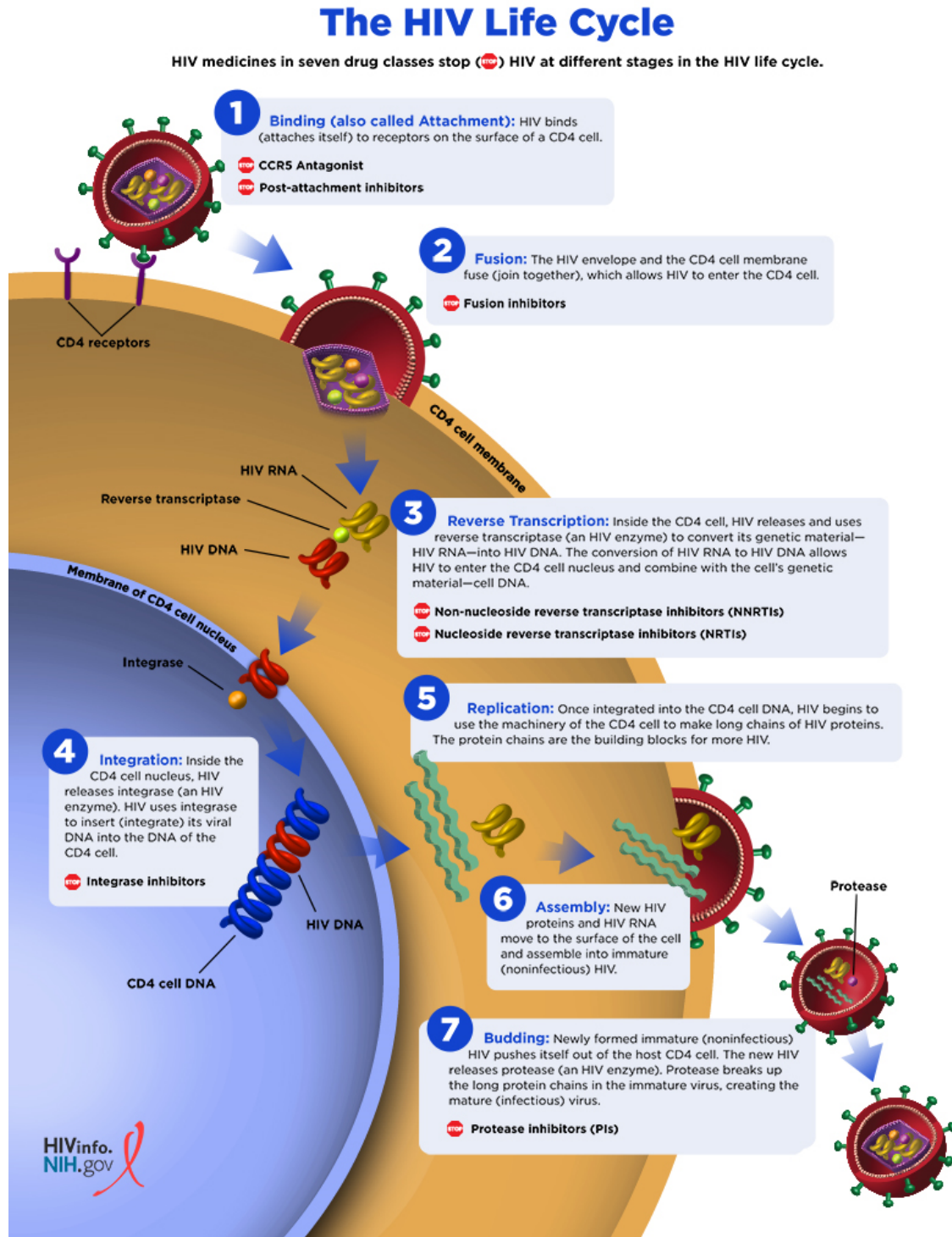


Figure 3.2 – The seven steps of the HIV replication cycle. Figure extracted from [NIH, 2021b]

3.1.1.4 Natural HIV disease progression and immune response

The dynamic of the interaction between HIV and the immune system is highly related to the clinical course/symptoms of HIV infection. In the blood, HIV viruses are quantified by RT-PCR amplification methods [Fiebig et al., 2003] given the so-called viral load defined as the concentration of the copies of HIV RNA in blood. In parallel, the quantification of the CD4+ T cells, termed CD4 count, is widely used as surrogate marker for disease progression, as CD4+ T cells represent the major HIV target cells [Cenderello and De Maria, 2016], and is usually made by flow cytometry techniques evaluating. Without treatment, the natural progression of the disease can be divided into three phases (Figure 3.3): (1) the acute phase (also termed the "phase of primary infection") lasting a dozen weeks after infection, the chronic phase (also termed "asymptomatic phase") that can last months to years depending on the people, and AIDS referred as the most advanced stage of the infection. **In this work we will focus on individuals that are in the clinical latency phase.**

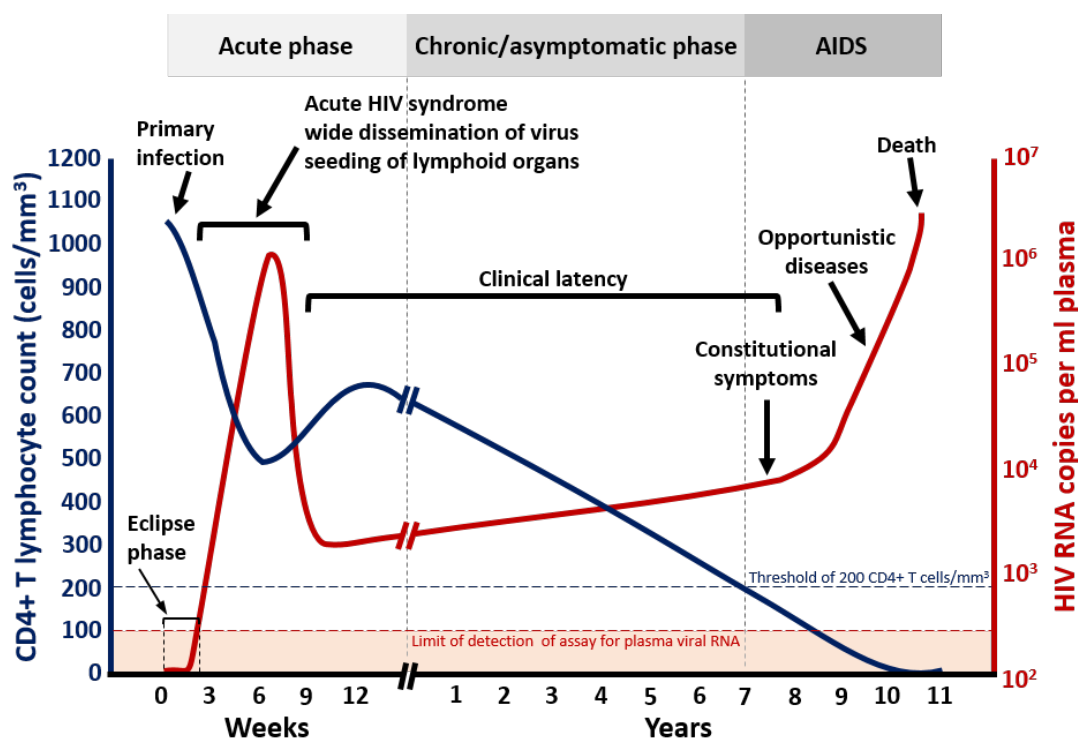


Figure 3.3 – Natural HIV disease progression. Dynamics of the HIV RNA load and CD4 count over the three clinical phases of HIV infection. *Figure adapted from [O'Brien and Hendrickson, 2013] and [McMichael et al., 2010].*

3.1.2 Treatment strategy

Nowadays, no effective drugs have been developed to eradicate HIV. Nevertheless, some HIV-infected people have shown an ability to long-term control of the virus replication in the absence of treatment following an early initiation of antiretroviral therapy (ART) [Sáez-Ciri3n et al., 2013]. Moreover, two individuals worldwide have been reported as cured of HIV [Leal et al., 2020]. Both of them, undergoing allogeneic haematopoietic stem-cell transplantation procedures using cells from CCR5 Δ 32/ Δ 32 donors to cure their respective myeloid leukemia and Hodgkin's lymphoma, display today undetectable HIV viral load after years of ART interruption [Hütter et al., 2009; Gupta et al., 2019]. Although this procedure cannot be seen as potential standard treatment against HIV due to its high risk of mortality, it provides hope to find a curative treatment one day.

3.1.2.1 Antiretroviral therapies

The generic term "antiretroviral" was introduced to refer to any drug used to prevent retrovirus' replication. Initially developed as monotherapies, antiretroviral therapies (ART) comprise today a combination of antiretroviral drugs developed to block the virus replication at different stages. Historically presented in 1996 at the International AIDS conference in Vancouver as "Highly active antiretroviral therapy" (HAART) [Vella et al., 2012], these combined therapies are more generally termed combination antiretroviral therapies (cART) today. Despite the lack of curative treatment against HIV, the development of ART allowed to significantly reduce the number of AIDS-related deaths, enhancing life expectancy and improve the daily life of HIV-infected people. In particular, HIV patients under ART have the opportunity to retrieve their normal life expectancy (e.g. up to 80 years for a 35-year-old HIV-positive person) [May et al., 2014]. By blocking viral replication, ART aim at reducing HIV viral load until an undetectable level and maintaining this level which progressively leads to the recovery of the immune system functionality, mostly depicted by the increasing level of CD4+ cell count. By maintaining an undetectable viral load level, ART also allow to reduce the HIV transmission. In this thesis, we will not detail in great extend the list of antiretroviral and their combination in cART.

Despite the success of the latest generation of ART which transformed a fatal disease into a chronic and manageable ones, HIV-infected people are still facing some difficulties that should be kept in mind. In particular, three types of treatment failure can be characterized: clinical, immunological and virological failures [Lenjiso et al., 2019]. The clinical failure is mainly driven by the appearance of adverse effects. The immuno-

logical failure was defined by the WHO as a decrease of CD4+ T cell count at or below 250 cells/mm³ (pre-therapy baseline being below 350 cells/mm³), or a 50% decrease from the peak of CD4+ T cell count during the treatment, or a persistent CD4+ T cell count below 100 cells/mm³ after ART initiation [WHO, 2017; Asefa et al., 2019; Dessie et al., 2021]. In this thesis, we particularly focus on a concept related to virological failure which refers to the difficulty for a patient to reduce and maintain its viral load at a low level [NIH, 2021a]. More specifically, the WHO defines it as the virologic response of a patient having a HIV RNA load above the threshold of 1000 copies/mL for at least two consecutive measurements in a 3-months interval after a minimum of 6 months of a given ART regimen, and assuming a perfect adherence [WHO, 2017].

3.1.2.2 Therapeutic vaccines as functional cure against HIV

cART have been proven to be highly efficient to suppress HIV viral load and reduce morbidity and mortality in infected people. Nevertheless, as mentioned above, some patients can face cART failures. Moreover, cART is expensive and there is a burden of a daily lifelong treatment [Cohn et al., 2020]. Despite their ability to maintain viral loads at an undetectable level, when successful, HIV infection persists in all individuals on treatment, cART being not able to totally eradicate the infection. Consequently, cART interruption will irremediably results in a viral load rebound within a few weeks without any further intervention. This rebound results from the existence of a latent HIV-1 reservoir [Barton et al., 2016] which is defined as a pool of long-lived/memory infected CD4+ T cells [Wong et al., 1997; Finzi et al., 1997; Murray et al., 2016] that are in a latent state (i.e. transcriptionally silent) but keep the ability to produce infectious virions after cART interruption [Vanhamel et al., 2019]. This HIV-1 reservoir is established in the early phase of the infection [Chun et al., 1998] and is expected to have a half-life of several years [Bachmann et al., 2019]. Although multiple studies have shown that the total size of this latent reservoir, including multiple distinct small reservoirs, should be limited by the earliness of the beginning of the antiretroviral treatment [Strain et al., 2005; Jain et al., 2013] and that its size seems to slowly decrease over time [Chomont et al., 2009], the eradication of the HIV reservoir represents a major challenge and induces a growing interest for the development of curative treatments.

Over the last decades, significant advances in our knowledge about the immune system and the HIV-1 reservoir allowed to propose and develop multiple potential therapeutic vaccines. However, the ability of the HIV virus to escape immune system made the development of efficient vaccines difficult. Multiple therapeutic approaches have been tested in clinical trials, but no relevant results have been obtained up to date [Larijani et al., 2019]. In the frame of this thesis, we focused exclusively on three different

vaccine therapeutic approaches: (a) IL-2 immunotherapies, (b) dendritic-cell vaccines and (c) the prime-boost therapeutic immunization including the recombinant DNA vaccine GTU-MultiHIB B and the lipopeptide vaccine (HIV-LIPO-5). The reader can refer to [Pham and Mesplède, 2018; Larijani et al., 2019] for a broader review about therapeutic strategies against HIV. Due to the absence of relevant surrogate immune marker of the viral load after cART interruption and thus accounting for virological control an/or the reduction of the size of the HIV-1 reservoir, analytical treatment interruption (ATI) is today the only available tool to assess the efficacy of the tested intervention and thus its ability to control the viral replication cART [Julg et al., 2019; Zheng et al., 2021].

3.1.2.3 Analytical treatment interruption

Over the years, many types of analytical treatment interruption have been used according to the type of trials and the therapeutic strategy evaluated. Our work being focused on HIV therapeutic vaccines we only considered trials with ATI evaluated after discontinuation of all interventions, meaning cART in our case. Moreover, we considered ATI trial that have been designed to ensure the safety of the patients. As a matter of fact, cART interruption representing an increasing risk for patients due to virological rebound, ATI are designed as short-term cART interruption period (e.g. around 12-16 weeks) and imply an intensive monitoring of patient viral loads [Lau et al., 2019]. Moreover, these study require the definition of multiple primary outcomes to characterize the viral rebound but also a list of prematurely cART resumption criteria to ensure, once again, the safety of the patients. As reviewed by Julg et al. [2019] following a consensus meeting about the recommendations for ATI in HIV trials, two major criteria endpoints are used to evaluate the vaccine efficacy according to the objectives of the study: the time to viral rebound, considered as the safest endpoint, when the curative properties of the therapeutic strategies is triggered, and the viral setpoint when the control of HIV infection is investigated. The time to rebound is currently defined as the time during which the viral load is maintained below a given threshold (e.g limit of detection). This endpoint has been used as primary outcome in many studies [Rasmussen et al., 2014; Mothe et al., 2015; Scheid et al., 2016; Bar et al., 2016; Sneller et al., 2017; Kroon et al., 2020]. While the time to rebound is more related to the characteristics of the virus and/or the HIV-1 reservoir, the setpoint, being defined as the stabilization of the viral load after an increased dynamics, is more related to the properties of the immune system to fight the viral infection. Accordingly, a low setpoint results in a better control of the infection. Contrary to the time to rebound which is considered as the safest endpoint being observed in the early part of the dynamics, the observation of the setpoint requires a longer follow-up increasing substantially the risk for the patients. In

fact, this endpoint being reached only after the rebound of the viral load, patients must be observed for several weeks with high viral load [Zheng et al., 2021]. Due to early cART resumption, under certain circumstances, the setpoint might be not observed for some patients. In addition to these two commonly used virological endpoints, other primary outcomes are commonly used to understand the viral kinetics. For example, we can define the peak of the viral dynamics or the area under the curve.

The research was carried out within the protocol of the EHVA T02 (NCT04120415) phase II HIV therapeutic vaccine trial with a 12-ATI week to evaluate and compare the efficacy of three vaccine arms with MVA HIV-B, vedolizumab and placebo. Our work consisted of determining the optimal criteria for the endpoints. Specifically, the setpoint was initially assumed to be optimal. However, because it is not always observed in patients, we attempted to find an early surrogate endpoint for the setpoint. Using data from three different HIV vaccine therapy trials with a protocol very similar to EHVA T02, we attempted to find this/these surrogate marker(s), which then became the primary endpoint of the EHVA T02 clinical trial. Ultimately, another version of the protocol of EHVA T02 used the outcome we identified in the following study as the primary endpoint. This work was the subject of an article in preparation, which can be found in the next section.

3.2 Optimization of the choice of primary endpoint in HIV therapeutic vaccine trial

This work was conducted in deep collaboration with the Vaccine Research Institute.

Optimization of the choice of primary endpoint in HIV therapeutic vaccine trials

Alexandre Marie^{1,2}, Prague Mélanie^{1,2}, Thiébaud Rodolphe^{1,2}, coauthors², and VRI studygroup²

¹Bordeaux University, Department of Public Health, INSERM UMR 1219, Bordeaux Population Health Research Centre, Inria SISTM, Bordeaux, France

²Vaccine Research Institute, Créteil, France

Abstract: HIV therapeutic vaccine development is an important component in the search for long-term HIV viral control strategies. Vaccine efficacy is assessed in trials with analytical treatment interruption (ATI) in which antiretroviral treatments are interrupted over a period of time. The setpoint is a major criterion used to estimate the ability of the tested vaccine to control viraemia. However, this latter can not always be observed. Consequently, we aim at identifying easily measurable and accurate viral load endpoint defined as an early surrogate of the viral setpoint during ATI. We propose a descriptive data analysis of three clinical trials to identify this optimal endpoint and highlight the good properties of the area under the HIV RNA load curve to be used as primary endpoint.

Keywords: HIV , therapeutic vaccine , ATI , setpoint , descriptive analysis , AUC

Introduction

Antiretroviral treatments (ART) have proven to be highly efficient to suppress HIV viral load and to reduce morbidity and mortality in infected people, representing today one of the most effective treatment to fight HIV in the absence of curative ones. Transforming fatal HIV infection into a chronic daily manageable disease (Deeks et al. 2013), ART are still subject to some disadvantages and limitations that can rapidly lead to adherence issues, such as the burden of a daily lifelong treatment, the cost of this latter, their toxicity or the development of drug resistance, among others (Cohn et al. 2020, Dybul et al. 2021). Moreover, ART can not eliminate latent HIV reservoir (Vanham & Van Gulck 2012, Vella et al. 2012, Barton et al. 2016) which irremediably results in viral load rebound after any ART interruption period. The eradication of the HIV reservoir represents today a major challenge and induces a growing interest for the development of curative treatment, such as HIV therapeutic vaccines. These alternative strategies aim at stimulating the immune system of HIV-infected people to induce or improve the immune response to HIV (Larijani et al. 2019) resulting in the suppression or at least the control of HIV replication in the absence of ART (Leal et al. 2020). The absence of relevant surrogate immune marker of the viral load after ART interruption makes analytical treatment interruption (ATI) the most suitable approach to assess HIV therapeutic vaccine efficacy in controlled clinical trials (Julg et al. 2019, Leal et al. 2020, Lévy et al. 2021). ATI represents short-term period(s) of ART interruption, following vaccine injection, during which free-of-ART HIV-infected patients undergo virological rebound and are closely and intensively monitored to prevent any uncontrolled increase of viral load. Similarly to more classic clinical trials, the assessment of the HIV therapeutic vaccine efficacy, and thus their ability to avoid or to control the viral rebound, requires the definition criteria endpoints. As reported by Julg et al. (2019) following the consensus meeting about the recommendations for ATI in HIV research trials, two major criteria endpoints are recommended to evaluate vaccine efficacy according to the objective of the study: the time to rebound as a test of cure, and the setpoint of rebound as a test of control of the infection, as targeted by many developed therapeutics. Commonly defined as the time during which viral load remains undetectable in the organism, the time to rebound occurs in the early part of the viral rebound dynamics minimizing the duration of the period of ART interruption and consequently the risk for patients.

At the opposite, the setpoint, being defined as the stabilization of the viral rebound, requires a longer follow-up to be observed increasing significantly the risk for the patients. To ensure patient safety, ART resumption criteria are carefully defined in ATI protocols. In addition to patient's wishes, non-related HIV clinical reasons or the observation of side effects, criteria defining a threshold of tolerated viral load and/or CD4+ T cell count measures are usually considered, compelling premature ART resumption. Consequently, the primary outcome defined as the setpoint of the viral rebound can not always be observed.

In this context, the objective of our work is to identify virological descriptors that could be used as an early surrogate of the setpoint, and thus by extension to the control of the viral infection during ATI. To this end, we propose to analyse viral load dynamics collected in three different HIV therapeutic vaccine clinical trials using descriptive analysis of these trajectories. The work is organized as follows: in a first part, materials and methods are described including the presentation of the data, the definition of the descriptors defined to describe viral load trajectories and the various analyses performed on them such as a correlation analyse. In the second part, we present the results of these analysis and identify the area under the curve as the optimal surrogate endpoint. Finally, we summarize and discuss our results.

Materials and Methods

Virologic measurements

In this work, we considered the data of three HIV therapeutic vaccine trials using ATI to evaluate the virological efficacy of interventions in maintaining low viral replication after ART interruption.

The first study is the VRI02 ANRS 149 LIGHT trial (Lévy et al. 2021), registered at ClinicalTrials.gov under the number NCT01492985, referred as LIGHT in the following. LIGHT is a multicenter, double-blind, placebo-controlled, randomized Phase II clinical trial evaluating the safety and immunogenicity of a therapeutic prime-boost vaccine strategy against HIV-1. As shown in Figure 1, the prime-boost therapeutic immunization is based on three doses of a recombinant DNA vaccine (GTU-MultiHIV B) as prime vaccination at weeks 0, 4 and 12, followed by two doses of a lipopeptide vaccine (HIV-LIPO-5) as boost vaccination at weeks 20 and 24. This trial included a total number of 103 HIV infected patients treated with cART for at least 6 months before their inclusion and exhibiting plasma HIV RNA load < 50 copies/mL and CD4+ T cell count \geq 600 cells/mm³. Participants were randomly assigned, with a 2:1 ratio, into two groups to receive either the prime-boost therapeutic vaccine strategy (n=68, vaccine group) or placebo (n=35, placebo group). At week 36, antiretroviral treatments were interrupted for patients with plasma HIV RNA load < 50 copies/mL and CD4+ T cell counts \geq 600 cells/mm³ until week 48. During this 12-week ATI period, patients were regularly monitored in particular with immunological (CD4+ and CD8+T cell counts) and plasma HIV RNA load measurements every two weeks (weeks 36, 38, 40, 42, 44, 46, 46 and 48). In this study, the primary endpoint was defined as the maximum HIV RNA load value (in log₁₀ copies/ml) reached during the ATI. Many different clinical, virological and immunological secondary endpoints were defined (the reader may refer to (Lévy et al. 2012) for the exhaustive list of secondary endpoints), in particular CD4+ T cell counts and HIV RNA load at different timepoints (weeks 40, 44, 48 and 74), the percentage of patients maintaining their viral loads below 10 000 copies/mL at the end of the ATI or the percentage of patients resuming prematurely their cART. In our analysis, we included only the 89 participants who started ATI at week 36 (n=32 in placebo group and n=57 in vaccine group).

The second study is the ANRS 118 ILIADE trial (Lévy et al. 2012), registered at ClinicalTrials.gov under the number NCT00071890, referred as ILIADE in the following. ILIADE is a multicenter, open-label, two parallel group randomized Phase II/III clinical trial evaluating the benefit of IL-2 immunotherapy in the maintenance of low viral replication after ART interruption and the ability to keep a level of CD4+ T cell count above 350 cells/mm³. As shown in Figure 2, the IL-2 therapy consisted in three cycles of recombinant

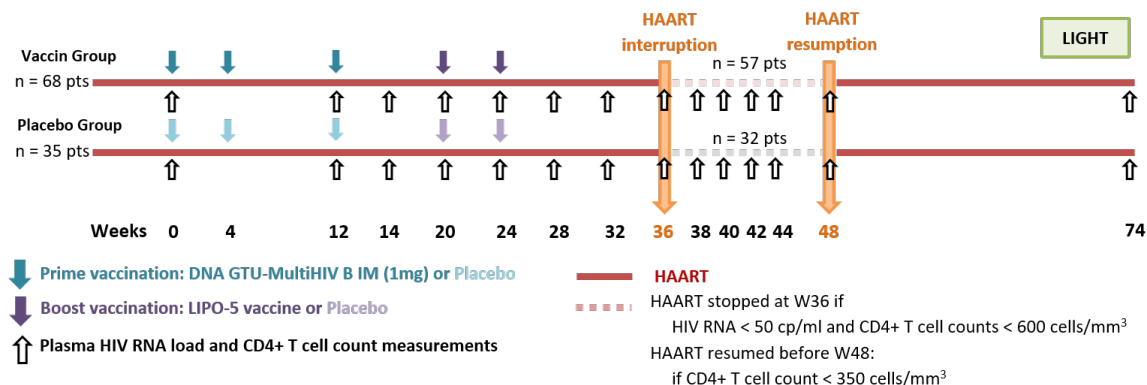


Figure 1 – VRI02 ANRS 149 LIGHT HIV vaccine trial - Study design

IL-2 (2 injections of 6×10^6 international units (IU) per day for 5 days) subcutaneously injected at weeks 0, 8 and 16. This trial included 148 HIV-infected patients treated with cART for at least 1 year before the study, exhibiting plasma HIV RNA load < 50 copies/mL and CD4+ T cell counts ≥ 500 cells/mm³ for at least 3 months before their inclusion and having a nadir (lowest value reached) of CD4+ T cell counts > 200 cells/mm³ before the study. Participants were randomly assigned, with a 1:1 ratio, into two groups to either receive IL-2 subcutaneous therapy (n=81, IL-2 group) or not (n=67, control group). At week 24, patients with CD4+ T cell counts ≥ 500 cells/mm³ stopped ART until reaching a CD4+ T cell counts lower than 350 cells/mm³ or in case of personal or medical requirements. From their inclusion to week 72, patients were monitored every 8 weeks (weeks 24, 32, 40, 48, 56, 64 and 72). After week 72, an extended period of ATI was proposed to participants, under the same conditions, up to week 228. In this trial, the primary endpoint was the cumulative proportion of subjects over the 72-week ATI period filling the following conditions of success: (1) ART interruption at week 24, (2) no CD4+ T cells counts below 350 cells/mm³ for two consecutive measures, (3) no cART resumption before week 72, (4) no AIDS-related events and (5) no loss to follow-up. Secondary immunological endpoints were defined as changes from baseline in T cell counts (CD4 and CD8) and in plasma HIV RNA load (the reader can refer to (Lévy et al. 2012) for an exhaustive list of all secondary endpoints). In our analysis, we included only the 140 participants who received at least one dose of the treatment and initiated ATI at week 24 (n=63 in control group and n=77 in IL2-group).

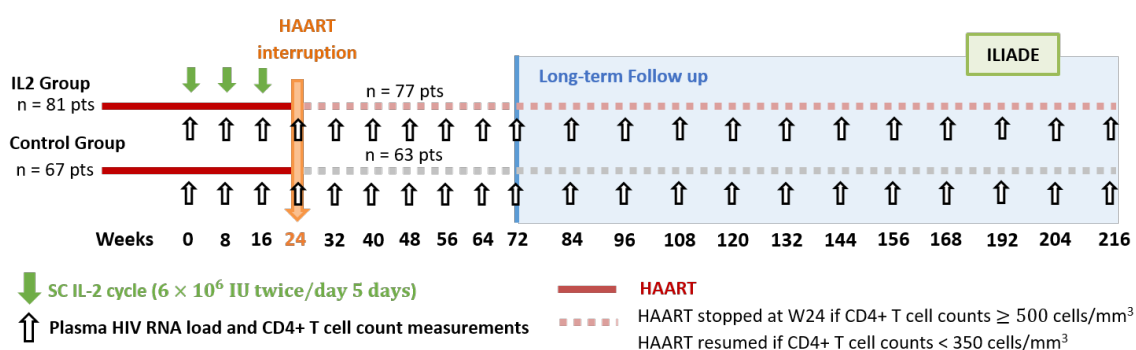


Figure 2 – ANRS 118 ILIADE HIV vaccine trial - Study design

The third study is the ANRS/VRI DALIA trial (Cobb et al. 2011, Lévy et al. 2014, Thiébaud et al. 2019), registered at ClinicalTrials.gov under the number NCT00796770, referred as DALIA in the following. DALIA is a single-center, single arm phase I clinical trial, conducted in the USA, evaluating the effects of a dendritic cell vaccine loaded with five HIV-derived lipopeptides on the immune system and the control of viral

replication. The trial included 19 infected patients treated with ART before the study and exhibiting plasma HIV RNA load < 50 copies/mL and CD4+ T cell counts > 500 cells/mm³ for at least 3 months before their inclusion and having a nadir of CD4+ T cell counts ≥ 300 cells/mm³ and never experienced AIDS-related events. The therapeutic strategy consisted in four vaccinations with dendritic-cell vaccine at weeks 0, 4, 8 and 12 (see Figure 3). At weeks 24, patients with plasma HIV RNA load < 400 copies/mL interrupted cART for 24 weeks. During the 24-week ATI period, patients were monitored every 1 to 4 weeks with measurements of plasma HIV RNA load and CD4+ T cells counts and could prematurely resume ART in case of immunological failure characterized by a CD4+ T cell counts dropping below 350 cells/mm³, with confirmation two weeks later with additional measurements, or in case of personal or medical requirement. In this vaccine trial, the primary endpoint was a safety endpoint defined as the occurrence of adverse event while the secondary endpoints corresponded to the proportion of cART resumption, CD4+ T cells count dropping below 350 cells/mm³ and the occurrence of AIDS-related or serious non-AIDS-related events.

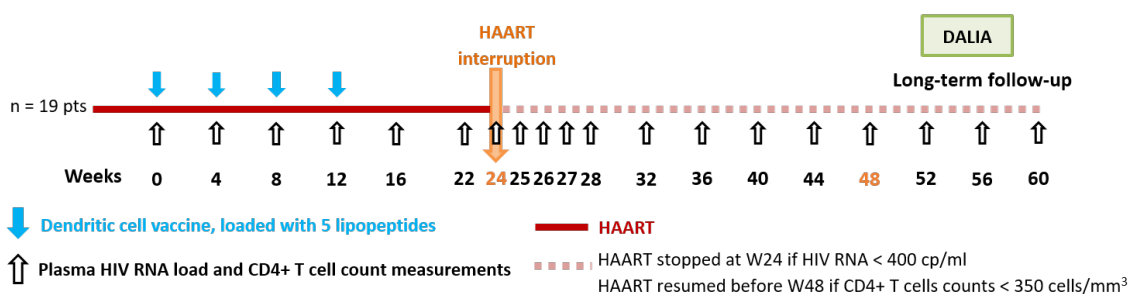


Figure 3 – ANRS/VRI DALIA HIV vaccine trial - Study design

Based on these three studies, we analyzed the HIV viral load trajectories collected for a total of 248 participants. In the following, time of viral load measurements were re-scaled within each study in order to consider the time of ART interruption as the initial time ($t=0$).

Definition of the descriptors of the viral dynamics

To analyze the dynamics of viral rebound induced by the interruption of the antiretroviral treatments and identify endpoints that could be used in HIV clinical trials to assess vaccine efficacy, we performed a descriptive analyse of these trajectories. In the following, we noted $Y_{ij} = Y_i(t_{ij})$ the HIV RNA load measured during ATI for the i th patient at the time t_{ij} , for $i \in \{1, \dots, N\}$ and $j \in \{1, \dots, n_i\}$. Numerous endpoints, defined as summary measures, were evaluated to describe viral dynamics. Throughout the rest of this work, these virological indicators are termed "descriptors".

As shown in the Figure 4, five main descriptors were defined to describe the viral dynamics. The objective of this work being to identify early surrogates of the setpoint, this latter was the first descriptor included in our analysis. Furthermore, as mentioned in Julg et al. (2019), we considered the time to viral rebound as the second most recommended endpoint in ATI protocols. The time to viral rebound, defining the time required to observe a rebound of viraemia after cART interruption, was mathematically evaluated as the delay between the cART interruption and the first detectable HIV RNA load. For each individual, the time of cART interruption being set at 0, the TTR of the i th patient is given as follows:

$$TTR_i = \min(\{t_{ij} | Y_{ij} > LOD_i\})$$

where LOD_i corresponds to the limit of detection related to the patient i . In particular, the limit of detection was 40 copies/mL in LIGHT and 50 copies/mL in both ILIADE and DALIA. Viral blips (e.g. viral replication < 100 copies/mL) before the true viral rebound were ignored. In addition to the setpoint and the TTR, we included three other main descriptors: the peak of the dynamics defined as the first local maximum, the slope

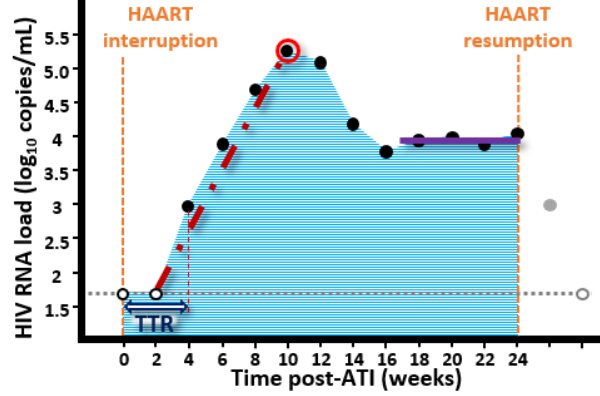


Figure 4 – Graphic illustration of the virological descriptors. Dots and circles represent a typical HIV RNA load dynamics in HIV infected patient after cART interruption and display respectively detectable and undetectable measures. The period of ATI is delimited by the vertical orange dashed lines. The virological descriptors are: (1) the peak (red circle) defined as the the first local maximum, (2) the slope of the rebound (red dotdashed line) defined as the slope between the last undetectable measure and the peak, (3) the setpoint (violet solid line) representing the plateau reached after the peak, (4) the time to rebound (TTR) (blue horizontal arrow) defined as the time from cART interruption to the first detectable measure, (5) the Area under the curve (AUC) (blue area) defined as the area under the HIV RNA load curve during ATI. The horizontal gray dotted line represents the limit of detection.

of the viral rebound defined as the slope between the last undetectable observation after cART interruption and the peak, and the AUC described as the area under the HIV RNA load curve while the patient is free of cART (see Figure 4). Accordingly, we evaluated these descriptors via equations 1, 2 and 3 respectively.

$$\text{Peak}_i = Y_i(T_i^{\text{peak}}) \quad (1)$$

$$\text{Slope}_i = \frac{\text{Peak}_i - \text{LOD}_i}{T_i^{\text{peak}} - T_i^{\text{LOD}}} \quad (2)$$

$$\text{AUC}_i = \int_{\text{ATI}} Y_i(t) dt \simeq \sum_{j=2}^{n_i} \frac{(t_{ij} - t_{ij-1})}{2} (Y_{ij} + Y_{ij-1}) \quad (3)$$

where T_i^{peak} and T_i^{LOD} are respectively the time at which the peak of the viral dynamics is reached and the time of the last undetectable measure and are defined as $T_i^{\text{peak}} = \min(\{t_{ij} | Y_{ij-1} \leq Y_{ij} \ \& \ Y_{ij} \geq Y_{ij+1}\})$ and $T_i^{\text{LOD}} = \max(\{t_{ij} | \forall j' \leq j, Y_{ij'} \leq \text{LOD}_i\})$. Similarly to the TTR, individual adjustment of the peak and the slope of the rebound were performed in case of viral blips. To approximate the calculation of the integral defining the AUC, the classic trapezoid method was used. Nevertheless, being calculated as an integral over the ATI period, the AUC is directly dependent on its duration and as described in data, the expected time of ATI differed from a trial to another: a 12-week ATI in LIGHT, a minimum of 48-week ATI in ILIADE and a minimum of 24-week ATI in DALIA. To take into account this variability in the calculation of the AUC but also the variability at the individual level resulting, for example, from an early cART resumption, a normalized version of the AUC was evaluated, as widely used in the literature (Brundage et al. 2018, Hill et al. 2018, Zecca et al. 2019, Kosulin et al. 2019). Accordingly, we defined the normalized (also termed time-averaged) AUC (nAUC) as the AUC divided by the individual duration of ATI:

$$\text{nAUC}_i = \frac{1}{T_i} \sum_{j=2}^{n_i} \frac{(t_{ij} - t_{ij-1})}{2} (Y_{ij} + Y_{ij-1}) \quad (4)$$

with T_i being the duration in week of ATI for the i th patient. Based on this definition, the nAUC is a virological descriptor that can be compared between trials or individuals.

As previously mentioned, a strict definition of the setpoint was more difficult to establish. In the literature, multiple definitions of this endpoint can be found. This criterion characterizing the stabilization of the viral dynamics, this heterogeneity results from the absence of a clear definition a stabilized dynamics as well as its high dependence on the design of the study. In particular, the observation of a setpoint is conditioned by the duration of the ATI period (the longer the ATI period, the more possible its observation), and the time between two virological measurements. Because of these differences of protocols, we initially estimated setpoints based on visual inspection of individual trajectories. Afterwards, an algorithm was derived to retrieve similar results. Accordingly, in our analysis, setpoints were defined for patients having at least two observations after the peak of their dynamics and highlighting a stabilized dynamics. Dynamics were assumed as stable as long as a time point can be identified after the peak such that, from this time point, the mean of all the slopes between two consecutive observations is lower than a given threshold, in absolute value. If a such time of observation could be found, the setpoint was defined as the mean of observations from this specific time to the cART resumption. Mathematically, the setpoint itself were defined as follows:

$$T_i^{setpoint} = \min \left(\left\{ t_{ij} | j \leq n_i - 1, t_{ij} > T_i^{peak}, \frac{\sum_{j'=j}^{n_i-1} \frac{Y_{i,j'+1} - Y_{i,j'}}{t_{i,j'+1} - t_{i,j'}}}{n_i - 1 - j'} \leq \text{Thresh} \right\} \right)$$

$$\text{Setpoint}_i = \text{mean} \left(\{Y_{ij} | t_{ij} \geq T_i^{setpoint}\} \right) \quad (5)$$

where $T_i^{setpoint}$ is the time of the beginning of the setpoint and $Thres$ the threshold value characterizing stabilization of the dynamics. This variable was fixed at $0.109 \log_{10} \text{ cp/mL/week}$ to retrieve closed results to those found during the initial estimation.

In addition to these five main descriptors, many others have been studied (results not shown) such as (1) the time of the peak, as previous mentioned (T_i^{peak}), (2) the composite, defined as the slope between the time of cART interruption and the peak, (3) the maximum value of the viral dynamics, defined as the global maximum of the dynamics, (4) the fold change, defined as the ratio between the first two detectable values divided by the delay between these two measures, (6) the doubling time, defined as the time needed to double the viral load at the beginning of the rebound using the first two detectable measures. However, in this paper, we mainly focused on the TTR, the setpoint, the peak, the slope and the nAUC being the descriptors depicting the more interesting results.

Analyse and comparison of descriptors

To analyze the viral dynamics observed in the three trials, the 248 HIV-infected patients were subdivided into five groups according to their trial and group of treatment: (1) LIGHT Placebo, (2) LIGHT Vaccine, (3) ILIADE IL-2, (4) ILIADE Control and (5) DALIA. Despite the absence of treatment in both LIGHT Placebo and ILIADE Control, these two groups remained as distinct because of their difference of study design and more specifically the duration of the ATI period and the delay between two HIV RNA load measurements.

A preliminary descriptive analysis of the viral dynamics during ATI at the different time points was performed to describe and summarize the dynamics within each group. This analysis was conducted to identify potential differences of the viral dynamics between the groups of treatment which could impact the estimation and the comparison of the virological descriptors across the groups. Statistical differences of HIV RNA load were evaluated at each time point, using classic two-sample two-sided t-tests, with a confidence level of 0.95, implemented in R. For each comparison, a prior F test comparing the variances of

the two compared samples allowed to determine whether a pooled variance t-test or a Welch's t-test should be performed. In the case of comparison of groups originating from distinct trials, comparisons were performed at the time points shared by the two compared groups. In that way we compared groups from LIGHT and ILIADE only at weeks 0 and 8, from LIGHT and DALIA at weeks 0, 2, 4, 8 and 12 and from ILIADE and DALIA at weeks 0, 8, 16, 24 and 32. To take into account the number of t-test performed, p-values were adjusted for test multiplicity with Benjamini and Hochberg (1995) correction (Benjamini & Hochberg 1995) using the classic R function *p.adjust*.

In a second time, a descriptive analysis of the virological descriptors, defined in the previous section and estimated for all the patients, was performed. Similarly to the previous analysis, statistical differences of the descriptors using t-tests and test multiplicity was conducted to identify similarities and/or differences across the five groups of patients.

The main objective of this work being to identify potential early surrogate of the setpoint, correlations between the different virological descriptors within each group were evaluated. To avoid the restriction of the study of correlations to linear relationships, Spearman correlations (Wissler 1905) were calculated to identify monotonic functions between the descriptors. By definition, the Spearman correlation is a non-parametric measure evaluating a statistical difference between two rank variables. Let us note \mathbf{X} and \mathbf{Y} two variables and X_i and Y_i their respective i th observation, for $i \in \{1, \dots, N\}$. The Spearman correlation coefficient ρ between \mathbf{X} and \mathbf{Y} is given by:

$$\rho = \frac{\text{Cov}(R(\mathbf{X}), R(\mathbf{Y}))}{\sigma(R(\mathbf{X})) \times \sigma(R(\mathbf{Y}))}$$

with $R(\mathbf{X})$ and $R(\mathbf{Y})$ being the ranks of \mathbf{X} and \mathbf{Y} respectively, $\text{Cov}(R(\mathbf{X}), R(\mathbf{Y}))$ the covariance of the ranks variables and $\sigma(R(\mathbf{X}))$ and $\sigma(R(\mathbf{Y}))$ their standard deviations. Once again, p-values of these different statistical tests were adjusted for multiplicity.

Impact of the upper threshold of viral load defining study dropout

To ensure the safety of HIV-infected patients undergoing ATIs, cART resumption criteria are carefully defined in the protocol. Despite the large number of HIV therapeutic vaccine trials conducted so far using ATI to assess vaccine efficacy, no really consensus has been fixed about the cART resumption criteria. Mostly chosen as virological endpoints, these latter are usually chosen according to the objective of the study. As aforementioned, in addition to non-HIV related causes or the evidence of disease progression with HIV-related symptoms, virological or CD4 count criteria are usually determined. This work being initiated to identify the optimal primary outcome to use in the HIV vaccine trial EHVA T02, we mainly focused on the envisaged virological cART resumption criteria: the resumption of cART when the viral load rebound above a given threshold. Based on the recommendations of Julg et al. (2019), several values of this threshold were explored and more particularly 10 000, 50 000 and 100 000 cp/mL representing respectively 4, 4.7 and 5 \log_{10} cp/mL. In this following, this virological threshold is termed "right censoring threshold" as it represents an upper boundary of the viral inducing study dropout.

As shown in Figure 5a, we studied the effect of the right censoring threshold on the value of the nAUC and by extension on its ability to remain a surrogate of the setpoint. In other words, we studied the impact of missing data, induced by early cART resumption, on the calculation of the correlation between the setpoint and the nAUC. Let us note X the right censoring threshold and TTX and nAUC_X the time interval and the nAUC calculated from cART interruption to the first observation above the threshold X . As widely encountered in protocols, we also evaluated the relevance of considering a confirmation measure before any validation of cART resumption. In that respect, we studied the scenario in which cART is resumed as soon as the HIV RNA load exceed the right censoring threshold at two consecutive time points. We note TTX^{conf} and nAUC_X^{conf} the time interval and the nAUC calculated from cART interruption to the

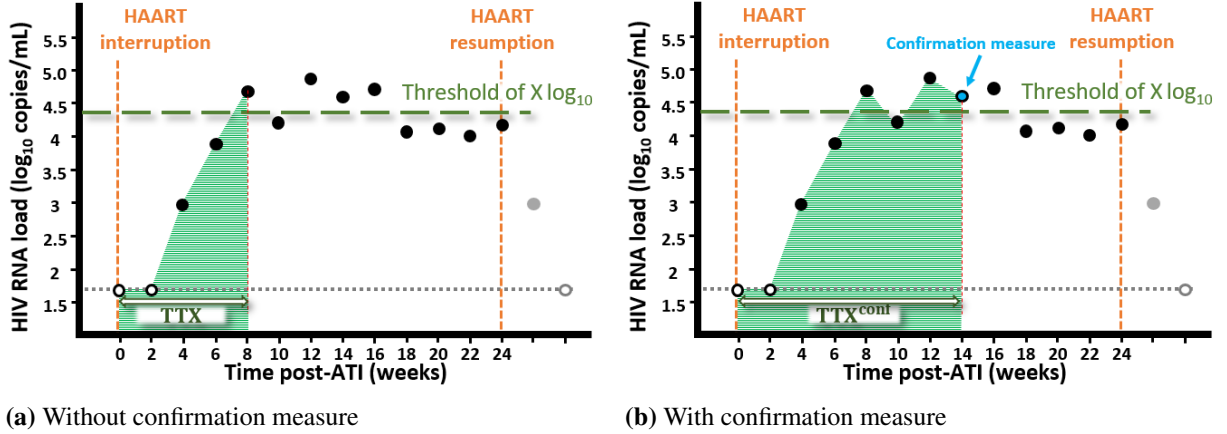


Figure 5 – Graphical illustration of the nAUC in the presence of a right censoring threshold. The vertical green long-dashed lines represent the threshold of $X \log_{10}$ copies/mL of HIV RNA load. On the figure (a), the green area represents the AUC calculated without confirmation measure (AUC_X), meaning from the cART interruption to the first observation above the threshold X . On the figure (b), the green area represents the AUC calculated with a confirmation measure (blue dot) (AUC_X^{conf}), meaning from the cART interruption to the first two consecutive observations above the threshold X .

confirmation measure. Mathematically, the two right censored nAUC can be written as follows for the i th patient:

$$nAUC_{X,i} = \frac{1}{TTX_i} \sum_{j=2}^{J_{X,i}} \frac{(t_{ij} - t_{ij-1})}{2} (Y_{ij} + Y_{ij-1})$$

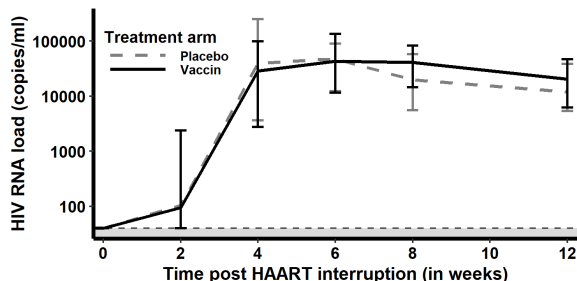
$$nAUC_{X,i}^{conf} = \frac{1}{TTX_i^{conf}} \sum_{j=2}^{\tilde{J}_{X,i}} \frac{(t_{ij} - t_{ij-1})}{2} (Y_{ij} + Y_{ij-1})$$

where $J_{X,i}$ and $\tilde{J}_{X,i}$ are respectively the number of the first observation of the i th subject above X and above X with the previous observation also above X , and are defined as $J_{X,i} = \min(\{j \in \{1, \dots, n_i\} | Y_{ij} \geq X, \forall j' < j, Y_{ij'} < X\} \cup \{n_i\})$ and $\tilde{J}_{X,i} = \min(\{j \in \{1, \dots, n_i\} | Y_{ij} \geq X, Y_{ij-1} \geq X, \forall j' < j-1, Y_{ij'} < X\} \cup \{n_i\})$. In both scenarios, if the condition of cART resumption is not met, nAUC is calculated as previously defined in equation 4. As shown in Figure 5 and similarly to the previous study, right censored nAUC are calculated on observation in \log_{10} scale.

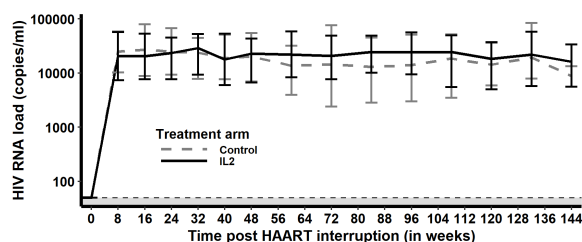
As first analysis, we evaluated within each of the five groups of treatment the correlations between the setpoint and both $nAUC_X$ and $nAUC_X^{conf}$. The right censoring threshold X was then set at three distinct values: 100 000, 50 000 and 10 000 copies/mL. Showing a significant decrease of the correlation coefficient as well as a loss of significance under some conditions, a second analysis was performed to identify the optimal conditions allowing to keep the highest significant correlation as possible between the setpoint and the nAUC. To this end, the same correlations were calculated for a threshold X ranging from 2.0 to 6.0 \log_{10} copies/mL. In both parts of this work, we kept for the setpoint the values estimated without right censoring of the viral load, assumed to be the "true" values of the descriptor.

Results

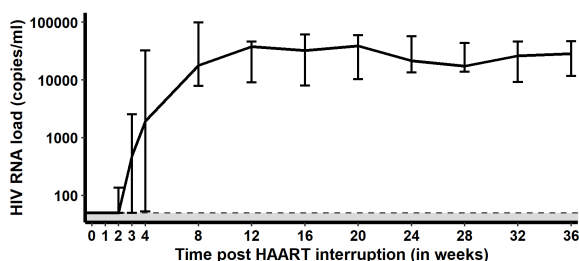
Descriptive analysis of the data



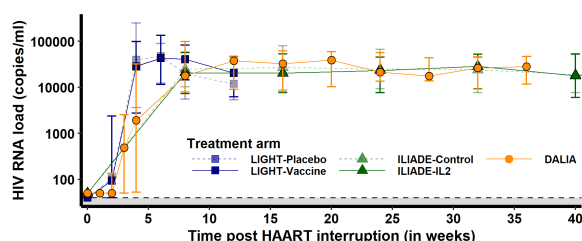
(a) **LIGHT trial:** 12-week ATI period with monitoring every two weeks.



(b) **ILIADE trial:** 144-week ATI period, with monitoring every 8 weeks.



(c) **DALIA trial:** 36-week ATI period with monitoring every 1 to 4 weeks.



(d) Comparison of the 3 trials during the first 40 weeks of ATI.

Figure 6 – HIV RNA load dynamics in the three HIV therapeutic vaccine trials LIGHT, ILIADE and DALIA during the period of cART interruption. Solid and dashed lines represent medians in therapeutic groups and control/placebo groups respectively, and error bars represent the interquartile range (IQR). Grey area correspond to the limit of detection (40 copies/mL in LIGHT and 50 copies/mL in ILIADE and DALIA). In (d), blue squares, green triangles and orange circles represent the mean observations in LIGHT, ILIADE and DALIA respectively.

As preliminary work, we conducted a descriptive analysis of the dynamics of the viral rebound after cART interruption within and across the five groups of treatment. The plasma HIV RNA load measures obtained during the ATI period for the 248 HIV-1 infected patients are summarized in Table 1. As shown in Figures 6a and 6b, comparable dynamics were observed between the two groups LIGHT Placebo and LIGHT Vaccine, and between ILIADE Control and ILIADE IL2, respectively. These results were confirmed by the absence of statistical significant differences at each time point between the two compared groups (lowest p-value in LIGHT: 0.95 ; lowest p-value in ILIADE: 0.79). Similarly, as displayed in the Figure 6d comparing the dynamics of the five groups of treatment during the first 40 weeks of ATI, HIV-infected patients enrolled in DALIA showed similar viral load measurements, in average, than those in ILIADE (Control and IL2) at week 8, 16, 24 and 32 with p-values closed to 1. Nevertheless, it is important to keep in mind that comparisons were performed at specific time points and thus it does not signify that the overall dynamics are similar. Due to the difference in protocol between LIGHT and ILIADE, only a single time point is shared between the 4 groups, at week 8. Once again, no statistical differences were highlighted at this time point between the groups, as shown by the overlapped confidence intervals in Table 1. Finally, while the comparisons of the groups LIGHT Placebo and LIGHT Vaccine with DALIA at week 0, 2, 4, 8 and 12 concluded to the absence of statistical differences between their respective viral load measurements, after multiplicity corrections these results were less obvious than the previous ones at week 2 and 4. In particular, p-values of 0.07 were found at week 4 for both LIGHT Placebo and LIGHT Vaccine and at week 2 for LIGHT vaccine, and a p-value of 0.1 at week 2 for the comparison between DALIA and LIGHT Placebo.

Table 1 – Plasma HIV RNA load, in log₁₀ scale, (in copies/mL) in each group of treatment of the three HIV vaccine trials, LIGHT, ILIADE and DALIA, in ATI period.

Weeks post-HAART interruption		LIGHT (n=89)		ILIADE (n=140)		DALIA (n=19)
		Placebo (n=32)	Vaccine (n=57)	Control (n=63)	IL2 (n=77)	
W0	Number part.	32	57	63	77	19
	Censored (%)	31 (97)	56 (98)	57 (90)	72 (94)	19 (100)
	Mean [IQR]	1.65 [1.60 ; 1.60]	1.60 [1.60 ; 1.60]	1.81 [1.70 ; 1.70]	1.76 [1.70 ; 1.70]	1.70 [1.70 ; 1.70]
W1	Number part.					18
	Censored (%)					17 (95)
	Mean [IQR]					1.75 [1.70 ; 1.70]
W2	Number part.	32	57			18
	Censored (%)	14 (44)	23 (40)			11 (61)
	Mean [IQR]	2.56 [1.60 ; 3.36]	2.54 [1.60 ; 3.38]			2.05 [1.70 ; 2.13]
W3	Number part.					19
	Censored (%)					8 (42)
	Mean [IQR]					2.79 [1.67 ; 3.39]
W4	Number part.	32	55			19
	Censored (%)	3 (9)	8 (15)			5 (26)
	Mean [IQR]	4.21 [3.54 ; 5.36]	4.12 [3.44 ; 4.99]			3.26 [1.72 ; 4.51]
W6	Number part.	31	55			
	Censored (%)	2 (6)	4 (7)			
	Mean [IQR]	4.40 [4.08 ; 4.95]	4.33 [4.06 ; 5.13]			
W8	Number part.	29	50	61	76	19
	Censored (%)	1 (3)	3 (6)	2 (3)	4 (5)	2 (11)
	Mean [IQR]	4.16 [3.74 ; 4.76]	4.31 [4.16 ; 4.92]	4.28 [4.01 ; 4.76]	4.17 [3.86 ; 4.76]	4.15 [3.90 ; 4.99]
W12	Number part.	25	46			17
	Censored (%)	1 (4)	3 (7)			0 (0)
	Mean [IQR]	3.98 [3.73 ; 4.58]	4.07 [3.79 ; 4.67]			4.36 [3.96 ; 4.66]
W16	Number part.			59	72	17
	Censored (%)			2 (3)	2(3)	1 (6)
	Mean [IQR]			4.26 [3.94 ; 4.90]	4.21 [3.89 ; 4.73]	4.27 [3.91 ; 4.79]
W20	Number part.					16
	Censored (%)					1 (6)
	Mean [IQR]					4.31 [4.01 ; 4.76]
W24	Number part.			55	70	16
	Censored (%)			2 (4)	3 (4)	0 (0)
	Mean [IQR]			4.21 [3.98 ; 4.83]	4.16 [3.88 ; 4.65]	4.15 [4.13 ; 4.75]
W28	Number part.					10
	Censored (%)					1 (10)
	Mean [IQR]					4.04 [4.14 ; 4.64]
W32	Number part.			47	66	6
	Censored (%)			2 (4)	3 (5)	1 (17)
	Mean [IQR]			4.09 [3.89 ; 4.65]	4.22 [3.97 ; 4.72]	3.97 [3.95 ; 4.66]
W36	Number part.					6
	Censored (%)					1 (17)
	Mean [IQR]					4.01 [4.06 ; 4.67]
W40	Number part.			44	65	
	Censored (%)			2 (4)	1 (2)	
	Mean [IQR]			4.18 [3.88 ; 4.71]	4.17 [3.78 ; 4.73]	
W48	Number part.			40	63	
	Censored (%)			1 (3)	1 (2)	
	Mean [IQR]			4.13 [3.84 ; 4.73]	4.14 [3.83 ; 4.63]	
W60	Number part.			35	57	
	Censored (%)			1 (3)	1 (2)	
	Mean [IQR]			3.92 [3.60 ; 4.50]	4.14 [3.92 ; 4.77]	
W72	Number part.			35	55	
	Censored (%)			1 (3)	1 (2)	
	Mean [IQR]			4.05 [3.38 ; 4.88]	4.22 [3.88 ; 4.69]	
W84	Number part.			29	50	
	Censored (%)			1 (3)	0 (0)	
	Mean [IQR]			3.99 [3.46 ; 4.65]	4.24 [4.00 ; 4.69]	
W96	Number part.			26	49	
	Censored (%)			1 (4)	1 (2)	
	Mean [IQR]			3.97 [3.47 ; 4.70]	4.24 [3.97 ; 4.75]	

As shown by the lower mean viral load and the highest percentage of censored data in DALIA compared to LIGHT groups (see Table 1), these results seemed in accordance with a slower viral rebound in patients

Table 2 – Descriptive analysis of the virological descriptors in the five groups of treatment.

	LIGHT (n=89)		ILIADE (n=140)		DALIA (n=19)
	Placebo (n=32)	Vaccine (n=57)	Control (n=63)	IL2 (n=77)	
Time to rebound (TTR) - weeks					
N(%)	31 (97)	54 (95)	59 (94)	77 (100)	19 (100)
Median [IQR]	2.00 [2.00 ; 4.00]	2.00 [2.00 ; 4.00]	8.00 [8.00 ; 8.00]	8.00 [8.00 ; 8.00]	3.00 [2.00 ; 6.00]
Peak - log₁₀ copies/mL					
N(%)	32 (100)	57 (100)	61 (97)	77 (100)	19 (100)
Median [IQR]	4.96 [4.57 ; 5.74]	4.96 [4.62 ; 5.36]	4.57 [4.21 ; 5.01]	4.66 [4.19 ; 4.99]	4.94 [4.10 ; 5.18]
Slope - log₁₀ copies/mL/week					
N(%)	31 (97)	54 (95)	55 (87)	76 (99)	19 (100)
Median [IQR]	0.84 [0.55 ; 1.07]	0.75 [0.57 ; 1.00]	0.29 [0.15 ; 0.37]	0.22 [0.14 ; 0.35]	0.52 [0.36 ; 0.89]
Normalized AUC (nAUC) - log₁₀ copies/mL					
N(%)	32 (100)	57 (100)	61 (97)	77 (100)	19 (100)
Median [IQR]	3.74 [3.31 ; 4.18]	3.80 [3.32 ; .20]	4.19 [3.74 ; 4.43]	4.25 [3.81 ; 4.50]	4.00 [3.68 ; 4.29]
Setpoint - log₁₀ copies/mL					
N(%)	20 (62)	31 (54)	48 (76)	70 (91)	17 (89)
Median [IQR]	4.29 [3.87 ; 4.71]	4.59 [4.20 ; 4.88]	4.32 [3.82 ; 4.71]	4.39 [3.91 ; 4.70]	4.38 [4.05 ; 4.55]
Time to setpoint - weeks					
N(%)	20 (62)	31 (54)	47 (75)	70 (91)	17 (89)
Median [IQR]	8.00 [6.00 ; 8.00]	8.00 [6.00 ; 8.00]	16.00 [16.00 ; 24.00]	16.00 [16.00 ; 24.00]	12.00 [8.00 ; 16.00]

enrolled in DALIA. A deeper analysis of the comparison of LIGHT and DALIA viral load measurements in particular at week 4 may be relevant afterwards.

To conclude, no significant differences were observed between the five groups of treatment at the distinct time points. However, it is important to keep in mind that these results are influenced by the duration of the ATI period and the delay between two HIV RNA load measurements and that these two elements could influence the estimation of the virological descriptors. This dependence highlights the interest for modeling work.

Descriptive analysis of the virological descriptors

As described in Materials and Methods (see section *Definition of the descriptors of the viral dynamics*), we focused our analysis on five virological descriptors: the time to rebound, the peak, the slope, the setpoint and the normalized AUC of the viral rebound. As described in Table 2 summarizing their distributions for each of the five groups, these latter were evaluated considering the viral load in log₁₀ scale.

In addition to these virological indicators, we initially analyzed the time required to reach the setpoint. As displayed in Figure 7f, the distributions of this specific time across the groups of treatment are highly heterogeneous. In particular, the time to setpoint is highly trial-specific and is significantly higher in ILIADE than in both LIGHT (p-value < 10⁻⁴) and DALIA (p-value < 0.001) trials and significantly higher in DALIA than in LIGHT (p-value < 0.001). In LIGHT, the estimation of the time to setpoint was conditioned by the short 12-week ATI and the delay of two weeks between observations. Indeed, our definition of the setpoint requiring a minimum of two observations after the peak, the time limit for the beginning of the setpoint was 8 weeks after cART interruption, which corresponds to the value found in 51% of the patients. The high percentages of patients for whom no stabilization of the dynamics was observed (38% in LIGHT Placebo and 46% in LIGHT Vaccine) are in accordance with this limitation. The significantly higher time to setpoint observed in both ILIADE and DALIA compared to LIGHT mostly resulted from the longer duration of ATI in these two trials. As a matter of fact, the majority of their patients showed a time to setpoint higher than 12 weeks: 98% and 71% respectively. This results highlights the importance of the choice of the ATI period. A short period of cART interruption is safer for patients but can prevent a good observation of the setpoint. Furthermore, it confirms the interest of finding early surrogates of the setpoint, especially for trials with short-term ATI. While the estimated time to setpoint appeared as well distributed among DALIA's patients with a robust mean, estimations in ILIADE are directly impacted by the choice of the interval between two virological measurements. Although the longer follow-up of patients allowed to reach higher values of

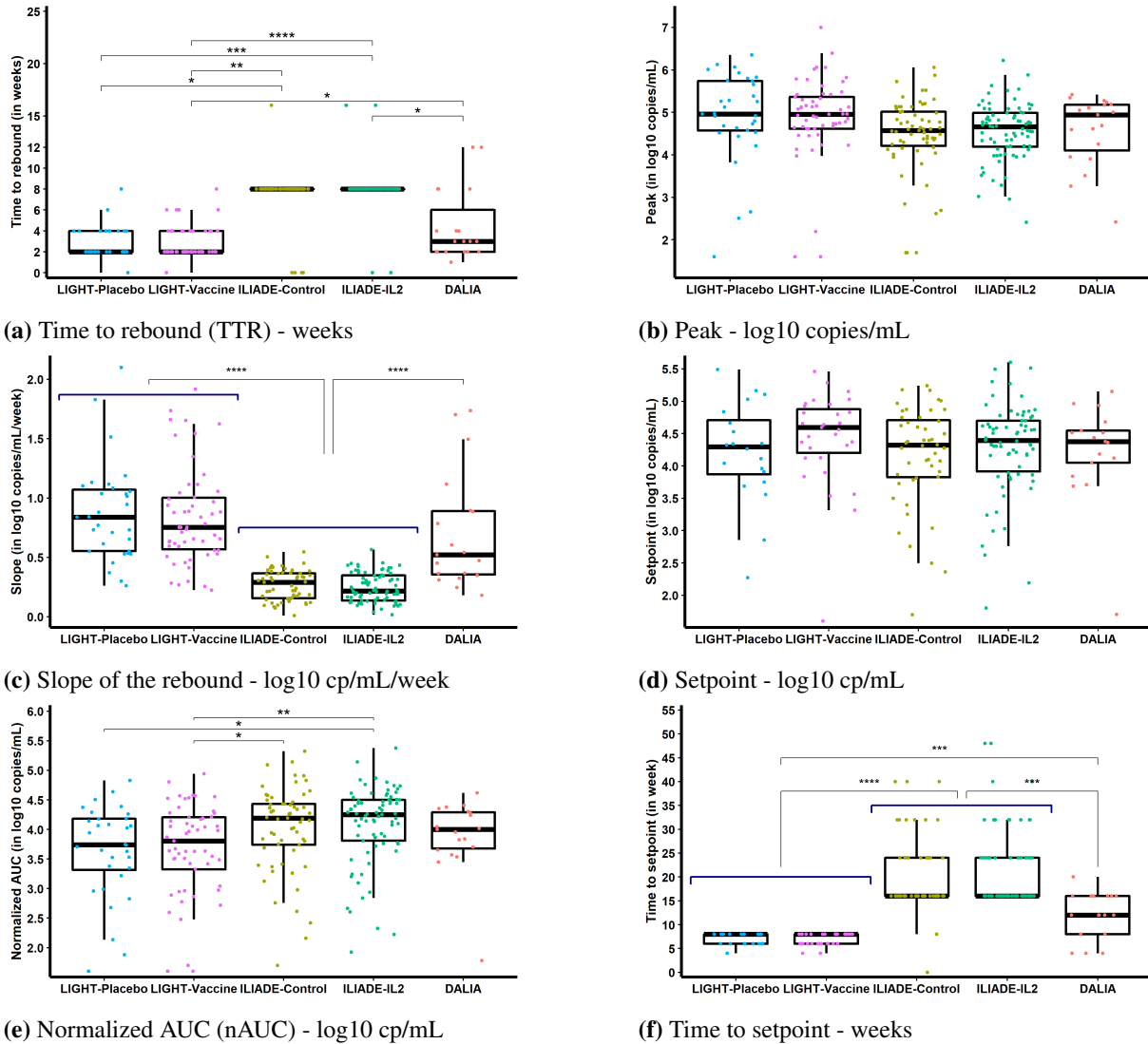


Figure 7 – Descriptive analysis of the descriptors. Comparison of the estimated descriptors between the five groups of treatments: LIGHT-placebo, LIGHT-vaccine, ILIADE-Control, ILIADE-IL2 and DALIA. Classic t-test were performed to compare mean values between the groups and p-values were adjusted for test-multiplicity with Benjamini and Hochberg correction. P-values of significant differences are displayed above brackets with (*): $p \leq 0.05$, (**): $p \leq 0.01$, (***): $p \leq 0.001$, (****): $p \leq 0.0001$

the time to setpoint, the lower bound of this distribution was fixed by the interval of 8 weeks between two measures.

Despite the dependency of the time required to reach a setpoint on the virological monitoring, no statistical differences of the setpoint were observed across the five groups of treatment (see Figure 7d), with mean values ranging from 4.29 to 4.59 log₁₀ copies/mL. Similarly, comparable values of the peak were observed in the five groups.

The analysis of the slope of the rebound seemed to reinforce the impact of the interval between two observations on the observed dynamics of the viral rebound, and more specifically on the early part of this dynamics. As shown in Figure 7c, the slopes estimated in ILIADE were significantly lower than the slopes estimated on both LIGHT and DALIA groups, with the mean value in ILIADE (both groups pooled)

being 70% lower than in LIGHT (both groups pooled) and 64% lower than in DALIA. On the opposite, no statistical differences were observed between LIGHT and DALIA. By definition, the slope is estimated between the last undetectable observation and the peak. However, the value of the peak and the limit of detection being comparable between the groups, this latter is only dependent on the interval between the last undetectable observation and the time of the peak, or by extension on the TTR and the time of the peak. As displayed in Figure 7a or summarized in Table 2, the time to rebound is significantly higher in ILIADE than in the two other trials. This difference results from the fact that the first detectable measures is mostly observed before the week 8 in LIGHT and DALIA and thus before the first observation collected in ILIADE after cART interruption. The time required to reach the peak is consequently higher in ILIADE, which explained the lower estimations of the slope.

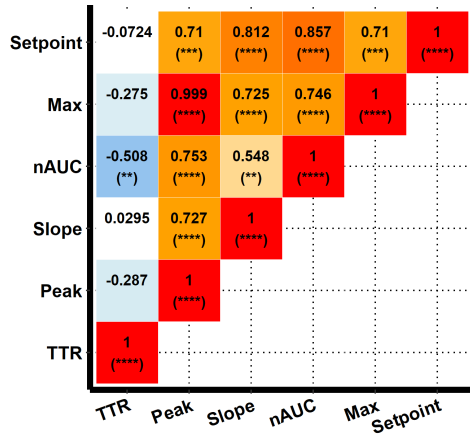
Finally, the analysis of the normalized AUC displayed quite comparable results between the groups of treatment, even though this descriptor was significantly slightly higher in ILIADE than in LIGHT. This difference can be explained by the difference of follow-up between the two trials. In particular, despite the normalization of the AUC, the dynamics after the week 12 in ILIADE being characterized by higher observations than the nAUC estimated in LIGHT, as shown by the value of the setpoint, the longer follow up in ILIADE allowed to progressively increase the value of its nAUC. In other words, the longer follow-up with stabilized dynamics allowed to progressively reduce the weight of the first low observations in the AUC calculation. As shown in Table 2, the gap between the values of the setpoint and the nAUC in ILIADE (0.13 and 0.14 \log_{10} cp/mL in Control and IL2 groups, resp) is significantly lower than in LIGHT (0.55 and 0.79 \log_{10} cp/mL in Placebo and Vaccine groups, resp) and DALIA (0.38 \log_{10} cp/mL), with p-values lower than 0.0001 and 0.01 respectively. Accordingly, this descriptive analysis highlighted the influence of the times of observations on the estimation of the descriptors.

Study of the correlations between the descriptors

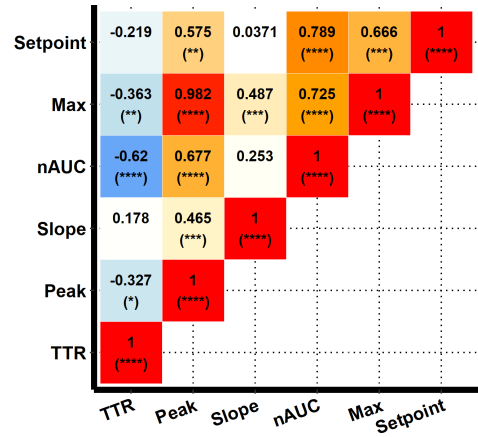
The preliminary descriptive analysis of the dynamics of the viral rebound showed no statistical differences between the dynamics of the five groups of treatment. Nevertheless, the descriptive analysis of the virological descriptors highlighted different patterns according to the descriptors of interest. In particular, this analysis pointed out the high dependency of the time to viral rebound, the slope of the rebound and the time to the setpoint on the study design. By contrast, the distributions of the individual estimations of the descriptor of interest, the setpoint, appeared as comparable between the five groups. The objective of this work being to identify early surrogate of the setpoint, the peak and the nAUC of the viral dynamics depicting quite constant distributions between the groups, these latter appeared as the more promising candidates.

In Figure 8, the results of the Spearman correlation analysis conducted to identify potential relationships between the descriptors are given. Despite the difference of virological monitoring and the duration of ATI between the five groups of treatment, correlation matrices display strong similarities in the type of relationships linking the descriptors. In addition to the five main descriptors described in Material and Methods (see section *Definition of the descriptors of the viral dynamics*), we added the maximum value of the viral replication in this analysis. As expected, the peak and the maximum value are significantly and highly positively correlated in all groups. In LIGHT and DALIA (Figures 8a, 8b and 8e), the correlations being higher than 0.974 and given their definition, the two descriptors are assumed to be equal for almost all patients. The variation between them could then be induced by measurement errors in the HIV RNA load observations. In ILIADE, smaller correlation coefficients were estimated with values approximating 0.80. These weaker correlations result from the loss of the long-term virological control in some patients. Leading to a sharp increased HIV RNA load dynamics at the end of the dynamics (after the setpoint) requiring cART resumption, this loss of control induced an higher maximum value than the peak.

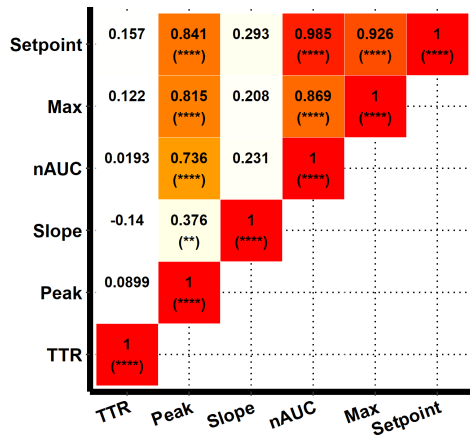
This correlation analysis pointed out the absence of the correlations between the time to rebound and both the slope and the setpoint. The TTR and the setpoint are two virological endpoint widely recommended to assess vaccine efficacy in HIV therapeutic vaccine trials (Julg et al. 2019). While the TTR is usually



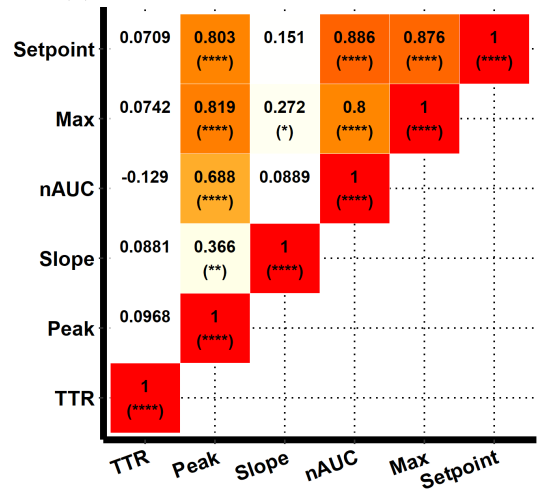
(a) LIGHT Placebo



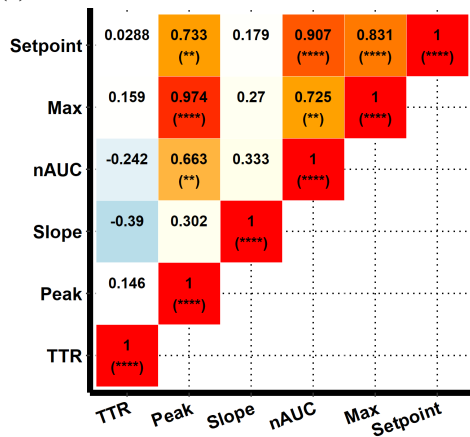
(b) LIGHT Vaccine



(c) ILIAD Control



(d) ILIAD IL2



(e) DALIA

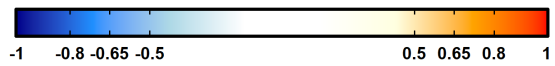


Figure 8 – Spearman correlation matrices of the virological descriptors. Heatmaps of the Spearman correlations between the five main descriptors and the maximum value. Color gradient represents the magnitude of the correlations with the red and the blue scales indicating positive and negative correlations, respectively. P values, adjusted for test multiplicity with Benjaminin and Hochberg correction, are given in brackets such as: (*): $p \leq 0.05$, (**): $p \leq 0.01$, (***): $p \leq 0.001$, (****): $p \leq 0.0001$.

used to evaluate the curative effect of the vaccine, the setpoint is used when the ability of the therapeutic treatment to control the virological rebound, and by extension the HIV reservoir, is evaluated. The absence of correlation between these two endpoints emphasizes this differentiation and shows the impossibility to use the TTR as surrogate of the setpoint in ATI. The two weak and non-significant relationships of the TTR with the setpoint and the slope suggest an independence between the time required to reach visible viral replication and both the speed of the rebound and the viral level at which the HIV RNA load dynamics could stabilize after the peak in the settings of these trials. In other words, the virological rebound being related the HIV reservoir, the capacity of the immune system to control the virus as well as the speed of the rebound are not conditioned by the reactivation of the reservoir. In addition to the slope and the setpoint, the TTR appears as uncorrelated to the peak of the rebound. Consequently, the magnitude of the rebound is not directly linked to the time required to reach visible viral replication.

As shown in Figure 8, we identified a low significant and positive correlation between the slope and the peak of the rebound for all groups, except for LIGHT placebo. According to the sign of the correlation coefficients, the magnitude of the rebound might be related to its speed such that the faster the viral rebound, the stronger it is. However, the absence of significance of this relationship in DALIA as well as the value of the correlation coefficients might mitigate this result.

The most unexpected result revealed in the correlation matrices, apart from the one of the group LIGHT Placebo, is the absence of correlation between the slope and the setpoint. In that respect, the ability of a patient and its immune system to control the viral replication is independent from the speed of the rebound and thus the power of the viral reservoir to restart the viral replication and widespread the virus in the human body. This result translates the fact that a patient with a strong HIV reservoir, inducing a fast rebound and overwhelming the immune system after cART interruption, can have a strong enough adaptive immune system to better control the virus at the end than an individual with a weaker reservoir. This non-significant relationship being observed in both therapeutic and control groups, the control of the virus is not induced by the vaccine efficacy. Finally, these non-significant relationships spotlight the absence of correlation between the early part of the viral rebound dynamics, which is mostly related to the action of the HIV reservoir, and the end of the dynamics which characterize the ability of the immune system to control the virus.

In the five groups of treatment, strong significant and positive correlations were identified between the setpoint and both the peak and the nAUC of the viral dynamics. The correlations between the setpoint the peak, ranging from 0.575 to 0.841, indicate that the lower the magnitude of the rebound, the more the patient is able to stabilize his viral load at a low level. Despite the strength of these correlations, within each group the relationship between the nAUC and the setpoint is described by higher correlation coefficient, ranging from 0.789 to 0.985. In both DALIA and ILIADE, correlations appear as stronger than in LIGHT. This result is accordance with the fact for patients showing an immune control of the virus, the longer the follow-up, the more the nAUC is correlated to the setpoint. As a matter, as already mentioned in the descriptive analysis of the nAUC, the more longer and stable the follow-up, the more the weight of the beginning of the dynamics in nAUC calculation decreases. In other words, assuming a patient infinitely, when the time of the follow-up tends to infinity, the nAUC tends to the setpoint. Nevertheless, even in a short-term follow-up like in LIGHT, nAUC is strongly correlated with the setpoint. Moreover, contrary to the peak which characterizes the dynamics only at a specific time, the nAUC is able to reflect the entire dynamics and its evolution can be followed over time.

To conclude, among all of our virological descriptors, the nAUC appears as the most reliable one to be used as surrogate of the setpoint. In the following of this work, we focused only on the nAUC.

The crucial choice of the right censoring threshold of the viral load inducing study dropout

The results of the correlation analysis evaluating the impact the right censoring of the viral load on the correlation between the true setpoint and the censored nAUC is displayed in Figure 9. In particular, we studied six scenarios: (1) correlation between the setpoint and $nAUC_{100000}$, (2) correlation between the

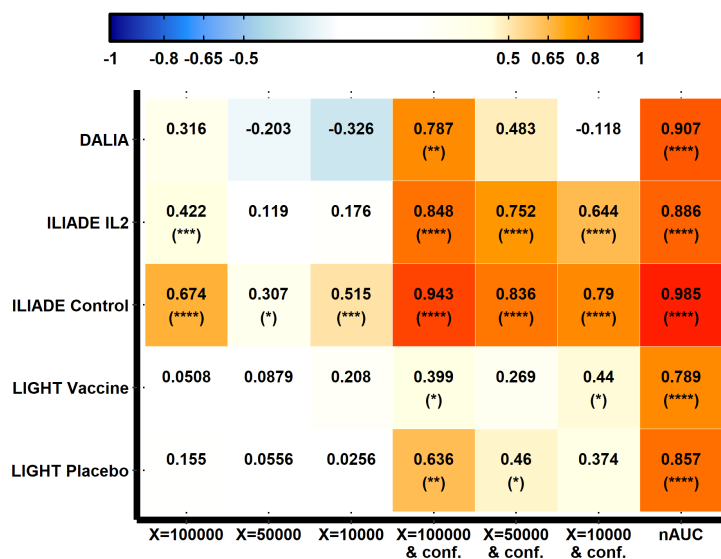


Figure 9 – Spearman correlations between the setpoint and the right censored nAUC. Each row represents the heatmap of the correlations between the setpoint and the right censored nAUC within one of the five groups of treatment. The first three columns show the correlation with the nAUC censored at the level X, without confirmation measure and the following three columns show the same correlation with a confirmation measure. The last column represents the correlations without any right censoring of the nAUC. Three for the threshold X were considered: 100 000, 50 000 and 10 000 cp/mL. Color gradient represents the magnitude of the correlations with the red and the blue scales indicating positive and negative correlations, respectively. P values, adjusted for test multiplicity with Benjaminin and Hochberg correction, are given in brackets such as: (*): $p \leq 0.05$, (**): $p \leq 0.01$, (***): $p \leq 0.001$, (****): $p \leq 0.0001$.

setpoint and $nAUC_{50000}$, (3) correlation between the setpoint and $nAUC_{10000}$, (4) correlation between the setpoint and $nAUC_{100000}^{conf}$, (5) correlation between the setpoint and $nAUC_{50000}^{conf}$ and (6) correlation between the setpoint and $nAUC_{10000}^{conf}$. To evaluate the impact of the right censoring on the magnitude and the significance of the correlation between the two descriptors of interest, we compared the results for each scenario to the correlations obtained in the previous analysis between the setpoint and nAUC (column 7 in Figure 9). Without confirmation measures, the significance of the correlations between the two descriptors is lost in most of the cases. Except for ILIADE depicting significantly positive correlations for the highest threshold value for ILIADE IL2 and for the values of X for ILIADE control, all other correlation coefficients were estimated as lower than 0.326, in absolute value. The nAUC being evaluated here as surrogate of the setpoint characterising the efficacy of the vaccine the control the viral replication after cART interruption, the use of such cART resumption criteria would led to a wrong conclusion about the vaccine efficacy. The high correlation obtained in ILIADE for the threshold of 100 000 copies/mL, compared to LIGHT and DALIA, could be explained by the longer time interval between two observations. As a matter of fact, the peak of the dynamics for these groups being mostly observed before the week 8 and higher than 10 000 copies/mL (see Figure 7b), the probability to be censored before the patients enrolled in ILIADE is extremely high. The consideration of a measure of confirmation allows to retrieve higher positive correlation coefficients. In particular, the choice of the highest value of the right censoring threshold exhibits significant and positive correlations for the five groups. To conclude, as expected, these initial results pointed out the necessity of using a confirmation measure and consider the highest value of the right censoring threshold as possible. Indeed, both of these elements allow a longer follow-up of the patient. Consequently, the difficulty results in the identification of the value of the threshold allowing the right balance between the longer and the safer follow-up for the patients.

The estimation of the correlation between the setpoint and both the $nAUC_X$ and $nAUC_X^{conf}$ for a right censoring threshold ranging from 10^2 to 10^6 (or 2.0 to 6.0 \log_{10} copies/mL) allowed to graphically visualize the dependence of the correlation coefficient to the value of the threshold and confirmed the necessity of a confirmation measure.

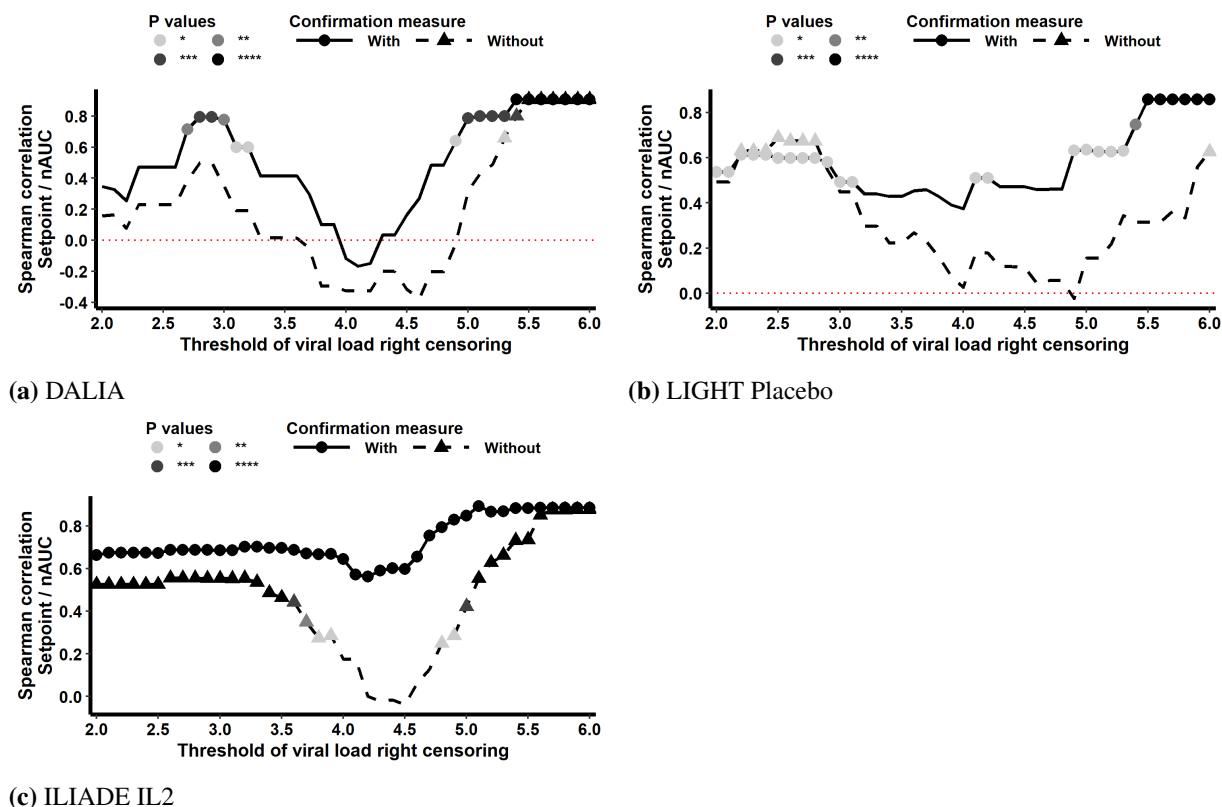


Figure 10 – Evolution of the correlation between the setpoint and nAUC as function of the right censoring threshold. The y-axis represents the values of the right censoring threshold, and the y-axis the Spearman correlation coefficient between the setpoint and the censored nAUC. The setpoint estimated on the raw data (without right censoring) is considered. Solid lines and dashed lines represent the results with and without a confirmation measure in the calculation of the nAUC. Significant correlations are highlighted by colored circles (with confirmation measure) and triangles (without confirmation measure). The darker the dots, the more significant the correlation. The vertical red dotted line display the transition from positive and negative correlations.

In Figure 10, displaying the results for the two groups DALIA and LIGHT Placebo (Figures 10a and 10b), whatever the value of the right censoring threshold, the consideration of a confirmation measure before cART resumption provides an higher correlation than without it. Moreover, two ranges of threshold lead to the possibility of significant correlations: a) lower than 3.0 and b) higher than 5.0 \log_{10} copies/mL. The first one arises from the fact that a too low cut-off only select data closed to the limit of detection and on a really short follow-up which reduce the variability of the estimated nAUC. Despite the significance of these relationships, the choice of such low threshold has no biological sense as no viral rebound can be observed or at least initiated. Accordingly, the choice of a threshold higher than 100 000 copies/mL with a confirmation measure seems to be the optimal scenario to retrieve a significant and positive correlation closed to the one estimated without right censoring. Moreover, as showed on the Figure, the use of a threshold between 3 000 and 50 000 \log_{10} copies/mL is not advised for those data. In ILIAD trial (see Figure 10c), despite the impact of the large time interval between two observations on the value and the significance of correlations,

results confirm the benefit of the confirmation measure and the additional care required for right censoring thresholds between 10 000 and 100 000 copies/mL.

Discussion

In this work, we analyzed the dynamics of the viral rebound induced by cART interruption in HIV therapeutic vaccine trials. We applied a descriptive method breaking down the viral dynamics as a multitude of virological descriptors and using Spearman correlations to determine the one that could be used as an early surrogate of the setpoint, and by extension a primary outcome in trials assessing vaccine efficacy. The descriptive and correlation analysis of these virological descriptors on data from the three HIV trials LIGHT, ILIADE and DALIA allowed us to identify the nAUC as the optimal endpoint. In addition to the nAUC, the peak of the rebound depicted similar properties than nAUC. Furthermore, this study gave us the opportunity to highlight unexpected properties of the dynamics of the viral rebound. Due to the absence of significant correlations of the time to rebound and the slope with the setpoint, we found a total independence between the early part of the dynamics and the stabilization of the viral load after the peak. By extension, these results could be explained by the interplay of two immunological mechanisms: the activation of the HIV reservoir causing the relaunch of viral replication, and the efficacy of the adaptive immune system to counteract the spread of the virus and control, at least for short-term periods, the viraemia of the host. Finally, the consideration of an upper virological threshold as cART resumption criteria allowed to identify the value of 100,000 copies/mL as an acceptable viraemia cut-off to maintain the optimal properties of the nAUC as primary outcome. However, we pointed out the necessity of a confirmation measure validate cART resumption inducing study dropout.

Initiated during the protocol development of the HIV-1 therapeutic vaccine trial EHVA T02 (NCT04120415), these findings allowed to optimize the choice of its primary and secondary outcomes and cART resumption criteria during ATI. Accordingly to our results, the AUC was defined as the primary outcome while the time from cART interruption to the right censoring threshold of 100,000 copies/mL, with a confirmation measure, as well as the peak and the setpoint were used as secondary outcomes. Finally, in addition to the commonly defined criteria, a confirmed rebound of the viral load above the virological threshold of 100,000 copies/mL was used as preliminary cART resumption criteria.

Although this work provided crucial results, our approach has some limitations. First of all, we performed our analysis as a pure descriptive method considering HIV RNA load measurements as the true observations. Therefore, all measurement errors, arising for instance from measurement techniques, were neglected. By definition, this omission led to a greater or lesser underestimation of the variability of our data. Statistical tests performed on this work, such as t-tests or Spearman correlations, being dependent on the variance of our data, the underestimation of the variance may lead to biased results (Ree & Carretta 2006). In particular, the greater the measurement error, the more the chance to wrongly conclude to non-significant result increases (Charter 1997). To overcome this issue, some corrections have been proposed to take into account error measurements in classic statistics (Durvasula et al. 2012, Kitagawa et al. 2018, Kim & Wilhelm 2021).

As widely mentioned in the Results section, the estimation of the virological descriptors, and by extension the results and the conclusion of this work, are highly dependent on the designs of the three studied trials (LIGHT, ILIADE and DALIA). In particular, we showed that the variability of the ATI period influenced the calculation of the nAUC and the time interval between two observations may play a role on the estimation of the peak, the TTR or the slope. For that reason, we mainly focused on the results obtained on DALIA to optimize the protocol of EHVA T02, these two latter having quite closed study design.

Another limitation of the proposed approach is the fact that we limited the analysis to HIV RNA load dynamics. As a matter of fact, CD4+ T cell being the main target cells of HIV virus, CD4 count are widely monitored in HIV vaccine trials and a lower bound of CD4 count is usually defined as cART resumption

criteria (e.g. 350 cells/mm³ in EHVA T02). The combined analysis of HIV RNA load and CD4 count may lead to a more global overview of the situation and even identify descriptors of CD4 count dynamics (e.g. initial value, slope of the decrease, setpoint) as new surrogate of the virological setpoint. Similarly, baseline and demographic characteristics of the patients could bring additional information. In particular, additional work may be conducted to identify whether some characteristics are specific to good responders by adjusting virological descriptors for patient characteristic. Trials with high samples should be considered for this type of analysis to ensure the power of the results.

Finally, as mentioned in the descriptive analysis, the estimation of virological descriptors is highly dependent on the study design. Accordingly, the extension of this work to a modeling approach, using in particular mechanistic models based on ordinary differential equations, appears as relevant and could allow to integrate both viral load and CD4 count in the analysis.

References

- Barton, K., Winckelmann, A. & Palmer, S. (2016), 'Hiv-1 reservoirs during suppressive therapy', *Trends in microbiology* **24**(5), 345–355.
- Benjamini, Y. & Hochberg, Y. (1995), 'Controlling the false discovery rate: a practical and powerful approach to multiple testing', *Journal of the Royal statistical society: series B (Methodological)* **57**(1), 289–300.
- Brundage, T. M., Vainorius, E., Chittick, G. & Nichols, G. (2018), 'Brincidofovir decreases adenovirus viral burden, which is associated with improved mortality in pediatric allogeneic hematopoietic cell transplant recipients', *Biology of Blood and Marrow Transplantation* **24**(3), S372.
- Charter, R. (1997), 'Effect on measurement error on tests of statistical significance', *Journal of clinical and experimental neuropsychology* **19**(3), 458–462.
- Cobb, A., Roberts, L. K., Palucka, A. K., Mead, H., Montes, M., Ranganathan, R., Burkeholder, S., Finholt, J. P., Blankenship, D., King, B. et al. (2011), 'Development of a hiv-1 lipopeptide antigen pulsed therapeutic dendritic cell vaccine', *Journal of immunological methods* **365**(1-2), 27–37.
- Cohn, L. B., Chomont, N. & Deeks, S. G. (2020), 'The biology of the hiv-1 latent reservoir and implications for cure strategies', *Cell host & microbe* **27**(4), 519–530.
- Deeks, S. G., Lewin, S. R. & Havlir, D. V. (2013), 'The end of aids: Hiv infection as a chronic disease', *The lancet* **382**(9903), 1525–1533.
- Durvasula, S., Sharma, S. & Carter, K. (2012), 'Correcting the t statistic for measurement error', *Marketing Letters* **23**(3), 671–682.
- Dybul, M., Attoye, T., Baptiste, S., Cherutich, P., Dabis, F., Deeks, S. G., Dieffenbach, C., Doehle, B., Goodenow, M. M., Jiang, A. et al. (2021), 'The case for an hiv cure and how to get there', *The Lancet HIV* **8**(1), e51–e58.
- Hill, J. A., Mayer, B. T., Xie, H., Leisenring, W. M., Huang, M.-L., Stevens-Ayers, T., Milano, F., Delaney, C., Jerome, K. R., Zerr, D. M. et al. (2018), 'Kinetics of double-stranded dna viremia after allogeneic hematopoietic cell transplantation', *Clinical Infectious Diseases* **66**(3), 368–375.
- Julg, B., Dee, L., Ananworanich, J., Barouch, D. H., Bar, K., Caskey, M., Colby, D. J., Dawson, L., Dong, K. L., Dubé, K. et al. (2019), 'Recommendations for analytical antiretroviral treatment interruptions in hiv research trials—report of a consensus meeting', *The lancet HIV* **6**(4), e259–e268.
- Kim, D. & Wilhelm, D. (2021), Powerful t-tests in the presence of nonclassical measurement error, Technical report, cemmap working paper.
- Kitagawa, T., Nybom, M. & Stuhler, J. (2018), Measurement error and rank correlations, Technical report, cemmap working paper.
- Kosulin, K., Pichler, H., Lawitschka, A., Geyeregger, R. & Lion, T. (2019), 'Diagnostic parameters of adenoviremia in pediatric stem cell transplant recipients', *Frontiers in microbiology* **10**, 414.

- Larijani, M. S., Ramezani, A. & Sadat, S. M. (2019), 'Updated studies on the development of hiv therapeutic vaccine', *Current HIV research* **17**(2), 75–84.
- Leal, L., Fehér, C., Richart, V., Torres, B. & García, F. (2020), 'Antiretroviral therapy interruption (ati) in hiv-1 infected patients participating in therapeutic vaccine trials: surrogate markers of virological response', *Vaccines* **8**(3), 442.
- Lévy, Y., Lacabaratz, C., Lhomme, E., Wiedemann, A., Bauduin, C., Fenwick, C., Foucat, E., Surenaud, M., Guillaumat, L., Boilet, V. et al. (2021), 'A randomized placebo-controlled efficacy study of a prime boost therapeutic vaccination strategy in hiv-1-infected individuals: Vri02 anrs 149 light phase ii trial', *Journal of Virology* **95**(9), e02165–20.
- Lévy, Y., Thiébaud, R., Gougeon, M.-L., Molina, J.-M., Weiss, L., Girard, P.-M., Venet, A., Morlat, P., Poirier, B., Lascaux, A.-S. et al. (2012), 'Effect of intermittent interleukin-2 therapy on cd4+ t-cell counts following antiretroviral cessation in patients with hiv', *Aids* **26**(6), 711–720.
- Lévy, Y., Thiébaud, R., Montes, M., Lacabaratz, C., Sloan, L., King, B., Pérusat, S., Harrod, C., Cobb, A., Roberts, L. K. et al. (2014), 'Dendritic cell-based therapeutic vaccine elicits polyfunctional hiv-specific t-cell immunity associated with control of viral load', *European journal of immunology* **44**(9), 2802–2810.
- Ree, M. J. & Carretta, T. R. (2006), 'The role of measurement error in familiar statistics', *Organizational Research Methods* **9**(1), 99–112.
- Thiébaud, R., Hejblum, B. P., Hocini, H., Bonnabau, H., Skinner, J., Montes, M., Lacabaratz, C., Richert, L., Palucka, K., Banchereau, J. et al. (2019), 'Gene expression signatures associated with immune and virological responses to therapeutic vaccination with dendritic cells in hiv-infected individuals', *Frontiers in immunology* **10**, 874.
- Vanham, G. & Van Gulck, E. (2012), 'Can immunotherapy be useful as a “functional cure” for infection with human immunodeficiency virus-1?', *Retrovirology* **9**(1), 1–21.
- Vella, S., Schwartländer, B., Sow, S. P., Eholie, S. P. & Murphy, R. L. (2012), 'The history of antiretroviral therapy and of its implementation in resource-limited areas of the world', *Aids* **26**(10), 1231–1241.
- Wissler, C. (1905), 'The spearman correlation formula', *Science* **22**(558), 309–311.
- Zecca, M., Wynn, R., Dalle, J.-H., Feuchtinger, T., Vainorius, E., Brundage, T. M., Chandak, A., Mozaffari, E., Nichols, G. & Locatelli, F. (2019), 'Association between adenovirus viral load and mortality in pediatric allo-hct recipients: the multinational advance study', *Bone marrow transplantation* **54**(10), 1632–1642.

3.3 Perspectives

The descriptive data analysis performed on multiple clinical trials allowed us to identify the time-averaged AUC as a valid and powerful surrogate endpoint for the setpoint. Nevertheless, in this analysis, we did not directly consider the effect that missing data could have on this criteria. Consequently, we propose in the next chapter (Chapter 4) an extension of this work to evaluate the impact of missing data, induced by premature ART resumption (or study dropout), on the AUC calculation and we present a parametric statistical test evaluating the difference of AUC between two groups of treatment when data are subject to both left-censoring and study dropout.

Chapter 4

Endpoints in HIV therapeutic vaccine trials

Abstract: In this chapter, we focus on the development of a robust statistical test to compare between different treatment groups summary statistics of longitudinal dynamics, such as the area under the curve of the outcome of interest (AUC). In particular, we are interested in the case of longitudinal data affected by MAR monotonic missing data due to study dropouts, leading to biases in the calculation of AUC. We then propose a parametric test based on spline mixed-effects models to account for this bias. In a simulation of two-arm trials, we demonstrate the good statistical performances of this test compared to commonly used ad hoc methods as well as to a nonparametric test. Continuing from the previous chapter, we apply this methodology in the context of two clinical trials of therapeutic vaccines against HIV that require interruption of antiretroviral treatment (ART) to account for vaccine efficacy. AUC is then used as the criterion for endpoint and viral load level as the criterion for early ART treatment resumption and thus study discontinuation. A preliminary work to extend this method to mechanistic models based on ordinary differential equations is also proposed at the end of the chapter and consists of a comparison of three models to describe viral load rebound after ART interruption.

Keywords: HIV ; Therapeutic vaccine ; ATI ; Efficacy ; AUC ; Missing data ; Study dropout ; Censoring ; Bias ; Parametric test ; Mixed-effects model ; Clinical trial

Dissemination:

▷ **Publication in international peer-reviewed journal**

[Alexandre, M., Prague, M., & Thiébaud, R. \(2021\). Between-group comparison of area under the curve in clinical trials with censored follow-up: Application to HIV therapeutic vaccines. *Statistical Methods in Medical Research*, 30\(9\), 2130-2147.](#)

▷ **Written communication (poster) at international conference**

[Alexandre M, Prague M, Lévy Y, Thiébaud R. Comparison of AUC in clinical trials with follow-up censoring: Application to HIV therapeutic vaccines. *International Society for Clinical Biostatistics*, Krakow, Poland, 2020 \(Online\).](#)

▷ **Oral communication at national conference**

[Alexandre M, Prague M, Thiébaud R. Comparaison d'AUC entre groupe de traitement dans des essais avec censure de suivi : Application aux vaccins thérapeutiques contre le VIH. *Young Statisticians and Probabilists*, France, 2021 \(Online\)](#)

[Alexandre M, Prague M, Thiébaud R. Méthodes de comparaison d'aires sous la courbe dans des essais cliniques avec arrêt prématuré du suivi : Application aux vaccins thérapeutiques contre le VIH. *Journées de Statistique*, Nice, France, 2021 \(Online\).](#)

4.1 Introduction of the context

In the previous chapter, we identified, with a method based on the descriptive analysis of the virological trajectories, a statistically relevant surrogate marker of the HIV therapeutic vaccine efficacy. In particular, we pointed out that, in therapeutic vaccine trials using virological rebound dynamics induced by cART discontinuation (ATI) to account for vaccine efficacy, AUC is a good surrogate endpoint of the setpoint. Still positioning ourselves in the context of the design of the protocol of the phase II HIV therapeutic vaccine study EHVA T02 (NCT04120415), we want to be able to use the AUC to compare the vaccine efficacy between the different treatment arms.

In longitudinal studies, AUC is a measure widely used to summarize trajectories, either at individual or populational levels, and compared between groups of treatment (e.g. vaccinated group and placebo group) to evaluate some properties of the developed drugs. In the context of HIV-1 treatment development, AUC of plasma HIV RNA load, reflecting the total viral exposure over a period of time, is increasingly used to compare treatment effect between groups of treatment. For example, as described by [Li et al. \[2014\]](#), the time-averaged AUC was used as co-primary endpoint in a placebo-controlled trial evaluating the effect of a therapeutic rAd5 HIV-1 gag vaccine on the HIV-reservoir during a 16 week-ATI period. Since the AUC is defined as a summary measure, the use of classic statistical tests comparing means between treatment groups, such as the two-sample students parametric t-test [[Kim, 2015](#)] or the non-parametric Wilcoxon rank sum test [[Divine et al., 2013](#)], seems relevant. The null hypothesis is then defined as the equality of the mean AUCs or the identity of the AUC distribution [[Spritzler et al., 2008](#)]. Nevertheless, the specificity of the context of ATI requires special cares to develop a statistical test with great properties. In therapeutic vaccine trials with ATI period, the increasing risks of virological relapse incurred by HIV-infected patients while free of cART, makes prematurely cART resumption plausible. In particular, as studied in the previous chapter, cART resumption criteria are directly defined in the protocol to ensure patient safety, such as a right censoring threshold. Once cART prematurely resumed, the evaluation of the treatment efficacy is no longer possible for the given patient. Consequently, cART resumption is considered as a study dropout and all observations obtained from that specific time are categorized as missing data. Using the classification of missing data previously introduced in Chapter 2 (see section 2.2.1), early resumption of antiretroviral treatment in ATI period induces monotonic (once missing, always missing) MAR missing data. In the previous work, we pointed out the necessity to take into account a confirmation measure in the AUC calculation in

order to maintain a relevant association between the AUC and the setpoint. The benefit provided by this additional measure can be explained by the fact that, in presence of missing data, the AUC calculation is biased [Bell et al., 2014; Spritzler et al., 2008] (see Figure 4.1(a)). Despite the robustness of the classic statistical in the case of complete data, these later must be carefully used in the presence of missing data. In most cases, these tests are applied without any consideration of the incompleteness of the data which can lead to a biased estimate of the AUC calculation and consequently to a potential biased conclusion. In addition to missing data, it should be kept in mind that left-censoring may also be a source of bias in AUC calculation.

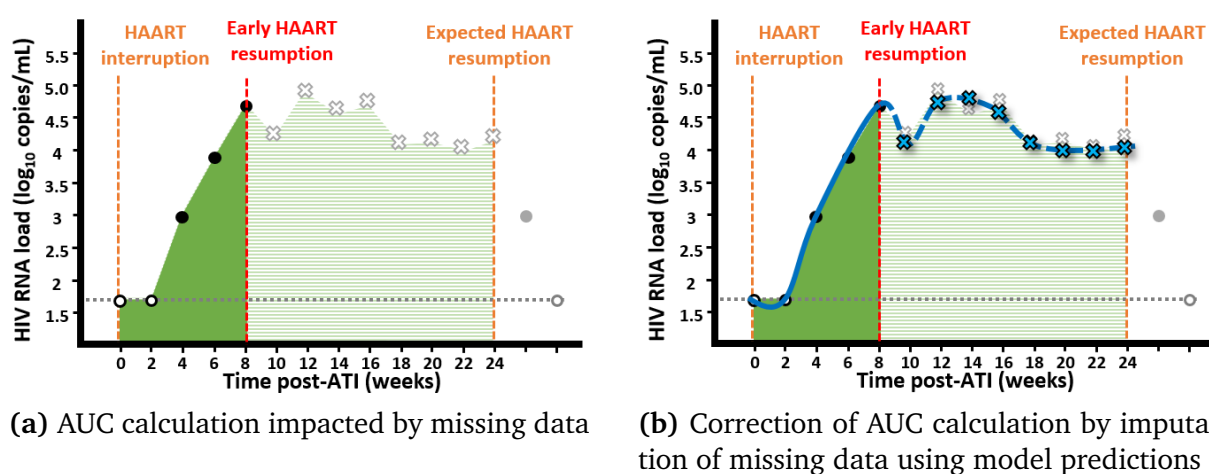


Figure 4.1 – Impact of early cART resumption on AUC calculation. Example of virological rebound dynamics after cART interruption impacted by a study dropout inducing missing data. Vertical orange dashed lines represent the expected duration of ATI. The vertical dashed red line display the premature cART resumption. White and black filled circles represent the observed data, either impacted or not by left-censoring, while gray crosses represent missing data, meaning data that should have been observed without early cART resumption. Dark green colored area displays the AUC calculated from cART interruption to the true cART resumption while the light green area displays the additional area that should have been calculated without study dropout. On Figure (b), blue crosses display data imputed as the predictions of a mathematical model estimated on observed data and the solid and dashed blue lines represent the estimation and the prediction of the model, respectively.

Accordingly, we aimed at proposing a statistical test comparing the AUC between groups of treatment taken into account MAR monotonic missing data as well as left-censored data. We proposed a statistical parametric test for AUC based on splines-based MEMs. As shown in Figure 4.1(b), the underlying idea behind this statistical test is that biased calculation of AUC could be corrected by "imputing" missing data using a mathematical model (e.g. mixed-effects model, mechanistic model) estimated on all patients via a population approach.

4.2. Between-group comparison of area under the curve in clinical trials with censored follow-up

This work was the subject of an article published in *Statistical Methods in Medical Research: Vol 30, Issue 9, 2021, Pages 2130-2147*, [[Alexandre et al., 2021](#)]. Supplementary information related to this article are available in Appendix A.

4.2 Between-group comparison of area under the curve in clinical trials with censored follow-up

Between-group comparison of area under the curve in clinical trials with censored follow-up: Application to HIV therapeutic vaccines

Statistical Methods in Medical Research
0(0) 1–18

© The Author(s) 2021

Article reuse guidelines:

sagepub.com/journals-permissions

DOI: 10.1177/09622802211023963

journals.sagepub.com/home/smm

Marie Alexandre^{1,2} , Mélanie Prague^{1,2} and Rodolphe Thiébaud^{1,2}

Abstract

In clinical trials, longitudinal data are commonly analyzed and compared between groups using a single summary statistic such as area under the outcome versus time curve (AUC). However, incomplete data, arising from censoring due to a limit of detection or missing data, can bias these analyses. In this article, we present a statistical test based on splines-based mixed-model accounting for both the censoring and missingness mechanisms in the AUC estimation. Inferential properties of the proposed method were evaluated and compared to ad hoc approaches and to a non-parametric method through a simulation study based on two-armed trial where trajectories and the proportion of missing data were varied. Simulation results highlight that our approach has significant advantages over the other methods. A real working example from two HIV therapeutic vaccine trials is presented to illustrate the applicability of our approach.

Keywords

Area under the curve, longitudinal data, statistical test, mixed-effects model, study drop out, left-censoring

1 Introduction

The area under the curve (AUC) is a summary measure commonly used in various applications when the outcome of interest is based on a quantitative variable such as a biomarker concentration. In pharmacokinetics, the AUC of the drug concentration versus time is typically analyzed to account for drug exposure and clearance from the body¹ or to evaluate the bioequivalence of vaccines,² or the quality of life by summarizing individual scores.^{3–6} In preclinical cancer drug screening tumor xenograft experiments, the ratio or the difference of AUC can be used to replace the commonly used treatment-to-control ratio^{7,8} or summarize symptoms⁹ to evaluate therapy effectiveness. In infectious diseases, the AUC can summarize the exposure to the HIV virus¹⁰ or influenza.^{11,12} When AUC is an outcome to be compared between arms in a clinical trial, estimates can be biased because of incomplete data. Two frequent sources for the lack of completeness can arise: censoring due to a limit of detection (LOD) of assay and study drop out.

In this context, various methods for the calculation of AUC have been proposed. Allisson et al.¹³ and Venter et al.¹⁴ compared different approaches based on incremental AUC. Incremental AUC consists in computing the AUC only for observations that are above a threshold, which can be viewed as particularly compelling when there

¹University of Bordeaux, Inria Bordeaux Sud-Ouest, Inserm, Bordeaux Population Health Research Center, SISTM Team, France

²Data Science Division, Vaccine Research Institute (VRI), Créteil, France

Corresponding author:

Mélanie Prague, University of Bordeaux, Inria Bordeaux Sud-Ouest, Inserm, Bordeaux Population Health Research Center, SISTM Team, UMR 1219, F-33000 Bordeaux, France.

Email: melanie.prague@inria.fr

is left-censored observations. However, Potteiger et al.¹⁵ pointed out the potential bias in resulting conclusions when using incremental AUC even in presence of complete data. Wilding et al.¹⁶ have developed an approach to evaluate treatment effect by comparing longitudinal data from two groups of patients through AUC calculation when data are subject to missing completely at random (MCAR) missingness process. Bell et al.¹⁷ extended this method to missing at random (MAR) data and incorporated the within-subject variability through random effects using linear mixed effects models (LMEMs). In both cases, the comparison of the mean AUC using maximum likelihood (ML) between groups was more robust than the comparison of the average individuals' AUC with standard two-sample t -tests. Furthermore, the estimation of the mean AUC using LMEM can be adapted to outcomes subject to left-censoring.¹⁸

In this paper, we propose a statistical parametric test for AUC based on splines-based MEMs which is extending the previously described approaches by adding flexibility in the modeling, accounting for left-censored data and dealing with MAR monotonic censored follow-up. Estimation of parameters in LMEMs model is possible using ML-based approach leading to robust inference in presence of right-censored¹⁹ and left-censored outcome.^{20,21} To do so, we use an expectation-maximization EM algorithm for computing the maximum likelihood in nonlinear mixed effects models with censored response as describe in Vaida et al.²²

Multiple other non-parametric approaches have been developed to solve this type of problem. Schisterman and Rotnizky²³ developed a semi-parametric estimator of a K-sample U-statistic when data are missing at random combining information from both outcomes and auxiliary variables. Thereafter, Spritzler et al.²⁴ extended these results by proposing a valid semi-parametric two-sample test of equal AUC when observations are MAR monotonic and/or missing completely at random (MCAR). Both works are based on weighting approaches and thus require strong assumptions on the missing data process. Alternative non parametric tests have been developed by Vardi et al.²⁵ based on permutation tests. However, parametric approaches may help in the situation of incomplete data.

This work was motivated by the evaluation of HIV therapeutic vaccine in clinical trials where high rate of censoring can occur. The goal of the vaccines in HIV-infected patients is to boost the immune system to control the viral replication when antiretroviral treatments (ART) are interrupted. Hence, analytical treatment interruption (ATI) is the ultimate way to assess the ability of new vaccine strategies to control viral replication after ART discontinuation.²⁶ However, HIV-infected patients undergoing ATIs are subject to high risks of immune damage with expansion of the existing reservoir, clinical symptoms, resistance emergence, increased risk of HIV transmission as well as loss of therapeutic benefits from ART.^{27,28} Therefore, ATI periods are short and patients are followed carefully. Specification of criteria determining ART resumption may vary from one study to another: development of Grade-3 adverse events or AIDS-related events, the CD4 cell count fell below 350 cells/mm³, or a HIV RNA load exceeding a given virologic threshold.²⁹⁻³⁴ Following these criteria, ART resumption may occur before the end of the planned ATI period leading to missing data comparable to study drop out. Also, HIV RNA viral load is subject to left censoring due to LOD usually around 50 copies/mL.²⁰ Therefore, the comparison of AUC in HIV therapeutic vaccine trials constitutes a particularly relevant context for the application of the method described in the paper.

The article is structured as follows. In section 2, we briefly describe two HIV therapeutic vaccine studies which motivated the development of our ML based-model proposed approach to estimate the difference of mean AUCs between two groups of patients when observations are left-censored and subject to follow-up censoring presented in section 3. In section 4, we investigate the inferential properties of this method and compare them with both traditional methods and a non-parametric test through simulation studies. To illustrate the applicability of the approach, we provide a real working example from the two motivating examples in section 5. To conclude, we summarize the paper and propose future research in section 6.

2 Motivating examples

In this paper, we focus on two HIV therapeutic vaccine trials testing the efficacy of vaccines through ART interruption in HIV-1-infected patients. The first one is the HIV therapeutic vaccine trial VRI02 ANRS 149 LIGHT.³⁵ This study is a randomized double-blind, two-arm placebo-controlled Phase-II trial. Its primary objective was to evaluate the virological efficacy after ART interruption of a therapeutic immunization compared to a placebo. The therapeutic immunization is based on a recombinant DNA vaccine (GTU-MultiHIV B) and a lipopeptide vaccine (LIPO-5). This study enrolled 105 patients (35 in the placebo control group vs. 70 in the

vaccinated group) whose 91 of them (32 placebo and 59 vaccinated) experienced ATI. HIV RNA load was repeatedly measured at times 0, 2, 4, 6, 8 and 12 weeks after ATI. The second study is the HIV therapeutic vaccine trial ANRS 093 Vac-IL2 (Vac-IL2).³⁶ This study is a randomized two-arm placebo-controlled Phase-II trial enrolling 71 patients (37 in the control group and 34 in the vaccinated group). Its primary objective was to evaluate the immunogenicity of a therapeutic immunization strategy combining two different vaccines, recombinant ALVAC-HIV (vCP1433) and Lipo-6T (HIV-1 lipopeptides), followed by the administration of subcutaneous interleukin-2 (IL-2). Therapeutic immunization was followed by 12 weeks of ATI with repeated measures of HIV RNA load at times 0, 1, 2, 3, 4, 6, 8, 10, 12 weeks after ATI.

3 Method

3.1 Definition of the AUC by interpolation method

We consider N subjects divided into G vaccine arms, with $N = \sum_{g=1}^G n_g$, with n_g being the number of patient in group g . Let $Y_{ij,g}$ be the response measured for the subject i belonging to group g at its j th time point, $t_{ij,g}$, with $i \in \{1, \dots, N\}$, $j \in \{1, \dots, m_i\}$ and $g \in \{1, \dots, G\}$. Moreover, we define $\{t_{ij,g}\}$ as the set of time points at which data are observed for the patient i and $m_i = |\{t_{ij,g}\}|$ the cardinal of this set. At group level, we equivalently note $\{t_{j,g}\} = \cup_{i \in g} (\{t_{ij,g}\})$ the set of time points at which outcome of interest is measured for at least one patient in g , whose m_g is the cardinal. As defined, this framework allows the consideration of unbalanced group design and group-specific time points. The area under the response of interest curve can be calculated by the trapezoid interpolation method. The AUC summary measure for the i th subject belonging to the group g and summary statistics for the entire group g can then be approximated by the following equations. Without loss of generality, we define the lower limit of the integration interval as well as the first time point in each group as zero

$$\text{AUC}_i = \int_0^{T_i} Y_{i,g}(t) dt \simeq \sum_{j=2}^{m_i} \frac{(t_{ij,g} - t_{ij-1,g})}{2} (Y_{ij,g} + Y_{ij-1,g})$$

$$\text{AUC}_g = \int_0^{T_g} \bar{Y}_g(t) dt \simeq \sum_{j=2}^{m_g} \frac{(t_{j,g} - t_{j-1,g})}{2} (\bar{Y}_{j,g} + \bar{Y}_{j-1,g})$$

where $\bar{Y}_{j,g}$ is defined as the mean value of the outcome Y in the g th group at its j th time point, $\bar{Y}_{j,g} = \frac{1}{n_g} \sum_{i \in g} Y_{ij,g}$, $T_i = \max_j(\{t_{ij,g}\})$ and $T_g = \max_j(\{t_{j,g}\})$ the individual and group time of follow-up. Whereas the trapezoid method is known as the cumulative area over $m - 1$ time period in which the value of interest Y is approximated by a straight line between two adjacent points (t_{j-1}, y_{j-1}) and (t_j, y_j) , two other interpolation methods have been studied in this work to approximate AUC using either global or piecewise cubic polynomials instead of linear function: (1) the Lagrange method and (2) the Spline method (see Online Appendices A and B for more details, respectively). These methods are not described in the main body of the article as they provide similar results to the described trapezoid interpolation method.

When calculating individual's AUC, it is usual to divide the AUC by the delay of follow-up to take into account the variability in follow-up due to early drop-out for example.³⁷⁻⁴⁰ Although we propose in this article a method based on modeling that would allow to work directly on the raw AUC, we will use a normalized AUC (nAUC), that is the AUC divided by the number of days/weeks of follow-up, for the sake of comparison with individual level methods. The nAUC are given by equations (1) and (2)

$$n\text{AUC}_i = \frac{1}{T_i} \int_0^{T_i} Y_{i,g}(t) dt \simeq \frac{1}{T_i} \sum_{j=2}^{m_i} \frac{(t_{ij,g} - t_{ij-1,g})}{2} (Y_{ij,g} + Y_{ij-1,g}) \quad (1)$$

$$n\text{AUC}_g = \frac{1}{T_g} \int_0^{T_g} \bar{Y}_g(t) dt \simeq \frac{1}{T_g} \sum_{j=2}^{m_g} \frac{(t_{j,g} - t_{j-1,g})}{2} (\bar{Y}_{j,g} + \bar{Y}_{j-1,g}) \quad (2)$$

3.2 Estimation of nAUC by mixed effects model

We assume the MEM given by equation (3) to describe the outcome $Y_{ij,g}$ of the subject i in the group g_i at the j th time point

$$Y_{ij,g_i} = f_0(t_{ij,g_i}) + \sum_{g=1}^G \mathbb{1}_{[g_i=g]} \times F_g(t_{ij,g}) + h_i(t_{ij,g_i}) + \varepsilon_{ij} \quad (3)$$

where the function f_0 gathers all non-group-specific terms, e.g. an intercept, the functions F_g are non-linear smooth functions of time describing the fixed effect specific to each group and h_i are polynomial time-dependent random effects modeling the inter-individual variability. In the following, the functions F_g are set to linear combinations such as $F_g(t_{ij,g}) = \sum_{k=1}^{K_g} \beta_k^g f_k^g(t_{ij,g})$ where K_g is the number of time-dependent components describing the group-specific dynamics, e.g. spline basis, and β_k^g are the regression coefficients.

For generalization purpose, the LMEM given in equation (3) can be re-expressed with matrix formulation as follow

$$Y = X_0\gamma + X\beta + Zb + \varepsilon$$

where Y is the vector of the outcome of interest, X_0 , X , and Z are respectively the design matrices for the non-group- and group-specific fixed effects and random effects. Because vaccine or randomized controlled trials involve often adjustment of treatment effects on covariates, such as baseline covariates, the use of MEM allows it through the definition of the design matrices, whether at population, group or individual level. The vectors γ , β and b are the unknown non group- and group-specific fixed parameters and the random parameters respectively, while ε is the vector of error terms supposedly normally distributed such as $\mathbb{E}(\varepsilon) = \mathbf{0}$ and $\text{Var}(\varepsilon) = \Theta$. Moreover, we assume that $\mathbb{E}(b) = \mathbf{0}$ and $\text{Var}(b) = \Omega$, with $b \perp \varepsilon$. By construction, the matrix X is defined as a diagonal block matrix such as $X = \text{diag}(X_1, \dots, X_G)$, where each sub-matrix X_g is group-specific. Similarly, the vector β can be written as $\beta^T = (\beta^{1T}, \dots, \beta^{GT})$, each vector β^g being only specific to the group g . It can be demonstrated that the estimate of the nAUC in group g (2) can be re-expressed as a linear combination of the responses at each time, as

$$n\text{AUC}_g = \frac{1}{T_g} \sum_{j=1}^{m_g} w_{j,g} \bar{Y}_{j,g} = \frac{1}{T_g} \mathbf{w}_g^T \bar{\mathbf{Y}}_g \quad (4)$$

where $\mathbf{w}_g = (w_{1,g}, \dots, w_{m_g,g})^T$, $\bar{\mathbf{Y}}_g = (\bar{Y}_{1,g}, \dots, \bar{Y}_{m_g,g})^T$, with

$$w_{j,g} = \begin{cases} \frac{t_{j+1,g} - t_{j,g}}{2}, & j = 1 \\ \frac{t_{j,g} - t_{j-1,g}}{2}, & j = m_g \\ \frac{t_{j+1,g} - t_{j-1,g}}{2}, & \text{otherwise} \end{cases} \quad (5)$$

In our method, the approximation of the summary statistics nAUC is obtained post-estimation of the MEM parameters. To this end, we denote $\hat{\boldsymbol{\mu}}_g = \mathbb{E}(\hat{\mathbf{Y}}_g)$ being the expected value of the estimation of Y in the g th group, where $\hat{\boldsymbol{\mu}}_g = (\hat{\mu}_{1,g}, \dots, \hat{\mu}_{m_g,g})^T$ with $\hat{\mu}_{j,g} = \mathbb{E}(\hat{Y}_{j,g})$ and $\hat{\mathbf{Y}}_g = (\hat{Y}_{1,g}, \dots, \hat{Y}_{m_g,g})^T$. It follows that $\hat{\mu}_{j,g}$ is expressed as a linear combination of the fixed parameter estimates denoted $\hat{\boldsymbol{\beta}}$ and $\hat{\boldsymbol{\gamma}}$ for the group- and non-group-specific. Indeed, by noting $X_0^{[g]}$ the sub-matrix of X_0 corresponding to the group g , we obtain $\hat{\boldsymbol{\mu}}_g = X_0^{[g]} \hat{\boldsymbol{\gamma}} + X_g \hat{\boldsymbol{\beta}}^g$ leading to

$$\hat{\mu}_{j,g} = \sum_{v=1}^{\dim(\hat{\boldsymbol{\gamma}})} X_{0jv}^{[g]} \cdot \hat{\gamma}_v + \sum_{v=1}^{K_g} X_{g jv} \cdot \hat{\beta}_v^g$$

Replacing $\bar{\mathbf{Y}}_g$ by $\hat{\boldsymbol{\mu}}_g$ in equation (4), the approximation of nAUC in the group g , $n\widehat{\text{AUC}}_g$, can be written as

$$n\widehat{\text{AUC}}_g = \frac{1}{T_g} \mathbf{w}_g^T \hat{\boldsymbol{\mu}}_g \quad (6)$$

3.3 Statistical testing of difference between groups

We want to identify whether or not two groups of treatment can be differentiated by their mean value of the area under the response curve. Consequently, we defined the hypotheses of interest for the two compared groups g and \tilde{g} as the equality and the difference of their nAUC for the null hypothesis, H_0 and the alternative one, H_1 , respectively.

While the mechanism of follow-up censoring and the resulting missing data have no direct impact on the method of the MEM estimation, the statistical test must be written to take it into account. The presence of informative censoring impacting directly the time of follow-up and thus the time interval of AUC calculation for each group, $[0, T_g]$, the statistical test is build to compare the mean value of AUC on the same time interval. To do this, we define the upper integration limit for nAUC calculation as $T = \min(T_g, T_{\tilde{g}})$ given the time restricted nAUC for each group calculated as

$$n\widehat{\text{AUC}}_g^{\text{rest}} = \frac{1}{T} \int_0^T \widehat{\mu}_g(t) dt \simeq \frac{1}{T} \mathring{\omega}_g^T \widehat{\mu}_g^{\text{rest}} \quad (7)$$

where $\mathring{\omega}_g = (\omega_{1,g}, \dots, \omega_{m_g,g})^T$ and $\widehat{\mu}_g^{\text{rest}} = (\widehat{\mu}_{1,g}, \dots, \widehat{\mu}_{m_g,g})^T$ with $m_g = |\{t_{j,g} | t_{j,g} \leq T\}|$.

Based on equation (7) of the approximation of nAUC in the group g , the test hypotheses may be re-expressed in terms of model fixed parameters such as

$$H_0 : n\widehat{\text{AUC}}_g^{\text{rest}} = n\widehat{\text{AUC}}_{\tilde{g}}^{\text{rest}} \iff \frac{1}{T} \mathring{\omega}_g^T (\mathring{X}_0^{[g]} \widehat{\gamma} + \mathring{X}_g \widehat{\beta}^g) = \frac{1}{T} \mathring{\omega}_{\tilde{g}}^T (\mathring{X}_0^{[\tilde{g}]} \widehat{\gamma} + \mathring{X}_{\tilde{g}} \widehat{\beta}^{\tilde{g}}) \quad (8)$$

$$H_1 : n\widehat{\text{AUC}}_g^{\text{rest}} \neq n\widehat{\text{AUC}}_{\tilde{g}}^{\text{rest}} \iff \frac{1}{T} \mathring{\omega}_g^T (\mathring{X}_0^{[g]} \widehat{\gamma} + \mathring{X}_g \widehat{\beta}^g) \neq \frac{1}{T} \mathring{\omega}_{\tilde{g}}^T (\mathring{X}_0^{[\tilde{g}]} \widehat{\gamma} + \mathring{X}_{\tilde{g}} \widehat{\beta}^{\tilde{g}})$$

where $(g, \tilde{g}) \in (1, \dots, G)^2, g \neq \tilde{g}$ and $\mathring{X}_0^{[g]}$ and \mathring{X}_g , respectively, defined as $X_0^{[g]}$ and X_g but restricted to the time interval $[0, T]$. Because β and γ are the parameters of a mixed model and assuming normality hypothesis, it follows that their respective maximum likelihood estimates are approximately normally distributed following the laws $\mathcal{N}(\widehat{\beta}, \widehat{\text{Var}}(\widehat{\beta}))$ and $\mathcal{N}(\widehat{\gamma}, \widehat{\text{Var}}(\widehat{\gamma}))$ and implies that both $\widehat{\mu}_g^{\text{rest}}$ and $n\widehat{\text{AUC}}_g^{\text{rest}}$ are normally distributed. Let note $\widehat{\Sigma}$ the variance-covariance matrix of the estimated fixed parameters given by the inverse of the Fisher information matrix and $\widehat{\Sigma}^g$ the sub-variance covariance matrix of $(\widehat{\gamma}^T, \widehat{\beta}^{gT})^T \in \mathcal{M}_{\dim(\widehat{\gamma}) + K_{g,1}}(\mathbb{R})$. By construction we obtain, $\mathbb{E}(\widehat{\mu}_g^{\text{rest}}) = \mathring{X}_0^{[g]} \widehat{\gamma} + \mathring{X}_g \widehat{\beta}^g$, $\text{Var}(\widehat{\mu}_g^{\text{rest}}) = (\mathring{X}_0^{[g]} \mathring{X}_g) \widehat{\Sigma}^g (\mathring{X}_0^{[g]} \mathring{X}_g)^T$ and $\mathbb{E}(n\widehat{\text{AUC}}_g^{\text{rest}}) = \frac{1}{T} \mathring{\omega}_g^T \mathbb{E}(\widehat{\mu}_g^{\text{rest}})$, $\text{Var}(n\widehat{\text{AUC}}_g^{\text{rest}}) = \frac{1}{T^2} \mathring{\omega}_g^T (\mathring{X}_0^{[g]} \mathring{X}_g) \widehat{\Sigma}^g (\mathring{X}_0^{[g]} \mathring{X}_g)^T \mathring{\omega}_g$. Consequently, the asymptotic normal distribution of the estimated difference of the restricted nAUC between the two groups can be inferred with

$$\Delta n\widehat{\text{AUC}}_{g-\tilde{g}}^{\text{rest}} \sim \mathcal{N}\left(\mathbb{E}\left(\Delta n\widehat{\text{AUC}}_{g-\tilde{g}}^{\text{rest}}\right), \text{Var}\left(\Delta n\widehat{\text{AUC}}_{g-\tilde{g}}^{\text{rest}}\right)\right)$$

with $\mathbb{E}(\Delta n\widehat{\text{AUC}}_{g-\tilde{g}}^{\text{rest}}) = \frac{1}{T} \mathring{\omega}_{\tilde{g}}^T \mathbb{E}(\widehat{\mu}_{\tilde{g}}^{\text{rest}}) - \frac{1}{T} \mathring{\omega}_g^T \mathbb{E}(\widehat{\mu}_g^{\text{rest}})$ and $\text{Var}(\Delta n\widehat{\text{AUC}}_{g-\tilde{g}}^{\text{rest}}) = \mathring{\omega}^T (\mathring{X}_0 \mathring{X}) \widehat{\Sigma} (\mathring{X}_0 \mathring{X}) \mathring{\omega}$, $\mathring{\omega} \in \mathcal{M}_{m_g + m_{\tilde{g}}, 1}(\mathbb{R})$ being defined as $\frac{1}{T} (\mathring{\theta}^T, \mathring{\omega}_{\tilde{g}}^T)^T - \frac{1}{T} (\mathring{\omega}_g^T, \mathring{\theta}^T)^T$. For a test of the null hypothesis defined in equation (8), we can build the standard normally distributed Z-statistic given by

$$Z = \frac{\Delta n\widehat{\text{AUC}}_{g-\tilde{g}}^{\text{rest}}}{\sqrt{\text{Var}\left(\Delta n\widehat{\text{AUC}}_{g-\tilde{g}}^{\text{rest}}\right)}}$$

Under the null hypothesis, the Z-statistics follows a $\mathcal{N}(0, 1)$. By weighted averaging incomplete measures, the impact of potential heteroscedasticity is reduced due to the AUC-based approach. If still variance heterogeneity

between the group occur, the Z-statistics can be modified into a Student's t -test like statistics with degree of freedom τ (equals to ∞ in case of Z-statistic). As matter of fact, in case of remaining heterogeneity, data specific to each group should be fitted with specific and independent mixed effects model. The T-statistic resulting from this procedure will differ from our Z-statistic by its standard deviation simply defined as the squared root of the sum of the variances of the group-specific nAUC, and with a degree of freedom defined by the Satterthwaite approximation^{41,42}

$$\tau = \frac{\left(\text{Var}\left(\widehat{nAUC}_g^{\text{rest}}\right) + \text{Var}\left(\widehat{nAUC}_{\bar{g}}^{\text{rest}}\right) \right)^2}{\frac{\text{Var}\left(\widehat{nAUC}_g^{\text{rest}}\right)}{n_g-1} + \frac{\text{Var}\left(\widehat{nAUC}_{\bar{g}}^{\text{rest}}\right)}{n_{\bar{g}}-1}}$$

Similarly, in case of small sample size, our Z-test can be modified into Student's t -test with degree of freedom defined by the Kenward-Roger approximation.⁴³ Similarly to Bailer,⁴⁴ a $100(1-\alpha)\%$ confidence interval for $\Delta n\widehat{AUC}_{g-\bar{g}}^{\text{rest}}$ can be derived from the statistic, as

$$\Delta n\widehat{AUC}_{g-\bar{g}}^{\text{rest}} \pm z_{\tau, \alpha/2} \sqrt{\text{Var}\left(\Delta n\widehat{AUC}_{g-\bar{g}}^{\text{rest}}\right)}$$

where $z_{\tau, \alpha/2}$ is the $(1-\alpha/2)100^{\text{th}}$ percentile of the distribution.

An extension to k-sample design is straightforward deriving a one-way ANOVA testing the equality of normalized AUCs. Similarly to our Z-statistics, nAUCs are compared on the same interval of calculation $[0, T]$ with $T = \min_{g \in \{1, \dots, G\}}(T_g)$.

$$\begin{cases} H_0 : n\widehat{AUC}_1^{\text{rest}} = n\widehat{AUC}_2^{\text{rest}} = \dots = n\widehat{AUC}_K^{\text{rest}} , \\ H_1 : \exists(i, j) | n\widehat{AUC}_i^{\text{rest}} \neq n\widehat{AUC}_j^{\text{rest}} \end{cases}$$

where K is the number of groups compared by the k-sample test, $K \leq G$. Similarly to classic one-way ANOVA, we define the statistic F following Fisher law as

$$F = \frac{\frac{SS_{\text{between}}}{K-1}}{\frac{SS_{\text{within}}}{N_K - K}} \sim F(K-1, N_K - K)$$

where $N_K = \sum_{g=1}^K n_g$ and SS_{between} and SS_{within} define respectively the inter- and intra-group variability and are calculated as

$$SS_{\text{between}} = \sum_{g=1}^K n_g \left(n\widehat{AUC}_g^{\text{rest}} - \frac{1}{K} \sum_{k=1}^K n\widehat{AUC}_k^{\text{rest}} \right)^2$$

$$SS_{\text{within}} = \sum_{g=1}^K n_g^2 \text{Var}(n\widehat{AUC}_g^{\text{rest}})$$

4 Simulation study

In this section, we conduct a simulation study to analyze the statistical properties of our approach. The simulation setting is driven by the motivating examples described in section 2.

4.1 Generation of simulated data

We simulate longitudinal data mimicking a randomized HIV therapeutic vaccine trial involving two groups of treatment in which the outcome of interest is the HIV RNA load measurement. We simulated data using a LMEM as described by (9)

$$Y_{ij,g} = \gamma_0 + \mathbb{1}_{[g=1]} \sum_{k=1}^{K_1} \beta_k^1 \phi_k^1(t_{ij,1}) + \mathbb{1}_{[g=2]} \sum_{k=1}^{K_2} \beta_k^2 \phi_k^2(t_{ij,2}) + b_{0i} + \sum_{k=1}^{K_i} b_{ki} \Psi_k^i(t_{ij,g}) + \varepsilon_{ij} \quad (9)$$

where $Y_{ij,g}$ is the outcome of the i th subject belonging to the g th group at the j th time point where $i \in \{1, \dots, n_g\}$, $j \in \{1, \dots, m_g\}$ and $g \in \{1, 2\}$. In this model, the non-group-specific function f_0 is a global intercept labeled γ_0 , while random effects are described by individual smooth cubic B-splines curves defined as linear combination of the cubic B-spline basis $\Psi^i = (\Psi_1^i, \dots, \Psi_{K_i}^i)^T$ with $\mathbf{b}_i = (b_{1i}, \dots, b_{K_i i})^T$ as regression coefficients, $\forall i \in \{1, \dots, N\}$, $N = n_1 + n_2$. Similarly, the group-specific fixed effects are modeled by cubic B-spline curves with $\phi^g = (\phi_1^g, \dots, \phi_{K_g}^g)^T$ and $\beta^g = (\beta_1^g, \dots, \beta_{K_g}^g)^T$ as spline basis and regression coefficients, respectively. Random effects describing the inter-individual variability are assumed to be normally distributed $\mathbf{b} \sim \mathcal{N}(\mathbf{0}, \Omega)$ as well as the error terms $\varepsilon_{ij} \sim \mathcal{N}(0, \sigma_\varepsilon^2)$. Based on the HIV RNA load data from the Vac-IL2 trial (see section 2, *Motivating Examples*), we evaluated the regression coefficient estimates γ_0 , β^1 , β^2 and \mathbf{b} as well as the parameters K_g and K_i being respectively the number of spline basis involved in the group-specific and individual spline curves. The model involving a global intercept γ_0 , the splines basis have been built without including intercept terms making K_g and K_i equal to the sum of the number of internal knots and the degree (fixed at 3 in our case) of the respective spline curves.

For the purpose of examining the properties of the proposed approach developed to test the equality of nAUCs, we generate numerous vaccine trials. As illustrated in Figure 1, we simulated two types of mean trajectory profiles: one in which the timing of viral rebound is similar in control and treatment group but the magnitude of the rebound may differ, and one in which the timing of viral rebound is expected to be longer in the treatment group compared to the control group. Finally, outcomes are measured at a constant time interval such as $t = (0, 1, 2, \dots, 24)^T$ weeks and the number of patients by group $n = n_1 = n_2$ varied amongst 20, 50 and 100. They reproduce the trajectories found in the Vac-IL2 and LIGHT trials (see section 2, *Motivating Examples*). Based on the Vac-IL2 data, we set the values of $\sigma_\varepsilon^2 = 0.2$, the fixed intercept $\gamma_0 = -0.44$ and the fixed parameters of the first group of treatment ($g = 1$) seen as the control group, β^1 (see Table 1). The five fixed parameters of the treatment group in both profiles β^2 have been chosen such as given values of ΔnAUC_{1-2} are targeted to specific values. To test the properties of the method, we simulated data with ΔnAUC_{1-2} taking values of 0, -0.1 and $-0.25 \log_{10}$ cp/ml. We defined the number of fixed splines basis as $K_1 = K_2 = 5$ for both profiles with the two internal knots fixed at (0.25, 5.62) weeks for both groups in profile 1 and (0.25, 5.62) and (3.23, 7.63) weeks in profile 2 for control and vaccine groups, respectively. Similarly, we fixed the number of random spline basis $K_i = 5$ with (2.0, 4.5) weeks as internal knots in profile 1 and (2.0, 4.5) and (5.0, 8.0) weeks in Profile 2 for control and vaccine groups, respectively. Number and positions of internal knots have been optimally chosen on Vac-IL2 data by applying the R-package *freenknotspline*⁴⁵ using AIC as optimization criterion.

The covariance matrix of the random effects Ω is defined as diagonal such as $\Omega = \sigma_b^2 \mathbf{I}_{K_i+1}$ where the value of σ_b^2 has been chosen according to the targeted values of $\text{Var}(\text{nAUC}_g)$. The estimated variances of nAUC were 0.027 and 0.021, respectively, in the control and the treatment group in Vac-IL2 trial. Hence, in simulations, we tested the impact of the intra-group variability when $\text{Var}(\text{nAUC}_g)$ was equal to 0.02 and 0.1, in both groups.

We generated MAR monotonic missing data as follows. For each subject i at each time point j , the outcome $Y_{ij,g}$ was labeled as missing if $Y_{ij,g} \in \{Y_{ij,g} | \exists j' \leq j, \{Y_{ij',g} \geq \alpha\} \cap \{Y_{ij'-1,g} \geq \alpha\}\}$, with α being a fixed threshold. A patient dropped out from the trial if his/her HIV RNA load exceeded the threshold α at two consecutive time points. The subsequent measurements were considered as missing. We investigated the impact of the missing data on the robustness of the method by considering three values for the threshold α : 100,000 ($5 \log_{10}$), 50,000 ($\sim 4.7 \log_{10}$) and 10,000 ($4 \log_{10}$) cp/ml. As illustrated in Figure 2 for the profile 1, the percentage of drop-out in each trial was inversely linked to the value of α . Due to the difference of nAUC between the two groups, each

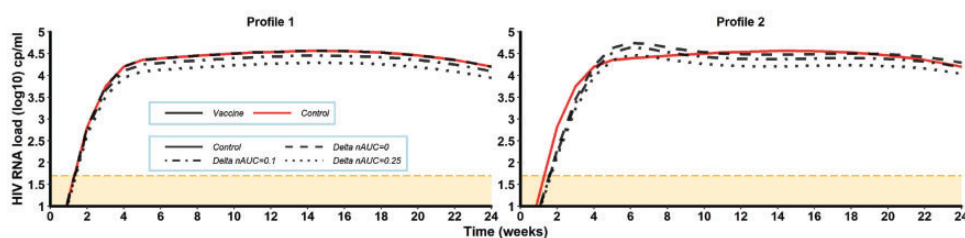


Figure 1. Simulated mean trajectories of HIV RNA load over time for both profiles 1 and 2. Note: Red solid line represents Group 1 (Control), dashed, dot dashed and dotted lines represent Group 2 (treatment) when $\Delta nAUC$ with Group 1 is equal to 0, -0.1 and -0.25 , respectively. Orange dashed line and area delimit the $LOD = \log_{10}(50)$. LOD: limit of detection.

Table 1. Fixed parameter values used to simulate control and vaccine groups for both profiles, according to $\Delta nAUC$ values.

Treatment group	Profile 1	Profile 2
Control group, β^1	($-0.55, 4.72, 4.96, 5.18, 4.64$)	($-0.55, 4.72, 4.96, 5.18, 4.64$)
$\Delta nAUC = 0, \beta^2$	($-0.55, 4.72, 4.96, 5.18, 4.64$)	($1.38, 5.57, 4.53, 5.20, 4.74$)
$\Delta nAUC = 0.1, \beta^2$	($-0.54, 4.61, 4.85, 5.07, 4.54$)	($1.35, 5.44, 4.43, 5.09, 4.63$)
$\Delta nAUC = 0.25, \beta^2$	($-0.52, 4.46, 4.69, 4.90, 4.39$)	($1.31, 5.26, 4.28, 4.92, 4.48$)

Note: The value of the global intercept was fixed at $\gamma_0 = -0.44$.

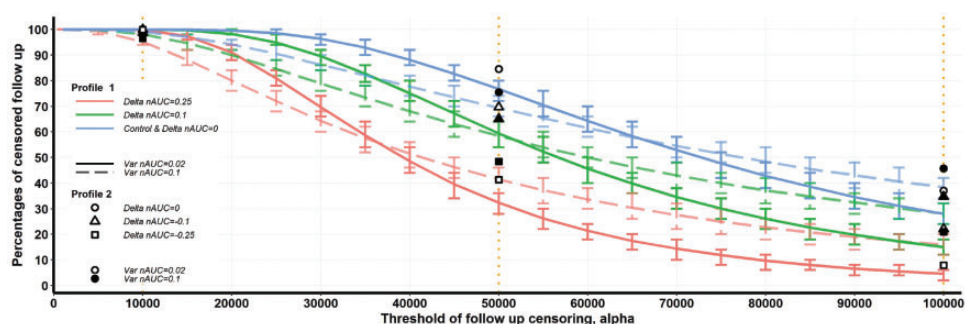


Figure 2. Percentages of censored follow-up when data simulated by both profiles are impacted by the threshold of lost of follow-up α . Note: Lines display percentages obtained for the profile 1 with solid and dashed lines representing data simulated with $Var(nAUC) = 0.02$ and 0.1 , respectively. Blue lines describe both Group 1 (Control) and Group 2 (treatment) when $\Delta nAUC$ with Group 1 is equal to 0, green and pink lines represent Group 2 when $\Delta nAUC = 0.1$ and 0.25 , respectively. Marks display percentages obtained for the Profile 2 with empty and full marks representing data simulated with $Var(nAUC) = 0.02$ and 0.1 , respectively. The squares, triangles and circles describe Group 2 when $\Delta nAUC = 0, 0.1$ and 0.25 with the control group in blue, respectively. Vertical dotted lines highlight the positions of $\alpha = 100,000, 50,000$ and $10,000$ cp/ml.

value of α generated both equal ($\Delta nAUC = 0$, blue curves) and unequal ($\Delta nAUC \neq 0$, blue curve for control and green/pink curves for treatment group) drop-out rates. While $\alpha = 100,000$ cp/ml led to approximately 30% of drop-out in control group and respectively 30%, 15% and 5% in treatment group when $\Delta nAUC = 0, 0.1$ and 0.25 , for $Var(nAUC) = 0.02$, these percentages increased respectively until 75%, 75%, 60% and 35% for $\alpha = 50,000$. Finally, the choice of $\alpha = 10,000$ allowed to test the method with extremely high percentages of drop-out which were in the neighborhood of 100%. The consideration of the second profile of data simulation led to a slight increase of these percentages of approximately 7% when the variance of $nAUC$ was equal to 0.1 and 10% for 0.02 .

We also generated left-censored outcomes using the limit of detection for viral load at $50 \sim 1.7 \log_{10}$ cp/ml, which has been chosen in accordance with values typically encountered in our motivating examples. This choice of LOD generated mean percentages of undetectable data in each group ranging from 7.30% to 7.70% for profile 1 and from 7.30% to 8.70% for profile 2, representing approximately two time points with undetectable outcome over 25.

4.2 Analysis of simulated data

We analyzed the simulated data using a well-specified model. Formulas for nAUC are derived from equation (9). MEM estimations took into account left-censored outcomes using an hybrid EM-algorithm implemented in the R-package *lmecc*.⁴⁶ Let note $(\widehat{\gamma}_0, \widehat{\boldsymbol{\beta}}^1, \widehat{\boldsymbol{\beta}}^2)^T$ the vector of the estimated fixed parameters where $\widehat{\boldsymbol{\beta}}^g = (\widehat{\beta}_1^g, \dots, \widehat{\beta}_{K_g}^g)^T$, for $g \in \{1, 2\}$. Using the model in equation (9), the expected value of Y in the g th group at any time $t_{j,g}$ is $\widehat{\mu}_{j,g} = \widehat{\gamma}_0 + \sum_{k=1}^{K_g} \widehat{\beta}_k^g \phi_k^g(t_{j,g})$, which allows to approximate the nAUC in each group, its variance and the difference in nAUC as follows

$$\begin{aligned} n\widehat{\text{AUC}}_g &= K_{\gamma g} \widehat{\gamma}_0 + \sum_{k=1}^{K_g} \widehat{\beta}_k^g C_{kg} \\ \Delta n\widehat{\text{AUC}}_{1-2} &= \widehat{\gamma}_0 (K_{\gamma 2} - K_{\gamma 1}) + \sum_{k=1}^{K_2} \widehat{\beta}_k^2 C_{k2} - \sum_{k=1}^{K_1} \widehat{\beta}_k^1 C_{k1} \\ \text{Var}(n\widehat{\text{AUC}}_g) &= (K_{\gamma g})^2 \text{Var}(\widehat{\gamma}_0) + \sum_{k=1}^{K_g} (C_{kg})^2 \text{Var}(\widehat{\beta}_k^g) + 2 \sum_{k=1}^{K_g-1} \sum_{\bar{k}=k+1}^{K_g} C_{kg} C_{\bar{k}g} \text{Cov}(\widehat{\beta}_k^g, \widehat{\beta}_{\bar{k}}^g) \\ &\quad + 2 \sum_{k=1}^{K_g} K_{\gamma g} C_{kg} \text{Cov}(\widehat{\gamma}_0, \widehat{\beta}_k^g) \end{aligned}$$

where C_{kg} and $K_{\gamma g}$ are defined by $C_{kg} = \frac{1}{T_g} \sum_{j=2}^{m_g} \frac{(t_{j,g} - t_{j-1,g})}{2} [\phi_k^g(t_{j,g}) + \phi_k^g(t_{j-1,g})]$ and $K_{\gamma g} = \frac{2}{T_g} \sum_{j=2}^{m_g} \frac{(t_{j,g} - t_{j-1,g})}{2}$.

For each combination of simulated datasets and missing data patterns, 1000 replications were performed with the objective of evaluating the robustness of the method to test the equality of areas under the curves between the two groups through its type-I error, its power and the bias in the estimation of the difference of nAUC. We compared the results provided by our method with a standard two-sample t -test for the difference of nAUC between the two groups, i.e. $H_0 : \overline{n\text{AUC}}_2 - \overline{n\text{AUC}}_1 = 0$ where $\overline{n\text{AUC}}_g = \frac{1}{n_g} \sum_{i=1}^{n_g} n\text{AUC}_i$ with $n\text{AUC}_i$ defined by equation (1). We performed this test without accounting for missing data and using two common ad hoc approaches: the last observation carried forward (LOCF) where missing data are imputed by the last observed value before the follow-up censoring, and the mean imputation where missing observations are imputed by the mean of the observations before this follow-up censoring.

In addition to the standard two-sample t -test, we compared our method with the t -test version of the non-parametric two-sample test proposed by Vardi et al.²⁵ This test was developed to compare a one-dimensional variable such as AUC between two groups of treatment when individual follow-up is subject to informative homogeneous or heterogeneous censoring. In order to be able to compare the results provided by this test and our method, we applied this test to normalized AUC. The test is based on U-statistics defined as

$$U_{m_1, m_2} = \frac{1}{m_1 m_2} \sum_{i_1=1}^{m_1} \sum_{i_2=1}^{m_2} D_{i_1, i_2}$$

where m_1 and m_2 are respectively the number of subjects in the first and the second compared groups, g_1 and g_2 , while D_{i_1, i_2} is defined as the paired cross-treatment contrast for the cross-treatment pair $(i_1, i_2) \in g_1 \times g_2$

$$\begin{aligned} D_{i_1, i_2} &= \frac{1}{T_{i_1} \wedge T_{i_2}} \int_0^{T_{i_1} \wedge T_{i_2}} [Y_{i_2, g_2}(t) - Y_{i_1, g_1}(t)] dt \\ &= \frac{1}{T_{i_1} \wedge T_{i_2}} \left[\text{AUC}_{i_2} \Big|_{[0, T_{i_1} \wedge T_{i_2}]} - \text{AUC}_{i_1} \Big|_{[0, T_{i_1} \wedge T_{i_2}]} \right] \end{aligned}$$

where $T_{i_1} \wedge T_{i_2} = \min(T_{i_1}, T_{i_2})$. The variable D_{i_1, i_2} is then defined as the difference of nAUC between the subjects i_1 and i_2 , restricted to their common time of follow-up. Similarly to the simulation studies conducted in their paper, we defined the variance of the U-statistic as equation (2.15) in Vardi's paper²⁵

$$\hat{\sigma}_{m_1, m_2}^2 = \sum_{i_1=1}^{m_1} \frac{(\bar{D}_{i_1.} - \bar{D}_{..})^2}{m_1(m_1 - 1)} + \sum_{i_2=1}^{m_2} \frac{(\bar{D}_{.i_2} - \bar{D}_{..})^2}{m_2(m_2 - 1)}$$

where $\bar{D}_{i_1.} = \sum_{i_2} D_{i_1, i_2}/m_2$, $\bar{D}_{.i_2} = \sum_{i_1} D_{i_1, i_2}/m_1$ and $\bar{D}_{..} = U_{m_1, m_2}$ and we considered the following null hypothesis H_0 : the distribution of D is symmetric about 0.

Five procedures are then compared for testing the equality of nAUC including three ad hoc methods respectively called Indiv. nAUC Data, Indiv. nAUC LOCF and Indiv. nAUC Mean Imp., the non-parametric test called NP nAUC and our approach called MEM nAUC.

4.3 Simulation results

The results of our simulations evaluating the robustness of the test of equality of nAUC are displayed in Table 2. Although only results for simulations involving $n_g = 50$ patients by group are presented in the main body of the article, extended results for $n_g = 20$ and 100 can be found in Online Appendix C, Tables C.2a and C.3a. In these simulations, as expected with a well-specified model, when there is no censored follow-up and no left censoring using individual nAUC, non-parametric approach or our method based on MEM nAUC are identical in term of type-I error, which are kept to their nominal level of 5% (between 0.044 and 0.06). However, the power seems to be consistently higher for MEM nAUC in particular when the inter-individual variability is high. When introducing the LOD at 50 cp/ml, the results are similar for profile 1 but tend to show a superiority of MEM nAUC for profile 2 in which there are a larger number of left-censored observations due to delay in viral rebound in one group. This is explained by the fact that MEM nAUC, contrary to individual nAUC involved either in indiv. nAUC or NP nAUC methods, accounts for left censoring instead of considering censored data fixed to their censorship level value. When the threshold of HIV RNA defining drop-out, α , is equal to 100,000 and 50,000 cp/ml, all individual methods (with or without adjustment for missing data) fail in term of type-I error in the second profile with lagged increasing trajectories of viral load (see Figure 1). Even when the type-I error is controlled such as for profile 1 (with the same shape of mean trajectories see Figure 1), the power for raw data and mean imputation approaches is low for most settings. While the NP nAUC method shows controlled type-I error between 0.048 and 0.057 for profiles 1 and 2 when α is equal to 100,000 cp/ml and for profile 1 when the threshold is equal to 50,000 cp/ml, we observe an inflation of the type-I error up to 0.075 for the second profile. On the contrary, the MEM nAUC method shows type-I error between 0.048 and 0.064 for profiles 1 and 2. When variability is low, the power is also good and higher than 76% for the two methods. In all cases, the power found in these settings is similar in magnitude to the power obtained when there is no censored follow-up and no left censoring for viral load. When the threshold α is equal to 10,000 copies/ml, while all individual methods and the non-parametric approach fail to control the type-I error for the profile 2, our approach MEM nAUC successfully gets a type-I error around the nominal value for both profiles. This result is mainly driven by the difference of the shapes of the mean trajectories for the two compared groups in Profile 2. In fact, as shown in Figure 1, the difference of nAUC appears as quite homogeneously distributed over the time of follow-up in profile 1 leading to robust results for all methods despite an early drop out for a high percentage of subjects. However, in profile 2, the value of $\Delta nAUC$ resulting from the compensation of the beginning and the end of the dynamics, only the parametric method is able to capture the true difference of nAUC regardless of the premature censored follow-up for more than 80% of individuals.

In addition, we graphically illustrated the estimated bias and standard error for $\Delta nAUC$ obtained for each method in Figure 3. For all profiles, when there is no drop-out or when the threshold α is high enough (equal to 100,000 and 50,000 cp/ml), the bias is closer to 0 for MEM nAUC compared to other methods. Also, the standard error of $\Delta nAUC$ calculated with MEM nAUC is similar to the non-parametric approach and closer to all the ad hoc individual methods to the theoretical values of standard error of $\Delta nAUC$, respectively 0.028 for $\text{Var}(nAUC) = 0.02$ and 0.063 for $\text{Var}(nAUC) = 0.1$. This mostly explains the comparable robustness between MEM nAUC and NP nAUC and their better performances in term of power compared to individual methods. When α is equal to 10,000 cp/ml, the inflated type-I errors observed for individual and non-parametric methods

Table 2. Comparison of the robustness of the test of equality of nAUC calculated as individual summary measures and mixed model summary statistics.

Data pattern	Methods	Profile 1				Profile 2				
		ΔnAUC	Type-I error	Power	Type-I error	Power	Type-I error	Power		
			0	-0.1	-0.25	0	-0.1	-0.25		
LOD	α	Var(nAUC)	0.02	0.1	0.02	0.1	0.02	0.1	0.02	0.1
		Indiv. nAUC	0.060	0.060	1.00	0.96	0.046	0.053	0.94	0.35
		NP nAUC	0.060	0.046	1.00	0.96	0.046	0.053	0.94	0.35
		MEM nAUC	0.059	0.055	1.00	0.99	0.044	0.056	0.95	0.44
		Control	0	0	0	0	0	0	0	0
Mean missing rate (%) ^a		Treatment	0	0	0	0	0	0	0	0
		Indiv. nAUC	0.056	0.049	1.00	0.97	0.062	0.063	0.89	0.30
		NP nAUC	0.056	0.049	1.00	0.97	0.062	0.063	0.89	0.30
		MEM nAUC	0.063	0.053	1.00	0.97	0.047	0.055	0.94	0.37
		Control	0	0	0	0	0	0	0	0
Mean missing rate (%)		Treatment	0	0	0	0	0	0	0	0
		Indiv. nAUC	0.060	0.054	1.00	0.79	0.540	0.526	0.92	0.37
		1. Data	0.052	0.045	1.00	0.96	0.281	0.170	0.31	0.11
		2. LOCF	0.059	0.053	1.00	0.80	0.529	0.500	0.83	0.65
		3. Mean Imp.	0.053	0.053	1.00	0.96	0.057	0.053	0.79	0.32
1.10 ⁵		NP nAUC	0.064	0.054	1.00	0.96	0.053	0.060	0.92	0.35
		MEM nAUC	28	38	27	39	28	38	28	38
		Control	28	38	27	39	28	38	28	38
		Treatment	28	38	5	16	37	46	22	8
		Indiv. nAUC	0.050	0.052	0.05	0.16	0.946	0.881	0.82	0.79
5.10 ⁴		1. Data	0.046	0.051	1.00	0.95	0.483	0.233	0.11	0.06
		2. LOCF	0.051	0.050	1.00	0.17	0.940	0.845	0.81	0.76
		3. Mean Imp.	0.048	0.053	1.00	0.93	0.069	0.075	0.77	0.44
		NP nAUC	0.063	0.060	1.00	0.95	0.048	0.051	0.76	0.31
		MEM nAUC	77	69	77	69	77	69	77	69
Mean missing rate (%)		Control	77	69	77	69	77	69	77	69
		Treatment	77	69	58	41	85	76	70	41
		Indiv. nAUC	0.041	0.057	0.06	0.07	0.894	0.868	0.91	0.87
		1. Data	0.058	0.043	0.20	0.68	0.555	0.421	0.18	0.11
		2. LOCF	0.039	0.050	0.04	0.07	0.746	0.725	0.83	0.76
1.10 ⁴		3. Mean Imp.	0.055	0.053	0.43	0.77	0.972	0.651	1.00	0.92
		NP nAUC	0.059	0.058	0.31	0.60	0.051	0.073	0.23	0.19
		MEM nAUC	100	99	100	99	100	99	100	99
		Control	100	99	100	95	100	100	100	99
		Treatment	100	99	98	100	100	99	100	99

AUC: area under the curve; nAUC: normalized AUC; NP: non parametric; Individual ad hoc methods (Indiv. nAUC): 1. Data: raw data, 2. LOCF: last observation carried forward, 3. Mean Imp.: mean imputation.

^a Missing rate: Percentage of subjects dropping out before the end of the study.

Note: Individual trajectories are subject to missing data and/or limit of detection. Simulations were performed for $n_g = 50$ subjects by group, mean trajectories following both profiles and for 1000 replications.

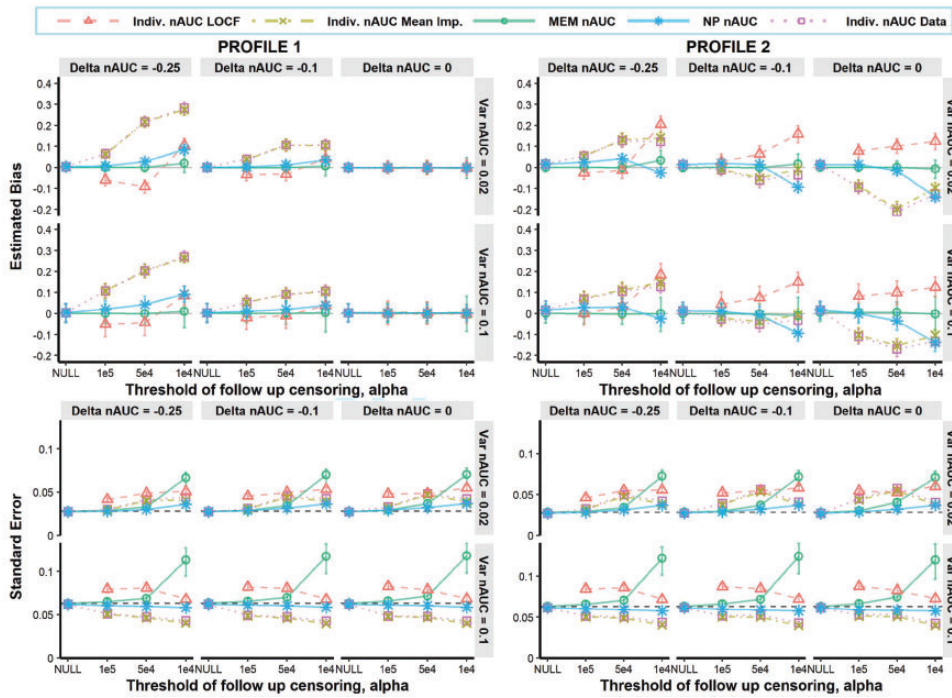


Figure 3. Comparison of the estimated bias and standard error of $\Delta nAUC$ obtained by the three individual methods Indiv. nAUC Data, Indiv. nAUC LOCF, Indiv. nAUC Mean Imp., the non-parametric test Non Param. and our method MEM nAUC. Both criteria were estimated for data subject to a LOD, with or without censored follow-up, with $n_g = 50$ subjects by group, mean trajectories following both profiles, for 1000 replications. Note: Pink dashed lines and triangles represent Ind. nAUC LOCF, green dot-dashed lines and crosses represent Indiv. nAUC Mean Imp., green solid lines and circles represent MEM nAUC, blue solid lines and stars represent NP nAUC and purple dotted lines with squares represent Indiv. nAUC Data. In standard Error plots, black dashed lines display the theoretical values (0.028 when $\text{Var}(nAUC) = 0.02$ and 0.063 for 0.1); LOCF: last observation carried forward.

are explained by biased estimates of $\Delta nAUC$ which are not compensated by an increased value of the standard error, unlike the MEM nAUC method.

4.4 Relaxing the correct model specification assumption

The validity of the method relies on the correct specification of the MEM as described in equation (3) in the section Method. To relax this assumption, we conducted additional simulations to evaluate the method when data are fitted with another MEM. To evaluate the performances in a setting closer to real-data, the number and position of the knots in the MEM defined in equation (9) were also estimated with the data. We used the R-package *freeknotspline* to estimate and replace the two sets of fixed two internal knots (2.0, 4.5) and (5.0, 8.0) involved in the build of group-specific spline curves by a set of knots optimizing the fit of data. Moreover, spline basis was built with external knots chosen as $(0, T_g)$ instead of $(0, 24)$ considering the real observed time of follow-up, which can be modified with censored follow-up. For each simulation, the number of internal knots for a given group is optimized between 1 and 3 as well as their position using AIC as optimization criterion. Three other selection criteria have been tested: BIC, adjAIC, adjGCV and compared to AIC. Similar results of power and type-I error have been obtained for the four criteria (results not shown). Spline basis involved in random effects were similarly built chosen $(0, T_i)$ as boundary knots and the number of internal knots chosen between 1 and 2. This adaptive feature of the model allows to build group-specific spline basis taken into account both left-censored and missing data. The results obtained by this model are displayed in Table 3 for $n_g = 50$ subjects by group. Similar results are presented in Online Appendix C in Tables C.2b and C.3b for $n_g = 20$ and 100, respectively.

In all settings except for high level of censored follow-up with $\alpha = 10,000$, using adaptive MEM led to equivalent type-I error (between 0.046 and 0.063 instead of 0.044 and 0.064) and power than with the well-specified model, for both profiles. Using adaptive MEM slightly increased the type-I error when the threshold for drop-out

Table 3. Robustness of the test of equality of nAUC calculated as mixed model summary statistics considering the MEM (9) with adaptive spline basis.

Data pattern	Method	Profile 1			Profile 2							
		Type-I error	Power		Type-I error	Power						
		0	-0.1	-0.25	0	-0.1	-0.25					
LOD	α	0.02	0.1	0.02	0.1	0.02	0.1	0.02	0.1	0.02	0.1	
50	Var(nAUC)	0.060	0.060	0.96	0.41	1.00	0.99	0.99	0.054	0.95	0.42	1.00
	Adap. MEM	0.063	0.056	0.95	0.35	1.00	0.97	0.97	0.051	0.94	0.37	1.00
5.10 ⁴	Adap. MEM	0.060	0.054	0.94	0.33	1.00	0.96	0.96	0.060	0.91	0.35	1.00
	Adap. MEM	0.060	0.059	0.84	0.31	1.00	0.95	0.95	0.050	0.77	0.30	1.00
	Adap. MEM	0.070	0.061	0.31	0.17	0.89	0.54	0.54	0.078	0.26	0.17	0.83

AUC: area under the curve; nAUC: normalized AUC; LOD: limit of detection.

Note: Individual trajectories are subject to missing data and/or LOD. Simulations were performed for $n_g=50$ subjects by group, mean trajectories following both profiles and for 1000 replications.

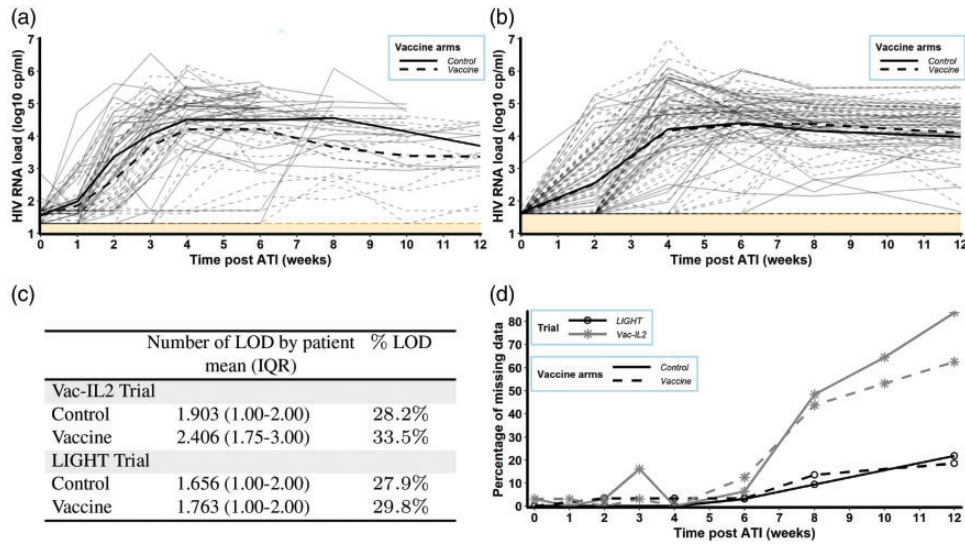


Figure 4. Exploratory plots and table for the control and vaccine groups from the Vac-IL2 and LIGHT HIV therapeutic vaccine trials. Observations are subject to LODs of 40 cp/ml or 20 and 50 cp/ml for LIGHT and Vac-IL2 trial, respectively. LOD: limit of detection. (a) Outcome trajectories for the control and vaccine groups of the Vac-IL2 HIV therapeutic vaccine trial, with two LOD = $\log_{10}(50)$ and $\log_{10}(20)$ cp/ml. (b) Outcome trajectories for the control and vaccine groups of the LIGHT HIV therapeutic vaccine trial, with LOD = $\log_{10}(40)$ cp/ml. (c) Mean number by patient and global percentage of observations below the LOD. (d) Percentage of missing data over time. Note: In (a) and (b), thick lines describe mean dynamics and thin lines individual ones, solid lines represent control group and dashed lines represent vaccine group. In (d), black lines with circles describe data from LIGHT trial, grey lines with crosses describe data from Vac-IL2 trial, solid lines represent control groups and dashed lines represent vaccine groups.

is 10,000 (between 0.061 and 0.078 instead of 0.051 and 0.073), while the estimated power remained unchanged. Altogether, even when the MEM structure is not known, this simulation shows that it is possible to use adaptive MEM for the modeling of the marker trajectories without invalidating the method, making it more relevant on real data.

5 Application on real clinical data

As illustrative examples, we applied the presented approach to the log-transformed HIV RNA load data from the Vac-IL2 and LIGHT trials (see section 2, Motivating Examples). Exploratory plots of the individual and mean HIV RNA load dynamics for control and vaccine groups are shown in Figure 4(a) and (b), for VAC-IL2 and LIGHT trials, respectively. As illustrated in table in Figure 4(c), longitudinal data in both trials are subject to left-censoring. While two values of LOD are considered in Vac-IL2 trial, 20 and 50 cp/ml (~ 1.3 and $1.7 \log_{10}$ cp/ml), impacting a total of 28.2% and 33.5% of observations for control and vaccine groups, only a LOD at 40 cp/ml ($\sim 1.6 \log_{10}$ cp/ml) is involved in LIGHT trial, leading to 27.9% and 29.8% of observations in the respective groups. In addition to left-censoring, those data are impacted by drop-outs. In LIGHT trial, ART resumption was required in case of serious AIDS or non-AIDS adverse events, when two consecutive of CD4+ T cells counted below 350 cells/mm³ within at least a two weeks' time interval as well as for specific patient or physician willingness. Approximately 20% of patients were concerned by these rules and resumed ART before the end of the predefined 12 weeks of ATI (see Figure 4(d)) being considered as drop-outs. In Vac-IL2 trial, 63% and 84% of drop-outs occurred in vaccine and control group respectively, as the result of HIV RNA load exceeding 50,000 cp/ml at four or six weeks post-ATI or exceeding 10,000 cp/ml after eight weeks of ART interruption.

We applied the proposed approach discussed in the manuscript using the MEM described by equation (9) where the number and the position of internal knots for both population and individual levels are optimized on data using the R-package *freenkspline* and AIC criteria. Also, the structure of the covariance matrix of random effects being unknown, we estimated this matrix as unstructured instead of diagonal. Moreover, we verified the applicability of our method on these real data by checking the normality of the distribution of the residuals provided by the MEM as well as the homoscedasticity of its error model for both trials (see Online Appendix E). We compared the results obtained by our approach, where the difference of nAUC between the two groups of

Table 4. Summary of results from both Vac-IL2 and LIGHT studies.

Methods	Estimate (SE)	95% CI	p -value	Estimate (SE)	95% CI	p -value
	Vac-IL2 trial			LIGHT trial		
Data	-0.346 (0.170)	[-0.680; -0.013]	0.046	-0.030 (0.175)	[-0.312; 0.372]	0.864
LOCF	-0.382 (0.198)	[-0.770; 0.007]	0.060	-0.018 (0.186)	[-0.382; 0.346]	0.924
Mean Imp.	-0.345 (0.312)	[-0.957; 0.266]	0.276	0.217 (0.245)	[-0.263; 0.697]	0.959
NP nAUC	-0.349 (0.205)	[-0.751; 0.053]	0.089	0.042 (0.178)	[-0.306; 0.390]	0.813
Adap. MEM	-0.459 (0.213)	[-0.877; -0.041]	0.031	0.095 (0.216)	[-0.329; 0.519]	0.660

SE: standard error; CI: confidence interval; NP: non parametric; Individual ad hoc methods (Indiv. nAUC): 1. Data: raw data, 2. LOCF: last observation carried forward, 3. Mean Imp.: mean imputation.

treatment is calculated with fixed parameter estimates, with the traditional ones where the nAUC is calculated using the trapezoidal method for every individual and compared at group level with a two-sample t -test. Similarly to the study of simulated data, estimates of individual nAUCs are computed using either log-transformed raw data without any transformation, LOCF or mean imputation ad hoc approaches. In addition, we applied the non-parametric approach NP nAUC briefly defined in section 4, Simulation study. The results are gathered in Table 4. In vac-IL2, the proposed approach concluded a significant difference between the two groups of treatment with a p -value of 0.031. Similar result is obtained with raw data with p -value slightly lower than 0.05. However, both LOCF, mean imputation ad hoc methods and non-parametric method are unable to reject the null hypothesis. All the tests lead to the same conclusion of no difference between groups in the LIGHT study. Considering the mean trajectories of the control and vaccine groups displayed in Figure 4(a) and (b), all the results obtained with our new approach are consistent with expected conclusions.

6 Discussion

In this paper, we proposed a splines-MEM based approach to estimate and compare the normalized area under the longitudinal outcome curve when observations are subject to left-censoring, induced by an LOD, and MAR monotonic missing data, due to drop-out. We demonstrated in a simulation study that incomplete data leads to biased estimates of nAUC resulting in invalid inferences regarding the difference in nAUC between groups with individual methods even when using simple ad hoc missing data correction, such as LOCF and mean imputation. Compared to the latter, we illustrated the superiority of our approach in term of type-I error and power. In addition, although the non-parametric approach developed by Vardi et al.²⁵ provided as robust statistical properties as our proposed method while the percentages of left-censored data remained lower than 50%, corresponding to a threshold of ART resumption higher than 100,000 copies/ml, the lack of information induced by higher percentages of drop out resulted in weaker results under certain conditions of simulation and more biased estimations of the difference of nAUC. We also highlighted that when the amount of data with drop-out is as high as 80% such as in a situation when ART are resumed if HIV RNA viral load exceeds 10,000 copies/mL in ATI trial, only the parametric approach appeared efficient to compare nAUC between groups. An application of two ATI trials for HIV illustrates the superiority of our method on real data.

Limitations of the proposed method include some assumptions induced by the use of MEM such as the normality and the homoscedasticity. However, we demonstrated that on clinical data these assumptions are realistic. As briefly noticed in section 3 (*Method*), two other versions of the proposed method are presented in Online Appendix replacing the estimation of $\Delta nAUC$ through the most commonly used trapezoid method by its estimation with either Lagrange or Spline interpolation methods. No significant differences of robustness have been observed in the application of those three methods on our well defined and tightened simulated trial designs. However, Lagrange and Splines methods could present more robust results in case of sparse designs. Also, in our simulations, we assumed a balanced longitudinal design with equal number of measurements and constant time points for every subject. Although clinical trials are commonly designed with the same monitoring for all participants, in reality the observed follow-up may deviate from the expected one. Moreover, some clinical trials could be designed to compare different monitoring designs among group in addition to treatment efficacy. As defined, the proposed method, being based on a discrete method of AUC calculation, should be biased by unbalanced times of measurements among groups with varying number of time points as well as different and irregular time steps between groups. As mentioned by Chandrasekhar et al.,¹⁸ the consideration of time as continuous variable

in the AUC calculation could be a solution to handle this problem. To this end, we could either refine the time grid to mimic continuous time in the AUC calculation step, or use more complex AUC approximation methods such as Gaussian quadrature methods. The choice of Gaussian quadrature methods requires thus the use of a resampling procedure, such as bootstrapping to estimate the standard error. In clinical trials, the sample size calculation, resulting in the determination of the number of participants in each arm needed to detect a clinically relevant treatment effect, is one of the major steps in designing the study. The proposed statistics being defined as classical Z-statistics, typical formulas of sample size calculation can be derived from it. As defined by Hazra et al.,⁴⁷ the general formula for two-sided test can be given by $n = (Z_{1-\alpha/2} + Z_{1-\beta})^2 \times \sigma^2 / \delta^2$ where α represents the accepted type-I error, β the type-II error, σ the standard deviation of the outcome being studied and δ the size effect defined as the targeted $\Delta nAUC/2$ in our case. Adjusted formulas can also be derived from this latter to account for unequal sized groups or unequal variance of outcomes using pooled variances. Simulations can be found in Online Appendix (see Figure F.1 in Online Appendix F) and showed good concordance between theoretical and practical power when there is no missing data. When missing data arise due to left censoring (LOD) or informative drop out, one need to take it into account in the sample size calculation.

The simulation study has been led under model correct specification assumption, i.e. the model used to analyse the data corresponds to the true data generation process. We further relaxed this assumption by using adaptive splines model for which some parameters, such as the location and number of knots for splines are supposed unknown.

Various extensions of this work could be guided to address the problem when there are a high proportion of drop-outs. The incorporation of prior information could be done through several ways. The study of more constrained splines through the addition of penalty on spline coefficients (P-splines)⁴⁸ or monotony and boundary conditions⁴⁹ (natural splines) is an option. In the same perspective, future research aims to extend this method to the use of mechanistic models.⁵⁰ In addition to introducing biological interpretation of the parameters, these models could incorporate more easily additional information such as asymptotic behaviors with steady states.

Acknowledgements

The authors thank the Vaccine Research Institute and the ANRS as sponsors and the LIGHT and VAC-IL2 study groups for sharing the data used in this article. Numerical computations were in part carried out using the PlaFRIM experimental testbed, supported by Inria, CNRS (LABRI and IMB), Université de Bordeaux, Bordeaux INP and Conseil Régional d'Aquitaine (see <https://www.plafrim.fr/>). The authors thank Dr Torsten Hothorn and two anonymous reviewers for constructive comments on the manuscript. The research has been initiated in the contest of the EHVA T01 trial which is supported by the European Union's Horizon 2020 Research and Innovation Programme (grant numbers 681032) and the Swiss Government (grant number 15 0337).

Declaration of conflicting interests

The author(s) declared no potential conflicts of interest with respect to the research, authorship, and/or publication of this article.


Funding

The author(s) received no financial support for the research, authorship, and/or publication of this article.

Additional information

Web Appendix is available with this paper at the Statistical Methods in Medical Research website. R Code implementing the method is available on github at <https://github.com/marie-alexandre/AUCcomparison.git>. A reference manual has been included in the package (https://github.com/marie-alexandre/AUCcomparison/blob/master/Reference_manual.pdf) describing how to implement the proposed method.

ORCID iD

Marie Alexandre  <https://orcid.org/0000-0002-3557-7075>

References

1. Scheff JD, Almon RR, DuBois DC, et al. Assessment of pharmacologic area under the curve when baselines are variable. *Pharmaceut Res* 2011; **28**: 1081–1089.

2. Heldens J, Weststrate M and Van den Hoven R. Area under the curve calculations as a tool to compare the efficacy of equine influenza vaccines – a retrospective analysis of three independent field trials. *J Immunol Methods* 2002; **264**: 11–17.
3. Lydick E, Epstein R, Himmelberger D, et al. Area under the curve: a metric for patient subjective responses in episodic diseases. *Qual Life Res* 1995; **4**: 41–45.
4. Neoptolemos JP, Stocken DD, Friess H, et al. A randomized trial of chemoradiotherapy and chemotherapy after resection of pancreatic cancer. *N Engl J Med* 2004; **350**: 1200–1210.
5. Schleyer E, Kühn S, Rührs H, et al. Oral idarubicin pharmacokinetics – correlation of trough level with idarubicin area under curve. *Leukemia* 1996; **10**: 707–712.
6. Duh MS, Lefebvre P, Fastenau J, et al. Assessing the clinical benefits of erythropoietic agents using area under the hemoglobin change curve. *The Oncologist* 2005; **10**: 438–448.
7. Hothorn LA. Statistical analysis of in vivo anticancer experiments: tumor growth inhibition. *Drug Inform J* 2006; **40**: 229–238.
8. Wu J and Houghton PJ. Interval approach to assessing antitumor activity for tumor xenograft studies. *Pharmaceut Stat* 2010; **9**: 46–54.
9. Qian W, Parmar M, Sambrook R, et al. Analysis of messy longitudinal data from a randomized clinical trial. *Stat Med* 2000; **19**: 2657–2674.
10. Cole SR, Napravnik S, Mugavero MJ, et al. Copy-years viremia as a measure of cumulative human immunodeficiency virus viral burden. *Am J Epidemiol* 2010; **171**: 198–205.
11. Ramos EL, Mitcham JL, Koller TD, et al. Efficacy and safety of treatment with an anti-m2e monoclonal antibody in experimental human influenza. *J Infect Dis* 2015; **211**: 1038–1044.
12. Calfee DP, Peng AW, Cass LM, et al. Safety and efficacy of intravenous zanamivir in preventing experimental human influenza a virus infection. *Antimicrob Agents Chemother* 1999; **43**: 1616–1620.
13. Allison DB, Paultre F, Maggio C, et al. The use of areas under curves in diabetes research. *Diabetes Care* 1995; **18**: 245–250.
14. Venter C, Slabber M and Vorster H. Labelling of foods for glycaemic index-advantages and problems. *South African J Clin Nutr* 2003; **16**: 118–126.
15. Potteiger J, Jacobsen D and Donnelly J. A comparison of methods for analyzing glucose and insulin areas under the curve following nine months of exercise in overweight adults. *Int J Obesity* 2002; **26**: 87–89.
16. Wilding GE, Chandrasekhar R and Hutson AD. A new linear model-based approach for inferences about the mean area under the curve. *Stat Med* 2012; **31**: 3563–3578.
17. Bell ML, King MT and Fairclough DL. Bias in area under the curve for longitudinal clinical trials with missing patient reported outcome data: summary measures versus summary statistics. *SAGE Open* 2014; **4**: 2158244014534858.
18. Chandrasekhar R, Shi Y, Hutson AD, et al. Likelihood-based inferences about the mean area under a longitudinal curve in the presence of observations subject to limits of detection. *Pharmaceut Stat* 2015; **14**: 252–261.
19. Little R and An H. Robust likelihood-based analysis of multivariate data with missing values. *Stat Sin* 2004; **14**: 949–968.
20. Jacqmin-Gadda H, Thiébaud R, Chêne G, et al. Analysis of left-censored longitudinal data with application to viral load in HIV infection. *Biostatistics* 2000; **1**: 355–368.
21. Thiébaud R and Jacqmin-Gadda H. Mixed models for longitudinal left-censored repeated measures. *Comput Meth Progr Biomed* 2004; **74**: 255–260.
22. Vaida F and Liu L. Fast implementation for normal mixed effects models with censored response. *J Comput Graph Stat* 2009; **18**: 797–817.
23. Schisterman E and Rotnitzky A. Estimation of the mean of a k-sample u-statistic with missing outcomes and auxiliaries. *Biometrika* 2001; **88**: 713–725.
24. Spritzler J, DeGruttola VG and Pei L. Two-sample tests of area-under-the-curve in the presence of missing data. *Int J Biostat* 2008; **4**.
25. Vardi Y, Ying Z and Zhang CH. Two-sample tests for growth curves under dependent right censoring. *Biometrika* 2001; **88**: 949–960.
26. Garner SA, Rennie S, Ananworanich J, et al. Interrupting antiretroviral treatment in HIV cure research: scientific and ethical considerations. *J Virus Eradict* 2017; **3**: 82.
27. Li JZ, Etemad B, Ahmed H, et al. The size of the expressed HIV reservoir predicts timing of viral rebound after treatment interruption. *AIDS* 2016; **30**: 343.
28. Henderson GE, Peay HL, Kroon E, et al. Ethics of treatment interruption trials in HIV cure research: addressing the conundrum of risk/benefit assessment. *J Med Ethics* 2018; **44**: 270–276.
29. Sneller MC, Justement JS, Gittens KR, et al. A randomized controlled safety/efficacy trial of therapeutic vaccination in HIV-infected individuals who initiated antiretroviral therapy early in infection. *Sci Transl Med* 2017; **9**: eaan8848.
30. Sued O, Ambrosioni J, Nicolás D, et al. Structured treatment interruptions and low doses of il-2 in patients with primary HIV infection. inflammatory, virological and immunological outcomes. *PLoS One* 2015; **10**: e0131651.

31. Lévy Y, Thiébaud R, Montes M, et al. Dendritic cell-based therapeutic vaccine elicits polyfunctional hiv-specific t-cell immunity associated with control of viral load. *Eur J Immunol* 2014; **44**: 2802–2810.
32. Pollard RB, Rockstroh JK, Pantaleo G, et al. Safety and efficacy of the peptide-based therapeutic vaccine for hiv-1, vacc-4x: a phase 2 randomised, double-blind, placebo-controlled trial. *Lancet Infect Dis* 2014; **14**: 291–300.
33. Bar KJ, Sneller MC, Harrison LJ et al. Effect of HIV antibody vrc01 on viral rebound after treatment interruption. *N Engl J Med* 2016; **375**: 2037–2050.
34. Fagard C, Le Braz M, Günthard H, et al. A controlled trial of granulocyte macrophage-colony stimulating factor during interruption of HAART. *AIDS* 2003; **17**: 1487–1492.
35. Palich R, Ghosn J, Chaillon A, et al. Viral rebound in semen after antiretroviral treatment interruption in an HIV therapeutic vaccine double-blind trial. *AIDS* 2019; **33**: 279–284.
36. Lévy Y, Gahéry-Ségard H, Durier C, et al. Immunological and virological efficacy of a therapeutic immunization combined with interleukin-2 in chronically hiv-1 infected patients. *AIDS* 2005; **19**: 279–286.
37. Brundage TM, Vainorius E, Chittick G, et al. Brincidofovir decreases adenovirus viral burden, which is associated with improved mortality in pediatric allogeneic hematopoietic cell transplant recipients. *Biol Blood Marrow Transplant* 2018; **24**: S372.
38. Hill JA, Mayer BT, Xie H, et al. Kinetics of double-stranded DNA viremia after allogeneic hematopoietic cell transplantation. *Clin Infect Dis* 2018; **66**: 368–375.
39. Zecca M, Wynn R, Dalle JH, et al. Association between adenovirus viral load and mortality in pediatric allo-HCT recipients: the multinational advance study. *Bone Marrow Transplant* 2019; **54**: 1632–1642.
40. Kosulin K, Pichler H, Lawitschka A, et al. Diagnostic parameters of adenoviremia in pediatric stem cell transplant recipients. *Front Microbiol* 2019; **10**: 414.
41. Satterthwaite FE. An approximate distribution of estimates of variance components. *Biometr Bull* 1946; **2**: 110–114.
42. Hrong-Tai Fai A and Cornelius PL. Approximate f-tests of multiple degree of freedom hypotheses in generalized least squares analyses of unbalanced split-plot experiments. *J Stat Comput Simulat* 1996; **54**: 363–378.
43. Kenward MG and Roger JH. Small sample inference for fixed effects from restricted maximum likelihood. *Biometrics* 1997; **53**: 983–997.
44. Bailer AJ. Testing for the equality of area under the curves when using destructive measurement techniques. *J Pharmacokinet Biopharmaceut* 1988; **16**: 303–309.
45. Spiriti S, Smith P and Lecuyer P. *freeknotsplines: algorithms for implementing free-knot splines*, 2018, R package version 1.0.1, <https://cran.r-project.org/web/packages/freeknotsplines/index.html>.
46. Vaida F and Liu L. *lme4: linear mixed-effects models with censored responses*, 2012. . R package version 1.0, <https://CRAN.R-project.org/package=lme4> (accessed 8 June 2021).
47. Hazra A and Gogtay N. Biostatistics series module 5: determining sample size. *Ind J Dermatol* 2016; **61**: 496.
48. Eilers PH and Marx BD. Flexible smoothing with b-splines and penalties. *Stat Sci* 1996; **11**: 89–102.
49. Laurini MP and Moura M. Constrained smoothing b-splines for the term structure of interest rates. *Insurance* 2010; **46**: 339–350.
50. Perelson AS and Ribeiro RM. Introduction to modeling viral infections and immunity. *Immunol Rev* 2018; **285**: 5.
51. Berrut JP and Trefethen LN. Barycentric Lagrange interpolation. *SIAM Rev* 2004; **46**: 501–517.

4.3 Perspectives

In this chapter, we focused on the evaluation of vaccine efficacy in HIV therapeutic vaccine trials with ATI using AUC as primary outcome. We proposed a parametric statistical test based on splines-MEM to assess the difference of AUC between vaccine and placebo group taking into account both left-censoring and monotonic pattern of missingness of observations induced by study dropout. This work highlighted the good statistical properties of this test that appeared as robust to MAR monotonic missing data. Moreover, we showed the superiority of this approach compared to imputation methods that are commonly used in longitudinal studies as well as its ability to outperform a non-parametric test, developed by [Vardi et al. \[2001\]](#) in the same context, to deal with bias of AUC calculation induced by high level of missing data.

For sake of continuity with the results of the previous section and for fair comparison with individual methods, the methodology has been derived to compare the normalized AUC between groups of treatment. However, it is important to underline that, by construction, the normalization has no effect on the statistical test. Only the temporal restriction compelling the comparison of groups on the same time interval plays a role on the statistical properties.

Although the proposed method allowed to reduce the bias induced by monotonic missing data in the calculation of AUC, another source of bias should be carefully considered: the choice of the method used to approximate the AUC. As a matter of fact, the calculation of the AUC requires integral approximation methods that have been performed in this work on each interval delimited by two observations. We derived the framework for the three basic methods of approximation: (1) the trapezoid method which is the most commonly used in this type of work, (2) the Lagrange interpolation method and (3) the Spline interpolation method, all three of them providing quite similar results. However, as discussed in the paper, this conclusion could have been driven by the choice of the non-sparse design of the simulation study. For further developments, the use of less coarse approximation methods could be expected, such as Gaussian quadrature [[Place and Stach, 1999](#)]. Another possibility could be to significantly reduce the time step used in the AUC calculation with the simple methods. Nevertheless, as depicted by equation (7) in the article above, the approximation of the integral is directly dependent on the number of observations/time points used to calculate the AUC. Consequently, the more the time grid is chosen thin, the more the calculation is time consuming. In randomized studies, time of observations must be carefully chosen

in order to miss as less as possible information that could be crucial for the evaluation of the study endpoint.

From a theoretical point of view, it would be interesting to extend the proposed statistical test to NMAR longitudinal data, which is also referred as informative and non-ignorable dropout. In this case, the majority of the methods used to handle missing data such as univariate/multivariate analysis of variance (ANOVA/MANOVA), MEM or single and multiple imputations methods, are not appropriate and irremediably lead to biased results. The difficult results in the fact that the probability of dropout is assumed to be related to the value of the observation that should have been observed in absence of missing data. Two types of joint models have been widely reviewed for this specific case: the selection models and the mixture-pattern models. The general idea of these models consist in jointly estimate the model for longitudinal data and the probability of missingness. These two classes of joint models differ in the manner to define the dependence between the two models. While selection models condition the probability of missingness on the variable outcome, and thus on unobserved outcomes, the pattern-mixture models condition the model for longitudinal outcomes on process of missingness requiring explicit assumptions about the unobserved responses [Little, 1993; Fitzmaurice, 2003; Lu, 2014; Nakai and Ke, 2011]. In particular, the use of these joint-models may be relevant to integrate multiple sources of missingness [Moore et al., 2017].

Two related significant limitations of the proposed approach are: (1) the necessity to know the literal expression of the function describing the outcome variables and (2) the development of the method only in the case of linear models. These two limitations enabled us to express the AUC directly as a linear function of the model parameters (see equation (8) of the article). To extend the method to non-linear models, the main difficulty resides in the estimation of the variance of the AUC. During the thesis, we started to work on the extension of the method to non-linear model with known literal expression, such as the Gompertz model [Vaghi et al., 2020], and we adapted our statistical test using the Taylor theorem [Papanicolaou, 2009] to approximate the variance of AUCs (results not shown). Thereafter, we adapted the methodology to all models by using the model predictions of the outcome to estimate the AUC within each group of treatment and by considering a bootstrap approach based on population parameters sampling, using the Fisher Information matrix, to approximate the variance of AUCs within each group.

Finally, an interesting extension of the proposed statistical test is its adaptation to mechanistic models. As a matter of fact, while the use of splines functions in the MEM easily allowed to model flexible dynamics characterizing the virological rebound, these models remain purely descriptive. On the opposite, mechanistic models could allow to incorporate more biological aspect in the modeling and thus could provide potential information about vaccine-induced immune response. Moreover, these models could give the opportunity to fill some lack of information provided by the early study dropout by incorporating additional data such as CD4+T cell count. However, numerous models with variable complexity and based on different biological hypothesis can be used to describe the same dynamics and provide similar fits. The common approach consists in using model selection methods based on selection criteria like AIC, BIC, etc, to select the optimal model for the given criteria. However, the optimal selected model can be highly dependent on the selection criteria [Zhang et al., 2014]. After selecting the single so-called optimal model, the uncertainty introduced by the model selection is usually ignored [Hjort and Claeskens, 2003]. Moreover, the developed statistical test being a parametric test, this latter should be dependent on model misspecification. Consequently, to take into account all of these limits, we are currently trying to extend the statistical parametric test to the model averaging [Buckland et al., 1997]. More specifically, we focus on its frequentist version [Yang, 2001; Hansen, 2007; Liang et al., 2011] applied to mechanistic ODE-based models. Briefly, this approach consists in defining a variable of interest (e.g. parameters, outcomes) as the weighted sum of this same variables estimated by different models, with the weights being usually defined as a function of the likelihood of the models. This work was initiated during the second year of this thesis but was put on hold due to the urgency of the project about SARS-CoV-2 presented in the next chapter.

Additional work: Mechanistic modelling of viral rebound in HIV vaccine trials

For the purpose of the extension of the proposed approach to mechanistic models and model averaging, an additional work was performed and has done the subject of a poster at the Population Approach Group in Europe (PAGE) annual meeting in 2019, in Stockholm. The poster is available in Appendix B.

The objective of this work was to model the viral rebound during ATI using multiple mechanistic ODE-based models and to compare their ability to well fit and predict the data and consequently to capture the variability in the trajectories of the viral rebound. We firstly used models found on the literature, for which we studied the identifiability with the software DAISY, before estimating them on LIGHT data by performing sensitivity analysis and using a population approach (see section 2.3). In particular, we

considered a multivariate observation model with two outcomes: the viral load and the CD4+ T cell count. Based on these estimations, models were compared on the basis of their values of Akaike information criterion (AIC) and the root mean squared error (RMSE). In a second time, we used data from ILIADE (data described in Chapter 3) as external data validation. To this end, population parameters of the models were considered as fixed at the values estimated on LIGHT data and only random effects were update on this new dataset. Similar to the previous analysis, models, and their ability to predict data from another trial, were compared on the AICs and RMSEs. As described in the poster (see Appendix B), we especially focused on three ODE-based models: (1) the well-known target-cell model developed by Perelson [Perelson et al., 1996] and already presented in section 2.3.4, (2) the activated-cell model (or delayed target-cell model in the poster) widely described and studied by Prague et al. [2012] and accounting for an additional state for quiescent target-cells and (3) the model developed by [Prague et al., 2019] integrating the interactions of the target cells and the virus with the immune system represented by the precursor and effector immune cells. In addition to the contribution of immune cells, the third model integrated the reactivation of the HIV-1 reservoir (i.e. infected cells) as a stochastic event. The comparison of the model on LIGHT data identified the second model and the third model as the best ones in terms of AIC and RMSE on viral load respectively while the three models appeared as equivalent in term of RMSE on CD4+ T cell trajectories. The application of the models on ILIADE data highlighted their ability to predict dynamics of new individuals and led to similar results in terms of model comparisons. To conclude, this work highlighted the best ability of the model integrating immune control to fit the viral load trajectories but interestingly not the CD4+ T cell count. These results are in accordance with our willingness to use model averaging and take advantage of multiple models and their ability to well fit at least a part of the dynamics.

In the next chapters, we exclusively focus on the development of mechanistic ODE-based models either in a project conducted to identify mechanistic correlate of protection against SARS-CoV-2 in NHP studies (Chapter 5) or in a project conducted to evaluate the longevity of the humoral response induced by an Ebola vaccine (Chapter 6).

Chapter 5

Mechanistic correlates of protection in vaccine trial: application to SARS-CoV-2.

Abstract: In this chapter, we focus on evaluating vaccine efficacy in the context of the current SARS-CoV-2 pandemic. After setting the context of the unprecedented vaccine development in which this work is taking place, we recall the need to find good correlate of protection (CoP) to accelerate the development of an effective vaccine. In particular, we note that no CoP have yet been identified that are causally linked to the protective effects of vaccines, also called mechanistic CoP. We then focus on the contribution of within-host mechanistic modeling to understanding the biological and immunological mechanisms of this viral infection, as well as the mechanisms of transmission within a population. We finally propose a method for identifying mechanistic CoP in preclinical studies that combines modeling of viral dynamics by mechanistic models and a model building strategy to down-select time-dependent immunological markers. By applying this method to data from three vaccine studies, we highlight the robustness of the results found with this method compared with commonly used purely descriptive approaches and its contribution to the identification of underlying immunological mechanisms.

Keywords: SARS-CoV-2 ; vaccine ; correlate of protection ; within-host modelling ; mechanistic model ; ordinary differential equation ; immune marker ; preclinical study ; binding antibody ; neutralization ; viral infectivity ; covariate

Dissemination:

▷ **Editorial in international peer-reviewed journal**

Prague, M., Alexandre, M., Thiébaud, R., & Guedj, J. (2022). [Within-host models of SARS-CoV-2: What can it teach us on the biological factors driving virus pathogenesis and transmission?](#). *Anaesthesia Critical Care & Pain Medicine*, 101055.

▷ **Publication in revision in international peer-reviewed journal**

Alexandre, M., Marlin, R., Prague, M., Coleon, S., Kahlaoui, N., Cardinaud, S., ... & Thiébaud, R. (2021). [SARS-CoV-2 mechanistic correlates of protection: insight from modelling response to vaccines](#). *bioRxiv - Under revision in Elife*

▷ **Oral communication at international conference**

Alexandre M, Prague M, Thiébaud R and the VRI/CEA group. [Accounting for time-dependant confounding variables in mechanistic ODE model: simulations and application to vaccine trial](#). *International Society for Clinical Biostatistics* , Lyon, France, 2021 (Online).

5.1 Biological and clinical context

5.1.1 General introduction on COVID-19

5.1.1.1 The COVID-19 pandemics

Coronavirus disease (COVID-19) is an infectious disease caused by the severe acute respiratory syndrome coronavirus 2 (SARS-CoV-2) virus. Officially named by the WHO in February 11, 2020 [Wu et al., 2020], COVID-19 emerged at the end of 2019 in Wuhan, China, with the first case related on 12 December 2019 [Zhou et al., 2020], before rapidly spreading and infecting numerous countries over the world in the following months. Becoming a global health threat and causing an unprecedented pandemic, on January 30, 2020, COVID-19 was declared as a Public Health Emergency of International Concern by the WHO under the recommendations of the Emergency Committee [WHO, 2019b] and a pandemic on March 11, 2020 [WHO, 2020d]. From December 12, 2019 to March 02, 2022, 437 338 859 confirmed cases and 5962 972 SARS-CoV-2-related deaths were reported worldwide to WHO [WHO, 2022b].

5.1.1.2 The SARS-CoV-2 virus

Coronaviruses belongs to the subfamily Coronavirinae, in the family of Coronaviridae, which contains four genera: Alphacoronavirus and Betacoronavirus infecting mammals and Gammacoronavirus and Deltacoronaviruses infecting only birds [Schoeman and Fielding, 2019; Hasöksüz et al., 2020]. Today, seven coronaviruses infecting humans have been reported. While four of them are responsible for mild to moderate illness, the three others induce severe to lethal respiratory illness: the severe acute respiratory syndrome coronavirus identified in 2003 in China with 8098 cases and 774 deaths related [CDC, 2017a; WHO, 2003], the Middle East respiratory syndrome coronavirus emerged in 2012 in Saudi Arabia and responsible 2600 cases and 943 deaths related in 2022 [CDC, 2017b; WHO, 2019a; ECDC, 2022] and the SARS-CoV-2.

The SARS-CoV-2 belongs to betacoronavirus genus. Its genome is a single-stranded positive sense RNA encapsulated into a capsid composed of nucleocapsid protein (N) ensuring its binding within the virion. As shown on figure 5.1, this structure is itself contains into an envelop composed of three structural proteins: membrane proteins (M), spike proteins (S) and envelope proteins (E) [Wang et al., 2020]. Each of these four structural proteins (N, M, S and E) plays an individual role in the replication cycle of the virus. The SARS-CoV-2 replication cycle can be subdivided into multiple steps (see Figure 5.2). The reader can refer to [Hardenbrook and Zhang, 2022; V'kovski et al., 2021; Zhang and Tang, 2020], among others, for deeper description of the replication

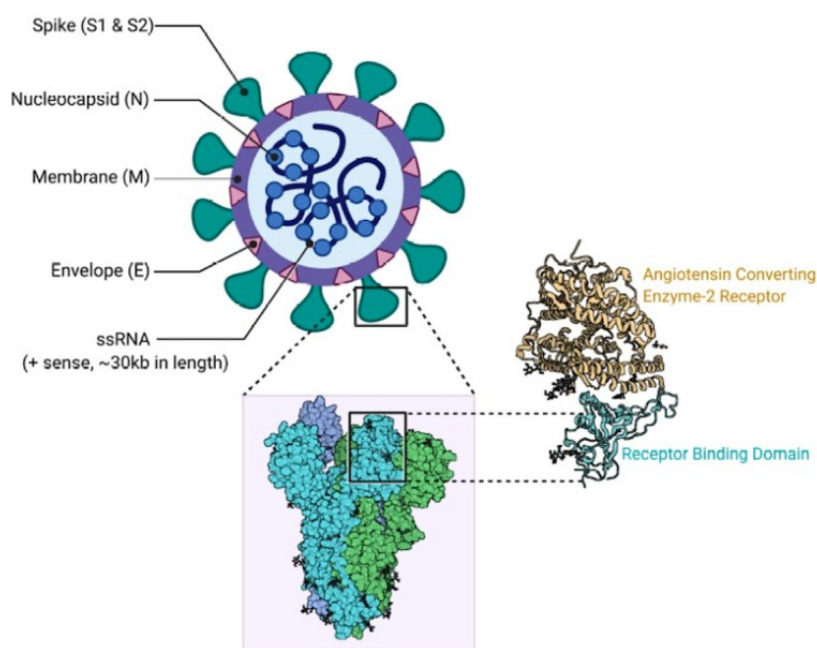


Figure 5.1 – The Structure of SARS-CoV-2 virus and ACE2 protein. *This figure was extracted from [Hasöksüz; 2020].*

cycle. The SARS-CoV-2 life cycle begins with the attachment and the entry of the virus into the host cell that is mediated by the spike protein. The receptor binding domain (RBD), located on one of the two segments constituting the spike protein (S1) recognizes and binds to the angiotensin-converting enzyme 2 (ACE2) receptor located on the surface of host cells, in particular on its endothelial cells [Shang et al., 2020]. After the entry into the cell and the fusion between the viral envelope and the membrane of the host cell, the viral genome is released into the cytoplasm of the cell (uncoating), and translated into replicase proteins. Viral RNA synthesis is then performed followed by the assembly of the replication-transcription complexes and the transcription of the four structural viral proteins (N, S, M, E) from the RNA genome. Viral proteins S, M and E are then inserted into the endoplasmic reticulum membrane while multiple copies of proteins N are responsible for packaging the viral RNA into ribonucleoprotein complexes (nucleocapsid) in the cytoplasm [Hardenbrook and Zhang, 2022]. Endoplasmic reticulum moves then to the endoplasmic reticulum-Golgi intermediate compartment to merge with the nucleocapsid and assembles the virion. Finally, the small protein E, which constitutes a major component of the viral envelope, mediates the budding and the release of the virion outside the host cell [Mandala et al., 2020].

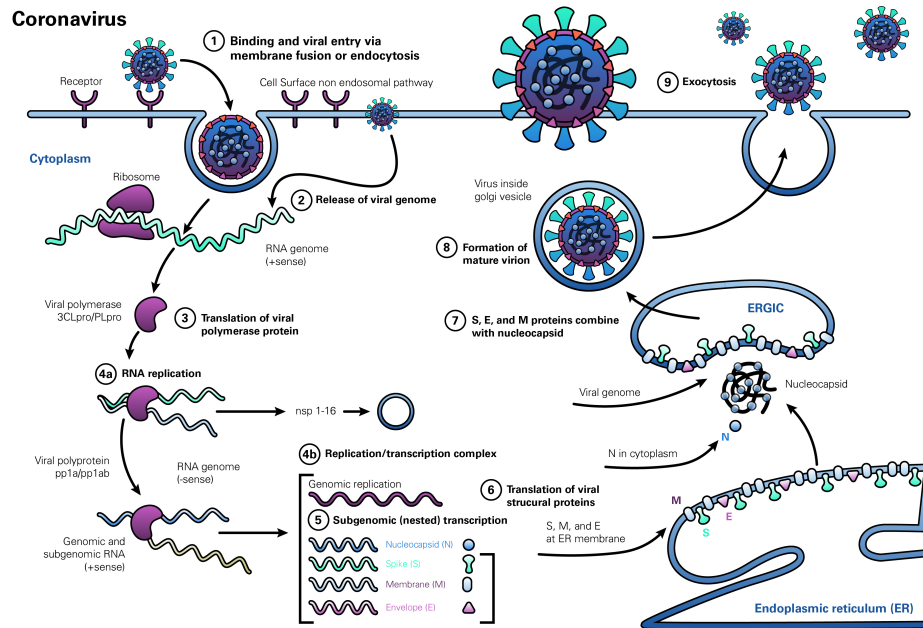


Figure 5.2 – Replication cycle of SARS-CoV-2. Figure extracted from [Burmer et al., 2020]

5.1.2 Vaccine development

5.1.2.1 An unprecedented worldwide effort

Since the beginning of the COVID-19 pandemic, the development of vaccines for SARS-CoV-2 moved at an unprecedented speed. Started in March 2020 with the first phase I clinical trial, on March 3, 2022, 189 vaccine candidates are evaluated in a total of 650 vaccine trials (numbers extracted from [COVID-19 vaccine tracker, 2020]). As shown in Table 5.1, these vaccine candidates are varied belonging to eight distinct vaccine platforms. Six of them are based on viral components: (1) protein subunit vaccine, (2) virus-like particle vaccine, (3) DNA- and (4) RNA-based vaccine, (5) non-replicating and (6) replicating viral vectored vaccine. The two others platforms are vaccines based on the whole virus, either live-attenuated or inactivated. Among them, protein subunit vaccines are the most numerous, with more than a third of vaccine candidates.

To date, based on their efficacy to prevent COVID-19, 10 COVID-19 vaccines have been granted an Emergency use listing (EUL) by the WHO [WHO, 2022a]. Created in response to the 2014-2016 Ebola outbreak in West Africa, the EUL identifies unlicensed treatments like vaccines or therapeutics that have proven to be safe and efficient enough to be used mainly during public health emergency of international concern (PHEIC) [WHO, 2020c]. Among these granted vaccines, five have been approved by

Table 5.1 – Number of vaccines candidates in clinical development. Vaccines candidates are splitted according to the phase of development and the vaccine platforms. Data were extracted from [COVID-19 vaccine tracker, 2020] on March 3, 2022.

	Phase I	Phase II	Phase III	Approved ¹	WHO , EUL ²	Total
Protein Subunit	11	26	26	13	2	63
Virus-like protein	0	5	2	1	0	7
DNA	6	6	4	1	0	16
RNA	8	18	11	3	2	37
Non replicating viral vector	12	7	9	6	3	28
Replicating viral vector	3	3	2	0	0	8
Inactivated	5	3	13	11	3	21
Live attenuated	1	0	0	0	0	1
Total	46	68	67	35	10	181

¹ Vaccines that have been approved by at least one country over the world.

² Vaccines granted an Emergency use listing (EUL) by the WHO

the European Medicines Agency (EMA) [EMA, 2020b,e,a,d,c], three have been granted an emergency use authorization (EUA) by the FDA [FDA, 2021c,b, 2022] and two have been formally approved by the FDA [FDA, 2021a,d]. Both of these vaccines belong to the RNA vaccine platform and demonstrated high efficacy. The BNT162b2 COVID-19 vaccine (Pfizer) is a nucleoside-modified RNA vaccine encoding the SARS-CoV-2 spike protein developed by BioNTech and Pfizer and is the first COVID-19 vaccine that has been granted an EUA on December 11, 2020 and approved by the FDA on July 16, 2021. Initially recommended to prevent COVID-19 for people older than 16 years based on its high efficacy after two doses (95% [90.3% ; 97.6%]) evaluated in a pivotal efficacy trial conducted on more than 40 000 persons [Polack et al., 2020], this vaccine demonstrated an efficacy of 100% [75.3% ; 100%] [Frenck Jr et al., 2021] on adolescents from 12 to 15 years. The BNT162b2 COVID-19 vaccine was additionally granted on May 10, 2021 for 12 to 15 aged people. Today, Phase I dose-finding study as well as a Phase II/III trial (still ongoing) are conducted on children from 6 months to 11 years to assess safety, immunogenicity and efficacy with encouraging first results of 90% [67.7% ; 98.3%] vaccine efficacy [Walter et al., 2022].

The mRNA-1273 COVID-19 vaccine (Moderna) is a nucleoside-modified RNA vaccine encoding the SARS-CoV-2 spike protein developed by Moderna Biotech and is the second COVID-19 vaccine that has been granted an EUA on December 19, 2020 and approved by the FDA on August 06, 2021. The vaccine was recommended to prevent severe COVID-19 disease for adults based on its efficacy after two doses (94.1% [89.3% ; 96.8%]) evaluated in a phase III RCT enrolling more than 30 000 persons [Baden et al., 2020]. Currently, Phase II/III RCT is conducted to evaluate its safety on 12 to 17 years adolescents, with first conclusive results [Ali et al., 2021].

5.1.2.2 The necessity to identify immune correlates of protection

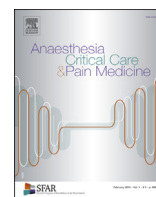
Despite the efficacy of these vaccines currently used on a large scale population, many challenges point out the need to continue vaccine development [Wouters et al., 2021]: the considerable worldwide demand for vaccine doses causing manufacturing challenges, the lack of information about the longevity of the vaccine efficacy, and thus the time interval between two injections, as well as about the vaccine efficacy in specific population (e.g. immunosuppressed individuals, pregnant women). In addition, as shown with the emergence of the different variants of concern, the efficacy of these vaccines, which are based on the original Wuhan SARS-CoV-2 spike, and/or the longevity of the vaccine-induced response can be significantly decreased [Castro Dopico et al., 2022; Shepherd et al., 2022]. In particular, since the emergence of the B.1.1.529 (omicron) variant, declared as variant of concern on November 26, 2021 by the WHO [WHO, 2021a], a faster decrease of vaccine effectiveness was observed during the omicron wave, whether for the mRNA-1273 or the BNT162b2 COVID-19 vaccine [Collie et al., 2021; Hansen et al., 2021; Abu-Raddad et al., 2022; Tseng et al., 2022]. To accelerate the vaccine development and more specifically the approval of vaccine candidates in specific populations, the identification of immune correlate of protection (CoP) (see chapter 1 for further information about CoP) is highly requested. However, no SARS-CoV-2 CoP has been currently identified [Gilbert et al., 2022; Perry et al., 2022]. Although both natural infection and vaccination against SARS-CoV-2 induce protection against future infections, the underlying immune mechanisms and the longevity of the induced protection remain unclear. Moreover, the lack of standardization of laboratory assays makes the identification of CoP more difficult [Zhu et al., 2022]. In a systemic review, Perry et al. [2022] reported a large number of studies identifying a robust association between antibodies levels, in particular neutralizing and anti-S antibody, and VE, viral load levels or risk of infection. Even though these results tend to support antibody as potential CoP [Feng et al., 2021; Gilbert et al., 2022; Cromer et al., 2022; Goldblatt et al., 2022; Castro Dopico et al., 2022], other results show contradictory results. For instance, some individuals have been infected despite their high levels of neutralizing antibodies while other studies pointed out the importance of other components in the induction of the protection. In particular, we know that both humoral and cellular responses play a role in protection [McMahan et al., 2021]. Consequently, all of these results tend to conclude that antibodies (neutralizing and anti-S) may be relevant CoP but not an absolute one for the moment.

Although many analysis have been conducted to evaluate correlates of protection [Yu et al., 2020b; Corbett et al., 2021b; Vidal et al., 2021; Corbett et al., 2021a; McMa-

han et al., 2021], none of them has been conducted to evaluate mechanistic CoP, as defined in chapter 1 and 2, meaning with a causal relationship between the surrogate marker and the clinical outcome of interest. While Gilbert et al. [2021] developed a causal inference approach to evaluate CoP in clinical trials using only vaccine arms, we proposed in this chapter a mathematical framework based on mechanistic models to identify mechanistic correlate of protection. We applied this methodology on data collected in three preclinical studies performed on non-human primates assessing efficacy of vaccines for SARS-CoV-2. This work has been the subject of an article currently under revision in *Elife*.

In addition, the interest of our team for the within-host modeling and its application on the context of the COVID-19 pandemic gave us the opportunity to realize an editorial, to which I participated to the writing, for the journal *Anaesthesia Critical Care & Pain Medicine* on the benefit of using within-host models and their application on SARS-CoV-2 [Prague et al., 2022].

5.2 Editorial about within-host models and their application on SARS-CoV-2



Editorial

Within-host models of SARS-CoV-2: What can it teach us on the biological factors driving virus pathogenesis and transmission?



ARTICLE INFO

Keywords:

Antiviral treatment
Host–pathogen interaction
Immunity
Mathematical modelling
Virus dynamics

Viral dynamics is a field of research that develops mathematical models based on biological knowledge to characterise the evolution of virological and immunological markers during infection. Analogous to epidemiological models, these models view the human body as a series of compartments composed of different cell or virus types that evolve over time (Fig. 1, panel “within-host modelling”).

In its most basic formulation, the model assumes three compartments: free virus particles infect target cells, which become productively infected cells, that are then gradually lost as a result of viral cytopathicity and/or immune response. Analogous to epidemiological models, one can define a “within-host” basic reproductive ratio (R_0) that quantifies how many infected cells arise from a single infected cell at the beginning of infection and depends on the balance between the processes of virus production and elimination. When $R_0 > 1$, the virus grows exponentially until most target cells are depleted. Thereafter, the virus declines rapidly at a rate that reflects the loss of infected cells that can either be eliminated or cured of their viral content. Over the past 30 years, many models have been developed that go beyond this simple “target-cell limited model” and incorporate more biological processes: the intracellular life cycle, the role of the innate and adaptive immune response, virus mutation, or pharmacological interventions [1] for a comprehensive set of reviews for various infectious diseases. In the context of SARS-CoV-2 infection, viral dynamic models are used for three main purposes: (i) characterising the association of viral load with transmission and with clinical evolution, (ii) optimising treatment and vaccine strategies, and (iii) understanding the viral-host interactions.

From a public health perspective, these models can quantify the parameters that determine the kinetics of viral load and its distribution in the population. An important observation that has been made is that the peak of viral load coincides with the

symptom onset, at least in the pre-vaccination and Omicron era [2–4]. This means that patients may shed large amounts of virus in the few days that precede their symptom onset, and underscores the problem of infections occurring during the pre-symptomatic phase of the disease. When longitudinal studies are nested within epidemiological studies, longitudinal profiles of individuals can be used to assess the heterogeneity of viral dynamics, and evaluate the impact of variants of concern or vaccination [5,6], or suggest strategies to improve testing strategies [3,5,7]. If both the index and its high risk contacts are followed prospectively [8], modelling can also be used to reconstruct viral load at the time of contact, and explore the accrued risk of transmission caused by increased levels of viral shedding and temporal changes in infectiousness [9] (Fig. 1 arrow 1).

In the past, these models have also been widely used to optimise antiviral therapies (Fig. 1, arrow 2). By fitting frequent nasopharyngeal viral load data, it was found that R_0 was close to 10, albeit with variability across studies [10,11]. As the within-host equivalent of the herd immunity threshold, antiviral treatment must be above $1 - 1/R_0 = 90\%$ to dramatically reduce viral replication. Given the *in vitro* estimated drug EC_{50} (half maximal effective concentration) and their pharmacological properties, we have shown that repurposed antiviral agents (e.g., hydroxychloroquine, lopinavir, remdesivir, favipiravir) are unlikely to achieve this pharmacodynamic target, anticipating the negative outcome of all trials evaluating these molecules [10]. In the new era of monoclonal antibodies (mAbs), we still lack exhaustive analyses of viral kinetics during treatment. Analyses in the macaque model of COVA1-18 suggest that the efficacy of mAbs in blocking *de novo* cell infection in the upper and lower respiratory tract may exceed 95% [12], which is consistent with the impressive results of several mAbs in phase 3 clinical trials. Modelling analyses are now urgently needed to explore the causal pathways between antiviral effect, viral dynamics and clinical benefit. In particular, it is still unclear whether monoclonal antibodies might also be beneficial when administered at a later stage of infection. In an analysis of hospitalised patients from the French COVID-19 cohort, we showed that viral dynamics after admission was an independent factor associated with mortality [4]. With a treatment reducing viral production by 90%, the time to viral clearance can be shortened by more than 2 days on average, which could lead to a reduction in mortality of approximately 25% in high-risk patients (age ≥ 65 years with risk factors). Interestingly, the results of the Recovery trial supported these predictions; REGN-COV reduced

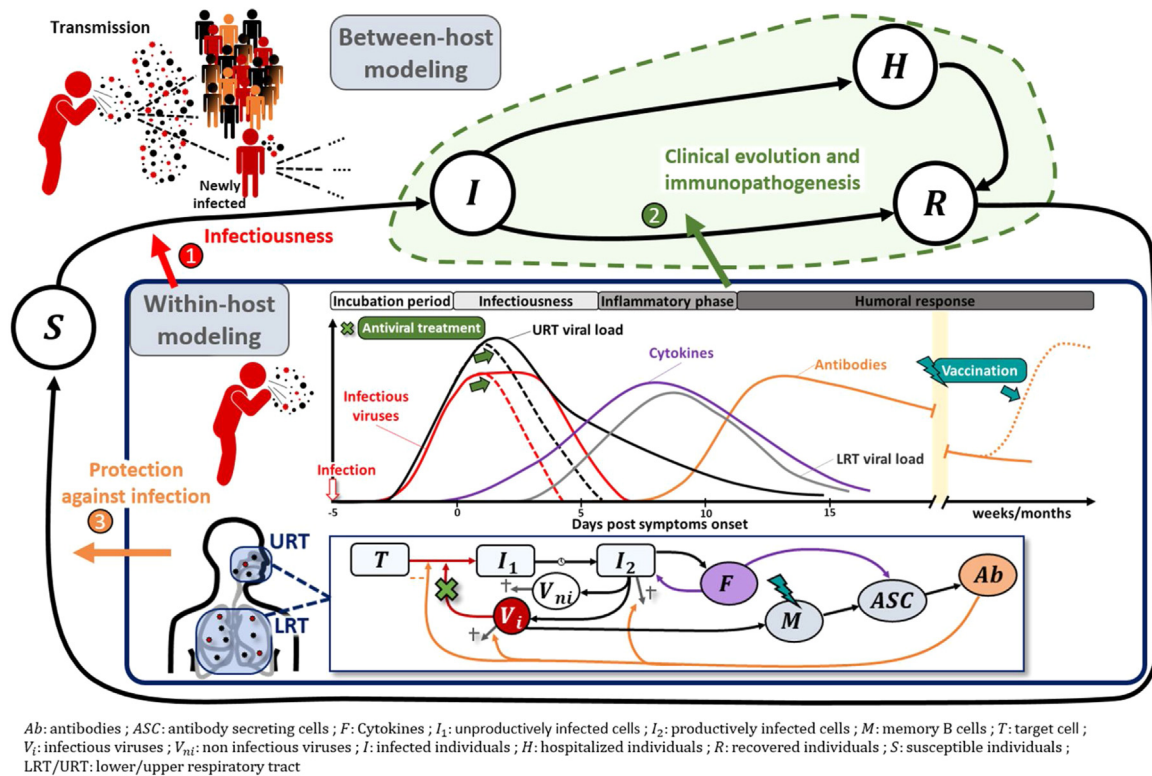


Fig. 1. Within-host models during the dynamics of an acute viral infection.

Models are used to understand the evolution of the viro-immunological response during an infection. As such, they can be used to disentangle the factors associated with (1) enhanced infectiousness during acute infection (2) progression towards a severe disease, and how to prevent it via pharmacological interventions (3) protection against infection via previous infection or vaccination.

mortality by 30% in patients who were seronegative at inclusion, a marker strongly associated with high viral load. Studies such as the randomised clinical trial Discovery (NCT 04315948) are now ongoing to examine the extent to which antiviral treatment may be relevant in hospitalised patients who had a high viral load at inclusion (Fig. 1, arrow 2).

Depending on the data collected, models may also provide insights into the role of the immune response on viral clearance. Several models have challenged the hypothesis of peak viral load being primarily caused by cell depletion, and have proposed models in which the innate [3] or adaptive immune response [4,11] plays a key role in viral clearance. These models can also be used to reproduce patterns observed in some patients, such as bimodal peak in viral load. However, these models are often limited by the difficulty of collecting frequent viral load and immunological data, which poses problems in parameter identifiability and leads to large uncertainty in parameter estimates.

For this reason, characterisation of the adaptive immune response within the host is often considered a separate problem. First, integrative analyses of multiple immunological markers can help understand the hyper inflammation and cytokine storm associated with clinical complications [13]. For instance, markers such as CD177 have been shown to be associated with disease progression and predict the course of patient hospitalisation trajectory [14]. Then, modelling the cellular and molecular determinants of the duration of antibody response is key to realistic prediction of epidemic dynamics, taking into account waning immunity (Fig. 1 arrow 3). Hence, the within-host modelling of Ebola vaccine response based on early phase 1 trial data has revealed the long-term duration of the response [15]. In what follows, we will focus on vaccination, but similar considerations can be applied to

natural infection. Of note, natural immunity confers at least similar [16] or longer-lasting and stronger protection against infection [17]. Binding and neutralising antibodies are clearly associated with protection against infection [18,19]. This means that the effect of vaccines on disease transmission and/or severity could be captured by these immunological markers, called correlates of protection (CoP). Defining such markers is critical to accelerate the development of new vaccines and vaccination strategies [20]. The use of within-host mathematical models can help in this investigation to define mechanistic CoP, which is directly related to the protective mechanism triggered by the vaccine, and thus causally responsible [21]. Therefore, within-host models help quantifying the effect of vaccines on the infection of new cells by SARS-CoV-2 through neutralisation [22]. Recent studies have also shown that neutralisation measured *in vitro* or *in vivo* is a reasonable mechanistic correlate of protection [19,23]. Finding good correlates of protection is particularly challenging in the context of an ever-evolving virus, where variants of concern (VoC) frequently emerge. Indeed, for each VoC, vaccine protection against transmission and hospitalisation needs to be rapidly assessed [24]. In addition, multiple mechanisms, and thus multiple biomarkers, could contribute to the protective efficacy of a vaccine. In the case of SARS-CoV-2, the role of T-cell responses has also been highlighted [25]. Therefore, expanding the framework for within-host modelling to integrate high-dimensional data generated in current immunological studies is promising research.

Conflicts of interest

The authors declare that they have no conflict of interest.

Acknowledgement

This work has received funding from the French Agency for Research on AIDS and Emerging Infectious Diseases via the EMERGEN project (ANRS0151).

References

- [1] Perelson AS, Ribeiro RM. Introduction to modeling viral infections and immunity. *Immunol Rev* 2018;285:5–8. <http://dx.doi.org/10.1111/immr.12700>.
- [2] He X, Lau EH, Wu P, Deng X, Wang J, Hao X, et al. Temporal dynamics in viral shedding and transmissibility of COVID-19. *Nat Med* 2020;26:672–5. <http://dx.doi.org/10.1038/s41591-020-0869-5>.
- [3] Ke R, Zitzmann C, Ho DD, Ribeiro RM, Perelson AS. In vivo kinetics of SARS-CoV-2 infection and its relationship with a person's infectiousness. *Proc Natl Acad Sci* 2021;118(49). <http://dx.doi.org/10.1073/pnas.2111477118>.
- [4] Néant N, Lingas G, Le Hingrat Q, Ghosn J, Engelmann I, Lepiller Q, et al. Modeling SARS-CoV-2 viral kinetics and association with mortality in hospitalized patients from the French COVID cohort. *Proc Natl Acad Sci* 2021;118(8). <http://dx.doi.org/10.1073/pnas.2017962118>.
- [5] Kissler SM, Fauver JR, Mack C, Olesen SV, Tai C, Shiue KY, et al. Viral dynamics of acute SARS-CoV-2 infection and applications to diagnostic and public health strategies. *PLoS Biol* 2021;19e3001333. <http://dx.doi.org/10.1371/journal.pbio.3001333>.
- [6] Kissler SM, Fauver JR, Mack C, Tai CG, Breban MI, Watkins AE, et al. Viral dynamics of SARS-CoV-2 variants in vaccinated and unvaccinated persons. *N Engl J Med* 2021;385:2489–91. <http://dx.doi.org/10.1056/NEJMc2102507>.
- [7] Ejima K, Kim KS, Iwanami S, Fujita Y, Li M, Zoh RS, et al. Time variation in the probability of failing to detect a case of polymerase chain reaction testing for SARS-CoV-2 as estimated from a viral dynamics model. *J R Soc Interface* 2021;18. <http://dx.doi.org/10.1098/rsif.2020.0947>.
- [8] Marks M, Millat-Martinez P, Ouchi D, Roberts C, Alemany A, Corbacho-Monné M, et al. Transmission of COVID-19 in 282 clusters in Catalonia, Spain: a cohort study. *Lancet Infect Dis* 2021;21(5):629–36. [http://dx.doi.org/10.1016/S1473-3099\(20\)30985-3](http://dx.doi.org/10.1016/S1473-3099(20)30985-3).
- [9] Marc A, Kerioui M, Blanquart F, Bertrand J, Mitjà O, Corbacho-Monné M, et al. Quantifying the relationship between SARS-CoV-2 viral load and infectiousness. *eLife* 2021;10e69302. <http://dx.doi.org/10.7554/eLife.69302>.
- [10] Gonçalves A, Bertrand J, Ke R, Comets E, de Lamballerie X, Malvy D, et al. Timing of antiviral treatment initiation is critical to reduce SARS-CoV-2 viral load. *CPT Pharmacometrics Syst Pharmacol* 2020;9:509–14. <http://dx.doi.org/10.1002/psp4.12543>.
- [11] Goyal A, Cardozo-Ojeda EF, Schiffer JT. Potency and timing of antiviral therapy as determinants of duration of SARS-CoV-2 shedding and intensity of inflammatory response. *Sci Adv* 2020;6eabc7112. <http://dx.doi.org/10.1126/sciadv.abc7112>.
- [12] Maisonnasse P, Aldon Y, Marc A, Marlin R, Dereuddre-Bosquet N, Kuzmina NA, et al. COVA1-18 neutralizing antibody protects against SARS-CoV-2 in three preclinical models. *Nat Commun* 2021;12:6097. <http://dx.doi.org/10.1038/s41467-021-26354-0>.
- [13] Chen G, Wu D, Guo W, Cao Y, Huang D, Wang H, et al. Clinical and immunological features of severe and moderate coronavirus disease 2019. *J Clin Invest* 2020;130:2620–9. <http://dx.doi.org/10.1172/JCI137244>.
- [14] Lévy Y, Wiedemann A, Hejblum BP, Durand M, Lefebvre C, Surénaud M, et al. CD177, a specific marker of neutrophil activation, is associated with coronavirus disease 2019 severity and death. *iScience* 2021;24:102711. <http://dx.doi.org/10.1016/j.isci.2021.102711>.
- [15] Pasin C, Balelli I, Van Effelther T, Bockstal V, Solfrosi L, Prague M, et al. Dynamics of the humoral immune response to a prime-boost ebola vaccine: quantification and sources of variation. *J Virol* 2019;93. <http://dx.doi.org/10.1128/JVI.00579-19>.
- [16] Kojima N, Klausner JD. Protective immunity after recovery from SARS-CoV-2 infection. *Lancet Infect Dis* 2022;22:12–4. [http://dx.doi.org/10.1016/S1473-3099\(21\)00676-9](http://dx.doi.org/10.1016/S1473-3099(21)00676-9).
- [17] Gazit S, Shlezinger R, Perez G, Lotan R, Peretz A, Ben-Tov A, et al. Comparing SARS-CoV-2 natural immunity to vaccine-induced immunity: reinfections versus breakthrough infections (preprint). *MedRxiv* 2021. <http://dx.doi.org/10.1101/2021.08.24.21262415>.
- [18] Feng S, Phillips DJ, White T, Sayal H, Aley PK, Bibi S, et al. Correlates of protection against symptomatic and asymptomatic SARS-CoV-2 infection. *Nat Med* 2021;27:2032–40. <http://dx.doi.org/10.1038/s41591-021-01540-1>.
- [19] Khoury DS, Cromer D, Reynaldi A, Schlub TE, Wheatley AK, Juno JA, et al. Neutralizing antibody levels are highly predictive of immune protection from symptomatic SARS-CoV-2 infection. *Nat Med* 2021;27:1205–11. <http://dx.doi.org/10.1038/s41591-021-01377-8>.
- [20] Jin P, Li J, Pan H, Wu Y, Zhu F. Immunological surrogate endpoints of COVID-2019 vaccines: the evidence we have versus the evidence we need. *Sig Transduct Target Ther* 2021;6:48. <http://dx.doi.org/10.1038/s41392-021-00481-y>.
- [21] Plotkin SA, Gilbert PB. Nomenclature for immune correlates of protection after vaccination. *Clin Infect Dis* 2012;54:1615–7. <http://dx.doi.org/10.1093/cid/cis238>.
- [22] Alexandre M, Marlin R, Prague M, Coleon S, Kahlaoui N, Cardinaud S, et al. SARS-CoV-2 mechanistic correlates of protection: insight from modelling response to vaccines (preprint). *BioRxiv* 2021. <http://dx.doi.org/10.1101/2021.10.29.466418>.
- [23] Gilbert PB, Montefiori DC, McDermott AB, Fong Y, Benkeser D, Deng W, et al. Immune correlates analysis of the mRNA-1273 COVID-19 vaccine efficacy clinical trial. *Science* 2022;375:43–50. <http://dx.doi.org/10.1126/science.abm3425>.
- [24] Higdon MM, Wahl B, Jones CB, Rosen JG, Truelove SA, Baidya A, et al. A systematic review of COVID-19 vaccine efficacy and effectiveness against SARS-CoV-2 infection and disease (preprint). *MedRxiv* 2021. <http://dx.doi.org/10.1101/2021.09.17.21263549>.
- [25] Sette A, Crotty S. Adaptive immunity to SARS-CoV-2 and COVID-19. *Cell* 2021;184(4):861–80. <http://dx.doi.org/10.1016/j.cell.2021.01.007>.

Mélanie Prague^{a,b,1,*}, Marie Alexandre^{a,b}, Rodolphe Thiébaud^{a,b}, Jérémie Guedj^{c,1}

^aUniv. Bordeaux, Department of Public Health, INSERM UMR 1219 Bordeaux Population Health Research Centre, Inria SISTM, Bordeaux, France

^bVaccine Research Institute, Créteil, France

^cUniversité de Paris, IAME, INSERM, F-75018 Paris, France

*Corresponding author at: Université de Bordeaux 146 rue Léon-Saignat CS 61292 33076 BORDEAUX CEDEX
E-mail address: melanie.prague@inria.fr (M. Prague)

¹Contributed equally.

Available online

5.3 Model building strategy in mechanistic model to identify mechanistic correlates of protection in NHP pre-clinical trials

This work was conducted in deep collaboration with the vaccine research Institut and the Infectious Disease Models and Innovative Therapies research infrastructure, coordinated by the CEA (Commissariat à l'énergie atomique et aux énergies alternatives) and involving partnerships between CEA, Pasteur Institut, Inserm and ANRS, among others.

Title: Modelling the response to vaccine in Non-Human Primates to define SARS-CoV-2 mechanistic correlates of protection

Authors: Marie Alexandre¹, Romain Marlin^{2,†}, Mélanie Prague^{1,†}, Séverin Coleon^{3,4}, Nidhal Kahlaoui², Sylvain Cardinaud^{3,4}, Thibaut Naninck², Benoit Delache², Mathieu Surenaud^{3,4}, Mathilde Galhaut², Nathalie Dereuddre-Bosquet², Mariangela Cavarelli², Pauline Maisonnasse², Mireille Centlivre^{3,4}, Christine Lacabaratz^{3,4}, Aurelie Wiedemann^{3,4}, Sandra Zurawski⁵, Gerard Zurawski⁵, Olivier Schwartz^{3,6,7}, Rogier W Sanders⁸, Roger Le Grand², Yves Levy^{3,4,9}, Rodolphe Thiébaud^{1,3,10,*}

Affiliations:

¹ Univ. Bordeaux, Department of Public Health, Inserm Bordeaux Population Health Research Centre, Inria SISTM, UMR 1219; Bordeaux, France.

² Center for Immunology of Viral, Auto-immune, Hematological and Bacterial diseases (IMVA-HB/IDMIT), Université Paris-Saclay, Inserm, CEA; Fontenay-aux-Roses, France.

³ Vaccine Research Institute; Creteil, France.

⁴ Inserm U955, Equipe 16; Créteil, France.

⁵ Baylor Scott and White Research Institute and INSERM U955; Dallas, Texas, United States of America.

⁶ Virus & Immunity Unit, Department of Virology, Institut Pasteur; Paris, France.

⁷ CNRS UMR 3569; Paris, France.

⁸ Department of Medical Microbiology, Amsterdam UMC, University of Amsterdam, Amsterdam Infection & Immunity Institute; 1105 AZ Amsterdam, the Netherlands.

⁹ AP-HP, Hôpital Henri-Mondor Albert-Chenevier, Service d'Immunologie Clinique et Maladies Infectieuses; Créteil, France.

¹⁰ CHU Bordeaux, Department of Medical information; Bordeaux, France.

*Corresponding author: Prof Rodolphe Thiébaud

Bordeaux University, Departement of Public Health
146 Rue Leo Saignat, 33076 Bordeaux Cedex, France
rodolphe.thiebaud@u-bordeaux.fr

[†] These authors contributed equally to this work.

31 **One Sentence Summary:** A model-based approach for modelling the immune control of viral dynamics is
32 applied to quantify the effect of several SARS-CoV-2 vaccine platforms and to define mechanistic correlates
33 of protection.

34
35 **Abstract:** The definition of correlates of protection is critical for the development of next generation SARS-
36 CoV-2 vaccine platforms. Here, we propose a model-based approach for identifying mechanistic correlates
37 of protection based on mathematical modelling of viral dynamics and data mining of immunological
38 markers. The application to three different studies in non-human primates evaluating SARS-CoV-2 vaccines
39 based on CD40-targeting, two-component spike nanoparticle and mRNA 1273 identifies and quantifies
40 two main mechanisms that are a decrease of rate of cell infection and an increase in clearance of infected
41 cells. Inhibition of RBD binding to ACE2 appears to be a robust mechanistic correlate of protection across
42 the three vaccine platforms although not capturing the whole biological vaccine effect. The model shows
43 that RBD/ACE2 binding inhibition represents a strong mechanism of protection which required significant
44 reduction in blocking potency to effectively compromise the control of viral replication.

45
46 **Key words:** SARS-CoV-2, Correlate of protection, Neutralization, Vaccines
47
48

49 INTRODUCTION

50 There is an unprecedented effort for SARS-CoV-2 vaccine development with 294 candidates currently
51 evaluated (1). However, variants of concern have emerged before the vaccine coverage was large enough
52 to control the pandemics (2). Despite a high rate of vaccine protection, these variants might compromise
53 the efficacy of current vaccines (3–6). Control of the epidemic by mass vaccination may also be
54 compromised by unknown factors such as long-term protection and the need of booster injections in
55 fragile, immuno-compromised, elderly populations, or even for any individual if protective antibody levels
56 wane. Furthermore, the repeated use of some of the currently approved vaccine could be compromised
57 by potential adverse events or by immunity against vaccine viral vectors (7). Finally, the necessity to
58 produce the billions of doses required to vaccinate the world's population also explains the need to
59 develop additional vaccine candidates.

60
61 The identification of correlates of protection (CoP) is essential to accelerate the development of new
62 vaccines and vaccination strategies (8, 9). Binding antibodies to SARS-CoV-2 and *in vitro* neutralization of
63 virus infection are clearly associated with protection (10–13). However, the respective contribution to
64 virus control *in vivo* remains unclear (14), and many other immunological mechanisms may also be
65 involved, including other antibody-mediated functions (antibody-dependent cellular cytotoxicity,
66 antibody-dependent complement deposition, antibody-dependent cellular phagocytosis (11, 15, 16)), as
67 well as T cell immunity (17). Furthermore, correlates of protection may vary between the vaccine
68 platforms (18–21).

69 Non-human primate (NHP) studies offer a unique opportunity to evaluate early markers of protective
70 response (22, 23). Challenge studies in NHP allow the evaluation of vaccine impact on the viral dynamics
71 in different tissue compartments (upper and lower respiratory tract) from day one of virus exposure (11,

72 15, 24). Such approaches in animal models may thus help to infer, for example, the relation between early
73 viral events and disease or the capacity to control secondary transmissions.

74 Here, we propose to apply a model-based approach on NHP studies to evaluate i) the immune mechanisms
75 involved in the vaccine response, and ii) the markers capturing this/these effect(s) leading to identification
76 of mechanisms of protection and definition of mechanistic CoP (25). First, we present a mechanistic
77 approach based on ordinary differential equation (ODE) models reflecting the virus-host interaction
78 inspired from models proposed for SARS-CoV-2 infection (26–31) and other viruses (32–35). The proposed
79 model includes several new aspects refining the modeling of viral dynamics *in vivo*, in addition to the
80 integration of vaccine effect. A specific inoculum compartment allows distinguishing the virus coming from
81 the challenge inoculum and the virus produced *de novo*, which is a key point in the context of efficacy
82 provided by antigen specific pre-existing immune effectors induced by the vaccine. Then, an original data
83 mining approach is implemented to identify the immunological biomarkers associated with specific
84 mechanisms of vaccine-induced protection.

85 We apply our approach to a recently published study (36) testing a protein-based vaccine targeting the
86 receptor-binding domain (RBD) of the SARS-CoV-2 spike protein to CD40 (α CD40.RBD vaccine). Targeting
87 vaccine antigens to dendritic cells via the surface receptor CD40 represents an appealing strategy to
88 improve subunit-vaccine efficacy (37–40) and for boosting natural immunity in SARS-CoV-2 convalescent
89 NHP.

90 We show that immunity induced by natural SARS-CoV-2 infection, as well as vaccine-elicited immune
91 responses contribute to viral load control by i) blocking new infection of target cells and ii) by increasing
92 the loss of infected cells. The modelling showed that antibodies inhibiting binding of RBD domain to ACE2
93 correlated with blockade of new infections and RBD binding antibodies correlate with the loss of infected
94 cells, reflecting importance of additional antibody functionalities. The role of RBD/ACE2 binding inhibition
95 has been confirmed in two other vaccine platforms.

96 97 RESULTS

98 A new mechanistic model fits the *in vivo* viral load dynamics in nasopharyngeal and tracheal 99 compartments

100 The mechanistic model aims at capturing the viral dynamics following challenge with SARS-CoV-2 virus in
101 NHP. For that purpose, we used data obtained from 18 cynomolgus macaques involved in the vaccine
102 study reported by Marlin et al (36) and exposed to a high dose (1×10^6 pfu) of SARS-CoV-2 administered via
103 the combined intra-nasal and intra-tracheal route. The viral dynamics during the primary infections were
104 characterized by a peak of genomic RNA (gRNA) production three days post-infection in both tracheal and
105 nasopharyngeal compartments, followed by a decrease toward undetectable levels beyond day 15 (**Figure
106 1 – figure supplement 1**). At the convalescent phase (median 24 weeks after the primary infection), 12
107 macaques were challenged with SARS-CoV-2 a second time, four weeks after being randomly selected to
108 receive either a placebo (n=6) or a single injection of the α CD40.RBD vaccine (n=6) (**Figure 1A**). A third
109 group of 6 naïve animals were infected at the same time. Compared to this naïve group, viral dynamics
110 were blunted following the second challenge of convalescent animals with the lowest viral load observed
111 in vaccinated animals (**Figure 1B, Figure 1 - figure supplement 2**).

112 We developed a mathematical model to better characterize the impact of the immune response on the
113 viral gRNA and subgenomic RNA (sgRNA) dynamics, adapted from previously published work (26, 27, 41),

114 which includes uninfected target cells (T) that can be infected (I_1) and produce virus after an eclipse phase
115 (I_2). The virus generated can be infectious (V_i) or non-infectious (V_{ni}). Although a single compartment for
116 *de novo* produced viruses (V) could be mathematically considered, two distinct ODE compartments were
117 assumed for a better understanding of the model. We completed the model by a compartment for the
118 inoculum to distinguish between the injected virus (V_s) and the virus produced *de novo* by the host (V_i and
119 V_{ni}). In both compartments of the upper respiratory tract (URT), the trachea and nasopharynx, viral
120 dynamics were distinctively described by this model (**Figure 2A**). Viral exchange between the two
121 compartments was tested (either from the nasopharynx to the trachea or vice versa). However, as
122 described in the literature (28, 42, 43) and demonstrated by the additional modeling work in Appendix 1
123 “Model building”, viral transport within the respiratory tract plays a negligible role in viral kinetics
124 compared with viral clearance. Consequently, no exchange was considered in the model. Using the gRNA
125 and sgRNA viral loads, we jointly estimated (i.e., shared random effects and covariates) the viral infectivity
126 (β), the viral production rate (P) and the loss rate of infected cells (δ) in the two compartments. We
127 assumed that gRNA and sgRNA were proportional to the free virus and the infected cells, respectively. This
128 modeling choice relied on both biological and mathematical reasons (see section Methods for more
129 details). Due to identifiability issues, the duration of the eclipse phase ($1/k$), the clearance of free viruses
130 from the inoculum (c_i) and produced *de novo* (c) were estimated separately by profile likelihood and
131 assumed to be identical in the two compartments of the URT. In addition, infectious and non-infectious
132 viruses were assumed to be cleared at the same rate. We estimated the viral infectivity at 0.95×10^{-6} ($CI_{95\%}$
133 [0.18×10^{-6} ; 4.94×10^{-6}]) (copies/ml) $^{-1}$ day $^{-1}$ in naïve animals, which is in the range of previously reported
134 modelling results whether in the case of SARS-CoV-2 virus (27, 29), or influenza (32, 33). We found
135 estimates of the loss rates of infected cells of 1.04 ($CI_{95\%}$ [0.79; 1.37]) day $^{-1}$, corresponding to a mean half-
136 life of 0.67 day. This estimation was consistent with previously published results obtained on SARS-CoV-2
137 virus showing the mean value of this parameter ranging from 0.60 to 2 days $^{-1}$ (i.e., half-life between 0.35
138 and 1.16 days) (26–30). The eclipse phase (3 days $^{-1}$) was found similar to the values commonly used in the
139 literature (26, 30, 32, 41). Here, we distinguished the clearance of the inoculum which was much higher
140 (20 virions day $^{-1}$) as compared to the clearance of the virus produced *de novo* (3 virions day $^{-1}$). While the
141 half-life of the virus *de novo* produced usually approximates 1.7 hours (i.e., $c=10$ day $^{-1}$) (26, 28, 30, 32),
142 because of this distinction, our model provided a higher estimation of 5.5 hours which remained in
143 accordance with the estimations obtained by Baccam et al. (2006) (41) on influenza A. Furthermore, the
144 viral production by each infected cells was estimated to be higher in the nasopharyngeal compartment
145 (12.1×10^3 virions/cell/day, $CI_{95\%}$ [3.15×10^3 ; 46.5×10^3]) as compared to the tracheal compartment (0.92×10^3
146 virions/cell/day, $CI_{95\%}$ [0.39×10^3 ; 2.13×10^3]). These estimations are in agreement with the observation of
147 the intense production of viral particles by primary human bronchial epithelial cells in culture (44). In
148 particular, they are in the range of estimates obtained within the URT, either in NHP (28) or in humans
149 (29), with the product pxT_0 equals to 15.1×10^8 ($CI_{95\%}$ [3.98×10^8 ; 58.1×10^8]) and 0.21×10^8 ($CI_{95\%}$ [0.088×10^8 ;
150 0.48×10^8]) virions/ml/day in the nasopharynx and the trachea, respectively. By allowing parameters to
151 differ between animals (through random effects), the variation of cell infectivity and of the loss rate of
152 infected cells captured the observed variation of the dynamics of viral load. The variation of those
153 parameters could be partly explained by the group to which the animals belong reducing the unexplained
154 variability of the cell infectivity by 66% and of the loss rate of infected cells by 54% (**Supplementary file 1**).
155 The model fitted well the observed dynamics of gRNA and sgRNA (**Figure 2B**).

156

157 **Modelling of the dynamics of viral replication argues for the capacity of α CD40.RBD vaccine to block** 158 **virus entry into host cells and to promote the destruction of infected cells**

159 We distinguish the respective contribution of the vaccine effect and post-infection immunity on the
160 reduction of the cell infection rate and the increase of the clearance of infected cells. Because blocking *de*

161 *novo* infection and promoting the destruction of infected cells would lead to different viral dynamics
162 profile (**Figure 2 – figure supplement 1**), we were able to identify the contribution of each mechanism by
163 estimating the influence of the vaccine compared to placebo or naive animals on each model parameter.
164 The α CD40.RBD vaccine reduced by 99.6% the infection of target cells in the trachea compared to the
165 naïve group. The estimated clearance of infected cells was 1.04 day^{-1} (95% CI 0.75; 1.45) in naïve macaques.
166 It was increased by 80% ($1.86/\text{day}^{-1}$) in the convalescent macaques vaccinated by α CD40.RBD or not.

167 The mechanistic model allows predicting the dynamics of unobserved compartments. Hence, a very early
168 decrease of the target cells (all cells expressing ACE2) as well as of the viral inoculum which fully
169 disappeared from day 2 onward were predicted (**Figure 2C**). In the three groups, the number of infected
170 cells as well as infectious viral particles increased up to day 2 and then decreased. We show that this viral
171 dynamic was blunted in the vaccinated animals leading to a predicted maximum number of infectious viral
172 particles in the nasopharynx and the trachea below the detection threshold (**Figure 2C**). The number of
173 target cells would be decreased by the infection in the naïve and the convalescent groups, whereas it
174 would be preserved in vaccinated animals.

175

176 **The RBD-ACE2 binding inhibition is the main mechanistic CoP explaining the effect of the α CD40.RBD** 177 **vaccine on new cell infection**

178 In our study (36), an extensive evaluation of the immunological response has been performed with
179 quantification of spike binding antibodies, antibodies inhibiting the attachment of RBD to ACE2, antibodies
180 neutralizing infection, SARS-CoV-2-specific CD4⁺ and CD8⁺ T cells producing cytokines and serum cytokine
181 levels (**Figure 3, Figure 1 - figure supplement 3, 4, 5**). Therefore, based on our mechanistic model we
182 investigated if any of these markers could serve as a mechanistic CoP. Such a CoP should be able to capture
183 the effect of the natural immunity following infection, associated or not to the vaccine (group effect)
184 estimated on both the rate of cell infection and the rate of the loss of infected cells. To this aim, we
185 performed a systematic screening by adjusting the model for each marker and we compared these new
186 models with the model without covariates and with the model adjusted for the groups. In particular, our
187 approach allowed us to benefit from all the information provided by the overall dynamics of the
188 immunological markers after the exposure by integrating them as time-varying covariates (see the
189 methods section for a detailed description of the algorithm). We demonstrate that the RBD-ACE2 binding
190 inhibition measure is sufficient to capture most of the effect of the groups on the infection of target cells
191 (**Figure 4A, 4B**). The integration of this marker in the model explains the variability of the cell infection rate
192 with greater certainty than the group of intervention, reducing the unexplained variability by 87%
193 compared to 66% (**Supplementary file 1**). The marker actually takes into account the variation between
194 animals within the same group. Hence, it suggests that the levels of anti-RBD antibodies induced by the
195 vaccine that block attachment to ACE2 are highly efficient at reflecting the neutralization of new infections
196 *in vivo*. Furthermore, when taking into account the information provided by the RBD-ACE2 binding
197 inhibition assay, the effect of the group of intervention was no longer significant (**Supplementary file 1**).
198 Finally, we looked at the estimated viral infectivity according to the binding inhibition assay in each animal.
199 A positive dependence was found between the viral infectivity and the RBD-ACE2 binding inhibition
200 measure, linking an increase of 10^3 AU of the marker, whether over time or between animals, with an
201 increase of 1.8% (95CI% [1.2%; 2.3%]) of the viral infectivity (see **Supplementary file 4**). Accordingly, the
202 values at the time of exposure were not overlapping at all, distinguishing clearly the vaccinated and
203 unvaccinated animals (see **Figure 4C**).

204

205 In the next step, several markers (IgG binding anti-RBD antibodies, CD8⁺ T cells producing IFN- γ) appeared
206 to be associated to the rate of loss of infected cells (**Figure 4 – figure supplement 1A**). Both specific
207 antibodies and specific CD8⁺ T cells are mechanisms commonly considered important for killing infected
208 cells. We retained the anti-RBD binding IgG Ab that were positively associated to the increase of the loss
209 of infected cells. For unknown reason the IFN- γ response was high in unstimulated conditions in the naïve
210 group. Thus, although this marker was associated with a decrease of the loss rate of infected cells, it
211 appears essentially here as an indicator of the animal group. Further studies would be needed to fully
212 confirm the place of IFN- γ response as a mechanistic marker.

213 A large part of the variation of the infection rate (71%) and loss rate of infected cells (60%) were captured
214 by the two markers of CoP: the RBD-ACE2 binding inhibition and the anti-RBD binding Ab concentration.
215 Using the estimated parameters, the effective reproduction number could be calculated (R) which is
216 representing the number of cells secondarily infected by virus from one infected cell (**Figure 4D**). When
217 looking at this effective reproduction number according to the groups, the vaccinated animal presented
218 from the first day of challenge an effective R below 1 meaning that no propagation of the infection started
219 within the host. These results were consistent when taking the value of RBD-ACE2 binding inhibition at the
220 time of the challenge without considering the evolution of the inhibition capacity over time (**Figure 4 -**
221 **figure supplement 1B**). This means that the dynamics of the viral replication is impacted very early during
222 the infection process in immunized (i.e., both convalescent and vaccinated) animals and that vaccinated
223 animals were protected from the beginning by the humoral response. Then, we looked at the threshold of
224 the markers of interest leading to the control of the within-host infection (as defined by $R < 1$) which was
225 around 30 000 AU for the RBD-ACE2 binding inhibition assay. For the animals in the naïve and the
226 convalescent groups, the observed values of binding inhibition measured by ECL RBD (the lower the better)
227 and of IgG anti-RBD binding antibodies (the higher the better) led to $R > 1$, whereas in vaccinated animals,
228 the value of ECL RBD led to $R < 1$. Therefore, our modeling study shows that the inhibition of binding of RBD
229 to ACE2 by antibodies is sufficient to control initial infection of the host (**Figure 4E**). According to the
230 observed value of ECL RBD in vaccinated animals (e.g., 66 AU in **Figure 4E**), a decrease of more than 2 \log_{10}
231 of the inhibition capacity (to reach 81 000 AU), due to variant of concern (VoC) or waning of immunity,
232 would have been necessary to impair the control of the within-host infection. Moreover, a decrease of the
233 neutralizing activity (i.e., increased ECL) could be compensated by an increase of cell death as measured
234 by an increase of binding IgG anti-RBD as a surrogate. As an example, increasing IgG anti-RBD from 2.5 to
235 10 in the animal MF7 of the convalescent group would lead to a control of the infection.

236 In conclusion, the α CD40.RBD vaccine-elicited humoral response leads to the blockade of new cell
237 infection that is well captured by measure of the inhibition of attachment of the virus to ACE2 through the
238 RBD domain of the spike protein. Hence, the inhibition of binding of RBD to ACE2 is a promising
239 mechanistic CoP. Indeed, this CoP fulfils the three criteria of leading to the best fit (lower BIC), the best
240 explanation of inter-individual variability, and fully captured the effect of the group of intervention.

241 242 **The model revealed the same CoP related to another protein-based vaccine but not with mRNA-1273** 243 **vaccine**

244 We took the opportunity of another study testing a two-component spike nanoparticle protein-based
245 vaccine performed in the same laboratory and using the same immune and virological assays (45),
246 measured only at the time of exposure, for applying the proposed model and methodology. In this study,
247 6 animals were vaccinated and compared to 4 naïve animals (**Figure 5A, 5B**). The good fit of the data
248 (**Figure 5C, 5D**) allows for estimating the effect of the vaccine that appeared here also to decrease the
249 infectivity rate (by 99%) and increase the clearance of the infected cells by 79%. Looking at the best
250 mechanistic CoP following the previously described strategy, we ended here again with the inhibition of

251 RBD binding to ACE2 as measured by ECL RBD. In fact, this marker measured at baseline before challenge
252 fulfilled the three criteria: i) it led to the best model in front of a model adjusted for group effect, ii) it
253 rendered the group effect non-significant and iii) it explained around 71% of the infectivity rate variability,
254 compared to 65% of variability explained by the groups. Interestingly, here again, the inhibition assay led
255 to a clear separation of the estimated rate of infectivity between vaccinees and the placebo group (**Figure**
256 **5E**).

257 Finally, we applied our approach to a published NHP study performed to evaluate several doses of mRNA-
258 1273 vaccine (24). Using available data, we compared the viral dynamics in the 100 µg, 10 µg and placebo
259 groups, enrolling a total of 12 rhesus macaques in a 1:1:1 ratio. Similar to the previous study, only immune
260 markers measured at the time of exposure were available in this study, in addition to viral dynamics. We
261 started from the same model as defined previously. We estimated a reduction of the infection rate by 97%
262 but we did not find any additional effect. Looking at potential mechanistic CoP, we retained neutralization
263 as measured on live cells with Luciferase marker. Although this marker led to the best fit and replaced the
264 group effect (which was non-significant after adjustment for the marker), it explained only 15% of the
265 variability of estimated viral infectivity, while 19% were explained by the groups.

266 In conclusion, we demonstrated, based upon challenge studies in NHP vaccinated with two different
267 protein-based vaccine platforms that both vaccines lead to the blockade of new cell infection. Neutralizing
268 antibodies likely represent a consistent mechanistic correlate of protection. This could change across
269 vaccine platforms especially because mechanisms of action are different.

270

271 **DISCUSSION**

272 We explored the mechanistic effects of three SARS-CoV-2 vaccines and assessed the quality of markers as
273 mechanistic CoP (mCoP). This model showed that neutralizing and binding antibodies, elicited by a non-
274 adjuvanted protein-based vaccine targeting the RBD of spike to the CD40 receptor of antigen presenting
275 cells are reliable mCoP. Interestingly, we found the simpler and easier to standardize and implement
276 binding inhibition assay may be more relevant to use as a correlate of protection than cell-culture
277 neutralization assays. This result has been replicated in another study testing a nanoparticle spike vaccine.
278 The model was able to capture the effect of the vaccines on the reduction of the rate of infection of target
279 cells and identified additional effects of vaccines beyond neutralizing antibodies. This latter consisted of
280 increasing the loss rate of infected cells which was better reflected by the IgG binding antibodies and CD8⁺
281 T cell responses in the case of the CD40-targeting vaccine. One limitation of our study is that the prediction
282 potential of our model relies on the range of the immune markers measured. However, our approach
283 would allow a full exploitation of the data generated as in systems serology where non-neutralizing Ab
284 functions, such as Ab-dependent cellular cytotoxicity (ADCC), Ab-dependent cellular phagocytosis (ADCP),
285 Ab-dependent complement deposition (ADCD), and Ab-dependent respiratory burst (ADRB) are explored
286 (46). The role of ADCC in natural infection has been previously shown (47), ADCD in DNA vaccine recipients
287 (11) and with Ad26 vaccine (48). Here, we extended significantly these data by modelling the viral dynamic,
288 showing that two other protein-based vaccines exert an additional effect on infected cell death which
289 relied on the level of IgG anti-RBD binding antibodies especially for the CD40.RBD targeting vaccine.
290 Measurements of other non-neutralizing Ab functions would probably also capture this additional effect.

291

292 The next question after determining which marker is a valid mCoP is to define the concentration that leads
293 to protection, looking for a threshold effect that will help to define an objective (10, 49). In the context of
294 SARS-CoV-2 virus, several emerged variants are leading to a significant reduction of viral neutralization as
295 measured by various approaches. However, a 20-fold reduction of viral neutralization might not translate

296 in 20-fold reduction of vaccine efficacy (50). First, there are many steps between viral neutralization and
297 the reduction of viral infectivity or the improvement of clinical symptoms. Second, the consequences of a
298 reduction of viral neutralization could be alleviated by other immunological mechanisms not compromised
299 by the variant. In the context of natural immunity, when the level of neutralizing antibodies was below a
300 protective threshold, the cellular immune response appeared to be critical (17, 51). We showed with our
301 model that an improvement of infected cell destruction could help to control the within-host infection and
302 is quantitatively feasible.

303 The control of viral replication is the key for reducing infectivity (52, 53) as well as disease severity (54,
304 55). According to our non-linear model linking the neutralization to the viral replication, a decrease of 4 to
305 20-fold in neutralization as described for the variants of concern (4, 6) is not enough, especially in the
306 context of the response to CD40.RBD targeting vaccine, to compromise the control of viral replication. The
307 results showing a conserved effectiveness of mRNA vaccines in humans infected by the alpha or beta
308 variants (56), although a decrease of neutralization has been reported (4), are consistent with this
309 hypothesis. However, this is highly dependent upon the mode of action of currently used vaccines and
310 upon the VoC that may much more compromise the neutralization but being also intrinsically less
311 pathogenic such as Omicron (57).

312
313 The analysis performed extended significantly the observation of associations between markers as
314 previously reported for SARS-CoV-2 vaccine (11) and other vaccines (58) because it allows a more causal
315 interpretation of the effect of immune markers. However, our modelling approach requires the *in vivo*
316 identification of the biological parameters under specific experimentations. On the other hand, the
317 estimation of parameters included in our model also provided information on some aspect of the virus
318 pathophysiology. Notably, we found an increased capacity of virion production in nasopharynx compared
319 to the trachea which could be explained by the difference in target cells according to the compartment
320 (59). This result needs to be confirmed as it may also be the consequence of a different local immune
321 response (60). The choice of the structural model defining the host-pathogen interaction is a fundamental
322 step in the presented approach. Here, it was well guided by the biological knowledge, the existing models
323 for viral dynamics (34, 61, 62) and the statistical inference allowing the selection of the model that best fit
324 the data. Nevertheless, many modeling choices for the statistical model were made in this approach and
325 more theoretical work evaluating the robustness of the results in their regards may be relevant for future
326 works. In particular, we could relax the constraint of linear interpolation of marker dynamics by using
327 simple regression models, allowing in the same time the integration of error model to account for
328 measurement error for time-varying covariates (63–65). Moreover, by construction, we assumed similar
329 interindividual variability and effects of covariates within the two URT compartments as well as similar
330 values for the viral infectivity and the loss rate of infected cells. Viral load dynamics measured in lungs
331 being different from those in the URT (66, 67), the relaxation of this hypothesis of homogeneous
332 physiological behavior in the URT may be pertinent to extend the model to the LRT. Finally, it should be
333 underlined that the dynamics of the immune response has not been modelled as suggested for instance
334 for B cell response (68). This clearly constitutes the next step after the selection of the markers of interest
335 as done in the present work.

336
337 In conclusion, the modelling of the response to two new promising SARS-CoV-2 vaccines in NHP revealed
338 a combination of effects with a blockade of new cell infections and the destruction of infected cells. For
339 these two vaccines, the antibody inhibiting the attachment of RBD to ACE2, appeared to be a very good
340 surrogate of the vaccine effect on the rate of infection of new cells and therefore could be used as a
341 mechanistic CoP. This modelling framework contributes to the improvement of the understanding of the

342 immunological concepts by adding a quantitative evaluation of the contributions of different mechanisms
343 of control of viral infection. In terms of acceleration of vaccine development, our results may help to
344 develop vaccines for “hard-to-target pathogens”, or to predict their efficacy in aging and particular
345 populations (69). It should also help in choosing vaccine dose, for instance at early development (70) as
346 well as deciding if and when boosting vaccination is needed in the face of waning protective antibody
347 levels (71, 72), at least in NHP studies although the framework could be extended to human studies using
348 mixed approaches of within and between hosts modelling (73) providing that enough information is
349 collected.

350

351 **MATERIALS AND METHODS**

352 **Experimental model and subjects details**

353 *Cynomolgus* macaques (*Macaca fascicularis*), aged 37-66 months (18 females and 13 males) and
354 originating from Mauritian AAALAC certified breeding centers were used in this study. All animals were
355 housed in IDMIT facilities (CEA, Fontenay-aux-roses), under BSL2 and BSL-3 containment when necessary
356 (Animal facility authorization #D92-032-02, Préfecture des Hauts de Seine, France) and in compliance with
357 European Directive 2010/63/EU, the French regulations and the Standards for Human Care and Use of
358 Laboratory Animals, of the Office for Laboratory Animal Welfare (OLAW, assurance number #A5826-01,
359 US). The protocols were approved by the institutional ethical committee “Comité d’Ethique en
360 Expérimentation Animale du Commissariat à l’Energie Atomique et aux Energies Alternatives” (CEtEA #44)
361 under statement number A20-011. The study was authorized by the “Research, Innovation and Education
362 Ministry” under registration number APAFIS#24434-2020030216532863v1.

363

364 **Evaluation of anti-Spike, anti-RBD and neutralizing IgG antibodies**

365 *Anti-Spike IgG were titrated by multiplex bead assay.* Briefly, Luminex beads were coupled to the Spike
366 protein as previously described (74) and added to a Bio-Plex plate (BioRad). Beads were washed with PBS
367 0.05% tween using a magnetic plate washer (MAG2x program) and incubated for 1h with serial diluted
368 individual serum. Beads were then washed and anti-NHP IgG-PE secondary antibody (Southern Biotech,
369 clone SB108a) was added at a 1:500 dilution for 45 min at room temperature. After washing, beads were
370 resuspended in a reading buffer 5 min under agitation (800 rpm) on the plate shaker then read directly on
371 a Luminex Bioplex 200 plate reader (Biorad). Average MFI from the baseline samples were used as
372 reference value for the negative control. Amount of anti-Spike IgG was reported as the MFI signal divided
373 by the mean signal for the negative controls.

374

375 *Anti-RBD and anti-Nucleocapside (N) IgG* were titrated using a commercially available multiplexed
376 immunoassay developed by Mesoscale Discovery (MSD, Rockville, MD) as previously described (75).
377 Briefly, antigens were spotted at 200–400 µg/mL in a proprietary buffer, washed, dried and packaged for
378 further use (MSD® Coronavirus Plate 2). Then, plates were blocked with MSD Blocker A following which
379 reference standard, controls and samples diluted 1:500 and 1:5000 in diluent buffer were added. After
380 incubation, detection antibody was added (MSD SULFO-TAGTM Anti-Human IgG Antibody) and then MSD
381 GOLDTM Read Buffer B was added and plates read using a MESO QuickPlex SQ 120MM Reader. Results
382 were expressed as arbitrary unit (AU)/mL.

383

384 *Anti-RBD and anti-N IgG* were titrated by ELISA. The Nucleocapsid and the Spike RBD domain (Genbank #
385 NC_045512.2) were cloned and produced in *E. Coli* and CHO cells, respectively, as previously described
386 (37). Antigens were purified on C-tag column (Thermo Fisher) and quality-controlled by SDS-PAGE and for
387 their level of endotoxin. Antigens were coated in a 96 wells plates Nunc-immuno Maxisorp (Thermo Fisher)
388 at 1 $\mu\text{g}/\text{mL}$ in carbonate buffer at 4°C overnight. Plates were washed in TBS tween 0.05% (Thermo Fisher)
389 and blocked with PBS 3% BSA for 2 hours at room temperature. Samples were then added, in duplicate, in
390 serial dilution for 1 hour at RT. Non-infected NHP sera were used as negative controls. After washing, anti-
391 NHP IgG coupled with HRP (Thermo Fisher) was added at 1:20,000 for 45 min at RT. After washing, TMB
392 substrate (Thermo Fisher) was added for 15 min at RT and the reaction was stopped with 1M sulfuric acid.
393 Absorbance of each well was measured at 450 nm (reference 570 nm) using a Tristar2 reader (Berthold
394 Technologies). The EC_{50} value of each sample was determined using GraphPad Prism 8 and antibody titer
395 was calculated as $\log(1/\text{EC}_{50})$.

396
397 *The MSD pseudo-neutralization assay* was used to measure antibodies neutralizing the binding of the spike
398 protein to the ACE2 receptor. Plates were blocked and washed as above, assay calibrator (COVID- 19
399 neutralizing antibody; monoclonal antibody against S protein; 200 $\mu\text{g}/\text{mL}$), control sera and test sera
400 samples diluted 1:10 and 1:100 in assay diluent were added to the plates. Following incubation of the
401 plates, an 0.25 $\mu\text{g}/\text{mL}$ solution of MSD SULFO-TAGTM conjugated ACE-2 was added after which plates were
402 read as above. Electro-chemiluminescence (ECL) signal was recorded.

403
404 **Viral dynamics modelling**

405 The mechanistic approach we developed to characterize the impact of the immune response on the viral
406 gRNA and sgRNA dynamics relies on a mechanistic model divided in three layers: firstly, we used a
407 mathematical model based on ordinary differential equations to describe the dynamics in the two
408 compartments, the nasopharynx and the trachea. Then we used a statistical model to take into account
409 both the inter-individual variability and the effects of covariates on parameters. Finally, we considered an
410 observation model to describe the observed \log_{10} viral loads in the two compartments.

411 For the mathematical model, we started from previously published models (26, 27, 41) where the
412 nasopharynx and trachea were respectively described by a target cell limited model, with an eclipse phase,
413 as model of acute viral infection assuming target-cell limitation (33). We completed the model by adding
414 a compartment for the inoculum that distinguishes the injected virus (V_s) from the virus produced *de novo*
415 (V_i and V_{ni}). To our knowledge, this distinction has not been proposed in any previous work. Two main
416 reasons led us to make this choice. First, it allowed us to study the dynamics of the inoculum, in particular
417 during the early phase of viral RNA load dynamics. Second, as described in more detail below, it gave us
418 the opportunity to use all the information provided by the preclinical studies, such as the known number
419 of inoculated virions, to define the initial conditions of the ODE model rather than estimating or randomly
420 fixing them for V_i and V_{ni} , as is usually done. Consequently, for each of the two compartments, the model
421 included uninfected target cells (T) that can be infected (I_1) either by infectious viruses (V_i) or inoculum
422 (V_s) at an infection rate β . After an eclipse phase, infected cells become productively infected cells (I_2) and
423 can produce virions at rate P and be lost at a per capita rate δ . The virions generated can be infectious (V_i)
424 with proportion μ while the $(1-\mu)$ remaining proportion of virions is non-infectious (V_{ni}). Mathematically,
425 a single compartment (V) for *de novo* produced virions could be considered in the model, with μV and $(1-$
426 $\mu)V$ representing the respective contributions of infectious and non-infectious viruses to the biological
427 mechanisms. However, to have a better visual understanding of the distinction between the two types of
428 viruses, we wrote the model with distinct compartments, V_i and V_{ni} .

429 Finally, virions produced *de novo* and those from the inoculum are cleared at a rate c and c_i respectively.
 430 Distinct clearances were considered to account for the effects of experimental conditions on viral
 431 dynamics. In particular, it is hypothesized that, animals being locally infected with large numbers of virions,
 432 a large proportion of it is assumed to be rapidly eliminated by swallowing and natural downstream influx,
 433 in contrast to the *de novo* produced virions. However, it is important to keep in mind that this distinction
 434 was possible because of the controlled experimental conditions performed in animals, (i.e., exact timing
 435 and amount of inoculated virus known, and frequent monitoring during the early phase of the viral
 436 dynamics). Because of identifiability issues, similar clearances for infectious and non-infectious viruses
 437 were used. Accordingly, the model can be written as the following set of differential equations, where the
 438 superscript X denotes the compartment of interest (N, nasopharynx or T, trachea):

$$\begin{cases}
 \frac{dT^X}{dt} = -\beta^X V_i^X T^X - \mu \beta^X V_s^X T^X \\
 \frac{dI_1^X}{dt} = \beta^X V_i^X T^X + \mu \beta^X V_s^X T^X - k I_1^X \\
 \frac{dI_2^X}{dt} = k I_1^X - \delta^X I_2^X \\
 \frac{dV_i^X}{dt} = \mu P^X I_2^X - c V_i^X - \beta^X V_i^X T^X \\
 \frac{dV_{ni}^X}{dt} = (1 - \mu) P^X I_2^X - c V_{ni}^X \\
 \frac{dV_s^X}{dt} = -c_i V_s^X - \mu \beta^X V_s^X T^X \\
 T^X(t=0) = T_0^X ; I_1^X(t=0) = 0 ; I_2^X(t=0) = 0 \\
 V_i^X(t=0) = 0 ; V_{ni}^X(t=0) = 0 ; V_s^X(t=0) = V_{S,0}^X
 \end{cases} \quad (1)$$

439 where $T^X(t=0)$, $I_1^X(t=0)$, $I_2^X(t=0)$, $V_i^X(t=0)$, $V_{ni}^X(t=0)$ and $V_s^X(t=0)$ are the initial conditions
 440 at the time of exposure. The initial concentration of target cells, that are the epithelial cells expressing the
 441 ACE2 receptor, is expressed as $T_0^X = \frac{T_0^{X,nbc}}{W^X}$ where $T_0^{X,nbc}$ is the initial number of cells and W^X is the volume
 442 of distribution of the compartment of interest (see the subsection "Consideration of the volume of
 443 distribution"). Each animal was exposed to 1×10^6 pfu of SARS-CoV-2 representing a total of 2.19×10^{10}
 444 virions. Over the total inoculum injected (5 mL), 10% (0.5 mL) and 90% (4.5 mL) of virions were respectively
 445 injected by the intra-nasal route and the intra-tracheal route leading to the following initial concentrations
 446 of the inoculum within each compartment : $V_{S,0}^N = \frac{0.10 \times \text{Inoc}_0}{W^N}$ and $V_{S,0}^T = \frac{0.90 \times \text{Inoc}_0}{W^T}$, with Inoc_0 the number
 447 of virions injected via the inoculum.

448 Using the gRNA and sgRNA viral loads, we estimated the viral infectivity, the viral production rate and the
 449 loss rate of infected cells within each of the two compartments of the URT (**Supplementary file 2**). To
 450 account for inter-individual variability and covariates, each of those three parameters was described by a
 451 mixed-effect model and jointly estimated between the two compartments as follows:

$$\left\{ \begin{array}{l} \log_{10}(\beta_i^N) = \beta_0 + \phi_{conv}^\beta \times \mathbb{I}_{group=conv} + \phi_{CD40}^\beta \times \mathbb{I}_{group=CD40} + u_i^\beta \\ \beta_i^T = \beta_i^N \times \exp(f_\beta^T) \\ \log(\delta_i^N) = \log(\delta_0) + \phi_{conv}^\delta \times \mathbb{I}_{group=conv} + \phi_{CD40}^\delta \times \mathbb{I}_{group=CD40} + u_i^\delta \\ \delta_i^T = \delta_i^N \times \exp(f_\delta^T) \\ \log(P_i^N) = \log(P_0) + \phi_{conv}^P \times \mathbb{I}_{group=conv} + \phi_{CD40}^P \times \mathbb{I}_{group=CD40} + u_i^P \\ P_i^T = P_i^N \times \exp(f_P^T) \end{array} \right. \quad (2)$$

452 where β_0 , $\log(\delta_0)$ and $\log(P_0)$ are the fixed effects, $\{\phi_{conv}^\theta | \theta \in \{\beta, \delta, P\}\}$ and $\{\phi_{CD40}^\theta | \theta \in \{\beta, \delta, P\}\}$ are
453 respectively the regression coefficients related to the effects of the group of convalescent and α CD40.RBD
454 vaccinated animals for the parameters β , δ and P , and u_i^θ is the individual random effect for the parameter
455 θ , which is assumed to be normally distributed with variance ω_θ^2 . A log-transformation was adopted for
456 the parameters δ and P to ensure their positivity while a \log_{10} -transformation was chosen for viral
457 infectivity to also improve the convergence of the estimation. Because of the scale difference between the
458 parameter β and the other parameters (see **Supplementary file 2**), the mere use of the log-transformation
459 for this parameter led to convergence issues. The use of a \log_{10} -transformation allowed to overcome this
460 problem. Moreover, as shown in Equation (2), a joint estimation of the parameters β , δ and P between the
461 two compartments of the URT was considered. In this regard, a homogeneous interindividual variability
462 within the URT was assumed as well as a similar contribution of the covariates to the value of the
463 parameters. Parameters in the trachea were then either equal or proportional to those in the nasopharynx.
464 This modeling choice, resulting in a smaller number of parameters to be estimated, was made mainly to
465 address identifiability issues and to increase the power of the estimation. All other parameters included in
466 the target-cell limited models were assumed to be fixed (see the subsection "Parameter estimation" for
467 more details).

468 In practice, after the selection of the optimal statistical model (see Appendix 1 "Model Building"), random
469 effects were added only to the parameters β and δ (i.e., $\omega_\beta \neq 0$, $\omega_\delta \neq 0$, and $\omega_P = 0$), and the estimation of
470 multiple models identified the viral production rate P as the only parameter taking different values
471 between the trachea and nasopharynx. (i.e., $\beta^N = \beta^T$ with $f_\beta^T = 0$, $\delta^N = \delta^T$ with $f_\delta^T = 0$, while $P^N \neq P^T$). Finally, the
472 adjustment of the model for the categorical covariates of groups of treatment, natural infection and/or
473 vaccination, identified β and δ as the parameters with a statistically significant effect of these covariates
474 (i.e., $\phi_{conv}^P = 0$ and $\phi_{CD40}^P = 0$).

475
476 For the observation model, we jointly described genomic and subgenomic viral loads in the two
477 compartments of the URT. We defined genomic viral load, which characterizes the total viral load observed
478 in a compartment (nasopharynx or trachea), as the sum of inoculated virions (\mathbf{V}_s), infectious (\mathbf{V}_i) and non-
479 infectious virions (\mathbf{V}_{ni}). The sgRNA was described as proportional to the infected cells ($\mathbf{I}_1 + \mathbf{I}_2$). This choice
480 was driven by two main reasons. First, sgRNA is only transcribed in infected cells (76). Second, as described
481 by Miao et al. (2011) (77), to overcome identifiability issues between the parameters $\boldsymbol{\beta}$ and \boldsymbol{P} typically
482 observed in target-cell limited models. The comparison of the two observation models describing sgRNA
483 as either proportional to virions produced *de novo* ($\mathbf{V}_i + \mathbf{V}_{ni}$) or proportional to infected cells ($\mathbf{I}_1 + \mathbf{I}_2$)
484 confirmed this conclusion. In addition to a better BICc value (-25 points) compared with the first model,
485 the second one allowed the estimation of both $\boldsymbol{\beta}$ and \boldsymbol{P} by counteracting identifiability problems faced
486 with the first model (results not shown). Accordingly, the \log_{10} -transformed gRNA and sgRNA of the i th
487 animal at the j th time point in compartment X (nasopharynx or trachea), denoted $gRNA_{ij}^X$ and $sgRNA_{ij}^X$
488 respectively, were described by the following equations:

$$\begin{cases} gRNA_{ij}^X = \log_{10}[V_i^X + V_{ni}^X + V_s^X](\Theta_i^X, t_{ij}) + \varepsilon_{ij,g}^X & \varepsilon_{ij,g}^X \sim \mathcal{N}(0, \sigma_{gX}^2) \\ sgRNA_{ij}^X = \alpha_{sgRNA} \times \log_{10}[I_1^X + I_2^X](\Theta_i^X, t_{ij}) + \varepsilon_{ij,sg}^X & \varepsilon_{ij,sg}^X \sim \mathcal{N}(0, \sigma_{sgX}^2) \end{cases} \quad (3)$$

489 where Θ_i^X is the set of parameters of the subject i for the compartment X and ε are the additive normally
 490 distributed measurement errors.

491

492 Consideration of the volume of distribution

493 To define the concentration of inoculum within each compartment after injection, nasopharyngeal and
 494 tracheal volumes of distribution, labelled W^N and W^T respectively, were needed. Given the estimated
 495 volumes of the trachea and the nasal cavities in four monkeys similar to our 18 macaques (**Figure 2 - figure**
 496 **supplement 2A-C**) and the well documented relationship between the volume of respiratory tract and
 497 animal weights (78), the volume of distribution of each compartment was defined as a step function of
 498 NHP weights:

$$\begin{aligned} W_i^N &= \begin{cases} 4 & \text{if Weight}_i \leq 4.5 \\ 5.5 & \text{otherwise} \end{cases} \\ W_i^T &= \begin{cases} 2 & \text{if Weight}_i \leq 4.5 \\ 3 & \text{otherwise} \end{cases} \end{aligned} \quad (4)$$

499 Where Weight_i is the weight of the monkey i in kgs. Using equation (4) and weights of our 18 NHPs (mean=
 500 4.08 ; [Q1 ; Q3] = [3.26 ; 4.77]), we estimated $W^T = 2$ and $W^N = 4$ mL for a third of them ($n=12$) (**Figure 2 -**
 501 **figure supplement 2D**), leading to the initial concentration of target cells T_0^X (see “Viral dynamics
 502 modeling” for equation) fixed at 3.13×10^4 cells.mL⁻¹ and 1.13×10^4 cells.mL⁻¹ in nasopharynx and trachea
 503 respectively. Similarly, their initial concentrations of challenge inoculum $V_{S,0}^X$ were fixed at 5.48×10^8
 504 copies.mL⁻¹ and 9.86×10^9 copies.mL⁻¹ in nasopharynx and trachea resp. For the last third of NHPs ($n=6$),
 505 $W^T = 3$ and $W^N = 5.5$ mL leading to T_0^X fixed at 2.27×10^4 cells.mL⁻¹ in nasopharynx and 7.50×10^3 cells.mL⁻¹
 506 in trachea while $V_{S,0}^X$ was fixed at 3.98×10^8 copies.mL⁻¹ in nasopharynx and 6.57×10^9 copies.mL⁻¹ in trachea.
 507 Through this modeling, we assumed a homogenous distribution of injected virions and target cells within
 508 nasopharyngeal and tracheal compartments. In addition, the natural downward flow of inoculum towards
 509 lungs, at the moment of injection, was indirectly taken into account by the parameter of inoculum
 510 clearance, c_i .

511

512 Parameter estimation

513 Among all parameters involved in the three layers of the mechanistic model, some of them have been
 514 fixed based on experimental settings and/or literature. That is the case of the proportion of infectious virus
 515 (μ) that has been fixed at 1/1000 according to previous work (28) and additional work (results not shown)
 516 evaluating the stability of the model estimation according to the value of this parameter. The initial
 517 number of target cells, that are the epithelial cells expressing the ACE2 receptor, $T_0^{X,nbc}$ was fixed at
 518 1.25×10^5 cells in the nasopharynx and 2.25×10^4 cells in trachea (28) (**Supplementary file 2**). The duration
 519 of the eclipse phase ($1/k$), the clearance of the inoculum (c_i) and the clearance of the virus produced *de*
 520 *novo* (c) were estimated by profile likelihood. The profile likelihood consists in defining a grid of values for
 521 the parameters to be evaluated and sequentially fixing these parameters to one of these combinations of
 522 values. The model and all the parameters that are not fixed are then estimated by maximizing the log-
 523 likelihood. In this process, all parameters that are assumed to be fixed in the model (i.e., μ and the initial
 524 conditions) are held fixed. Finally, the optimal set of parameters is chosen as the one optimizing the log-
 525 likelihood. Although the available data did not allow the direct estimation of these three parameters, the

526 use profile likelihood enabled the exploration of various potential values for k , c and c_i . In a first step, we
527 explored the 18 models resulting from the combination of 3 values of $k \in \{1, 3, 6\} \text{ day}^{-1}$ and 6 values for c
528 $\in \{1, 5, 10, 15, 20, 30\} \text{ day}^{-1}$, assuming that the two parameters of virus clearance were equal, as first
529 approximation. As shown in **Supplementary file 3a**, an eclipse phase of 8 hours ($k=3$) and virus clearance
530 higher than 15 virions per day led to lowest values of $-2\log$ -likelihood ($-2LL$, the lower the better). In a
531 second step, we fixed the parameter k at 3 day^{-1} and estimated the 70 models resulting from the
532 combination of 10 values for $c \in \{1, 2, 3, 4, 5, 10, 15, 20, 25, 30\} \text{ day}^{-1}$ and 7 values for $c_i \in \{1, 5, 10, 15, 20,$
533 $25, 30\} \text{ day}^{-1}$ (**Supplementary file 3b**). The distinction of the two parameters of free virus clearance enabled
534 to find much lower half-life of inoculum (~ 50 minutes) than half-life of virus produced *de novo* (~ 5.55
535 hours), with $c=3 \text{ day}^{-1}$ compared to $c_i=20 \text{ day}^{-1}$.

536
537 Once all these parameters have been fixed, the estimation problem was restricted to the determination
538 of the viral infectivity β , the viral production rate P , the loss rate of infected cells δ for each compartment,
539 the parameter α_{vls_g} in the observation model, regression coefficients for groups of intervention
540 (ϕ_{conv}, ϕ_{DC40}) and standard deviations for both random effects (ω) and error model (σ). The estimation
541 was performed by Maximum likelihood estimation using a stochastic approximation EM algorithm
542 implemented in the software Monolix (<http://www.lixoft.com>). Furthermore, we performed a bootstrap
543 procedure with replacement (79) (50 samples) on the optimal model to obtain and verify the robustness
544 of the estimates (see **Supplementary file 2** for the results), and to reduce potential overfitting that could
545 result from the small number of NHPs. Selection of the compartment effect on parameters (β, δ, P) as well
546 as random effects and covariates on the statistical model (2) was performed by the estimation of several
547 models that were successively compared according to the corrected Bayesian information criterion (BICc)
548 (to be minimized). After the removal of random effect on the viral production ($\omega_P = 0$) allowing the
549 reduction of the variance on the two other random effects, all combinations of compartment effects were
550 evaluated, leading to the final selection of a single effect on P ($f_\beta^T = f_\delta^T = 0$). Then, the effect of group
551 intervention was independently added on model parameters among β, δ, P and c . Once the group effect
552 on the viral infectivity identified as the best one, the addition of a second effect on the remaining
553 parameters was tested, resulting in the selection of the loss rate of infected cells. Finally, the irrelevance
554 of the addition of a third effect was verified.

555 The possibility of migration of free plasma virus between the nasopharynx and the trachea was tested.
556 However, as widely described in the literature, the transport of viral particles within the respiratory tract
557 is negligible in the viral dynamics and is difficult to estimate. The reader can refer to Appendix 1 “Model
558 building” for an additional modelling work conducted to estimate this exchange and provided the same
559 conclusion. Accordingly, the two compartments of the URT were assumed are distinct in our model.

560

561 **Algorithm for automatic selection of biomarkers as CoP**

562 After identifying the effect of the group of intervention on both the viral infectivity (β) and the loss rate of
563 infected cells (δ), we aimed at determining whether some immunological markers quantified in the study
564 could capture this effect. Nowadays, many methods for selecting constant covariates already exist (80)
565 and are implemented in software like Monolix. However, these latter do not allow time-varying covariates.
566 In this section, we present the algorithm we implemented to select time-varying covariates. We proposed
567 a classical stepwise data-driven automatic covariate modelling method (**Figure 4 - figure supplement 2**).
568 However, initially implemented to select covariates from more than 50 biomarkers, computational time
569 restricted us to consider only a forward selection procedure. Nevertheless, the method can be easily
570 extended to classical stepwise selection in which both forward selection and backward elimination are

571 performed sequentially. Although the method was developed for time-varying covariates, it can also be
572 applied to constant covariates.

573 At the initialization step ($k=0$) (see **Figure 4 – figure supplement 2**), the algorithm requests 3 inputs: (1) a
574 set of potential M covariates, labelled Marker_m for $m \in \{1, \dots, M\}$ (e.g., immunological markers) ; (2) a set of
575 P parameters on which covariates could be added, labelled θ_p for $p \in \{1, \dots, P\}$ (e.g. β and δ) ; and (3) an
576 initial model (e.g., the model without covariates), labelled M^0 , with θ_p^0 being the definition of the
577 parameter θ_p . At each step $k > 0$, we note M^{k-1} the current model resulting in the model built in the step $k-1$.
578 Then each combination of markers and parameters that have not already been added in M^{k-1} , labelled
579 r ($r \in \{\text{Marker } m \otimes \theta_p \notin M^{k-1} \mid m \in \{1, \dots, M\}, p \in \{1, \dots, P\}\}$), are considered and tested in an
580 univariate manner (each relation r is independently added in M^{k-1} and ran). To this end, the parameter θ_p
581 involved in this relationship r is modified as $\theta_p^k(t) = \theta_p^{k-1}(t) \times \exp(\phi_m^p \times \text{Marker}_m(t))$, where ϕ_m^p is the
582 regression coefficient related the marker and $\text{Marker}_m(t)$ being the trajectory of the marker over time,
583 while other parameters remain unchanged ($\forall \theta_q \notin r, \theta_q^k(t) = \theta_q^{k-1}(t)$). Once all these models evaluated,
584 the one with the optimal value of a given selection criterion defining the quality of the fits (e.g., the lowest
585 BICc value) is selected and compared to the model M^{k-1} . If the value of the criterion is better than the one
586 found for M^{k-1} , then this model is defined as the new current model, M^k , and the algorithm moves to the
587 step $k+1$. Otherwise, the algorithm stops. The algorithm can also be stopped at the end of a fixed number
588 of step K .

589 The objective of this algorithm being to identify mechanistic correlates of protection, at each step, the
590 selected model should respect, in addition to the best fits criterion, the 2 other criteria defining mCoP
591 meaning the ability to capture the effect of the group of intervention and the ability to better explain the
592 variability on individual parameters than the model adjusted for the group effect. To this end, we verify
593 that in the selected model additionally adjusted for the group of intervention, the group effect appears as
594 non-significantly different from 0 using a Wald-test. Then, we check that the variances of random effects
595 in the selected model are lower or equal to the ones obtained in the model adjusted only for the group
596 effect.

597

598 **Modelling hypothesis for time-dependent covariates in our application**

599 Using a population-based approach to estimate our mechanistic model and similar to the adjustment of
600 the model for constant covariates (e.g., groups of intervention), time-varying covariates are incorporated
601 into the statistical model as individual-specific explanatory variables in the mixed-effects models. To
602 implement the algorithm for selecting the time-varying covariates, many modeling choices were made.
603 First, targeting covariates able to fully replace the group of intervention, we kept a similar mathematical
604 relationship between parameters and immune markers than the one used with the constant covariate (see
605 Equation (2)). Accordingly, we adjusted the model parameters additively in logarithmic scale. In this
606 regard, at each step k ($k > 0$), the parameter θ_p was defined as $\log(\theta_p^k(t)) = \log(\theta_p^{k-1}(t)) + \phi_m^p \times$
607 $\text{Marker}_m(t)$. However, this choice may affect the results and other choices may be more relevant under
608 different conditions. Second, because immune markers are observed only at discrete time points, whereas
609 the estimation of the model is performed in a continuous way, we introduced immune markers as time-
610 varying covariates using linear interpolation. Lets denote $\text{Marker}_{i,j}$ the value of the marker observed for
611 the i th animal at the j th time point, with $i \in \{1, \dots, n\}$ and $j \in \{1, \dots, J\}$. By linear interpolation, the time-
612 continuous marker was defined as, $\forall t > 0$,

$$\begin{aligned}
\text{Marker}_i^{\text{int}}(t) &= \sum_{j=1}^{J-1} \mathbb{I}_{[t_j; t_{j+1}[}(t) \left[\frac{\text{Marker}_{i,j+1} - \text{Marker}_{i,j}}{t_{j+1} - t_j} t + \frac{\text{Marker}_{i,j} t_{j+1} - \text{Marker}_{j+1} t_j}{t_{j+1} - t_j} \right] \\
&+ \mathbb{I}_{t \geq t_j}(t) \times \text{Marker}_{i,j}
\end{aligned}$$

As previously described in the Results section, three different studies were considered in this work: a main study reported by Marlin et al. (36) testing the α CD40.RBD vaccine, and two additional studies (24, 45) evaluating a two-component spike nanoparticle vaccine and the mRN-1273 vaccine, respectively. In the main study, the method was applied with both time-varying covariates and constant covariates for which only baseline value was considered, such that $\text{Marker}_i(t) = \text{Marker}_i(t=0)$ (see **Supplementary file 1**). For the other two studies, only the baseline values were considered as covariates, the dynamics being not available. To assess the robustness of the results, several selection criteria were tested: AIC, BIC, log-likelihood, the percentage of explained interindividual variability, and similar results were obtained for all (results not shown). Moreover, as presented in Appendix 2 “BICc as selection criteria and multiple testing adjustment”, we verified the robustness of the use of BIC as selection criteria despite the multiplicity of the tests. The identification of antibodies inhibiting the attachment of the RBD domain to the ACE2 receptor (ECLRBD) as the first time-varying CoP led to the definition of the time-varying viral infectivity for the i -th animal as described in Equation (5), while the selection anti-RBD IgG-binding antibodies (IggRBD) led to the elimination rate of infected cells given in Equation (6).

$$\beta_i(t) = 10^{\beta_0 + u_i^\beta} \times \exp(\phi_{ecl}^\beta \times \text{ECLRBD}_i^{\text{int}}(t)) \quad (5)$$

$$\delta_i(t) = \delta_0 \times \exp(\phi_{igg}^\delta \times \text{IggRBD}_i^{\text{int}}(t) + u_i^\delta) \quad (6)$$

Quantification and statistical analysis

In each of the three studies used in this work, no statistical tests were performed on the raw data (i.e., observations), whether for viral load or for immune marker measurements, to identify statistical differences between treatment groups, as the statistical analyses were already been performed in the respective papers. Statistical significance of the effect of groups in model estimation is indicated in the tables by stars: *, $p < 0.05$; **, $p < 0.01$; ***, $p < 0.001$ and were estimated by Wald tests (Monolix® software version 2019R1).

Model parameters were estimated with the SAEM algorithm (Monolix® software version 2019R1). Graphics were generated using R version 3.6.1 and Excel 2016 and details on the statistical analysis for the experiments can be found in the accompanying figure legends. Horizontal red dashed lines on graphs indicate assay limit of detection.

643 **References and Notes**

- 644 1. World Health Organisation, COVID-19 vaccine tracker and landscape (2021) (available at
645 <https://www.who.int/publications/m/item/draft-landscape-of-covid-19-candidate-vaccines>).
- 646 2. S. Cobey, D. B. Larremore, Y. H. Grad, M. Lipsitch, Concerns about SARS-CoV-2 evolution should not hold back
647 efforts to expand vaccination. *Nat Rev Immunol* **21**, 330–335 (2021).
- 648 3. A. Kuzmina, Y. Khalaila, O. Voloshin, A. Keren-Naus, L. Boehm-Cohen, Y. Raviv, Y. Shemer-Avni, E. Rosenberg, R.
649 Taube, SARS-CoV-2 spike variants exhibit differential infectivity and neutralization resistance to convalescent or post-
650 vaccination sera. *Cell host & microbe* **29**, 522-528.e2 (2021).
- 651 4. D. Planas, T. Bruel, L. Grzelak, F. Guivel-Benhassine, I. Staropoli, F. Porrot, C. Planchais, J. Buchrieser, M. M. Rajah,
652 E. Bishop, M. Albert, F. Donati, M. Prot, S. Behillil, V. Enouf, M. Maquart, M. Smati-Lafarge, E. Varon, F. Schortgen, L.
653 Yahyaoui, M. Gonzalez, J. De Sèze, H. Péré, D. Veyer, A. Sève, E. Simon-Lorière, S. Fafi-Kremer, K. Stefic, H. Mouquet,
654 L. Hocqueloux, S. van der Werf, T. Prazuck, O. Schwartz, Sensitivity of infectious SARS-CoV-2 B.1.1.7 and B.1.351
655 variants to neutralizing antibodies. *Nat Med* **27**, 917–924 (2021).
- 656 5. Y. Lustig, I. Nemet, L. Kliker, N. Zuckerman, R. Yishai, S. Alroy-Preis, E. Mendelson, M. Mandelboim, Neutralizing
657 Response against Variants after SARS-CoV-2 Infection and One Dose of BNT162b2. *New England Journal of Medicine*
658 **384**, 2453–2454 (2021).
- 659 6. D. Zhou, W. Dejnirattisai, P. Supasa, C. Liu, A. J. Mentzer, H. M. Ginn, Y. Zhao, H. M. E. Duyvesteyn, A. Tuekprakhon,
660 R. Nutalai, B. Wang, G. C. Paesen, C. Lopez-Camacho, J. Slon-Campos, B. Hallis, N. Coombes, K. Bewley, S. Charlton,
661 T. S. Walter, D. Skelly, S. F. Lumley, C. Dold, R. Levin, T. Dong, A. J. Pollard, J. C. Knight, D. Crook, T. Lambe, E.
662 Clutterbuck, S. Bibi, A. Flaxman, M. Bittaye, S. Belij-Rammerstorfer, S. Gilbert, W. James, M. W. Carroll, P. Klenerman,
663 E. Barnes, S. J. Dunachie, E. E. Fry, J. Mongkolsapaya, J. Ren, D. I. Stuart, G. R. Screaton, Evidence of escape of SARS-
664 CoV-2 variant B.1.351 from natural and vaccine-induced sera. *Cell* **184**, 2348-2361.e6 (2021).
- 665 7. A. Greinacher, T. Thiele, T. E. Warkentin, K. Weisser, P. A. Kyrle, S. Eichinger, Thrombotic Thrombocytopenia after
666 ChAdOx1 nCov-19 Vaccination. *The New England journal of medicine* **384**, 2092–2101 (2021).
- 667 8. T. Koch, S. C. Mellinghoff, P. Shamsrizi, M. M. Addo, C. Dahlke, Correlates of Vaccine-Induced Protection against
668 SARS-CoV-2. *Vaccines* **9**, 238 (2021).
- 669 9. P. Jin, J. Li, H. Pan, Y. Wu, F. Zhu, Immunological surrogate endpoints of COVID-2019 vaccines: the evidence we
670 have versus the evidence we need. *Signal transduction and targeted therapy* **6**, 48 (2021).
- 671 10. D. S. Khoury, D. Cromer, A. Reynaldi, T. E. Schlub, A. K. Wheatley, J. A. Juno, K. Subbarao, S. J. Kent, J. A. Triccas,
672 M. P. Davenport, Neutralizing antibody levels are highly predictive of immune protection from symptomatic SARS-
673 CoV-2 infection. *Nat Med* **27**, 1205–1211 (2021).
- 674 11. J. Yu, L. H. Tostanoski, L. Peter, N. B. Mercado, K. McMahan, S. H. Mahrokhian, J. P. Nkolola, J. Liu, Z. Li, A.
675 Chandrashekar, D. R. Martinez, C. Loos, C. Atyeo, S. Fischinger, J. S. Burke, M. D. Slein, Y. Chen, A. Zuiani, F. J. N. Lellis,
676 M. Travers, S. Habibi, L. Pessaint, A. Van Ry, K. Blade, R. Brown, A. Cook, B. Finneyfrock, A. Dodson, E. Teow, J. Velasco,
677 R. Zahn, F. Wegmann, E. A. Bondzie, G. Dagotto, M. S. Gebre, X. He, C. Jacob-Dolan, M. Kirilova, N. Kordana, Z. Lin, L.
678 F. Maxfield, F. Nampanya, R. Nityanandam, J. D. Ventura, H. Wan, Y. Cai, B. Chen, A. G. Schmidt, D. R. Wesemann, R.
679 S. Baric, G. Alter, H. Andersen, M. G. Lewis, D. H. Barouch, DNA vaccine protection against SARS-CoV-2 in rhesus
680 macaques. *Science (New York, N.Y.)* **369**, 806–811 (2020).
- 681 12. K. A. Earle, D. M. Ambrosino, A. Fiore-Gartland, D. Goldblatt, P. B. Gilbert, G. R. Siber, P. Dull, S. A. Plotkin, Evidence
682 for antibody as a protective correlate for COVID-19 vaccines. *Vaccine* **39**, 4423–4428 (2021).
- 683 13. S. Feng, D. J. Phillips, T. White, H. Sayal, P. K. Aley, S. Bibi, C. Dold, M. Fuskova, S. C. Gilbert, I. Hirsch, H. E.
684 Humphries, B. Jepson, E. J. Kelly, E. Plested, K. Shoemaker, K. M. Thomas, J. Vekemans, T. L. Villafana, T. Lambe, A. J.
685 Pollard, M. Voysey, Correlates of protection against symptomatic and asymptomatic SARS-CoV-2 infection. *Nat Med*
686 **27**, 2032–2040 (2021).
- 687 14. S. J. Zost, P. Gilchuk, R. E. Chen, J. B. Case, J. X. Reidy, A. Trivette, R. S. Nargi, R. E. Sutton, N. Suryadevara, E. C.
688 Chen, E. Binshtein, S. Shrihari, M. Ostrowski, H. Y. Chu, J. E. Didier, K. W. MacRenaris, T. Jones, S. Day, L. Myers, F.

- 689 Eun-Hyung Lee, D. C. Nguyen, I. Sanz, D. R. Martinez, P. W. Rothlauf, L.-M. Bloyet, S. P. J. Whelan, R. S. Baric, L. B.
690 Thackray, M. S. Diamond, R. H. Carnahan, J. E. Crowe, Rapid isolation and profiling of a diverse panel of human
691 monoclonal antibodies targeting the SARS-CoV-2 spike protein. *Nature medicine* **26**, 1422–1427 (2020).
- 692 15. N. B. Mercado, R. Zahn, F. Wegmann, C. Loos, A. Chandrashekar, J. Yu, J. Liu, L. Peter, K. McMahan, L. H.
693 Tostanoski, X. He, D. R. Martinez, L. Rutten, R. Bos, D. van Manen, J. Vellinga, J. Custers, J. P. Langedijk, T. Kwaks, M.
694 J. G. Bakkers, D. Zuijdgeest, S. K. Rosendahl Huber, C. Atyeo, S. Fischinger, J. S. Burke, J. Feldman, B. M. Hauser, T. M.
695 Caradonna, E. A. Bondzie, G. Dagotto, M. S. Gebre, E. Hoffman, C. Jacob-Dolan, M. Kirilova, Z. Li, Z. Lin, S. H.
696 Mahrokhian, L. F. Maxfield, F. Nampanya, R. Nityanandam, J. P. Nkolola, S. Patel, J. D. Ventura, K. Verrington, H. Wan,
697 L. Pessaint, A. Van Ry, K. Blade, A. Strasbaugh, M. Cabus, R. Brown, A. Cook, S. Zouantchangadou, E. Teow, H.
698 Andersen, M. G. Lewis, Y. Cai, B. Chen, A. G. Schmidt, R. K. Reeves, R. S. Baric, D. A. Lauffenburger, G. Alter, P. Stoffels,
699 M. Mammen, J. Van Hoof, H. Schuitemaker, D. H. Barouch, Single-shot Ad26 vaccine protects against SARS-CoV-2 in
700 rhesus macaques. *Nature* **586**, 583–588 (2020).
- 701 16. A. Tauzin, M. Nayrac, M. Benlarbi, S. Y. Gong, R. Gasser, G. Beaudoin-Bussi eres, N. Brassard, A. Laumaea, D.
702 V ezina, J. Pr evost, S. P. Anand, C. Bourassa, G. Gendron-Lepage, H. Medjahed, G. Goyette, J. Niessl, O. Tastet, L.
703 Gokool, C. Morrisseau, P. Arlotto, L. Stamatas, A. T. McGuire, C. Larochelle, P. Uchil, M. Lu, W. Mothes, G. De Serres,
704 S. Moreira, M. Roger, J. Richard, V. Martel-Laferr ere, R. Duerr, C. Tremblay, D. E. Kaufmann, A. Finzi, A single dose of
705 the SARS-CoV-2 vaccine BNT162b2 elicits Fc-mediated antibody effector functions and T cell responses. *Cell Host &*
706 *Microbe* **29**, 1137-1150.e6 (2021).
- 707 17. K. McMahan, J. Yu, N. B. Mercado, C. Loos, L. H. Tostanoski, A. Chandrashekar, J. Liu, L. Peter, C. Atyeo, A. Zhu, E.
708 A. Bondzie, G. Dagotto, M. S. Gebre, C. Jacob-Dolan, Z. Li, F. Nampanya, S. Patel, L. Pessaint, A. Van Ry, K. Blade, J.
709 Yalley-Ogunro, M. Cabus, R. Brown, A. Cook, E. Teow, H. Andersen, M. G. Lewis, D. A. Lauffenburger, G. Alter, D. H.
710 Barouch, Correlates of protection against SARS-CoV-2 in rhesus macaques. *Nature* **590**, 630–634 (2021).
- 711 18. S. A. Plotkin, Complex Correlates of Protection After Vaccination. *Clinical Infectious Diseases* **56**, 1458–1465
712 (2013).
- 713 19. S. A. Plotkin, Updates on immunologic correlates of vaccine-induced protection. *Vaccine* **38**, 2250–2257 (2020).
- 714 20. S. B. Bradfute, S. Bavari, Correlates of immunity to filovirus infection. *Viruses* **3**, 982–1000 (2011).
- 715 21. G. Dagotto, J. Yu, D. H. Barouch, Approaches and Challenges in SARS-CoV-2 Vaccine Development. *Cell Host &*
716 *Microbe* **28**, 364–370 (2020).
- 717 22. C. Mu oz-Fontela, W. E. Dowling, S. G. P. Funnell, P.-S. Gsell, A. X. Riveros-Balta, R. A. Albrecht, H. Andersen, R.
718 S. Baric, M. W. Carroll, M. Cavaleri, C. Qin, I. Crozier, K. Dallmeier, L. de Waal, E. de Wit, L. Delang, E. Dohm, W. P.
719 Duprex, D. Falzarano, C. L. Finch, M. B. Frieman, B. S. Graham, L. E. Gralinski, K. Guilfoyle, B. L. Haagmans, G. A.
720 Hamilton, A. L. Hartman, S. Herfst, S. J. F. Kaptein, W. B. Klimstra, I. Knezevic, P. R. Krause, J. H. Kuhn, R. Le Grand, M.
721 G. Lewis, W.-C. Liu, P. Maisonnasse, A. K. McElroy, V. Munster, N. Oreshkova, A. L. Rasmussen, J. Rocha-Pereira, B.
722 Rockx, E. Rodr guez, T. F. Rogers, F. J. Salguero, M. Schotsaert, K. J. Stittelaar, H. J. Thibaut, C.-T. Tseng, J. Vergara-
723 Alert, M. Beer, T. Brasel, J. F. W. Chan, A. Garc a-Sastre, J. Neyts, S. Perlman, D. S. Reed, J. A. Richt, C. J. Roy, J. Segal es,
724 S. S. Vasan, A. M. Henao-Restrepo, D. H. Barouch, Animal models for COVID-19. *Nature* **586**, 509–515 (2020).
- 725 23. N. Eyal, M. Lipsitch, How to test SARS-CoV-2 vaccines ethically even after one is available. *Clin Infect Dis* , ciab182
726 (2021).
- 727 24. K. S. Corbett, B. Flynn, K. E. Foulds, J. R. Francica, S. Boyoglu-Barnum, A. P. Werner, B. Flach, S. O’Connell, K. W.
728 Bock, M. Minai, B. M. Nagata, H. Andersen, D. R. Martinez, A. T. Noe, N. Douek, M. M. Donaldson, N. N. Nji, G. S.
729 Alvarado, D. K. Edwards, D. R. Flebbe, E. Lamb, N. A. Doria-Rose, B. C. Lin, M. K. Louder, S. O’Dell, S. D. Schmidt, E.
730 Phung, L. A. Chang, C. Yap, J.-P. M. Todd, L. Pessaint, A. Van Ry, S. Browne, J. Greenhouse, T. Putman-Taylor, A.
731 Strasbaugh, T.-A. Campbell, A. Cook, A. Dodson, K. Steingrebe, W. Shi, Y. Zhang, O. M. Abiona, L. Wang, A. Pegu, E. S.
732 Yang, K. Leung, T. Zhou, I.-T. Teng, A. Widge, I. Gordon, L. Novik, R. A. Gillespie, R. J. Loomis, J. I. Moliva, G. Stewart-
733 Jones, S. Himansu, W.-P. Kong, M. C. Nason, K. M. Morabito, T. J. Ruckwardt, J. E. Ledgerwood, M. R. Gaudinski, P. D.
734 Kwong, J. R. Mascola, A. Carfi, M. G. Lewis, R. S. Baric, A. McDermott, I. N. Moore, N. J. Sullivan, M. Roederer, R. A.
735 Seder, B. S. Graham, Evaluation of the mRNA-1273 Vaccine against SARS-CoV-2 in Nonhuman Primates. *The New*
736 *England journal of medicine* **383**, 1544–1555 (2020).

- 737 25. S. A. Plotkin, P. B. Gilbert, Nomenclature for Immune Correlates of Protection After Vaccination. *Clinical Infectious*
738 *Diseases* **54**, 1615–1617 (2012).
- 739 26. A. Gonçalves, J. Bertrand, R. Ke, E. Comets, X. de Lamballerie, D. Malvy, A. Pizzorno, O. Terrier, M. Rosa Calatrava,
740 F. Mentré, P. Smith, A. S. Perelson, J. Guedj, Timing of Antiviral Treatment Initiation is Critical to Reduce SARS-CoV-2
741 Viral Load. *CPT: Pharmacometrics & Systems Pharmacology* **9**, 509–514 (2020).
- 742 27. K. S. Kim, K. Ejima, S. Iwanami, Y. Fujita, H. Ohashi, Y. Koizumi, Y. Asai, S. Nakaoka, K. Watashi, K. Aihara, R. N.
743 Thompson, R. Ke, A. S. Perelson, S. Iwami, A quantitative model used to compare within-host SARS-CoV-2, MERS-
744 CoV, and SARS-CoV dynamics provides insights into the pathogenesis and treatment of SARS-CoV-2. *PLoS biology* **19**,
745 e3001128 (2021).
- 746 28. A. Gonçalves, P. Maisonnasse, F. Donati, M. Albert, S. Behillil, V. Contreras, T. Naninck, R. Marlin, C. Solas, A.
747 Pizzorno, J. Lemaitre, N. Kahlaoui, O. Terrier, R. Ho Tsong Fang, V. Enouf, N. Dereuddre-Bosquet, A. Brisebarre, F.
748 Touret, C. Chapon, B. Hoen, B. Lina, M. Rosa Calatrava, X. de Lamballerie, F. Mentré, R. Le Grand, S. van der Werf, J.
749 Guedj, SARS-CoV-2 viral dynamics in non-human primates. *PLoS computational biology* **17**, e1008785 (2021).
- 750 29. S. Wang, Y. Pan, Q. Wang, H. Miao, A. N. Brown, L. Rong, Modeling the viral dynamics of SARS-CoV-2 infection.
751 *Mathematical biosciences* **328**, 108438 (2020).
- 752 30. A. Marc, M. Kerioui, F. Blanquart, J. Bertrand, O. Mitjà, M. Corbacho-Monné, M. Marks, J. Guedj, S. E. Cobey, J.
753 W. Van der Meer, Eds. Quantifying the relationship between SARS-CoV-2 viral load and infectiousness. *eLife* **10**,
754 e69302 (2021).
- 755 31. R. Ke, C. Zitzmann, D. D. Ho, R. M. Ribeiro, A. S. Perelson, In vivo kinetics of SARS-CoV-2 infection and its
756 relationship with a person's infectiousness. *Proceedings of the National Academy of Sciences* **118**, e2111477118
757 (2021).
- 758 32. M. A. Myers, A. P. Smith, L. C. Lane, D. J. Moquin, R. Aogo, S. Woolard, P. Thomas, P. Vogel, A. M. Smith, J. T.
759 Schiffer, S. L. Sawyer, J. T. Schiffer, Eds. Dynamically linking influenza virus infection kinetics, lung injury,
760 inflammation, and disease severity. *eLife* **10**, e68864 (2021).
- 761 33. P. Baccam, C. Beauchemin, C. A. Macken, F. G. Hayden, A. S. Perelson, Kinetics of Influenza A Virus Infection in
762 Humans. *Journal of Virology* **80**, 7590–7599 (2006).
- 763 34. A. Goyal, L. E. Liao, A. S. Perelson, Within-host mathematical models of hepatitis B virus infection: Past, present,
764 and future. *Current Opinion in Systems Biology* **18**, 27–35 (2019).
- 765 35. A. Goyal, R. M. Ribeiro, A. S. Perelson, The Role of Infected Cell Proliferation in the Clearance of Acute HBV
766 Infection in Humans. *Viruses* **9**, 350 (2017).
- 767 36. R. Marlin, V. Godot, S. Cardinaud, M. Galhaut, S. Coleon, S. Zurawski, N. Dereuddre-Bosquet, M. Cavarelli, A.-S.
768 Gallouët, P. Maisonnasse, L. Dupaty, C. Fenwick, T. Naninck, J. Lemaitre, M. Gomez-Pacheco, N. Kahlaoui, V.
769 Contreras, F. Relouzat, R. H. T. Fang, Z. Wang, J. Ellis, C. Chapon, M. Centlivre, A. Wiedemann, C. Lacabaratz, M.
770 Surenaud, I. Szurgot, P. Liljeström, D. Planas, T. Bruel, O. Schwartz, S. van der Werf, G. Pantaleo, M. Prague, R.
771 Thiébaud, G. Zurawski, Y. Lévy, R. L. Grand, Targeting SARS-CoV-2 receptor-binding domain to cells expressing CD40
772 improves protection to infection in convalescent macaques. *Nat Commun* **12**, 5215 (2021).
- 773 37. A.-L. Flamar, S. Zurawski, F. Scholz, I. Gayet, L. Ni, X.-H. Li, E. Klechevsky, J. Quinn, S. Oh, D. H. Kaplan, J.
774 Banchereau, G. Zurawski, Noncovalent assembly of anti-dendritic cell antibodies and antigens for evoking immune
775 responses in vitro and in vivo. *Journal of immunology (Baltimore, Md. : 1950)* **189**, 2645–55 (2012).
- 776 38. G. Zurawski, X. Shen, S. Zurawski, G. D. Tomaras, D. C. Montefiori, M. Roederer, G. Ferrari, C. Lacabaratz, P. Klucar,
777 Z. Wang, K. E. Foulds, S.-F. Kao, X. Yu, A. Sato, N. L. Yates, C. LaBranche, S. Stanfield-Oakley, K. Kibler, B. Jacobs, A.
778 Salazar, S. Self, W. Fulp, R. Gottardo, L. Galmin, D. Weiss, A. Cristillo, G. Pantaleo, Y. Levy, Superiority in Rhesus
779 Macaques of Targeting HIV-1 Env gp140 to CD40 versus LOX-1 in Combination with Replication-Competent NYVAC-
780 KC for Induction of Env-Specific Antibody and T Cell Responses. *Journal of Virology* **91**, e01596-16.

- 781 39. L. Cheng, Q. Wang, G. Li, R. Banga, J. Ma, H. Yu, F. Yasui, Z. Zhang, G. Pantaleo, M. Perreau, S. Zurawski, G.
782 Zurawski, Y. Levy, L. Su, TLR3 agonist and CD40-targeting vaccination induces immune responses and reduces HIV-1
783 reservoirs. *The Journal of clinical investigation* **128**, 4387–4396 (2018).
- 784 40. V. Godot, C. Tcherakian, L. Gil, I. Cervera-Marzal, G. Li, L. Cheng, N. Ortonne, J.-D. Lelièvre, G. Pantaleo, C. Fenwick,
785 M. Centlivre, H. Mouquet, S. Cardinaud, S. M. Zurawski, G. Zurawski, P. Milpied, L. Su, Y. Lévy, TLR-9 agonist and
786 CD40-targeting vaccination induces HIV-1 envelope-specific B cells with a diversified immunoglobulin repertoire in
787 humanized mice. *PLoS pathogens* **16**, e1009025 (2020).
- 788 41. P. Baccam, C. Beauchemin, C. A. Macken, F. G. Hayden, A. S. Perelson, Kinetics of Influenza A Virus Infection in
789 Humans. *Journal of Virology* **80**, 7590–7599 (2006).
- 790 42. R. Ke, C. Zitzmann, R. M. Ribeiro, A. S. Perelson, *Kinetics of SARS-CoV-2 infection in the human upper and lower*
791 *respiratory tracts and their relationship with infectiousness* (medRxiv, 2020;
792 <https://www.medrxiv.org/content/10.1101/2020.09.25.20201772v1>).
- 793 43. L. Pinky, C. W. Burke, C. J. Russell, A. M. Smith, Quantifying dose-, strain-, and tissue-specific kinetics of
794 parainfluenza virus infection. *PLOS Computational Biology* **17**, e1009299 (2021).
- 795 44. R. Robinot, M. Hubert, G. D. de Melo, F. Lazarini, T. Bruel, N. Smith, S. Levallois, F. Larrous, J. Fernandes, S.
796 Gellenoncourt, S. Rigaud, O. Gorgette, C. Thouvenot, C. Trébeau, A. Mallet, G. Duménil, S. Gobaa, R. Eournay, P.-M.
797 Lledo, M. Lecuit, H. Bourhy, D. Duffy, V. Michel, O. Schwartz, L. A. Chakrabarti, SARS-CoV-2 infection induces the
798 dedifferentiation of multiciliated cells and impairs mucociliary clearance. *Nat Commun* **12**, 4354 (2021).
- 799 45. P. J. M. Brouwer, M. Brinkkemper, P. Maisonnasse, N. Dereuddre-Bosquet, M. Grobden, M. Claireaux, M. de Gast,
800 R. Marlin, V. Chesnais, S. Diry, J. D. Allen, Y. Watanabe, J. M. Giezen, G. Kerster, H. L. Turner, K. van der Straten, C. A.
801 van der Linden, Y. Aldon, T. Naninck, I. Bontjer, J. A. Burger, M. Poniman, A. Z. Mykytyn, N. M. A. Okba, E. E. Schermer,
802 M. J. van Breemen, R. Ravichandran, T. G. Caniels, J. van Schooten, N. Kahlaoui, V. Contreras, J. Lemaître, C. Chapon,
803 R. H. T. Fang, J. Villaudy, K. Sliepen, Y. U. van der Velden, B. L. Haagmans, G. J. de Bree, E. Ginoux, A. B. Ward, M.
804 Crispin, N. P. King, S. van der Werf, M. J. van Gils, R. Le Grand, R. W. Sanders, Two-component spike nanoparticle
805 vaccine protects macaques from SARS-CoV-2 infection. *Cell* **184**, 1188-1200.e19 (2021).
- 806 46. A. W. Chung, M. P. Kumar, K. B. Arnold, W. H. Yu, M. K. Schoen, L. J. Dunphy, T. J. Suscovich, N. Frahm, C. Linde,
807 A. E. Mahan, M. Hoffner, H. Streeck, M. E. Ackerman, M. J. McElrath, H. Schuitemaker, M. G. Pau, L. R. Baden, J. H.
808 Kim, N. L. Michael, D. H. Barouch, D. A. Lauffenburger, G. Alter, Dissecting Polyclonal Vaccine-Induced Humoral
809 Immunity against HIV Using Systems Serology. *Cell* **163**, 988–98 (2015).
- 810 47. J. Dufloo, L. Grzelak, I. Staropoli, Y. Madec, L. Tondeur, F. Anna, S. Pelleau, A. Wiedemann, C. Planchais, J.
811 Buchrieser, R. Robinot, M.-N. Ungeheuer, H. Mouquet, P. Charneau, M. White, Y. Lévy, B. Hoen, A. Fontanet, O.
812 Schwartz, T. Bruel, Asymptomatic and symptomatic SARS-CoV-2 infections elicit polyfunctional antibodies. *Cell*
813 *reports. Medicine* **2**, 100275 (2021).
- 814 48. G. Alter, J. Yu, J. Liu, A. Chandrashekar, E. N. Borducchi, L. H. Tostanoski, K. McMahan, C. Jacob-Dolan, D. R.
815 Martinez, A. Chang, T. Anioke, M. Lifton, J. Nkolola, K. E. Stephenson, C. Atyeo, S. Shin, P. Fields, I. Kaplan, H. Robins,
816 F. Amanat, F. Krammer, R. S. Baric, M. Le Gars, J. Sadoff, A. M. de Groot, D. Heerwegh, F. Struyf, M. Douoguih, J. van
817 Hoof, H. Schuitemaker, D. H. Barouch, Immunogenicity of Ad26.COVS vaccine against SARS-CoV-2 variants in
818 humans. *Nature* **596**, 268–272 (2021).
- 819 49. P. Jin, J. Li, H. Pan, Y. Wu, F. Zhu, Immunological surrogate endpoints of COVID-2019 vaccines: the evidence we
820 have versus the evidence we need. *Signal transduction and targeted therapy* **6**, 48 (2021).
- 821 50. K. R. W. Emary, T. Golubchik, P. K. Aley, C. V Ariani, B. Angus, S. Bibi, B. Blane, D. Bonsall, P. Cicconi, S. Charlton,
822 E. A. Clutterbuck, A. M. Collins, T. Cox, T. C. Darton, C. Dold, A. D. Douglas, C. J. A. Duncan, K. J. Ewer, A. L. Flaxman,
823 S. N. Faust, D. M. Ferreira, S. Feng, A. Finn, P. M. Folegatti, M. Fuskova, E. Galiza, A. L. Goodman, C. M. Green, C. A.
824 Green, M. Greenland, B. Hallis, P. T. Heath, J. Hay, H. C. Hill, D. Jenkin, S. Kerridge, R. Lazarus, V. Libri, P. J. Lillie, C.
825 Ludden, N. G. Marchevsky, A. M. Minassian, A. C. McGregor, Y. F. Mujadidi, D. J. Phillips, E. Plested, K. M. Pollock, H.
826 Robinson, A. Smith, R. Song, M. D. Snape, R. K. Sutherland, E. C. Thomson, M. Toshner, D. P. J. Turner, J. Vekemans,
827 T. L. Villafana, C. J. Williams, A. V. S. Hill, T. Lambe, S. C. Gilbert, M. Voysey, M. N. Ramasamy, A. J. Pollard, COVID-19

828 Genomics UK consortium, AMPHEUS Project, Oxford COVID-19 Vaccine Trial Group, Efficacy of ChAdOx1 nCoV-19
829 (AZD1222) vaccine against SARS-CoV-2 variant of concern 202012/01 (B.1.1.7): an exploratory analysis of a
830 randomised controlled trial. *Lancet (London, England)* **397**, 1351–1362 (2021).

831 51. A. Chandrashekar, J. Liu, A. J. Martinot, K. McMahan, N. B. Mercado, L. Peter, L. H. Tostanoski, J. Yu, Z. Maliga, M.
832 Nekorchuk, K. Busman-Sahay, M. Terry, L. M. Wrijil, S. Ducat, D. R. Martinez, C. Atyeo, S. Fischinger, J. S. Burke, M. D.
833 Slein, L. Pessaint, A. Van Ry, J. Greenhouse, T. Taylor, K. Blade, A. Cook, B. Finneyfrock, R. Brown, E. Teow, J. Velasco,
834 R. Zahn, F. Wegmann, P. Abbink, E. A. Bondzie, G. Dagotto, M. S. Gebre, X. He, C. Jacob-Dolan, N. Kordana, Z. Li, M.
835 A. Lifton, S. H. Mahrokhian, L. F. Maxfield, R. Nityanandam, J. P. Nkolola, A. G. Schmidt, A. D. Miller, R. S. Baric, G.
836 Alter, P. K. Sorger, J. D. Estes, H. Andersen, M. G. Lewis, D. H. Barouch, SARS-CoV-2 infection protects against
837 rechallenge in rhesus macaques. *Science (New York, N.Y.)* **369**, 812–817 (2020).

838 52. N. H. L. Leung, D. K. W. Chu, E. Y. C. Shiu, K.-H. Chan, J. J. McDevitt, B. J. P. Hau, H.-L. Yen, Y. Li, D. K. M. Ip, J. S. M.
839 Peiris, W.-H. Seto, G. M. Leung, D. K. Milton, B. J. Cowling, Respiratory virus shedding in exhaled breath and efficacy
840 of face masks. *Nat Med* **26**, 676–680 (2020).

841 53. M. Marks, P. Millat-Martinez, D. Ouchi, C. h Roberts, A. Alemany, M. Corbacho-Monné, M. Ubals, A. Tobias, C.
842 Tebé, E. Ballana, Q. Bassat, B. Baro, M. Vall-Mayans, C. G-Beiras, N. Prat, J. Ara, B. Clotet, O. Mitjà, Transmission of
843 COVID-19 in 282 clusters in Catalonia, Spain: a cohort study. *The Lancet Infectious Diseases* **21**, 629–636 (2021).

844 54. N. Néant, G. Lingas, Q. L. Hingrat, J. Ghosn, I. Engelmann, Q. Lepiller, A. Gaymard, V. Ferré, C. Hartard, J.-C.
845 Plantier, V. Thibault, J. Marlet, B. Montes, K. Bouiller, F.-X. Lescure, J.-F. Timsit, E. Faure, J. Poissy, C. Chidiac, F. Raffi,
846 A. Kimmoun, M. Etienne, J.-C. Richard, P. Tattevin, D. Garot, V. L. Moing, D. Bachelet, C. Tardivon, X. Duval, Y.
847 Yazdanpanah, F. Mentré, C. Laouénan, B. Visseaux, J. Guedj, for the F. C. C. I. and F. C. S. Groups, Modeling SARS-
848 CoV-2 viral kinetics and association with mortality in hospitalized patients from the French COVID cohort. *PNAS* **118**
849 (2021), doi:10.1073/pnas.2017962118.

850 55. C. Gutmann, K. Takov, S. A. Burnap, B. Singh, H. Ali, K. Theofilatos, E. Reed, M. Hasman, A. Nabeebaccus, M. Fish,
851 M. J. McPhail, K. O’Gallagher, L. E. Schmidt, C. Cassel, M. Rienks, X. Yin, G. Auzinger, S. Napoli, S. F. Mujib, F. Trovato,
852 B. Sanderson, B. Merrick, U. Niazi, M. Saqi, K. Dimitrakopoulou, R. Fernández-Leiro, S. Braun, R. Kronstein-
853 Wiedemann, K. J. Doores, J. D. Edgeworth, A. M. Shah, S. R. Bornstein, T. Tonn, A. C. Hayday, M. Giacca, M. Shankar-
854 Hari, M. Mayr, SARS-CoV-2 RNAemia and proteomic trajectories inform prognostication in COVID-19 patients
855 admitted to intensive care. *Nat Commun* **12**, 3406 (2021).

856 56. T. Charmet, L. Schaeffer, R. Grant, S. Galmiche, O. Chény, C. Von Platen, A. Maurizot, A. Rogoff, F. Omar, C. David,
857 A. Septfons, S. Cauchemez, A. Gaymard, B. Lina, L. H. Lefrancois, V. Enouf, S. van der Werf, A. Mailles, D. Levy-Bruhl,
858 F. Carrat, A. Fontanet, Impact of original, B.1.1.7, and B.1.351/P.1 SARS-CoV-2 lineages on vaccine effectiveness of
859 two doses of COVID-19 mRNA vaccines: Results from a nationwide case-control study in France. *The Lancet Regional*
860 *Health - Europe* **8**, 100171 (2021).

861 57. T. Nyberg, N. M. Ferguson, S. G. Nash, H. H. Webster, S. Flaxman, N. Andrews, W. Hinsley, J. L. Bernal, M. Kall, S.
862 Bhatt, P. Blomquist, A. Zaidi, E. Volz, N. A. Aziz, K. Harman, S. Funk, S. Abbott, T. Nyberg, N. M. Ferguson, S. G. Nash,
863 H. H. Webster, S. Flaxman, N. Andrews, W. Hinsley, J. Lopez Bernal, M. Kall, S. Bhatt, P. Blomquist, A. Zaidi, E. Volz,
864 N. Abdul Aziz, K. Harman, S. Funk, S. Abbott, R. Hope, A. Charlett, M. Chand, A. C. Ghani, S. R. Seaman, G. Dabrera, D.
865 De Angelis, A. M. Presanis, S. Thelwall, R. Hope, A. Charlett, M. Chand, A. C. Ghani, S. R. Seaman, G. Dabrera, D. De
866 Angelis, A. M. Presanis, S. Thelwall, Comparative analysis of the risks of hospitalisation and death associated with
867 SARS-CoV-2 omicron (B.1.1.529) and delta (B.1.617.2) variants in England: a cohort study. *The Lancet* **399**, 1303–1312
868 (2022).

869 58. K. E. Kester, J. F. Cummings, O. Ofori-Anyinam, C. F. Ockenhouse, U. Krzych, P. Moris, R. Schwenk, R. A. Nielsen,
870 Z. Debebe, E. Pinelis, L. Juompan, J. Williams, M. Dowler, V. A. Stewart, R. A. Wirtz, M.-C. Dubois, M. Lievens, J. Cohen,
871 W. R. Ballou, D. G. Heppner, RTS,S Vaccine Evaluation Group, Randomized, double-blind, phase 2a trial of falciparum
872 malaria vaccines RTS,S/AS01B and RTS,S/AS02A in malaria-naive adults: safety, efficacy, and immunologic associates
873 of protection. *The Journal of infectious diseases* **200**, 337–46 (2009).

- 874 59. K. J. Travaglini, A. N. Nabhan, L. Penland, R. Sinha, A. Gillich, R. V Sit, S. Chang, S. D. Conley, Y. Mori, J. Seita, G. J.
875 Berry, J. B. Shrager, R. J. Metzger, C. S. Kuo, N. Neff, I. L. Weissman, S. R. Quake, M. A. Krasnow, A molecular cell atlas
876 of the human lung from single-cell RNA sequencing. *Nature* **587**, 619–625 (2020).
- 877 60. A. Pizzorno, B. Padey, T. Julien, S. Trouillet-Assant, A. Traversier, E. Errazuriz-Cerda, J. Fouret, J. Dubois, A.
878 Gaymard, F.-X. Lescure, V. Dulière, P. Brun, S. Constant, J. Poissy, B. Lina, Y. Yazdanpanah, O. Terrier, M. Rosa-
879 Calatrava, Characterization and Treatment of SARS-CoV-2 in Nasal and Bronchial Human Airway Epithelia. *Cell*
880 *Reports Medicine* **1**, 100059 (2020).
- 881 61. A. Gonçalves, P. Maisonnasse, F. Donati, M. Albert, S. Behillil, V. Contreras, T. Naninck, R. Marlin, C. Solas, A.
882 Pizzorno, J. Lemaitre, N. Kahlaoui, O. Terrier, R. H. T. Fang, V. Enouf, N. Dereuddre-Bosquet, A. Brisebarre, F. Touret,
883 C. Chapon, B. Hoen, B. Lina, M. R. Calatrava, X. de Lamballerie, F. Mentré, R. L. Grand, S. van der Werf, J. Guedj, SARS-
884 CoV-2 viral dynamics in non-human primates. *PLOS Computational Biology* **17**, e1008785 (2021).
- 885 62. A. P. Smith, D. J. Moquin, V. Bernhauerova, A. M. Smith, Influenza Virus Infection Model With Density Dependence
886 Supports Biphasic Viral Decay. *Frontiers in Microbiology* **9** (2018).
- 887 63. U. G. Dafni, A. A. Tsiatis, Evaluating surrogate markers of clinical outcome when measured with error. *Biometrics*
888 **54**, 1445–1462 (1998).
- 889 64. R. J. Carroll, D. Ruppert, L. A. Stefanski, C. M. Crainiceanu, *Measurement Error in Nonlinear Models: A Modern*
890 *Perspective, Second Edition* (Chapman and Hall/CRC, New York, ed. 2, 2006).
- 891 65. L. Wu, *Mixed Effects Models for Complex Data* (Chapman and Hall/CRC, New York, 2009).
- 892 66. G. Lui, L. Ling, C. K. Lai, E. Y. Tso, K. S. Fung, V. Chan, T. H. Ho, F. Luk, Z. Chen, J. K. Ng, K. Chow, P. K. Cheng, R. C.
893 Chan, D. N. Tsang, C. D. Gomersall, D. S. Hui, P. K. Chan, Viral dynamics of SARS-CoV-2 across a spectrum of disease
894 severity in COVID-19. *Journal of Infection* **81**, 318–356 (2020).
- 895 67. A. Goyal, E. R. Duke, E. F. Cardozo-Ojeda, J. T. Schiffer, Mathematical modeling explains differential SARS CoV-2
896 kinetics in lung and nasal passages in remdesivir treated rhesus macaques. *Biorxiv*, 2020.06.21.163550 (2020).
- 897 68. I. Balelli, C. Pasin, M. Prague, F. Crauste, T. V. Effelterre, V. Bockstal, L. Solforosi, R. Thiébaud, A model for
898 establishment, maintenance and reactivation of the immune response after vaccination against Ebola virus. *Journal*
899 *of Theoretical Biology* **495**, 110254 (2020).
- 900 69. A. J. Pollard, E. M. Bijker, A guide to vaccinology: from basic principles to new developments. *Nature reviews.*
901 *Immunology* **21**, 83–100 (2021).
- 902 70. S. J. Rhodes, J. Guedj, H. A. Fletcher, T. Lindenstrøm, T. J. Scriba, T. G. Evans, G. M. Knight, R. G. White, Using
903 vaccine Immunostimulation/Immunodynamic modelling methods to inform vaccine dose decision-making. *NPI*
904 *vaccines* **3**, 36 (2018).
- 905 71. C. Gaebler, Z. Wang, J. C. C. Lorenzi, F. Muecksch, S. Finkin, M. Tokuyama, A. Cho, M. Jankovic, D. Schaefer-
906 Babajew, T. Y. Oliveira, M. Cipolla, C. Viant, C. O. Barnes, Y. Bram, G. Breton, T. Hägglöf, P. Mendoza, A. Hurley, M.
907 Turroja, K. Gordon, K. G. Millard, V. Ramos, F. Schmidt, Y. Weisblum, D. Jha, M. Tankelevich, G. Martinez-Delgado, J.
908 Yee, R. Patel, J. Dizon, C. Unson-O'Brien, I. Shimeliovich, D. F. Robbiani, Z. Zhao, A. Gazumyan, R. E. Schwartz, T.
909 Hatzioannou, P. J. Bjorkman, S. Mehandru, P. D. Bieniasz, M. Caskey, M. C. Nussenzweig, Evolution of antibody
910 immunity to SARS-CoV-2. *Nature* **591**, 639–644 (2021).
- 911 72. K. Vanshylla, V. Di Cristanziano, F. Kleipass, F. Dewald, P. Schommers, L. Gieselmann, H. Gruell, M. Schlotz, M. S.
912 Ercanoglu, R. Stumpf, P. Mayer, M. Zehner, E. Heger, W. Johannis, C. Horn, I. Suárez, N. Jung, S. Salomon, K. A.
913 Eberhardt, B. Gathof, G. Fätkenheuer, N. Pfeifer, R. Eggeling, M. Augustin, C. Lehmann, F. Klein, Kinetics and
914 correlates of the neutralizing antibody response to SARS-CoV-2 infection in humans. *Cell host & microbe* **29**, 917-
915 929.e4 (2021).
- 916 73. A. Goyal, D. B. Reeves, J. T. Schiffer, Multi-scale modelling reveals that early super-spreader events are a likely
917 contributor to novel variant predominance. *Journal of The Royal Society Interface* **19**, 20210811.

- 918 74. C. Fenwick, A. Croxatto, A. T. Coste, F. Pojer, C. André, C. Pellaton, A. Farina, J. Campos, D. Hacker, K. Lau, B.-J.
919 Bosch, S. Gonseth Nussle, M. Bochud, V. D’Acremont, D. Trono, G. Greub, G. Pantaleo, Changes in SARS-CoV-2 Spike
920 versus Nucleoprotein Antibody Responses Impact the Estimates of Infections in Population-Based Seroprevalence
921 Studies. *Journal of Virology* **95**, e01828-20.
- 922 75. M. Johnson, H. R. Wagstaffe, K. C. Gilmour, A. L. Mai, J. Lewis, A. Hunt, J. Sirr, C. Bengt, L. Grandjean, D. Goldblatt,
923 Evaluation of a novel multiplexed assay for determining IgG levels and functional activity to SARS-CoV-2. *Journal of*
924 *clinical virology : the official publication of the Pan American Society for Clinical Virology* **130**, 104572 (2020).
- 925 76. S. G. Sawicki, D. L. Sawicki, S. G. Siddell, A Contemporary View of Coronavirus Transcription. *Journal of Virology*
926 **81**, 20–29 (2007).
- 927 77. H. Miao, X. Xia, A. S. Perelson, H. Wu, On Identifiability of Nonlinear ODE Models and Applications in Viral
928 Dynamics. *SIAM Review* **53**, 3–39 (2011).
- 929 78. B. Asgharian, O. Price, G. McClellan, R. Corley, D. R. Einstein, R. E. Jacob, J. Harkema, S. A. Carey, E. Schelegle, D.
930 Hyde, J. S. Kimbell, F. J. Miller, Development of a rhesus monkey lung geometry model and application to particle
931 deposition in comparison to humans. *Inhalation toxicology* **24**, 869–99 (2012).
- 932 79. H.-T. Thai, F. Mentré, N. H. G. Holford, C. Veyrat-Follet, E. Comets, Evaluation of bootstrap methods for estimating
933 uncertainty of parameters in nonlinear mixed-effects models: a simulation study in population pharmacokinetics.
934 *Journal of Pharmacokinetics and Pharmacodynamics* **41**, 15–33 (2014).
- 935 80. M. Z. I. Chowdhury, T. C. Turin, Variable selection strategies and its importance in clinical prediction modelling.
936 *Fam Med Community Health* **8**, e000262 (2020).

937
938

939 **Acknowledgments:** We would like to thank J. Guedj and O. Terrier for fruitful discussions on the model
940 definition. We thank S. Langlois, J. Demilly, N. Dhooge, P. Le Calvez, M. Potier, J. M. Robert, T. Prot, and C.
941 Dodan for the NHP experiments; L. Bossevot, M. Leonec, L. Moenne-Loccoz, M. Calpin-Lebreau, and J.
942 Morin for the RT-qPCR, ELISpot and Luminex assays, and for the preparation of reagents; A-S. Gallouët, M.
943 Gomez-Pacheco and W. Gros for NHP T-cell assays and flow cytometry; B. Fert for her help with the CT
944 scans; M. Barendji, J. Dinh and E. Guyon for the NHP sample processing; S. Keyser for the transports
945 organization; F. Ducancel and Y. Gorin for their help with the logistics and safety management; I. Mangeot
946 for here help with resources management and B. Targat contributed to data management. The monkey
947 and syringe pictures in Fig.1 was created with BioRender.com. This work was supported by INSERM and
948 the Investissements d’Avenir program, Vaccine Research Institute (VRI), managed by the ANR under
949 reference ANR-10-LABX-77-01. MA has been funded by INRIA PhD grant. The Infectious Disease Models
950 and Innovative Therapies (IDMIT) research infrastructure is supported by the “Programme Investissements
951 d’Avenir”, managed by the ANR under reference ANR-11-INBS-0008. The Fondation Bettencourt Schueller
952 and the Region Ile-de-France contributed to the implementation of IDMIT’s facilities and imaging
953 technologies used to define volume of respiratory tract. The NHP study received financial support from
954 REACTing, the Fondation pour la Recherche Medicale (FRM; AM-CoV-Path). We thank Lixoft SAS for their
955 support. Numerical computations were in part carried out using the PlaFRIM experimental testbed,
956 supported by Inria, CNRS (LABRI and IMB), Université de Bordeaux, Bordeaux INP and Conseil Régional
957 d’Aquitaine (see <https://www.plafrim.fr>). We thank Miles Davenport and Frederik Graw as Senior Editor
958 and Reviewing Editor of our paper, respectively, and the three anonymous reviewers for their time and
959 their constructive comments.

960
961

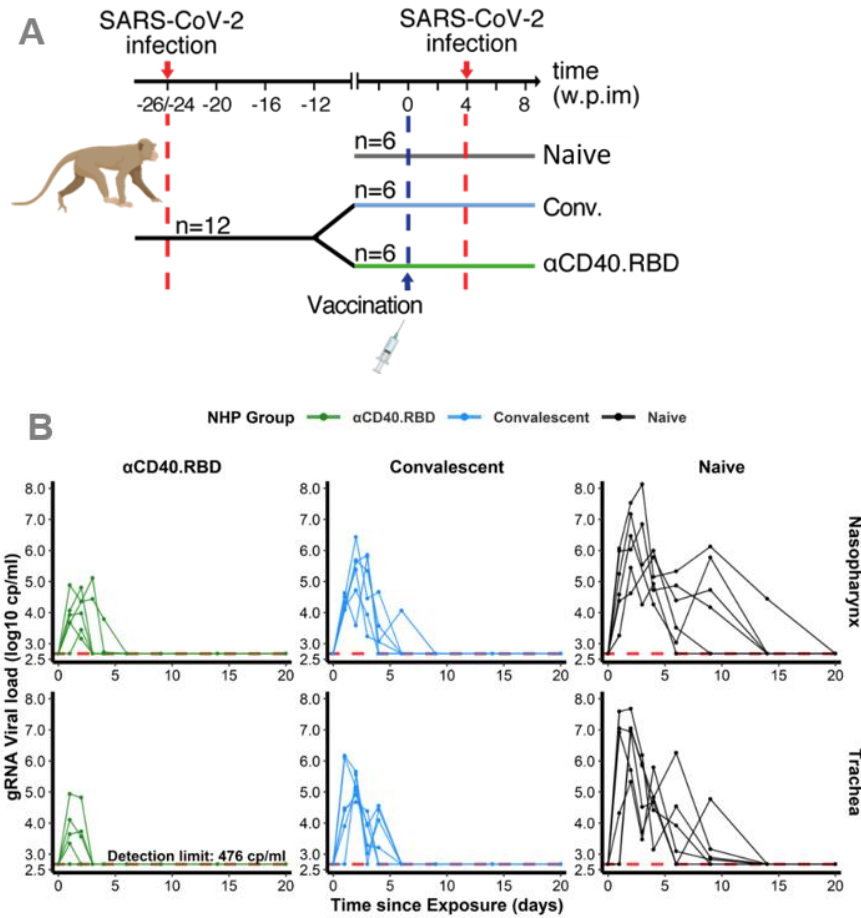
962 **Competing interests:** Authors declare that they have no competing interests

963 **Data and materials availability:** No unique reagents were generated for this study.

964 All raw data used in this analysis are provided as additional files. Otherwise source data are provided with
965 the paper, gathering data from 1) the study (36) used in this analysis, which are also directly available
966 online in the section **Source data** of this related paper (<https://www.nature.com/articles/s41467-021-25382-0#Sec17>) ; 2) the study (45) used in this analysis, which are also available from the corresponding
967 authors of the related paper and 3) the study (24) used in this analysis, which are also available online in
968 the section **Supplementary Material** of the related paper, excel file labelled (“Supplementary Appendix
969 2”). The original code (mlxtran models and R) as well as model definition files including the full list of
970 parameters used are available and free-of-cost on github (Inria SISTM Team) at the following link:
971 <https://github.com/sistm/SARSCoV2modelingNHP>.
972

973 **Figures**

974



975 **Figure 1. Design of the study 1 and viral dynamics.**

976 **(A) Study design.** Cynomolgus macaques (*Macaca fascicularis*), aged 37-58 months (8 females and 13

977 males). 24-26 weeks post infection with SARS-CoV-2, twelve of these animals were randomly assigned in

978 two experimental groups. The convalescent vaccinated group (n=6) received 200 μ g of α CD40.RBD

979 vaccine. The other six convalescent animals were used as controls. Additional six age matched (43.7

980 months \pm 6.76) cynomolgus macaques from same origin were included in the study as controls naive from

981 any exposure to SARS-CoV-2. Four weeks after immunization, all animals were exposed to a total dose of

982 10^6 pfu of SARS-CoV-2 virus via the combination of intra-nasal and intra-tracheal routes. In this work, only

983 data collected from the 2nd exposure were considered. **(B)** Individual \log_{10} transformed gRNA viral load

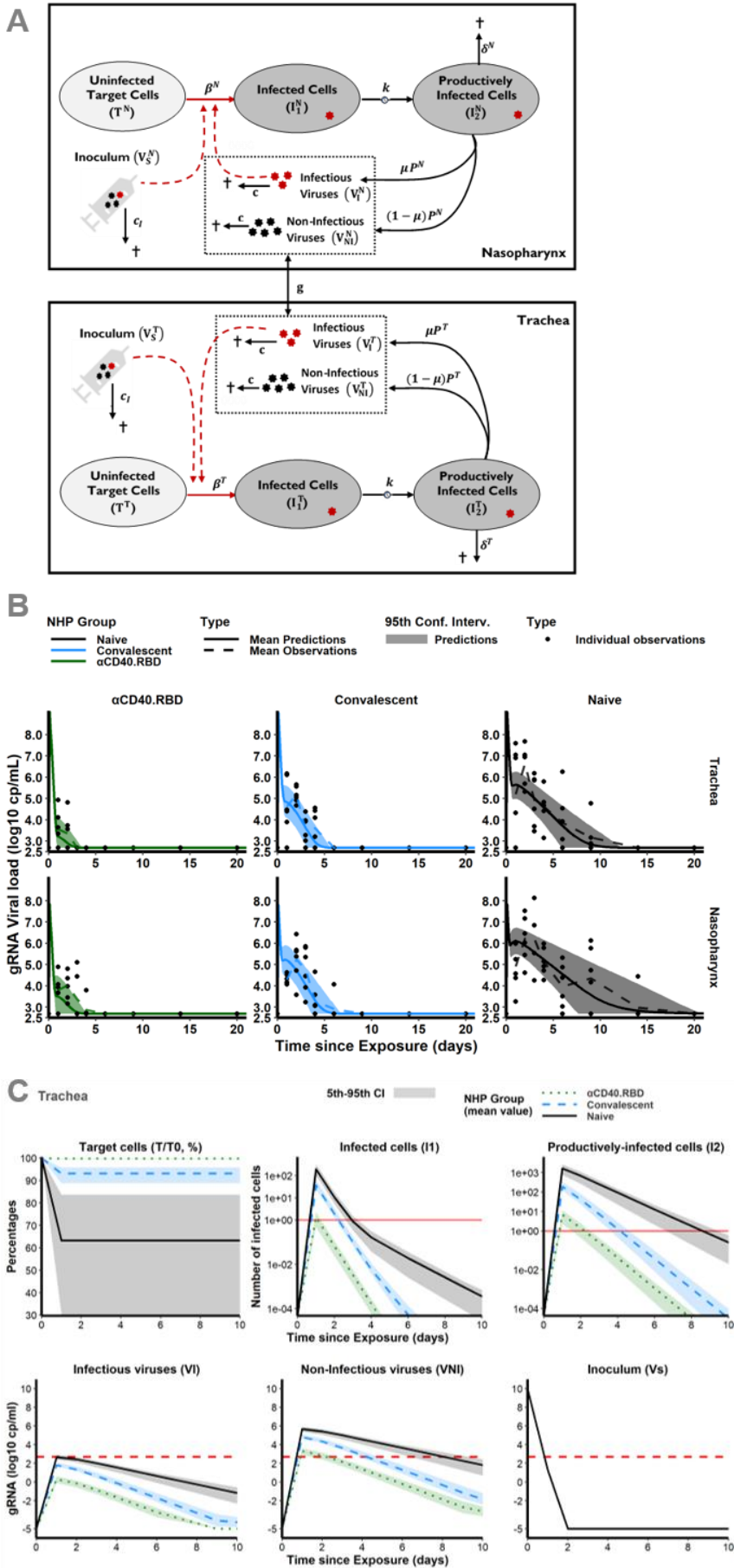
984 dynamics in nasopharyngeal swabs (top) and tracheal swabs (bottom) after the initial exposure to SARS-

985 CoV-2 in naive macaques (black, right) and after the second exposure in convalescent (blue, middle) and

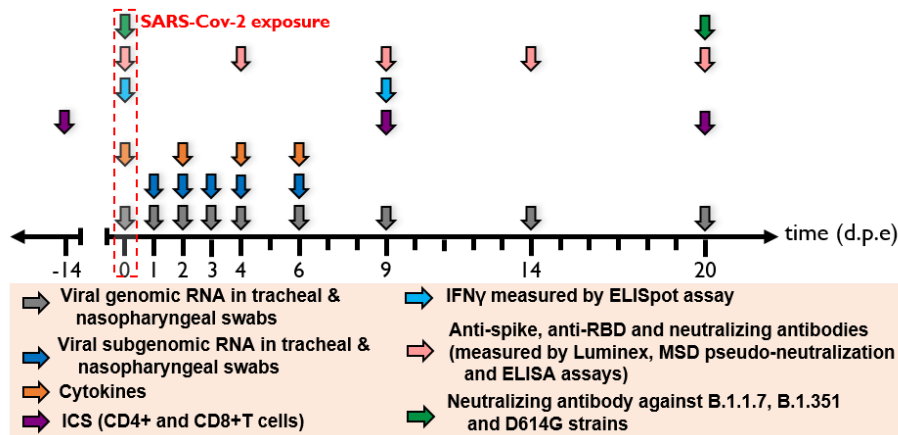
986 α CD40.RBD-vaccinated convalescent (green, left) groups. Horizontal red dashed lines indicate the limit of

987 quantification.

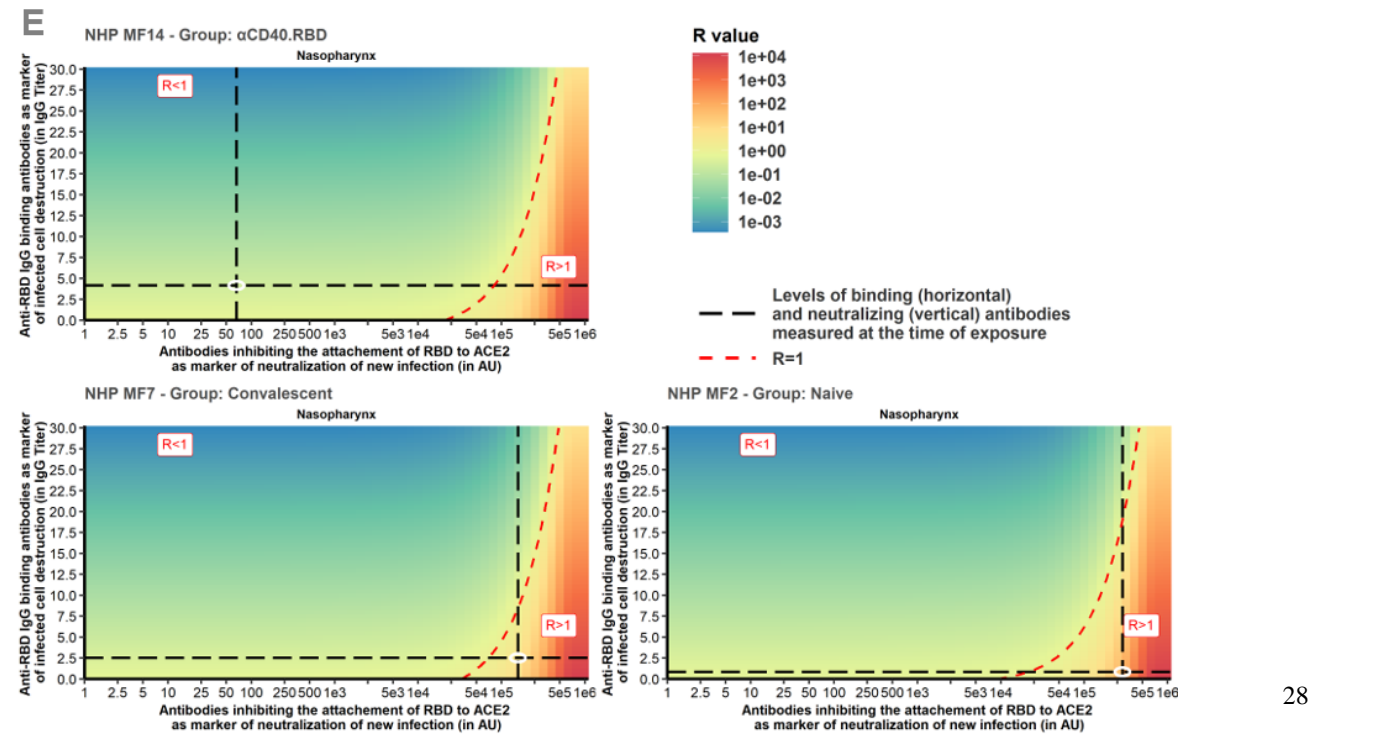
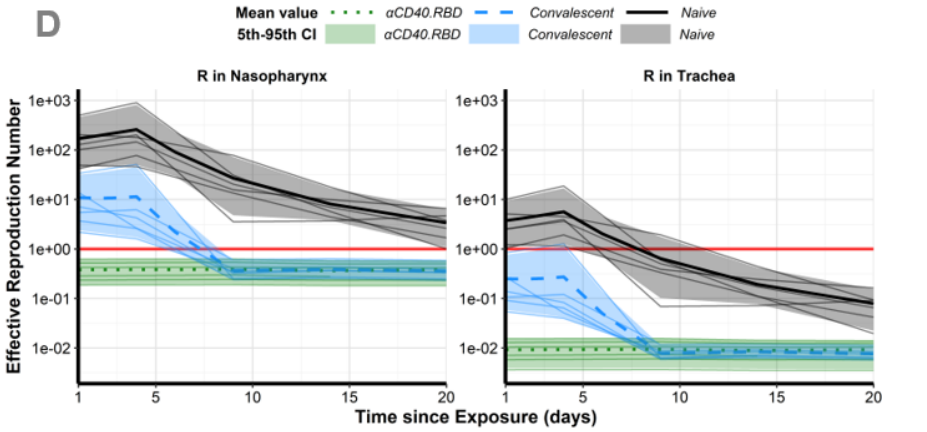
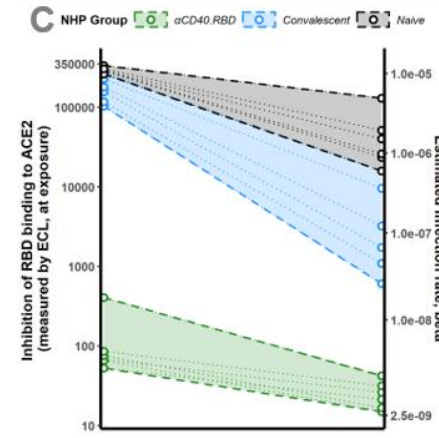
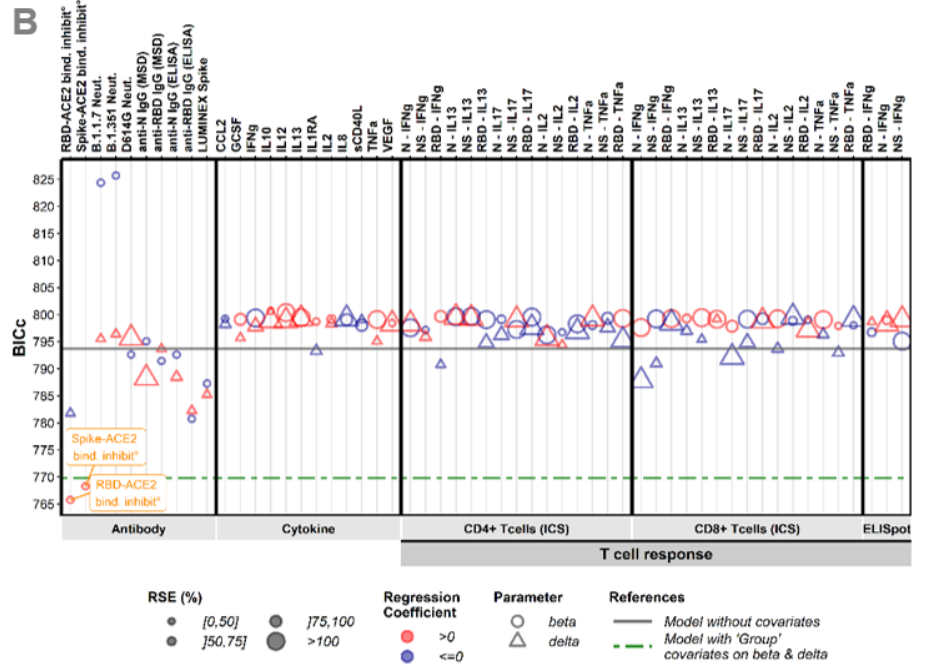
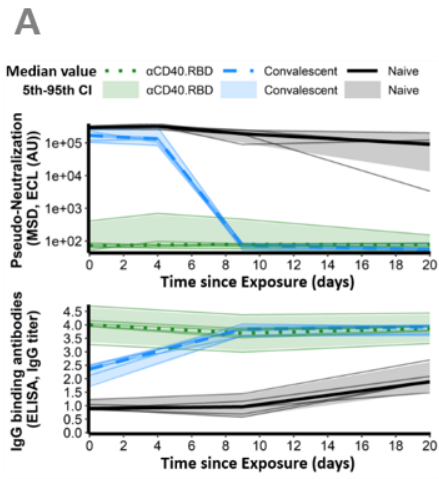
988



990 **Figure 2. Mechanistic modelling.**
 991 **(A)** Description of the model in the two compartments: the nasopharynx and the trachea. **(B)** Model fit to
 992 the \log_{10} transformed observed gRNA viral loads in tracheal (top) and nasopharyngeal (bottom)
 993 compartments after the initial exposure to SARS-CoV-2 in naive macaques (black, right) and after the
 994 second exposure in convalescent (blue, middle) and vaccinated (green, left) animals.
 995 Thick solid and dashed lines indicate mean viral load dynamics predicted and observed, respectively.
 996 Shaded areas indicate the 95% confidence intervals of the predictions. Dots represents observations. **(C)**
 997 Model predictions of unobserved quantities in the tracheal compartment for naive (black, solid lines),
 998 convalescent (blue, dashed lines) and vaccinated (green, dotted lines) animals: target cells as percentage
 999 of the value at the challenge (top, left), infected cells (top, middle), productively infected cells (top, right),
 1000 inoculum (bottom, right), infectious (bottom, left) and non-infectious virus (bottom, middle). Thick lines
 1001 indicate mean values over time within each group. Shaded areas indicate the 95% confidence interval.
 1002 Horizontal dashed red lines indicate the limit of quantification and horizontal solid red lines highlight the
 1003 threshold of one infected cell.
 1004
 1005
 1006



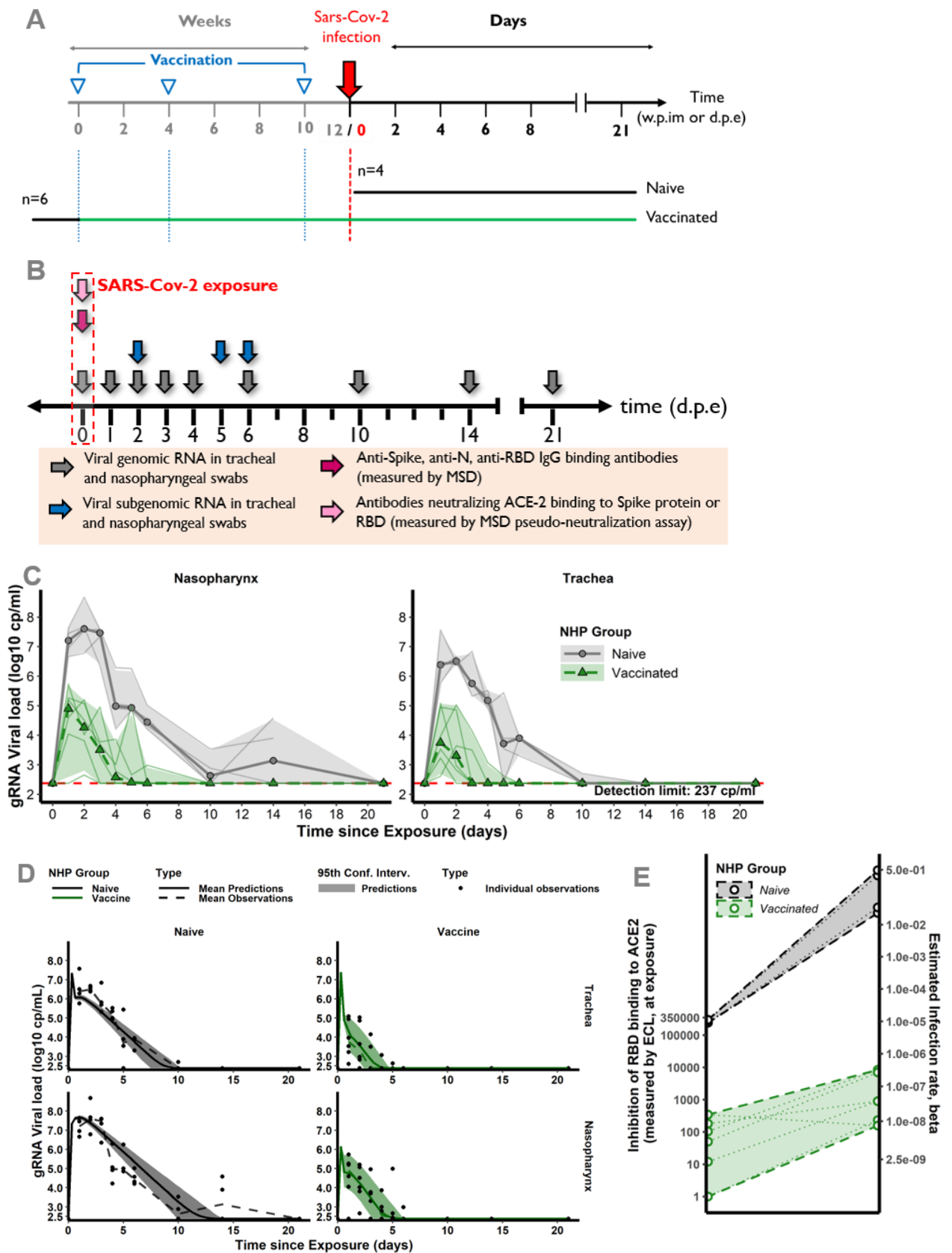
1007 **Figure 3. Harvest times and measurements.**
 1008 Nasopharyngeal and tracheal fluids, were collected at 0, 1, 2, 3, 4, 6, 9, 14 and 20 days post exposure
 1009 (d.p.e) while blood was taken at 0, 2, 4, 6, 9, 14 and 20 d.p.e. Genomic and subgenomic viral loads were
 1010 measured by RT-qPCR. Anti-Spike IgG sera were titrated by multiplex bead assay, Anti-RBD and anti-
 1011 Nucleocapside (N) IgG were titrated using a commercially available multiplexed immunoassay developed
 1012 by Mesoscale Discovery (MSD, Rockville, MD). The MSD pseudo-neutralization assay was used to measure
 1013 antibodies neutralizing the binding of the spike protein and RBD to the ACE2 receptor. Neutralizing
 1014 antibodies against B.1.1.7, B.1.351 and D614G strains were measured by S-Fuse neutralization assay and
 1015 expressed as ED50 (Effective dose 50%). T-cell responses were characterized as the frequency of PBMC
 1016 expressing cytokines (IL-2, IL-17 a, IFN- γ , TNF-a, IL-13, CD137 and CD154) after stimulation with S or N
 1017 sequence overlapping peptide pools. IFN- γ ELISpot assay of PBMCs were performed on PBMC stimulated
 1018 with RBD or N sequence overlapping peptide pools and expressed as spot forming cell (SFC) per 1.0×10^6
 1019 PBMC.
 1020
 1021



1023 **Figure 4. Immune markers.**

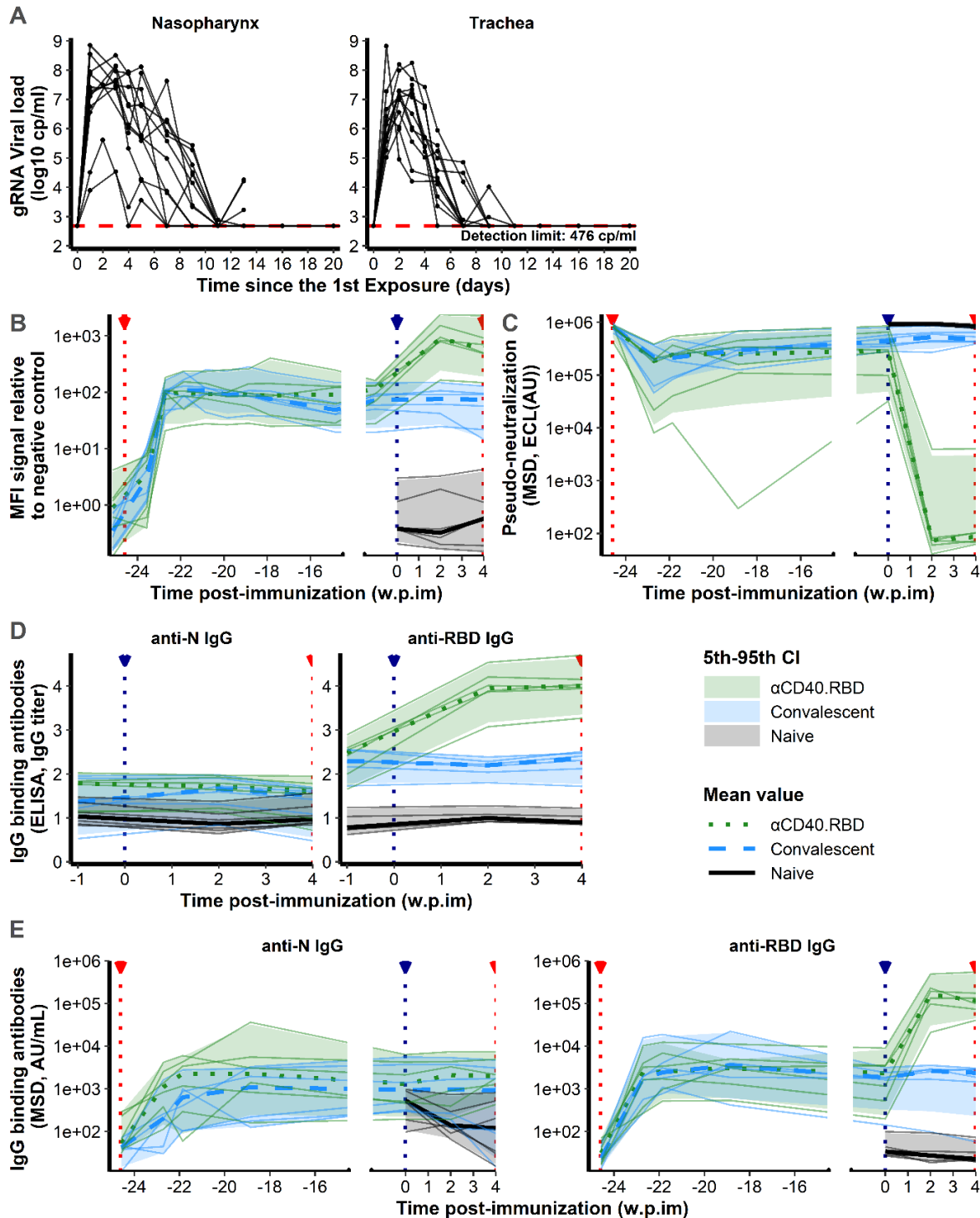
1024 **(A) Dynamics of biomarker selected as mCoP.** Quantification of antibodies inhibiting RBD-ACE2 binding,
1025 measured by the MSD pseudo-neutralization assay (ECL, in AU) (top) and anti-RBD IgG titrated by ELISA
1026 assay (in IgG titer) (bottom). Thin lines represent individual values. Thick lines indicate medians of
1027 observations within naïve (black, solid line), convalescent (blue, dashed line) and α CD40.RBD-vaccinated
1028 convalescent (green, dotted line) animals. Shaded areas indicate 5th-95th confidence intervals of
1029 observations. **(B) Systematic screening of effect of the markers.** For every single marker, a model has been
1030 fitted to explore whether it explains the variation of the parameter of interest better or as well than the
1031 group indicator. Parameters of interest were β , the infection rate of ACE2+ target cells, and δ , the loss rate
1032 of infected cells. Models were compared according to the Bayesian Information Criterion (BIC), the lower
1033 being the better. The green line represents the reference model that includes the group effect
1034 (naive/convalescent/vaccinated) without any adjustment for immunological marker (see **Figure 3** for more
1035 details about measurement of immunological markers). **(C) Thresholds of inhibition of RBD-ACE2 binding.**
1036 Estimated infection rate (in $(\text{copies/mL})^{-1} \text{ day}^{-1}$) of target cells according to the quantification of antibodies
1037 inhibiting RBD-ACE2 (in ECL) at exposure. Thin dotted lines and circles represent individual values of
1038 infection rates (right axis) and neutralizing antibodies (left axis). Shaded areas delimit the pseudo-
1039 neutralization / viral infectivity relationships within each group. **(D) Reproduction number over time.** Model
1040 predictions of the reproduction number over time in the trachea (right) and nasopharynx (left). The
1041 reproduction number is representing the number of infected cells from one infected cell if target cells are
1042 unlimited. Below one, the effective reproduction number indicates that the infection is going to be cured.
1043 Horizontal solid red lines highlight the threshold of one. Same legend than A). **(E) Conditions for controlling**
1044 **the infection.** Basic reproduction number (R_0) at the time of the challenge according to the levels of
1045 antibodies inhibiting RBD-ACE2 binding (the lower the better) and of anti-RBD IgG binding antibodies (the
1046 higher the better) assuming they are mechanistic correlates of blocking new cell infection and promoting
1047 infected cell death, respectively. The red area with $R > 1$ describes a situation where the infection is
1048 spreading. The green area with $R < 1$ describes a situation where the infection is controlled. The dotted red
1049 line delimitates the two areas. Black long dashed lines represent the values of neutralizing and binding
1050 antibodies measured at exposure. Observed values for three different animals belonging to the naive
1051 (bottom, right), convalescent (bottom, left) and vaccinated (top, left) groups are represented. For each
1052 animal, individual values of R_0 were estimated considering their individual values of the model parameters
1053 (β and δ).

1054



1056 **Figure 5. The second study testing two-component spike nanoparticle vaccine.**
1057 **(A)** Study design. Cynomolgus macaques were randomly assigned in two experimental groups. Twelve,
1058 eight and two weeks post-infection with SARS-CoV-2 virus, six of them were successively immunized with
1059 50 µg of SARS-CoV-2 S-I53-50NP vaccine. The four other animals received no vaccination. Two weeks after
1060 the final immunization, all monkeys were exposed to a total dose of 10⁶ pfu of SARS-CoV-2 virus via intra-
1061 nasal and intra-tracheal routes. **(B)** Harvest times and measurements. Nasopharyngeal and tracheal fluids
1062 were collected at 0, 1, 2, 3, 4, 5, 6, 10, 14 and 21 d.p.e while blood was taken at 0, 2, 4, 6, 10, 14 and 21
1063 d.p.e. Genomic and subgenomic viral loads were measured by RT-qPCR. Anti-Spike, anti-RBD and anti-
1064 Nucleocapside (N) IgG were titrated using a multiplexed immunoassay developed by Mesoscale Discovery
1065 (MSD, Rockville, MD) and expressed in AU/mL. The MSD pseudo-neutralization assay was used to quantify
1066 antibodies neutralizing the binding of the spike protein and RBD domain to the ACE2 receptor and results
1067 were expressed in ECL. **(C)** Genomic viral load dynamics in nasopharyngeal and tracheal swabs after the
1068 exposure to SARS-Cov-2 in naïve (black, solid line) and vaccinated (green, dashed line) animals. Thin lines
1069 represent individual values. Thick lines indicate medians within each group. **(D)** Model fit to the log₁₀-
1070 transformed observed gRNA viral load in nasopharynx and trachea after the exposure to SARS-CoV-2 in
1071 naïve and vaccinated macaques. Solid thin lines indicate individual dynamics predicted by the model
1072 adjusted for groups. Thick dashed lines indicate mean viral load over time. **(E)** Thresholds of inhibition of
1073 RBD-ACE2 binding. Estimated infection rate of target cells ((copies/mL)-1day⁻¹) according to the
1074 quantification of antibodies inhibiting RBD-ACE2 binding (ECL) at exposure for naïve (black) and vaccinated
1075 (green) animals. Thin dotted lines and circles represent individual infection rates (right axis) and
1076 neutralizing antibodies (left axis). Thick dashed lines and dashed areas delimit the pseudo-neutralization /
1077 viral infectivity relationships within each group. (C,D) Horizontal red dashed lines represent the limit of
1078 quantification and shaded areas the 95% confidence intervals.

Supplementary Figures and Tables



1080

1081

1082

1083

1084

1085

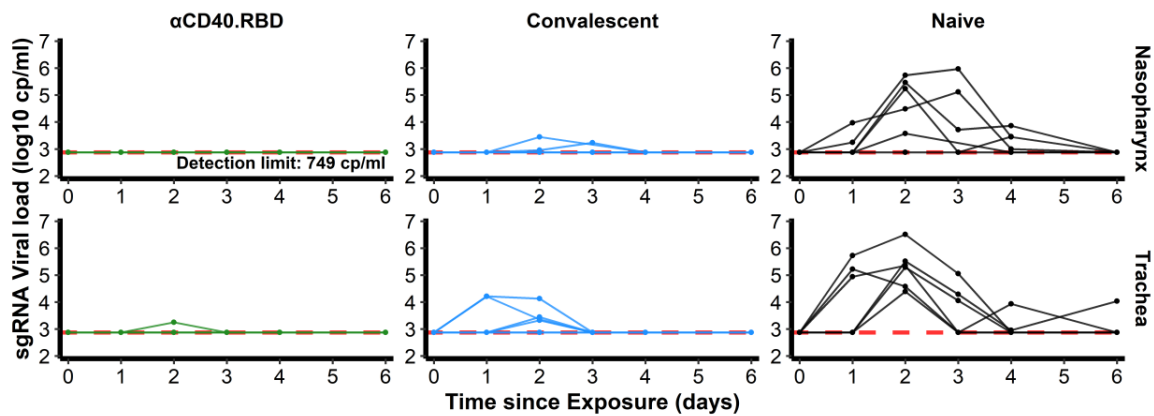
1086

Figure 1 – figure supplement 1. Viral dynamics after the first exposure to SARS-CoV-2 and biomarker measurements from the first to the second exposure to SARS-CoV-2.

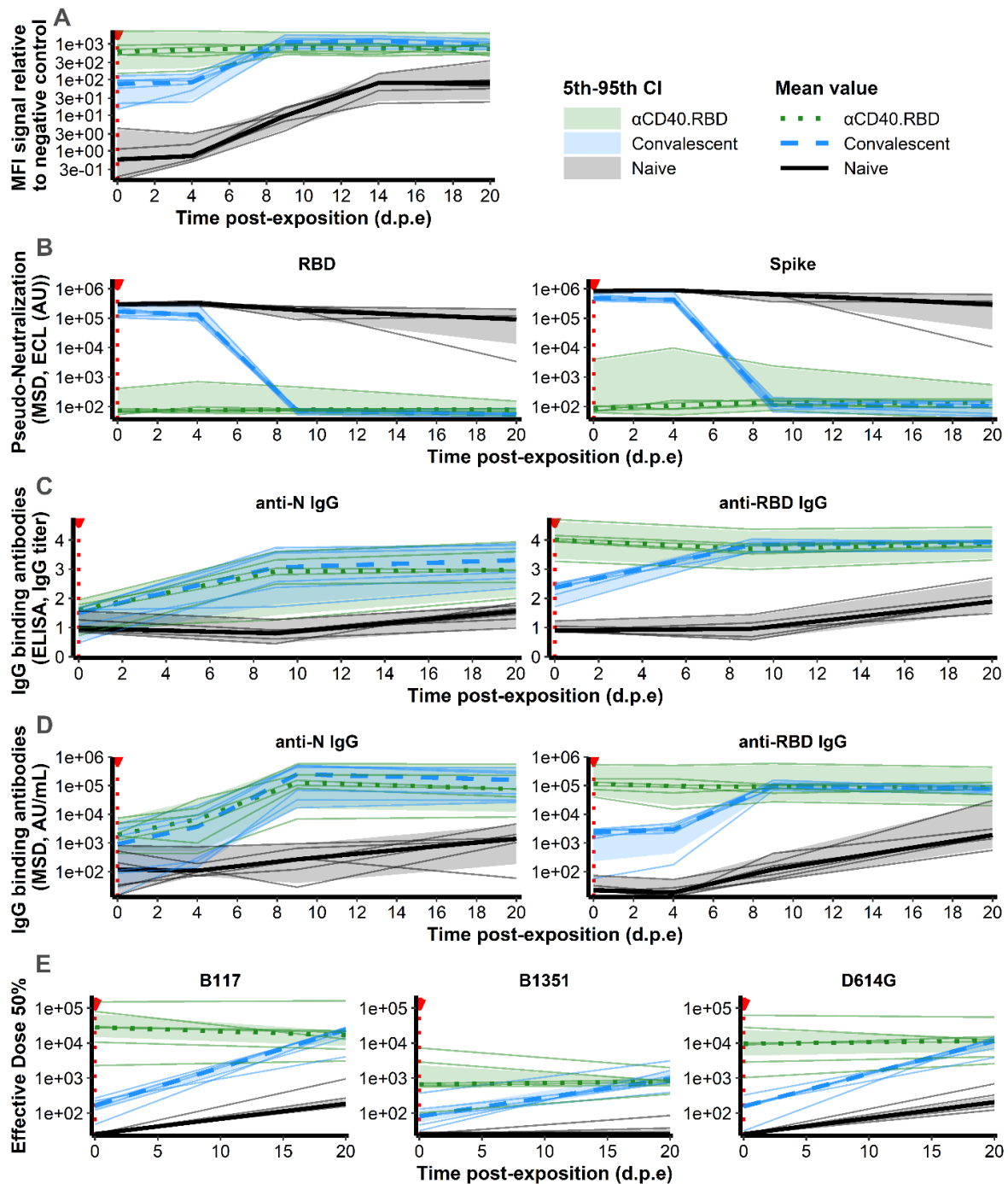
(A) Individual log₁₀ transformed gRNA viral load dynamics in nasopharyngeal (left) and tracheal (right) swabs after the initial exposure to SARS-CoV-2 in naive macaques (n=12). Solid lines represent individual values. Horizontal red dashed lines indicate the limit of quantification. **(B)** Relative MFI of IgG binding to SARS-CoV-2 Spike protein, measured using a Luminex-based serology assay, in serum samples, after the initial exposure

1087 to SARS-CoV-2. **(C)** Quantification of antibodies inhibiting the attachment of Spike protein to ACE2 receptor
 1088 in NHP serum, measured by the Mesoscale Discovery (MSD, Rockville, MD) pseudo-neutralization assay.
 1089 Results are expressed as ECL (ECL, Electro-chemiluminescence) in AU. **(D)** Quantification of SARS-CoV-2 IgG
 1090 binding N or RBD domain measured in the serum of NHPs titrated by ELISA assay. Results are expressed in IgG
 1091 titer. **(E)** Quantification of SARS-CoV-2 IgG binding N and RBD domain measured in the serum of NHPs using
 1092 a multiplexed solid-phase chemiluminescence assay. Results are expressed in AU/mL. **(B-E)** Results are
 1093 obtained after the initial exposure to SARS-CoV-2 at -24.9 weeks post-immunization (w.p.im) in convalescent
 1094 (n=6, blue, dashed line) and α CD40.RBD-vaccinated convalescent (n=6, green, dotted line) animals and at 4
 1095 w.p.im in naive (n=6, black, solid line) animals. Thin lines represent individual values. Thick lines indicate
 1096 medians within each group and shaded areas indicate 5th-95th confidence intervals. The red (-24.6 and 4.0
 1097 w.p.im) and blue (0 w.p.im) lines highlight viral exposure and vaccination respectively.

1098
 1099



1100
 1101 **Figure 1 - figure supplement 2. Subgenomic viral dynamics after the second exposure to SARS-CoV-2.**
 1102 Individual log₁₀ transformed subgenomic (gRNA) viral load dynamics in nasopharyngeal (top) and tracheal
 1103 (bottom) swabs after the initial exposure to SARS-CoV-2 in naive macaques (n=6, black, right) and after the
 1104 second exposure in convalescent (n=6, blue, middle) and α CD40.RBD-vaccinated convalescent (n=6, green,
 1105 left) groups. Horizontal red dashed lines indicate the limit of quantification.



1106
1107

1108

1109

1110

1111

1112

1113

1114

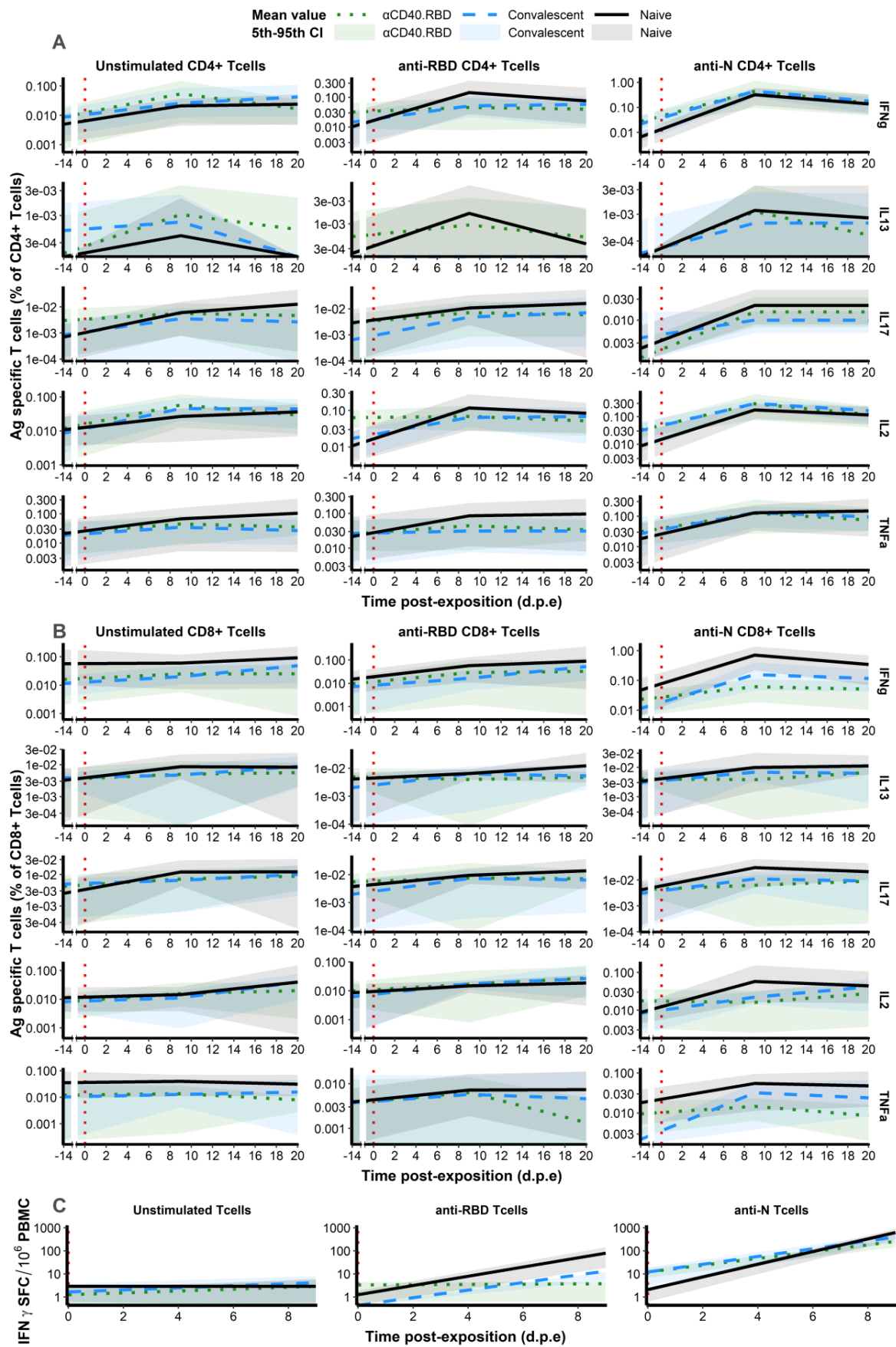
1115

1116

Figure 1 – figure supplement 3. Antibody measurements after the second exposure to SARS-CoV-2.

(A) Relative MFI of IgG binding to SARS-CoV-2 Spike protein, measured using a Luminex-based serology assay, in serum samples, after the second exposure to SARS-CoV-2. (B) Quantification of antibodies inhibiting that attachment of RBD domain or Spike protein to ACE2 receptor in NHP serum, measured by the Mesoscale Discovery (MSD, Rockville, MD) pseudo-neutralization assay, after the second exposure to SARS-CoV-2. Results are expressed as ECL, in AU. (C) Quantification of SARS-CoV-2 IgG binding N or RBD domain measured in the serum of NHPs titrated by ELISA assay, after the second exposure to SARS-CoV-2. Results are expressed in Ig titer. (D) Quantification of SARS-CoV-2 IgG binding N or RBD domain measured in the serum of NHPs using a multiplexed solid-phase chemiluminescence assay, after the second exposure to SARS-CoV-2. Results

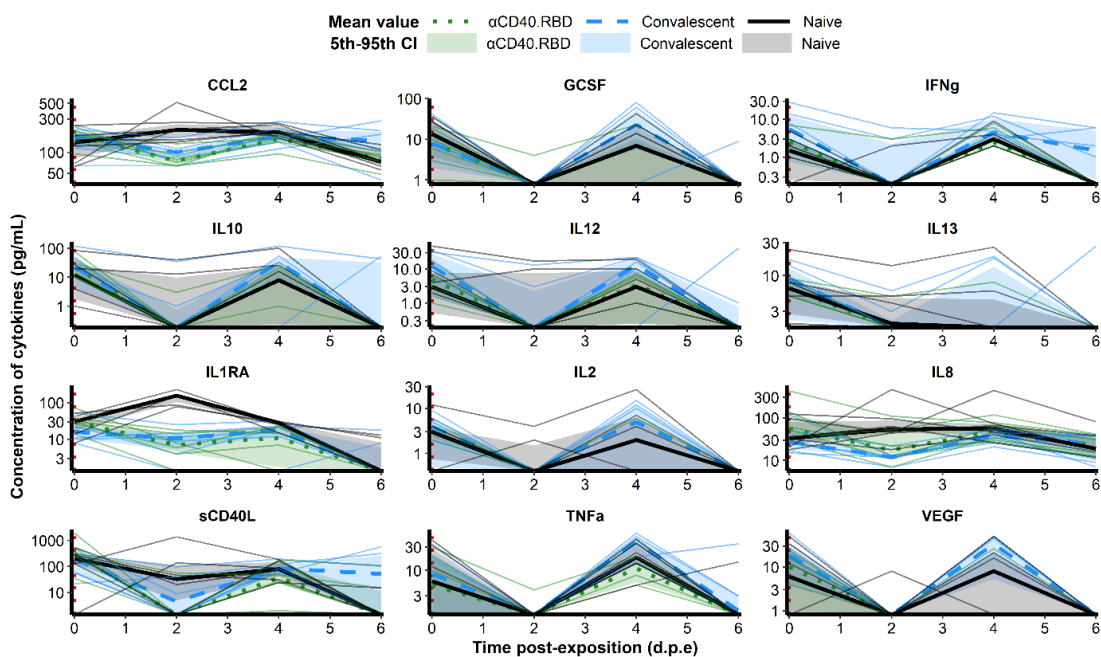
1117 are expressed in AU/mL. **(E)** Quantification of neutralizing antibodies against B.1.1.7, B.1.351 and D614G
1118 SARS-CoV-2 strains measured in the serum of NHPs using S-Fuse neutralization assay, after the second
1119 exposure to SARS-CoV-2 (measured only at the exposure and 20 days post-exposure (d.p.e)). Results are
1120 expressed as ED50 (Effective dose 50%). **(A-E)** Results are obtained after the initial exposure to SARS-CoV-2
1121 in naive macaques (n=6, black, solid line) and after the second exposure in convalescent (n=6, blue, dashed
1122 line) and α CD40.RBD-vaccinated convalescent (n=6, green, dotted line) animals. Thin lines represent
1123 individual values. Thick lines indicate medians within each group and shaded areas indicate 5th-95th
1124 confidence intervals. Red dotted vertical lines highlight the viral exposure.
1125



1127 **Figure 1 – figure supplement 4. Antigen-specific T-cell responses in NHPs after the second exposure to SARS-**
 1128 **CoV-2.**

1129 **(A-B)** Frequency of IFN γ ⁺ (first line), IL-13⁺ (second line), IL-17⁺ (third line), IL-2⁺ (fourth line) or TNF α ⁺ (fifth line)
 1130 antigen-specific CD4⁺ Tcells (CD154⁺) and CD8⁺ Tcells (CD137⁺) in the total CD4⁺ Tcell (A) or CD8⁺ Tcell (B)
 1131 population in NHP serum. PBMCs were stimulated *ex-vivo* overnight with medium (left), SARS-CoV-2 RBD
 1132 (middle) or N (right) overlapping peptide pools. T-cell responses being not measures at the challenge,
 1133 measured obtained 14 days pre-exposure were added. **(C)** Antigen-specific T-cell responses in NHPs. T-cells
 1134 were analyzed by ELISpot after *ex-vivo* stimulation with SARS-CoV-2 RBD or N overlapping peptide pools and
 1135 plotted as spot-forming cells (SFC) per 1.0x10⁶ PBMCs. **(A-C)** Results are obtained after the initial exposure
 1136 to SARS-CoV-2 in naive macaques (n=6, black, solid line) and after the second exposure in convalescent (n=6,
 1137 blue, dashed line) and α CD40.RBD-vaccinated convalescent (n=6, green, dotted line) animals. Thin lines
 1138 represent individual values. Thick lines indicate medians within each group and shaded areas indicate 5th-
 1139 95th confidence intervals. Red dotted vertical lines highlight the viral exposure.

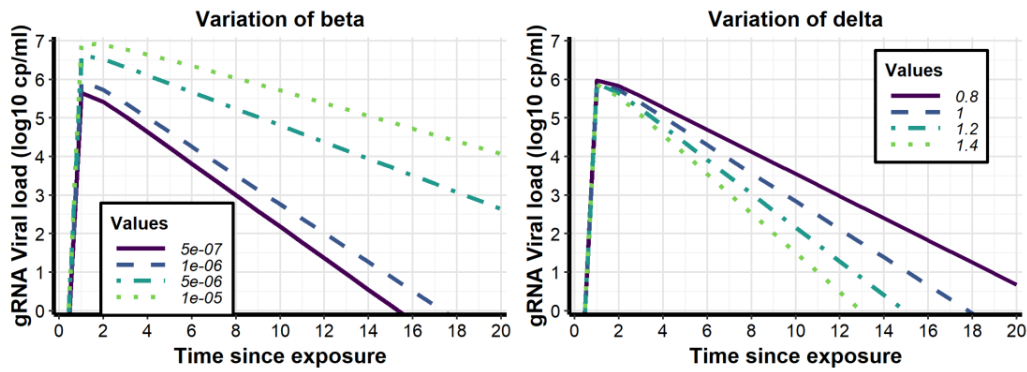
1140



1141

1142 **Figure 1 – figure supplement 5. Cytokines and chemokines in the plasma in NHPs after the second exposure**
 1143 **to SARS-CoV-2.**

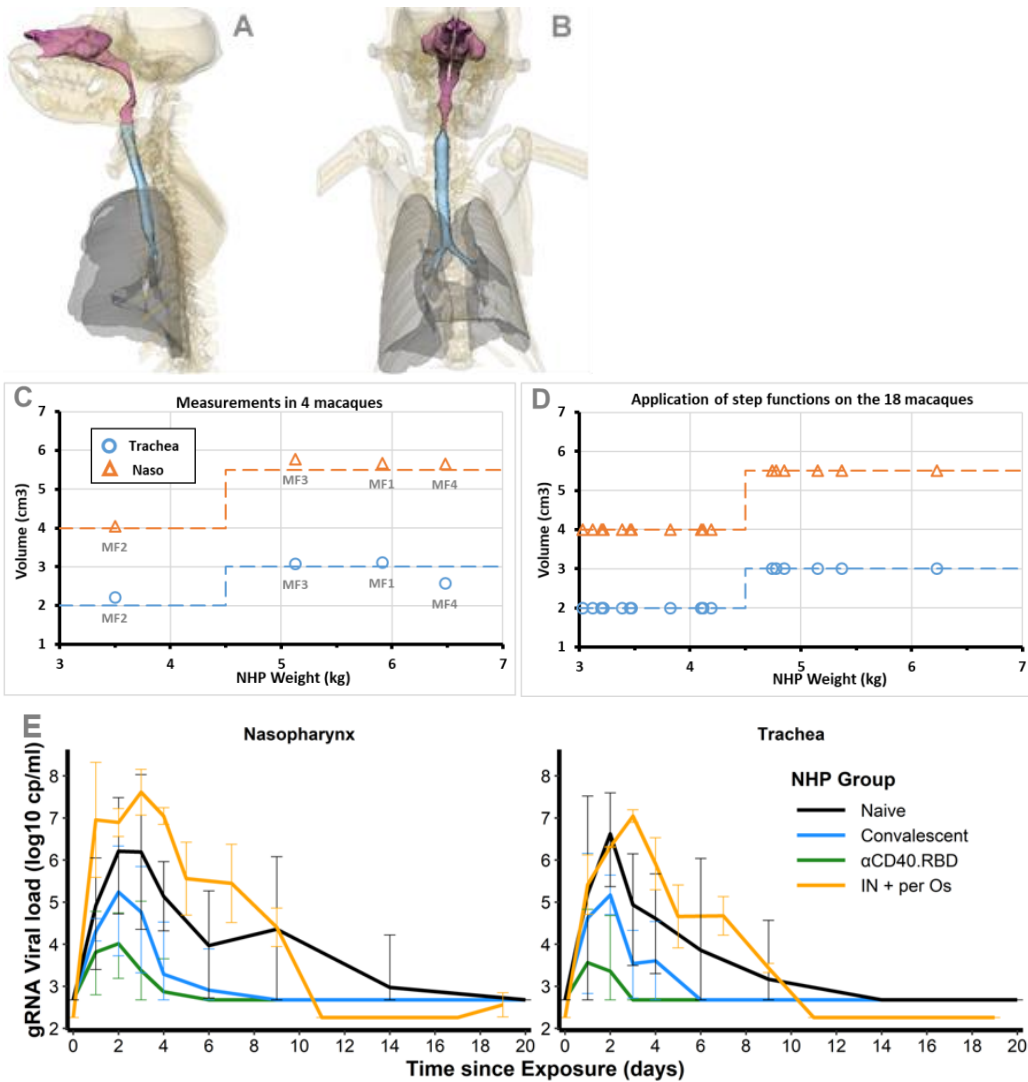
1144 Plasma concentration of 12 cytokines and chemokines in pg/mL. Results are obtained after the initial
 1145 exposure to SARS-CoV-2 in naive macaques (n=6, black, solid line) and after the second exposure in
 1146 convalescent (n=6, blue, dashed line) and α CD40.RBD-vaccinated convalescent (n=6, green, dotted line)
 1147 animals. Thin lines represent individual values. Thick lines indicate medians within each group and shaded
 1148 areas indicate 5th-95th confidence intervals. Red dotted vertical lines highlight the viral exposure.



1149
1150
1151
1152
1153
1154
1155
1156

Figure 2 - figure supplement 1. Modelling of the viral dynamics using mechanistic model.

Examples simulated genomic viral load dynamics for different values of viral infectivity (β , left) or loss rate of infected cells (δ , right) showing the effect of either blocking de novo infection or promoting the destruction of infected cells on viral dynamics profile. Except for β or δ , all other parameters were fixed at a given value.

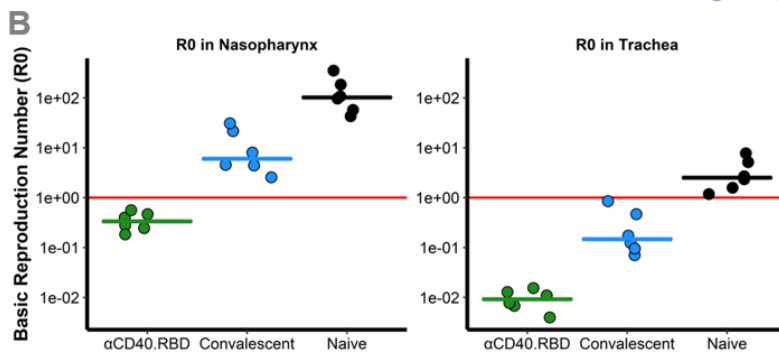
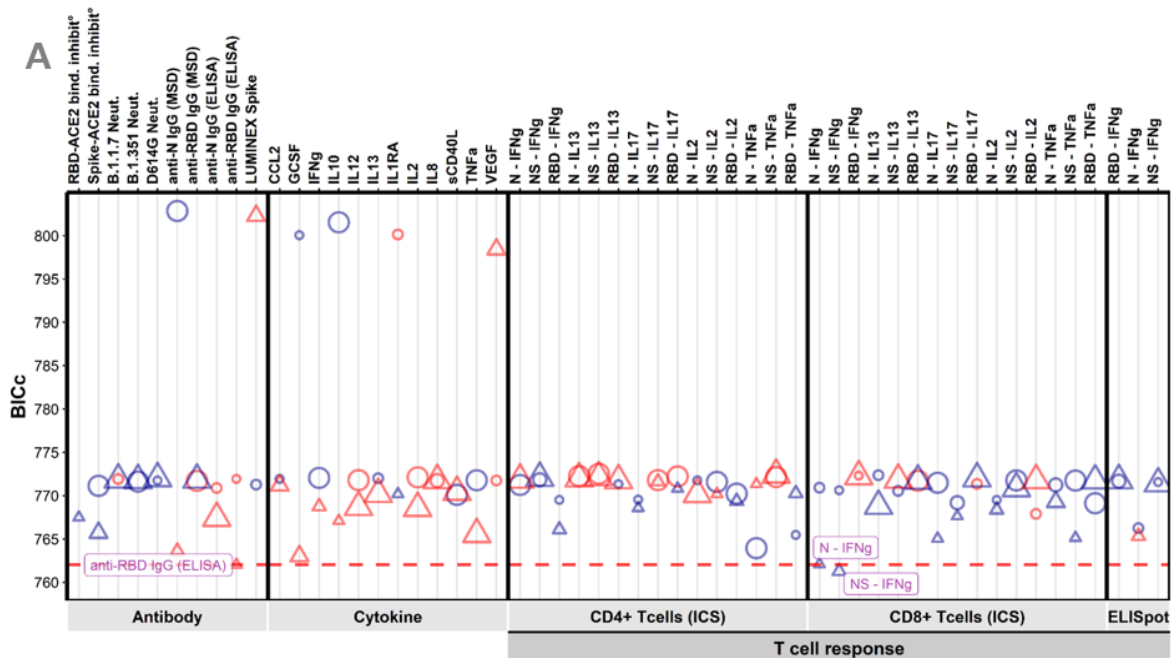


1157
1158

1159
1160
1161
1162
1163
1164
1165
1166
1167
1168
1169
1170
1171
1172
1173
1174

Figure 2 - figure supplement 2. Modelling of the dynamics of viral replication.

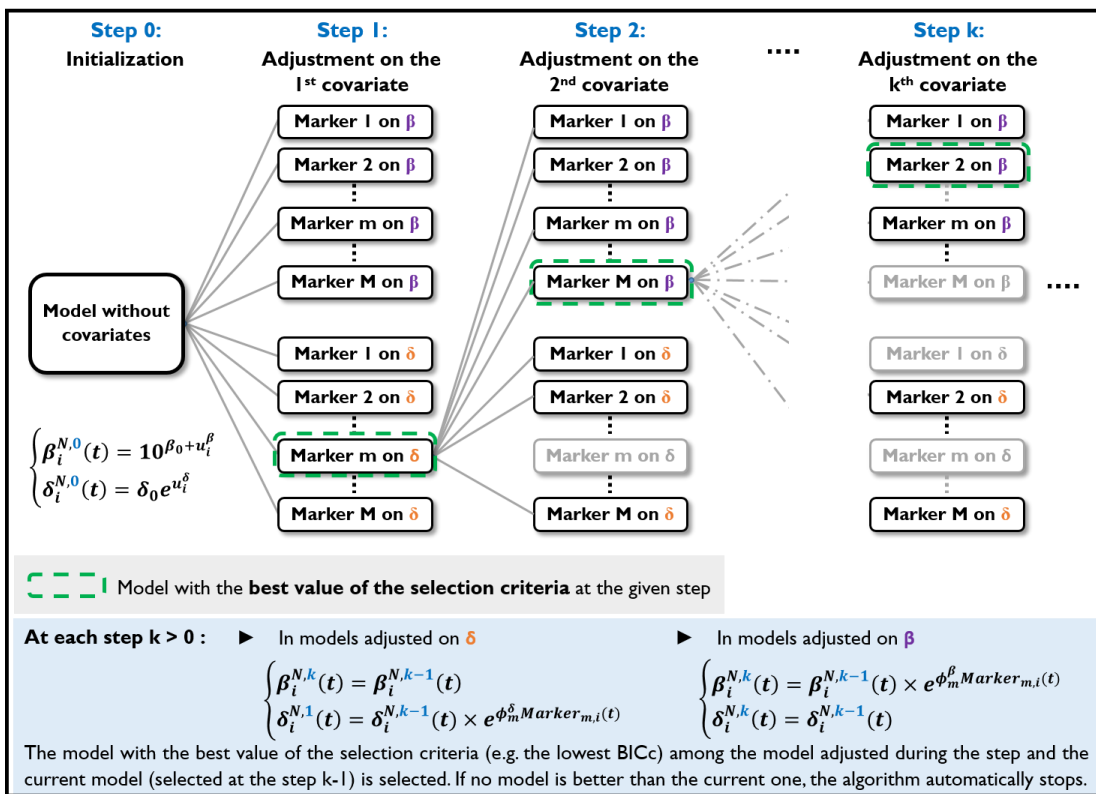
(A) Sagittal view of the 3D representation of the NHP respiratory system. **(B)** Coronal view of the 3D representation of the NHP respiratory system. (A-B) Lungs are colored in grey, Trachea and Nasal regions in blue and purple respectively. **(C)** Relationship between the weights (in kgs) measured in 4 NHPs and the estimation of the volume of their tracheal (blue circles) and nasal (orange triangles) regions (in cm³). Measurements were obtained on NHPs similar to the 18 macaques of our study. Orange and blue dashed lines represent the step function used to describe this relationship with a breakpoint at 4.5 kg. **(D)** Volumes of the tracheal (blue circles) and nasal (orange triangles) regions estimated for the 18 macaques using the step function defined in the subfigure C and their weights. **(E)** Mean gRNA load dynamics in nasopharyngeal (left) and tracheal (right) swabs after the initial exposure to SARS-CoV-2 in naive macaques (n=6, black) and after the second exposure in convalescent (n=6, blue) and α CD40.RBD-vaccinated convalescent (n=6, green) macaques. Two additional macaques (IN + per Os, orange) were initially exposed to SARS-CoV-2 via intra-nasal (0.5mL of inoculum) and intra-gastric (4.5 mL) routes instead of intra-nasal (0.5 mL of inoculum) and intra-tracheal (4.5 mL) routes as defined in the study. Solid lines represent mean values and error bars indicate the 5th-95th confidence intervals.



1175
1176
1177

1178 **Figure 4 – figure supplement 1. Immune markers selection and Basic reproduction number.**

1179 **(A) Systematic screening of effect of the markers (Step 2).** For every single marker, a model, already adjusted
 1180 on viral infectivity with antibodies inhibiting the attachment of RBD domain to ACE2 receptor, has been fitted
 1181 to explore whether it explains the variation of the parameter of interest better or as well than the model of
 1182 reference. Parameters of interest were β , the infection rate of ACE2+ target cells and δ , the loss rate of
 1183 infected cells. Models were compared according to the Bayesian Information Criterion (BIC), the lower being
 1184 the better. The red dashed line represents the reference model that includes the group effect (naive/
 1185 convalescent/vaccinated) on the parameter δ and with adjustment of pseudo-neutralization on β . **(B)**
 1186 *Reproduction number at the time of exposure.* Model predictions of the reproduction number at the time of
 1187 exposure (R_0) in the tracheal (right) and nasopharyngeal (left) compartments for naive (black), convalescent
 1188 (blue) and α CD40.RBD-vaccinated convalescent (green) animals. The reproduction number is representing
 1189 the number of infected cells from one infected cell if target cells are unlimited. When this effective
 1190 reproduction number is below 1, it means that the infection is going to be cured. The values of R_0 were
 1191 estimated by the model with viral infectivity (β) and loss rate of infected cells (δ) adjusted on pseudo-
 1192 neutralization and anti-RBD IgG binding antibodies titrated by ELISA assay respectively measured only at the
 1193 time of challenge. Horizontal solid red lines highlight the threshold of the reproduction number equals to one.
 1194



1195 **Figure 4 - figure supplement 2. Flow chart of the algorithm for automatic selection of covariate.**

1196 At the initialization step of our study, the model without covariates is considered as initial the model, all
 1197 immunological markers are seen as potential covariates (Marker) and $\{\beta, \delta\}$ is defined as the set of parameters
 1198 on which covariates can be added. At each, all the marker-parameter relationships that have not already been
 1199 added to the current model are added in an univariate manner to this model and ran. Among all the tested
 1200 models, the one with the optimal value of selection criteria (e.g. lowest BICc) is selected (green dashed
 1201 rectangle) and compared to the current model. If this one is better, it becomes the new current model and
 1202 the algorithm moves to the step k+1. Otherwise, the algorithm stops.
 1203
 1204

Supplementary file 1. Criteria defining RBD-ACE2 binding inhibition (studies testing two-component spike nanoparticle vaccine) or neutralization measured on live cells with luciferase marker (mRNA-1273) as mechanistic correlate of protection of the vaccine on new cell infection. Studies are labelled Study 1 and Study 2 for the main and the additional studies testing two-component spike nanoparticle vaccine, respectively and mRNA-1273 for the third study evaluating several doses of mRNA-1273 vaccine.

Model	Study 1		Study 2		mRNA-1273
	RBD-ACE2 binding inhibition on β	RBD-ACE2 binding inhibition on β	RBD-ACE2 binding inhibition on β	RBD-ACE2 binding inhibition on β	Neutralization on β
Type of covariates added in the model	Time-varying	Baseline	Baseline	Baseline	Baseline
Criterion 1	793.71	793.71	427.63	469.13	
Without adjustment					
Group effect (β and δ)	772.34	772.34	404.80	468.70	
Best fits (BICc Value)	765.76	765.22	413.35	467.21	
Marker effect only (β)	762.69	762.53	407.66		
Marker (β) and Group (δ) effects					
Criterion 2	Conv: -0.747** (0.255)	Conv: -0.747** (0.255)	Vacc: -6.01**** (0.8)	10 μ g: -0.267 (0.578)	
Group effect (β and δ)	Conv-CD40: -2.38*** (0.265)	Conv-CD40: -2.38*** (0.265)		100 μ g: -1.6** (0.621)	
Group effect (Value (Sd))	Conv: 0.00428 (1.71)	Conv: 0.303 (0.864)	Vacc: 2.31 (1.18)	10 μ g: 0.105(0.646)	
	Conv-CD40: 0.1 (2.79)	Conv-CD40: 0.362 (1.14)		100 μ g: 3.10-4 (0.84)	
Criterion 3	β : 65.5 %	β : 65.5 %	β : 64.9 %	β : 18.5 %	
Group effect (β and δ)	δ : 54 %	δ : 54 %	δ : 58.2 %	δ : 4.6%	
Expl. variability for β or δ (relative % ¹)	β : 87.4 %	β : 82.7 %	β : 70.8 %	β : 15.4 %	
	δ : 27.1 %	δ : 31.6 %	δ : -17%	δ : 19.1 %	
Marker effect (β)	β : 79 %	β : 75.4 %	β : 66 %		
Marker (β) and Group (δ) effects	δ : 56.7 %	δ : 65.6 %	δ : 69.9 %		

¹ Relative percentage of inter-individual variability compared to variability obtained on model without any adjustment ; $100 \cdot (x \cdot 100) / ref$
* $P < 0.05$, ** $P < 0.01$, *** $P < 0.001$, **** $P < 1e-4$, Wald test for fold change different from 1

Supplementary file 2. Model parameters for viral dynamics in both the nasopharynx and the trachea estimated by the model adjusted for groups of intervention, either as a single estimation or using a bootstrap procedure with replacement. For the bootstrap procedure, 50 iterations were performed.

Param.	Meaning	Value [95% CI]	Bootstrap	Unit
β	Viral infectivity in the naive group ($\times 10^{-6}$)	0.95 [0.18 ; 4.94]	0.91 [0.12 ; 7.03]	(copies/ml) ⁻¹ day ⁻¹
	Fold change in the convalescent group	0.18 [0.04 ; 0.88]**	0.15 [0.04 ; 0.58]	
	Fold change in the Conv-CD40 group	0.004 [0.001 ; 0.029]***	0.006 [0.001 ; 0.04]	
δ	Loss rate of infected cells in the naive group	1.04 [0.79 ; 1.37]	1.09 [0.74 ; 1.60]	day ⁻¹
	Fold change in the convalescent group	1.79 [1.21 ; 2.66]**	1.70 [1.08 ; 2.66]	
	Fold change in the Conv-CD40 group	1.80 [1.17 ; 2.75]**	2.00 [0.94 ; 4.27]	
P^N	Viral production rate in the naso. ($\times 10^3$)	12.1 [3.15 ; 46.5]	10.1 [1.16 ; 87.7]	virions.(cell.day) ⁻¹
P^T	Viral production rate in the trachea ($\times 10^3$)	0.92 [0.39 ; 2.13]	0.86 [0.08 ; 9.19]	virions.(cell.day) ⁻¹
α_{vIsg}	Infected cells and sgRNA viral load ratio	1.39 [1.01 ; 1.76]	1.42 [0.99 ; 2.02]	Virions.cell ⁻¹
k	Eclipse rate	3	3	day ⁻¹
c	Clearance of <i>de novo</i> produced viruses	3	3	day ⁻¹
c_i	Clearance of inoculum	20	20	day ⁻¹
μ	Percentage of infectious viruses	10^{-3}	10^{-3}	
$T_0^{X, nbc}$	Initial number of target cells	1.25×10^5 (Naso.)	1.25×10^5 (Naso.)	cells
		2.25×10^4 (Trachea)	2.25×10^4 (Trachea)	
$Inoc_0$	Number of virions inoculated	2.19×10^{10}	2.19×10^{10}	virions
ω_β	SD of random effect on $\log_{10} \beta$	0.366 [0.160 ; 0.571]	0.319 [0.111 ; 0.527]	
ω_δ	SD of random effect on δ	0.170 [-0.089 ; 0.429]	0.122 [-0.039 ; 0.283]	
σ_{vLn}	SD of error model IgRNA in naso.	1.27 [1.01 ; 1.53]	1.24 [0.96 ; 1.51]	
σ_{vLt}	SD of error model IgRNA in trachea	1.09 [0.90 ; 1.28]	1.09 [0.92 ; 1.26]	
σ_{sgvLn}	SD of error model sgRNA in naso	1.41 [0.97 ; 1.85]	1.35 [1.08 ; 1.61]	
σ_{sgvLt}	SD of error model sgRNA in trachea	1.62 [1.11 ; 2.13]	1.53 [1.15 ; 1.92]	

Conv-CD40 group: group of convalescent NHPs being vaccinated ; **SD:** Standard deviation ; * $P < 0.05$, ** $P < 0.01$, *** $P < 0.001$, wald test for fold change different from 1

Supplementary file 3a. Values of -2LL estimated on models with viral clearance ($c=c_l$) and eclipse phase rate k fixed at different values.

c	k	1	3	6
1		1285.29	1286.42	1289.54
5		871.38	864.50	866.80
10		773.74	764.29	768.18
15		749.67	738.71	742.12
20		749.44	738.40	740.98
30		750.00	739.51	741.34

Supplementary file 3b. Values of -2LL estimated on models with inoculum clearance c_l and clearance of virus de novo produced c fixed at different values. The eclipse phase rate was fixed at $k=3 \text{ day}^{-1}$.

c	c_l	1	5	10	15	20	25	30
1		1286.42	873.30	777.21	753.72	754.14	754.32	754.75
2		1286.70	864.90	760.94	734.03	734.14	733.94	734.95
3		1286.41	864.58	760.69	734.71	733.85	734.87	734.48
4		1286.33	864.22	761.78	735.91	735.16	735.42	736.14
5		1286.38	864.50	762.69	737.13	735.85	736.37	736.69
10		1286.55	865.48	764.29	738.38	737.56	737.89	738.13
15		1286.23	865.12	764.79	738.71	737.54	738.17	738.75
20		1285.96	865.19	764.78	738.86	738.40	738.25	739.30
25		1286.28	864.93	764.97	739.20	738.05	738.37	739.34
30		1286.45	864.77	765.16	739.01	738.13	738.58	739.51

Supplementary file 4. Model parameters for viral dynamics in both the nasopharynx and the trachea estimated by the model with the viral infectivity adjusted for ACE2-RBD binding inhibition and the loss rate of infected cells adjusted for the group of treatment, either as single estimation or using a bootstrap procedure with replacement. For the bootstrap procedure, 50 iterations were performed.

Param.	Meaning	Value [95% CI]	Bootstrap	Unit
β	Infection rate with ECLRBBD=0 AU ($\times 10^{-8}$)	0.80 [0.21 ; 3.01]	0.82 [0.13 ; 5.13]	(copies/ml) ⁻¹ day ⁻¹
	Fold Δ ECLRBBD = 10^3 AU	1.018 [1.012 ; 1.023]	1.017 [1.012 ; 1.022]	
δ	Loss rate of infected cells	1.00 [0.76 ; 1.33]	1.02 [0.80 ; 1.30]	day ⁻¹
	Fold change in the convalescent group	1.78 [1.21 ; 2.61]**	1.74 [1.24 ; 2.46]	
	Fold change in the Conv-CD40 group	2.18 [1.24 ; 3.84]**	2.17 [0.82 ; 5.74]	
P^N	Viral production rate in the naso. ($\times 10^3$)	9.87 [2.86 ; 34.06]	8.92 [0.42 ; 191]	virions.(cell.day) ⁻¹
P^T	Viral production rate in the trachea ($\times 10^3$)	0.71 [0.16 ; 3.18]	0.62 [0.02 ; 19.7]	virions.(cell.day) ⁻¹
α_{vlsq}	Infected cells and sgRNA viral load ratio	1.33 [1.02 ; 1.74]	1.32 [0.91 ; 1.90]	Virions.cell ⁻¹
k	Eclipse rate	3	3	day ⁻¹
c	Clearance of <i>de novo</i> produced viruses	3	3	day ⁻¹
c_I	Clearance of inoculum	20	20	day ⁻¹
μ	Percentage of infectious viruses	10^{-3}	10^{-3}	
$T_0^{X,abc}$	Initial number of target cells	1.25×10^5 (Naso.)	1.25×10^5 (Naso.)	cells
		2.25×10^4 (Trachea)	2.25×10^4 (Trachea)	
$Inoc_0$	Number of virions inoculated	2.19×10^{10}	2.19×10^{10}	virions
ω_β	SD of random effect on $\log_{10} \beta$	0.223 [-0.059 ; 0.505]	0.205 [0.011 ; 0.399]	
ω_δ	SD of random effect on δ	0.196 [-0.090 ; 0.482]	0.079 [-0.092 ; 0.250]	
σ_{vln}	SD of error model gRNA in naso.	1.13 [0.91 ; 1.34]	1.13 [0.90 ; 1.36]	
σ_{vlt}	SD of error model gRNA in trachea	1.25 [1.02 ; 1.48]	1.27 [1.07 ; 1.48]	
σ_{sgvln}	SD of error model sgRNA in naso	1.57 [1.09 ; 2.04]	1.62 [1.30 ; 1.94]	
σ_{sgvlt}	SD of error model sgRNA in trachea	1.33 [0.96 ; 1.70]	1.36 [1.15 ; 1.56]	

Conv-CD40 group: group of convalescent NHPs being vaccinated ; * $P < 0.05$, ** $P < 0.01$, *** $P < 0.001$, wald test for fold change different from 1

Appendix 1 - Model building

In the model presented in the manuscript, we considered the two compartments of the upper respiratory tract (URT), trachea and nasopharynx, as two distinct compartments (i.e. without transfer of virus between them), as described by equation (1). In each of them, the viral dynamics are described by a target-cell limited model augmented with a compartment describing the dynamics of the inoculated virus (V_s). Moreover, in the statistical model describing the model parameters, the three parameters β , δ and P were assumed as jointly estimated between the two compartments, with shared random effects and covariates and considering that parameters β and δ are equal in both trachea and nasopharynx ($\beta^T = \beta^N$, $\delta^T = \delta^N$).

$$\left\{ \begin{array}{l} \frac{dT^N}{dt} = -\beta^N V_i^N T^N - \mu \beta^N V_s^N T^N \\ \frac{dI_1^N}{dt} = \beta^N V_i^N T^N + \mu \beta^N V_s^N T^N - k I_1^N \\ \frac{dI_2^N}{dt} = k I_1^N - \delta^N I_2^N \\ \frac{dV_i^N}{dt} = \mu P^N I_2^N - c V_i^N - \beta^N V_i^N T^N \\ \frac{dV_{ni}^N}{dt} = (1 - \mu) P^N I_2^N - c V_{ni}^N \\ \frac{dV_s^N}{dt} = -c_i V_s^N - \mu \beta^N V_s^N T^N \end{array} \right. \quad \left\{ \begin{array}{l} \frac{dT^T}{dt} = -\beta^T V_i^T T^T - \mu \beta^T V_s^T T^T \\ \frac{dI_1^T}{dt} = \beta^T V_i^T T^T + \mu \beta^T V_s^T T^T - k I_1^T \\ \frac{dI_2^T}{dt} = k I_1^T - \delta^T I_2^T \\ \frac{dV_i^T}{dt} = \mu P^T I_2^T - c V_i^T - \beta^T V_i^T T^T \\ \frac{dV_{ni}^T}{dt} = (1 - \mu) P^T I_2^T - c V_{ni}^T \\ \frac{dV_s^T}{dt} = -c_i V_s^T - \mu \beta^T V_s^T T^T \end{array} \right. \quad (7)$$

Initially, random effects were added on the three parameters. However, taken into consideration identifiability issues that are usually encountered between the viral infectivity (β) and the viral production (P), we decided to remove the possibility of inter-individual variability on the parameter P . This choice was also driven by multiple model estimations showing less robust estimations when variability was allowed in both parameters β and P . In particular, the estimate of the viral production was impacted by a ratio between the parameter and its standard error (RSE) higher than 100%.

Comparison of the parameters between the tracheal and the nasopharyngeal compartments

To decide which of these three parameters were assumed to be equal between the two compartments, all possibilities were tested and compared, using the BICc as selection criteria. As shown in **Table 1**, we started with the model in which all parameters were equal between the two compartments and we progressively relaxed this hypothesis. During this step, no exchange of virions between the two compartments of the URT was possible ($g=0$). Once all models estimated, we kept the one with the lowest value of BICc, meaning with the highest negative difference of BICc compared to the initial model. We identified the model with only the viral production varying between the two compartments as the best one to fit the data.

Table 1. Comparison of models evaluating the difference of viral infectivity (β), loss of infected cells (δ) and viral production (P) between the nasopharynx and the trachea.

Model tested	Statistical model	Δ BICc
Initial model	$\beta^T = \beta^N$ $\delta^N = \delta^T$ $P^N = P^T$ Variability on β and δ	
Model with different β	$\beta^T \neq \beta^N$ $\delta^N = \delta^T$ $P^N = P^T$ Variability on β and δ	-17.31
Model with different δ	$\beta^T = \beta^N$ $\delta^N \neq \delta^T$ $P^N = P^T$ Variability on β and δ	-14.38
Model with different P	$\beta^T = \beta^N$ $\delta^N = \delta^T$ $P^N \neq P^T$ Variability on β and δ	-25.24

Model with different β and δ	$\beta^T \neq \beta^N$ $\delta^N \neq \delta^T$ $P^N = P^T$ Variability on β and δ	-13.00
Model with different β and P	$\beta^T \neq \beta^N$ $\delta^N = \delta^T$ $P^N \neq P^T$ Variability on β and δ	-19.19
Model with different δ and P	$\beta^T = \beta^N$ $\delta^N \neq \delta^T$ $P^N \neq P^T$ Variability on β and δ	-19.47
Model with different β , δ and P	$\beta^T \neq \beta^N$ $\delta^N \neq \delta^T$ $P^N \neq P^T$ Variability on β and δ	-13.39

Identification of group effects

Once the structure of the statistical model defined, we tried to identify on which parameters an effect of the group of treatment could be identified and by extension on which biological mechanisms. In this step, we were interested in four parameters: β , δ , P and c, the latter being the clearance of *de novo* produced virions. In the study, three groups of treatments were considered as constant categorical covariates: Naïve, convalescent and convalescent vaccinated. We performed a forward selection approach using the BICc as selection criteria to find the best model, using the model without covariate as initial model. At each step the model decreasing the most the value of the BICc is selected and the procedure stops once the BICc does not decrease anymore. At each step of the procedure, the statistical significance of covariate added into the model was verified via a Wald test. As shown in **Table 2**, the selected model identified a group effect on the viral infectivity and the loss rate of infected cells.

Table 2. Comparison of models evaluating the adjustment of the viral infectivity (β), the loss rate of infected cells (δ), the viral production (P) and the viral clearance (c) for the groups of treatment. The group of naïve animals is assumed as the group of reference.

Step	Model tested	Statistical model	$\Delta BICc$
1	Initial Model: Model without group effects	$\beta = 10^{(\beta_0)}$ $\delta = \delta_0$ $P = P_0$ $c = c_0$	
	Model with group effect on β	$\beta = 10^{(\beta_0 + \phi_{conv}^\beta + \phi_{CD40}^\beta)}$ $\delta = \delta_0$ $P = P_0$ $c = c_0$	-21.5
	Model with group effect on δ	$\beta = 10^{\beta_0}$ $\delta = \delta_0 \exp(\phi_{conv}^\delta + \phi_{CD40}^\delta)$ $P = P_0$ $c = c_0$	-16.62
	Model with group effect on P	$\beta = 10^{\beta_0}$ $\delta = \delta_0$ $P = P_0 \exp(\phi_{conv}^P + \phi_{CD40}^P)$ $c = c_0$	+9.68
	Model with group effect on c	$\beta = 10^{\beta_0}$ $\delta = \delta_0$ $P = P_0$ $c = c_0 \exp(\phi_{conv}^c + \phi_{CD40}^c)$	+9.20
2	Initial Model: Model with group effect on β	$\beta = 10^{(\beta_0 + \phi_{conv}^\beta + \phi_{CD40}^\beta)}$ $\delta = \delta_0$ $P = P_0$ $c = c_0$	

	Model with group effect on β and δ	$\beta = 10^{(\beta_0 + \phi_{conv}^\beta + \phi_{CD40}^\beta)}$ $\delta = \delta_0 \exp(\phi_{conv}^\delta + \phi_{CD40}^\delta)$ $P = P_0$ $c = c_0$	-2.48
	Model with group effect on β and P	$\beta = 10^{(\beta_0 + \phi_{conv}^\beta + \phi_{CD40}^\beta)}$ $\delta = \delta_0$ $P = P_0 \exp(\phi_{conv}^P + \phi_{CD40}^P)$ $c = c_0$	+12.25
	Model with group effect on β and c	$\beta = 10^{(\beta_0 + \phi_{conv}^\beta + \phi_{CD40}^\beta)}$ $\delta = \delta_0$ $P = P_0$ $c = c_0 \exp(\phi_{conv}^c + \phi_{CD40}^c)$	+11.97
3	Initial Model: Model with group effect on β and δ	$\beta = 10^{(\beta_0 + \phi_{conv}^\beta + \phi_{CD40}^\beta)}$ $\delta = \delta_0 \exp(\phi_{conv}^\delta + \phi_{CD40}^\delta)$ $P = P_0$ $c = c_0$	
	Model with group effect on β , δ and P	$\beta = 10^{(\beta_0 + \phi_{conv}^\beta + \phi_{CD40}^\beta)}$ $\delta = \delta_0 \exp(\phi_{conv}^\delta + \phi_{CD40}^\delta)$ $P = P_0 \exp(\phi_{conv}^P + \phi_{CD40}^P)$ $c = c_0$	+10.88
	Model with group effect on β , δ and c	$\beta = 10^{(\beta_0 + \phi_{conv}^\beta + \phi_{CD40}^\beta)}$ $\delta = \delta_0 \exp(\phi_{conv}^\delta + \phi_{CD40}^\delta)$ $P = P_0$ $c = c_0 \exp(\phi_{conv}^c + \phi_{CD40}^c)$	+11.61

Based on all these results, the optimal statistical model with adjustment for groups of treatment was defined as follows:

$$\begin{cases} \log_{10}(\beta_i) = \beta_0 + \phi_{conv}^\beta \times \mathbb{I}_{i \in conv} + \phi_{CD40}^\beta \times \mathbb{I}_{i \in CD40} + u_i^\beta \\ \log(\delta_i) = \log(\delta_0) + \phi_{conv}^\delta \times \mathbb{I}_{i \in conv} + \phi_{CD40}^\delta \times \mathbb{I}_{i \in CD40} + u_i^\delta \\ \log(P_i^N) = \log(P_0) \\ P_i^T = P_i^N \times \exp(f_P^T) \end{cases}$$

Exchange of viruses between the nasopharyngeal and tracheal compartments

Afterwards, we tested the possibility of an exchange of free plasma virus from between the two compartments of the URT. We made the hypothesis of a constant first order exchange and we tested the addition a transfer of virions from nasopharyngeal to tracheal compartments and vice versa, with a migration rate g_{NT} and g_{TN} respectively. To this end, equations of infectious (V_i) and non-infectious (V_{ni}) viruses in Equation (1) between the two compartments were linked as follows:

$$\begin{aligned} \frac{dV_i^T}{dt} &\mapsto \frac{dV_i^T}{dt} - g_{TN}V_i^T + g_{NT}V_i^N & \frac{dV_{ni}^T}{dt} &\mapsto \frac{dV_{ni}^T}{dt} - g_{TN}V_{ni}^T + g_{NT}V_{ni}^N \\ \frac{dV_i^N}{dt} &\mapsto \frac{dV_i^N}{dt} + g_{TN}V_i^T - g_{NT}V_i^N & \frac{dV_{ni}^N}{dt} &\mapsto \frac{dV_{ni}^N}{dt} + g_{TN}V_{ni}^T - g_{NT}V_{ni}^N \end{aligned} \quad (8)$$

with the arrow symbolizing the modification of the equations defined in (1) and g_{NT} and g_{TN} being two positive rates. As a first step, we tried to estimate either bidirectional or one of the two unidirectional transfers using the data from the 18 NHPs of the first study described in the main paper. However, data were too sparse to bring enough information to get estimations. Consequently, as a second step, additional data were used: two naïve macaques were exposed to the same dose (1×10^6 pfu) of SARS-CoV-2 than the 18 NHPs of the main study. However, instead of being inoculated via intra-tracheal (4.5 mL) and intra-nasal (0.5 mL) routes, these latter received inoculum via intra-gastric (4.5 mL) and intra-nasal (0.5 mL) routes. Similar to the main study, the viral gRNA dynamics in both tracheal and nasopharyngeal compartments were repeatedly measured during the 20 days following the challenge (**Figure S9E**).

These two additional macaques having not received intra-tracheal inoculum, viral dynamics measured in this same compartment was expected to come from (at least partially) an exchange with the nasopharynx and thus bring information about it. However, having only two macaques without virions inoculated via intra-tracheal route, no enough information were available to totally estimate the model with exchanges. Consequently, these two additional NHPs having similar characteristics than the 18 NHPs involved in the main study, we made the assumption that the viral

dynamics in nasopharynx after inoculation and the viral dynamics in the trachea, once the transfer initiated, should be described by the same model (without inoculum in trachea) and those by the same parameters. We expected that the difference of dynamics in trachea between these two set of macaques could allow an estimation of the parameters g_{TN} and/or g_{NT} . For that reason, we estimated the model in equation (1) using data from the 18 NHPs of the main study. Then using the data from the two additional NHPs, and assuming all parameters of the model resulting from equations (8) as fixed (see **Table S2**), except g_{TN} and g_{NT} , we tried to quantify the transfers of virions.

The estimation of multiple models on those two animals tended to conclude that only a unidirectional transfer of viruses from the nasopharyngeal to the tracheal compartment should be explored, with an estimation of g_{NT} ranging from 0.9 to 2.5 day^{-1} . Once these values quantified, we tried to update/re-estimate the model, initially estimated on the 18 NHPs, using only a unidirectional transfer from nasopharynx to trachea and fixing the value of the migration rate at the different values aforementioned. However, all tested values of g_{NT} led irremediably to a degradation of the model with an increase of at least 2 points of BICc.

An estimation of the parameter g_{NT} by profile likelihood (results not shown) led to a strictly increasing profile of the likelihood (the lower the better) and was thus no more conclusive. Consequently, no exchange of virions were assumed in the final model and the parameters g_{NT} and g_{TN} were fixed at 0 day^{-1} .

Appendix 2 - BICc as selection criteria and multiple testing adjustment

In the case of classic covariate selection approaches using p-values as selection criteria, particular attention must be paid to take into account the dependence of the results on the number tests performed.

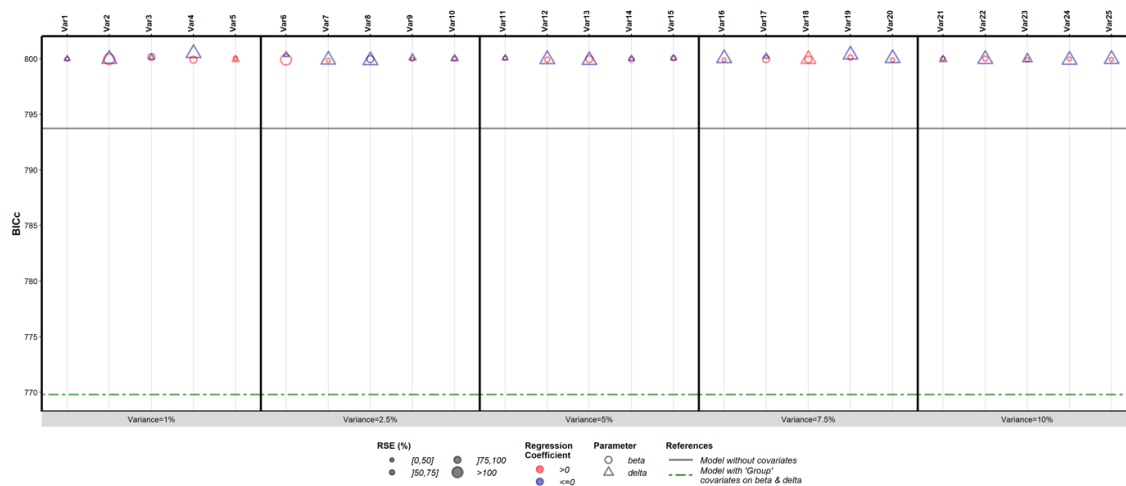
Over the years, multiple corrections have been proposed to adjust results for test multiplicity (e.g. Bonferroni correction, Benjamini & Hochberg correction among others).

Although we verified the significance of the covariate selected in our model, our covariate selection approach relies on the corrected Bayesian information criteria (BICc). To ensure the robustness of the BICc as selection criterion despite the multiplicity of the tests, we performed an additional simulation work.

We simulated $M=25$ longitudinal variables for 18 individuals and with similar time points than those found on our data, meaning at days 0, 4, 9 and 20 post-infection. Variables were simulated as white noise random variables such that for the i th subject at the j th time point, the m th variable was defined as $X_{ij}^m \sim \mathcal{N}(0, \sigma^2)$, with $m=1, \dots, M$. In our simulations, we tested 5 values for the variance σ^2 ranging from 1 to 10% (5 variables simulated for each value of σ).

Assuming these variables as our time-varying covariates, we applied the forward selection approach used in our method by testing each of them in a univariate manner of both β and δ .

As shown in **Appendix2 - figure 1**, the 50 models built to evaluate the adjustment of either β or δ for the simulated variables provide similar results in term of BICc, and thus whatever the value of the standard deviation σ used. Consequently, these results appear as quite robust to the multiplicity of the test. Moreover, as expected, adjustments for white-noise random variables depict the degradation of the model in comparison to the model without covariates.



Appendix 2 - figure 1. Results of the forward selection approach applied on the 25 simulated white-noise random variables. The discrete x-axis represents the different variables and the y-axis represents the values of the BICc. Circles and triangles correspond to the results obtained with the parameters β or δ adjusted for the variables. The vertical solid black line represents the value of the BICc obtained with the model without covariates while the vertical dashed green line highlights the value of the criterion obtained with both β and δ adjusted for the groups of treatment.

5.4 Perspectives

In this chapter, we focused on the identification of SARS-CoV-2 mechanistic correlate of protection. To this end, we proposed a mathematical framework coupling the mechanistic modelling of the viral dynamics and a time-varying covariate selection algorithm. The distinct application of this approach on data collected in three different preclinical studies on NHPs evaluating three different SARS-CoV-2 vaccines allowed us to identify the blockage of the viral infectivity as the main mechanism of action of these three vaccines and the decrease of the loss rate of infected cells as the second mechanism of two of them. Moreover, the data mining performed by the covariate selection approach gave us the opportunity to identify the inhibition of the attachment of the RBD domain to ACE2 host cell receptor as a strong mechanism of protection across the different studies.

In this work, we proposed to identify mechanistic immune correlates of protection among a large set of immune markers by integrating them either as constant (measures at baseline) or linearly interpolated time-varying covariates in the statistical model describing the model parameters. However, this modeling choice shows some limitations that could be further discussed and lead to additional works.

The first limitation that can be pointed out is the integration of immune markers in the model as perfectly measured variables. Indeed, in particular in the case of time varying covariates, no error model has been introduced in the statistical model to account for measurement errors. As widely discussed in the literature on the topic of regression models [Wang and Davidian, 1996; Carroll et al., 1997; Tosteson et al., 1998; Carroll et al., 2006], measurement errors on time-varying covariates are well-known as source of bias in estimated regression coefficients. The naive approach consisting in omit measure imperfections in the estimation of the association between a time-varying covariate and a longitudinal outcome tends to underestimate this association with a regression coefficient biased toward the null [Prentice, 1982]. As mentioned by Dafni and Tsiatis [1998], this point is particularly relevant in clinical trials with the evaluation of the relationship between a surrogate marker and a clinical outcome. The biased estimation of this association can in fact lead to wrong conclusions about the potential surrogate endpoint. To identify and quantify this bias in the case of our study, we performed an additional simulation work conducted in the framework of the internship of a Master 2 student that I had the opportunity to co-supervise with Pr. Rodolphe Thiébaud. In this additional work, we focused only on the immune marker quantifying the inhibi-

tion of the attachment between the RBD domain and the ACE2 receptor as the main CoP found in our model. Simulations consisted in simulating trajectories of this time-varying covariate, using a simple logistic regression model estimated on raw data, by varying the variance of the error model. Applying our ODE-based model with these different simulated trajectories of the covariate integrated in the statistical model as linearly interpolated time-varying covariates, we were able to observe this dependency between the under-estimation of the regression coefficient and the magnitude of the measurement error. As shown in Figure 5.3 displaying these results, only a small bias on our regression coefficient, quantifying the association between the viral load and the surrogate marker, was found with an underestimation of approximately -5% (IQR: [-15% ; 4.9%]). Many methods have been proposed in the literature to overcome this

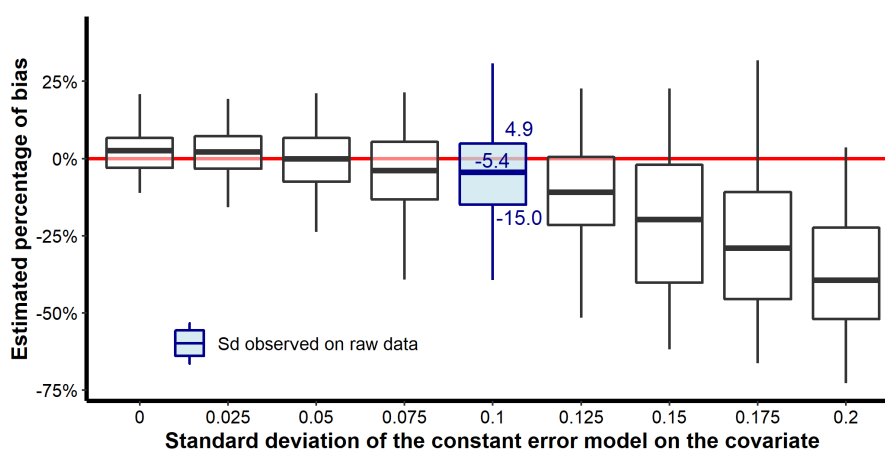


Figure 5.3 – Bias of the regression coefficient as a function of the variability of the measurement error. The x-axis represents the standard deviation of the error model used to simulate the time-varying covariate. The y-axis represents the percentage of bias obtained on the estimated regression coefficient quantifying the association between the viral load and the surrogate marker. A total of 50 simulations were performed for each value of the standard deviation. In blue are displayed the results obtained for the value of the standard deviation found on observed data. The vertical red solid line displays the threshold of unbiased results.

issue, such as regression calibration methods, likelihood or Bayesian methods [Fuller, 1987; Gustafson, 2003; Carroll et al., 2006; Wu, 2009]. While the latter two methods imply strong assumptions on the covariate distribution, classic three-step calibration methods or the closely related two-step approach proposed by Dafni and Tsiatis [1998] may be considered. In particular, a possible solution to overcome this issue would be to consider a coupled estimation of a regression model for the trajectories of the immune marker (e.g. logistic regression) and the ODE model for the outcome variable, in which covariate values would be directly replaced by the estimates of the regression model.

Another limitation of the proposed approach that could be mentioned is the non-inclusion of the effect the clinical outcome on the surrogate marker. Indeed, in our modeling approach, we considered the direct effect an immune marker (e.g. the pseudo-neutralization of RBD-ACE2 attachment) on the viral load, but we ignored the influence of the viral load on the marker. Ignoring this retroactive effect could lead to a biased estimation of their interaction. To overcome this problem, we proposed to augment the mechanistic model by directly integrating the selected immune markers into the mechanistic model (ongoing work). In particular, we propose to integrate the humoral immune response via antibody compartment(s). Based on multiple modeling works of the humoral response [Wang et al., 2014; Miao et al., 2016; Clapham et al., 2016; Pasin, 2018; Mutua et al., 2019b; Hattaf, 2020; Fatehi et al., 2021] and results presented on our paper, we derived the model presented in Figure 5.4 and Equation 5.1, where the subscript X stands for the upper respiratory tract compartments (N:Nasopharynx and T:Trachea). Moreover, we modified the observational model to incorporate both binding antibodies and neutralization (ECLRBD) observations (see Equation 5.2). In both systems of equations, modifications brought to the model presented in our paper were colored in blue.

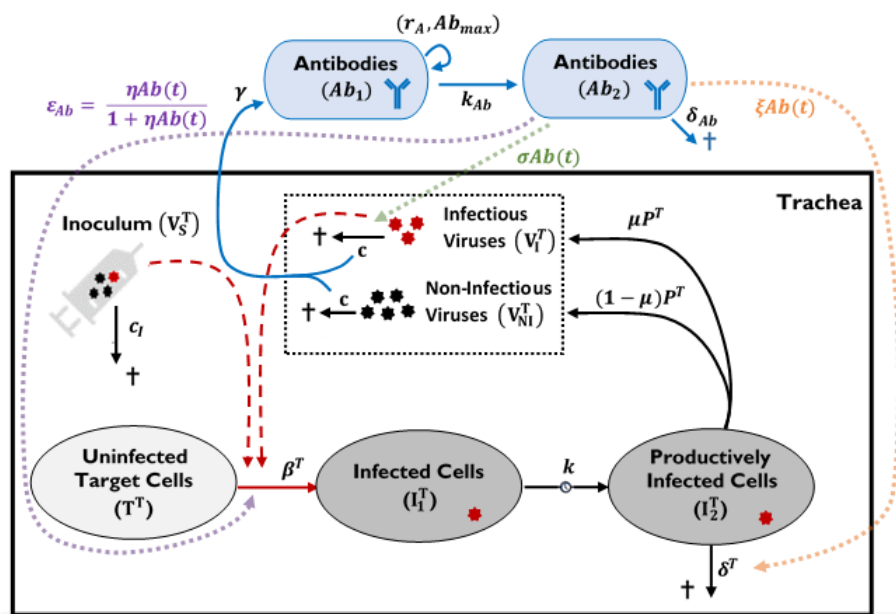


Figure 5.4 – Diagram of the model coupling both virological and humoral immune responses. This diagram displays the interactions between the antibodies and the virological components in the tracheal compartment. Additional components, in comparison to the initial model, are colored in blue (antibodies, Ab), purple (effect Ab on the decrease of the viral infectivity), orange (effect of Ab on increase of the death rate of infected cells) and green (effect of Ab on the increase of the virus clearance)

$$\left\{ \begin{array}{l}
 \frac{dT^X}{dt} = -\left(1 - \frac{\eta Ab_2}{(1 + \eta Ab_2)}\right) \beta V_i^X T^X - \mu \left(1 - \frac{\eta Ab_2}{(1 + \eta Ab_2)}\right) \beta V_s^X T^X \\
 \frac{dI_1}{dt} = \left(1 - \frac{\eta Ab_2}{(1 + \eta Ab_2)}\right) \beta V_i^X T^X + \mu \left(1 - \frac{\eta Ab_2}{(1 + \eta Ab_2)}\right) \beta V_s^X T^X - k I_1^X \\
 \frac{dI_2^X}{dt} = k I_1^X - \delta I_2^X - \xi Ab_2 I_2^X \\
 \frac{dV_i^X}{dt} = \mu P^X I_2^X - c V_i^X - \left(1 - \frac{\eta Ab_2}{(1 + \eta Ab_2)}\right) \beta V_i^X T^X - \sigma Ab_2 V_i^X \\
 \frac{dV_{ni}^X}{dt} = (1 - \mu) P^X I_2^X - c V_{ni}^X - \sigma Ab_2 V_{ni}^X \\
 \frac{dV_s^X}{dt} = -c_i V_s^X - \mu \left(1 - \frac{\eta Ab_2}{(1 + \eta Ab_2)}\right) \beta V_s^X T^X \\
 \frac{dAb_1}{dt} = \gamma (V_i^N + V_{ni}^N + V_i^T + V_{ni}^T) + r_{Ab} \left(1 - \frac{Ab_1}{Ab_{max}}\right) Ab_1 - k_{Ab} Ab_1 \\
 \frac{dAb_2}{dt} = k_{Ab} Ab_1 - \sigma Ab_2 (V_i^N + V_{ni}^N + V_i^T + V_{ni}^T) - \xi Ab_2 (I_2^N + I_2^T) - \delta_{Ab} Ab_2
 \end{array} \right. \quad (5.1)$$

$$\left\{ \begin{array}{l}
 gRNA_{ij}^X = \log_{10} [(V_i^X + V_{ni}^X + V_s^X)(\Theta_i^X, t_{ij})] + \varepsilon_{ij,g}^X \\
 sgRNA_{ij}^X = \alpha_{sgRNA} \times \log_{10} [(I_1^X + I_2^X)(\Theta_i^X, t_{ij})] + \varepsilon_{ij,sg}^X \\
 IgGRBD_{ij} = \log_{10} [Ab_2(\Theta_i, t_{ij})] + \varepsilon_{ij,bAb} \\
 ECLRBD_{ij} = A \times \left(1 - \frac{\eta Ab_2^n}{1 + \eta Ab_2^n}\right) + B + \varepsilon_{ij,ecl}
 \end{array} \right. \quad (5.2)$$

Afterwards, it would be interesting to use this type of model coupling both the viral load dynamics and the humoral response to improve the design of preclinical trials. In particular, we could use it to get information about the longevity of the immune response, the time required before the next vaccination, the comparison of multiple homologous and/or heterologous vaccine regimen or the effect of variants of concern on the vaccine efficacy. In a similar context, we studied in the next chapter the longevity of the humoral immune response to a two-dose heterologous Ebola vaccine using mechanistic modeling.

Finally, it could be interesting to extend this model in order to use it on human data. In this work, we only focus on data obtained in NHPs. However, the proposed methodology to identify mechanistic correlates of protection can not be directly applied on human data. Indeed, in preclinical studies the dynamics of the viral load is used to evaluate the efficacy of the vaccine, outcome which is possible only in controlled

studies performed on animals as time of infection is perfectly known and viral load measurements are performed regularly and repeatedly on a daily scale (in particular at the beginning of the dynamics). In humans, monitoring being performed on a larger time scale, from weeks to months, this type of outcome is much more difficult to get as viral load is only observable in the few days following infection. Accordingly, the model used in our approach should be modified to integrate clinical outcomes usually used in clinical trials, such as occurrence of side effects or specific symptoms. To this end, models such as survival model used to jointly estimate a time-to-event process and longitudinal process could be envisaged.

PART III

Humoral response dynamics

Chapter 6

Evaluation of the longevity of the humoral immune response of Ebola vaccine

Abstract: In contrast to the previous chapters, which focused mainly on viral dynamics, in this chapter we are interested in assessing the longevity of the humoral immune response triggered by Ebola virus vaccination. In particular, we focus on heterologous dual vaccination with the viral vectors Ad26.ZEBOV and MVA-BN -Filo, which was developed by Janssen Pharmaceutical and tested in several phase I to III clinical trials. We present a mechanistic model based on ordinary differential equations describing the dynamics of antibodies produced by two populations of secreting cells (ASCs). This model was previously estimated using data from three phase I trials with 1 year of follow-up. Using data from 498 subjects from 3 phase II /IIB trials followed up to 2 years after the first vaccination, we now demonstrate the robustness of this model as well as its good quality of long-term prediction. We take advantage of the larger number of participants and longer follow-up time to re-estimate the model using a population-based approach. In particular, we show longer survival of long-lived ASCs than previously estimated, and we confirm longer persistence of antibodies in Europeans than in Africans. We also find an effect of participant age and sex on the decline in humoral dynamics. Estimating this model using longer-term data, as well as estimating models that combine both establishment and maintenance of the humoral response, would allow us to confirm and refine these results. They are briefly described at the end of this chapter.

Keywords: Ebola ; humoral response ; vaccine ; longevity ; mechanistic model ; ordinary differential equation ; population approach ; model building

Dissemination:

▷ **Article in preparation**

Alexandre, M., EBOVAC 1 and EBOVAC 2 consortia, Prague, M. & Thiébaud, R. [Evaluation and prediction of the long-term humoral immune response induced by the two-dose heterologous Ad26.ZEBOV, MVA-BN-Filo vaccine regimen against Ebola.](#)

▷ **Oral communication at international conference**

Alexandre M, Prague M, Clairon Q, Van Effelterre T, Thiébaud R. [Dynamics of the humoral immune response to a two-dose heterologous vaccine regimen against Ebola virus. Population Approach Group in Europe \(PAGE\), 2021 \(Online\).](#)

Alexandre M, Prague M, Clairon Q, Van Effelterre T, Thiébaud R. [Dynamics of the humoral immune response to a two-dose heterologous vaccine regimen against Ebola virus. Workshop on Modelling Immunity, Toronto, Canada, 2021 \(Online\).](#)

6.1 Biological and clinical context

6.1.1 General introduction on Ebola virus disease

Ebola virus disease (EVD) is a severe and often fatal disease for humans inducing severe hemorrhagic fever caused by Ebola virus (EBOV) that have discovered in 1976 in South Sudan and Democratic Republic of Congo (DRC) [Johnson et al., 1977; WHO, 2021c].

Ebola viruses are filoviruses [Kuhn et al., 2019] belonging to the Ebolavirus genus which includes six virus species [Zheng et al., 2015]: Bundibugyo ebolavirus (BOMV), Reston ebolavirus (RESTV), Sudan ebolavirus (SUDV), Taï Forest ebolavirus TAFV), Zaire ebolavirus (ZEBOV), and Bombali ebolavirus (BOMV) - the most recently discovered in 2018 in Guinea [Goldstein et al., 2018]. SUDV, ZEBOV and BOMV are responsible for the majority of disease in humans with case fatality rates ranging from 25% to 90%.

As filovirus, EBOV is shaped as a long filament containing a single negative-sense RNA genome encoding for 7 structural proteins including in particular a nucleoprotein (NP) and glycoprotein (GP) which cover the surface of the virion. The GP plays a crucial role in cell attachment, fusion and entry [Rougeron et al., 2015; Friedrich et al., 2012] and will therefore be capital for vaccine development against EVD [Venkatraman et al., 2018]. Only transmitted between humans by direct blood, body fluids or skin contacts [Rewar and Mirdha, 2014], EBOV has an incubation period from 2 to 21 days [Kortepeter et al., 2011], and is followed by sudden "flu-like" symptoms onset (flu, fatigue, headache, muscle pain), before evolving into more alarming symptoms like vomiting, diarrhoea, respiratory and neurological symptoms, haemorrhagic complications or organ failures [Goeijenbier et al., 2014].

6.1.2 Ebola outbreaks and actual epidemiological context

Ebola virus is known to cause outbreaks periodically and mostly in Africa. Since its emergence in 1976, more than 30 outbreaks occurred in Africa and some cases were reported in Europe, USA, Philippines and Russia [Coltart et al., 2017; CDC, 2021a,b; WHO, 2021c]. The 2014-2016 outbreak in West Africa was unprecedented, whether in terms of number of cases with more than 28 000 infected people and 11 000 deaths, speed of the spread of the epidemic, geographical distribution or effective actions of governmental or non-governmental organizations [Coltart et al., 2017; Kamorudeen et al., 2020]. Emerging in Guinea in 2013, the virus rapidly spread to two neighbouring countries, Liberia and Sierra Leone before reaching other countries in Africa (Senegal,

Mali, Nigeria), in Europe (UK, Spain, Italy) and the USA. On August 8, 2014, WHO declared the Public Health Emergency of International Concern (PHEIC) and lasted until March 29, 2016 [CDC, 2019]. This unprecedented epidemiological context for Ebola virus led to a significant acceleration of the vaccine development. In particular, it conducted to the launch of the Innovative Medicines Initiatives (IMI) Ebola+ Program funding 12 project such as the EBOVAC consortium, gathering the EBOVAC1, EBOVAC2 and EBOVAC3 projects, aiming at assessing the safety, tolerability and immunogenicity of two-dose vaccine regimen developed by Jansen Pharmaceutical. In the frame of this thesis, we focused exclusively on EBOVAC 1 and EBOVAC 2 projects.

More recently, the 2018-2020 Ebola outbreak that occurred in DRC was declared as the second largest in history with 3 481 cases and 2 299 deaths. This 10th outbreak in DRC started in the eastern part of the country and was declared in North Kivu on 1 August 2018. The spread of the virus to border country, Uganda, led to the declaration of the Public Health Emergency of International Concern by the WHO on July 17, 2019 [Aruna et al., 2019]. Thanks to the collaborations of the DRC Government, the WHO, the engagement of multiple communities and the development of efficient therapeutics elicited by the 2014-2016 outbreak, the vaccination of hundred thousands of people highly participated to the control of the epidemic on June 25, 2020 [WHO, 2020a].

The most recent outbreak was declared in North Kivu province of the Democratic Republic of Congo on February 7, 2021. A total of 11 confirmed cases and 6 deaths were related during this outbreak which was rapidly controlled due to the help of the WHO experts and the vaccination of approximately 2000 people considered at high risk. The end of the outbreak was declared three months later, on May 3, 2021 [WHO, 2021b].

6.1.3 Ebola vaccine development

The vaccine development against Ebola started in the 1970's with the emergence of the disease. Vaccine clinical trials conducted on human require a lot of resources, money and time and are expected to be used on a large scale to be cost-effective for pharmaceutical company. Consequently, before 2013, the limited number of human candidates for vaccine trials due to the low number of infected people during outbreaks as well as their sporadic nature limited the access to efficacy data and prevented the commercial interest for vaccine license [Marzi and Mire, 2019]. No licensed therapeutic treatment were then available on the market before 2014. With the 2014-2016 West Africa outbreak, vaccine development was significantly accelerated and provided optimal conditions for testing EBOV vaccine candidates that have already been evaluated

in NHPs models [Marzi and Mire, 2019]. To date, a large number of vaccine candidates are under development at different trial stages. In particular, seven vaccine regimens mostly based on vectored vaccines and DNA-based vaccines have been widely tested [Matz et al., 2019] and two of them have been approved [WHO, 2020b]. In the following, although a larger number of vaccines has been developed and tested in preclinical and clinical trials over the years, we mostly focus on the vaccine regimen studied in the modeling work presented in this chapter: the two-dose heterologous prophylactic vaccine regimen against EVD using Ad26.ZEBOV as first vaccination and MVA-BN-Filo as booster vaccination developed by Jansen pharmaceutical (Ad26.ZEBOV/MVA-BN-Filo). Nevertheless, Ebola vaccine development has been widely reviewed and readers can refer to these papers for a broader overview: [Venkatraman et al., 2018; Suschak and Schmaljohn, 2019; Marzi and Mire, 2019; Matz et al., 2019; Feldmann et al., 2020; Sharma et al., 2021].

Ad26.ZEBOV is a non-replicant vectored vaccine (i.e. containing viral genetic material encapsulated inside another harmless virus than can not replicate) and more specifically a recombinant human adenovirus serotype 26 expressing the full length Mayinga GP of the EBOV. The safety and the protective efficacy of this adenovirus was investigated by [Geisbert et al., 2011] who demonstrated its protective effect with 75% of survival. Nevertheless, similar to other adenoviruses, this vector showed a limited protective effect in time. In parallel, the multivalent version of the modified vaccinia Ankara (MVA) vector, expressing the GP of the virus strains EBOV, SUDV and MARV, as well as the NP from Tai Forest strain (MVA-BN-Filo), was tested in clinical trials. Identified as effective vaccines, MVA-vector vaccines were rapidly identified as vectors increasing the longevity of the adenovirus-induced immune response when used as booster vaccination [Suschak and Schmaljohn, 2019; Stanley et al., 2014; Venkatraman et al., 2019; Ewer et al., 2016; Tapia et al., 2016].

As aforementioned, in this work, we focused exclusively on the two-dose Ad26.ZEBOV / MVA-BN-Filo vaccine strategy which has been approved by the EMA in July 2020 [EMA, 2020; Johnson, 2020] to prevent Ebola virus disease in individuals older than 1 year. To evaluate this vaccine strategy, multiple Phase I to III clinical trials have been conducted, in particular by the IMI via the EBOVAC Consortia funded to assessing the safety, tolerability and immunogenicity of this specific vaccine regimen. Today, the clinical program includes four Phase I clinical trials evaluating different combinations and schedules of this heterologous strategy. Performed on healthy volunteers in US, UK and Africa, these studies showed that the vaccine regimen is well-tolerated

and highly immunogenic against Ebola. Based on these results, eight Phase II studies and eight Phase III studies were conducted to broader assess the safety and the immunogenicity of the specific Ad26.ZEBOV/MVA-BN-Filo vaccine regimen for different schedule and on specific populations. Among all of these trials, our work focused on the data from three of the four Phase I clinical trials as well as two Phase II and I Phase IIB studies. The three Phase I clinical trials were randomized, placebo-controlled, observer-blind studies conducted on healthy adults in UK (NCT02313077) [Milligan et al., 2016; Winslow et al., 2017], Kenya (NCT02376426) [Mutua et al., 2019a] and Tanzania/Uganda (NCT02376400) [Anywaine et al., 2019]. These participants received as prime/boost vaccination either Ad26.ZEBOV then MVA-BN-Filo or MVA-BN-Filo then Ad26.ZEBOV with an interval of 28 or 56 days between the two vaccinations. The two Phase II clinical trials (NCT02416453 and NCT02564523) were conducted as randomized, observer-blind, placebo-controlled, parallel group, multicenter studies evaluating the safety, tolerability and immunogenicity of the Ad26.ZEBOV/MVA-BN-Filo vaccine regimen with an interval between the two vaccinations of either 28, 56 or 84 days. The first one was realized in Europe (France and UK) on healthy adults and shown a well-tolerability and a persisting humoral immune response for at least 1 year [Pollard et al., 2021] while the second one was conducted on adults and children from 1 to 17 years, with adults being either healthy or infected by HIV. [Anywaine et al., 2022; Barry et al., 2021]. Finally, the Phase IIB study (NCT02509494) is double-blinded, placebo-controlled study conducted in Sierra Leone on Adults and children randomized to receive either Ad26.ZEBOV/MVA-BN-Filo vaccine regimen with 56 days between the two vaccinations or placebo [Ishola et al., 2022]. While participants from the first five studies were followed for 1 year after the first vaccination, a sub-group of participants in the last one were monitored for two years.

In addition to these six clinical trials, multiple Phase II and III studies are currently ongoing to evaluate the Ad26.ZEBOV/MVA-BN-Filo vaccine regimen in distinct population such as the Phase II trial conducted in DRC on high risk population represented by health care providers (NCT04186000) or the study realized in Guinea and Sierra Leone in 4-11 months infants (NCT03929757). Moreover, some studies have been funded to get an extended follow up of the participants, from 2 to 5 years, in order to provide more information about the longevity of the humoral response. That is the case for instance of the Phase IIB study called PREVAC (NCT02876328) [Badio et al., 2021] conducted on healthy participants in Guinea, Mali and Sierra Leone and evaluating the safety and the immunogenicity of three vaccine strategies in adults and children: Ad26.ZEBOV/MVA-BN-Filo, a single dose of rVSV Δ G-ZEBOV-GP (the second approved

vaccine regimen to prevent Ebola virus disease) and two doses of rVSV Δ G-ZEBOV-GP, that have been extended up to 5 years under the PREVAC-UP project.

Despite the significance advances made these last years in vaccine development against Ebola virus, crucial points about vaccination and immunity are still under investigation, such as the protection and the duration of the vaccine immunity [Sharma et al., 2021]. Due to the sporadic nature of Ebola outbreaks and the globally low number of related cases, the direct evaluation of the vaccine efficacy in human remains difficult. A surrogate endpoint/correlate of protection is then requested to assess vaccine efficacy and preclinical studies are essential to identify this CoP. Although non CoP has been clearly identified today, as reviewed by Longet et al. [2021], many clinical and preclinical studies have conducted since the emergence of Ebola virus in which survival has been associated with a strong humoral response. In addition, recent analysis of Phase II/III clinical trial assessing rVSV Δ G-ZEBOV-GP vaccine efficacy [Grais et al., 2021] or preclinical studies [Meyer et al., 2021] testing other candidate vaccines, identified binding antibodies has highly associated with vaccine induced protection. Moreover, they pointed out the superiority of binding antibodies as candidate correlate of protection in comparison to neutralizing antibodies. Nevertheless, it is important to keep in mind that the cellular might also be seen has a good correlate of protection [Stanley et al., 2014; Ruibal et al., 2016; Speranza et al., 2018]. Based on all these results, although no CoP has been identified, the binding antibody response is widely used as the immune marker studied to assess vaccine efficacy.

Contrary to the work presented in the previous chapter on SARS-CoV-2, we didn't work on the evaluation of the vaccine induced protection and the identification of a correlate of protection for Ebola virus. This time, we focused on the second aforementioned crucial point currently investigated in vaccine development against Ebola: the longevity of the vaccine-induced immunity.

6.2 Evaluation of the durability of the humoral response

To evaluate the longevity of the immune response, we take over the work done by Pasin [2018], in which a mechanistic model of the humoral response have built and estimated on data from the 3 Phase I trials of the EBOVAC consortium mentioned above. We extended this work to the aggregated data from both the Phase I trials and the 3 Phase II /IIb clinical studies presented in the previous paragraphs. The large number of participants as well as the longer follow-up observed in Phase II trials and the increased

heterogeneity of the data allowed us to improve our knowledge about the durability of the humoral immune response and to identify factors influencing these dynamics. As presented in chapter 2 (see section 2.3), we considered in this work a mechanistic ODE-base model estimated by the SAEM algorithm in a population approach. This work has been the subject of a paper under preparation for submission and was conducted as part of EBOVAC 1 and EBOVAC 2 projects.

Evaluation and prediction of the long-term humoral immune response induced by the two-dose heterologous Ad26.ZEBOV, MVA-BN-Filo vaccine regimen against Ebola

Marie Alexandre,^{a,b} EBOVAC 1 and EBOVAC 2 consortia,^c Mélanie Prague,^{a,b,*} Rodolphe Thiébaud,^{a,b,*,†}

^aBordeaux University, Department of Public Health, Inserm UMR 1219 Bordeaux Population Health Research Center, Inria SISTM ; Bordeaux, France

^bVaccine Research Institute; Créteil, France

^cJanssen Pharmaceutical N. V., Beerse, Belgium

* These authors contributed equally to this work

ABSTRACT The persistence of the long-term immune response induced by the heterologous Ad26.ZEBOV, MVA-BN -Filo two-dose vaccination regimen against Ebola has been investigated in several clinical trials. Longitudinal data on IgG-binding antibody concentrations were analyzed from 487 participants enrolled in six phase I and phase II clinical trials conducted by the EBOVAC1 and EBOVAC2 consortia. A model based on ordinary differential equations describing the dynamics of antibodies and short- and long-lived antibody-secreting cells (ASCs) was used to model the humoral response from 7 days after the second vaccination to a follow-up period of 2 years. Using a population-based approach, we first assessed the robustness of the model, which was originally estimated based on phase I data, against all data. Then we assessed the longevity of the humoral response and identified factors that influence these dynamics. We estimated a half-life of the long-lived ASC of at least 15 years and found an influence of geographic region, sex, and age on the humoral response dynamics, with longer antibody persistence in Europeans and women and higher production of antibodies in younger subjects.

KEYWORDS: Antibody response longevity, Ebola, mechanistic modeling, vaccine

INTRODUCTION

The 2014-2016 Ebola virus disease (EBOV) outbreak in West Africa and the current SARS-CoV-2 pandemic have led to accelerated development of vaccines to control the spread of infection and reduce the severity of disease in infected individuals. As a result, effective vaccines were developed and became available quickly after the outbreak of the epidemics. In the case of Ebola, the recombinant replication-competent vesicular stomatitis viral vectored vaccine (Ervebo) was approved by the FDA in December 2019 (1) and used during epidemics through a ring vaccination strategy. The heterologous prime-boost strategy, combining immunizations with Ad26.ZEBOV (Zabdeno) and MVA-BN -Filo (Mvabea), was approved by the European Commission in March 2021 (2) under exceptional circumstances for use in children and adults. An important question for those who have already been vaccinated and for using the vaccines for a preventive strategy to control the occurrence of outbreaks is the duration of protection conferred by vaccination.

In the context of rapid vaccine development, long-term follow-up in large populations of vaccinated persons, as with older vaccines, is not possible (3, 4). When data are sparse, mathematical modelling is helpful because it can provide estimates of the duration of response by using additional information from biological knowledge about the vaccine mechanism and biological parameters. It is also helpful in quantifying the effect of factors that influence the response to the vaccine. This type of work is performed by modelling the dynamics of one or several markers that could be considered as good correlates of protection (5). Vaccine efficacy and mechanisms of action have been evaluated for various infectious diseases, such as influenza (6, 7, 8), yellow fever (9, 10), Zika (11), or

40 more recently SARS-CoV-2 (12). In the case of the Ad26.ZEBOV and MVA-BN-Filo vaccine strategy, the concentration
 41 of binding antibodies is considered a good correlate of protection (13) and was used for the FDA Animal Rule (14).

42 In a previous work, (15), we used a mathematical model for antibody-secreting cell (ASC) dynamics that distin-
 43 guishes between short-lived and long-lived cells (SL and LL, respectively), and we estimated the model parameters
 44 using the data from the first phase 1 studies available. We found that antibody production is maintained by the
 45 population of long-lived cells with an estimated half-life of at least 5 years. New data from three phase 2 studies
 46 (16, 17, 18) conducted in two international consortia (EBOVAC1 and EBOVAC2) gave the opportunity to validate the
 47 model and better characterise factors associated to the variation of the antibody response.

48 RESULTS

49 **Descriptive analysis of the data.** The baseline and demographic characteristics of the 487 participants in-
 50 cluded into the study are shown in Table 1. In all the results hereafter, test multiplicity with Benjamini and
 51 Hochberg correction (19) has been used (see section Materials and Methods for more details). Comparable base-
 52 line characteristic in terms of age, body mass index (BMI) and weight are observed in European subjects across
 53 the Phase-I and II clinical studies (all p-values > 0.80). Similarly, no differences are observed in Africa across trials
 54 and sites in term of weight however BMI appears as significantly higher in east African subjects (+6%, pvalue=0.007)
 55 than in west African ones, and participants in EBL2002 tended to be older (34 vs 27 years, p-value < 0.001). Euro-
 56 pean participants were significantly older than African (41 vs 29 years, p-value < 0.001). Similarly, BMI and weight
 57 (p-values < 0.001 in both cases) were significantly higher in European subjects than in African ones (+13% and +18%,
 58 resp).

TABLE 1 Demographic and baseline characteristics of participants.

	Phase-I trials			Phase-II trials				Total
	Europe	East Africa		Europe	East Africa	West Africa	West Africa	
	UK	Kenya	Tanz./Ug.	UK/France	Ken./Tanz.	BFA/IVC	Sierra Leone	
	EBL1001	EBL1003	EBL1004	EBL2001	EBL2002	EBL3001		
Part., no.	14	15	15	71	79	58	235	487
Sex								
Men	4 (29%)	11 (73%)	10 (67%)	32 (45%)	45 (57%)	44 (75%)	203 (86%)	349 (72%)
Women	10 (71%)	4 (27%)	5 (33%)	39 (55%)	34 (43%)	14 (24%)	32 (14%)	138 (28%)
Age (yrs)	37.6 (9.3)	23.7 (2.8)	26.5 (6.8)	41.2 (14.7)	34.1 (13.5)	34.1 (10.8)	27.2 (10.0)	31.3 (12.4)
BMI (kg/m ²)	26.1 (3.3)	22.5 (4.1)	22.9 (4.2)	25.4 (4.5)	23.8 (4.0)	23.0 (3.4)	21.9 (3.3)	23.0 (3.9)

Data are n (%) or mean (SD). Only healthy adults receiving Ad26.ZEBOV followed by MVA-BN-Filo 56 days later were selected within each of the 6 trials. UK = United Kingdom, Tanz. = Tanzania, Ug. = Uganda, BFA = Burkina Faso, IVC = Ivory Coast.

59 Figure 1 shows the dynamics of antibody concentrations (median and interquartile ranges) 7 days after the
 60 second vaccination for each study. In addition, Table 2 summarizes antibody concentrations observed at prede-
 61 fined harvest times. Only participants who had received both the first and second vaccinations were included
 62 in the analysis (a total of 135 participants were excluded). Similar dynamics were observed in all studies, with a
 63 peak 21 days after the second vaccination, followed by a biphasic decline up to 1 year after the first vaccination.
 64 Furthermore, the longer-term dynamics observed in EBL3001 suggest a stabilization of dynamics after the decline.

65 Antibody concentrations in European subjects showed no statistical difference at peak (21 days after the sec-
 66 ond vaccination) and 1 year after the first vaccination between the phase I (EBL1001) and phase II (EBL2001) clinical
 67 trials (pvalue=0.21 and 0.14, respectively). By contrast, the antibody concentrations of African participants were
 68 significantly lower in Phase-II studies than in Phase-I at the peak of the response (pvalue<0.001) with a mean
 69 value decreasing from 4.12 to 3.70 log₁₀ ELISA units/mL. This difference was mostly driven by the lower peaks of
 70 antibody concentrations measured in subjects from Sierra Leone (EBL3001) displaying a mean value being 13%
 71 lower than the Phase-I African subjects (pvalue < 0.001) while only a 6% decrease was observed in EBL2002 sub-
 72 jects (pvalue=0.003). One year after the first vaccination, this difference was less pronounced (2.47 vs 2.67 log₁₀,
 73 pvalue=0.019). The antibody concentration in European subjects 1 year after the first vaccination was significantly
 74 higher than in African (+24% pvalue < 0.001). Participants from the EBL1004 trial (Tanzania/Uganda) tended to have

TABLE 2 Ebola glycoprotein-specific binding antibody concentrations, in log₁₀ scale (in ELISA units/mL), in each study from 7 days after the second vaccination to study completion.

	Phase-I trials			Phase-II trials		
	EBL1001 (n=14) ^a	EBL1003 (n=15) ^a	EBL1004 (n=15) ^a	EBL2001 (n=71) ^a	EBL2002 (n=137) ^b	EBL3001 (n=235) ^c
Day 64 (7 days after the 2nd vaccination, MVA-BN-Filo)						
Number part.	14	15	15			
Responders [†]	14 (100%)	15 (100%)	15 (100%)			
Missing data	0 (0%)	0 (0%)	0 (0%)			
Mean [IQR]	3.19 [2.99 ; 3.48]	3.33 [2.90 ; 3.73]	3.09 [2.55 ; 3.58]			
Day 78 (21 days after the 2nd vaccination, MVA-BN-Filo)						
Number part.	14	15	15	70	137	231
Responders [†]	14 (100%)	15 (100%)	15 (100%)	70 (100 %)	137 (100%)	231 (100%)
Missing data	0 (0%)	0 (0%)	0 (0%)	1 (1%)	0 (0%)	4 (2%)
Mean [IQR]	3.88 [3.64 ; 4.10]	4.21 [3.96 ; 4.45]	4.03 [3.80 ; 4.31]	4.00 [3.79 ; 4.43]	3.88 [3.62 ; 4.16]	3.60 [3.34 ; 3.88]
Day 156 (155 days after the 1st vaccination, Ad26.ZEBOV)						
Number part.						42 [‡]
Responders [†]						42 (100%)
Missing data						1 (2%)
Mean [IQR]						2.73 [2.54 ; 3.00]
Day 180 (179 days after the 1st vaccination, Ad26.ZEBOV)						
Number part.	12	15	15		23 *	
Responders [†]	12 (100%)	15 (100%)	15 (100%)		23 (100%)	
Missing data	2 (14%)	0 (0%)	0 (0%)			
Mean [IQR]	3.47 [3.29 ; 3.60]	3.00 [2.67 ; 3.20]	2.97 [2.71 ; 3.25]		2.70 [2.47 ; 2.85]	
Day 240 (239 days after the 1st vaccination, Ad26.ZEBOV)						
Number part.	13	15	15			
Responders [†]	13 (100 %)	15 (100%)	15 (100%)			
Missing data	1 (7%)	0 (0%)	0 (0%)			
Mean [IQR]	3.35 [3.20 ; 3.41]	2.66 [2.22 ; 2.93]	2.83 [2.56 ; 3.09]			
Day 360/365 (1 year after the 1st vaccination, Ad26.ZEBOV)						
Number part.	12	15	15	51	134	207
Responders [†]	12 (100%)	15 (100%)	15 (100%)	51 (100%)	134 (100%)	205 (99%)
Missing data	2 (14%)	0 (0%)	0 (0%)	20 (28%)	3 (2%)	28 (12 %)
Mean [IQR]	3.24 [3.09 ; 3.33]	2.61 [2.40 ; 2.96]	2.74 [2.46 ; 3.06]	3.07 [2.89 ; 3.28]	2.54 [2.26 ; 2.78]	2.44 [2.11 ; 2.68]
Day 540 (539 days after the 1st vaccination, Ad26.ZEBOV)						
Number part.						33 [‡]
Responders [†]						33 (100%)
Missing data						10 (23%)
Mean [IQR]						2.43 [2.15 ; 2.68]
Day 720 (2 years after the 1st vaccination, Ad26.ZEBOV)						
Number part.						190
Responders [†]						184 (97%)
Missing data						45 (19 %)
Mean [IQR]						2.45 [2.19 ; 2.69]

IQR = Interquartile range = 75% confidence intervals. ^a Participants receiving the 2nd vaccination in the protocol-defined window of 57 ± 1 day. ^b Participants receiving the 2nd vaccination in the protocol-defined window of 57±3 days. ^c Participants receiving the 2nd vaccination in the protocol-defined window of 57 ± 1 week. * Refers to participants enrolled in EBL 2002 having an additional timepoint, initially scheduled for subjects who do not receive a second vaccination because of a study pause. † Refers to the number of participants with uncensored antibody concentration meaning with value higher than the LLOQ and is expressed as n/N (%) where n is the number of responders at that timepoint and N the the total number of participants with data at the first and the second vaccination and at that time point. ‡ Refers only to 43 participants enrolled in a substudy to receive a third dose (Ad26.ZEBOV) two years after the first vaccination.

75 a slightly better antibody concentration compared to other Africans (p-value=0.02).

76

77 **Mechanistic model of the humoral response.** To better identify the factors associated to the dynamic of the
78 antibody response and to predict its duration, we used a model initially applied by (15) in Phase-I trials evaluating
79 the two-dose heterologous Ad26.ZEBOV, MVA-BN-Filo vaccine regimen. In this mechanistic model, antibodies are

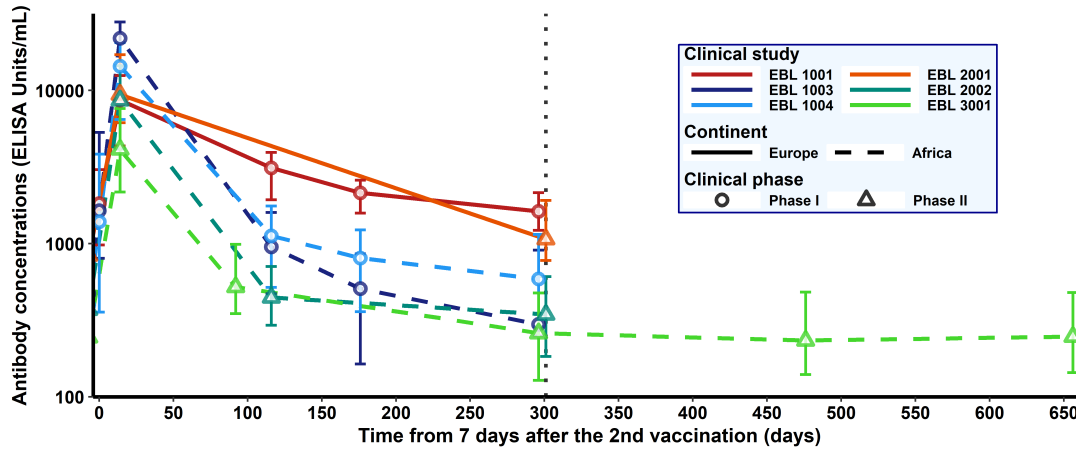


FIG 1 Dynamics of Ebola GP-specific binding antibody concentrations, in \log_{10} scale (in ELISA units/mL), in each clinical study from 7 days after the second vaccination. Each color correspond to a clinical study (red:EBL1001, dark blue:EBL1003, light blue:EBL1004, orange:EBL2001, turquoise:EBL2002, light green:EBL3001). Solid and dashed lines represent medians in European and African subjects respectively. Circles correspond to Phase-I studies and triangles to Phase-II studies. Error bars correspond to 25th-75th confidence intervals. The vertical dotted line represents the first year after the first vaccination.

80 assumed to be produced by plasma cells (antibody-secreting cells, ASCs) divided into two distinct sub-populations
 81 characterized by their lifespan: short-lived (SL) and long-lived (LL). For various infectious diseases, a rapid expansion
 82 of Ag-specific ASCs in blood peaking on day 7 post-infection or vaccination, followed by a fast depletion is
 83 observed (20, 21). Therefore, a strictly decreasing dynamics was considered from 7 days after the second vacci-
 84 nation for the two compartments of plasma cells assuming no additional exposure to the antigen. A schematic
 85 diagram of the mathematical model used to describe the humoral response from 7 days after the second vacci-
 86 nation is displayed in Figure 2. This simple model relied on three biological processes. LL and SL ASCs decay with
 87 time at rate δ_L and δ_S , respectively, and produce antibodies at rates θ_L and θ_S . Finally, antibodies are assumed
 88 to decay over time at rate δ_{Ab} . Baseline level of ASCs being unknown, the parameters $\phi_L = \theta_L L_0$ and $\phi_S = \theta_S S_0$,
 89 representing the respectively influx of LL and SL ASCs, were defined (see [Materials and Methods - Mathematical](#)
 90 [model of antibody kinetics](#). for more details).

91

92 **Quality of model's prediction.** Using parameter estimations obtained by (15) on humoral response observed
 93 in Phase-I trials, we evaluated the robustness of the model and predictive abilities.

94 First, we looked at the capacity of the model to capture the dynamic of the antibodies during the first year of
 95 vaccination based on the previously estimated parameters in a new population of participants. Fixing antibody,
 96 short- and long-lived ASCs half-live at 24 days, 3.0 days and 6.0 years, respectively, as well as SL ASCs influx param-
 97 eter at 2755 ELISA units/mL/day and LL ASCs influx parameter at 16.6 and 70.7 ELISA units/mL/day for African and
 98 European subjects (see [Materials and Methods - Evaluation of the model quality of prediction](#). for more details),
 99 only random effects (i.e. individual deviation from population mean) for the 487 subjects were evaluated using
 100 empirical bayes estimates (EBEs). Restricted to the first year following the first vaccination, the model allowed
 101 to fit well the antibody concentrations (see Figure A1). In addition, the overall percentage of observations falling
 102 within the 95% individual prediction intervals (also referred as the percentage of coverage) was evaluated at 99.8%
 103 (100% for each trial except for EBL1003 with 97.3%). The root mean squared error (RMSE) was consistent with a
 104 relatively small average difference between observations and predictions estimated at $0.081 \log_{10}$ ELISA units/ml
 105 (RMSE=0.102 and 0.075 \log_{10} ELISA units/ml in Phase-I and Phase-II studies, resp). These results confirmed the abil-
 106 ity of the model, estimated only with data from phase 1 trials, to capture the antibody response in all additional
 107 participants included in phase 2 trials.

108 Then, we looked at the ability of the model to predict long-term antibody concentration beyond 12 months.

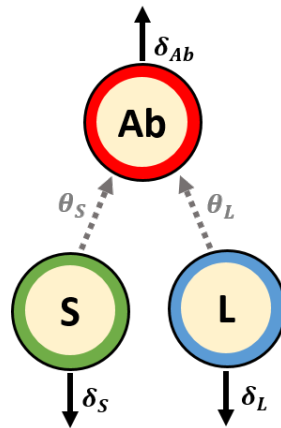


FIG 2 Schematic diagram of the model describing the humoral immune response from 7 days after the 2nd vaccination. *S* and *L* stand for short- and long-lived ASCs respectively and *Ab* for antibodies. The parameters δ_S , δ_L and δ_{Ab} are respectively the decay rates of SL ASCs, LL ASCs and antibodies while θ_S and θ_L represent the production rates of antibodies by SL and LL ASCs.

109 Individual parameters assessed for the early part of the dynamics of humoral responses were then used to pre-
 110 dict long-term antibody responses between 1 and 2 years after the first vaccination. As described in Table 2, only
 111 subjects from the EBL3001 clinical trial contributed to this analysis because they were the only ones with a follow-
 112 up beyond 12 months. As shown in Figure 3, the model demonstrated high quality long-term predictions with
 113 approximately 90% of the observed antibody concentrations falling within the 95% individual prediction intervals.
 114

115 **Update of the knowledge about the longevity of the humoral immune response.** The model was pretty
 116 good to forecast long-term humoral response. However, the increase of the RMSE and the decrease of the per-
 117 centage of coverage for EBL3001 subjects beyond 12 months (from 7 days after the second vaccination ; RMSE,
 118 before 12 months: 0.079 and after 12 months: 0.313 ; Coverage, before 12 months: 100% and after 12 months:
 119 90.58%) motivated an update of the parameters using all available data from the phase 1 and 2 trials. We firstly
 120 focused on the half-life of LL ASCs, $\log(2)/\delta_L$. The estimation of the lower bound of the loss rate of LL ASCs δ_L was
 121 performed with a profile likelihood. Thanks to the longer follow-up available the previous estimation of 5 years
 122 for the lower bound of the half-life of LL ASCs has been updated to 15 years (Figure 4). Hence, long-lived antibody
 123 secreting cells being non-proliferating cells (22), half of LL ASCs produced at the latest 7 days after the second
 124 vaccination and producing antibodies should persist at least 15 years. Given this result, further estimations were
 125 performed considering the parameter δ_L as fixed at the corresponding value of a lifespan of 15 years.

126 The application of three algorithms of covariate selection (SCM, COSSAC and SAMBA ; see [Materials and Meth-](#)
 127 [ods - Update and re-estimation of the model.](#) for more details) enabled us to identify factors influencing the
 128 dynamics of the humoral response. Although methods of covariate search differ from an algorithm to another,
 129 the adjustment of the biological parameters of the model for demographic and baseline characteristics selected
 130 by the different methods were quite consistent. All procedures led to the selection of an effect of continent, sex
 131 and age on antibody responses.

132 The best model estimated an effect of continent on ϕ_L (see Table 3 presenting a summary of parameter esti-
 133 mations). The mean value of ϕ_L was estimated at 38.1 ELISA units/mL.days⁻¹ in Europe compared to 10.3 ELISA
 134 unit/mL.days⁻¹ in African subjects. These results are accordance with the previous ones obtained with Phase 1
 135 trials (15).

136 By adding more information with Phase 2 trials data, we also identified the sex as another significant covariate
 137 for explaining the inter-individual variability of the decay rate of antibodies. Indeed, we estimated that antibodies
 138 have a significantly higher half-lives in women (p-value estimated by wald test <0.001) with an increase of the decay
 139 rate of 38% (95% confidence interval (CI): [19% ; 59%]) for men as compared to women.

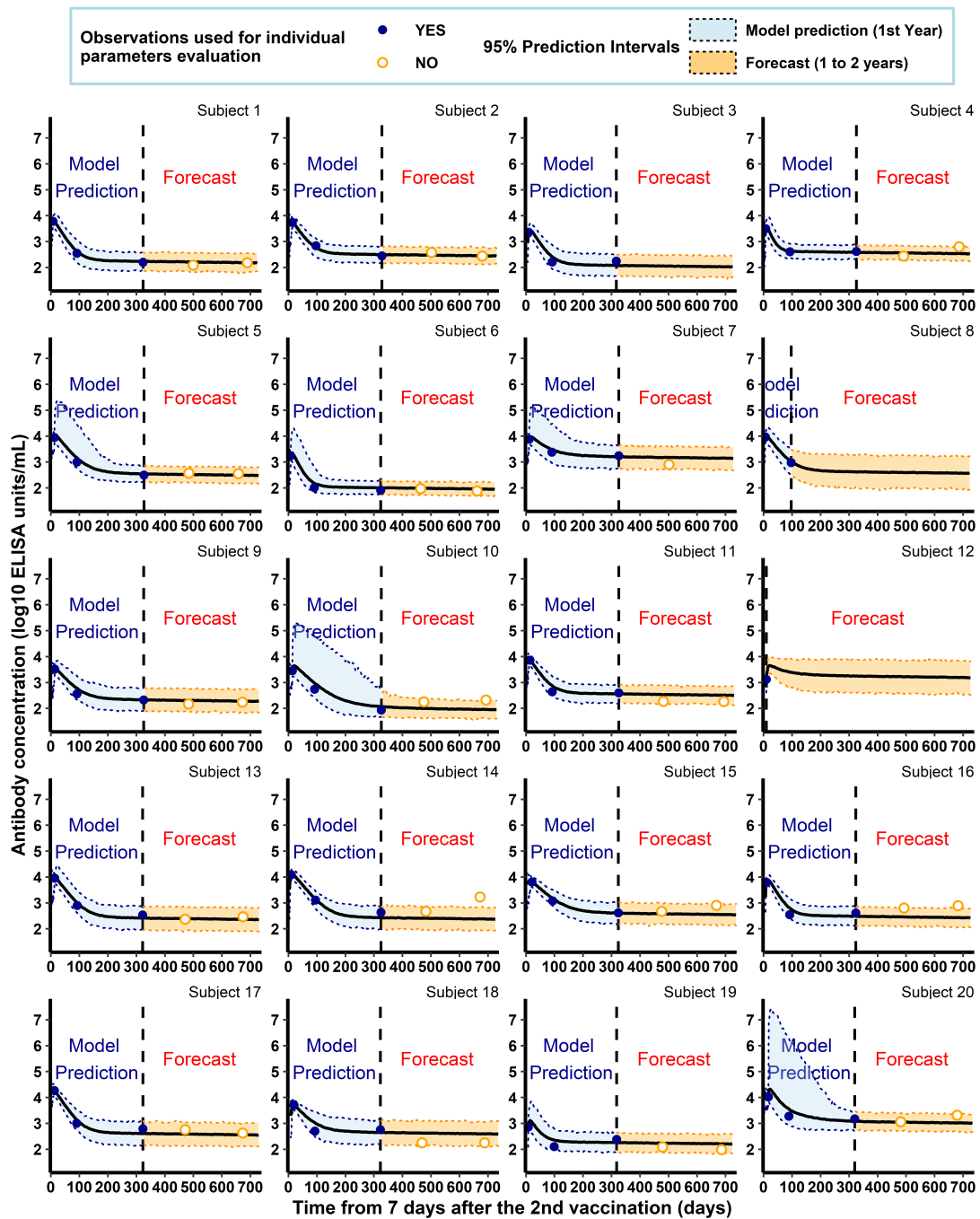


FIG 3 Individual antibody concentrations predicted by the model, estimated on Phase-I data, for random sample of subjects of the clinical study EBL3001. Each subplot represents the individual antibody dynamics (in \log_{10} ELISA units/mL) from 7 days after the 2nd vaccination. For each subject, the vertical dashed line represents the time limit (1 year after the first vaccination) between the predictions (in blue) and the forecasts (in orange). Plain blue dots correspond to observations used to evaluate individual parameters while orange circles are long-term observations not used in parameter estimation. Shaded areas correspond to 95% individual prediction intervals (accounting for the uncertainty on the individual parameter estimation and the measurement error) and the solid lines correspond to the prediction of the model.

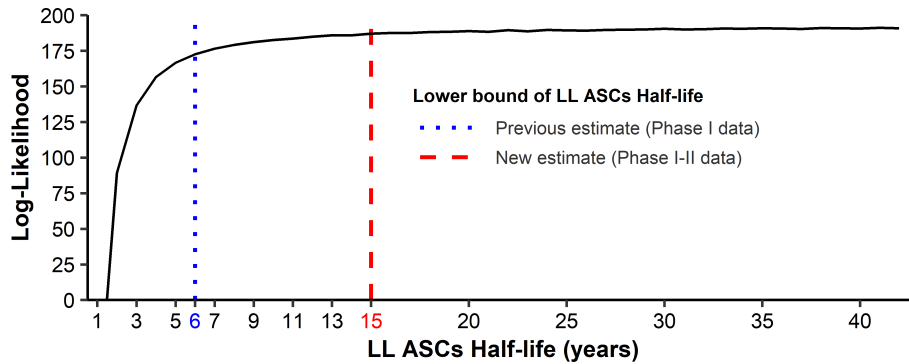


FIG 4 Profile likelihood on parameter δ_L . The y-axis corresponds to the non-penalized log-likelihood computed by importance sampling for several values of LL ASCs half-life which needs to be maximized. The blue dotted vertical line represents the lower bound of LL ASCs half-life estimated by profile likelihood by (15) on Phase-I data. The red dashed vertical line represents the newly estimated lower bound using Phase-I and II data.

140 We also found that older age was associated to a decrease of the influx of short-lived ASCs (parameter ϕ_S). A
 141 31 years old subjects (ages are assumed to be centered, see Table 1) displayed a mean value of SL ASCs influx of
 142 3045 ELISA units/mL.days⁻¹ (see Table 3). For one year older the influx of SL ASCs is decreased by 6% (95% CI: [4%
 143 ; 8%].

144

145 Once the optimal covariate structure identified, we estimated the value of the parameters of the model as
 146 shown in Table 3 providing the model parameters estimated by (15) on Phase-I data as well as the model pa-
 147 rameters obtained on combined Phase-I and II data. The Figure 5 displays the dynamics estimated by the model
 148 highlighting the goodness of fit of the data.

149 Compared with the estimates we obtained from the phase I data, the new estimates show a decrease in the
 150 magnitude of the ϕ_L parameter. This decrease is likely due to the significant increase in the half-life of the LL ASC
 151 from 6 to 15 years. Nevertheless, the mean ϕ_L remained four times higher in Europe than in Africa, as (15) approx-
 152 imated using Phase I data (4.3 times higher in Europe than in Africa). For the dynamics of SL ASCs, the parameter
 153 estimates remained quite stable, between the newly estimated model and the earlier estimates. As noted above,
 154 the information gained from longer follow-up allowed an update of the lower bound of the LL ASC decay rate.
 155 Similarly, the use of many additional subjects improved the precision of the model parameter estimates. Indeed,
 156 the confidence intervals in the new estimates have become narrower, whether for the parameters ϕ_L , ϕ_S , or δ_S ,
 157 and are mostly included within the confidence intervals of the old estimates. Finally, comparison of the model
 158 estimates showed a slight increase in inter-individual variability for the parameters ϕ_L and δ_{Ab} in the new model
 159 compared with the old one. The latter may be due to the use of additional data collected in a more heterogeneous
 160 population than in phase I studies. On the contrary, adjustment of the parameter ϕ_S for the age of the participants
 161 allowed to reduce the unexplained inter-individual variability for the same parameter by 24%.

162 We examined the ability of our model to predict the response for new participants by performing Monte Carlo
 163 cross-validation (MCCV) and using RMSE and percent coverage as quality criteria for prediction. (See [Materials
 164 and Methods - Update and re-estimation of the model.](#) for more details). The results of this analysis were
 165 summarised in Figure 6, where these two criteria are displayed as functions of the percentages of subjects used in
 166 the training dataset. Finally, despite the wide range of percentages tested for the split of train and test, the quality
 167 of the model prediction was very stable. The mean RMSE gradually decreased from 0.0857 to 0.0816 log₁₀ ELISA
 168 units/mL until it reached the values of 0.0843 log₁₀ ELISA units/mL when 100% of the data are used to estimate the
 169 models. The mean percentage of coverage remained higher than 95% even when only 20% of participants were
 170 used to estimate the model. Consequently, the model showed reasonably good quality in predicting the humoral
 171 immune response from 7 days after the second vaccination to two years after the first vaccination.

TABLE 3 Model parameters estimated on Phase-I participants by (15) and the new estimates obtained on pooled Phase-I and Phase-II data.

Parameter	Meaning	Phase-I data		Phase-I & II data	
		Mean	95% CI	Mean	95% CI
Fixed Effects					
δ_{Ab}	antibody decay rate (day ⁻¹)	0.029	[0.027 ; 0.033]		
Women				0.0260	[0.022 ; 0.0299]
Men				0.0358	[0.0292 ; 0.0439]
$\log(2)/\delta_{Ab}$	antibody half-life (days)	24	[22 ; 26]		
Women				26.7	[23.2 ; 30.7]
Men				19.4	[15.8 ; 23.7]
δ_S	SL ASCs decay rate (day ⁻¹)	0.231	[0.15 ; 0.36]	0.305	[0.257 ; 0.361]
$\log(2)/\delta_S$	SL ASCs half-life (days)	3.0	[1.9 ; 4.7]	2.28	[1.92 ; 2.70]
δ_L	LL ASCs decay rate (year ⁻¹)	3.16×10^{-4}	$[1.46 ; 7.03] \times 10^{-4}$	1.25×10^{-4}	
$\log(2)/\delta_L$	LL ASCs half-life (years)	6.0	[2.7 ; 13]	15.0	
ϕ_S	SL ASCs influx (EU/mL/day)	2755	[1852 ; 4100]		
Mean Age (31.3 years)				3045	[2297 ; 4036]
FC Δ Age = + 1 year*				0.939	[0.917 ; 0.962]
ϕ_L	LL ASCs influx (EU/mL/day)				
African subj.		16.6	[13.7 ; 20.1]	10.3	[9.09 ; 11.8]
Eur. subj.		70.7	[54.0 ; 92.7]	38.1	[28.2 ; 51.3]
Random Effects					
ω_{ϕ_S}	Sd of RE on ϕ_S	0.92	[0.83 ; 1.01]	0.704	[0.524 ; 0.884]
ω_{ϕ_L}	Sd of RE on ϕ_L	0.85	[0.78 ; 0.92]	0.879	[0.804 ; 0.953]
$\omega_{\delta_{Ab}}$	Sd of RE on δ_{Ab}	0.30	[0.24 ; 0.36]	0.354	[0.285 ; 0.422]
Error Model					
σ_{Ab}	Sd of error model	0.10	[0.10 ; 0.10]	0.107	[0.102 ; 0.113]

CI: Confidence interval ; EU: ELISA units ; FC: Fold change ; LL ASCs: long-lived antibody secreting cells ; RE: Random effects ; SL ASCs: short-lived antibody secreting cells ; Sd: Standard deviation. * Represents the multiplicative factor to apply to the value of ϕ_S , obtained for the mean age, for an increase of the age of subjects of 1 year: $\phi_S(\text{Mean Age} + 1 \text{ yr}) = \phi_S(\text{Mean Age}) \times \text{FC}(\Delta\text{Age}=+1)$.

172 DISCUSSION

173 With this modeling work, we evaluated the good quality of the long-term predictions of the mechanistic model
 174 developed by (15) that considers two populations of ASCs. Using a relatively small number of participants who
 175 followed four different vaccination regimens (only 177 - 25% - of whom followed of the vaccination regimen of
 176 interest in this study), we demonstrated with new data and a longer follow-up that the model had good quality
 177 long-term predictions of humoral response. In particular, the model was able to capture well the dynamics in
 178 participants who showed a lower antibody response. Re-estimation of the model with a longer-term follow-up
 179 allowed us to update the value of the lower limit of the LL ASC half-life and showed that the longevity of LL plasma
 180 cells is higher than previously estimated. In addition, we confirmed an influence of the geographic region on the
 181 long-term dynamics of the humoral response, as found in the first study. Furthermore, by considering additional
 182 data accounting for greater variability in humoral response as well as in demographic characteristics, we were able
 183 to identify two additional factors that influence the establishment and longevity of the vaccine-induced response.
 184 We found that the age of the participants may influence the initial magnitude of the humoral response through
 185 its impact on the dynamics of SL ASCs. We also found that the decrease in antibody response over time may be
 186 influenced by sex. In particular, we found that antibody concentration decreased more slowly in women. Finally,
 187 re-estimating the model with more participants allowed us to update the estimates of the model parameters while
 188 decreasing uncertainty as shown by narrower confidence intervals.

189 The values of the parameter estimates appear to be consistent with the literature. In particular, the mean val-
 190 ues obtained for the half-life of the antibodies are consistent with the literature, which supports a half-life between

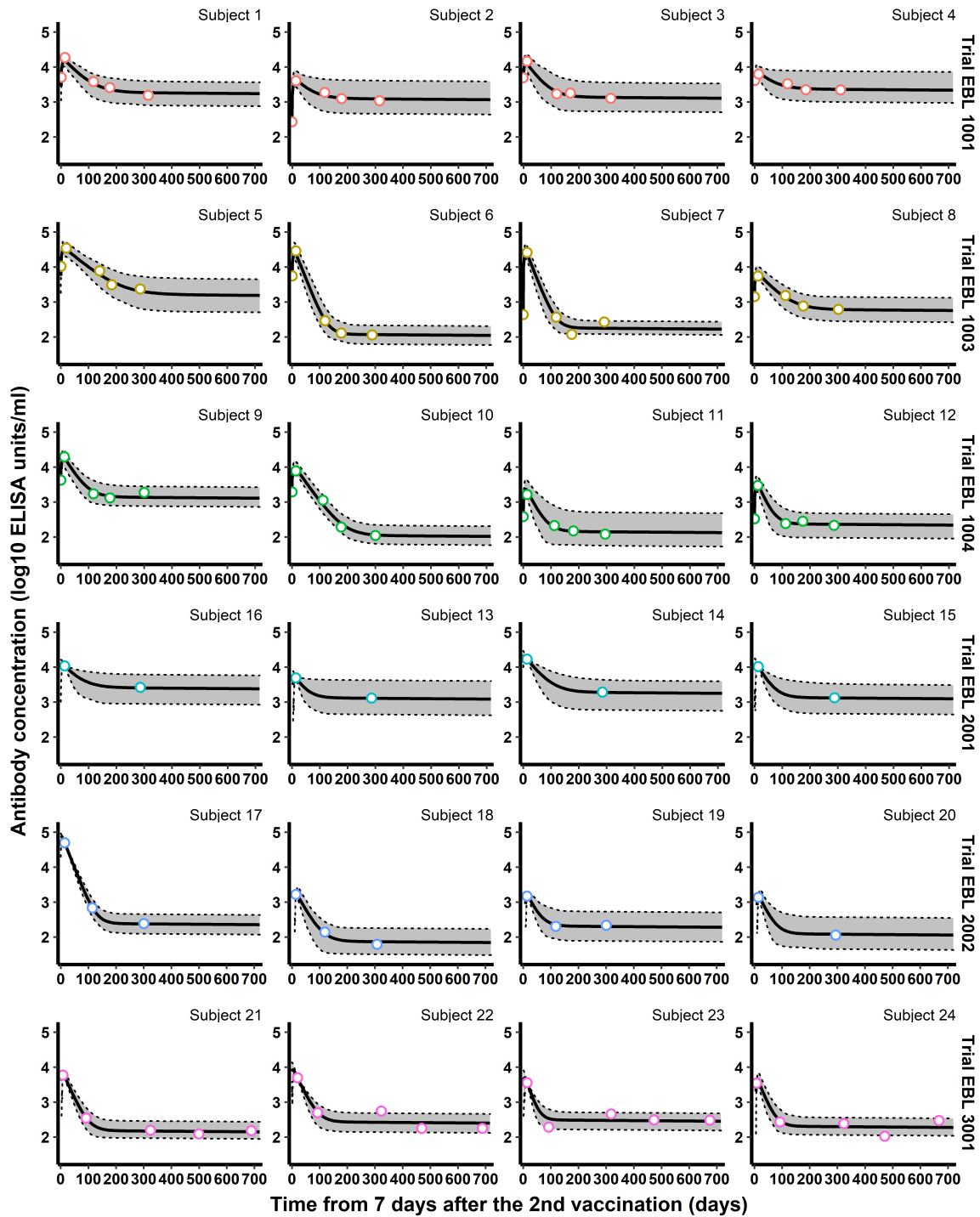


FIG 5 Individual antibody concentrations estimated by the model for random sample of subjects from the 6 clinical studies. Each subplot represents the individual antibody dynamics (in \log_{10} ELISA units/mL) from 7 days after the 2nd vaccination to 2 years. Colored circles correspond to observations used to estimate the model. The solid thick lines correspond to the individual dynamics and the 95% individual confidence intervals (accounting for the uncertainty of the estimation of the individual parameters only) are delimited by the shaded areas.

191 20 and 50 days (23, 24, 25, 26, 27, 28, 29). Indeed, the parameter δ_{Ab} was estimated to values corresponding to a
 192 mean half-life of 19 to 27 days.

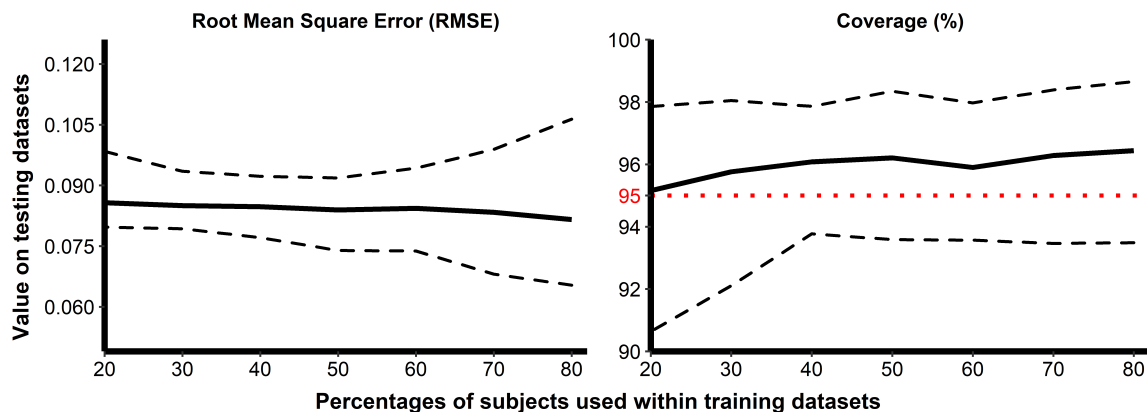


FIG 6 Evaluation of the ability of the model to predict unseen data using Monte-Carlo Cross-validation. The predictive quality was assessed by the evaluation of two criteria: the RMSE (left side) and the percentage of coverage (right side). The x-axis corresponds to the percentages of subjects randomly selected for the training dataset and the y-axis to the value of criteria calculated on testing dataset. Hundred replicates were performed for each train-test split percentage. Solid lines display the values of criteria and dashed lines, the 95% confidence intervals. The horizontal red dotted line on the right side displays the threshold of 95%.

193 The cause of the influence of the geographic region on the humoral response to vaccine is still unknown.
 194 Malaria has been one of the co-infection suspected to play a role in compromising the immune response (30,
 195 31, 32). Nevertheless, these results should be interpreted cautiously, as simple nonspecific cross-reactivity could
 196 also be responsible for this association (31). Chronic parasitic infections have also been suspected (33) such as
 197 schistosomiasis (34). Both hypotheses are currently explored in the EBOVAC consortia. The role of microbiota
 198 on the modulation of the immune responses to vaccination is a new research area (35). The modelling result
 199 presented here could help in exploring the causal effect of co-infections by orienting toward a mechanism that is
 200 compromising the production of long-lived antibody secreting cells.

201 We also found a different clearance of antibodies between men and women. As described by (36) or more recently
 202 by (37), many mechanisms may be responsible for sex-specific differences in vaccine-induced immunity, whether
 203 the direct or indirect effect of sex chromosomes through sex chromosome-encoded genes and sex hormones
 204 (oestrogen, testosterone, steroid, ...) or environmental exposures. These factors may then influence humoral
 205 immunity by inducing epigenetic and microbiological modifications and enhancing or altering the function of some
 206 immune cells. Consequently, the observed sex difference in antibody persistence may in fact summarise the
 207 significant contribution of sex to these unobserved mechanisms. The precise mechanism leading to a quicker
 208 clearance of the antibodies in men remain to be explored. The influence of age on the response to vaccine is
 209 known but the characterisation of its effect through the production of short-lived antibody secreting cells should be
 210 confirmed. Some studies have noted a decrease in plasma cells and memory B cells proliferation with age, usually
 211 peaking in childhood before progressively decreasing over time. The decrease in the percentage of memory B cells
 212 and plasma cells in humans appears to be observed primarily in peripheral blood. However, (38) has noted an
 213 age-related decline in the number of plasma cells in human bone marrow, which could be triggered by a reduction
 214 in germinal center responses. In addition, the decrease in B-cells production with age could result from a decrease
 215 in the diversity of naïve B cells (39). Indeed, the change in bone marrow with age could lead to a decrease in the
 216 number of survival niches, resulting in a decrease in naïve B cell production and a shift in the ratio of naïve to
 217 memory B cells (40). Consequently, this loss of diversity should lead to a decrease in the absolute number of early
 218 B cells progenitors. Nevertheless, identification of the age-related decline in SL ASC influx in our model should be
 219 viewed with caution because participants older than 65 years were not represented in the cohorts analyzed.

220 In conclusion, the dynamical model constructed from early phase 1 data has demonstrated is predictive capacity
 221 with longer follow-up and updated estimates give promising results for the duration of the immune response.
 222 The variation of the immune response to the vaccine endorses the impact of geographic situation, sex and age.

223 MATERIALS AND METHODS

224 **Immunogenicity measurements.** We considered data from six studies aiming at evaluating the safety, tol-
225 erability and immunogenicity of two-dose vaccine regimens with Ad26.ZEBOV and MVA-BN-Filo. Ad26.ZEBOV is
226 a monovalent, recombinant, E1/E3-deleted, replication-defective, adenovirus type 26 vector vaccine expressing
227 Ebola virus Mayinga variant GP, produced in PER.C6 human cells and injected in a single dose of 5×10^{10} viral
228 particles. MVA-BN-Filo is a recombinant, replication-defective, modified vaccinia Ankara vector vaccine expressing
229 Mayinga variant GP, Sudan virus Gulu variant GP, Marburg virus Musoke variant GP, and Tai Forest nucleoprotein.
230 This multivalent vaccine was produced in chicken fibroblasts and injected in a dose of 1×10^8 median tissue culture
231 infective dose (TCID₅₀). Three of the six studies are randomized, observer-blinded, placebo-controlled Phase-I tri-
232 als on healthy volunteers aged 18 to 50 years. These studies were performed in four countries: United-Kingdom
233 (UK), Kenya, Tanzania and Uganda. Results of the trials were previously described by (41) and (42) for UK (study
234 registered at ClinicalTrials.gov, NCT02313077, and labelled EBL1001 here) , (43) for Kenya (study registered at
235 ClinicalTrials.gov, NCT02376426, and labelled EBL1003 here) and (44) for Tanzania/Uganda (study registered at
236 ClinicalTrials.gov, NCT02376400, and labelled EBL1004 here). In addition, we considered data from two random-
237 ized, observer-blinded placebo-controlled, parallel-group phase-II trials on healthy volunteers aged 18 to 65 or 75
238 years. These studies were performed in 6 countries: UK, France, Kenya, Uganda, Burkina Faso and Ivory Coast.
239 We refer to (16) for detailed description of results in the European trial and to (17) for the African trial (two studies
240 registered at ClinicalTrials.gov, NCT02416453 and NCT02564523, and labelled EBL2001 and EBL2002 here respec-
241 tively for the European and African studies). The last study is a combined open-label, non-randomized stage 1, and
242 a randomized, observer-blinded, placebo-controlled stage 2 phase-II trial on healthy adults. This study was con-
243 ducted in Sierra Leone aimed also to evaluate the long-term immunogenicity and the humoral immune memory
244 induced by the vaccine regimen. Results of this trial were described by (18) (study registered at ClinicalTrials.gov,
245 NCT02509494, and labelled EBL3001 here).

246 In Phase-I trials, participants were equally randomized into four vaccination regimens: two with MVA-BN-Filo
247 as first vaccination at day 1, followed by Ad26.ZEBOV on day 29 or 57, and two with Ad26.ZEBOV as prime vaccine
248 on day 1, followed by MVA-BN-Filo on day 29 or 57. Within each regimen, subjects received either active vaccine
249 or placebo in a 5:1 ratio. In the study EBL2001, participants in Cohorts I-III were equally randomized into three
250 parallel groups in which they received Ad26.ZEBOV as first vaccine on day 1, followed by MVA-BN-Filo on day 29,
251 57 or 85. This first cohort was excluded from the analysis as subjects were enrolled to provide data only on safety
252 and the timing of anti-Ebola virus GP ASCs responses. Within each group, participants received active vaccines or
253 placebo in a 14:1 or 10:3 ratios in cohorts II and III respectively. In the study EBL2002, healthy adults (Cohort I)
254 were equally randomized into the same three parallel groups with an active vaccine: placebo ratio of 5:1. Adults
255 HIV-infected patients (Cohort IIa) and healthy children (Cohorts IIb and III) were not included in the analysis. Finally,
256 in the study EBL3001, participants received either Ad26.ZEBOV as first vaccination on day 1 followed by MVA-BN-
257 Filo on day 57, or MenACWY vaccine on day 1 and placebo on day 57, with a ratio of 1:0 and 3:1 in stage 1 and 2
258 respectively. In the analysis, only subjects receiving Ad26.ZEBOV as first vaccination on day 1 and MVA-BN-Filo as
259 second vaccination on day 57 (Ad26/MVA D57) were included, which corresponded to a total of 487 subjects over
260 all studies, whom 44 in Phase-I studies, 71 in EBL2001, 137 in EBL2002 and 235 in EBL3001.

261 Subjects were followed up to 1 year after the first vaccination in all the studies with longitudinal immuno-
262 genicity measurements performed on blood samples. As shown in Figure 7, for the vaccine regimen of interest,
263 immunogenicity samples were collected in all participants immediately before the administration of the first vac-
264 cination (Ad26.ZEBOV) on day 1, before the second vaccination (MVA-BN-Filo) on day 57, then 21 days after the
265 second dose at day 78 and 1 year after the first dose (at day 360 or 365 according to the trial). In phase-I trials,
266 additional samples were done at days 7, 29, 64, 180 and 240 while immunological assays were done on blood
267 samples taken at day 180 and day 156 in EBL2002 and EBL3001 respectively. Participants enrolled in EBL3001
268 were additionally followed up to 2 years after the first vaccination with blood samples collected every 6 months
269 after the first year. We analyzed total IgG Ebola virus GP-specific binding antibody concentrations measured by
270 an Ebola virus GP (kikwit strain) Filovirus Animal Non-Clinical Group ELISA. Being interested in the longevity of
271 the long-term immunity induced by the two-dose heterologous vaccine, similarly to (15), we mainly focused our
272 analysis on immunogenicity measurement sampled after the second vaccination.

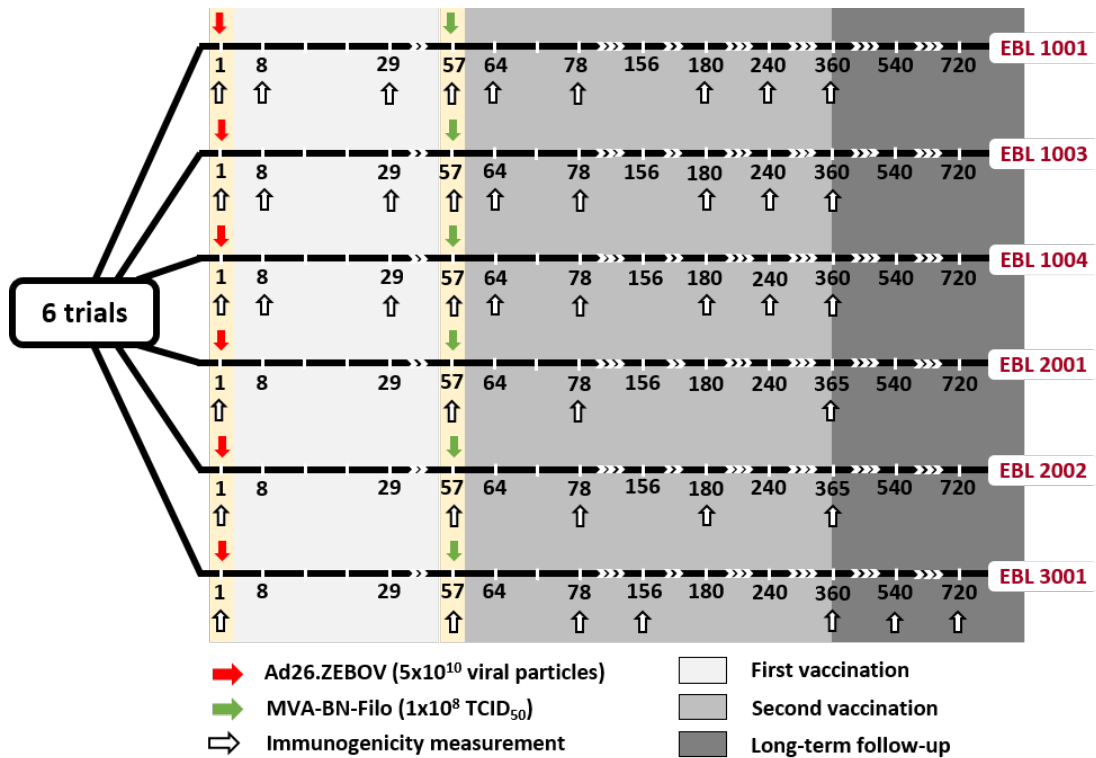


FIG 7 Design of EBOVAC 1 (EBL 1001, 1003, 1004 and 3001) and EBOVAC 2 (EBL 2001 and 2002) trials for participants receiving Ad26/MVA D57 as vaccine regimen. Immunogenicity measurements provide the concentration of IgG binding antibodies against Ebola measured by ELISA (units/mL).

274 **Statistical analysis.** A preliminary descriptive analysis was performed on the baseline and demographic
 275 characteristics of participants to describe and summarize the basic features of the data. Statistical differences
 276 among groups of participants were evaluated using classic t-tests implemented in R and p-values where adjusted
 277 for test multiplicity with Benjamini and Hochberg correction (19) using the classic R function *p.adjust*. Similar analysis
 278 were performed on immunogenicity data measured at specific timepoints shared by the six trials (21 days
 279 after the second dose and 1 year after the first one) to identify potential subgroups of participants sharing the
 280 same dynamics. Finally, spearman correlations between antibody concentrations measured 21 days after the second
 281 vaccination and longer-term humoral responses were evaluated assuming adjustment for test multiplicity on
 282 p-values.

284 **Mathematical model of antibody kinetics.** To analyze the humoral immune response induced by the two-
 285 dose heterologous vaccine regimen Ad26.ZEBOV, MVA-BN-Filo against Ebola virus and evaluate the long-term
 286 immunogenicity, we used a mechanistic model divided into three parts. First of all, a mathematical model based
 287 on ordinary differential equations is defined to describe the dynamics of plasma cells and antibodies (3). As shown
 288 in Figure 2, antibodies are assumed to be produced by two plasma cell populations differentiated by their lifespan:
 289 short- and long-lived antibody secreting cells (ASCs). Consequently, the ODE-system contains three compartments:
 290 the short-lived ASCs (labelled S), the long-lived ASCs (labelled L) and the antibodies (Ab). Based on the hypothesis
 291 that antibody secreting cells peaked at day 7 post-infection/vaccination (20, 21), time was rescaled to consider only
 292 the antibody dynamics from 7 days after the second vaccination (day 64) during which plasma cells only decrease
 293 over time. As demonstrated by (15), the model can be written as a single equation (1).

294

$$\begin{cases} \frac{dAb}{dt} = \phi_S e^{-\delta_S t} + \phi_L e^{-\delta_L t} - \delta_{Ab} Ab \\ Ab(t=0) = Ab_0 \end{cases} \quad (1)$$

295 with δ_S , δ_L and δ_{Ab} representing the average decay rates of SL ASCs, LL ASCs and antibodies respectively. The
 296 parameters ϕ_S and ϕ_L are respectively the influx of SL and LL ASCs defined as $\phi_S = \theta_S S_0$ and $\phi_L = \theta_L L_0$ where
 297 $S_0 = S(t=0)$ and $L_0 = L(t=0)$ are the initial conditions at 7 days after the second vaccination while θ_S and θ_L
 298 are their respective antibody production rates. The initial antibody concentration Ab_0 is defined by the individual
 299 measure of antibody concentration at 7 days after the second vaccination. Keeping in mind that the antibody
 300 concentration can be unobserved at day 68 for some participants (see Figure 7), a lag-time was introduced in
 301 equation (1) labelled T_i representing the individual time interval the assumed initial time (day 64) and the first
 302 observation after this specific time. The equation can then be written as follows.

303

$$\begin{cases} \frac{dAb}{dt} = \phi_S e^{-\delta_S(t+T_i)} + \phi_L e^{-\delta_L(t+T_i)} - \delta_{Ab} Ab \\ Ab(t=0) = \widetilde{Ab}_0 \end{cases} \quad (2)$$

304 Based on this equation, time was rescaled for each individual such as the initial condition ($t=0$) coincide with the
 305 first observation following day 64. We estimated the five following biological parameters $\Psi = (\phi_S, \delta_S, \phi_L, \delta_L, \delta_{Ab})$.
 306 To account for inter-individual variability, we used a statistical model on which the five model parameters are
 307 assumed to be log-transformed, to ensure their positivity. Each parameter is then described by a mixed-effects
 308 model which can depends on covariates. Each individual parameter Ψ_k^i for the subject i can be defined as follows,
 309 for $k = \{1, \dots, 5\}$.

310

$$\log(\Psi_k^i) = \log(\Psi_{k,0}) + \beta_k Z_k^i + u_k^i \quad (3)$$

311 where Ψ_0 is the fixed effect, Z_k and β_k are respectively the vectors of explanatory variables and regression co-
 312 efficients related to the biological parameter Ψ_k , and u_k^i is the individual random effect assumed to be normally
 313 distributed with the variance ω_k^2 . Random effects were assumed to be independent from each other. Based on
 314 results obtained in the previous work (15), we assumed random effects on the influx parameters, ϕ_L and ϕ_S , and
 315 on the decay rate of antibodies δ_{Ab} .

316 For the observation model, we modeled the observed IgG binding antibody concentrations against the kikwit
 317 glycoprotein from the six studies by the Ab ODE-compartment. We assumed an additive error model normally
 318 distributed on the \log_{10} value of the antibody concentrations, with a variance σ_{Ab}^2 . The antibody concentration for
 319 patient i at the j th time is given by

320

$$Y(t_{ij}) = \log_{10} [Ab(\Psi^i, t_{ij})] + \varepsilon_{ij} \quad \varepsilon_{ij} \sim \mathcal{N}(0, \sigma_{Ab}^2) \quad (4)$$

321

322

323 **Model estimation.** Mathematical and practical identifiability has been assessed in previous work (15). Thus
 324 the parameter δ_L was estimated by profile likelihood (45) which consists in defining a grid of values for the parame-
 325 ter and to sequentially set the parameter δ_L at one of those different values and estimate the model by maximizing
 326 the log-likelihood, given that value of δ_L . The resulting profile shows the maximum possible log-likelihood for each
 327 value of δ_L and has its maximum at the maximum likelihood estimate $\hat{\delta}_L$. Other parameters were estimated by a
 328 population approach in which the model estimation relies on the estimation of the population parameters gath-
 329 ering parameter intercepts (Ψ_0), the regression coefficients (β), the standard deviation of random effects (ω) and
 330 the standard deviation of the error model (σ_{Ab}). Model estimation was performed by the Monolix @software ver-
 331 sions 2019R1 and 2019R2. This software uses the Stochastic Approximation Expectation-Maximization (SAEM) al-
 332 gorithm (46, 47) to estimate the population parameters with likelihood computed by importance sampling (48) and
 333 the fisher information matrix calculated by stochastic approximation. Once population parameters re-estimated,
 334 individual parameters are computed as Empirical bayes estimates (EBEs) representing the most likely values of
 335 the individual parameters given individual data and population parameters. EBEs are calculated as the mode of

336 the condition parameter distribution by Markov-Chain Monte-Carlo (MCMC) procedure (49) using the Metropolis-
 337 Hasting algorithm (50) to compute the conditional distribution and the Nelder-Mead Simplex algorithm (51) to
 338 maximize it.

339

340 **Evaluation of the model quality of prediction.** The mechanistic model described by equations 2, 3 and
 341 4, initially estimated on Phase-I data by (15), was validated on data from the six trials according to its quality of
 342 prediction. To this end, a two-step approach was applied: first, the robustness of the model was assessed by
 343 evaluating its ability to well predict antibody dynamics from 7 days post-second vaccination to 1 year after the first
 344 vaccination for all Phase-I and Phase-II subjects. Then, the ability of the model to forecast antibody concentration
 345 after 1 year following the first vaccination was evaluated. To investigate the robustness of the model initially
 346 estimated on Phase-I data, only data restricted to the first year following the first vaccination were used to stay
 347 in the scope of applicability of the model. Assuming fixed effects and regression coefficients of the population
 348 parameters ($\Psi_{k,0}$ and $\beta_k, \forall k \in \{1, \dots, 5\}$), distribution of random effects ($\sigma_k, \forall k \in \{1, \dots, 5\}$) as well as the standard
 349 deviation of the error model (σ_{Ab}) as fixed to previously obtained values, we evaluated individual parameters
 350 for the 487 participants, via the variables u_k^i , using the empirical bayes estimates (EBEs) approach implemented
 351 in Monolix. As shown in Table 3, we fixed the decay rate of antibodies (δ_{Ab}), SL ASCs (δ_S) and LL ASCs (δ_L) for
 352 corresponding half-lives of 24 days, 3 days and 6 years, respectively. The parameter ϕ_S was fixed at 2755 ELISA
 353 units/mL/day while ϕ_L was fixed at 16.6 ELISA units/mL/day for African subjects and 70.7 ELISA units/mL/day for
 354 European ones. East and West African subjects were assumed to share the same value of LL ASCs influx. Finally,
 355 standard deviations of the inter-individual variability on the three parameters ϕ_S , ϕ_S and δ_{Ab} were chosen as
 356 $\omega_{\phi_S} = 0.92$, $\omega_{\phi_L} = 0.85$ and $\omega_{\delta_{Ab}} = 0.30$. The parameter σ_{Ab} was fixed at 0.10 (see (15)). To stay consistent with
 357 the model built on Phase-I data, we assumed in the statistical model an adjustment for geographic region (binary
 358 variable equal to 0 in Africa and 1 in Europe) on ϕ_L , as shown on the following equation:

$$359 \quad \log(\phi_L^i) = \log(\phi_{L,0}) + \beta_{\phi_{L,Eur}} \times \mathbb{1}_{i \in Eur} + u_{\phi_L}^i \quad (5)$$

360 For each individual, the 95% prediction interval (52) of the antibody dynamics was calculated and the percentage of
 361 coverage, defined as the percentage of observations falling within the prediction interval, was assessed. Through
 362 these results, we highlighted the ability of the model to predict short-term antibody concentration (from 7 days
 363 after the second vaccination to 1 year after the first one). Once short-term predictions validated, individual pa-
 364 rameters, found on the first year of follow-up, were used to quantify the long-term forecast skills of the model. To
 365 this end, we used the model to make individual predictions of antibody concentration between 1 and 2 years after
 366 the first vaccination. Predictions were then compared to observations in EBL3001 trial (being the single trial with
 367 observed antibody concentrations measured after 1 year) and the percentage of observations falling within the
 368 95% individual prediction intervals was quantified. K-means clustering for longitudinal data (53) was performed to
 369 identify distinct trajectories of the dynamics of the humoral response. Using the kml R-package (54), trajectories
 370 of antibody concentration from 7 days after the second vaccination to 2 years after the first one were sequentially
 371 clustered into 2 and more clusters. Thereafter, we evaluated for each resulting partition the percentage of cover-
 372 age and the RMSE to investigate potential different prediction abilities according to underlying trajectories.

373

374 **Update and re-estimation of the model.** Once the quality of prediction of the mechanistic model evaluated,
 375 an update of the model was accomplished in order to improve biological knowledge about the longevity of the
 376 long-term immune response induced by the two-dose heterologous vaccine regimen, Ad26.ZEBOV, MVA-BN-Filo.
 377 The low number of subjects included into the three Phase-I trials (177 of whom only 44 received the Ad26/MVA D57
 378 vaccine regimen) as well as the short-term follow-up of their immune response up to 1 year after the first vaccina-
 379 tion tended to limit the precision of the estimation of the model parameters in the work conducted only on Phase-I
 380 trials. Despite the validation of the model according to its quality of prediction on additional data coming from
 381 the three Phase-II trials (EBL 2001, 2002 and 3001), a re-estimation of the model using antibody dynamics from
 382 the 487 participants was accomplished to enhance and reinforce our understanding of the underlying biological
 383 processes leading to the long-term immunity following vaccination against Ebola. Participants from Phase-I clinical

384 studies, being monitored only during the first year following the first vaccination, provided information only on
 385 the early phase of the humoral response. In particular, the lack of information on the long-term immunity made
 386 the estimation of the decay rate of the long-lived ASCs difficult. Long-lived ASCs being persistent plasma cells with
 387 a lifespan ranging from several months to lifetime (55, 56, 57, 22), only an approximation of the lower bound of
 388 the confidence interval of their half-life ($\log(2)/\delta_L$) was possible. Using additional data from Phase-II studies and
 389 in particular the humoral response measurements beyond 1 year, we performed a profile likelihood to identify
 390 whether enough information were available to precisely estimate the parameter δ_L . Considering the statistical
 391 model found by (15), the model was estimated for multiple values of LL ASCs half-life ranging from 1 to 40 years.
 392 The profile likelihood was then drawn by maximizing the log-likelihood, computed by importance sampling (48),
 393 for each of those related models.

394 As first estimation, a sequential Bayesian estimation was envisaged, that is using information provided by
 395 Phase-I studies only through informative prior distribution for parameters. Maximum A posteriori (MAP) esti-
 396 mates, corresponding to a penalized maximum likelihood estimation (58), should then be obtained using humoral
 397 responses from only the 443 Phase-II subjects. However, the difference of sampling between Phase-I and II stud-
 398 ies, in particular the absence of data from 7 to 21 days after the second vaccination for Phase-II subjects (see
 399 Table 2), made the estimation of the model difficult. The lack of information at the early stage of the dynamics
 400 induced practical identifiability issues for the parameters δ_S and ϕ_S . To tackle this difficulty, all data were used
 401 to update the model. Random effects found on Phase-I trials were kept, considering inter-individual variability on
 402 the parameter δ_{Ab} as well as on the ASCs influx, ϕ_L and ϕ_S .

403 The statistical model was updated by performing a covariate selection. We applied the classic stepwise co-
 404 variate modeling (SCM) algorithm (59, 60) which is a stepwise procedure with a forward selection followed by a
 405 backward elimination. In the forward selection, each parameter-covariate relationship is tested in turn and the re-
 406 lationship improving the model criteria (a corrected version of the Bayesian information criterion, BICc) the most
 407 is kept (the lower the better). Then the addition of a second covariate is tested. In the backward elimination,
 408 the removal of each parameter-covariate relationship selected in the first step is tested in an univariate manner.
 409 To verify the robustness of the results, two other algorithms of covariate selection in non-linear mixed effects
 410 models were performed, using BICc as model selection criteria: 1) the conditional sampling use for stepwise ap-
 411 proach based on correlation tests (COSSAC) (60), and 2) the stochastic approximation for model building algorithm
 412 (SAMBA) (61). The three algorithms were independently applied on an initial model without any covariates and
 413 tested the addition of the seven following potential covariates: Sex (=0 for women and =1 for men), Age, Weight,
 414 BMI, Continent (Europe/Africa), Region (Europe/East Africa/West Africa) and EBL 3001 (=1 for participants from
 415 EBL3001 and 1 otherwise). Covariates such as Age, BMI and Weight were centered around the mean value of
 416 the studied population (see Table 1). The parameter δ_L , facing some identifiability issues due to the lack of mea-
 417 surements beyond 2 years, was removed from the covariate selection procedure. The statistical significance of
 418 selected covariates was then evaluated using a Wald-test. EBL3001 being the only study with a follow-up beyond
 419 1 year after the first vaccination and being conducted in a single country (Sierra Leone), the robustness of the re-
 420 sults was analyzed to verify the short-term relevance of the selected covariates. To this end, the same procedure
 421 was performed on the model already adjusted for the selected covariates but considering only data up to 1 year
 422 after the first vaccination. At the end of the covariate selection procedure, an optimal model was obtained with
 423 the following statistical model (see section Results - Update of the knowledge about the longevity of the humoral
 424 immune response. for more details).

$$425 \quad \begin{cases} \log(\phi_L^i) = \log(\phi_{L,0}) + \beta_{\phi_L, Eur} \times \mathbb{1}_{i \in Eur} + u_{\phi_L}^i \\ \log(\phi_S^i) = \log(\phi_{S,0}) + \beta_{\phi_S, Age} \times (Age_i - \overline{Age}) + u_{\phi_S}^i \\ \log(\delta_{Ab}^i) = \log(\delta_{Ab,0}) + \beta_{\delta_{Ab}, Men} \times \mathbb{1}_{i \in Men} + u_{\delta_{Ab}}^i \end{cases} \quad (6)$$

426 where Age_i and \overline{Age} are respectively the age of the subject i and the average age of the participants and with
 427 $u_{\phi_L}^i \sim \mathcal{N}(0, \omega_{\phi_L}^2)$, $u_{\phi_S}^i \sim \mathcal{N}(0, \omega_{\phi_S}^2)$ and $u_{\delta_{Ab}}^i \sim \mathcal{N}(0, \omega_{\delta_{Ab}}^2)$. Once the optimal model selected, the robustness of the
 428 convergence of the estimation was assessed by using the convergence assessment tool implemented in Monolix
 429 which evaluate the robustness of the SAEM algorithm for numerous initial conditions.

430 The predictive quality of the newly estimated model was assessed by performing a Monte-Carlo Cross-validation
431 (62). Subjects from the overall dataset were randomly splitted into a training and a testing dataset, given a train-
432 test split percentage. We paid attention to keep the same ratio of subjects within each of the two sub-datasets for
433 each trial. Once the model fitted on train data, EBEs resulting from this model were evaluated on test data followed
434 by the prediction of the individual antibody dynamics. Two criteria were then calculated on the testing dataset to
435 estimate how accurately the predictive model performs: the percentage of coverage (the higher the better) and the
436 RMSE (the lower the better). For each of the seven train-test split percentages {20%, 30%, 40%, 50%, 60%, 70%, 80%},
437 the procedure was replicated 100 times.

438 **SUPPLEMENTAL MATERIAL**

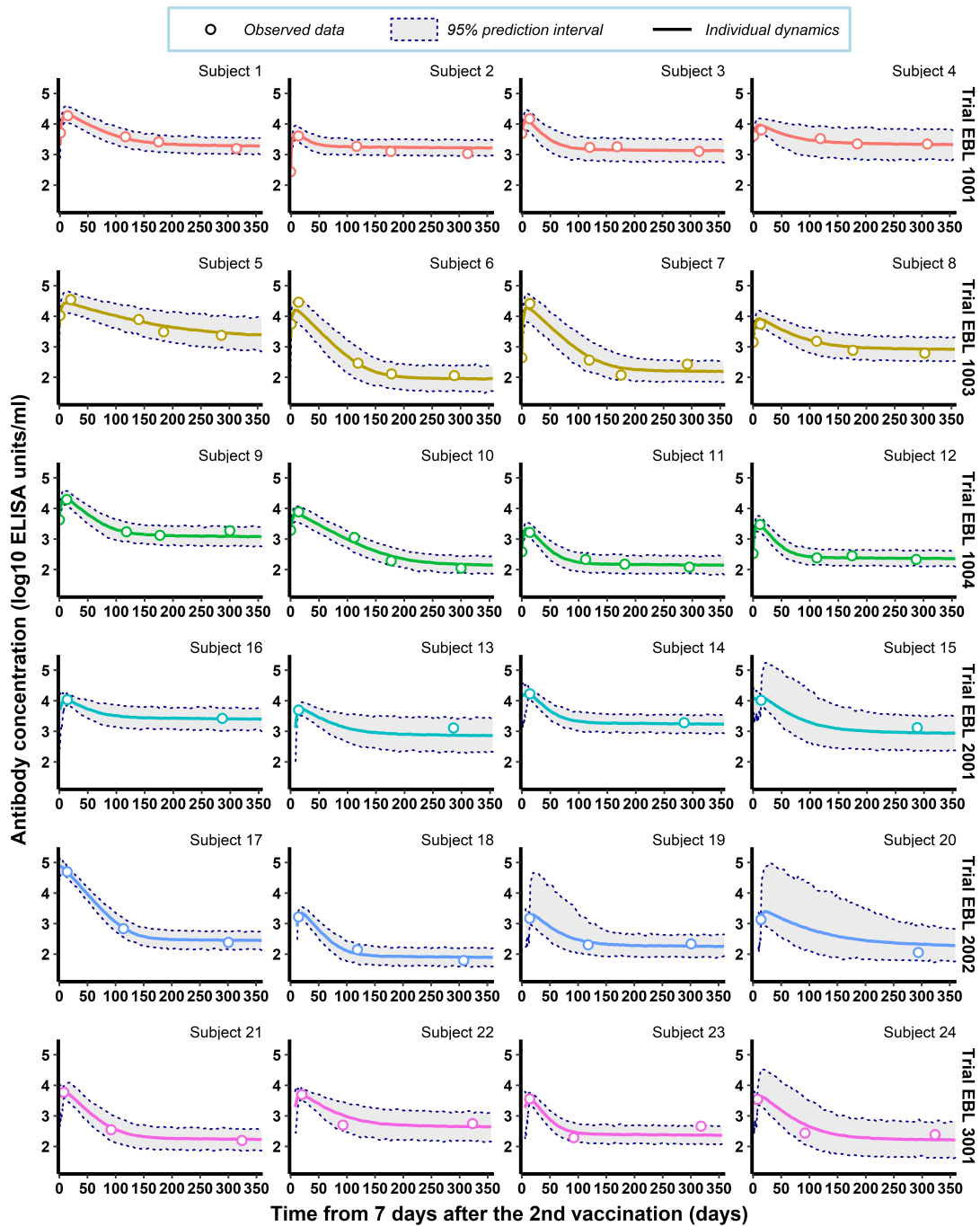


FIG A1 Individual antibody concentrations predicted by the mechanistic model estimated on data from Phase-I clinical studies only (clinical studies accounting for additional vaccine regimens than Ad26/MVA D57, see (15)). Each subplot represents the individual antibody dynamics (in log₁₀ ELISA units/mL) from 7 days after the 2nd vaccination to 1 year of follow up for random sample of 24 subjects from the 6 clinical studies. The solid thick lines correspond to the mean individual dynamics predicted by the model and colored circles correspond to observations (used to evaluate random effects using EBEs). Shaded areas correspond to the 95% individual prediction intervals (accounting for the uncertainty of the estimation of the individual parameters and the measurement error).

439 ACKNOWLEDGMENTS

440 MA has been funded by INRIA PhD grant. We thank Lixoft SAS for their support. Numerical computations were in
441 part carried out using the PlaFRIM experimental testbed, supported by Inria, CNRS (LABRI and IMB), Université de
442 Bordeaux, Bordeaux INP and Conseil Régional d'Aquitaine (see <https://www.plafrim.fr>).

443 REFERENCES

1. **Food and Drug Administration (FDA)**. 2019. First FDA-approved vaccine for the prevention of Ebola virus disease, marking a critical milestone in public health preparedness and response <https://www.fda.gov/news-events/press-announcements/first-fda-approved-vaccine-prevention-ebola-virus-disease-marking-critical-milestone-public-health>. (visited on 2022-01-03).
2. **European Commission (EC)**. 2021. Vaccine against Ebola: Commission grants new market authorizations https://ec.europa.eu/commission/presscorner/detail/en/IP_20_1248. (visited on 2022-01-03).
3. **Andraud M, Lejeune O, Musoro JZ, Ogunjimi B, Beutels P, Hens N**. 2012. Living on three time scales: the dynamics of plasma cell and antibody populations illustrated for hepatitis a virus. *PLoS computational biology* 8 (3):e1002418.
4. **Monath TP**. 2005. Yellow fever vaccine. *Expert review vaccines* 4 (4):553–574.
5. **Plotkin SA, Gilbert PB**. 2012. Nomenclature for immune correlates of protection after vaccination. *Clin Infect Dis* 54 (11):1615–1617.
6. **Pawelek KA, Huynh GT, Quinlivan M, Cullinane A, Rong L, Perelson AS**. 2012. Modeling within-host dynamics of influenza virus infection including immune responses. *PLoS computational biology* 8 (6):e1002588.
7. **Lee HY, Topham DJ, Park SY, Hollenbaugh J, Treanor J, Mosmann TR, Jin X, Ward BM, Miao H, Holden-Wiltse J, et al.**. 2009. Simulation and prediction of the adaptive immune response to influenza A virus infection. *J virology* 83 (14):7151–7165.
8. **Xie XT, Yitbarek A, Astill J, Singh S, Khan SU, Sharif S, Poljak Z, Greer AL**. 2021. Within-host model of respiratory virus shedding and antibody response to H9N2 avian influenza virus vaccination and infection in chickens. *Infect Dis Model* 6:490–502.
9. **Bonin CRB, Fernandes GC, dos Santos RW, Lobosco M**. 2017. A simplified mathematical-computational model of the immune response to the yellow fever vaccine. *In 2017 IEEE International Conference on Bioinformatics and Biomedicine (BIBM) IEEE*, p 1425–1432.
10. **Bonin CR, Fernandes GC, Dos Santos RW, Lobosco M**. 2018. A qualitatively validated mathematical-computational model of the immune response to the yellow fever vaccine. *BMC immunology* 19 (1):1–17.
11. **Best K, Perelson AS**. 2018. Mathematical modeling of within-host Zika virus dynamics. *Immunol reviews* 285 (1):81–96.
12. **Perelson AS, Ke R**. 2021. Mechanistic Modeling of SARS-CoV-2 and Other Infectious Diseases and the Effects of Therapeutics. *Clin Pharmacol & Ther* 109 (4):829–840.
13. **Roosendaal R, Hendriks J, van Effelterre T, Spiessens B, Dekking L, Solfrosi L, Czapska-Casey D, Bockstal V, Stoop J, Splinter D, et al.**. 2020. Nonhuman primate to human immunobridging to infer the protective effect of an Ebola virus vaccine candidate. *NPJ vaccines* 5 (1):1–11.
14. **Food and Drug Administration (FDA)**. 2015. Product Development Under the Animal Rule <https://www.fda.gov/media/88625/download>. (visited on 2022-01-03).
15. **Pasin C, Balelli I, Van Effelterre T, Bockstal V, Solfrosi L, Prague M, Douoguih M, Thiébaud R**. 2019. Dynamics of the humoral immune response to a prime-boost Ebola vaccine: quantification and sources of variation. *J virology* 93 (18):e00579–19.
16. **Pollard AJ, Launay O, Lelievre JD, Lacabaratz C, Grande S, Goldstein N, Robinson C, Gaddah A, Bockstal V, Wiedemann A, et al.**. 2021. Safety and immunogenicity of a two-dose heterologous Ad26. ZEBOV and MVA-BN-Filo Ebola vaccine regimen in adults in Europe (EBOVAC2): a randomised, observer-blind, participant-blind, placebo-controlled, phase 2 trial. *The Lancet Infect Dis* 21 (4):493–506.
17. **Barry H, Mutua G, Kibuuka H, Anywaine Z, Sirima SB, Meda N, Anzala O, Eholie S, Bétard C, Richert L, et al.**. 2021. Safety and immunogenicity of 2-dose heterologous Ad26. ZEBOV, MVA-BN-Filo Ebola vaccination in healthy and HIV-infected adults: A randomised, placebo-controlled Phase II clinical trial in Africa. *PLoS medicine* 18 (10):e1003813.
18. **Ishola D, Manno D, Afolabi MO, Keshinro B, Bockstal V, Rogers B, Owusu-Kyei K, Serry-Bangura A, Swaray I, Lowe B, et al.**. 2021. Safety and long-term immunogenicity of the two-dose heterologous Ad26. ZEBOV and MVA-BN-Filo Ebola vaccine regimen in adults in Sierra Leone: a combined open-label, non-randomised stage 1, and a randomised, double-blind, controlled stage 2 trial. *The Lancet Infect Dis*.
19. **Benjamini Y, Hochberg Y**. 1995. Controlling the false discovery rate: a practical and powerful approach to multiple testing. *J Royal statistical society: series B (Methodological)* 57 (1):289–300.
20. **Odendahl M, Mei H, Hoyer BF, Jacobi AM, Hansen A, Muehlinghaus G, Berek C, Hiepe F, Manz R, Radbruch A, et al.**. 2005. Generation of migratory antigen-specific plasma blasts and mobilization of resident plasma cells in a secondary immune response. *Blood* 105 (4):1614–1621.
21. **Huang KYA, Li CKF, Clutterbuck E, Chui C, Wilkinson T, Gilbert A, Oxford J, Lambkin-Williams R, Lin TY, McMichael AJ, et al.**. 2014. Virus-specific antibody secreting cell, memory B-cell, and sero-antibody responses in the human influenza challenge model. *The J infectious diseases* 209 (9):1354–1361.
22. **Khodadadi L, Cheng Q, Radbruch A, Hiepe F**. 2019. The maintenance of memory plasma cells. *Front immunology* 10:721.
23. **O'Dempsey T, McArdle T, Ceesay SJ, Secka O, Demba E, Banya W, Francis N, Greenwood BM**. 1996. Meningococcal antibody titres in infants of women immunised with meningococcal polysaccharide vaccine during pregnancy. *Arch Dis Childhood-Fetal Neonatal Ed* 74 (1):F43–F46.
24. **Zeitlin L, Cone RA, Moench TR, Whaley KJ**. 2000. Preventing infectious disease with passive immunization. *Microbes infection* 2 (6):701–708.
25. **Rosenthal KS, Tan MJ**. 2010. *Rapid Review Microbiology and*

- Immunology E-Book. Elsevier Health Sciences.
26. **Brinkhof MW, Mayorga O, Bock J, Heininger U, Herzog C.** 2013. Kinetics of maternally acquired anti-hepatitis A antibodies: prediction of waning based on maternal or cord blood antibody levels. *Vaccine* 31 (11):1490–1495.
 27. **Vilajeliu A, Ferrer L, Munrós J, Goncé A, López M, Costa J, Bayas JM, Group PW, et al.** 2016. Pertussis vaccination during pregnancy: antibody persistence in infants. *Vaccine* 34 (33):3719–3722.
 28. **Voysey M, Pollard AJ, Sadarangani M, Fanshawe TR.** 2017. Prevalence and decay of maternal pneumococcal and meningococcal antibodies: a meta-analysis of type-specific decay rates. *Vaccine* 35 (43):5850–5857.
 29. **Adaken C, Scott JT, Sharma R, Gopal R, Dicks S, Niazi S, Ijaz S, Edwards T, Smith CC, Cole CP, et al.** 2021. Ebola virus antibody decay–stimulation in a high proportion of survivors. *Nature* 590 (7846):468–472.
 30. **McArdle AJ, Turkova A, Cunningham AJ.** 2018. When do coinfections matter? *Curr opinion infectious diseases* 31 (3):209.
 31. **Mahon BE, Simon J, Widdowson MA, Samai M, Rogier E, Legardy-Williams J, Liu K, Schiffer J, Lange J, DeByle C, et al.** 2021. Baseline Asymptomatic Malaria Infection and Immunogenicity of rVSVΔG-ZEBOV-GP Vaccine: The Sierra Leone Trial to Introduce a Vaccine Against Ebola (STRIVE). *The J Infect Dis*.
 32. **Williamson W, Greenwood B.** 1978. Impairment of the immune response to vaccination after acute malaria. *The Lancet* 311 (8078):1328–1329.
 33. **Borkow G, Bentwich Z.** 2008. Chronic parasite infections cause immune changes that could affect successful vaccination. *Trends parasitology* 24 (6):243–245.
 34. **Dzhivhuho GA, Rehrl SA, Ndlovu H, Horsnell WG, Brombacher F, Williamson AL, Chege GK.** 2018. Chronic schistosomiasis suppresses HIV-specific responses to DNA-MVA and MVA-gp140 Env vaccine regimens despite antihelminthic treatment and increases helminth-associated pathology in a mouse model. *PLoS pathogens* 14 (7):e1007182.
 35. **Lynn DJ, Benson SC, Lynn MA, Pulendran B.** 2021. Modulation of immune responses to vaccination by the microbiota: implications and potential mechanisms. *Nat. Rev Immunol* p 1–14.
 36. **Markle J, Fish EN.** 2014. SexX matters in immunity. *Trends immunology* 35 (3):97–104.
 37. **Fischinger S, Boudreau CM, Butler AL, Streeck H, Alter G.** 2019. Sex differences in vaccine-induced humoral immunity. *Semin immunopathology* 41 (2):239–249.
 38. **Pritz T, Lair J, Ban M, Keller M, Weinberger B, Krismer M, Grubeck-Loebenstien B.** 2015. Plasma cell numbers decrease in bone marrow of old patients. *Eur journal immunology* 45 (3):738–746.
 39. **Trembl JF.** 2010. Pim kinases are required for short lived plasma cell responses by murine B cells. PhD thesis. University of Pennsylvania.
 40. **Siegrist CA, Aspinall R.** 2009. B-cell responses to vaccination at the extremes of age. *Nat. Rev Immunol* 9 (3):185–194.
 41. **Milligan ID, Gibani MM, Sewell R, Clutterbuck EA, Campbell D, Plested E, Nuthall E, Voysey M, Silva-Reyes L, McElrath MJ, et al.** 2016. Safety and immunogenicity of novel adenovirus type 26-and modified vaccinia ankara- vectored ebola vaccines: a randomized clinical trial. *Jama* 315 (15):1610–1623.
 42. **Winslow RL, Milligan ID, Voysey M, Luhn K, Shukarev G, Douoguih M, Snape MD.** 2017. Immune responses to novel adenovirus type 26 and modified vaccinia virus Ankara- vectored Ebola vaccines at 1 year. *Jama* 317 (10):1075–1077.
 43. **Mutua G, Anzala O, Luhn K, Robinson C, Bockstal V, Anumendem D, Douoguih M.** 2019. Safety and immunogenicity of a 2-dose heterologous vaccine regimen with Ad26. ZEBOV and MVA-BN-Filo Ebola vaccines: 12-month data from a phase 1 randomized clinical trial in Nairobi, Kenya. *The J infectious diseases* 220 (1):57–67.
 44. **Anywaine Z, Whitworth H, Kaleebu P, Praygod G, Shukarev G, Manno D, Kapiga S, Grosskurth H, Kalluvya S, Bockstal V, et al.** 2019. Safety and immunogenicity of a 2-dose heterologous vaccination regimen with Ad26. ZEBOV and MVA-BN-Filo Ebola vaccines: 12-month data from a phase 1 randomized clinical trial in Uganda and Tanzania. *The J infectious diseases* 220 (1):46–56.
 45. **Cole SR, Chu H, Greenland S.** 2014. Maximum likelihood, profile likelihood, and penalized likelihood: a primer. *Am journal epidemiology* 179 (2):252–260.
 46. **Kuhn E, Lavielle M.** 2005. Maximum likelihood estimation in nonlinear mixed effects models. *Comput statistics & data analysis* 49 (4):1020–1038.
 47. **Delyon B, Lavielle M, Moulines E.** 1999. Convergence of a stochastic approximation version of the EM algorithm. *Ann statistics* p 94–128.
 48. **Pinheiro JC, Bates DM.** 1995. Approximations to the log-likelihood function in the nonlinear mixed-effects model. *J computational Graph Stat* 4 (1):12–35.
 49. **Kuhn E, Lavielle M.** 2004. Coupling a stochastic approximation version of EM with an MCMC procedure. *ESAIM: Probab Stat* 8:115–131.
 50. **Chib S, Greenberg E.** 1995. Understanding the metropolis-hastings algorithm. *The american statistician* 49 (4):327–335.
 51. **Lagarias JC, Reeds JA, Wright MH, Wright PE.** 1998. Convergence properties of the Nelder–Mead simplex method in low dimensions. *SIAM J. on optimization* 9 (1):112–147.
 52. **Kümmel A, Bonate PL, Dingemans J, Krause A.** 2018. Confidence and prediction intervals for pharmacometric models. *CPT: pharmacometrics & systems pharmacology* 7 (6):360–373.
 53. **Genolini C, Falissard B.** 2010. kml: k-means for longitudinal data. *Comput Stat* 25 (2):317–328.
 54. **Genolini C, Alacoque X, Sentenac M, Arnaud C.** 2015. kml and kml3d: R Packages to Cluster Longitudinal Data. *J Stat Softw* 65 (4):1–34. <http://www.jstatsoft.org/v65/i04/>.
 55. **Slifka MK, Antia R, Whitmire JK, Ahmed R.** 1998. Humoral immunity due to long-lived plasma cells. *Immunity* 8 (3):363–372.
 56. **Radbruch A, Muehlinghaus G, Luger EO, Inamine A, Smith KG, Dörner T, Hiepe F.** 2006. Competence and competition: the challenge of becoming a long-lived plasma cell. *Nat Rev Immunol* 6 (10):741–750.
 57. **Hammarlund E, Thomas A, Amanna IJ, Holden LA, Slayden OD, Park B, Gao L, Slifka MK.** 2017. Plasma cell survival in the absence of B cell memory. *Nat communications* 8 (1):1–11.
 58. **Drylewicz J, Commenges D, Thiebaut R.** 2012. Maximum a posteriori estimation in dynamical models of primary HIV infection. *Stat Commun Infect Dis* 4 (1).
 59. **Jonsson EN, Karlsson MO.** 1998. Automated covariate model

- building within NONMEM. *Pharm research* 15 (9):1463–1468.
60. **Ayral G, Si Abdallah JF, Magnard C, Chauvin J.** 2021. A novel method based on unbiased correlations tests for covariate selection in nonlinear mixed effects models: The COSSAC approach. *CPT: pharmacometrics & systems pharmacology* 10 (4):318–329.
 61. **Prague M, Lavielle M.** 2021. SAMBA: a Novel Method for Fast Automatic Model Building in Nonlinear Mixed-Effects Models. *CPT: Pharmacometrics Syst Pharmacol*.
 62. **Picard RR, Cook RD.** 1984. Cross-validation of regression models. *J Am Stat Assoc* 79 (387):575–583.
 63. **Balelli I, Pasin C, Prague M, Crauste F, Van Effelterre T, Bockstal V, Solfrosi L, Thiebaut R.** 2020. A model for establishment, maintenance and reactivation of the immune response after vaccination against Ebola virus. *J theoretical biology* 495:110254.
 64. **Hochberg Y.** 1988. A sharper Bonferroni procedure for multiple tests of significance. *Biometrika* 75 (4):800–802.
 65. **Vanshylla K, Di Cristanziano V, Kleipass F, Dewald F, Schommers P, Gieselmann L, Gruell H, Schlotz M, Ercanoglu MS, Stumpf R, et al..** 2021. Kinetics and correlates of the neutralizing antibody response to SARS-CoV-2 infection in humans. *Cell host & microbe* 29 (6):917–929.
 66. **Zhang K, Ma ZG, Yang L, Kang W, Yin Y, Lau JYN.** 2020. Significant reduction of humoral response to SARS-CoV-2 4 months after the diagnosis of COVID-19. *Precis Clin Med*.
 67. **Schmetzer O, Flörcken A.** 2013. Sex differences in the drug therapy for oncologic diseases. *Sex gender differences pharmacology* p 411–442.
 68. **Klein A, Loewenstein A.** 2016. Therapeutic monoclonal antibodies and fragments: bevacizumab. *Retin Pharmacother* 55:232–245.
 69. **Blanco E, Pérez-Andrés M, Arriba-Méndez S, Contreras-Sanfeliciano T, Criado I, Pelak O, Serra-Caetano A, Romero A, Puig N, Remesal A, et al..** 2018. Age-associated distribution of normal B-cell and plasma cell subsets in peripheral blood. *J Allergy Clin Immunol* 141 (6):2208–2219.
 70. **WHO.** 2018. World malaria report 2018. World Health Organ Geneva.
 71. **Boscardin WJ, Taylor JM, Law N.** 1998. Longitudinal models for AIDS marker data. *Stat Methods Med Res* 7 (1):13–27.
 72. **Hill AL, Rosenbloom DI, Nowak MA, Siliciano RF.** 2018. Insight into treatment of HIV infection from viral dynamics models. *Immunol reviews* 285 (1):9–25.
 73. **Perelson AS, Ribeiro RM.** 2013. Modeling the within-host dynamics of HIV infection. *BMC biology* 11 (1):1–10.
 74. **Davenport MP, Ribeiro RM, Chao DL, Perelson AS.** 2004. Predicting the impact of a nonsterilizing vaccine against human immunodeficiency virus. *J virology* 78 (20):11340–11351.
 75. **Jones LE, Perelson AS.** 2002. Modeling the effects of vaccination on chronically infected HIV-positive patients. *JAIDS-HAGERSTOWN MD- 31* (4):369–377.
 76. **Thiébaud R, Jarne A, Routy JP, Sereti I, Fischl M, Ive P, Speck RF, d'Offizi G, Casari S, Commenges D, et al..** 2016. Repeated cycles of recombinant human interleukin 7 in HIV-infected patients with low CD4 T-cell reconstitution on antiretroviral therapy: results of 2 phase II multicenter studies. *Clin Infect Dis* 62 (9):1178–1185.

6.3 Perspectives

In this paper, we focused on the evaluation of the longevity of the humoral response induced by the two-dose heterologous Ad26.ZEBOV/MVA-BN-Filo vaccine regimen. To this end, we started by evaluating the robustness of the mechanistic ODE-based model developed by Pasin et al. [Pasin, 2018]. Estimated on Phase I data, we used humoral data collected in three Phase II/IIb clinical trials to assess the ability of the model to predict the long-term humoral immune response. Once its good quality of long-term predictions evaluated, the re-estimation of the model using all Phase I and II data allowed us to identify factors of variability of the humoral response. In particular, we showed that age, sex and geographical region have an impact on the magnitude and the durability of the humoral response. Moreover, the use of longer-term data gave us the possibility to update the lower bound of the half-life of long-lived antibody secreting cells.

In this work, we only focused on the longevity of the humoral response, without considering its establishment. In particular, as presented in the article, the mechanistic model used to estimate the dynamics of the humoral response does not integrate any compartment characterizing the stimulation of the immune system, which is only possible due to immunological memory. Accordingly, in our mechanistic model, no anamnestic response can be described. However, Balelli et al. [2020] proposed an extension of the model used in our analysis accounting for both memory B cells and antigens injected via vaccination (see Figure 6.1). By integrating these two compartments and fitting this model to data from the three Phase I trials of the EBOVAC 1 consortium, Balelli et al. had the opportunity to study the establishment of the humoral response following the first and the second vaccination. However, the estimation of this model required memory B cells data.

An interesting extension of this work would be to evaluate the robustness of this model on the Phase II data used in our modeling work. Moreover, in two of the three Phase II trials (EBL2002 and EBL3001), a subgroup of participants were challenged, either after one or two years, with a third dose, corresponding to a booster dose of Ad26.ZEBOV. Using these data, it would be interesting to evaluate the establishment of the humoral response following this third and study the longevity of the induced antibody response. Moreover, this type of work could give the opportunity to quantify whether the second and the third vaccination have a similar effect on the reactivation

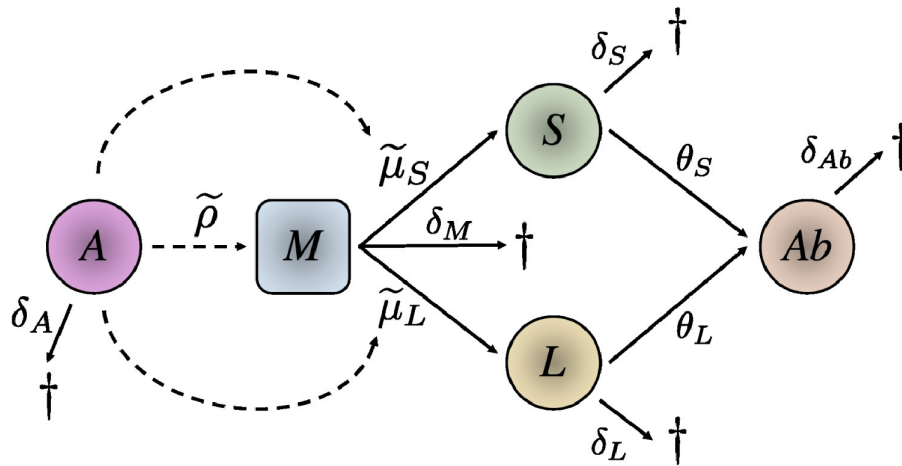


Figure 6.1 – Schematic diagram of the model describing both the establishment and the longevity of the humoral response following the first vaccination. A stands for vaccine antigen, M for memory B cells, S and L for short-lived and long-lived ASCs, respectively and Ab for antibodies. The parameters δ_A , δ_M , δ_L , δ_S and δ_{Ab} are respectively the decay rate of the corresponding cell populations, $\tilde{\rho}$ the generation rate of memory B cells by antigens, $\tilde{\mu}_S$ and $\tilde{\mu}_L$ correspond to the differentiation rate of memory B cells into SL and LL ASCs resp. and θ_L and θ_S represent their antibody production rates.

of the humoral response and whether a longer-term response could be induced by the third dose, in comparison to vaccine strategy with only two doses.

By extension, this type of work would provide us the opportunity to identify the optimal treatment strategy. In particular, the possibility to evaluate a multiple dose strategy would allow to predict the decrease of the humoral response after each dose and consequently to determine the optimal time before a third or a fourth injection. Moreover, the identification of the effect of covariates such as the age, the sex and the geographic region on the dynamics of the humoral response would give the opportunity to optimize the schedule of vaccine infections within specific populations. In addition to the optimization of the time between two vaccinations it could be interesting to work on the identification of the optimal vaccine vector to inject at each vaccination according to the considered population.

In the same vein as the work we performed on Phase II clinical trials, an interesting modelling work, that has been initiated during a Master 1 tutored project I had the opportunity to co-supervise with Dr. Mélanie Prague, is the evaluation of the mechanistic model on the Phase IIb study called PREVAC (NCT02876328), or even PREVAC-UP, assessing the safety and immunogenicity of three vaccine regimen on both adults and children: Ad26.ZEBOV/MVA-BN-Filo, a single dose of rVSV Δ G-ZEBOV-GP and two doses of rVSV Δ G-ZEBOV-GP. Indeed, a coupled estimation of the three vaccine regimen

would allowed to provide additional information on the distinct humoral responses induced by these different vaccine strategy. Moreover, it might be particularly interesting due to the fact that the shape of the response induced by these two vaccine vectors rVSV Δ G-ZEBOV-GP and Ad26.ZEBOV are different. This difference could results from the fact that rVSV Δ G-ZEBOV-GP is a live attenuated vaccine vector while Ad26.ZEBOV is a non-replicant adenovirus.

General discussion and conclusion

In this thesis, we have conducted works to better understand the complex interactions between the virus and the immune system after vaccination and we developed sophisticated mathematical tools to provide answers to major clinical questions concerning vaccine development. There is a great heterogeneity of the challenges addressed in these works:

- ▷ a variety of mathematical and statistical tools used and developed: descriptive analyses, statistical tests, linear and non-linear mixed effects models as well as mechanistic models, requiring an understanding of several estimation methods,
- ▷ the application of these tools in the study of three different infectious diseases: HIV, Ebola and COVID-19, involving an understanding of the mechanisms of action specific to each virus and their interactions with the immune system,
- ▷ the integration of the specificities of the varied epidemiological contexts in which these diseases are studied: chronic disease with a long incubation period for HIV, sporadic disease for Ebola (emerging only during multiple brief and quite localized outbreaks), and disease occurring in the context of a global pandemic still ongoing for SARS-CoV-2,
- ▷ the use of relatively varied data collected in both clinical and preclinical trials conducted in the context of the development of therapeutic vaccines for HIV and prophylactic ones for Ebola and SARS-CoV-2, not to mention the specificities relating to the case of SARS-CoV-2 due to the urgency of the unprecedented situation which has irremediably transcended the field of vaccine development and the study of infectious diseases in general.

Specifically, we demonstrated the power of mathematical modeling in evaluating vaccine efficacy by first proposing a descriptive analysis of data from multiple HIV clinical trials to identify AUC as the optimal primary end point in ATI protocol studies. This analysis allowed us to highlight the dependence that may exist between the choice of endpoint, the choice of ART resumption criteria, and the study design, underscoring the important contribution of dynamic models in optimizing the design of these studies.

Based on the results of this study, we developed a robust parametric statistical test built on linear mixed-effects models to compare AUC between different vaccination arms, taking into account the specificities of clinical trials with ART interruption, such as the presence of monotonic MAR missing data due to study dropouts. Despite the good statistical properties of this test, which has been shown to be more robust than existing nonparametric tests under the conditions of the simulations tested, it is important to consider the limitations of the proposed test due to possible model misspecification and the lack of integration of biological/immunological knowledge in model building. For this reason, we considered extending this test to NLME-ODE models as well as model averaging. Finally, we proposed a strategy for model building in a mechanistic model to identify immunologic correlates of protection that represent a critical concept (and alternative primary endpoint) to ensure effective and rapid vaccine development against SARS-CoV-2 among multiple time-dependent immunologic markers. In particular, application of this concept to three preclinical NHP studies investigating different vaccine strategies allowed us to identify blocking of viral infectivity as the main mechanism of action of these vaccines and the role of antibody neutralizing function in this mechanism of action. As a limitation of this work, we acknowledge that we assume that the immune markers have dynamics independent of the viruses. The addition of antibodies, particularly as compartments of the model, would provide an opportunity to account for the complex, nonlinear, and interdependent interaction between the virus and the immune system. Finally, in a final project, we were able to highlight the interest in mechanistic models to assess the longevity of the humoral response elicited by vaccination. Specifically, we proposed an analysis pipeline based on mixed-effects models to model the dynamics of the humoral response and predict the longevity of the response elicited by a two-dose heterologous vaccination strategy against Ebola virus. In addition, we used the modeling strategy to identify factors for variability in the antibody response. However, the mechanistic model used in this approach is limited to describing the decline in humoral dynamics after the second vaccination. Including new compartments in the model, such as the memory B-cell response, and estimating them in a larger number of patients and with follow-up beyond 2 years would allow us to expand the model's range of action and refine its estimation.

Many development perspectives are conceivable for the continuation of this work, whether in understanding the immunological responses triggered by vaccination or in developing efficient mathematical and statistical tools to optimize the evaluation of preventive and therapeutic vaccines. Moreover, in a more theoretical framework, various extensions of the mathematical tools used in our work can be explored to integrate them into a broader field: e.g. other infectious diseases or more generally in modeling based

on nonlinear mixed effects models.

This work highlights the utility of using sophisticated mathematical tools to analyze data from preclinical and clinical trials and to optimize the evaluation of therapeutic and prophylactic vaccines. As briefly discussed in Chapter 3, with the determination of AUC as the optimal end point in HIV vaccine trials using a descriptive approach, mathematical modeling and more accurate mechanistic models are also powerful tools that could be used to optimize the design of future trials. Unlike clinical trials, which are expensive and time-consuming to design regardless of study duration and limited in the number of designs/strategies tested, simulation tools can provide a tremendous opportunity to optimize study design and thus accelerate vaccine development. These simulated studies are referred to as "in silico" studies. Using data and estimations from previous studies, many designs can be tested and compared. For example, the number and timing of injections, the number of participants that must be recruited to achieve sufficient power to evaluate vaccine efficacy, and even the choice of immunogenicity measurements or determination of optimal endpoints can be explored based on the design. In addition to the clinical trial design tool, mechanistic models can be used directly to make medical decisions in trials based on prior observations and their predictive properties [Villain et al., 2019; Thiébaud et al., 2021; Pasin et al., 2018].

In this work, model averaging was introduced as a relevant mathematical tool and we started to model viral load dynamics in HIV treatment trials to compare vaccine efficacy under certain conditions (e.g., high percentage of missing data due to trial dropouts). When applied to mechanistic models based on ODEs, model averaging has mostly been considered as a way to solve the problem of model selection and misspecification. Although the use of model averaging in ODE models is becoming more widespread in the field of infectious disease modeling, this mathematical approach is still relatively new and feverish in its application. Model selection rather than model averaging methods are still strongly rooted in current biological works. In contrast, model averaging is widely used in finance and economics to model and predict data that contain a large amount of volatile and uncertain information. Similarly, model averaging could be used more widely to integrate and estimate the uncertainty of some model parameters. As shown in this work, mathematical and statistical tools such as profile likelihood analysis or sensitivity analysis are commonly used to estimate the values of parameters that cannot be directly estimated in the overall model. However, this type of approach relies on the concept of model selection. Apart from not taking into account the uncertainty about the value of the fixed parameters, the estimation of the other pa-

parameters of the structural ODE model does not depend on this uncertainty. As suggested by [Lingas et al., 2021], model averaging could be used to integrate information provided by all models estimated with different values of the problematic parameter (e.g., models estimated for the profile likelihood) and consequently bring more information about the parameter uncertainty into the resulting model.

Similarly, model averaging could be considered as an alternative approach to covariate selection [Jackson et al., 2009]. Similar to profile likelihood, covariate selection methods are equivalent to model selection approaches that use criteria such as AIC, BIC, and p-values to select the optimal model. Consequently, uncertainty in the selection of covariates is not considered in the estimation of this model. Moreover, in the case of multiple models with similar abilities to fit the data optimally, biological knowledge is required to select the best model. However, our biological knowledge is not always sufficient to make this possible. Consequently, we could use model averaging to combine all these models and integrate the information and uncertainties provided by all models (e.g., different mechanisms involved in the dynamics of a given outcome). This approach avoids the solution of a "wrongly" chosen model and thus a misspecification of the model.

Finally, an interesting extension of model averaging in modeling infectious disease dynamics is the consideration of time-varying weights. Indeed, this extension is often used in finance to account for structural changes over time [Sun et al., 2021]. Since this approach is usually defined with time-varying functions, it can be considered as an alternative way to define time-varying parameters. In addition, it allows for the addition of another layer/dynamic when modeling the dynamics of infectious diseases. For example, considering models that focus on describing different interactions between the virus and the immune system (e.g., humoral response, T-cell response, B-cell response, cytokines, ...), averaging over time-varying models could allow identifying the predominant mechanisms over time. However, this approach is severely limited by computational time and an extensive work remains to be done to apply this type of analysis to our problems.

In the present work, we have considered only virologic and immunologic markers. However, an interesting extension of the proposed work would be the integration of more diverse data. In particular, the integration of omics data seems relevant in the context of within-host modeling. However, the use of this type of data requires the consideration of methods for dealing with high-dimensional data (e.g., variable selection with ACP, lasso-based methods, ...). With these methods, we have the possibility to identify, for example, genes that might influence the value of certain parameters and

thus the underlying biological mechanisms. Accordingly, these coupled methods offer the possibility to estimate the efficacy of vaccines depending on the genetic heritage or characteristics of a given population. This approach may gradually lead to personalized medicines.

With the same idea of extending mathematical models to other types of data, an interesting perspective is to extend the work done in this paper by including a multiscale framework. Indeed, in this work we have focused exclusively on within-host modeling, specifically through mechanistic modeling and estimation using a population approach. However, in the case of an infectious disease such as COVID -19, we have shown in our editorial paper that within-host modeling can provide information on the transmission of the virus at the population level (inter-host modeling). Consequently, it seems reasonable to link the two scales by modeling both virus-immune dynamics and transmission dynamics. As described by [Dorratoltaj et al. \[2017\]](#), this type of two-scale approach can be useful to integrate and study mechanisms such as coinfection.

Similarly, within-host modeling can be extended by integrating phylogenetic data [[Alizon et al., 2011](#)]. While phylodynamic models have already been coupled with epidemiological models, in particular to derive properties of these models [[Volz et al., 2009](#)], phylodynamic models can also be used in the case of infectious diseases such as COVID-19 to integrate information on viral infectivity/virulence into within-host models. In particular, phylodynamic models can be used to estimate the virulence of the different viral strains and, in the case of SARS-CoV-2, the different variants of concerns (VoC) and integrate this knowledge directly into the estimation of viral infectivity. An estimate of vaccine efficacy could then be derived for each VoC. In other words, a coupled estimate of phylodynamics and mechanistic models within the host could provide an estimate of viral dynamics by integrating intrinsic properties of the virus derived from its genotype.

Bibliography

- Aalen O**, Borgan O, Gjessing H. Survival and event history analysis: a process point of view. Springer Science & Business Media; 2008.
- Aalen OO**. Dynamic modelling and causality. *Scandinavian Actuarial Journal*. 1987; 1987(3-4):177–190.
- Aalen OO**, Frigessi A. What can statistics contribute to a causal understanding? *Scandinavian Journal of Statistics*. 2007; 34(1):155–168.
- Aalen OO**, Røysland K, Gran JM, Ledergerber B. Causality, mediation and time: a dynamic viewpoint. *Journal of the Royal Statistical Society: Series A (Statistics in Society)*. 2012; 175(4):831–861.
- Abbas AK**, Lichtman AH, Pillai S, et al. Cellular and molecular immunology. 9th ed. Philadelphia: Saunders Elsevier; 2017.
- Abu-Raddad LJ**, Chemaitelly H, Ayoub HH, AlMukdad S, Tang P, Hasan MR, Coyle P, Yassine HM, Al-Khatib HA, Smatti MK, et al. Effectiveness of BNT162b2 and mRNA-1273 COVID-19 boosters against SARS-CoV-2 Omicron (B. 1.1. 529) infection in Qatar. *medRxiv*. 2022; .
- Alexandre M**, Prague M, Thiébaud R. Between-group comparison of area under the curve in clinical trials with censored follow-up: Application to HIV therapeutic vaccines. *Statistical Methods in Medical Research*. 2021; 30(9):2130–2147. doi: [10.1177/09622802211023963](https://doi.org/10.1177/09622802211023963).
- Ali K**, Berman G, Zhou H, Deng W, Faughnan V, Coronado-Voges M, Ding B, Dooley J, Girard B, Hillebrand W, et al. Evaluation of mRNA-1273 SARS-CoV-2 vaccine in adolescents. *New England Journal of Medicine*. 2021; 385(24):2241–2251.
- Alizon S**, Luciani F, Regoes RR. Epidemiological and clinical consequences of within-host evolution. *Trends in microbiology*. 2011; 19(1):24–32.
- Anywaine Z**, Barry H, Anzala O, Mutua G, Sirima SB, Eholie S, Kibuuka H, Bétard C, Richert L, Lacabaratz C, et al. Safety and immunogenicity of 2-dose heterologous Ad26. ZEBOV, MVA-BN-Filo Ebola vaccination in children and adolescents in Africa: A randomised, placebo-controlled, multicentre Phase II clinical trial. *PLoS medicine*. 2022; 19(1):e1003865.
- Anywaine Z**, Whitworth H, Kaleebu P, Praygod G, Shukarev G, Manno D, Kapiga S, Grosskurth H, Kalluvya S, Bockstal V, et al. Safety and immunogenicity of a 2-dose heterologous vaccination regimen with Ad26. ZEBOV and MVA-BN-Filo Ebola vaccines: 12-month data from a phase 1 randomized clinical trial in Uganda and Tanzania. *The Journal of infectious diseases*. 2019; 220(1):46–56.
- Arjas E**, Parner J. Causal reasoning from longitudinal data. *Scandinavian Journal of Statistics*. 2004; 31(2):171–187.
- Aruna A**, Mbala P, Minikulu L, Mukadi D, Bulemfu D, Edidi F, Bulabula J, Tshapenda G, Nsio J, Kitenge R, et al. Ebola virus disease outbreak—democratic republic of the Congo, August 2018–November 2019. *Morbidity and Mortality Weekly Report*. 2019; 68(50):1162.

- Asefa A, Asaye Z, Girma A, Hiko D. Predictors of Clinical and Immunological Failure Among Patients on First-Line Antiretroviral Therapy (ART) in Southwest Ethiopia. *HIV/AIDS (Auckland, NZ)*. 2019; 11:377.
- Bachmann N, von Siebenthal C, Vongrad V, Turk T, Neumann K, Beerenwinkel N, Bogojeska J, Fellay J, Roth V, Kok YL, et al. Determinants of HIV-1 reservoir size and long-term dynamics during suppressive ART. *Nature communications*. 2019; 10(1):1–11.
- Baden LR, El Sahly HM, Essink B, Kotloff K, Frey S, Novak R, Diemert D, Spector SA, Roupheal N, Creech CB, et al. Efficacy and safety of the mRNA-1273 SARS-CoV-2 vaccine. *New England Journal of Medicine*. 2020; .
- Badio M, Lhomme E, Kieh M, Beavogui AH, Kennedy SB, Doumbia S, Leigh B, Sow SO, Fusco D, Kirchoff M, et al. Partnership for Research on Ebola VACCination (PREVAC): protocol of a randomized, double-blind, placebo-controlled phase 2 clinical trial evaluating three vaccine strategies against Ebola in healthy volunteers in four West African countries. *Trials*. 2021; 22(1):1–15.
- Balelli I, Pasin C, Prague M, Crauste F, Van Effelterre T, Bockstal V, Solfrosi L, Thiebaut R. A model for establishment, maintenance and reactivation of the immune response after vaccination against Ebola virus. *Journal of Theoretical Biology*. 2020; 495:110254.
- Bar KJ, Sneller MC, Harrison LJ, Justement JS, Overton ET, Petrone ME, Salantes DB, Seamon CA, Scheinfeld B, Kwan RW, et al. Effect of HIV antibody VRC01 on viral rebound after treatment interruption. *New England Journal of Medicine*. 2016; 375(21):2037–2050.
- Barré-Sinoussi F, Chermann JC, Rey F, Nugeyre MT, Chamaret S, Gruest J, Dauguet C, Axler-Blin C, Vézinet-Brun F, Rouzioux C, et al. Isolation of a T-lymphotropic retrovirus from a patient at risk for acquired immune deficiency syndrome (AIDS). *Science*. 1983; 220(4599):868–871.
- Barry H, Mutua G, Kibuuka H, Anywaine Z, Sirima SB, Meda N, Anzala O, Eholie S, Bétard C, Richert L, et al. Safety and immunogenicity of 2-dose heterologous Ad26. ZEBOV, MVA-BN-Filo Ebola vaccination in healthy and HIV-infected adults: A randomised, placebo-controlled Phase II clinical trial in Africa. *PLoS medicine*. 2021; 18(10):e1003813.
- Barton K, Winckelmann A, Palmer S. HIV-1 reservoirs during suppressive therapy. *Trends in microbiology*. 2016; 24(5):345–355.
- Barton RR, Ivey Jr JS. Modifications of the Nelder-Mead simplex method for stochastic simulation response optimization. *Institute of Electrical and Electronics Engineers (IEEE)*; 1991.
- Basta NE and Moodie EMM on behalf of the VIPER (Vaccines, Infectious disease Prevention, and Epidemiology Research) Group COVID-19 Vaccine Development and Approvals Tracker Team (COVID-19 vaccine tracker), COVID-19 Vaccine Development and Approvals Tracker.; 2020. URL <https://covid19.trackvaccines.org/>, (visited on 2022-03-03).
- Bazzoli C, Retout S, Mentré F. Fisher information matrix for nonlinear mixed effects multiple response models: evaluation of the appropriateness of the first order linearization using a pharmacokinetic/pharmacodynamic model. *Statistics in medicine*. 2009; 28(14):1940–1956.
- Beal SL, Sheiner LB. Estimating population kinetics. *Critical reviews in biomedical engineering*. 1982; 8(3):195–222.
- Bebenek K, Abbotts J, Roberts JD, Wilson SH, Kunkel TA. Specificity and mechanism of error-prone replication by human immunodeficiency virus-1 reverse transcriptase. *Journal of Biological Chemistry*. 1989; 264(28):16948–16956.

- Bell ML, King MT, Fairclough DL. Bias in area under the curve for longitudinal clinical trials with missing patient reported outcome data: summary measures versus summary statistics. *Sage Open*. 2014; 4(2):2158244014534858.
- Berndt ER, Hall BH, Hall RE, Hausman JA. Estimation and inference in nonlinear structural models. In: *Annals of Economic and Social Measurement, Volume 3, number 4* NBER; 1974.p. 653–665.
- Best K, Perelson AS. Mathematical modeling of within-host Zika virus dynamics. *Immunological reviews*. 2018; 285(1):81–96.
- Bloom DE, Canning D, Weston M. The value of vaccination. In: *Fighting the Diseases of Poverty* Routledge; 2017.p. 214–238.
- Boscardin WJ, Taylor JM, Law N. Longitudinal models for AIDS marker data. *Statistical Methods in Medical Research*. 1998; 7(1):13–27.
- Boukhebza H, Bellon N, Limacher JM, Inchauspé G. Therapeutic vaccination to treat chronic infectious diseases: current clinical developments using MVA-based vaccines. *Human vaccines & immunotherapeutics*. 2012; 8(12):1746–1757.
- Box GE, Cox DR. An analysis of transformations. *Journal of the Royal Statistical Society: Series B (Methodological)*. 1964; 26(2):211–243.
- Breslow NE. Extra-Poisson variation in log-linear models. *Journal of the Royal Statistical Society: Series C (Applied Statistics)*. 1984; 33(1):38–44.
- Brisse M, Vrba SM, Kirk N, Liang Y, Ly H. Emerging concepts and technologies in vaccine development. *Frontiers in immunology*. 2020; 11:2578.
- Broniatowski M, Celeux G, Diebolt J. Reconnaissance de mélanges de densités par un algorithme d'apprentissage probabiliste. *Data analysis and informatics*. 1983; 3:359–373.
- Buckland ST, Burnham KP, Augustin NH. Model selection: an integral part of inference. *Biometrics*. 1997; p. 603–618.
- Burmer G, Burmer M, Pabuwal V, SARS-CoV-2 and COVID-19 Pathogenesis: A Review. Seattle, WA: LifeSpan BioSciences, Inc; 2020.
- Carroll RJ, Lin X, Wang N. Generalized linear mixed measurement error models. In: *Modelling Longitudinal and Spatially Correlated Data* Springer; 1997.p. 321–330.
- Carroll RJ, Ruppert D, Stefanski LA, Crainiceanu CM. Measurement error in nonlinear models: a modern perspective. Chapman and Hall/CRC; 2006.
- Castro Dopico X, Ols S, Loré K, Karlsson Hedestam GB. Immunity to SARS-CoV-2 induced by infection or vaccination. *Journal of Internal Medicine*. 2022; 291(1):32–50.
- Celeux G, Chauveau D, Diebolt J. On stochastic versions of the EM algorithm. PhD thesis, INRIA; 1995.
- Celeux G, Diebolt J. A random imputation principle: the stochastic EM algorithm. PhD thesis, INRIA; 1988.
- Celeux G, Diebolt J. A stochastic approximation type EM algorithm for the mixture problem. *Stochastics: An International Journal of Probability and Stochastic Processes*. 1992; 41(1-2):119–134.

Bibliography

- Cenderello G, De Maria A.** Discordant responses to cART in HIV-1 patients in the era of high potency antiretroviral drugs: clinical evaluation, classification, management prospects. *Expert review of anti-infective therapy.* 2016; 14(1):29–40.
- Centers for Disease Control and Prevention (CDC),** COVID-19 vaccines WHO EUL issued; 2017. URL <https://www.cdc.gov/sars/about/fs-sars.html>, (last reviewed on 2017-12-06, visited on 2022-03-03).
- Centers for Disease Control and Prevention (CDC),** Middle East Respiratory Syndrome (MERS); 2017. URL <https://www.cdc.gov/coronavirus/mers/about/index.html>, (last reviewed on 2019-08-02, visited on 2022-03-03).
- Centers for Disease Control (CDC),** 2014-2016 Ebola Outbreak in West Africa; 2019. URL <https://www.cdc.gov/vhf/ebola/history/2014-2016-outbreak/index.html>, (last reviewed on 2019-03-08, visited on 2022-03-01).
- Centers for Disease Control (CDC),** Ebola Virus Disease Distribution Map: Cases of Ebola Virus Disease in Africa Since 1976; 2021. URL <https://www.cdc.gov/vhf/ebola/history/distribution-map.html>, (last reviewed on 2021-06-21, visited on 2022-03-01).
- Centers for Disease Control (CDC),** History of Ebola Virus Disease (EVD) Outbreaks; 2021. URL <https://www.cdc.gov/vhf/ebola/history/distribution-map.html>, (last reviewed on 2022-02-22, visited on 2022-03-01).
- Chaplin DD.** Overview of the immune response. *Journal of Allergy and Clinical Immunology.* 2010; 125(2):S3–S23.
- Chen H, Geng Z, Jia J.** Criteria for surrogate end points. *Journal of the Royal Statistical Society: Series B (Statistical Methodology).* 2007; 69(5):919–932.
- Chen RT, Markowitz LE, Albrecht P, Stewart JA, Mofenson LM, Preblud SR, Orenstein WA.** Measles antibody: reevaluation of protective titers. *Journal of infectious diseases.* 1990; 162(5):1036–1042.
- Chia WN, Zhu F, Ong SWX, Young BE, Fong SW, Le Bert N, Tan CW, Tiu C, Zhang J, Tan SY, et al.** Dynamics of SARS-CoV-2 neutralising antibody responses and duration of immunity: a longitudinal study. *The Lancet Microbe.* 2021; .
- Chib S, Greenberg E.** Understanding the metropolis-hastings algorithm. *The american statistician.* 1995; 49(4):327–335.
- Chomont N, El-Far M, Ancuta P, Trautmann L, Procopio FA, Yassine-Diab B, Boucher G, Boulassel MR, Ghattas G, Brenchley JM, et al.** HIV reservoir size and persistence are driven by T cell survival and homeostatic proliferation. *Nature medicine.* 2009; 15(8):893–900.
- Chun TW, Engel D, Berrey MM, Shea T, Corey L, Fauci AS.** Early establishment of a pool of latently infected, resting CD4+ T cells during primary HIV-1 infection. *Proceedings of the National Academy of Sciences.* 1998; 95(15):8869–8873.
- Ciupe SM, Heffernan JM.** In-host modeling. *Infectious Disease Modelling.* 2017; 2(2):188–202.
- Ciupe SM, Ribeiro RM, Perelson AS.** Antibody responses during hepatitis B viral infection. *PLoS computational biology.* 2014; 10(7):e1003730.
- Clapham HE, Quyen TH, Kien DTH, Dorigatti I, Simmons CP, Ferguson NM.** Modelling virus and antibody dynamics during dengue virus infection suggests a role for antibody in virus clearance. *PLoS computational biology.* 2016; 12(5):e1004951.

- Cohn A**, Rodewald LE, Orenstein WA, Schuchat A. 73 - Immunization in the United States. In: Plotkin SA, Orenstein WA, Offit PA, Edwards KM, editors. *Plotkin's Vaccines (Seventh Edition)*, seventh edition ed. Elsevier; 2018.p. 1421–1440.e4. URL <https://www.sciencedirect.com/science/article/pii/B9780323357616000730>, doi: <https://doi.org/10.1016/B978-0-323-35761-6.00073-0>.
- Cohn LB**, Chomont N, Deeks SG. The biology of the HIV-1 latent reservoir and implications for cure strategies. *Cell host & microbe*. 2020; 27(4):519–530.
- Collie S**, Champion J, Moultrie H, Bekker LG, Gray G. Effectiveness of BNT162b2 vaccine against omicron variant in South Africa. *New England Journal of Medicine*. 2021; .
- Coltart CE**, Lindsey B, Ghinai I, Johnson AM, Heymann DL. The Ebola outbreak, 2013–2016: old lessons for new epidemics. *Philosophical Transactions of the Royal Society B: Biological Sciences*. 2017; 372(1721):20160297.
- Commenges D**, Gégout-Petit A. A general dynamical statistical model with causal interpretation. *Journal of the Royal Statistical Society: Series B (Statistical Methodology)*. 2009; 71(3):719–736.
- Commenges D**, Jacqmin-Gadda H, Proust C, Guedj J. A newton-like algorithm for likelihood maximization: The robust-variance scoring algorithm. *arXiv preprint math/0610402*. 2006; .
- Commenges D**, Sayyareh A, Letenneur L, Guedj J, Bar-Hen A. Estimating a difference of Kullback–Leibler risks using a normalized difference of AIC. *The Annals of Applied Statistics*. 2008; 2(3):1123–1142.
- Conway JM**, Ribeiro RM. Modeling the immune response to HIV infection. *Current opinion in systems biology*. 2018; 12:61–69.
- Corbett KS**, Nason MC, Flach B, Gagne M, O’Connell S, Johnston TS, Shah SN, Edara VV, Floyd K, Lai L, et al. Immune correlates of protection by mRNA-1273 vaccine against SARS-CoV-2 in nonhuman primates. *Science*. 2021; 373(6561):eabj0299.
- Corbett KS**, Werner AP, Connell SO, Gagne M, Lai L, Moliva JI, Flynn B, Choi A, Koch M, Foulds KE, et al. mRNA-1273 protects against SARS-CoV-2 beta infection in nonhuman primates. *Nature Immunology*. 2021; 22(10):1306–1315.
- Corey L**, Gilbert PB, Tomaras GD, Haynes BF, Pantaleo G, Fauci AS. Immune correlates of vaccine protection against HIV-1 acquisition. *Science translational medicine*. 2015; 7(310):310rv7–310rv7.
- Cromer D**, Steain M, Reynaldi A, Schlub TE, Wheatley AK, Juno JA, Kent SJ, Triccas JA, Khoury DS, Davenport MP. Neutralising antibody titres as predictors of protection against SARS-CoV-2 variants and the impact of boosting: a meta-analysis. *The Lancet Microbe*. 2022; 3(1):e52–e61.
- Dafni UG**, Tsiatis AA. Evaluating surrogate markers of clinical outcome when measured with error. *Biometrics*. 1998; p. 1445–1462.
- D’Argenio DA**, Wilson CB. A decade of vaccines: Integrating immunology and vaccinology for rational vaccine design. *Immunity*. 2010; 33(4):437–440.
- Davidian M**, Gallant AR. Smooth nonparametric maximum likelihood estimation for population pharmacokinetics, with application to quinidine. *Journal of Pharmacokinetics and Biopharmaceutics*. 1992; 20(5):529–556.
- Davidian M**, Gallant AR. The nonlinear mixed effects model with a smooth random effects density. *Biometrika*. 1993; 80(3):475–488.

Bibliography

- Dawid AP. Causal inference without counterfactuals. *Journal of the American statistical Association*. 2000; 95(450):407–424.
- Delany I, Rappuoli R, De Gregorio E. Vaccines for the 21st century. *EMBO molecular medicine*. 2014; 6(6):708–720.
- Delyon B, Lavielle M, Moulines E. Convergence of a stochastic approximation version of the EM algorithm. *Annals of statistics*. 1999; p. 94–128.
- Dempster AP, Laird NM, Rubin DB. Maximum likelihood from incomplete data via the EM algorithm. *Journal of the Royal Statistical Society: Series B (Methodological)*. 1977; 39(1):1–22.
- Dessie G, Mulugeta H, Wagnaw F, Zegeye A, Kiross D, Negesse A, Aynalem YA, Getaneh T, Ohringer A, Burrowes S. Immunological Treatment Failure Among Adult Patients Receiving Highly Active Antiretroviral Therapy in East Africa: A Systematic Review and Meta-Analysis. *Current Therapeutic Research*. 2021; 94:100621.
- Didelez V. Graphical models for composable finite Markov processes. *Scandinavian Journal of Statistics*. 2007; 34(1):169–185.
- Didelez V. Graphical models for marked point processes based on local independence. *Journal of the Royal Statistical Society: Series B (Statistical Methodology)*. 2008; 70(1):245–264.
- Dietz K, Heesterbeek J. Daniel Bernoulli’s epidemiological model revisited. *Mathematical biosciences*. 2002; 180(1-2):1–21.
- Divine G, Norton HJ, Hunt R, Dienemann J. A review of analysis and sample size calculation considerations for Wilcoxon tests. *Anesthesia & Analgesia*. 2013; 117(3):699–710.
- Dorratoltaj N, Nikin-Beers R, Ciupe SM, Eubank SG, Abbas KM. Multi-scale immunoepidemiological modeling of within-host and between-host HIV dynamics: systematic review of mathematical models. *PeerJ*. 2017; 5:e3877.
- Duval M. Modélisation et estimation de variances hétérogènes dans les modèles non-linéaires mixtes. PhD thesis, Paris, AgroParisTech; 2008.
- Duval M, Robert-Granié C. SAEM-MCMC: some criteria. hal-00189580. 2007; .
- Duval M, Robert-Granié C, Foulley JL. Estimation of heterogeneous variances in nonlinear mixed models via the SAEM-MCMC algorithm with applications to growth curves in poultry. *Journal de la Société Française de Statistique*. 2009; 150(2):65–83.
- D’arc M, Ayouba A, Esteban A, Learn GH, Boué V, Liegeois F, Etienne L, Tagg N, Leendertz FH, Boesch C, et al. Origin of the HIV-1 group O epidemic in western lowland gorillas. *Proceedings of the National Academy of Sciences*. 2015; 112(11):E1343–E1352.
- European Centre for Disease Prevention and Control (ECDC), Geographical distribution of confirmed MERS-CoV cases by reporting country from April 2012 to 31 January 2022; 2022. URL <https://www.ecdc.europa.eu/en/publications-data/geographical-distribution-confirmed-mers-cov-cases-reporting-country-april-2012-0>, (last reviewed on 2022-02-07, visited on 2022-03-03).
- European Medicine Agency (EMA), COVID-19 Vaccine Janssen; 2020. URL <https://www.ema.europa.eu/en/medicines/human/EPAR/covid-19-vaccine-janssen>, (visited on 2022-03-03).
- European Medicine Agency (EMA), EMA recommends first COVID-19 vaccine for authorisation in the EU; 2020. URL <https://www.ema.europa.eu/en/news/ema-recommends-first-covid-19-vaccine-authorisation-eu>, (visited on 2022-03-03).

Bibliography

- European Medicine Agency (EMA), EMA recommends Nuvaxovid for authorisation in the EU ; 2020. URL <https://www.ema.europa.eu/en/news/ema-recommends-nuvaxovid-authorisation-eu>, (visited on 2022-03-03).
- European Medicine Agency (EMA), Spikevax (previously COVID-19 Vaccine Moderna); 2020. URL <https://www.ema.europa.eu/en/medicines/human/EPAR/spikevax>, (visited on 2022-03-03).
- European Medicine Agency (EMA), Vaxzevria (previously COVID-19 Vaccine AstraZeneca) ; 2020. URL <https://www.ema.europa.eu/en/medicines/human/EPAR/vaxzevria-previously-covid-19-vaccine-astrazeneca>, (visited on 2022-03-03).
- European Medicines Agency (EMA), New vaccine for prevention of Ebola virus disease recommended for approval in the European Union; 2020. URL <https://www.ema.europa.eu/en/news/new-vaccine-prevention-ebola-virus-disease-recommended-approval-european-union>, (visited on 2022-03-01).
- Ewer K, Rampling T, Venkatraman N, Bowyer G, Wright D, Lambe T, Imoukhuede EB, Payne R, Fehling SK, Strecker T, Biedenkopf N, Krähling V, Tully CM, Edwards NJ, Bentley EM, Samuel D, Labbé G, Jin J, Gibani M, Minhinnick A, et al. A Monovalent Chimpanzee Adenovirus Ebola Vaccine Boosted with MVA. *New England Journal of Medicine*. 2016; 374(17):1635–1646. URL <https://doi.org/10.1056/NEJMoa1411627>, doi: [10.1056/NEJMoa1411627](https://doi.org/10.1056/NEJMoa1411627), PMID: 25629663.
- Fajnzylber J, Regan J, Coxen K, Corry H, Wong C, Rosenthal A, Worrall D, Giguel F, Piechocka-Trocha A, Atyeo C, et al. SARS-CoV-2 viral load is associated with increased disease severity and mortality. *Nature communications*. 2020; 11(1):1–9.
- Fatehi F, Bingham RJ, Dykeman EC, Stockley PG, Twarock R. Comparing antiviral strategies against COVID-19 via multiscale within-host modelling. *Royal Society Open Science*. 2021; 8(8):210082.
- Feghali CA, Wright TM, et al. Cytokines in acute and chronic inflammation. *Front Biosci*. 1997; 2(1):d12–d26.
- Feldmann H, Sprecher A, Geisbert TW. Ebola. *New England Journal of Medicine*. 2020; 382(19):1832–1842.
- Feng S, Phillips DJ, White T, Sayal H, Aley PK, Bibi S, Dold C, Fuskova M, Gilbert SC, Hirsch I, et al. Correlates of protection against symptomatic and asymptomatic SARS-CoV-2 infection. *Nature medicine*. 2021; 27(11):2032–2040.
- Fiebig EW, Wright DJ, Rawal BD, Garrett PE, Schumacher RT, Peddada L, Heldebrant C, Smith R, Conrad A, Kleinman SH, et al. Dynamics of HIV viremia and antibody seroconversion in plasma donors: implications for diagnosis and staging of primary HIV infection. *Aids*. 2003; 17(13):1871–1879.
- Fine PEM, Mulholland K, Scott JA, Edmunds WJ. 77 - Community Protection. In: Plotkin SA, Orenstein WA, Offit PA, Edwards KM, editors. *Plotkin's Vaccines (Seventh Edition)*, seventh edition ed. Elsevier; 2018.p. 1512–1531.e5. URL <https://www.sciencedirect.com/science/article/pii/B9780323357616000778>, doi: <https://doi.org/10.1016/B978-0-323-35761-6.00077-8>.
- Finzi D, Hermankova M, Pierson T, Carruth LM, Buck C, Chaisson RE, Quinn TC, Chadwick K, Margolick J, Brookmeyer R, et al. Identification of a reservoir for HIV-1 in patients on highly active antiretroviral therapy. *Science*. 1997; 278(5341):1295–1300.
- Fitzmaurice GM. Methods for handling dropouts in longitudinal clinical trials. *Statistica Neerlandica*. 2003; 57(1):75–99.

Bibliography

- Foged C. Subunit vaccines of the future: the need for safe, customized and optimized particulate delivery systems. *Therapeutic delivery*. 2011; 2(8):1057–1077.
- Food and Drug Administration (FDA), Surrogate Endpoint Resources for Drug and Biologic Development; 2018. URL <https://www.fda.gov/drugs/development-resources/surrogate-endpoint-resources-drug-and-biologic-development>, (visited on 2021-12-09).
- Food and drug Administration (FDA), FDA Approves First COVID-19 Vaccine; 2021. URL <https://www.fda.gov/news-events/press-announcements/fda-approves-first-covid-19-vaccine>, (visited on 2022-03-03).
- Food and drug Administration (FDA), Janssen Vaccine EUA and Resources - EUA letter of authorization; 2021. URL <https://www.janssenlabels.com/emergency-use-authorization/Janssen+COVID-19+Vaccine-EUA.pdf>, (visited on 2022-03-03).
- Food and drug Administration (FDA), Pfizer-BioNTech Vaccine EUA and Resources - EUA letter of authorization; 2021. URL <https://www.fda.gov/media/144412/download>, (visited on 2022-03-03).
- Food and drug Administration (FDA), Spikevax and Moderna COVID-19 Vaccine; 2021. URL <https://www.fda.gov/emergency-preparedness-and-response/coronavirus-disease-2019-covid-19/spikevax-and-moderna-covid-19-vaccine>, (visited on 2022-03-03).
- Food and Drug Administration (FDA), The Drug Development Process; 2021. URL <https://www.fda.gov/patients/drug-development-process>, (visited on 2021-12-07).
- Food and drug Administration (FDA), Moderna Vaccine EUA and Resources - EUA letter of authorization; 2022. URL <https://www.fda.gov/media/144636/download>, (visited on 2022-03-03).
- Fosen J, Ferkingstad E, Borgan Ø, Aalen OO. Dynamic path analysis—a new approach to analyzing time-dependent covariates. *Lifetime data analysis*. 2006; 12(2):143–167.
- Frangakis CE, Rubin DB. Principal stratification in causal inference. *Biometrics*. 2002; 58(1):21–29.
- Frenck Jr RW, Klein NP, Kitchin N, Gurtman A, Absalon J, Lockhart S, Perez JL, Walter EB, Senders S, Bailey R, et al. Safety, immunogenicity, and efficacy of the BNT162b2 Covid-19 vaccine in adolescents. *New England Journal of Medicine*. 2021; 385(3):239–250.
- Friedrich BM, Trefry JC, Biggins JE, Hensley LE, Honko AN, Smith DR, Olinger GG. Potential vaccines and post-exposure treatments for filovirus infections. *Viruses*. 2012; 4(9):1619–1650.
- Fuller W. *Measurement error models*, new york: Johnwiley. Fuller-Measurement Error Models 1987. 1987; .
- Gaffen SL, Liu KD. Overview of interleukin-2 function, production and clinical applications. *Cytokine*. 2004; 28(3):109–123.
- Gallo RC, Sarin PS, Gelmann E, Robert-Guroff M, Richardson E, Kalyanaraman V, Mann D, Sidhu GD, Stahl RE, Zolla-Pazner S, et al. Isolation of human T-cell leukemia virus in acquired immune deficiency syndrome (AIDS). *Science*. 1983; 220(4599):865–867.
- Geisbert TW, Bailey M, Hensley L, Asiedu C, Geisbert J, Stanley D, Honko A, Johnson J, Mulangu S, Pau MG, et al. Recombinant adenovirus serotype 26 (Ad26) and Ad35 vaccine vectors bypass immunity to Ad5 and protect nonhuman primates against ebolavirus challenge. *Journal of virology*. 2011; 85(9):4222–4233.

- Germain RN. Vaccines and the future of human immunology. *Immunity*. 2010; 33(4):441–450.
- Geweke J. Bayesian inference in econometric models using Monte Carlo integration. *Econometrica: Journal of the Econometric Society*. 1989; p. 1317–1339.
- Gilbert PB, Fong Y, Carone M. Assessment of immune correlates of protection via controlled vaccine efficacy and controlled risk. arXiv preprint arXiv:210705734. 2021; .
- Gilbert PB, Montefiori DC, McDermott AB, Fong Y, Benkeser D, Deng W, Zhou H, Houchens CR, Martins K, Jayashankar L, et al. Immune correlates analysis of the mRNA-1273 COVID-19 vaccine efficacy clinical trial. *Science*. 2022; 375(6576):43–50.
- Gilbert PB, Qin L, Self SG. Evaluating a surrogate endpoint at three levels, with application to vaccine development. *Statistics in medicine*. 2008; 27(23):4758–4778.
- Gill RD, Robins JM. Causal inference for complex longitudinal data: the continuous case. *Annals of Statistics*. 2001; p. 1785–1811.
- Girard MP, Koff WC. Human immunodeficiency virus vaccines. In: *Plotkin's Vaccines* Elsevier; 2018.p. 400–429.
- Goeijenbier M, Van Kampen J, Reusken C, Koopmans M, Van Gorp E. Ebola virus disease: a review on epidemiology, symptoms, treatment and pathogenesis. *Neth J Med*. 2014; 72(9):442–8.
- Goetz KB, Pfliegerer M, Schneider CK. First-in-human clinical trials with vaccines—what regulators want. *Nature biotechnology*. 2010; 28(9):910–916.
- Goldblatt D, Fiore-Gartland A, Johnson M, Hunt A, Bengt C, Zavadska D, Snipe HD, Brown JS, Workman L, Zar HJ, et al. Towards a population-based threshold of protection for COVID-19 vaccines. *Vaccine*. 2022; 40(2):306–315.
- Goldstein T, Anthony SJ, Gbakima A, Bird BH, Bangura J, Tremeau-Bravard A, Belaganahalli MN, Wells HL, Dhanota JK, Liang E, et al. The discovery of Bombali virus adds further support for bats as hosts of ebolaviruses. *Nature microbiology*. 2018; 3(10):1084–1089.
- Grais RF, Kennedy SB, Mahon BE, Dubey SA, Grant-Klein RJ, Liu K, Hartzel J, Collier BA, Welebob C, Hanson ME, et al. Estimation of the correlates of protection of the rVSVΔG-ZEBOV-GP Zaire ebolavirus vaccine: a post-hoc analysis of data from phase 2/3 clinical trials. *The Lancet Microbe*. 2021; 2(2):e70–e78.
- Granger CW. Investigating causal relations by econometric models and cross-spectral methods. *Econometrica: journal of the Econometric Society*. 1969; p. 424–438.
- Grassly NC, Fraser C. Mathematical models of infectious disease transmission. *Nature Reviews Microbiology*. 2008; 6(6):477–487.
- Green PJ. On use of the EM algorithm for penalized likelihood estimation. *Journal of the Royal Statistical Society: Series B (Methodological)*. 1990; 52(3):443–452.
- Guedj J, Thiébaud R, Commenges D. Maximum likelihood estimation in dynamical models of HIV. *Biometrics*. 2007; 63(4):1198–1206.
- Guideline IHT. General considerations for clinical trials E8. In: *International Conference on Harmonization of Technical Requirements for Registration of Pharmaceuticals for Human Use*; 1997. .
- Gupta RK, Abdul-Jawad S, McCoy LE, Mok HP, Peppia D, Salgado M, Martinez-Picado J, Nijhuis M, Wensing AM, Lee H, et al. HIV-1 remission following CCR5Δ32/Δ32 haematopoietic stem-cell transplantation. *Nature*. 2019; 568(7751):244–248.

- Gustafson P.** Measurement error and misclassification in statistics and epidemiology: impacts and Bayesian adjustments. CRC Press; 2003.
- Hanquet G, Valenciano M, Simondon F, Moren A.** Vaccine effects and impact of vaccination programmes in post-licensure studies. *Vaccine*. 2013; 31(48):5634–5642.
- Hansen BE.** Least squares model averaging. *Econometrica*. 2007; 75(4):1175–1189.
- Hansen CH, Schelde AB, Moustsen-Helms IR, Emborg HD, Krause TG, Mølbak K, Valentiner-Branth P, et al.** Vaccine effectiveness against SARS-CoV-2 infection with the Omicron or Delta variants following a two-dose or booster BNT162b2 or mRNA-1273 vaccination series: A Danish cohort study. *medRxiv*. 2021; .
- Hardenbrook NJ, Zhang P.** A structural view of the SARS-CoV-2 virus and its assembly. *Current opinion in virology*. 2022; 52:123–134.
- Harville DA.** Maximum likelihood approaches to variance component estimation and to related problems. *Journal of the American statistical association*. 1977; 72(358):320–338.
- Hasöksüz M, Kiliç S, Saraç F.** Coronaviruses and sars-cov-2. *Turkish journal of medical sciences*. 2020; 50(SI-1):549–556.
- Hattaf K.** Global stability and Hopf bifurcation of a generalized viral infection model with multi-delays and humoral immunity. *Physica A: Statistical Mechanics and Its Applications*. 2020; 545:123689.
- Hedeker D, Gibbons RD.** A random-effects ordinal regression model for multilevel analysis. *Biometrics*. 1994; p. 933–944.
- Heesterbeek H, Anderson RM, Andreasen V, Bansal S, De Angelis D, Dye C, Eames KT, Edmunds WJ, Frost SD, Funk S, et al.** Modeling infectious disease dynamics in the complex landscape of global health. *Science*. 2015; 347(6227).
- Hemelaar J.** The origin and diversity of the HIV-1 pandemic. *Trends in molecular medicine*. 2012; 18(3):182–192.
- Henderson DA.** Smallpox eradication. *Public health reports*. 1980; 95(5):422.
- Herz A, Bonhoeffer S, Anderson RM, May RM, Nowak MA.** Viral dynamics in vivo: limitations on estimates of intracellular delay and virus decay. *Proceedings of the National Academy of Sciences*. 1996; 93(14):7247–7251.
- Hjort NL, Claeskens G.** Frequentist model average estimators. *Journal of the American Statistical Association*. 2003; 98(464):879–899.
- Ho DD, Neumann AU, Perelson AS, Chen W, Leonard JM, Markowitz M.** Rapid turnover of plasma virions and CD4 lymphocytes in HIV-1 infection. *Nature*. 1995; 373(6510):123–126.
- Hoebe K, Janssen E, Beutler B.** The interface between innate and adaptive immunity. *Nature immunology*. 2004; 5(10):971–974.
- Holland PW.** Statistics and causal inference. *Journal of the American statistical Association*. 1986; 81(396):945–960.
- Honek J.** Preclinical research in drug development. *Medical Writing*. 2017; 26:5–8.
- Hudgens MG, Gilbert PB, Self SG.** Endpoints in vaccine trials. *Statistical methods in medical research*. 2004; 13(2):89–114.

Bibliography

- Hughes JP. Mixed effects models with censored data with application to HIV RNA levels. *Biometrics*. 1999; 55(2):625–629.
- Hughes MD. Analysis and design issues for studies using censored biomarker measurements with an example of viral load measurements in HIV clinical trials. *Statistics in medicine*. 2000; 19(23):3171–3191.
- Hütter G, Nowak D, Mossner M, Ganepola S, Müßig A, Allers K, Schneider T, Hofmann J, Kücherer C, Blau O, et al. Long-term control of HIV by CCR5 Delta32/Delta32 stem-cell transplantation. *New England Journal of Medicine*. 2009; 360(7):692–698.
- Iasonos A, O’Quigley J. Adaptive dose-finding studies: a review of model-guided phase I clinical trials. *Journal of Clinical Oncology*. 2014; 32(23):2505.
- Ibrahim JG, Molenberghs G. Missing data methods in longitudinal studies: a review. *Test*. 2009; 18(1):1–43.
- Ishola D, Manno D, Afolabi MO, Keshinro B, Bockstal V, Rogers B, Owusu-Kyei K, Serry-Bangura A, Swaray I, Lowe B, et al. Safety and long-term immunogenicity of the two-dose heterologous Ad26. ZEBOV and MVA-BN-Filo Ebola vaccine regimen in adults in Sierra Leone: A combined open-label, non-randomised stage 1, and a randomised, double-blind, controlled stage 2 trial. *The Lancet Infectious Diseases*. 2022; 22(1):97–109.
- Iwasaki A, Omer SB. Why and how vaccines work. *Cell*. 2020; 183(2):290–295.
- Iyer SS, Cheng G. Role of interleukin 10 transcriptional regulation in inflammation and autoimmune disease. *Critical Reviews™ in Immunology*. 2012; 32(1).
- Jackson CH, Thompson SG, Sharples LD. Accounting for uncertainty in health economic decision models by using model averaging. *Journal of the Royal Statistical Society: Series A (Statistics in Society)*. 2009; 172(2):383–404.
- Jacqmin-Gadda H, Thiébaud R, Chêne G, Commenges D. Analysis of left-censored longitudinal data with application to viral load in HIV infection. *Biostatistics*. 2000; 1(4):355–368.
- Jain V, Hartogensis W, Bacchetti P, Hunt PW, Hatano H, Sinclair E, Epling L, Lee TH, Busch MP, McCune JM, et al. Antiretroviral therapy initiated within 6 months of HIV infection is associated with lower T-cell activation and smaller HIV reservoir size. *The Journal of infectious diseases*. 2013; 208(8):1202–1211.
- Joffe MM, Greene T. Related causal frameworks for surrogate outcomes. *Biometrics*. 2009; 65(2):530–538.
- Johansen K, Pfeifer D, Salisbury D. 74 - Immunization in Europe. In: Plotkin SA, Orenstein WA, Offit PA, Edwards KM, editors. *Plotkin’s Vaccines (Seventh Edition)*, seventh edition ed. Elsevier; 2018.p. 1441–1465.e7. URL <https://www.sciencedirect.com/science/article/pii/B9780323357616000742>, doi: <https://doi.org/10.1016/B978-0-323-35761-6.00074-2>.
- Johnson J, Johnson & Johnson Announces European Commission Approval for Janssen’s Preventive Ebola Vaccine; 2020. URL <https://www.jnj.com/johnson-johnson-announces-european-commission-approval-for-janssens-preventive-ebola-vaccine> (visited on 2022-03-01).
- Johnson K, Webb P, Lange J, Murphy F, et al. Isolation and partial characterisation of a new virus causing acute haemorrhagic fever in Zaire. *Lancet*. 1977; p. 569–571.
- Joint United Nations Programme on HIV/AIDS (UNAIDS). Fact sheet – World AIDS day 2021. UNAIDS. 2021; URL https://www.unaids.org/sites/default/files/media_asset/UNAIDS_FactSheet_en.pdf, (visited on 2022-01-08).

Bibliography

- Joint United Nations Programme on HIV/AIDS (UNAIDS).** Global AIDS Strategy 2021-2026—End Inequalities; End AIDS. UNAIDS. 2021; URL https://www.unaids.org/sites/default/files/media_asset/global-AIDS-strategy-2021-2026_en.pdf, (visited on 2022-01-08).
- Joint United Nations Programme on HIV/AIDS (UNAIDS).** HIV estimates with uncertainty bounds 1990-Present. UNAIDS. 2021; URL https://www.unaids.org/en/resources/documents/2021/HIV_estimates_with_uncertainty_bounds_1990-present, (visited on 2022-01-08).
- Joint United Nations Programme on HIV/AIDS (UNAIDS).** UNAIDS Board adopts new global AIDS strategy which paves the way to end AIDS by 2030. UNAIDS (Press release). 2021; URL https://www.unaids.org/sites/default/files/20210325_PR_Strategy_en.pdf, (visited on 2022-01-08).
- Joint United Nations Programme on HIV/AIDS (UNAIDS).** UNAIDS data 2021. UNAIDS. 2021; URL https://www.unaids.org/sites/default/files/media_asset/JC3032_AIDS_Data_book_2021_En.pdf, (visited on 2022-01-08).
- Jones RH, Boadi-Boateng F.** Unequally spaced longitudinal data with AR (1) serial correlation. *Biometrics*. 1991; p. 161–175.
- Julg B, Dee L, Ananworanich J, Barouch DH, Bar K, Caskey M, Colby DJ, Dawson L, Dong KL, Dubé K, et al.** Recommendations for analytical antiretroviral treatment interruptions in HIV research trials—report of a consensus meeting. *The Lancet HIV*. 2019; 6(4):e259–e268.
- Kamorudeen RT, Adedokun KA, Olarinmoye AO.** Ebola outbreak in West Africa, 2014–2016: Epidemic timeline, differential diagnoses, determining factors, and lessons for future response. *Journal of Infection and Public Health*. 2020; 13(7):956–962.
- Kardani K, Bolhassani A, Shahbazi S.** Prime-boost vaccine strategy against viral infections: Mechanisms and benefits. *Vaccine*. 2016; 34(4):413–423.
- Kayser V, Ramzan I.** Vaccines and vaccination: history and emerging issues. *Human Vaccines & Immunotherapeutics*. 2021; p. 1–14.
- Kim TK.** T test as a parametric statistic. *Korean journal of anesthesiology*. 2015; 68(6):540.
- Kirchhoff F.** Immune evasion and counteraction of restriction factors by HIV-1 and other primate lentiviruses. *Cell host & microbe*. 2010; 8(1):55–67.
- Kondělková K, Vokurková D, Krejsek J, Borská L, Fiala Z, Ctírad A.** Regulatory T Cells (TREG) and Their Roles in Immune System With Respect to Immunopathological Disorders. *Acta medica (Hradec Kralove)*. 2010; 53(2):73–77.
- Kortepeter MG, Bausch DG, Bray M.** Basic clinical and laboratory features of filoviral hemorrhagic fever. *The Journal of infectious diseases*. 2011; 204(suppl_3):S810–S816.
- Kroon ED, Ananworanich J, Pagliuzza A, Rhodes A, Phanuphak N, Trautmann L, Mitchell JL, Chintanaphol M, Intasan J, Pinyakorn S, et al.** A randomized trial of vorinostat with treatment interruption after initiating antiretroviral therapy during acute HIV-1 infection. *Journal of virus eradication*. 2020; 6(3):100004.
- Kuhn E, Lavielle M.** Coupling a stochastic approximation version of EM with an MCMC procedure. *ESAIM: Probability and Statistics*. 2004; 8:115–131.
- Kuhn E, Lavielle M.** Maximum likelihood estimation in nonlinear mixed effects models. *Computational statistics & data analysis*. 2005; 49(4):1020–1038.

Bibliography

- Kuhn JH**, Amarasinghe GK, Basler CF, Bavari S, Bukreyev A, Chandran K, Crozier I, Dolnik O, Dye JM, Formenty PB, et al. ICTV virus taxonomy profile: Filoviridae. *The Journal of general virology*. 2019; 100(6):911.
- Laird NM**, Ware JH. Random-effects models for longitudinal data. *Biometrics*. 1982; p. 963–974.
- Larijani MS**, Ramezani A, Sadat SM. Updated studies on the development of HIV therapeutic vaccine. *Current HIV research*. 2019; 17(2):75–84.
- Lau JS**, Smith MZ, Lewin SR, McMahon JH. Clinical trials of antiretroviral treatment interruption in HIV-infected individuals. *Aids*. 2019; 33(5):773–791.
- Lavielle M**, Mentré F. Estimation of population pharmacokinetic parameters of saquinavir in HIV patients with the MONOLIX software. *Journal of pharmacokinetics and pharmacodynamics*. 2007; 34(2):229–249.
- Leal L**, Fehér C, Richart V, Torres B, García F. Antiretroviral therapy interruption (ATI) in HIV-1 infected patients participating in therapeutic vaccine trials: surrogate markers of virological response. *Vaccines*. 2020; 8(3):442.
- Lei M**, Baehr C, Del Moral P. Fisher information matrix-based nonlinear system conversion for state estimation. In: *IEEE ICCA 2010* IEEE; 2010. p. 837–841.
- Lenjiso GA**, Endale BS, Bacha YD. Clinical and immunological failure among HIV-positive adults taking first-line antiretroviral therapy in Dire Dawa, eastern Ethiopia. *BMC public health*. 2019; 19(1):1–10.
- Lesaffre E**, Spiessens B. On the effect of the number of quadrature points in a logistic random effects model: an example. *Journal of the Royal Statistical Society: Series C (Applied Statistics)*. 2001; 50(3):325–335.
- Levine RA**, Casella G. Implementations of the Monte Carlo EM algorithm. *Journal of Computational and Graphical Statistics*. 2001; 10(3):422–439.
- Li JZ**, Heisey A, Ahmed H, Wang H, Zheng L, Carrington M, Wrin T, Schooley RT, Lederman MM, Kuritzkes DR, et al. Relationship of HIV reservoir characteristics with immune status and viral rebound kinetics in an HIV therapeutic vaccine study. *AIDS (London, England)*. 2014; 28(18):2649.
- Liang H**, Zou G, Wan AT, Zhang X. Optimal weight choice for frequentist model average estimators. *Journal of the American Statistical Association*. 2011; 106(495):1053–1066.
- Lindstrom MJ**, Bates DM. Newton—Raphson and EM algorithms for linear mixed-effects models for repeated-measures data. *Journal of the American Statistical Association*. 1988; 83(404):1014–1022.
- Lindstrom MJ**, Bates DM. Nonlinear mixed effects models for repeated measures data. *Biometrics*. 1990; p. 673–687.
- Lingas G**, Néant N, Gaymard A, Belhadi D, Peytavin G, Hites M, Staub T, Greil R, Paiva JA, Poissy J, et al. Modeling remdesivir antiviral efficacy in COVID-19 hospitalized patients of the randomized, controlled, open-label DisCoVeRy trial. *medRxiv*. 2021; .
- Little RJ**. Pattern-mixture models for multivariate incomplete data. *Journal of the American Statistical Association*. 1993; 88(421):125–134.
- Little RJ**, Rubin DB. *Statistical analysis with missing data*, vol. 793. John Wiley & Sons; 2019.

Bibliography

- Lodoen MB, Lanier LL.** Natural killer cells as an initial defense against pathogens. *Current opinion in immunology*. 2006; 18(4):391–398.
- Lok J, Gill R, Van Der Vaart A, Robins J.** Estimating the causal effect of a time-varying treatment on time-to-event using structural nested failure time models. *Statistica Neerlandica*. 2004; 58(3):271–295.
- Longet S, Mellors J, Carroll MW, Tipton T.** Ebolavirus: comparison of survivor immunology and animal models in the search for a correlate of protection. *Frontiers in Immunology*. 2021; p. 3871.
- Lotka AJ.** *Elements of physical biology*. Williams & Wilkins; 1925.
- Lu K.** An analytic method for the placebo-based pattern-mixture model. *Statistics in Medicine*. 2014; 33(7):1134–1145.
- Lumley SF, O'Donnell D, Stoesser NE, Matthews PC, Howarth A, Hatch SB, Marsden BD, Cox S, James T, Warren F, et al.** Antibodies to SARS-CoV-2 are associated with protection against reinfection. *MedRxiv*. 2020; .
- Luo R, Zurakowski R.** Resistance risk management in hiv therapy switching with explicit quiescent t-cell modeling. *IFAC Proceedings Volumes*. 2008; 41(2):10325–10330.
- Lyles RH, Lyles CM, Taylor DJ.** Random regression models for human immunodeficiency virus ribonucleic acid data subject to left censoring and informative drop-outs. *Journal of the Royal Statistical Society: Series C (Applied Statistics)*. 2000; 49(4):485–497.
- Lynn HS.** Maximum likelihood inference for left-censored HIV RNA data. *Statistics in medicine*. 2001; 20(1):33–45.
- Mackenzie ML, Donovan C, McArdle B.** Regression spline mixed models: A forestry example. *Journal of agricultural, biological, and environmental statistics*. 2005; 10(4):394–410.
- Mandala VS, McKay MJ, Shcherbakov AA, Dregni AJ, Kolocouris A, Hong M.** Structure and drug binding of the SARS-CoV-2 envelope protein transmembrane domain in lipid bilayers. *Nature structural & molecular biology*. 2020; 27(12):1202–1208.
- Mankarious S, Lee M, Fischer S, Pyun K, Ochs H, Oxelius V, Wedgwood R.** The half-lives of IgG subclasses and specific antibodies in patients with primary immunodeficiency who are receiving intravenously administered immunoglobulin. *The Journal of laboratory and clinical medicine*. 1988; 112(5):634–640.
- Mann JM, Chin J, Piot P, Quinn T.** The international epidemiology of AIDS. *Scientific American*. 1988; 259(4):82–89.
- Market M, Angka L, Martel AB, Bastin D, Olanubi O, Tennakoon G, Boucher DM, Ng J, Ardolino M, Auer RC.** Flattening the COVID-19 curve with natural killer cell based immunotherapies. *Frontiers in Immunology*. 2020; 11:1512.
- Marquardt DW.** An algorithm for least-squares estimation of nonlinear parameters. *Journal of the society for Industrial and Applied Mathematics*. 1963; 11(2):431–441.
- Marzi A, Mire CE.** Current Ebola virus vaccine progress. *BioDrugs*. 2019; 33(1):9–14.
- Matz KM, Marzi A, Feldmann H.** Ebola vaccine trials: progress in vaccine safety and immunogenicity. *Expert review of vaccines*. 2019; 18(12):1229–1242.
- May MT, Gompels M, Delpuch V, Porter K, Orkin C, Kegg S, Hay P, Johnson M, Palfreeman A, Gilson R, et al.** Impact on life expectancy of HIV-1 positive individuals of CD4+ cell count and viral load response to antiretroviral therapy. *AIDS (London, England)*. 2014; 28(8):1193.

- McCullagh P, Nelder JA.** Generalized linear models. Routledge; 2019.
- McMahan K, Yu J, Mercado NB, Loos C, Tostanoski LH, Chandrashekar A, Liu J, Peter L, Atyeo C, Zhu A, et al.** Correlates of protection against SARS-CoV-2 in rhesus macaques. *Nature*. 2021; 590(7847):630–634.
- McMichael AJ, Borrow P, Tomaras GD, Goonetilleke N, Haynes BF.** The immune response during acute HIV-1 infection: clues for vaccine development. *Nature Reviews Immunology*. 2010; 10(1):11–23.
- McNab F, Mayer-Barber K, Sher A, Wack A, O’garra A.** Type I interferons in infectious disease. *Nature Reviews Immunology*. 2015; 15(2):87–103.
- Mentre F, Mallet A, Baccar D.** Optimal design in random-effects regression models. *Biometrika*. 1997; 84(2):429–442.
- Meyer M, Gunn BM, Malherbe DC, Gangavarapu K, Yoshida A, Pietzsch C, Kuzmina NA, Saphire EO, Collins PL, Crowe Jr JE, et al.** Ebola vaccine-induced protection in nonhuman primates correlates with antibody specificity and Fc-mediated effects. *Science translational medicine*. 2021; 13(602):eabg6128.
- Miao H, Teng Z, Kang C, Muhammadhaji A.** Stability analysis of a virus infection model with humoral immunity response and two time delays. *Mathematical Methods in the Applied Sciences*. 2016; 39(12):3434–3449.
- Milligan ID, Gibani MM, Sewell R, Clutterbuck EA, Campbell D, Plested E, Nuthall E, Voysey M, Silva-Reyes L, McElrath MJ, et al.** Safety and immunogenicity of novel adenovirus type 26–and modified vaccinia ankara–vectored ebola vaccines: a randomized clinical trial. *Jama*. 2016; 315(15):1610–1623.
- Moore CM, MaWhinney S, Forster JE, Carlson NE, Allshouse A, Wang X, Routy JP, Conway B, Connick E.** Accounting for dropout reason in longitudinal studies with nonignorable dropout. *Statistical methods in medical research*. 2017; 26(4):1854–1866.
- Moore TJ.** Deadly medicine: Why tens of thousands of patients died in America’s worst drug disaster. *Statistics in Medicine*. 1997; 16:2507–2510.
- Morris CN.** Parametric empirical Bayes inference: theory and applications. *Journal of the American statistical Association*. 1983; 78(381):47–55.
- Mothe B, Climent N, Plana M, Rosàs M, Jiménez JL, Muñoz-Fernández MÁ, Puertas MC, Carrillo J, Gonzalez N, León A, et al.** Safety and immunogenicity of a modified vaccinia Ankara-based HIV-1 vaccine (MVA-B) in HIV-1-infected patients alone or in combination with a drug to reactivate latent HIV-1. *Journal of Antimicrobial Chemotherapy*. 2015; 70(6):1833–1842.
- Murray AJ, Kwon KJ, Farber DL, Siliciano RF.** The latent reservoir for HIV-1: how immunologic memory and clonal expansion contribute to HIV-1 persistence. *The Journal of Immunology*. 2016; 197(2):407–417.
- Mutua G, Anzala O, Luhn K, Robinson C, Bockstal V, Anumendem D, Douoguih M.** Safety and immunogenicity of a 2-dose heterologous vaccine regimen with Ad26, ZEBOV and MVA-BN-Filo Ebola vaccines: 12-month data from a phase 1 randomized clinical trial in Nairobi, Kenya. *The Journal of infectious diseases*. 2019; 220(1):57–67.
- Mutua JM, Perelson AS, Kumar A, Vaidya NK.** Modeling the effects of morphine-altered virus specific antibody responses on HIV/SIV dynamics. *Scientific reports*. 2019; 9(1):1–11.
- Nakai M, Ke W.** Review of the methods for handling missing data in longitudinal data analysis. *International Journal of Mathematical Analysis*. 2011; 5(1):1–13.

- National Institutes of Health (NIH), Guidelines for the Use of Antiretroviral Agents in Adults and Adolescents Living with HIV; 2021. URL <https://clinicalinfo.hiv.gov/en/guidelines/adult-and-adolescent-arv/what-start-initial-combination-regimens-antiretroviral-naive>, (last reviewed on 2021-06-03 and visited on 2022-01-18).
- National Institutes of Health (NIH), The HIV Life Cycle; 2021. URL <https://hivinfo.nih.gov/understanding-hiv/fact-sheets/hiv-life-cycle>, (visited on 2022-01-08).
- Nelder JA, Mead R. A simplex method for function minimization. *The computer journal*. 1965; 7(4):308–313.
- Neyman JS. On the application of probability theory to agricultural experiments. essay on principles. section 9. (translated and edited by dm dabrowska and tp speed, statistical science (1990), 5, 465-480). *Annals of Agricultural Sciences*. 1923; 10:1–51.
- Nychka D. Some properties of adding a smoothing step to the EM algorithm. *Statistics & probability letters*. 1990; 9(2):187–193.
- O'Brien SJ, Hendrickson SL. Host genomic influences on HIV/AIDS. *Genome biology*. 2013; 14(1):1–13.
- Ochoa R. 14 - Pathology Issues in the Design of Toxicology Studies. In: HASCHEK WM, ROUSSEAU CG, WALLIG MA, editors. *Handbook of Toxicologic Pathology (Second Edition)*, second edition ed. San Diego: Academic Press; 2002.p. 307–326. URL <https://www.sciencedirect.com/science/article/pii/B9780123302151500156>, doi: <https://doi.org/10.1016/B978-012330215-1/50015-6>.
- Papanicolaou A. Taylor approximation and the delta method. *April*. 2009; 28:2009.
- Pasin C, Dufour F, Villain L, Zhang H, Thiébaud R. Controlling IL-7 injections in HIV-infected patients. *Bulletin of mathematical biology*. 2018; 80(9):2349–2377.
- Pasin C. Modélisation et optimisation de la réponse à des vaccins et à des interventions immunothérapeutiques: application au virus Ebola et au VIH. PhD thesis, Bordeaux; 2018.
- Pearl J. Direct and Indirect Effects. *Proceedings of the seventeenth conference on uncertainty in artificial intelligence*. 2001; p. 411–420.
- Pearl J. The Foundations of Causal Inference, *Sociological Methodology* (vol 40, pg 75, 2010). *SOCIOLOGICAL METHODOLOGY* 2011, VOL 41. 2011; 41:373–373.
- Pearl J. Causal diagrams for empirical research. *Biometrika*. 1995; 82(4):669–688.
- Pearl J. The foundations of causal inference. *Sociological Methodology*. 2010; 40(1):75–149.
- Pearl J, Robins JM. Probabilistic evaluation of sequential plans from causal models with hidden variables. In: *UAI*, vol. 95 Citeseer; 1995. p. 444–453.
- Pearl J, et al. *Models, reasoning and inference*. Cambridge, UK: CambridgeUniversityPress. 2000; 19.
- Perelson AS, Ke R. Mechanistic Modeling of SARS-CoV-2 and Other Infectious Diseases and the Effects of Therapeutics. *Clinical Pharmacology & Therapeutics*. 2021; 109(4):829–840.
- Perelson AS, Neumann AU, Markowitz M, Leonard JM, Ho DD. HIV-1 dynamics in vivo: virion clearance rate, infected cell life-span, and viral generation time. *Science*. 1996; 271(5255):1582–1586.

Bibliography

- Perry J, Osman S, Wright J, Richard-Greenblatt M, Buchan SA, Sadarangani M, Bolotin S. Does a humoral correlate of protection exist for SARS-CoV-2? A systematic review. medRxiv. 2022;
- Pham HT, Mesplède T. The latest evidence for possible HIV-1 curative strategies. *Drugs in context*. 2018; 7.
- Pinheiro JC. Linear Mixed Effects Models for Longitudinal Data. *Encyclopedia of Biostatistics*. 2005; 4.
- Pinheiro JC, Bates DM. Approximations to the log-likelihood function in the nonlinear mixed-effects model. *Journal of computational and Graphical Statistics*. 1995; 4(1):12–35.
- Place J, Stach J. Efficient numerical integration using gaussian quadrature. *Simulation*. 1999; 73(4):232–237.
- Plantier JC, Leoz M, Dickerson JE, De Oliveira F, Cordonnier F, Lemée V, Damond F, Robertson DL, Simon F. A new human immunodeficiency virus derived from gorillas. *Nature medicine*. 2009; 15(8):871–872.
- Plitnick LM. Global regulatory guidelines for vaccines. In: *Nonclinical development of novel biologics, biosimilars, vaccines and specialty biologics* Elsevier; 2013.p. 225–241.
- Plotkin S. History of vaccination. *Proceedings of the National Academy of Sciences*. 2014; 111(34):12283–12287.
- Plotkin SA. Correlates of protection induced by vaccination. *Clinical and vaccine immunology*. 2010; 17(7):1055–1065.
- Plotkin SA, Gilbert PB. Nomenclature for immune correlates of protection after vaccination. *Clinical Infectious Diseases*. 2012; 54(11):1615–1617.
- Plotkin SA, Plotkin SA. Correlates of vaccine-induced immunity. *Clinical infectious diseases*. 2008; 47(3):401–409.
- Plotkin SL, Plotkin SA. A short history of vaccination. *Vaccines*. 2004; 5:1–16.
- Polack FP, Thomas SJ, Kitchin N, Absalon J, Gurtman A, Lockhart S, Perez JL, Marc GP, Moreira ED, Zerbini C, et al. Safety and efficacy of the BNT162b2 mRNA Covid-19 vaccine. *New England Journal of Medicine*. 2020; .
- Pollard AJ, Launay O, Lelievre JD, Lacabaratz C, Grande S, Goldstein N, Robinson C, Gaddah A, Bockstal V, Wiedemann A, et al. Safety and immunogenicity of a two-dose heterologous Ad26. ZEBOV and MVA-BN-Filo Ebola vaccine regimen in adults in Europe (EBOVAC2): a randomised, observer-blind, participant-blind, placebo-controlled, phase 2 trial. *The Lancet Infectious Diseases*. 2021; 21(4):493–506.
- Prague M, Alexandre M, Thiébaud R, Guedj J. Within-host models of SARS-CoV-2: What can it teach us on the biological factors driving virus pathogenesis and transmission? *Anaesthesia Critical Care & Pain Medicine*. 2022; p. 101055.
- Prague M, Commenges D, Drylewicz J, Thiébaud R. Treatment monitoring of HIV-infected patients based on mechanistic models. *Biometrics*. 2012; 68(3):902–911.
- Prague M, Gerold JM, Balelli I, Pasin C, Li JZ, Barouch DH, Whitney JB, Hill AL. Viral rebound kinetics following single and combination immunotherapy for HIV/SIV. *BioRxiv*. 2019; p. 700401.
- Prentice RL. Covariate measurement errors and parameter estimation in a failure time regression model. *Biometrika*. 1982; 69(2):331–342.

Bibliography

- Prentice RL.** Surrogate endpoints in clinical trials: definition and operational criteria. *Statistics in medicine.* 1989; 8(4):431–440.
- Preston BD.** Error-prone retrotransposition: rime of the ancient mutators. *Proceedings of the National Academy of Sciences of the United States of America.* 1996; 93(15):7427.
- Qazi BS, Tang K, Qazi A.** Recent advances in underlying pathologies provide insight into interleukin-8 expression-mediated inflammation and angiogenesis. *International journal of inflammation.* 2011; 2011.
- Qin L, Gilbert PB, Corey L, McElrath MJ, Self SG.** A framework for assessing immunological correlates of protection in vaccine trials. *The Journal of infectious diseases.* 2007; 196(9):1304–1312.
- Rasmussen TA, Tolstrup M, Brinkmann CR, Olesen R, Erikstrup C, Solomon A, Winkelmann A, Palmer S, Dinarello C, Buzon M, et al.** Panobinostat, a histone deacetylase inhibitor, for latent-virus reactivation in HIV-infected patients on suppressive antiretroviral therapy: a phase 1/2, single group, clinical trial. *The lancet HIV.* 2014; 1(1):e13–e21.
- Retout S, Duffull S, Mentré F.** Development and implementation of the population Fisher information matrix for the evaluation of population pharmacokinetic designs. *Computer methods and Programs in Biomedicine.* 2001; 65(2):141–151.
- Rewar S, Mirdha D.** Transmission of Ebola virus disease: an overview. *Annals of global health.* 2014; 80(6):444–451.
- Richardson TS, Rotnitzky A.** Causal etiology of the research of James M. Robins. *Statistical Science.* 2014; 29(4):459–484.
- Riedel S.** Edward Jenner and the history of smallpox and vaccination. In: *Baylor University Medical Center Proceedings*, vol. 18 Taylor & Francis; 2005. p. 21–25.
- Robins J.** A new approach to causal inference in mortality studies with a sustained exposure period—application to control of the healthy worker survivor effect. *Mathematical modelling.* 1986; 7(9-12):1393–1512.
- Robins J.** A graphical approach to the identification and estimation of causal parameters in mortality studies with sustained exposure periods. *Journal of chronic diseases.* 1987; 40:139S–161S.
- Robins JM.** Marginal structural models. *American Statistical Association.* 1997; .
- Robins JM.** Marginal structural models versus structural nested models as tools for causal inference. In: *Statistical models in epidemiology, the environment, and clinical trials* Springer; 2000.p. 95–133.
- Robins JM, Blevins D, Ritter G, Wulfsohn M.** G-estimation of the effect of prophylaxis therapy for *Pneumocystis carinii* pneumonia on the survival of AIDS patients. *Epidemiology.* 1992; p. 319–336.
- Robins JM, Greenland S.** Identifiability and exchangeability for direct and indirect effects. *Epidemiology.* 1992; p. 143–155.
- Robins JM, Hernán MA.** Estimation of the causal effects of time-varying exposures. *Longitudinal data analysis.* 2009; 553:599.
- Roosendaal R, Solfrosi L, Stieh DJ, Serroyen J, Straetemans R, Dari A, Boulton M, Wegmann F, Rosendahl Huber SK, van der Lubbe JE, et al.** SARS-CoV-2 binding and neutralizing antibody levels after Ad26. COV2. S vaccination predict durable protection in rhesus macaques. *Nature communications.* 2021; 12(1):1–10.

- Rosenbaum PR. The consequences of adjustment for a concomitant variable that has been affected by the treatment. *Journal of the Royal Statistical Society: Series A (General)*. 1984; 147(5):656–666.
- Rougeron V, Feldmann H, Grard G, Becker S, Leroy EM. Ebola and Marburg haemorrhagic fever. *Journal of Clinical Virology*. 2015; 64:111–119. URL <https://www.sciencedirect.com/science/article/pii/S1386653215000281>, doi: <https://doi.org/10.1016/j.jcv.2015.01.014>.
- Rubin DB. Estimating causal effects of treatments in randomized and nonrandomized studies. *Journal of educational Psychology*. 1974; 66(5):688.
- Rubin DB. Inference and missing data. *Biometrika*. 1976; 63(3):581–592.
- Rubin DB. Assignment to treatment group on the basis of a covariate. *Journal of educational Statistics*. 1977; 2(1):1–26.
- Rubin DB. Multiple imputations in sample surveys—a phenomenological Bayesian approach to nonresponse. In: *Proceedings of the survey research methods section of the American Statistical Association*, vol. 1 American Statistical Association; 1978. p. 20–34.
- Rubin DB. Multiple imputation for nonresponse in surveys, vol. 81. John Wiley & Sons; 2004.
- Ruibal P, Oestereich L, Lüdtke A, Becker-Ziaja B, Wozniak DM, Kerber R, Korva M, Cabeza-Cabrerizo M, Bore JA, Koundouno FR, et al. Unique human immune signature of Ebola virus disease in Guinea. *Nature*. 2016; 533(7601):100–104.
- Sadat Larijani M, Sadat SM, Bolhassani A, Ramezani A. A shot at dendritic cell-based vaccine strategy against HIV-1. *Journal of Medical Microbiology and Infectious Diseases*. 2019; 7(4):89–92.
- Sáez-Cirióń A, Bacchus C, Hocqueloux L, Avettand-Fenoel V, Girault I, Lecuroux C, Potard V, Versmisse P, Melard A, Prazuck T, et al. Post-treatment HIV-1 controllers with a long-term virological remission after the interruption of early initiated antiretroviral therapy ANRS VISCONTI Study. *PLoS pathogens*. 2013; 9(3):e1003211.
- Salk JE, Menke Jr WJ, Francis Jr T. A clinical, epidemiological and immunological evaluation of vaccination against epidemic influenza. *American Journal of Epidemiology*. 1945; 42(1):57–93.
- Samson A, Lavielle M, Mentré F. Extension of the SAEM algorithm to left-censored data in nonlinear mixed-effects model: Application to HIV dynamics model. *Computational Statistics & Data Analysis*. 2006; 51(3):1562–1574.
- Sarafianos SG, Marchand B, Das K, Himmel DM, Parniak MA, Hughes SH, Arnold E. Structure and function of HIV-1 reverse transcriptase: molecular mechanisms of polymerization and inhibition. *Journal of molecular biology*. 2009; 385(3):693–713.
- Savic R, Lavielle M. Performance in population models for count data, part II: a new SAEM algorithm. *Journal of Pharmacokinetics and Pharmacodynamics*. 2009; 36(4):367–379.
- Schafer JL. *Analysis of incomplete multivariate data*. CRC press; 1997.
- Schafer JL. Multiple imputation: a primer. *Statistical methods in medical research*. 1999; 8(1):3–15.
- Scheid JF, Horwitz JA, Bar-On Y, Kreider EF, Lu CL, Lorenzi JC, Feldmann A, Braunschweig M, Nogueira L, Oliveira T, et al. HIV-1 antibody 3BNC117 suppresses viral rebound in humans during treatment interruption. *Nature*. 2016; 535(7613):556–560.

Bibliography

- Schoeman D**, Fielding BC. Coronavirus envelope protein: current knowledge. *Virology journal*. 2019; 16(1):1–22.
- Sela M**, Hilleman MR. Therapeutic vaccines: realities of today and hopes for tomorrow. *Proceedings of the National Academy of Sciences*. 2004; 101(suppl 2):14559–14559.
- Servín-Blanco R**, Zamora-Alvarado R, Gevorkian G, Manoutcharian K. Antigenic variability: obstacles on the road to vaccines against traditionally difficult targets. *Human vaccines & immunotherapeutics*. 2016; 12(10):2640–2648.
- Shang J**, Wan Y, Luo C, Ye G, Geng Q, Auerbach A, Li F. Cell entry mechanisms of SARS-CoV-2. *Proceedings of the National Academy of Sciences*. 2020; 117(21):11727–11734.
- Sharma AR**, Lee YH, Nath S, Lee SS. Recent developments and strategies of Ebola virus vaccines. *Current Opinion in Pharmacology*. 2021; 60:46–53.
- Sheiner LB**, Beal SL. Evaluation of methods for estimating population pharmacokinetic parameters. I. Michaelis-Menten model: routine clinical pharmacokinetic data. *Journal of pharmacokinetics and biopharmaceutics*. 1980; 8(6):553–571.
- Shenoy S**. SARS-CoV-2 (COVID-19), viral load and clinical outcomes; lessons learned one year into the pandemic: A systematic review. *World Journal of Critical Care Medicine*. 2021; 10(4):132.
- Shepherd BO**, Chang D, Vasan S, Ake J, Modjarrad K. HIV and SARS-CoV-2: Tracing a Path of Vaccine Research and Development. *Current HIV/AIDS Reports*. 2022; p. 1–8.
- Siettos CI**, Russo L. Mathematical modeling of infectious disease dynamics. *Virulence*. 2013; 4(4):295–306.
- Silverman B**, Jones M, Wilson J, Nychka D. A smoothed EM approach to indirect estimation problems, with particular reference to stereology and emission tomography. *Journal of the Royal Statistical Society: Series B (Methodological)*. 1990; 52(2):271–303.
- Sneller MC**, Justement JS, Gittens KR, Petrone ME, Clarridge KE, Proschan MA, Kwan R, Shi V, Blazkova J, Refsland EW, et al. A randomized controlled safety/efficacy trial of therapeutic vaccination in HIV-infected individuals who initiated antiretroviral therapy early in infection. *Science translational medicine*. 2017; 9(419):eaan8848.
- Sok D**, Burton DR. Recent progress in broadly neutralizing antibodies to HIV. *Nature immunology*. 2018; 19(11):1179–1188.
- Speranza E**, Ruibal P, Port JR, Feng F, Burkhardt L, Grundhoff A, Günther S, Oestereich L, Hiscox JA, Connor JH, et al. T-cell receptor diversity and the control of T-cell homeostasis mark Ebola virus disease survival in humans. *The Journal of infectious diseases*. 2018; 218(suppl_5):S508–S518.
- Spritzler J**, DeGruttola VG, Pei L. Two-sample tests of area-under-the-curve in the presence of missing data. *The international journal of biostatistics*. 2008; 4(1).
- Stanley DA**, Honko AN, Asiedu C, Trefry JC, Lau-Kilby AW, Johnson JC, Hensley L, Ammendola V, Abbate A, Grazioli F, et al. Chimpanzee adenovirus vaccine generates acute and durable protective immunity against ebolavirus challenge. *Nature medicine*. 2014; 20(10):1126–1129.
- Stiratelli R**, Laird N, Ware JH. Random-effects models for serial observations with binary response. *Biometrics*. 1984; p. 961–971.

Bibliography

- Strain MC**, Little SJ, Daar ES, Havlir DV, Günthard HF, Lam RY, Daly OA, Nguyen J, Ignacio CC, Spina CA, et al. Effect of treatment, during primary infection, on establishment and clearance of cellular reservoirs of HIV-1. *The Journal of infectious diseases*. 2005; 191(9):1410–1418.
- Sun Y**, Hong Y, Lee TH, Wang S, Zhang X. Time-varying model averaging. *Journal of Econometrics*. 2021; 222(2):974–992.
- Suschak JJ**, Schmaljohn CS. Vaccines against Ebola virus and Marburg virus: recent advances and promising candidates. *Human Vaccines & Immunotherapeutics*. 2019; 15(10):2359–2377.
- Tapia MD**, Sow SO, Lyke KE, Haidara FC, Diallo F, Doumbia M, Traore A, Coulibaly F, Kodio M, Onwuchekwa U, Szein MB, Wahid R, Campbell JD, Kieny MP, Moorthy V, Imoukhuede EB, Rampling T, Roman F, De Ryck I, Bellamy AR, et al. Use of ChAd3-EBO-Z Ebola virus vaccine in Malian and US adults, and boosting of Malian adults with MVA-BN-Filo: a phase 1, single-blind, randomised trial, a phase 1b, open-label and double-blind, dose-escalation trial, and a nested, randomised, double-blind, placebo-controlled trial. *The Lancet Infectious Diseases*. 2016; 16(1):31–42. URL <https://www.sciencedirect.com/science/article/pii/S147330991500362X>, doi: [https://doi.org/10.1016/S1473-3099\(15\)00362-X](https://doi.org/10.1016/S1473-3099(15)00362-X).
- Thiébaud R**, Jacqmin-Gadda H. Mixed models for longitudinal left-censored repeated measures. *Computer methods and programs in biomedicine*. 2004; 74(3):255–260.
- Thiébaud R**, Jacqmin-Gadda H, Babiker A, Commenges D, Collaboration C. Joint modelling of bivariate longitudinal data with informative dropout and left-censoring, with application to the evolution of CD4+ cell count and HIV RNA viral load in response to treatment of HIV infection. *Statistics in medicine*. 2005; 24(1):65–82.
- Thiébaud R**, Jacqmin-Gadda H, Lepout C, Katlama C, Costagliola D, Le Moing V, Morlat P, Chêne G, Group AS, et al. Bivariate longitudinal model for the analysis of the evolution of HIV RNA and CD4 cell count in HIV infection taking into account left censoring of HIV RNA measures. *Journal of biopharmaceutical statistics*. 2003; 13(2):271–282.
- Thiébaud R**, Villain L, Pasin C, Commenges D. Modelling the Response to Interleukin-7 Therapy in HIV-Infected Patients. In: *Mathematical, Computational and Experimental T Cell Immunology* Springer; 2021.p. 95–107.
- Tierney L**, Kadane JB. Accurate approximations for posterior moments and marginal densities. *Journal of the american statistical association*. 1986; 81(393):82–86.
- Tosteson TD**, Buonaccorsi JP, Demidenko E. Covariate measurement error and the estimation of random effect parameters in a mixed model for longitudinal data. *Statistics in Medicine*. 1998; 17(17):1959–1971.
- Tseng HF**, Ackerson BK, Luo Y, Sy LS, Talarico C, Tian Y, Bruxvoort K, Tupert JE, Florea A, Ku JH, et al. Effectiveness of mRNA-1273 against SARS-CoV-2 omicron and delta variants. *medRxiv*. 2022; .
- Ueckert S**, Mentré F. A new method for evaluation of the Fisher information matrix for discrete mixed effect models using Monte Carlo sampling and adaptive Gaussian quadrature. *Computational Statistics & Data Analysis*. 2017; 111:203–219.
- Ulmer JB**, Mason PW, Geall A, Mandl CW. RNA-based vaccines. *Vaccine*. 2012; 30(30):4414–4418.
- Vaghi C**, Rodallec A, Fanciullino R, Ciccolini J, Mochel JP, Mastri M, Poignard C, Ebos JM, Benzekry S. Population modeling of tumor growth curves and the reduced Gompertz model improve prediction of the age of experimental tumors. *PLoS computational biology*. 2020; 16(2):e1007178.

Bibliography

- Van Dyk DA, Tang R. The one-step-late PXEM algorithm. *Statistics and Computing*. 2003; 13(2):137–152.
- VanderWeele TJ. Surrogate measures and consistent surrogates. *Biometrics*. 2013; 69(3):561–565.
- Vanhamel J, Bruggemans A, Debyser Z. Establishment of latent HIV-1 reservoirs: what do we really know? *Journal of virus eradication*. 2019; 5(1):3–9.
- Vardi Y, Ying Z, Zhang CH. Two-sample tests for growth curves under dependent right censoring. *Biometrika*. 2001; 88(4):949–960.
- Vella S, Schwartländer B, Sow SP, Eholie SP, Murphy RL. The history of antiretroviral therapy and of its implementation in resource-limited areas of the world. *Aids*. 2012; 26(10):1231–1241.
- Venkatraman N, Ndiaye BP, Bowyer G, Wade D, Sridhar S, Wright D, Powlson J, Ndiaye I, Dièye S, Thompson C, et al. Safety and immunogenicity of a heterologous prime-boost Ebola virus vaccine regimen in healthy adults in the United Kingdom and Senegal. *The Journal of infectious diseases*. 2019; 219(8):1187–1197.
- Venkatraman N, Silman D, Folegatti PM, Hill AV. Vaccines against Ebola virus. *Vaccine*. 2018; 36(36):5454–5459.
- Vidal SJ, Collier ARY, Yu J, McMahan K, Tostanoski LH, Ventura JD, Aid M, Peter L, Jacob-Dolan C, Anioke T, et al. Correlates of neutralization against SARS-CoV-2 variants of concern by early pandemic sera. *Journal of Virology*. 2021; 95(14):e00404–21.
- Villain L, Commenges D, Pasin C, Prague M, Thiébaud R. Adaptive protocols based on predictions from a mechanistic model of the effect of IL7 on CD4 counts. *Statistics in medicine*. 2019; 38(2):221–235.
- Visseaux B, Damond F, Matheron S, Descamps D, Charpentier C. Hiv-2 molecular epidemiology. *Infection, Genetics and Evolution*. 2016; 46:233–240.
- Volterra V. Variations and fluctuations of the number of individuals in animal species living together. *Animal ecology*. 1926; p. 409–448.
- Volz EM, Kosakovsky Pond SL, Ward MJ, Leigh Brown AJ, Frost SD. Phylodynamics of infectious disease epidemics. *Genetics*. 2009; 183(4):1421–1430.
- Vonesh E, Chinchilli VM. Linear and nonlinear models for the analysis of repeated measurements. CRC press; 1996.
- Vonesh EF, Carter RL. Mixed-effects nonlinear regression for unbalanced repeated measures. *Biometrics*. 1992; p. 1–17.
- Vonesh EF, Wang H, Nie L, Majumdar D. Conditional second-order generalized estimating equations for generalized linear and nonlinear mixed-effects models. *Journal of the American Statistical Association*. 2002; 97(457):271–283.
- V'kovski P, Kratzel A, Steiner S, Stalder H, Thiel V. Coronavirus biology and replication: implications for SARS-CoV-2. *Nature Reviews Microbiology*. 2021; 19(3):155–170.
- Walter EB, Talaat KR, Sabharwal C, Gurtman A, Lockhart S, Paulsen GC, Barnett ED, Muñoz FM, Maldonado Y, Pahud BA, et al. Evaluation of the BNT162b2 Covid-19 vaccine in children 5 to 11 years of age. *New England Journal of Medicine*. 2022; 386(1):35–46.
- Wand MP. Smoothing and mixed models. *Computational statistics*. 2003; 18(2):223–249.

Bibliography

- Wang MY, Zhao R, Gao LJ, Gao XF, Wang DP, Cao JM. SARS-CoV-2: structure, biology, and structure-based therapeutics development. *Frontiers in cellular and infection microbiology*. 2020; p. 724.
- Wang N, Davidian M. A note on covariate measurement error in nonlinear mixed effects models. *Biometrika*. 1996; 83(4):801–812.
- Wang S, Zou D. Global stability of in-host viral models with humoral immunity and intracellular delays. *Applied Mathematical Modelling*. 2012; 36(3):1313–1322.
- Wang T, Hu Z, Liao F. Stability and Hopf bifurcation for a virus infection model with delayed humoral immunity response. *Journal of Mathematical Analysis and Applications*. 2014; 411(1):63–74.
- Wang W, Gindi G. Noise analysis of MAP-EM algorithms for emission tomography. *Physics in Medicine & Biology*. 1997; 42(11):2215.
- Wei GC, Tanner MA. A Monte Carlo implementation of the EM algorithm and the poor man's data augmentation algorithms. *Journal of the American statistical Association*. 1990; 85(411):699–704.
- Wei X, Ghosh SK, Taylor ME, Johnson VA, Emini EA, Deutsch P, Lifson JD, Bonhoeffer S, Nowak MA, Hahn BH, et al. Viral dynamics in human immunodeficiency virus type 1 infection. *Nature*. 1995; 373(6510):117–122.
- Weinberg GA, Szilagyi PG. Vaccine epidemiology: efficacy, effectiveness, and the translational research roadmap. *The Journal of infectious diseases*. 2010; 201(11):1607–1610.
- Welham SJ, Cullis BR, Kenward MG, Thompson R. A comparison of mixed model splines for curve fitting. *Australian & New Zealand Journal of Statistics*. 2007; 49(1):1–23.
- Wexler D, Bertelsen KM. A brief survey of first-in-human studies. *The Journal of Clinical Pharmacology*. 2011; 51(7):988–993.
- Williams DA. Extra-binomial variation in logistic linear models. *Journal of the Royal Statistical Society: Series C (Applied Statistics)*. 1982; 31(2):144–148.
- Winslow RL, Milligan ID, Voysey M, Luhn K, Shukarev G, Douoguih M, Snape MD. Immune responses to novel adenovirus type 26 and modified vaccinia virus Ankara–vectored Ebola vaccines at 1 year. *Jama*. 2017; 317(10):1075–1077.
- Wolfinger R. Laplace's approximation for nonlinear mixed models. *Biometrika*. 1993; 80(4):791–795.
- Wong JK, Hezareh M, Gunthard HF, Havlir DV, Ignacio CC, Spina CA, Richman DD. Recovery of replication-competent HIV despite prolonged suppression of plasma viremia. *Science*. 1997; 278(5341):1291–1295.
- World Health Organization and International Programme on Chemical Safety (WHO), Biomarkers in risk assessment : validity and validation. World Health Organization; 2001.
- World Health Organization (WHO), Severe Acute Respiratory Syndrome (SARS); 2003. URL https://www.who.int/health-topics/severe-acute-respiratory-syndrome#tab=tab_1, (visited on 2022-03-03).
- World Health Organization (WHO), WHO guidelines on clinical evaluation of vaccines. Regulatory expectations. 2001; 2007. URL https://www.who.int/biologicals/publications/clinical_guidelines_ecbs_2001.pdf?ua=1, (visited on 2021-12-08).

Bibliography

- World Health Organization (WHO), What's new in treatment monitoring: viral load and CD4 testing; 2017. URL <https://apps.who.int/iris/bitstream/handle/10665/255891/WHO-HIV-2017.22-eng.pdf>, (visited on 2022-01-24).
- World Health Organization (WHO), Middle East respiratory syndrome coronavirus (MERS-CoV); 2019. URL [https://www.who.int/news-room/fact-sheets/detail/middle-east-respiratory-syndrome-coronavirus-\(mers-cov\)](https://www.who.int/news-room/fact-sheets/detail/middle-east-respiratory-syndrome-coronavirus-(mers-cov)), (last reviewed on 2019-08-11, visited on 2022-03-03).
- World Health Organization (WHO), R&D Blueprint and COVID-19; 2019. URL <https://www.who.int/teams/blueprint/covid-19>, (visited on 2022-03-03).
- World Health Organization (WHO), 10th Ebola outbreak in the Democratic Republic of the Congo declared over; vigilance against flare-ups and support for survivors must continue; 2020. URL <https://www.who.int/news/item/25-06-2020-10th-ebola-outbreak-in-the-democratic-republic-of-the-congo-declared-over-vi>, (visited on 2022-03-01).
- World Health Organization (WHO), Ebola virus disease: Vaccines; 2020. URL <https://www.who.int/news-room/questions-and-answers/item/ebola-vaccines>, (visited on 2022-03-01).
- World Health Organization (WHO), Emergency use listing procedure; 2020. URL [https://www.who.int/publications/m/item/emergency-use-listing-procedure#:~:text=Emergency%20Use%20Listing%20\(EUL\)%20procedure,Ebola%20outbreak%20of%202014%2D2016](https://www.who.int/publications/m/item/emergency-use-listing-procedure#:~:text=Emergency%20Use%20Listing%20(EUL)%20procedure,Ebola%20outbreak%20of%202014%2D2016), (visited on 2022-03-03).
- World Health Organization (WHO), WHO Director-General's opening remarks at the media briefing on COVID-19 - 11 March 2020; 2020. URL <https://www.who.int/director-general/speeches/detail/who-director-general-s-opening-remarks-at-the-media-briefing-on-covid-19---11-march-2020>, (visited on 2022-03-03).
- World Health Organization (WHO), Classification of Omicron (B.1.1.529): SARS-CoV-2 Variant of Concern; 2021. URL [https://www.who.int/news/item/26-11-2021-classification-of-omicron-\(b.1.1.529\)-sars-cov-2-variant-of-concern](https://www.who.int/news/item/26-11-2021-classification-of-omicron-(b.1.1.529)-sars-cov-2-variant-of-concern), (visited on 2022-03-03).
- World Health Organization (WHO), Ebola outbreak 2021- North Kivu - Overview; 2021. URL <https://www.who.int/emergencies/situations/ebola-2021-north-kivu>, (visited on 2022-03-01).
- World Health Organization (WHO), Ebola virus disease fact sheet; 2021. URL <http://www.who.int/mediacentre/factsheets/fs103/en/>, (visited on 2021-03-01).
- World Health Organization (WHO), Vaccine efficacy, effectiveness and protection; 2021. URL <https://www.who.int/news-room/feature-stories/detail/vaccine-efficacy-effectiveness-and-protection>, (visited on 2021-12-08).
- World Health Organization (WHO), COVID-19 vaccines WHO EUL issued; 2022. URL <https://extranet.who.int/pqweb/vaccines/vaccinescovid-19-vaccine-eul-issued>, (visited on 2022-03-01).
- World Health Organization (WHO), WHO Coronavirus (COVID-19) Dashboard; 2022. URL <https://covid19.who.int/>, (visited on 2022-03-03).
- Wouters OJ, Shadlen KC, Salcher-Konrad M, Pollard AJ, Larson HJ, Teerawattananon Y, Jit M. Challenges in ensuring global access to COVID-19 vaccines: production, affordability, allocation, and deployment. *The Lancet*. 2021; 397(10278):1023–1034.

Bibliography

- Wright B. Chapter 2 - Clinical Trial Phases. In: Shamley D, Wright B, editors. *A Comprehensive and Practical Guide to Clinical Trials* Academic Press; 2017.p. 11–15. URL <https://www.sciencedirect.com/science/article/pii/B978012804729300002X>, doi: <https://doi.org/10.1016/B978-0-12-804729-3.00002-X>.
- Wright S. Correlation and Causation. *JouMal of. Agricultural Research*. 1921; .
- Wu H, Wu L. A multiple imputation method for missing covariates in non-linear mixed-effects models with application to HIV dynamics. *Statistics in medicine*. 2001; 20(12):1755–1769.
- Wu L. *Mixed effects models for complex data*. CRC press; 2009.
- Wu YC, Chen CS, Chan YJ. The outbreak of COVID-19: An overview. *Journal of the Chinese medical association*. 2020; 83(3):217.
- Xiao Y, Miao H, Tang S, Wu H. Modeling antiretroviral drug responses for HIV-1 infected patients using differential equation models. *Advanced drug delivery reviews*. 2013; 65(7):940–953.
- Xu X, Sneppen K. The timing of natural killer cell response in coronavirus infection: a concise model perspective. *bioRxiv*. 2021; .
- Yang Y. Adaptive regression by mixing. *Journal of the American Statistical Association*. 2001; 96(454):574–588.
- Yu F, Yan L, Wang N, Yang S, Wang L, Tang Y, Gao G, Wang S, Ma C, Xie R, et al. Quantitative detection and viral load analysis of SARS-CoV-2 in infected patients. *Clinical Infectious Diseases*. 2020; 71(15):793–798.
- Yu J, Tostanoski LH, Peter L, Mercado NB, McMahan K, Mahrokhian SH, Nkolola JP, Liu J, Li Z, Chandrashekar A, et al. DNA vaccine protection against SARS-CoV-2 in rhesus macaques. *Science*. 2020; 369(6505):806–811.
- Zarnitsyna VI, Gianlupi JF, Hagar A, Sego T, Glazier JA. Advancing therapies for viral infections using mechanistic computational models of the dynamic interplay between the virus and host immune response. *Current opinion in virology*. 2021; 50:103–109.
- Zhang X, Zou G, Liang H. Model averaging and weight choice in linear mixed-effects models. *Biometrika*. 2014; 101(1):205–218.
- Zhang Y, Tang LV. Overview of targets and potential drugs of SARS-CoV-2 according to the viral replication. *Journal of Proteome Research*. 2020; 20(1):49–59.
- Zheng H, Yin C, Hoang T, He RL, Yang J, Yau SST. Ebolavirus classification based on natural vectors. *DNA and cell biology*. 2015; 34(6):418–428.
- Zheng L, Tierney C, Bosch RJ. Analytical Treatment Interruption in HIV Trials: Statistical and Study Design Considerations. *Current HIV/AIDS Reports*. 2021; 18(5):475–482.
- Zhou P, Yang XL, Wang XG, Hu B, Zhang L, Zhang W, Si HR, Zhu Y, Li B, Huang CL, et al. A pneumonia outbreak associated with a new coronavirus of probable bat origin. *nature*. 2020; 579(7798):270–273.
- Zhu F, Althaus T, Tan CW, Costantini A, Chia WN, Chau NVV, Mattiuzzo G, Rose NJ, Voiglio E, Wang LF, et al. WHO international standard for SARS-CoV-2 antibodies to determine markers of protection. *The Lancet Microbe*. 2022; 3(2):e81–e82.
- Zurawski G, de Vries JE. Interleukin 13, an interleukin 4-like cytokine that acts on monocytes and B cells, but not on T cells. *Immunology today*. 1994; 15(1):19–26.

Appendices

Appendix A

Supplementary Materials - *Between-group comparison of area under the curve in clinical trials with censored follow-up: Application to HIV therapeutic vaccines*

Between-group comparison of area under the curve in clinical trials with censored follow-up: Application to HIV therapeutic vaccines

Marie Alexandre, Mélanie Prague, Rodolphe Thiébaud

Supplementary information

List of Appendices

A	Definition of the nAUC by Lagrange interpolation method	2
B	Definition of the nAUC by Spline interpolation method	7
C	Robustness of the test of equality of nAUC, 20 and 100 patients by group	13
D	Robustness of the test of equality of nAUC estimated with Lagrange and Spline interpolation methods	14
E	Study of the residuals of the mixed effects models applied on real clinical data	17
F	Study of the sample size	19

List of Tables in Appendices

Table C.1	Comparison of the robustness of the test of equality of nAUC - Trapezoid interpolation method - 20 patients by group	13
Table C.2	Comparison of the robustness of the test of equality of nAUC - Trapezoidal interpolation method - 100 patients by group	13
Table D.1	Comparison of the robustness of the test of equality of nAUC - Lagrange interpolation method - 20 patients by group	14
Table D.2	Comparison of the robustness of the test of equality of nAUC - Lagrange interpolation method - 50 patients by group	14
Table D.3	Comparison of the robustness of the test of equality of nAUC - Lagrange interpolation method - 100 patients by group	15
Table D.4	Comparison of the robustness of the test of equality of nAUC - Spline interpolation method - 20 patients by group	15
Table D.5	Comparison of the robustness of the test of equality of nAUC - Spline interpolation method - 50 patients by group	16
Table D.6	Comparison of the robustness of the test of equality of nAUC - Spline interpolation method - 100 patients by group	16

List of Figures in Appendices

Figure E.1	Study of the residuals of the MEM fitting real clinical data	18
Figure F.1	Study of Type-I Error and Power as function of Sample size	19

A Definition of the nAUC by Lagrange interpolation method

We consider a dataset labelled $\mathcal{D} = \{(t_j, y_j) | j = 1, \dots, m\}$ where y_j is defined as the value of the response y at the j th time point. Our objective is to approximate the area under the response curve on the interval $[t_1, t_m]$.

A.1 General description of the method

The Lagrange method is an interpolation method used to approximate polynomial functions. This method consists on an approximation of the functional value y (e.g. HIV RNA load curve) by a polynomial function of degree P , between two adjacent points (t_{j-1}, y_{j-1}) and (t_j, y_j) . For the sake of simplicity, we chose cubic polynomial functions as approximation fixing $P = 3$. However, equivalent method can be derived for higher values of P . We note $\tilde{y}_j: [t_{j-1}, t_j] \rightarrow \mathbb{R}$, the function approximating y on the interval $[t_{j-1}, t_j]$, with $(a_j, b_j, c_j, d_j)^T$ the vector of the $P + 1$ polynomial coefficients. By definition, \tilde{y}_j can be written

$$\tilde{y}_j(t) = a_j + b_j t + c_j t^2 + d_j t^3 \quad \forall t \in [t_{j-1}, t_j], \quad \forall j \in \{3, \dots, m-1\} \quad [\text{A.1}]$$

To estimate the vector of polynomial coefficients, this equation is fitted to the four $(P + 1)$ nearest data points (t_{j-2}, y_{j-2}) , (t_{j-1}, y_{j-1}) , (t_j, y_j) and (t_{j+1}, y_{j+1}) . As developed below, the use of the Lagrange multiplier formulas enables to estimate the four coefficients a_j, b_j, c_j and d_j . Once these coefficients estimated, the area under the approximation curve on the interval $[t_{j-1}, t_j]$ can be calculated by integrating [A.1] on its interval of definition.

$$\begin{aligned} \text{AUC}|_{[t_{j-1}, t_j]} &= \int_{t_{j-1}}^{t_j} \tilde{y}_j(t) dt \\ &= a_j(t_j - t_{j-1}) + \frac{b_j}{2}(t_j^2 - t_{j-1}^2) + \frac{c_j}{3}(t_j^3 - t_{j-1}^3) + \frac{d_j}{4}(t_j^4 - t_{j-1}^4) \end{aligned} \quad [\text{A.2}]$$

This method requiring four points of interpolation, whose one located before and another after the interval of interest, the calculation appears impossible on the first and last intervals $[t_1, t_2]$ and $[t_{m-1}, t_m]$. To overcome this problem, we reduce by one the degree of the polynomial function such as the response of interest y is then approximated by quadratic polynomial function ($P = 2$), using only three $(P + 1)$ points of interpolation instead of four.

$$\tilde{y}_j(t) = a_j + b_j t + c_j t^2 \quad \text{for} \quad \begin{cases} t_1 \leq t \leq t_2 \\ t_{m-1} \leq t \leq t_m \end{cases}$$

On the first interval $[t_1, t_2]_{(j=2)}$, the three chosen points are $(t_{j-1}, y_{j-1}) = (t_1, y_1)$, $(t_j, y_j) = (t_2, y_2)$ and $(t_{j+1}, y_{j+1}) = (t_3, y_3)$ whereas those points are $(t_{j-2}, y_{j-2}) = (t_{m-2}, y_{m-2})$, $(t_{j-1}, y_{j-1}) = (t_{m-1}, y_{m-1})$ and $(t_j, y_j) = (t_m, y_m)$ on the last one, $[t_{m-1}, t_m]_{(j=m)}$. As mentioned above, the three coefficients a_j, b_j and c_j are calculated through Lagrange multiplier formulas, leading to local approximations of AUC [A.3] and [A.4].

$$\text{AUC}|_{[t_1, t_2]} = a_2(t_2 - t_1) + \frac{b_2}{2}(t_2^2 - t_1^2) + \frac{c_2}{3}(t_2^3 - t_1^3) \quad [\text{A.3}]$$

$$\text{AUC}|_{[t_{m-1}, t_m]} = a_m(t_m - t_{m-1}) + \frac{b_m}{2}(t_m^2 - t_{m-1}^2) + \frac{c_m}{3}(t_m^3 - t_{m-1}^3) \quad [\text{A.4}]$$

Once all locals AUC estimated, the global AUC is defined as the cumulative area written:

$$\text{AUC} = \sum_{j=2}^m \text{AUC}|_{[t_{j-1}, t_j]} \quad [\text{A.5}]$$

A.2 Estimation of polynomial coefficients by Lagrange multiplier

The objective is to estimate the coefficients of the interpolation functions \tilde{y}_j , $\forall j \in \{2, \dots, m\}$. To this end, we use the Lagrange polynomials which enables to change the expressions of our polynomials \tilde{y} by definition of interpolation points. By noting $\{(x_0, y_0), \dots, (x_P, y_P)\}$ the set of distinct interpolation points on $[t_{j-1}, t_j]$, the polynomial function \tilde{y}_j can be rewrite in the Lagrange form as

$$\tilde{y}_j(t) = \sum_{p=0}^P y_p \underbrace{\left(\prod_{\substack{l=0 \\ l \neq p}}^P \frac{t - x_l}{x_p - x_l} \right)}_{\mathcal{L}_p(t)}$$

where \mathcal{L}_p is called the Lagrange polynomials. Thereafter, we decided to split our $m - 1$ intervals into two subsets due to the fact that the number of interpolation points used to approximate the function y impacts the shape of the Lagrange multiplier formulas. Consequently, we build the subset of *external intervals* corresponding to the first and last intervals within $P + 1 = 3$ interpolation points are involved. All the other intervals are gathered inside the second subset called *intern intervals*.

On internal intervals (cubic interpolations)

As previously mentioned, four interpolation points are used in each internal interval, therefore $P = 3$. By applying the Lagrange form⁵¹, we rewrite \tilde{y}_j as

$$\begin{aligned} \tilde{y}_j(t) &= y_0 \times \mathcal{L}_0(t) + y_1 \times \mathcal{L}_1(t) + y_2 \times \mathcal{L}_2(t) + y_3 \times \mathcal{L}_3(t) \\ &= y_0 \left(\frac{t - x_1}{x_0 - x_1} \times \frac{t - x_2}{x_0 - x_2} \times \frac{t - x_3}{x_0 - x_3} \right) + y_1 \left(\frac{t - x_0}{x_1 - x_0} \times \frac{t - x_2}{x_1 - x_2} \times \frac{t - x_3}{x_1 - x_3} \right) \\ &\quad + y_2 \left(\frac{t - x_0}{x_2 - x_0} \times \frac{t - x_1}{x_2 - x_1} \times \frac{t - x_3}{x_2 - x_3} \right) + y_3 \left(\frac{t - x_0}{x_3 - x_0} \times \frac{t - x_1}{x_3 - x_1} \times \frac{t - x_2}{x_3 - x_2} \right) \end{aligned}$$

To find the expressions of the polynomial coefficients, we bring together the terms linked to the same power of t and, by comparison with [A.1], we identify the four coefficients. Moreover, by replacing (x_0, y_0) by (t_{j-2}, y_{j-2}) , (x_1, y_1) by (t_{j-1}, y_{j-1}) , (x_2, y_2) by (t_j, y_j) and (x_3, y_3) by (t_{j+1}, y_{j+1}) , the definitions of the four coefficients a_j , b_j , c_j and d_j involved become

$$\begin{aligned} a_j &= - \sum_{p=0}^{P=3} \frac{y_{j-2+p} \prod_{\substack{l=0 \\ l \neq p}}^{P=3} t_{j-2+l}}{\prod_{\substack{l=0 \\ l \neq p}}^{P=3} (t_{j-2+p} - t_{j-2+l})} & b_j &= \sum_{p=0}^{P=3} \frac{y_{j-2+p} \sum_{\substack{l_1=0 \\ l_1 \neq p}}^{P-1=2} \sum_{\substack{l_2=l_1+1 \\ l_2 \neq p}}^{P=3} t_{j-2+l_1} \cdot t_{j-2+l_2}}{\prod_{\substack{l=0 \\ l \neq p}}^{P=3} (t_{j-2+p} - t_{j-2+l})} \\ c_j &= - \sum_{p=0}^{P=3} \frac{y_{j-2+p} \sum_{\substack{l=0 \\ l \neq p}}^{P=3} t_{j-2+l}}{\prod_{\substack{l=0 \\ l \neq p}}^{P=3} (t_{j-2+p} - t_{j-2+l})} & d_j &= \sum_{p=0}^{P=3} \frac{y_{j-2+p}}{\prod_{\substack{l=0 \\ l \neq p}}^{P=3} (t_{j-2+p} - t_{j-2+l})} \end{aligned}$$

On external intervals (quadratic interpolations)

Inside the two external intervals, only three interpolation points are considered ($P = 2$). By applying the same steps than in internal intervals, and replacing (x_0, y_0) by (t_1, y_1) , (x_1, y_1) by (t_2, y_2) and (x_2, y_2) by (t_3, y_3) on $[t_1, t_2]$ and (x_0, y_0) by (t_{m-2}, y_{m-2}) , (t_1, y_1) by (t_{m-1}, y_{m-1}) and (x_2, y_2) by (t_m, y_m) on $[t_{m-1}, t_m]$, we identify the six polynomial coefficients by

$$\begin{aligned}
a_2 &= \sum_{p=0}^{P=2} \frac{y_{1+p} \prod_{\substack{l=0 \\ l \neq p}}^{P=2} t_{1+l}}{\prod_{\substack{l=0 \\ l \neq p}}^{P=2} (t_{1+p} - t_{1+l})} & a_m &= \sum_{p=0}^{P=2} \frac{y_{m-2+p} \prod_{\substack{l=0 \\ l \neq p}}^{P=2} t_{m-2+l}}{\prod_{\substack{l=0 \\ l \neq p}}^{P=2} (t_{m-2+p} - t_{m-2+l})} \\
b_2 &= - \sum_{p=0}^{P=2} \frac{y_{1+p} \sum_{\substack{l=0 \\ l \neq p}}^{P=2} t_{1+l}}{\prod_{\substack{l=0 \\ l \neq p}}^{P=2} (t_{1+p} - t_{1+l})} & b_m &= - \sum_{p=0}^{P=2} \frac{y_{m-2+p} \sum_{\substack{l=0 \\ l \neq p}}^{P=2} t_{m-2+l}}{\prod_{\substack{l=0 \\ l \neq p}}^{P=2} (t_{m-2+p} - t_{m-2+l})} \\
c_2 &= \sum_{p=0}^{P=2} \frac{y_{1+p}}{\prod_{\substack{l=0 \\ l \neq p}}^{P=2} (t_{1+p} - t_{1+l})} & c_m &= \sum_{p=0}^{P=2} \frac{y_{m-2+p}}{\prod_{\substack{l=0 \\ l \neq p}}^{P=2} (t_{m-2+p} - t_{m-2+l})}
\end{aligned}$$

A.3 Literal expression of AUC

Based on the definitions of the polynomial coefficients established above and on equations [A.2], the literal expression of the AUC on intervals $[t_{j-1}, t_j]$, for $j = 3, \dots, m-1$, is given by

$$\begin{aligned}
\text{AUC}|_{[t_{j-1}, t_j]} &= a_j(t_j - t_{j-1}) + \frac{b_j}{2}(t_j^2 - t_{j-1}^2) + \frac{c_j}{3}(t_j^3 - t_{j-1}^3) + \frac{d_j}{4}(t_j^4 - t_{j-1}^4) \\
&= \sum_{p=0}^{P=3} \frac{y_{j-2+p}}{\prod_{\substack{l=0 \\ l \neq p}}^{P=3} (t_{j-2+p} - t_{j-2+l})} \times C_{[j][p]} \tag{A.6}
\end{aligned}$$

where

$$\begin{aligned}
C_{[j][p]} &= \left[- (t_j - t_{j-1}) \left(\prod_{\substack{l=0 \\ l \neq p}}^{P=3} t_{j-2+l} \right) + \frac{(t_j^2 - t_{j-1}^2)}{2} \left(\sum_{\substack{l_1=0 \\ l_1 \neq p}}^{P-1=2} \sum_{\substack{l_2=l_1+1 \\ l_2 \neq p}}^{P=3} t_{j-2+l_1} t_{j-2+l_2} \right) \right. \\
&\quad \left. - \frac{(t_j^3 - t_{j-1}^3)}{3} \left(\sum_{\substack{l=0 \\ l \neq p}}^{P=3} t_{j-2+l} \right) + \frac{(t_j^4 - t_{j-1}^4)}{4} \right]
\end{aligned}$$

Similarly, using equations [A.3] and [A.4], we found the following expressions on intervals $[t_1, t_2]$ and $[t_{m-1}, t_m]$.

$$\text{AUC}|_{[t_1, t_2]} = \sum_{p=0}^{P=2} \frac{y_{1+p}}{\prod_{\substack{l=0 \\ l \neq p}}^{P=2} (t_{1+p} - t_{1+l})} \times C_{[2][p]} \tag{A.7}$$

$$\text{AUC}|_{[t_{m-1}, t_m]} = \sum_{p=0}^{P=2} \frac{y_{m-2+p}}{\prod_{\substack{l=0 \\ l \neq p}}^{P=2} (t_{m-2+p} - t_{m-2+l})} \times C_{[m][p]} \tag{A.8}$$

where

$$C_{[2][p]} = (t_2 - t_1) \left(\prod_{\substack{l=0 \\ l \neq p}}^{P=2} t_{1+l} \right) - \frac{(t_2^2 - t_1^2)}{2} \left(\sum_{\substack{l=0 \\ l \neq p}}^{P=2} t_{1+l} \right) + \frac{(t_2^3 - t_1^3)}{3}$$

$$C_{[m][p]} = (t_m - t_{m-1}) \left(\prod_{\substack{l=0 \\ l \neq p}}^{P=2} t_{m-2+l} \right) - \frac{(t_m^2 - t_{m-1}^2)}{2} \left(\sum_{\substack{l=0 \\ l \neq p}}^{P=2} t_{m-2+l} \right) + \frac{(t_m^3 - t_{m-1}^3)}{3}$$

By combining [A.5], [A.6], [A.7] and [A.8], we obtain the expression of the global AUC.

$$\text{AUC} = \sum_{p=0}^{P=2} \left[\frac{y_{1+p} \times C_{[2][p]}}{\prod_{\substack{l=0 \\ l \neq p}}^{P=2} (t_{1+p} - t_{1+l})} + \frac{y_{m-2+p} \times C_{[m][p]}}{\prod_{\substack{l=0 \\ l \neq p}}^{P=2} (t_{m-2+p} - t_{m-2+l})} \right] + \sum_{j=3}^{m-1} \sum_{p=0}^{P=3} \frac{y_{j-2+p} \times C_{[j][p]}}{\prod_{\substack{l=0 \\ l \neq p}}^{P=3} (t_{j-2+p} - t_{j-2+l})} \quad [\text{A.9}]$$

A.4 Application of the Lagrange method with our mixed effect model

In this subsection, we develop literal expressions of the approximated normalized AUC in each group g and its variance, $\widehat{n\text{AUC}}_g$ and $\text{Var}(\widehat{n\text{AUC}}_g)$ respectively. We are also interested in the difference of nAUC between two given vaccine arms g and \tilde{g} labelled $\Delta \widehat{n\text{AUC}}_{g-\tilde{g}}$ as well as the resulting expression of its variance, $\text{Var}(\Delta \widehat{n\text{AUC}}_{g-\tilde{g}})$. As mentioned in the main body of the article, we note $Y_{i,j,g}$ the outcome of the subject i belonging to the group of treatment g at its j th time point $t_{i,j,g}$, where $i \in \{1, \dots, N\}$, $j \in \{1, \dots, m_i\}$ and $g \in \{1, \dots, G\}$. The outcome of interest Y is described by the linear mixed effects model given by

$$Y_{i,j,g_i} = f_0(t_{i,j,g_i}) + \sum_{g=1}^G \mathbb{1}_{[g_i=g]} \times F_g(t_{i,j,g}) + h_i(t_{i,j,g_i}) + \varepsilon_{ij}$$

where the function f_0 represents the non group-specific terms, the functions F_g are linear combinations of time-depending and group specific functions labelled f_g such as $F_g(t_{i,j,g}) = \sum_{k=1}^{K_g} \beta_k^g f_g^k(t_{i,j,g})$ and h_i are time-dependent functions describing inter-individual variability. Because, only f_0 and F_g functions are involved in literal expressions of interest, any further information are given to specify random effects. For sake of simplicity, we fixed the f_0 as global intercept, $f_0(t_{i,j,g}) = \gamma_0$. Consequently, the model can be re-write as

$$Y_{i,j,g_i} = \gamma_0 + \sum_{g=1}^G \mathbb{1}_{[g=g_i]} \times \sum_{k=1}^{K_g} \beta_k^g f_g^k(t_{i,j,g}) + h_i(t_{i,j,g_i}) + \varepsilon_{ij}$$

Based on this definition, the expected value of the estimation of Y in the g th group at the j th time point, $\widehat{\mu}_{j,g}$, is defined as

$$\widehat{\mu}_{j,g} = \widehat{\gamma}_0 + \sum_{k=1}^{K_g} \widehat{\beta}_k^g f_g^k(t_{j,g}) \quad [\text{A.10}]$$

where $\widehat{\gamma}_0$ and $\widehat{\beta}^g = (\widehat{\beta}_1^g, \dots, \widehat{\beta}_{K_g}^g)^T$ are maximum likelihood estimates of the fixed parameters of the MEM.

Literal expression of nAUC and its variance

The literal expression of the estimated nAUC in group g is obtained by replacing the outcome y_j in Equation [A.9] by [A.10] and dividing the resulting expression by the time of follow up T_g (as described in the main article). After rearranging the equation, it follows

$$\widehat{n\text{AUC}}_g = \widehat{\gamma}_0 K_{\gamma_0}^g + \sum_{k=1}^{K_g} \widehat{\beta}_k^g C_{k,g} \quad [\text{A.11}]$$

where

$$\left\{ \begin{array}{l} K_{\gamma_0}^g = \frac{1}{T_g} \left(\frac{P=2}{p=0} \left[\frac{C_{[2][p]}^g}{(t_{1+p,g} - t_{1+l,g})} + \frac{C_{[m_g][p]}^g}{(t_{m_g-2+p,g} - t_{m_g-2+l,g})} \right] + \frac{m_g-1}{j=3} \frac{P=3}{p=0} \frac{C_{[j][p]}^g}{(t_{j-2+p,g} - t_{j-2+l,g})} \right) \\ C_{k_g} = \frac{1}{T_g} \left(\frac{P=2}{p=0} \left[\frac{f_g^k(t_{1+p,g}) C_{[2][p]}^g}{(t_{1+p,g} - t_{1+l,g})} + \frac{f_g^k(t_{m_g-2+p,g}) C_{[m_g][p]}^g}{(t_{m_g-2+p,g} - t_{m_g-2+l,g})} \right] + \frac{m_g-1}{j=3} \frac{P=3}{p=0} \frac{f_g^k(t_{j-2+p,g}) C_{[j][p]}^g}{(t_{j-2+p,g} - t_{j-2+l,g})} \right) \\ C_{[2][p]}^g = (t_{2,g} - t_{1,g}) \frac{P=2}{l=0} t_{1+l,g} - \frac{(t_{2,g}^2 - t_{1,g}^2)}{2} \frac{P=2}{l \neq p} t_{1+l,g} + \frac{(t_{2,g}^3 - t_{1,g}^3)}{3} \\ C_{[m_g][p]}^g = (t_{m_g,g} - t_{m_g-1,g}) \frac{P=2}{l=0} t_{m_g-2+l,g} - \frac{(t_{m_g,g}^2 - t_{m_g-1,g}^2)}{2} \frac{P=2}{l \neq p} t_{m_g-2+l,g} + \frac{(t_{m_g,g}^3 - t_{m_g-1,g}^3)}{3} \\ C_{[j][p]}^g = -(t_{j,g} - t_{j-1,g}) \frac{P=3}{l=0} t_{j-2+l,g} + \frac{(t_{j,g}^2 - t_{j-1,g}^2)}{2} \frac{P-1=2}{l_1=0} \frac{P=3}{l_2=l_1+1} t_{j-2+l_1,g} \cdot t_{j-2+l_2,g} \\ - \frac{(t_{j,g}^3 - t_{j-1,g}^3)}{3} \frac{P=3}{l \neq p} t_{j-2+l,g} + \frac{(t_{j,g}^4 - t_{j-1,g}^4)}{4} \frac{l_1=0}{l_1 \neq p} \frac{l_2=l_1+1}{l_2 \neq p} \end{array} \right.$$

Based on the expression [A.11], we defined its variance

$$\begin{aligned} \text{Var}(\widehat{nAUC}_g) &= (K_{\gamma_0}^g)^2 \text{Var}(\widehat{\gamma}_0) + \sum_{k=1}^{K_g} (C_{k_g})^2 \text{Var}(\widehat{\beta}_k^g) + 2 \sum_{k=1}^{K_g-1} \sum_{\tilde{k}=k+1}^{K_g} C_{k_g} C_{\tilde{k}_g} \text{Cov}(\widehat{\beta}_k^g, \widehat{\beta}_{\tilde{k}}^g) \\ &\quad + 2K_{\gamma_0}^g \sum_{k=1}^{K_g} C_{k_g} \text{Cov}(\widehat{\gamma}_0, \widehat{\beta}_k^g) \end{aligned}$$

Literal expression of $\Delta nAUC$ and its variance

To define the literal expression of $\Delta nAUC$ identified as the difference of $nAUC$ between the groups of treatment g and \tilde{g} , we found the following equation

$$\Delta \widehat{nAUC}_{g-\tilde{g}} = \widehat{nAUC}_{\tilde{g}} - \widehat{nAUC}_g = \widehat{\gamma}_0 (K_{\gamma_0}^{\tilde{g}} - K_{\gamma_0}^g) + \sum_{k=1}^{K_{\tilde{g}}} \widehat{\beta}_k^{\tilde{g}} C_{k_{\tilde{g}}} - \sum_{k=1}^{K_g} \widehat{\beta}_k^g C_{k_g}$$

It follows the expression of its variance

$$\begin{aligned} \text{Var}(\Delta \widehat{nAUC}_{g-\tilde{g}}) &= (K_{\gamma_0}^{\tilde{g}} - K_{\gamma_0}^g)^2 \text{Var}(\widehat{\gamma}_0) + \sum_{k=1}^{K_{\tilde{g}}} (C_{k_{\tilde{g}}})^2 \text{Var}(\widehat{\beta}_k^{\tilde{g}}) + 2 \sum_{k=1}^{K_{\tilde{g}}-1} \sum_{\tilde{k}=k+1}^{K_{\tilde{g}}} C_{k_{\tilde{g}}} C_{\tilde{k}_{\tilde{g}}} \text{Cov}(\widehat{\beta}_k^{\tilde{g}}, \widehat{\beta}_{\tilde{k}}^{\tilde{g}}) \\ &\quad + \sum_{k=1}^{K_g} (C_{k_g})^2 \text{Var}(\widehat{\beta}_k^g) + 2 \sum_{k=1}^{K_g-1} \sum_{\tilde{k}=k+1}^{K_g} C_{k_g} C_{\tilde{k}_g} \text{Cov}(\widehat{\beta}_k^g, \widehat{\beta}_{\tilde{k}}^g) - 2 \sum_{k_0=1}^{K_{\tilde{g}}} \sum_{k_1=1}^{K_g} C_{k_0_{\tilde{g}}} C_{k_1_g} \text{Cov}(\widehat{\beta}_{k_0}^{\tilde{g}}, \widehat{\beta}_{k_1}^g) \\ &\quad + 2 (K_{\gamma_0}^{\tilde{g}} - K_{\gamma_0}^g) \left[\sum_{k=1}^{K_{\tilde{g}}} C_{k_{\tilde{g}}} \text{Cov}(\widehat{\gamma}_0, \widehat{\beta}_k^{\tilde{g}}) - \sum_{k=1}^{K_g} C_{k_g} \text{Cov}(\widehat{\gamma}_0, \widehat{\beta}_k^g) \right] \end{aligned} \quad [A.12]$$

Matrix formulation

As mentioned in the main article, the linear mixed effects model can be re-expressed through matrix formulation involving the re-expression of the $nAUC$. Similar to the trapezoid method, the $nAUC$ can be written as linear combination of the response

of interest at each time point, as

$$n\text{AUC}_g = \frac{1}{T_g} \sum_{j=1}^{m_g} \omega_{j,g}^{lagr} \bar{Y}_{j,g} = \frac{1}{T_g} \boldsymbol{\omega}_g^{lagr T} \bar{\mathbf{Y}}_g$$

where $\boldsymbol{\omega}_g^{lagr} = (\omega_{1,g}^{lagr}, \dots, \omega_{m_g,g}^{lagr})^T$, $\bar{\mathbf{Y}}_g = (\bar{Y}_{1,g}, \dots, \bar{Y}_{m_g,g})^T$, with

$$w_{j,g}^{lagr} = \begin{cases} \frac{C_{[2][j-1],g}}{P=2} + \sum_{p=3}^3 \frac{C_{[j-1+p][3-p],g}}{(j-1) \prod_{\substack{l=0, \\ l \neq (j-1)}} (t_{j,g} - t_{j-3+p+l,g})}, & j \in \{1, 2, 3\} \\ \frac{C_{[m_g][j-(m_g-2)],g}}{P=2} + \sum_{p=0}^{m_g-j} \frac{C_{[j-1+p][3-p],g}}{P=3 \prod_{\substack{l=0, \\ l \neq (3-p)}} (t_{j,g} - t_{j-3+p+l,g})}, & j \in \{m_g-2, m_g-1, m_g\} \\ \sum_{p=0}^3 \frac{C_{[j-1+p][3-p],g}}{P=3 \prod_{\substack{l=0, \\ l \neq (3-p)}} (t_{j,g} - t_{j-3+p+l,g})}, & \text{otherwise} \end{cases}$$

B Definition of the nAUC by Spline interpolation method

We consider a dataset labelled $\mathcal{D} = \{(t_j, y_j) | j = 1, \dots, m\}$ where y_j is defined as the value of the response y at the j th time point. Our objective is to approximate the area under the response curve on the interval $[t_1, t_m]$.

B.1 General description of the method

The spline method is an interpolation method providing approximation of smooth functions such as splines curves or polynomials functions. Similarly to the Lagrange method, this one consists on an approximation of the functional value y by polynomial functions of degree P where the global polynomial function of interpolation is replaced by local ones connected at fixed knots. In this interpolation method, the knots are directly defined as the data points. In addition, constraints of differentiability must be taken into account. In fact, splines are built in such way that both the fitted curve and its first $P - 1$ derivatives are continuously differentiable. For the sake of simplicity, we chose to fix $P = 3$. Consequently, on each interval $[t_{j-1}, t_j]$, the approximation function $\tilde{y}_j : [t_{j-1}, t_j] \rightarrow \mathbb{R}$ can be written as

$$\tilde{y}_j(t) = a_j + b_j t + c_j t^2 + d_j t^3 \quad \forall t \in [t_{j-1}, t_j], \quad \forall j \in \{2, \dots, m\} \quad [\text{B.1}]$$

Due to differentiability constraints, we want both the first and the second derivative of \tilde{y}_j to be continuous. Differentiating [B.1] twice, we obtain the linear expression in [B.2] which can be re-write, considering that $\tilde{y}_j''(t_{j-1}) = y_{j-1}''$ and $\tilde{y}_j''(t_j) = y_j''$, as [B.3]

$$\tilde{y}_j''(t) = 2c_j + 6d_j t \quad \forall t \in [t_{j-1}, t_j] \quad [\text{B.2}]$$

$$\tilde{y}_j''(t) = \frac{y_{j-1}''}{h_j} (t_j - t) + \frac{y_j''}{h_j} (t - t_{j-1}) \quad [\text{B.3}]$$

where $h_j = t_j - t_{j-1}$. We can then go back to the function \tilde{y} by integrating [B.3].

$$\tilde{y}_j'(t) = \frac{-y_{j-1}''}{2h_j} (t_j - t)^2 + \frac{y_j''}{2h_j} (t - t_{j-1})^2 + C_1 \quad [\text{B.4}]$$

$$\tilde{y}_j(t) = \frac{-y_{j-1}''}{6h_j} (t_j - t)^3 + \frac{y_j''}{6h_j} (t - t_{j-1})^3 + C_1 t + C_2 \quad [\text{B.5}]$$

where C_1 and C_2 are two integration constants. The relations between (y_{j-1}, y_j) and their second derivatives (y''_{j-1}, y''_j) can be found by evaluating [B.5] at both times t_{j-1} and t_j as

$$\begin{aligned} y_{j-1} &= \frac{y''_{j-1}}{6h_j} (t_j - t_{j-1})^3 + C_1 t_{j-1} + C_2 \\ y_j &= \frac{y''_j}{6h_j} (t_j - t_{j-1})^3 + C_1 t_j + C_2 \end{aligned}$$

The two integration constants C_1 and C_2 can be identified by solving the following system of two equations

$$\begin{cases} C_1 t_{j-1} + C_2 = y_{j-1} - \frac{y''_{j-1}}{6h_j} (t_j - t_{j-1})^3 \\ C_1 t_j + C_2 = y_j - \frac{y''_j}{6h_j} (t_j - t_{j-1})^3 \end{cases}$$

leading to the 2 following expressions

$$\begin{cases} C_1 = \frac{1}{h_j} (y_j - y_{j-1}) - \frac{h_j}{6} (y''_j - y''_{j-1}) \\ C_2 = \frac{1}{h_j} (y_{j-1} t_j - y_j t_{j-1}) - \frac{h_j}{6} (y''_{j-1} t_j - y''_j t_{j-1}) \end{cases}$$

Combining these two formulas with [B.4] and [B.5], we obtain:

$$\tilde{y}'_j(t) = \frac{-y''_{j-1}}{2h_j} (t_j - t)^2 + \frac{y''_j}{2h_j} (t - t_{j-1})^2 + \frac{1}{h_j} (y_j - y_{j-1}) - \frac{h_j}{6} (y''_j - y''_{j-1}) \quad [\text{B.6}]$$

$$\begin{aligned} \tilde{y}_j(t) &= \frac{y''_{j-1}}{6h_j} (t_j - t)^3 + \frac{y''_j}{6h_j} (t - t_{j-1})^3 + \frac{1}{h_j} [y_j (t - t_{j-1}) + y_{j-1} (t_j - t)] \\ &\quad - \frac{h_j}{6} [y''_{j-1} (t - t_{j-1}) + y''_j (t_j - t)] \end{aligned} \quad [\text{B.7}]$$

Our goal is to express the approximation function \tilde{y} as a function of our interpolation points corresponding to the data points $\{(t_j, y_j), \forall j \in \{1, \dots, m\}\}$. However, we can observe that the second derivatives y''_{j-1} and y''_j remain unknown. Consequently, we have to define them based on known variables such as $y_j, \forall j \in \{1, \dots, m\}$. To achieve this goal, let use the first derivative of \tilde{y}_j written in [B.6]. Because the data point (t_{j-1}, y_{j-1}) belongs to the two intervals $[t_{j-2}, t_{j-1}]$ and $[t_{j-1}, t_j]$, we can evaluate this equation and its equivalence on $[t_{j-1}, t_{j-1}]$ at time $t = t_{j-1}$, which gives the two following equations

$$y'_{j-1} = \begin{cases} \tilde{y}'_{j-1}(t_{j-1}) = \frac{h_{j-1}}{2} y''_{j-1} + \frac{(y_{j-1} - y_{j-2})}{h_{j-1}} - \frac{h_{j-1}}{6} (y''_{j-1} - y''_{j-2}) & \text{on } [t_{j-2}, t_{j-1}] \\ \tilde{y}'_j(t_{j-1}) = -\frac{h_j}{2} y''_{j-1} + \frac{(y_j - y_{j-1})}{h_j} - \frac{h_j}{6} (y''_j - y''_{j-1}) & \text{on } [t_{j-1}, t_j] \end{cases}$$

where $h_{j-1} = t_{j-1} - t_{j-2}$. By differentiability constraints ensuring the continuity of the first derivative, these two equations are supposed to be equal which provides the relationship between the zero and the second order of derivation of \tilde{y}_j .

$$\frac{h_{j-1}}{6} y''_{j-2} + \frac{(h_j + h_{j-1})}{3} y''_{j-1} + \frac{h_j}{6} y''_j = \frac{1}{h_j} (y_j - y_{j-1}) - \frac{1}{h_{j-1}} (y_{j-1} - y_{j-2}) \quad [\text{B.8}]$$

This equation allows us to generate $m - 2$ equations, for $j \in \{3, \dots, m\}$. Because m unknown y''_j must be defined, two additional equations are required. To this end, let consider two new equations defined by boundary conditions. Three types of splines-boundary conditions are commonly used. The Clamped or End-slope spline boundary conditions consider the first derivative at the endpoints as known such as $\tilde{y}'_2(t_1) = f'_1$ and $\tilde{y}'_m(t_m) = f'_m$. Using [B.6], we obtain the following two

$$B = \begin{bmatrix} [& & & B_1 & & &] \\ \frac{1}{h_2} & -(\frac{1}{h_3} + \frac{1}{h_2}) & \frac{1}{h_3} & 0 & \dots & \dots & 0 \\ 0 & \dots & \dots & \dots & \dots & \dots & \vdots \\ \vdots & \dots & \frac{1}{h_j} & -(\frac{1}{h_j} + \frac{1}{h_{j+1}}) & \frac{1}{h_{j+1}} & \dots & 0 \\ \vdots & \dots & \dots & \dots & \dots & \dots & \vdots \\ 0 & \dots & \dots & 0 & \frac{1}{h_{m-1}} & -(\frac{1}{h_m} + \frac{1}{h_{m-1}}) & \frac{1}{h_m} \\ [& & & B_m & & &] \end{bmatrix}$$

- Not-a-knot spline conditions:
 $B_1 = \mathbf{0} ; B_m = \mathbf{0}$
- Clamped conditions:
 $B_1 = (\frac{-1}{h_2}, \frac{1}{h_2}, \mathbf{0})$
 $B_m = (\mathbf{0}, \frac{1}{h_m}, \frac{-1}{h_m})$
- Natural spline conditions:
 $B_1 = \mathbf{0} ; B_m = \mathbf{0}$

We define the matrix $U \in \mathcal{M}_{m \times m}(\mathbb{R})$ as the product of the inverse matrix of A with B , $U = A^{-1}B$, therefore $Y'' = UY + A^{-1}F$. By definition of the matrix multiplication, the j th term of the vector Y'' can be written as linear combination of y_j , for $j \in \{1, \dots, m\}$:

$$y_j'' = \sum_{p=1}^m u_{jp} y_p + \sum_{p=1}^m a_{jp}^{-1} f_p \quad [\text{B.12}]$$

Once the vector Y'' estimated, the function $\tilde{y} : t \rightarrow \tilde{y}(t)$ can be defined through the equation [B.7].

B.2 Literal expression of AUC

The AUC on the interval $[t_{j-1}, t_j]$ can be calculated by integrating on its interval of definition the function \tilde{y}_j defined in [B.7].

$$\begin{aligned} \text{AUC}|_{[t_{j-1}, t_j]} &= \int_{t_{j-1}}^{t_j} \tilde{y}_j(t) dt \\ &= \int_{t_{j-1}}^{t_j} \left[\frac{y_{j-1}''}{6h_j} (t_j - t)^3 + \frac{y_j''}{6h_j} (t - t_{j-1})^3 + \frac{1}{h_j} [y_j(t - t_{j-1}) + y_{j-1}(t_j - t)] \right. \\ &\quad \left. - \frac{h_j}{6} [y_j''(t - t_{j-1}) + y_{j-1}''(t_j - t)] \right] dt \\ &= -\frac{h_j^3}{24} (y_j'' + y_{j-1}'') + \frac{1}{2} h_j (y_j + y_{j-1}) \end{aligned}$$

As cumulative area, the overall AUC on $[t_1, t_m]$ is equal to

$$\text{AUC} = \sum_{j=2}^m \left[-\frac{h_j^3}{24} (y_j'' + y_{j-1}'') + \frac{h_j}{2} (y_j + y_{j-1}) \right]$$

Considering the relationship between y_j'' and y_j in [B.12], we obtain the equation [B.13].

$$\text{AUC} = \sum_{j=2}^m \left[-\frac{h_j^3}{24} \sum_{p=1}^m ((u_{jp} + u_{j-1p}) y_p + (a_{jp}^{-1} + a_{j-1p}^{-1}) f_p) + \frac{h_j}{2} (y_j + y_{j-1}) \right] \quad [\text{B.13}]$$

B.3 Application of the Spline method with our mixed effects model

In this subsection, we develop the literal expressions of the approximated normalized AUC in each group g and its variance, $\widehat{n\text{AUC}}_g$ and $\text{Var}(\widehat{n\text{AUC}}_g)$ respectively. We are also interested in the difference of nAUC between two given vaccine arms g and \tilde{g} labelled $\Delta \widehat{n\text{AUC}}_{g-\tilde{g}}$ as well as the resulting expression of its variance, $\text{Var}(\Delta \widehat{n\text{AUC}}_{g-\tilde{g}})$. As mentioned in the main body of the article, we note $Y_{i,j,g}$ the outcome of the subject i belonging to the group of treatment g at its j th time point $t_{i,j,g}$, where $i \in \{1, \dots, N\}$, $j \in \{1, \dots, m_i\}$ and $g \in \{1, \dots, G\}$. The outcome of interest Y is described by the linear mixed effects model given by

$$Y_{ij,g_i} = f_0(t_{ij,g_i}) + \sum_{g=1}^G \mathbb{1}_{[g_i=g]} \times F_g(t_{ij,g}) + h_i(t_{ij,g_i}) + \varepsilon_{ij}$$

where the function f_0 represents the non group-specific terms, the functions F_g are linear combinations of time-depending and group specific functions labelled f_g such as $F_g(t_{ij,g}) = \sum_{k=1}^{K_g} \beta_k^g f_g^k(t_{ij,g})$ and h_i are time-dependent functions describing inter-individual variability. Because, only f_0 and F_g functions are involved in literal expressions of interest, any further information are given to specify random effects. For sake of simplicity, we fixed the f_0 as global intercept, $f_0(t_{ij,g}) = \gamma_0$. Consequently, the model can be re-write as

$$Y_{ij,g_i} = \gamma_0 + \sum_{g=1}^G \mathbb{1}_{[g=g_i]} \times \sum_{k=1}^{K_g} \beta_k^g f_g^k(t_{ij,g}) + h_i(t_{ij,g_i}) + \varepsilon_{ij}$$

Based on this definition, the expected value of the estimation of Y in the g th group at the j th time point, $\hat{\mu}_{j,g}$, is defined as

$$\hat{\mu}_{j,g} = \hat{\gamma}_0 + \sum_{k=1}^{K_g} \hat{\beta}_k^g f_g^k(t_{j,g}) \quad [\text{B.14}]$$

where $\hat{\gamma}_0$ and $\hat{\beta}^g = (\hat{\beta}_1^g, \dots, \hat{\beta}_{K_g}^g)^T$ are maximum likelihood estimates of the fixed parameters of the MEM.

Literal expression of nAUC and its variance

The literal expression of the estimated nAUC in group g is obtained by replacing the outcome y_j in Equation [B.13] by [B.14] and dividing the resulting expression by the time of follow up T_g (as described in the main article).

$$\widehat{nAUC}_g = \hat{\gamma}_0 K_{\gamma_0}^g + \sum_{k=1}^{K_g} \hat{\beta}_k^g C_{k_g} + K_g \quad [\text{B.15}]$$

where

$$\left\{ \begin{array}{l} K_{\gamma_0}^g = \frac{1}{T_g} \sum_{j=2}^{m_g} \left[-\frac{h_{j,g}^3}{24} \sum_{p=1}^{m_g} (u_{jp,g} + u_{j-1p,g}) + h_{j,g} \right] \\ C_{k_g} = \frac{1}{T_g} \sum_{j=2}^{m_g} \left[-\frac{h_{j,g}^3}{24} \sum_{p=1}^{m_g} (u_{jp,g} + u_{j-1p,g}) f_g^k(t_{p,g}) + \frac{h_{j,g}}{2} (f_g^k(t_{j,g}) + f_g^k(t_{j-1,g})) \right] \\ K_g = \frac{1}{T_g} \sum_{j=2}^{m_g} \left[-\frac{h_{j,g}^3}{24} \sum_{p=1}^{m_g} (a_{jp,g}^{-1} + a_{j-1p,g}^{-1}) f_{p,g} \right] \quad (\text{constant}) \end{array} \right.$$

Based on the expression [B.15] and knowing that K_g is a simple constant, we defined its variance

$$\begin{aligned} \text{Var}(\widehat{nAUC}_g) &= (K_{\gamma_0}^g)^2 \text{Var}(\hat{\gamma}_0) + \sum_{k=1}^{K_g} (C_{k_g})^2 \text{Var}(\hat{\beta}_k^g) + 2 \sum_{k=1}^{K_g-1} \sum_{\tilde{k}=k+1}^{K_g} C_{k_g} C_{\tilde{k}_g} \text{Cov}(\hat{\beta}_k^g, \hat{\beta}_{\tilde{k}}^g) \\ &\quad + 2K_{\gamma_0}^g \sum_{k=1}^{K_g} C_{k_g} \text{Cov}(\hat{\gamma}_0, \hat{\beta}_k^g) \end{aligned}$$

Literal expression of $\Delta nAUC$ and its variance

To define the literal expression of $\Delta nAUC$ built as the difference of nAUC between the groups of treatment g and \tilde{g} , we found

$$\begin{aligned} \Delta \widehat{nAUC}_{g-\tilde{g}} &= \widehat{nAUC}_{\tilde{g}} - \widehat{nAUC}_g \\ &= \hat{\gamma}_0 (K_{\gamma_0}^{\tilde{g}} - K_{\gamma_0}^g) + \sum_{k=1}^{K_{\tilde{g}}} \hat{\beta}_k^{\tilde{g}} C_{k_{\tilde{g}}} - \sum_{k=1}^{K_g} \hat{\beta}_k^g C_{k_g} + K_{\tilde{g}} - K_g \end{aligned}$$

By definition of the variance, we get a similar literal expression of $\text{Var} \Delta \widehat{nAUC}_{g-\tilde{g}}$ to the one obtained with the Lagrange method (see Equation [A.12]).

Matrix formulation

As mentioned in the main article, the linear mixed-effects model can be re-expressed through matrix formulation involving the re-expression of the nAUC. Similar to the trapezoid method, the nAUC can be written as linear combination of the response of interest at each time point, as

$$nAUC_g = \frac{1}{T_g} \sum_{j=1}^{m_g} [\omega_{j,g}^{spl} \bar{Y}_{j,g} + G_{j,g}] = \frac{1}{T_g} (\boldsymbol{\omega}_g^{spl T} \bar{\mathbf{Y}}_g + \mathbf{G}_g)$$

where $\boldsymbol{\omega}_g^{spl} = (\omega_{1,g}^{spl}, \dots, \omega_{m_g,g}^{spl})^T$, $\bar{\mathbf{Y}}_g = (\bar{Y}_{1,g}, \dots, \bar{Y}_{m_g,g})^T$ and $\mathbf{G}_g = (G_{1,g}, \dots, G_{m_g,g})^T$ with

$$\begin{aligned} \omega_{j,g}^{spl} &= \sum_{p=2}^{m_g} -\frac{h_{p,g}^3}{24} (u_{pj,g} + u_{p-1j,g}) + \begin{cases} \frac{t_{j+1,g} - t_{j,g}}{2}, & j = 1 \\ \frac{t_{j,g} - t_{j-1,g}}{2}, & j = m_g \\ \frac{t_{j+1,g} - t_{j-1,g}}{2}, & \text{otherwise} \end{cases} \\ &= \sum_{p=2}^{m_g} -\frac{h_{p,g}^3}{24} (u_{pj,g} + u_{p-1j,g}) + \omega_{j,g}^{trap} \\ G_{j,g} &= \sum_{p=2}^{m_g} [(a_{pj,g}^{-1} + a_{p-1j,g}^{-1}) f_{j,g}] \quad \forall j \in \{1, \dots, m_g\} \end{aligned}$$

with $\omega_{j,g}^{trap}$ defined in the main article by Equation [5] as the weights found for the trapezoid method.

C Robustness of the test of equality of nAUC, 20 and 100 patients by group

Table C.1. Comparison of the robustness of the test of equality of nAUC. Individual trajectories are subject to missing data and/or LOD. Simulations were performed for $n_g = 20$ subjects by group, mean trajectories following both profiles and for 1 000 replications.

Data Pattern	Methods	Profile 1			Profile 2		
		Type-I error	Power	Type-I error	Power	Type-I error	Power
LOD	$\Delta nAUC$	0	-0.1	-0.25	0	-0.1	-0.25
	$Var(nAUC)$	0.02	0.1	0.02	0.1	0.02	0.1
\emptyset	Indiv. nAUC	0.058	0.60	0.17	1.00	0.69	0.054
	NP nAUC	0.058	0.60	0.17	1.00	0.69	0.054
	MEM nAUC	0.061	0.70	0.63	0.22	1.00	0.80
50	Indiv. nAUC	0.063	0.64	0.61	1.00	0.72	0.057
	NP nAUC	0.063	0.64	0.61	1.00	0.72	0.057
	MEM nAUC	0.073	0.68	0.61	1.00	0.73	0.065
1.10 ⁵	Indiv. nAUC	0.056	0.61	0.27	0.09	0.94	0.44
	1. Data	0.052	0.59	0.45	1.00	0.66	0.138
	2. LOCF	0.056	0.62	0.27	0.09	0.95	0.44
5.10 ⁴	NP nAUC	0.056	0.68	0.55	1.00	0.67	0.066
	MEM nAUC	0.074	0.72	0.58	1.00	0.69	0.057
	Indiv. nAUC	0.059	0.63	0.06	0.11	1.11	0.639
1.10 ⁴	1. Data	0.050	0.55	0.39	0.17	0.99	0.62
	2. LOCF	0.057	0.65	0.07	0.06	1.11	0.12
	3. Mean Imp.	0.050	0.56	0.42	0.16	0.99	0.60
1.10 ⁴	NP nAUC	0.056	0.67	0.46	0.18	1.00	0.64
	MEM nAUC	0.066	0.72	0.46	0.18	1.00	0.64
	Indiv. nAUC	0.066	0.72	0.07	0.05	0.08	0.07
1.10 ⁴	1. Data	0.049	0.55	0.12	0.11	0.46	0.32
	2. LOCF	0.061	0.66	0.06	0.05	0.07	0.07
	3. Mean Imp.	0.045	0.55	0.19	0.13	0.82	0.42
1.10 ⁴	NP nAUC	0.034	0.74	0.16	0.12	0.75	0.42
	MEM nAUC	0.063	0.74	0.16	0.12	0.75	0.42
	Indiv. nAUC	0.066	0.72	0.07	0.05	0.08	0.07

(a) Results for nAUC calculated as individual summary measures and mixed model summary statistics provided by the well-specified MEM.

Data Pattern	Method	Profile 1			Profile 2		
		Type-I error	Power	Type-I error	Power	Type-I error	Power
LOD	$\Delta nAUC$	0	-0.1	-0.25	0	-0.1	-0.25
	$Var(nAUC)$	0.02	0.1	0.02	0.1	0.02	0.1
\emptyset	Adap. MEM	0.066	0.67	0.63	0.23	1.00	0.80
	Adap. MEM	0.071	0.71	0.62	0.20	1.00	0.72
	Adap. MEM	0.068	0.71	0.60	0.19	1.00	0.69
1.10 ⁵	Adap. MEM	0.064	0.69	0.46	0.18	1.00	0.64
	Adap. MEM	0.044	0.79	0.19	0.13	0.74	0.40
	Adap. MEM	0.068	0.81	0.19	0.14	0.60	0.37

(b) Results for nAUC calculated as mixed model summary statistics provided by the adaptive MEM.

Table C.2. Comparison of the robustness of the test of equality of nAUC. Individual trajectories are subject to missing data and/or LOD. Simulations were performed for $n_g = 100$ subjects by group, mean trajectories following both profiles and for 1 000 replications.

Data Pattern	Methods	Profile 1			Profile 2		
		Type-I error	Power	Type-I error	Power	Type-I error	Power
LOD	$\Delta nAUC$	0	-0.1	-0.25	0	-0.1	-0.25
	$Var(nAUC)$	0.02	0.1	0.02	0.1	0.02	0.1
\emptyset	Indiv. nAUC	0.062	0.52	1.00	0.56	1.00	1.00
	NP nAUC	0.062	0.52	1.00	0.56	1.00	1.00
	MEM nAUC	0.058	0.56	1.00	0.68	1.00	1.00
50	Indiv. nAUC	0.058	0.49	1.00	0.58	1.00	1.00
	NP nAUC	0.058	0.49	1.00	0.58	1.00	1.00
	MEM nAUC	0.059	0.54	1.00	0.58	1.00	1.00
1.10 ⁵	Indiv. nAUC	0.040	0.56	0.80	0.24	1.00	0.98
	1. Data	0.060	0.52	0.99	0.53	1.00	1.00
	2. LOCF	0.042	0.58	0.82	0.25	1.00	0.98
5.10 ⁴	NP nAUC	0.058	0.59	1.00	0.52	1.00	1.00
	MEM nAUC	0.060	0.57	1.00	0.54	1.00	1.00
	Indiv. nAUC	0.054	0.45	0.06	0.06	0.21	0.29
1.10 ⁴	1. Data	0.050	0.56	0.97	0.48	1.00	1.00
	2. LOCF	0.055	0.47	0.06	0.06	0.24	0.31
	3. Mean Imp.	0.061	0.54	0.98	0.45	1.00	1.00
1.10 ⁴	NP nAUC	0.055	0.51	0.99	0.49	1.00	1.00
	MEM nAUC	0.055	0.51	0.99	0.49	1.00	1.00
	Indiv. nAUC	0.054	0.66	0.06	0.05	0.21	0.09
1.10 ⁴	1. Data	0.056	0.54	0.36	0.24	0.96	0.95
	2. LOCF	0.051	0.63	0.06	0.05	0.17	0.07
	3. Mean Imp.	0.049	0.65	0.71	0.34	1.00	0.97
1.10 ⁴	NP nAUC	0.056	0.63	0.42	0.20	0.96	0.73
	MEM nAUC	0.056	0.63	0.42	0.20	0.96	0.73
	Indiv. nAUC	0.054	0.66	0.06	0.05	0.21	0.09

(a) Results for nAUC calculated as individual summary measures and mixed model summary statistics provided by the well-specified MEM.

Data Pattern	Method	Profile 1			Profile 2		
		Type-I error	Power	Type-I error	Power	Type-I error	Power
LOD	$\Delta nAUC$	0	-0.1	-0.25	0	-0.1	-0.25
	$Var(nAUC)$	0.02	0.1	0.02	0.1	0.02	0.1
\emptyset	Adap. MEM	0.054	0.53	1.00	0.67	1.00	1.00
	Adap. MEM	0.061	0.53	1.00	0.58	1.00	1.00
	Adap. MEM	0.058	0.59	1.00	0.54	1.00	1.00
1.10 ⁵	Adap. MEM	0.058	0.48	0.99	0.49	1.00	1.00
	Adap. MEM	0.059	0.69	0.40	0.19	0.94	0.69
	Adap. MEM	0.059	0.69	0.40	0.19	0.94	0.69

(b) Results for nAUC calculated as mixed model summary statistics provided by the adaptive MEM.

Note: AUC = area under the curve ; nAUC = normalized AUC ; NP = Non Parametric ; LOD = Limit of detection ; Individual adhoc methods (Indiv. nAUC) : 1. Data = Raw data, 2. LOCF = Last observation carried forward, 3. Mean Imp. = Mean Imputation.

D Robustness of the test of equality of nAUC estimated with Lagrange and Spline interpolation methods

Table D.1. Comparison of the robustness of the test of equality of nAUC calculated as individual summary measures and mixed model summary statistics. Individual trajectories are subject to missing data and/or limit of detection. Simulations were performed for $n_g = 20$ subjects by group, mean trajectories following both profiles and for 1 000 replications. Results obtained with the **Lagrange interpolation method**

Data Pattern	Methods	Profile 1			Profile 2		
		Type-I error	Power	Type-I error	Power	Type-I error	Power
LOD	$\Delta nAUC$	0	-0.1	-0.25	0	-0.1	-0.25
	$Var(nAUC)$	0.02	0.1	0.02	0.1	0.02	0.1
\emptyset	Indiv. nAUC	0.055	0.059	0.59	0.17	1.00	0.69
	NP nAUC	0.055	0.059	0.59	0.17	1.00	0.9
	MEM nAUC	0.069	0.072	0.63	0.23	1.00	0.80
50	Indiv. nAUC	0.063	0.062	0.61	0.18	1.00	0.72
	NP nAUC	0.063	0.062	0.61	0.18	1.00	0.72
	MEM nAUC	0.068	0.071	0.62	0.19	1.00	0.72
	Indiv. nAUC	0.057	0.063	0.27	0.09	0.94	0.44
	1. Data	0.054	0.059	0.45	0.18	1.00	0.66
	2. LOCF	0.058	0.063	0.27	0.09	0.95	0.44
	3. Mean Imp.	0.055	0.065	0.54	0.18	1.00	0.67
	NP nAUC	0.068	0.070	0.60	0.19	1.00	0.69
	MEM nAUC	0.061	0.063	0.06	0.06	0.11	0.11
	1. Data	0.050	0.056	0.39	0.17	0.99	0.62
	2. LOCF	0.057	0.064	0.07	0.06	0.11	0.12
	3. Mean Imp.	0.050	0.055	0.42	0.17	0.99	0.61
	NP nAUC	0.064	0.068	0.46	0.18	1.00	0.64
	MEM nAUC	0.064	0.068	0.46	0.18	1.00	0.64
	Indiv. nAUC	0.064	0.073	0.07	0.06	0.08	0.08
	1. Data	0.050	0.055	0.12	0.11	0.46	0.32
	2. LOCF	0.061	0.068	0.06	0.05	0.07	0.07
	3. Mean Imp.	0.044	0.055	0.19	0.12	0.82	0.41
	NP nAUC	0.033	0.071	0.16	0.12	0.74	0.41
	MEM nAUC	0.064	0.068	0.46	0.18	1.00	0.64
	Indiv. nAUC	0.064	0.073	0.07	0.06	0.08	0.08
	1. Data	0.050	0.055	0.12	0.11	0.46	0.32
	2. LOCF	0.061	0.068	0.06	0.05	0.07	0.07
	3. Mean Imp.	0.044	0.055	0.19	0.12	0.82	0.41
	NP nAUC	0.033	0.071	0.16	0.12	0.74	0.41
	MEM nAUC	0.064	0.068	0.46	0.18	1.00	0.64
	Indiv. nAUC	0.064	0.073	0.07	0.06	0.08	0.08
	1. Data	0.050	0.055	0.12	0.11	0.46	0.32
	2. LOCF	0.061	0.068	0.06	0.05	0.07	0.07
	3. Mean Imp.	0.044	0.055	0.19	0.12	0.82	0.41
	NP nAUC	0.033	0.071	0.16	0.12	0.74	0.41
	MEM nAUC	0.064	0.068	0.46	0.18	1.00	0.64
	Indiv. nAUC	0.064	0.073	0.07	0.06	0.08	0.08
	1. Data	0.050	0.055	0.12	0.11	0.46	0.32
	2. LOCF	0.061	0.068	0.06	0.05	0.07	0.07
	3. Mean Imp.	0.044	0.055	0.19	0.12	0.82	0.41
	NP nAUC	0.033	0.071	0.16	0.12	0.74	0.41
	MEM nAUC	0.064	0.068	0.46	0.18	1.00	0.64
	Indiv. nAUC	0.064	0.073	0.07	0.06	0.08	0.08
	1. Data	0.050	0.055	0.12	0.11	0.46	0.32
	2. LOCF	0.061	0.068	0.06	0.05	0.07	0.07
	3. Mean Imp.	0.044	0.055	0.19	0.12	0.82	0.41
	NP nAUC	0.033	0.071	0.16	0.12	0.74	0.41
	MEM nAUC	0.064	0.068	0.46	0.18	1.00	0.64
	Indiv. nAUC	0.064	0.073	0.07	0.06	0.08	0.08
	1. Data	0.050	0.055	0.12	0.11	0.46	0.32
	2. LOCF	0.061	0.068	0.06	0.05	0.07	0.07
	3. Mean Imp.	0.044	0.055	0.19	0.12	0.82	0.41
	NP nAUC	0.033	0.071	0.16	0.12	0.74	0.41
	MEM nAUC	0.064	0.068	0.46	0.18	1.00	0.64
	Indiv. nAUC	0.064	0.073	0.07	0.06	0.08	0.08
	1. Data	0.050	0.055	0.12	0.11	0.46	0.32
	2. LOCF	0.061	0.068	0.06	0.05	0.07	0.07
	3. Mean Imp.	0.044	0.055	0.19	0.12	0.82	0.41
	NP nAUC	0.033	0.071	0.16	0.12	0.74	0.41
	MEM nAUC	0.064	0.068	0.46	0.18	1.00	0.64
	Indiv. nAUC	0.064	0.073	0.07	0.06	0.08	0.08
	1. Data	0.050	0.055	0.12	0.11	0.46	0.32
	2. LOCF	0.061	0.068	0.06	0.05	0.07	0.07
	3. Mean Imp.	0.044	0.055	0.19	0.12	0.82	0.41
	NP nAUC	0.033	0.071	0.16	0.12	0.74	0.41
	MEM nAUC	0.064	0.068	0.46	0.18	1.00	0.64
	Indiv. nAUC	0.064	0.073	0.07	0.06	0.08	0.08
	1. Data	0.050	0.055	0.12	0.11	0.46	0.32
	2. LOCF	0.061	0.068	0.06	0.05	0.07	0.07
	3. Mean Imp.	0.044	0.055	0.19	0.12	0.82	0.41
	NP nAUC	0.033	0.071	0.16	0.12	0.74	0.41
	MEM nAUC	0.064	0.068	0.46	0.18	1.00	0.64
	Indiv. nAUC	0.064	0.073	0.07	0.06	0.08	0.08
	1. Data	0.050	0.055	0.12	0.11	0.46	0.32
	2. LOCF	0.061	0.068	0.06	0.05	0.07	0.07
	3. Mean Imp.	0.044	0.055	0.19	0.12	0.82	0.41
	NP nAUC	0.033	0.071	0.16	0.12	0.74	0.41
	MEM nAUC	0.064	0.068	0.46	0.18	1.00	0.64
	Indiv. nAUC	0.064	0.073	0.07	0.06	0.08	0.08
	1. Data	0.050	0.055	0.12	0.11	0.46	0.32
	2. LOCF	0.061	0.068	0.06	0.05	0.07	0.07
	3. Mean Imp.	0.044	0.055	0.19	0.12	0.82	0.41
	NP nAUC	0.033	0.071	0.16	0.12	0.74	0.41
	MEM nAUC	0.064	0.068	0.46	0.18	1.00	0.64
	Indiv. nAUC	0.064	0.073	0.07	0.06	0.08	0.08
	1. Data	0.050	0.055	0.12	0.11	0.46	0.32
	2. LOCF	0.061	0.068	0.06	0.05	0.07	0.07
	3. Mean Imp.	0.044	0.055	0.19	0.12	0.82	0.41
	NP nAUC	0.033	0.071	0.16	0.12	0.74	0.41
	MEM nAUC	0.064	0.068	0.46	0.18	1.00	0.64
	Indiv. nAUC	0.064	0.073	0.07	0.06	0.08	0.08
	1. Data	0.050	0.055	0.12	0.11	0.46	0.32
	2. LOCF	0.061	0.068	0.06	0.05	0.07	0.07
	3. Mean Imp.	0.044	0.055	0.19	0.12	0.82	0.41
	NP nAUC	0.033	0.071	0.16	0.12	0.74	0.41
	MEM nAUC	0.064	0.068	0.46	0.18	1.00	0.64
	Indiv. nAUC	0.064	0.073	0.07	0.06	0.08	0.08
	1. Data	0.050	0.055	0.12	0.11	0.46	0.32
	2. LOCF	0.061	0.068	0.06	0.05	0.07	0.07
	3. Mean Imp.	0.044	0.055	0.19	0.12	0.82	0.41
	NP nAUC	0.033	0.071	0.16	0.12	0.74	0.41
	MEM nAUC	0.064	0.068	0.46	0.18	1.00	0.64
	Indiv. nAUC	0.064	0.073	0.07	0.06	0.08	0.08
	1. Data	0.050	0.055	0.12	0.11	0.46	0.32
	2. LOCF	0.061	0.068	0.06	0.05	0.07	0.07
	3. Mean Imp.	0.044	0.055	0.19	0.12	0.82	0.41
	NP nAUC	0.033	0.071	0.16	0.12	0.74	0.41
	MEM nAUC	0.064	0.068	0.46	0.18	1.00	0.64
	Indiv. nAUC	0.064	0.073	0.07	0.06	0.08	0.08
	1. Data	0.050	0.055	0.12	0.11	0.46	0.32
	2. LOCF	0.061	0.068	0.06	0.05	0.07	0.07
	3. Mean Imp.	0.044	0.055	0.19	0.12	0.82	0.41
	NP nAUC	0.033	0.071	0.16	0.12	0.74	0.41
	MEM nAUC	0.064	0.068	0.46	0.18	1.00	0.64
	Indiv. nAUC	0.064	0.073	0.07	0.06	0.08	0.08
	1. Data	0.050	0.055	0.12	0.11	0.46	0.32
	2. LOCF	0.061	0.068	0.06	0.05	0.07	0.07
	3. Mean Imp.	0.044	0.055	0.19	0.12	0.82	0.41
	NP nAUC	0.033	0.071	0.16	0.12	0.74	0.41
	MEM nAUC	0.064	0.068	0.46	0.18	1.00	0.64
	Indiv. nAUC	0.064	0.073	0.07	0.06	0.08	0.08
	1. Data	0.050	0.055	0.12	0.11	0.46	0.32
	2. LOCF	0.061	0.068	0.06	0.05	0.07	0.07
	3. Mean Imp.	0.044	0.055	0.19	0.12	0.82	0.41
	NP nAUC	0.033	0.071	0.16	0.12	0.74	0.41
	MEM nAUC	0.064	0.068	0.46	0.18	1.00	0.64
	Indiv. nAUC	0.064	0.073	0.07	0.06	0.08	0.08
	1. Data	0.050	0.055	0.12	0.11	0.46	0.32
	2. LOCF	0.061	0.068	0.06	0.05	0.07	0.07
	3. Mean Imp.	0.044	0.055	0.19	0.12	0.82	0.41
	NP nAUC	0.033	0.071	0.16	0.12	0.74	0.41
	MEM nAUC	0.064	0.068	0.46	0.18	1.00	0.64
	Indiv. nAUC	0.064	0.073	0.07	0.06	0.08	0.08
	1. Data	0.050	0.055	0.12	0.11	0.46	0.32
	2. LOCF	0.061	0.068	0.06	0.05	0.07	0.07
	3. Mean Imp.	0.044	0.055	0.19	0.12	0.82	0.41
	NP nAUC	0.033	0.071	0.16	0.12	0.74	0.41
	MEM nAUC	0.064	0.068	0.46	0.18	1.00	0.64
	Indiv. nAUC	0.064	0.073	0.07	0.06	0.08	0.08
	1. Data	0.050	0.055	0.12	0.11	0.46	0.32
	2. LOCF	0.061	0.068	0.06	0.05	0.07	0.07
	3. Mean Imp.	0.044	0.055	0.19	0.12	0.82	0.41

Table D.3. Comparison of the robustness of the test of equality of nAUC calculated as individual summary measures and mixed model summary statistics. Individual trajectories are subject to missing data and/or limit of detection. Simulations were performed for $n_g = 100$ subjects by group, mean trajectories following both profiles and for 1 000 replications. Results obtained with the **Lagrange interpolation method**

Data Pattern	Methods	Profile 1			Profile 2		
		Type-I error	Power	Type-I error	Power	Type-I error	Power
LOD	$\Delta nAUC$	0	-0.1	-0.25	0	-0.1	-0.25
	$\text{Var}(nAUC)$	0.02	0.1	0.02	0.1	0.02	0.1
\emptyset	Indiv. nAUC	0.060	0.051	1.00	0.56	1.00	1.00
	NP nAUC	0.060	0.051	1.00	0.56	1.00	1.00
	MEM nAUC	0.058	0.056	1.00	0.68	1.00	1.00
50	Indiv. nAUC	0.056	0.049	1.00	0.58	1.00	1.00
	NP nAUC	0.056	0.049	1.00	0.58	1.00	1.00
	MEM nAUC	0.059	0.056	1.00	0.58	1.00	1.00
1.10 ⁵	Indiv. nAUC	0.038	0.057	0.80	0.25	1.00	0.98
	1. Data	0.060	0.053	0.99	0.53	1.00	1.00
	2. LOCF	0.042	0.058	0.81	0.25	1.00	0.98
5.10 ⁴	3. Mean Imp.	0.057	0.058	1.00	0.52	1.00	1.00
	NP nAUC	0.061	0.058	1.00	0.53	1.00	1.00
	MEM nAUC	0.052	0.045	0.06	0.06	0.21	0.28
1.10 ⁴	Indiv. nAUC	0.049	0.057	0.97	0.48	1.00	1.00
	1. Data	0.053	0.048	0.06	0.06	0.24	0.31
	2. LOCF	0.062	0.052	0.98	0.45	1.00	1.00
5.10 ⁴	3. Mean Imp.	0.056	0.051	0.99	0.48	1.00	1.00
	NP nAUC	0.051	0.065	0.07	0.06	0.11	0.12
	MEM nAUC	0.049	0.058	0.42	0.16	0.99	0.61
1.10 ⁴	Indiv. nAUC	0.064	0.069	0.46	0.18	1.00	0.64
	1. Data	0.065	0.071	0.07	0.05	0.08	0.07
	2. LOCF	0.049	0.055	0.12	0.11	0.46	0.32
5.10 ⁴	3. Mean Imp.	0.061	0.063	0.07	0.05	0.07	0.07
	NP nAUC	0.045	0.055	0.19	0.13	0.81	0.41
	MEM nAUC	0.035	0.075	0.17	0.12	0.76	0.42

Note: AUC = area under the curve ; nAUC = normalized AUC ; NP = Non Parametric ; LOD = Limit of detection ; Individual adhoc methods (Indiv. nAUC): 1. Data = Raw data, 2. LOCF = Last observation carried forward, 3. Mean Imp. = Mean Imputation.

Table D.5. Comparison of the robustness of the test of equality of nAUC calculated as individual summary measures and mixed model summary statistics. Individual trajectories are subject to missing data and/or limit of detection. Simulations were performed for $n_g = 50$ subjects by group, mean trajectories following both profiles and for 1 000 replications. Results obtained with the **Spline interpolation method**

Data Pattern	Methods	Profile 1			Profile 2		
		Type-I error	Power	Power	Type-I error	Power	Power
LOD	$\Delta nAUC$	0	-0.1	-0.25	0	-0.1	-0.25
	$\text{Var}(nAUC)$	0.02	0.1	0.02	0.1	0.02	0.1
\emptyset	Indiv. nAUC	0.059	0.046	0.95	0.33	1.00	0.96
	NP nAUC	0.059	0.046	0.95	0.33	1.00	0.96
	MEM nAUC	0.058	0.055	0.97	0.41	1.00	0.99
	MEM nAUC	0.059	0.049	0.96	0.35	1.00	0.97
50	Indiv. nAUC	0.059	0.049	0.96	0.35	1.00	0.97
	NP nAUC	0.059	0.049	0.96	0.35	1.00	0.97
	MEM nAUC	0.062	0.053	0.95	0.35	1.00	0.97
	MEM nAUC	0.060	0.053	0.49	0.16	1.00	0.80
1.10 ⁵	1. Data	0.054	0.045	0.84	0.32	1.00	0.96
	2. LOCF	0.059	0.053	0.51	0.16	1.00	0.81
	3. Mean Imp.	0.052	0.049	0.93	0.32	1.00	0.96
	MEM nAUC	0.064	0.053	0.94	0.33	1.00	0.97
5.10 ⁴	Indiv. nAUC	0.048	0.052	0.05	0.05	0.14	0.17
	1. Data	0.047	0.050	0.77	0.29	1.00	0.95
	2. LOCF	0.051	0.049	0.05	0.05	0.15	0.18
	3. Mean Imp.	0.049	0.053	0.81	0.27	1.00	0.93
1.10 ⁴	Indiv. nAUC	0.063	0.059	0.84	0.31	1.00	0.95
	1. Data	0.039	0.059	0.04	0.06	0.12	0.07
	2. LOCF	0.059	0.043	0.20	0.15	0.81	0.68
	3. Mean Imp.	0.037	0.051	0.04	0.06	0.10	0.07
1.10 ⁴	NP nAUC	0.055	0.055	0.43	0.19	1.00	0.76
	MEM nAUC	0.058	0.056	0.32	0.19	0.91	0.60
	MEM nAUC	0.050	0.063	0.71	0.33	1.00	0.93
	MEM nAUC	0.057	0.063	0.42	0.20	0.97	0.73

Note: AUC = area under the curve ; nAUC = normalized AUC ; NP = Non Parametric ; LOD = Limit of detection ; Individual adhoc methods (Indiv. nAUC): 1. Data = Raw data, 2. LOCF = Last observation carried forward, 3. Mean Imp. = Mean Imputation.

Table D.6. Comparison of the robustness of the test of equality of nAUC calculated as individual summary measures and mixed model summary statistics. Individual trajectories are subject to missing data and/or limit of detection. Simulations were performed for $n_g = 100$ subjects by group, mean trajectories following both profiles and for 1 000 replications. Results obtained with the **Spline interpolation method**

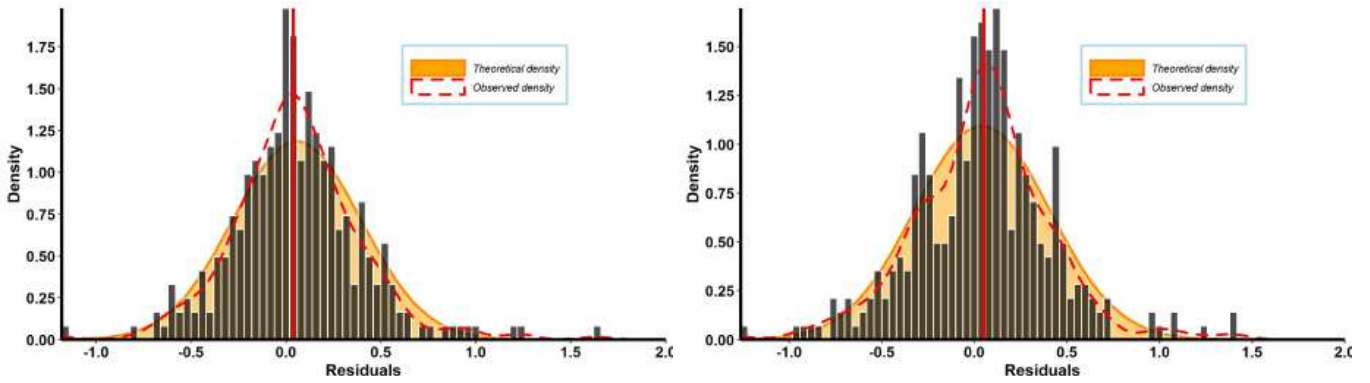
Data Pattern	Methods	Profile 1			Profile 2		
		Type-I error	Power	Power	Type-I error	Power	Power
LOD	$\Delta nAUC$	0	-0.1	-0.25	0	-0.1	-0.25
	$\text{Var}(nAUC)$	0.02	0.1	0.02	0.1	0.02	0.1
\emptyset	Indiv. nAUC	0.061	0.050	1.00	0.56	1.00	1.00
	NP nAUC	0.061	0.050	1.00	0.56	1.00	1.00
	MEM nAUC	0.058	0.056	1.00	0.68	1.00	1.00
	MEM nAUC	0.058	0.048	1.00	0.58	1.00	1.00
50	Indiv. nAUC	0.058	0.048	1.00	0.58	1.00	1.00
	NP nAUC	0.058	0.048	1.00	0.58	1.00	1.00
	MEM nAUC	0.059	0.054	1.00	0.58	1.00	1.00
	MEM nAUC	0.040	0.056	0.80	0.25	1.00	0.98
1.10 ⁵	1. Data	0.060	0.052	0.99	0.53	1.00	1.00
	2. LOCF	0.042	0.058	0.82	0.25	1.00	0.98
	3. Mean Imp.	0.058	0.060	1.00	0.52	1.00	1.00
	MEM nAUC	0.058	0.057	1.00	0.54	1.00	1.00
5.10 ⁴	Indiv. nAUC	0.054	0.045	0.06	0.06	0.23	0.30
	1. Data	0.050	0.056	0.97	0.48	1.00	1.00
	2. LOCF	0.055	0.046	0.06	0.06	0.24	0.32
	3. Mean Imp.	0.059	0.054	0.98	0.45	1.00	1.00
1.10 ⁴	Indiv. nAUC	0.058	0.063	0.71	0.33	1.00	0.97
	1. Data	0.054	0.067	0.07	0.05	0.21	0.09
	2. LOCF	0.057	0.054	0.36	0.24	0.96	0.95
	3. Mean Imp.	0.051	0.062	0.06	0.05	0.17	0.07
1.10 ⁴	NP nAUC	0.050	0.063	0.71	0.33	1.00	0.97
	MEM nAUC	0.057	0.063	0.42	0.20	0.97	0.73
	MEM nAUC	0.993	0.995	1.00	0.99	0.99	0.98
	MEM nAUC	0.826	0.632	0.28	0.16	0.20	0.25

E Study of the residuals of the mixed effects models applied on real clinical data.

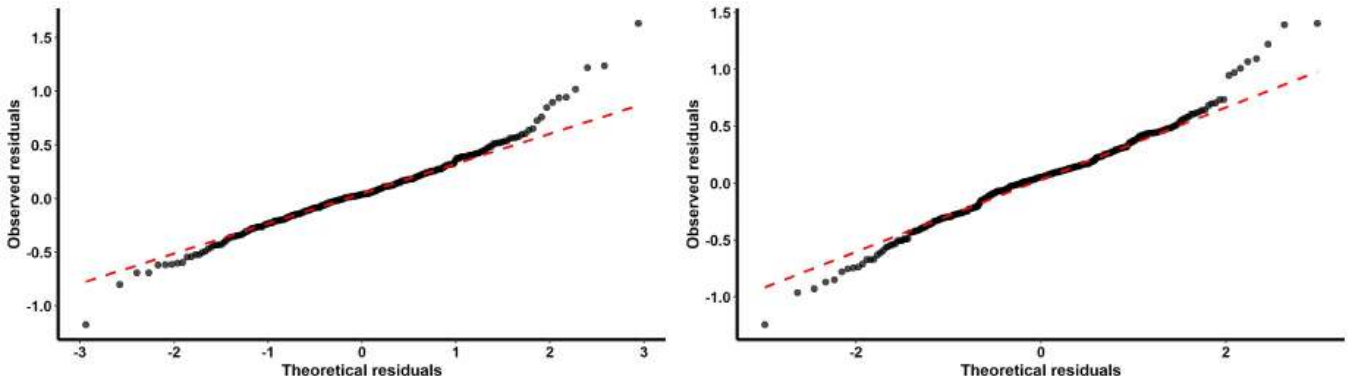
In order to verify the applicability of the developed method on the real clinical data, we checked for the two trials both the normality of the distribution of the residuals obtained by the mixed effects model and the homoscedasticity of its error model.

To evaluate the normality of the distribution of the residuals, we performed a Kolmogorov-Smirnov test on the residuals after removing the censored data. We obtained p-values of 0.1213 and 0.2347 for the LIGHT and VAC-IL2 trials respectively which tend to conclude that our residuals are normally distributed. We also used graphical validation and plotted both the distribution (Figure E.1a) and the QQplot (Figure E.1b) of the residuals obtained for the two clinical trials LIGHT and Vac-IL2.

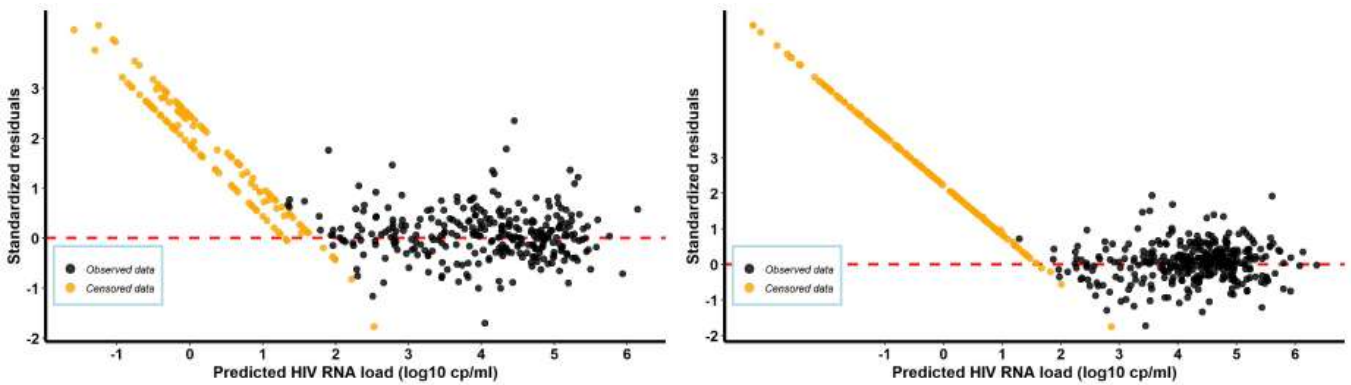
To evaluate the homoscedasticity of the error model of the mixed effects models, we performed a Breush-Pagan test on non-censored data and we plotted the residuals against the fitted values to check the dispersion of the residuals (Figure E.1c). We obtained p-values of 0.29 and 0.66 for the LIGHT and Vac-IL2 trials respectively, which tend to conclude the homoscedasticity of residuals can not be rejected for both trials



(a) Density of the residuals of the Vac-IL2 and LIGHT therapeutic vaccine trials on the left and right side respectively. Black histograms and red dashed lines represent observed densities while orange areas represent theoretical densities of the residuals defined by the mean and the standard deviation of the observed residuals.



(b) QQplot of the residuals of the Vac-IL2 and LIGHT therapeutic vaccine trials on the left and right side respectively.



(c) Residuals versus predicted HIV RNA load for the Vac-IL2 and LIGHT therapeutic vaccine trials on the left and right side respectively. Black dots represent observed data while orange dots represent left-censored data.

Figure E.1. Study of the residuals of the mixed effects model fitting HIV RNA load of the Vac-IL2 (left side) and LIGHT (right side) therapeutic vaccine trials.

F Study of the sample size

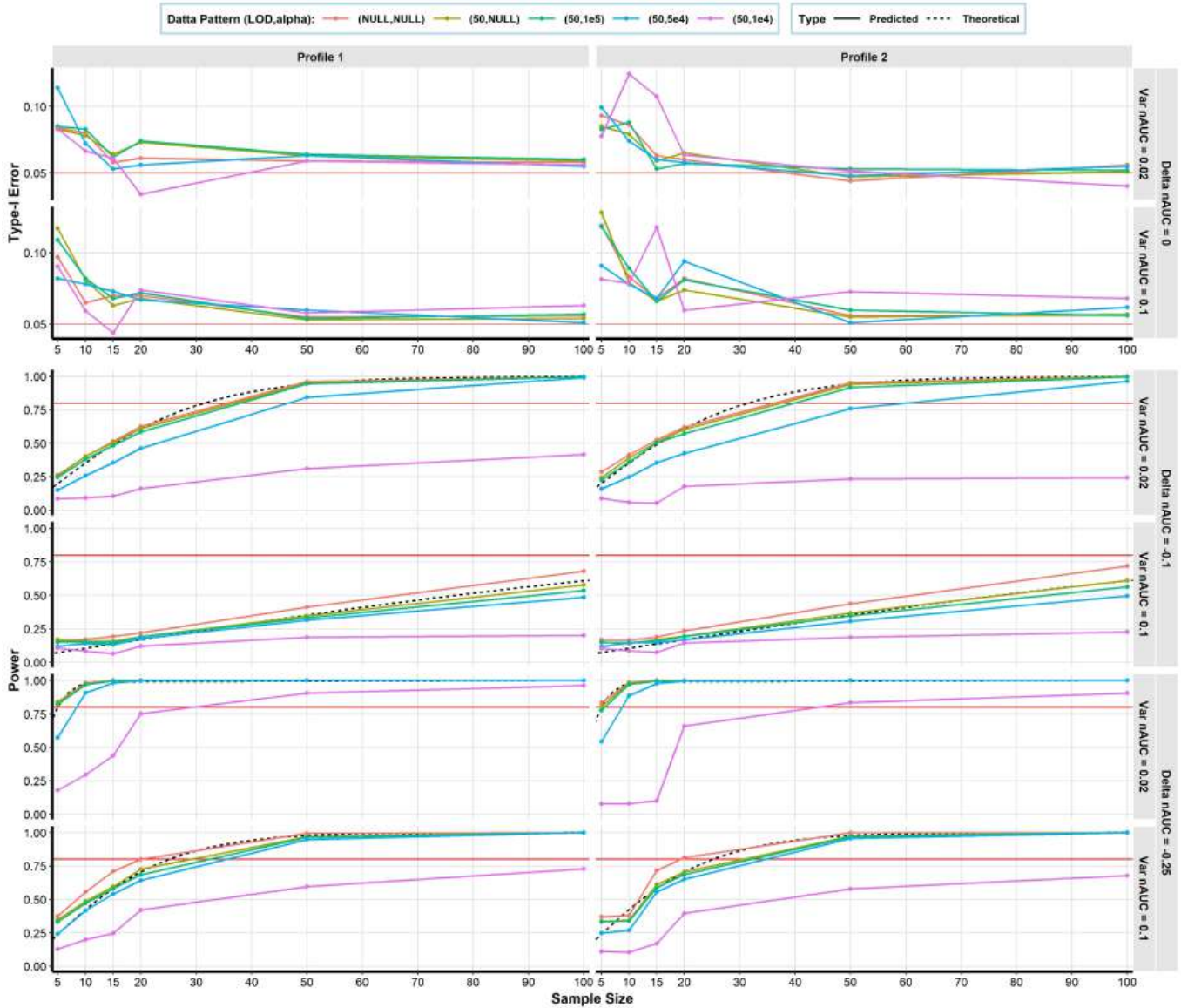


Figure F.1. Study of Type-I Error and Power as function of Sample size. Solid lines represent power and type-I error obtained by our MEM: in orange, without LOD or missing data ; in yellow, with LOD and without missing data ; in green, LOD with $\alpha = 100000$; in blue, LOD with $\alpha = 50000$ and in pink, LOD with $\alpha = 10000$ cp/ml. Dashed lines represent theoretical power provided by the formula (see section Discussion). The horizontal red lines display the threshold of 5% for type-I error and 80% for power.

Appendix B

Poster PAGE2019 - *Modeling Viral Load Rebound in HIV Therapeutic Vaccine Studies*

Modeling Viral Load Rebound in HIV Therapeutic Vaccine Studies

Alexandre Marie^{1,2,3,4,*}, Prague Mélanie^{1,2,3,4}, Lévy Yves^{4,5}, Thiébaud Rodolphe^{1,2,3,4}

¹ INRIA, SISTM Team, Bodeaux France ; ² INSERM U1219, Bodeaux France ; ³ University of Bodeaux, ISPED, Bodeaux France ; ⁴ Vaccine Research Institute, Créteil France ; ⁵ Hôpital Universitaire Henri-Mondor, Créteil France ; * marie.alexandre@inria.fr



INTRODUCTION

- ▷ The development of HIV therapeutic vaccine is ongoing.
- ▷ Their efficacy is typically assessed in Analytic treatment interruption (ATI) protocols trial, in which antiretroviral treatments (ART) are interrupted over a period of time.
- ▷ Dynamical modelling of the HIV immune system interaction after ART interruption could help in the evaluation of vaccine strategies and the understanding of their mechanism of action.

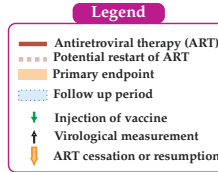
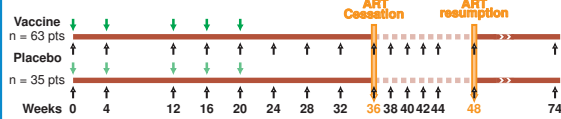
OBJECTIVES

- ▷ Find the best mechanistic model modelling the variability of the viral rebound after HIV therapeutic vaccination during ATI trials.

DATA FROM TWO VACCINE TRIALS WITH ATI

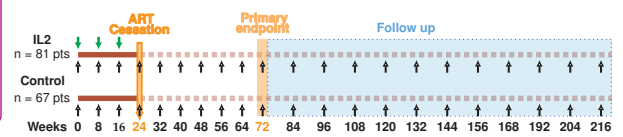
▷ VRI02 ANRS 149 LIGHT [1]

- ▷ Phase II double-blinded trial
- ▷ 98 HIV-infected patients receiving GTU®-MultiHIV B/LIPO-5 prime-boost vaccine or placebo.



▷ ANRS 118 ILIAD2 [2]

- ▷ Phase II-III, multicenter, randomized, open-label trial
- ▷ 148 HIV-infected patients receiving IL-2 or nothing

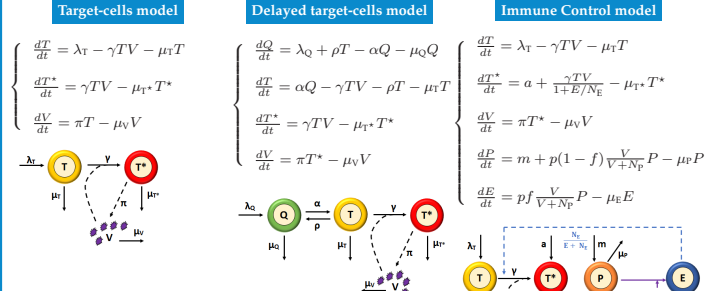


	Groups	Sample size	ATI time period	Time point on ATI	Primary endpoint
LIGHT	Vaccine + Placebo	63 + 35	12 Weeks: W36 → W48	6, every 2 weeks	Maximum value of plasma HIV-1 RNA
ILIAD2	IL-2 + Control	81 + 67	≥ 48 Weeks: W24 → W72	7, every 8 weeks & 11, every 12 weeks	Cumulative proportion of success through 72 weeks

MECHANISTIC MODELING

Mathematical model: Ordinary differential equations (ODE) modelling dynamics of viral load and CD4 count.

- ▷ Three compartments model [5]: $\frac{dT}{dt} = \lambda_T - \gamma TV - \mu_T T$
- ▷ Four compartments model [6]: $\frac{dT}{dt} = \lambda_Q + \rho T - \alpha Q - \mu_Q Q$
- ▷ Five compartments model [7]: $\frac{dT}{dt} = \lambda_T - \gamma TV - \mu_T T$



Variable	Description
Q	Quiescent CD4+ T cells
T	Activated uninfected CD4+ T cells
T*	Productively infected CD4+ T cells
V	Free HIV virus
P	Precursor immune cells
E	Effector immune cells

Parameter	Description	Parameter	Description
λ_T	Production rate of T cells	π	Virus production rate
λ_Q	Production rate of Q cells	μ_X	Death rate of X cells $X \in \{T, T^*, V, P, E\}$
m	Production rate of P cells	p	Maximum proliferation rate of immune cells
α	Activation rate of Q cells	f	Fraction of E cells that do not revert to memory
ρ	Reversion rate to the Q state	N_E	Concentration of E cells at which half-maximal inhibition occurs
a	Latent cell reactivation rate		
γ	Viral infectivity	N_P	VL at which half-maximal proliferation occurs

Immune control model:

- ▷ Account for stochastic reactivation of latently infected T cells (parameter a)
- ▷ Two regimes to consider: rare and frequent reactivation

$$a = f(R_0, t_a, p_{surv})$$

with R_0 as basic reproductive ratio, p_{surv} the probability of the long-term survival of the infection started from a single reactivating cell and t_a the average time between reactivation events of latently cells.

▷ Statistical Model: Mixed Effect model

We denote by ξ_i^l the l th individual biological parameter of the i th patient whose log-transformations, $\tilde{\xi}_i^l$ is defined by the sum of Fixed effects (average value in the population) and Random effects (inter-individual variability): for $i \in \{1, \dots, n\}$ and $l \in \{1, \dots, q\}$

$$\tilde{\xi}_i^l = (\tilde{\lambda}_i^l, \tilde{\gamma}_i^l, \dots, \tilde{\mu}_i^l)^T \quad \tilde{\xi}_i^l(t) = \phi_i + Z_i^l(t)\beta_l + \omega_i^l(t)u_i^l \quad \text{with } u_i^l \sim \mathcal{N}(0, I_q)$$

▷ Observational Model

Viral Load: $Y_{j1}^i = \log_{10} [V(t_{j1}^i, \xi^i(t_{j1}^i))] + \varepsilon_{j1}^i$ $\varepsilon_{j1}^i \sim \mathcal{N}(0, \sigma_{vl})$

CD4 count: $Y_{j2}^i = [(T + T^* + Q)(t_{j2}^i, \xi^i(t_{j2}^i))]^{0.25} + \varepsilon_{j2}^i$ $\varepsilon_{j2}^i \sim \mathcal{N}(0, \sigma_{cd4})$

- ▷ Practical identifiability (DAISY [8]) and sensibility analysis have been performed to evaluate models.
- ▷ SAEM algorithm [9] implemented in Monolix v.2018R2 is used to estimate parameters.

CONCLUSION & GOING FURTHER

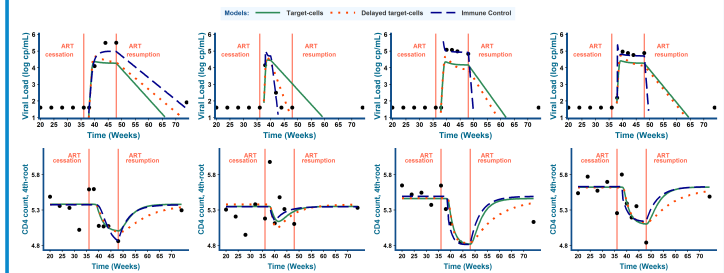
- ▷ Interestingly, the immune control model improve the fit of viral load but not CD4 count.
- ▷ Other models of immune control should be explored.
- ▷ Extension could include additional compartments and data from other immunological assays (Intracellular cytokine staining, transcriptomics, ...)

COMPARISON OF MODELS

▷ Estimation of the model parameters:

- Viral load and CD4 count data from LIGHT trial
- Comparison based on AIC and Root Mean Square Error (RMSE)

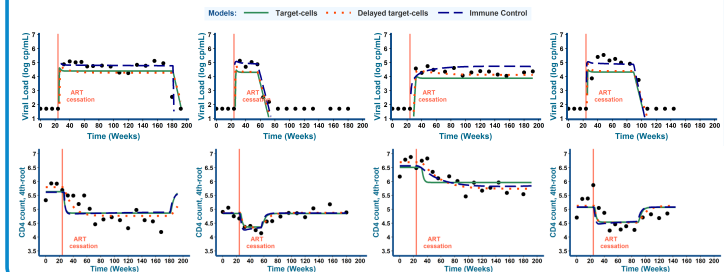
	Target-cells	Delayed target-cells	Immune Control
AIC	1738.871	1726.380	1753.840
RMSE VL	0.1462	0.1362	0.1039
RMSE CD4	0.0511	0.0510	0.0513



▷ External data validation:

- Use of parameters estimated on LIGHT
- Viral load and CD4 count data from ILIAD2 trial
- Comparison based on AIC and RMSE

	Target-cells	Delayed target-cells	Immune Control
AIC	8239.06	7335.73	7969.11
RMSE VL	0.1917	0.1651	0.1264
RMSE CD4	0.0771	0.0690	0.0786



REFERENCES

- Y. Lévy et al. (2016). Poster presented at HIV Research for Prevention.
- Y. Lévy et al. (2012). *Aids*.
- Y. Lévy et al. (2014). *European journal of immunology*.
- B. Juld et al. (2019). *The Lancet HIV*.
- AS Perelson et al. (2013). *BMC biology*.
- M. Prague et al. (2012). *Biometrics*.
- M. Maziane et al. (2015). *Acta biotheoretica*.
- G. Bellu et al. (2007). *Computer methods and programs in biomedicine*.
- E. Kuhn et al. (2005). *Computational statistics & Data analysis*.

Modélisation mécaniste et optimisation de la réponse vaccinale contre les maladies infectieuses: application au VIH, à Ebola et au SARS-CoV-2

Résumé : Le développement vaccinal contre les maladies infectieuses est un élément clé en santé publique. Dans ce contexte, la modélisation mathématique s'avère fondamentale pour bien comprendre la réponse immunitaire induite par la vaccination. L'objectif de ces travaux de thèse est de proposer des outils de modélisation et des méthodes d'analyse d'essais cliniques pour comprendre le mécanisme d'action de vaccins, dériver de bons critères de jugement d'efficacité et évaluer la longévité de la réponse immunitaire induite. Dans une première partie, nous nous intéressons aux vaccins thérapeutiques contre le VIH qui sont habituellement testés dans des essais cliniques requérant l'arrêt de traitements antirétroviraux. Ces essais présentent des données manquantes par sortie d'étude informative, i.e. les patients pour lesquels le vaccin est le moins efficace sont remis sous traitement précocement. Basé sur un modèle linéaire à effets mixtes nous évaluons les performances d'une méthode qui permet de comparer les aires sous les courbes de dynamique virale comme critère de jugement principal. Dans une seconde partie dédiée au développement vaccinal pour SARS-CoV-2, nous proposons une nouvelle méthode d'identification de corrélats de protection (CoP) basée sur une approche originale de sélection de variable dépendantes du temps dans les modèles non linéaires à effets mixtes, aussi appelé modèles mécanistes. Par son application à trois essais vaccinaux, nous identifions les mesures de neutralisation des anticorps comme CoP mécaniste. Dans une dernière partie dédiée à l'évaluation à long terme de la réponse anticorps à la vaccination Ebola, nous proposons des méthodes pour évaluer la robustesse sur de nouvelles données d'un modèle mécaniste de dynamique humorale précédemment établi sur des données précoces. Nous montrons que l'âge, le sexe et la localisation géographique sont identifiés comme facteurs de variabilité de la magnitude et de la longévité de la réponse humorale. Dans cette thèse, ces travaux ont à la fois permis de répondre à des questions cliniques de développement vaccinal avec des outils de modélisation statistiques mais plus largement participent à l'accélération du développement vaccinal.

Mots clés : Modélisation mécaniste ; Equations différentielles ordinaires ; Modèles à effets mixtes ; Vaccin ; Critères de jugement ; Corrélats de protection ; Réponse humorale ; Longévité ; VIH ; Ebola ; SARS-CoV-2

Mechanistic modeling and optimization of vaccine response in infectious diseases: application to HIV, Ebola and SARS-CoV-2

Abstract: Vaccine development against infectious diseases is a key element in public health. In this context, mathematical modeling is fundamental to better understand the vaccine-induced immune response. The objective of this thesis is to propose modeling tools and methods analysing clinical trials to better understand the mechanism of action of vaccines, to derive the right efficacy outcomes and to evaluate the longevity of the induced immune response. In a first part, we are interested in therapeutic HIV vaccines that are usually tested in clinical trials requiring discontinuation of antiretroviral therapy. These trials present missing data by informative study output, i.e. patients for whom the vaccine is less effective resume treatment early. Based on a linear mixed-effects model, we evaluate the performance of a method comparing areas under viral dynamics curves as the primary outcome. In a second part dedicated to SARS-CoV-2 vaccine development, we propose a new method for identifying correlates of protection based on an original approach of time-dependent variable selection in nonlinear mixed-effect models, otherwise known as mechanistic models. By applying it to three vaccine trials, we identify antibody neutralization measures as mechanistic CoP. In a final part dedicated to the long-term evaluation of the antibody response to Ebola vaccination, we propose methods to evaluate robustness on new data from a mechanistic model of humoral dynamics previously established on early data. We show that age, gender and geographical location are identified as factors of variability in the magnitude and longevity of the humoral response. In this thesis, these works allowed to answer clinical questions about vaccine development using statistical modeling tools and more broadly participate in the acceleration of vaccine development.

Keywords: Mechanistic modeling ; Ordinary differential equations ; Mixed-effects models ; Vaccine ; Criteria endpoint ; Correlate of protection ; Humoral response ; Longevity ; HIV ; Ebola ; SARS-CoV-2

Discipline: Santé publique - option Biostatistiques

Laboratoire: Unité INSERM U1219, Bordeaux Population Health Center - INRIA - Université de Bordeaux
146 Rue Léo Saignat 33000 Bordeaux, FRANCE